THE UNIVERSITY *of* LIVERPOOL
Department of Civil Engineering

A fundamental study into wet process modification of paving binders and mixtures by crumb rubber from used tyres

by

Ignacio Artamendi
BSc, MSc (Eng)

Thesis submitted in accordance with the requirements of
The University of Liverpool for the degree of Doctor in Philosophy

December 2003

ABSTRACT

This thesis describes an investigation into the effect of crumb rubber modifier (CRM) from tyre waste on the physico-chemical and rheological properties of bituminous binders produced by the wet process, which comprises blending the rubber and the bitumen at elevated temperature. Furthermore, the effect of these modified binders on the resulting engineering properties of bituminous mixtures is also investigated.

The blending process, which involves the dispersion of CRM into the bitumen under controlled time and temperature, results in interactions between the rubber particles and the bitumen. To understand the mechanism and factors affecting these interactions, swelling of truck and car-tyre rubbers by different solvents and bitumens was investigated. Results were analysed based on diffusion theory, which enables a kinetic parameter, the diffusion coefficient, to be calculated.

A Dynamic Shear Rheometer (DSR) was used to study the effect of blending (interaction) time and temperature on the rheological properties of the resulting modified binders. The effect of material variables, like rubber type, size and content, and bitumen grade and origin, on these properties was also investigated.

A laboratory mix design method for the determination of the required binder content based on the assessment of the aggregate packing characteristics and the resulting void structure was developed. Mixtures containing conventional and CRM binders were evaluated in terms of stiffness, resistance to moisture damage, permanent deformation and surface characteristics.

Fatigue life and low temperature fracture properties of the selected mixtures were also assessed. Fatigue testing was carried out in a four-point bending test apparatus under controlled strain and stress conditions. Fatigue lives were evaluated in terms of the number of cycles to 50 % stiffness reduction (N_f) and macro-crack formation (N_1). A damage parameter, based on the linear reduction in stiffness during a fatigue test, was adopted and a relationship was found between the rate of damage and the initial strain for both testing modes.

Refinements to a damage model developed elsewhere were introduced to counteract the variability due to dissipated energy effects manifested in the two modes of testing.

Low temperature fracture characteristics were obtained from three-point bending beam tests on notched specimens. Fracture resistance was evaluated following two approaches, namely linear elastic and elastic-plastic. Linear Elastic Fracture Mechanics approach enabled the determination of the critical stress intensity factor or fracture toughness (K_{IC}). Elastic-Plastic Fracture Mechanics approach, on the other hand, was used to determine the critical strain energy release rate or critical value of the J-integral (J_{IC}).

The implication of this work is that crumb rubber from used tyres should be seriously considered as and ingredient in asphalt for paving applications in the UK.

ACKNOWLEDGEMENT

I would like to express my most sincere thanks to my supervisor, Dr H. Khalid, Senior Lecturer in Civil Engineering, for his invaluable guidance and encouragement during all phases of this research. I would also like to thank to Dr G.C. Eastmond, Honorary Senior Fellow in Chemistry, for his guidance and advice on the chemical aspects of the research.

I am also grateful to all the technical staff and, in particular, to Mr. D. Searls, Highways Laboratory Technician, and Mr. A. Cowan for their assistance.

Finally, I would like to thank the Engineering and Physical Science Research Council and the industrial partners of the research project, Tarmac, J. Allcock & Sons, Shell and Rhusden Granulating Company, for their financial and technical support.

CONTENTS

Publications

Artamendi, I., Eastmond, G.C. and Khalid, H., (2002). "Influence of crumb rubber modifier (CRM) from tyre waste on the rheological properties of bituminous binders." Proc., 3rd Int. Conf. Bituminous Mixtures and Pavements, Thessaloniki, Greece, November 2002, pp. 65 – 74.

Khalid, H. and Artamendi, I., (2002). "Exploratory study to evaluate the properties of rubberised asphalt modified using the wet and dry processes." Proc., 3rd Int. Conf. Bituminous Mixtures and Pavements, Thessaloniki, Greece, November 2002, pp. 15 – 25

Artamendi, I. and Khalid, H. "Fatigue damage of crumb rubber modified mixtures". Paper accepted for the 5th Int. RILEM Conf. Cracking in pavements, May 2004, Limoges, France.

Artamendi, I. and Khalid, H. "Fracture characteristics of crumb rubber modified asphalt mixtures". Abstract accepted for the 3rd Euroasphalt & Eurobitume Congress, May 2004, Vienna, Austria.

LIST OF FIGURES

LIST OF TABLES

ABBREVIATIONS

AAV	Aggregate Abrasion Value
ADOT	Arizona Department of Transport
ASCE	American Society of Civil Engineers
ASTM	American Society of Testing and Materials
BBA	British Board of Agrèment
BSI	British Standards Institution
CDM	Compacted Density of the Mix
CDMA	Compacted Density of Mineral Aggregate
C_4H_6	Butadiene
C_5H_8	Isoprene
C_8H_8	Styrene
CRM	Crumb Rubber Modifier
C.R.U.M.B	Crumb Rubber Universal Marketing Bureau
DSR	Dynamic Shear Rheometer
DTT	Direct Tension Test
ECM	Effective Crack Model
EPFM	Elastic-Plastic Fracture Mechanics
EU	European Union
EVA	Ethylene Vinyl Acetate
FHWA	Federal Highway Administration
GPC	Gel Permeation Chromatography
HMA	Hot Mix Asphalt
IRIS	Innovative Rheological Interface Software
ISTEA	Intermodal Surface Transportation Efficiency Act
ITFT	Indirect Tensile Fatigue Test
ITSM	Indirect Tensile Stiffness Modulus
ITT	Indirect Tension Test
KSR	Bitumen of Kuwaiti (Middle East) origin
LEFM	Linear Elastic Fracture Mechanics
LVDT	Linear Variable Differential Transducer
LVER	Linear Viscoelastic Region
NAT	Nottingham Asphalt Tester

NCHRP	National Co-operative Highway Research Program
NR	Natural Rubber
Pen	Penetration (dmm)
PMBs	Polymer Modified Binders
PRADO	PRogramme for Asphalt mix Design and Optimisation
PSV	Polished Stone Value
RAP	Reclaimed Asphalt Pavement
RLA	Repeated Load Axial (test)
RMA	Rubber Manufactures Association
RPA	Rubber Pavement Association
SAM	Stress absorbing membrane
SAMI	Stress-absorbing membrane interlayer
SARA	Saturates, Aromatics, Resins and Asphaltenes (fractions)
SBR	Styrene Butadiene Rubber
SBS	Styrene Butadiene Styrene
SG	Specific Gravity
SGM	Specific Gravity of the Mix
SGMA	Specific Gravity of Mineral Aggregate
SHRP	Strategic Highway Research Program
SIPC	Shell International Petroleum Company
STD	Standard Deviation
TAI	The Asphalt Institute
TCU	Temperature Control Unit
TFOT	Thin Film Oven Test
TRB	Transportation Research Board
TRL	Transport Research Laboratory
TSRST	Thermal Stress Restrained Specimen Test
UTGW	Used Tyre Working Group
VEN	Bitumen of Venezuelan origin
VIM	Voids in the Mix
VMA	Voids in Mineral Aggregate
VPO	Vapor Pressure Osmometry

Chapter 1

INTRODUCTION

Chapter 1

INTRODUCTION

1.1 THE PROBLEM OF USED TYRES

Disposal of used tyres has become a significant environmental issue that requires urgent attention. In the UK, the Environment Agency has given warning that up to 13 million tyres are already stockpiled in fields and quarries that never intended to store them. The biggest tyre dump in Britain is at Heyope, in Powys, Wales, which holds 9 million tyres. For eleven years there has been an intense fire deep inside the dump, which has yet to be extinguished.

Moreover, every year over 40 million tyres are taken off vehicles in the UK. Although around 70 % of these tyres are reused, recycled or burned for fuel, the remaining 30 %, around 12 million, are simply put on legal or illegal dumpsites, with no disposal route.

At present, garages have to pay disposal companies up to £1 to dispose of each car tyre, rising to £7 for a truck tyre. However, many used tyres are illegally dumped, as it is more convenient than recycling them. The Environment Agency estimates that it costs local authorities £2.8 million a year to clear up these illegal dumps.

The problem is further aggravated as, with effect from July 2003, a new EU Landfill Directive prohibits landfill of whole tyres and, with effect from July 2006, of shredded tyres. In addition to this, the End-of-life Vehicle Directive requires the reuse, recycling and recovery of vehicle components to be raised to 85% by 2007.

In order to meet the above Directives, the UK tyre industry will have to develop an appropriate infrastructure to absorb the tyres previously land-filled. Currently, a variety of reuse, recycling and recovery industries exist in the UK. The largest

consumers of used tyres include retread manufactures, landfill engineering, crumb rubber production and as fuel in cement kilns.

1.2 SCOPE OF THE RESEARCH

Of the available methods of recycling tyres, the use of crumb rubber in asphalt presents one of the most attractive options. Firstly, a large amount of tyres could be disposed of through their use in the production of asphalt for the construction and rehabilitation of the transport infrastructure. Secondly, it could enhance the engineering properties and, consequently, the performance of bituminous materials used in paving applications.

Crumb Rubber Modifier (CRM), a general term for used tyre rubber that is reduced in size and is used as an asphalt modifier, has been added to asphalt either in the wet or dry process. The wet process involves dispersing the crumb rubber particles in the bitumen under controlled conditions of time, temperature and mixing shear rate to produce a rubber-modified binder. This modified binder is then mixed with aggregate to form a bituminous mixture. In the dry process, on the other hand, the crumb rubber is mixed with the aggregates before incorporating the bitumen into the mixture. The rubber particles, thus, act as a partial replacement to some of the aggregate sizes. Typically, maximum size of the CRM particles used in the wet process ranges from 2 mm to 0.2 mm, whereas larger sizes, ranging from 2 mm to 6 mm, are used in the dry process.

Both, the wet and dry processes have a long history of laboratory research and field performance. Historically, tyre rubber was used as an asphalt modifier in an attempt to improve the performance of asphalt pavement mixtures. More recently, tyre rubber has been incorporated in asphalt mixtures as a means to alleviate the environmental problem of used tyre storage and disposal.

In the UK, the use of crumb rubber in asphalt has been very limited. Of the very rare instances, Colas Ltd. in 1998, laid the first trial asphalt surfacing containing rubber granulates using the dry process. Until now, however, there has been no

focused research or field trials in which crumb rubber has been added to asphalt mixtures using the wet method.

It is clear, therefore, that the UK lacks experience in the use of crumb rubber in bituminous binders and mixtures produced by the wet process. Concerted research is, therefore, needed to develop a basic understanding of how these rubber-modified binders and mixtures are produced and perform, while helping to reduce the tyre waste problem.

Bahia and Davies (1994) claimed that during the wet process, the two materials interact as bitumen components migrate into the rubber causing it to swell. Swelling also depletes the bitumen of the absorbed components and, consequently, modifies its properties. Therefore, the properties of both, the rubber and the bitumen will change affecting the final rubber-modified bitumen. To investigate the swelling phenomenon, an experimental procedure, which involved the immersion of rubber monoliths in various solvents and bitumens, has been developed. This procedure permitted to identify the type of substances preferentially absorbed by the rubbers. It also provided a tool to assess the extent and rate of swelling under conditions close to those employed in the production of CRM binders.

Bituminous binders are considered as viscoelastic materials and their rheological properties depend on both, temperature and rate of loading. Typically, rotational viscometers are used to characterise the high temperature properties associated with mixing and construction conditions, whereas dynamic and creep tests are employed to characterise their behaviour at temperatures and loading times associated with service conditions.

CRM binders' properties are affected by a large number of variables. These can be classified into material and process variables. Material variables include rubber content, size and source (car or truck tyre), and bitumen origin and grade. Process variables, on the other hand, include the temperature and duration within which the CRM binders are produced.

In this study, the effect of material variables on binders' properties was investigated by means of dynamic mechanical tests performed in a Dynamic Shear Rheometer (DSR), under a wide range of temperatures and frequencies (loading times). The method of time-temperature superposition was used to separate the dependencies of the materials behaviour, which enabled the effect of CRM modification to be evaluated.

Viscoelastic properties of various CRM binders produced under different conditions of time and temperature were obtained, and the changes in these properties were related to the main interaction mechanisms occurring during the production of CRM binders, i.e. particle swelling and degradation It has been reported (Abdelrahman and Carpenter, 1999) that swelling and degradation of CRM particles are accompanied by changes in viscoelastic properties of the binders. In addition to this, a method was developed to isolate bitumen from CRM-bitumen blends. Properties of these isolated (filtered) binders, after interaction with the rubber, were evaluated to assess the effect of interaction on the bitumen matrix.

Creep tests have also been used to study the viscoelastic properties of bituminous binders. Zanzotto and Kennepohl (1996) carried out creep and creep recovery test to investigate the degradation of CRM in bitumen by heat and shear. In this study, creep and creep recovery tests performed in the DSR were used to evaluate the effects of material and process variables on binders' properties.

Once a CRM binder is produced, it is then mixed with aggregates to form a bituminous mixture. The performance of a mixture is mainly affected by viscoelastic properties of the binder, aggregate characteristics and the volumetric composition of its components. Volumetric design of asphalt mixtures has been traditionally based on recipe specifications and/or empirical tests, such us the Marshall test. These approaches, however, do not provide any fundamental engineering properties of the material neither consider the characteristics of the aggregates.

The method proposed here for the design of bituminous mixtures is based upon the examination of the compacted aggregate structure. Work by Lees (1970) demonstrated how dense gradings could be developed by sequentially blending binary aggregate combinations. The required binder content is then determined through the assessment of the aggregate packing characteristics. Following this approach, close-graded mixtures containing a conventional and two modified binders with CRM from truck and from car tyres were designed for use as wearing courses. The selection of the mixtures was based on performance-related properties.

One of the consequences of the rubber-bitumen interaction is the migration of bitumen components into the rubber, which leads the rubber to swell and the bitumen to harden. It may be envisaged that while these effects could lead to an improvement in the mixture's resistance to permanent deformation, its fatigue and low temperature cracking properties could be adversely affected since it might lead to embrittlement of the mixture.

Fatigue cracking is one of the major load-related distresses experienced in asphalt pavements and occurs when a bituminous layer is subjected to repeated loading under the passing traffic. In the laboratory, fatigue life is typically assessed by repeated-load bending tests applied either under controlled stress or strain modes. Fatigue failure has been defined in different ways depending on the mode of loading. Failure in controlled strain and stress modes has been traditionally defined as 50 and 10 % reduction in the initial stiffness, respectively. These definitions, however, are arbitrary and do not represent the state of the material.

Hopman et al. (1989) introduced an energy ratio based on the dissipated energy concept and defined failure as the number of cycles (N_1) where cracks are considered to initiate. The N_1 criterion represents the same state of the material for controlled stress and strain modes. It is, however, more difficult and subjective to define for strain mode than for stress mode.

A different approach to characterise fatigue has been proposed by Di Benedetto et al. (1996). They identified the existence of a stage during a fatigue test, which accounted for most of the fatigue life, where the reduction in the stiffness modulus with number of load applications was approximately linear. Based on this, a damage parameter is introduced and the change of this parameter with number of cycles is used to depict damage due to fatigue. Furthermore, the model proposed by Di Benedetto et al. introduces an energy term to counteract the variability due to dissipated energy effects in the two modes of loading. A useful development to this model would be a method to deduce unique fatigue damage parameters that are independent of fatigue testing mode.

Low temperature cracking can also lead to serious damage to asphalt pavement structures. It occurs when the shrinkage stresses caused by thermal contraction of a bituminous layer are greater than the tensile strength of the material. Traditionally, low temperature cracking has been evaluated by standard test methods, such us indirect and direct tension and bending tests. These methods, however, can only reveal the properties of a homogeneous material without defects or flaws. Fracture mechanics theory, on the other hand, considers the state of stress in such flaws and provides failure criteria for materials in the presence of cracks.

Bituminous mixtures can exhibit both brittle and ductile fracture, depending on the state of stress at failure, which, in turn depends on factors such us temperature, loading conditions and inherent properties of the material. For brittle fracture, the stress intensity factor (K), based on linear elastic fracture mechanics theory, has been used to describe asphalt fracture. The stress intensity factor criterion postulates that fracture occurs when K reaches a critical value, K_{IC}, known as fracture toughness. A number of studies, however, indicated the shortcomings of using linear elastic theory for the analysis of asphalt fracture due to the non-linear behaviour of the material (Dongre et al., 1989 and Kim and El Hussein, 1997).

An alternative parameter, the J-integral, has been developed for assessing the fracture resistance of a material experience both elastic and plastic deformation.

In the development of this parameter, the deformation theory of plasticity was applied, thus, the stresses and strains in an elastic-plastic material are considered to be the same as for a nonlinear elastic material with the same stress-strain curve. It is seen then that the *J*-integral is analogous to *K* for the case of elastic behaviour. Based on this parameter, failure occurs when the *J*-integral reaches some critical value, J_{IC}.

The critical strain energy release rate or critical value of the *J*-integral, J_{IC}, has been used to study the fracture characteristics of bituminous mixtures. Work by Dongre et al. (1989) showed that the J_{IC} fracture parameter was sensitive to binder and mix properties, whereas the K_{IC} parameter was not as sensitive as J_{IC}.

In the present study, the low temperature fracture properties of mixtures containing CRM from truck and from car tyres were investigated. Monotonic three-point bending tests of notched specimens were undertaken to determine the load-deflection curves. The two approaches referred to above, i.e. K_{IC} and J_{IC} were used to characterise the materials' fracture resistance.

1.3 RESEARCH OBJECTIVES

The research work presented in this thesis aims to assess the effect of CRM modification on binder and mixture properties. The outcome of the research could enhance the level of confidence of the UK paving industry in these relatively novel materials, which, in turn, could help to reduce the problem of used tyre disposal.

The specific objectives are as follows:

- To assess the current UK situation with respect to used tyre processing and disposal.

- To develop a suitable laboratory method to study the swelling of tyre rubbers by bitumen and to evaluate the extent and rate of swelling by determining the equilibrium swelling uptake and the kinematic parameter 'diffusion coefficient'.

- To achieve a basic understanding of the effect that material variables such us CRM content, size and type, and bitumen origin have on binder viscosity with regard to mixing and construction conditions.

- To evaluate the effect of CRM content and type on the binder's viscoelastic properties over wide range of frequencies and/or temperatures as related to during in-service conditions.

- To investigate the effects of process variables, temperature and time, on the rheological properties CRM binders by means of dynamic and creep and recovery testing.

- To assess the effect that absorption of bitumen components by the rubber has on the bitumen matrix by measuring the viscoelastic properties of isolated bitumens after interaction with CRM.

- To develop a mix design procedure based on the aggregates' internal void structure and aiming to optimise performance-related properties, for bituminous mixtures for used as wearing courses containing CRM from two origins truck and car tyres.

- To characterise the effect of CRM origin on the mixture fatigue life and, to apply and implement a fatigue damage model developed elsewhere to depict fatigue damage independent of test mode.

- To adopt linear elastic and elastic-plastic fracture mechanics analysis to characterise low temperature fracture properties of mixtures containing CRM from truck and car tyres.

1.4 CONTENTS OF THESIS

1.4.1 Chapter 2: Use of crumb rubber in road applications

This chapter introduces the problems associated with the disposal of used tyres and the different methods of processing them. Particular attention is given to the processing of used tyres into crumb rubber as a recycling option. Furthermore, the chapter provides background information about the use of crumb rubber in asphalt for pavement applications.

1.4.2 Chapter 3: Rubber-bitumen interaction

In this chapter, the nature of the rubber-bitumen interaction and, in particular, the swelling phenomenon, is investigated. The chapter contains the results of swelling tests, which involved the immersion of rubber in various solvents and bitumens. Furthermore, swelling data is analysed based on the diffusion theory. From this analysis, the diffusion coefficients are determined and evaluated.

1.4.3 Chapter 4: Rheology

This chapter presents the results of an investigation into the effects of CRM on the rheological properties of bituminous binders. CRM binders were characterised in terms of their viscosities at high temperature and their viscoelastic properties at intermediate temperatures. Furthermore, the effects of production conditions of temperature and time on the CRM binders' properties were also investigated.

1.4.4 Chapter 5: Mix design and evaluation

This chapter describes a procedure for the design of bituminous mixtures. The procedure is based on the assessment of the void distribution in a compacted aggregate structure. Following this approach, a conventional and two modified mixtures containing CRM from truck and from car tyres were designed and evaluated. Mixtures were evaluated in terms of stiffness, resistance to permanent deformation, moisture damage and surface characteristics.

1.4.5 Chapter 6: Fatigue resistance

This chapter contains a detailed analysis of the fatigue test results obtained from four-point bending tests. The mixtures investigated had been previously designed in Chapter 5. Fatigue lives were given in terms of the number of cycles to failure and to macro-crack formation. A fatigue damage parameter was introduced and the rate of damage was used to characterise the fatigue resistance of the mixtures.

1.4.6 Chapter 7: Fracture and low temperature cracking

This chapter presents the low temperature fracture characteristic of the mixtures designed in Chapter 5. A fracture mechanics approach based on linear-elastic and elastic-plastic theory is followed for the analysis of the fracture test data.

1.4.7 Chapter 8: Conclusions and recommendations

This chapter summarises the findings of the research project and suggest further areas of investigation in the topic of CRM binders and mixtures.

Chapter 2

USE OF CRUMB RUBBER IN ROAD APPLICATIONS

Chapter 2

USE OF CRUMB RUBBER IN ROAD APPLICATIONS

2.1 USED TYRES

2.1.1 Introduction

Tyres play a vital role in today's society as we rely on them to travel and to transport food and other goods. There are over 121 million tyres on vehicles in Great Britain, a number which is increasing. Moreover, the numbers of vehicles and distances travelled have more than doubled in 30 years so more and more tyres are being used each year.

Traditionally, when the tyres have come to the end of their life they have been considered as waste. Historically, industry has focussed on the disposal of used tyres rather than on recapturing the economic value of the resources incorporated in the tyres. As a consequence, the applications for used tyres have been of low economic value resulting in low volumes of recycling, accumulation of tyre stockpiles, and an industry characterized by low profitability.

Used tyres are one of the most visible of waste products and the accumulation of discarded tyres is increasing worldwide at an alarming rate. Only in the USA, it is estimated that 3 billion tyres are currently found in landfills and stockpiles across the country and this is growing by approximately 200 million annually (Epps, 1994).

Although essentially inert in the natural environment, used tyres illegally dumped or stockpiled present a considerable fire risk. Uncontrolled burning of tyres produces substances which can harm the environment. These can affect air and water quality, and contaminate soil and vegetation. Black smoke, and other pollutants are also released into the atmosphere. Water used to control the fire or rainfall causes these pollutants to be washed into the ground or to runoff into nearby watercourses.

2.1.2 Used tyre processing and disposal

Currently, there are various methods of used tyres disposal that can be broadly classified as reuse, recycling, energy and material recovery, and landfill. A brief description of these methods is presented below.

2.1.2.1 Reuse

The term reuse covers all those tyres which are ultimately returned to their originally intended use on the road and applies to both part-worn tyres, where tyres with useful life remaining can be refitted to vehicles, and retreaded tyres. Retreading involves removing or 'buffing off' the remainder of worn tread, overlaying a new strip of rubber and remoulding. Retreading minimises tyre waste by increasing the life of post consumer tyres, thus reducing the volume of tyres disposed of annually.

2.1.2.2 Recycling

The use of tyres for landfill engineering applications is the most common engineering use of waste tyres. The used of tyres as a leachate drainage layers substituting for the use of conventional aggregate in the construction of new landfill cells is well proven. Other uses include road and sea embankments, slope stabilisation, highway construction, drainage culvert beds and others.

Used tyres can also be processed into rubber shred and crumb. Shredding involves the mechanical shearing of the whole tyre into pieces ranging from 25 – 300 mm in size, and it is primarily a pre-treatment for other uses. Crumbing, on the other hand, usually comprises removal of the steel and fabric component and further reduction of rubber shred to crumb (granular) rubber. Traditional end-use markets for granulate rubber include carpet underlay and sports and safety surfacings. Further markets include rubber crumb in road surfaces and as aggregate replacement in concrete.

2.1.2.3 Recovery

Used tyres are also disposed of through combustion in waste-to-energy schemes. Rubber in tyres consists of around 60 % hydrocarbons, which is a store of energy that can be recovered by incineration. Used tyres can beneficially replace some of the fossil fuels traditionally used in the cement making process. Furthermore, used tyres can be burnt in dedicated incinerators to produce electricity for use by industry and local communities. The main drawback of this technology is that tyres, when burning, produce large amounts of black smoke and sulphur dioxide, which cause air pollution. Thus, the costs of controlling these emissions contribute to the increase in investment costs, which can be up to ten times as those burning with liquid fuel.

Another form of, in this case, material recovery is pyrolysis. Pyrolysis is the thermal degradation of a material in the absence of oxygen, which in the case of tyres generates gas, oil, carbon char and steel. A proportion of the resultant gas and oil can be used to fuel the process. Novel reprocessing techniques such us pyrolysis are beginning to be considered as a mean of tyre recovery. However, as with any new process, one of the greatest obstacles is translating laboratory theory to a commercially viable plant.

2.1.2.4 Landfill

Tyres can be landfilled both whole and in shredded form. However, disposal of used tyres in landfill makes no use of the natural resources used in tyre manufacture and is the least sustainable option.

2.1.3 The UK situation

The disposal of used tyres in the UK is a significant issue that cannot be neglected. In the UK, over 40 million tyres are taken off vehicles every year accounting for a total amount of around 430,000 tonnes per year. Presently the UK recovers value from around 70 % of these tyres through reuse, recycling and energy recovery. Of the remaining 30 %, around 12 million used tyres, the vast majority are stockpiled, dumped or go to landfill (UTWG, 2000) (see **Figure 2.1**).

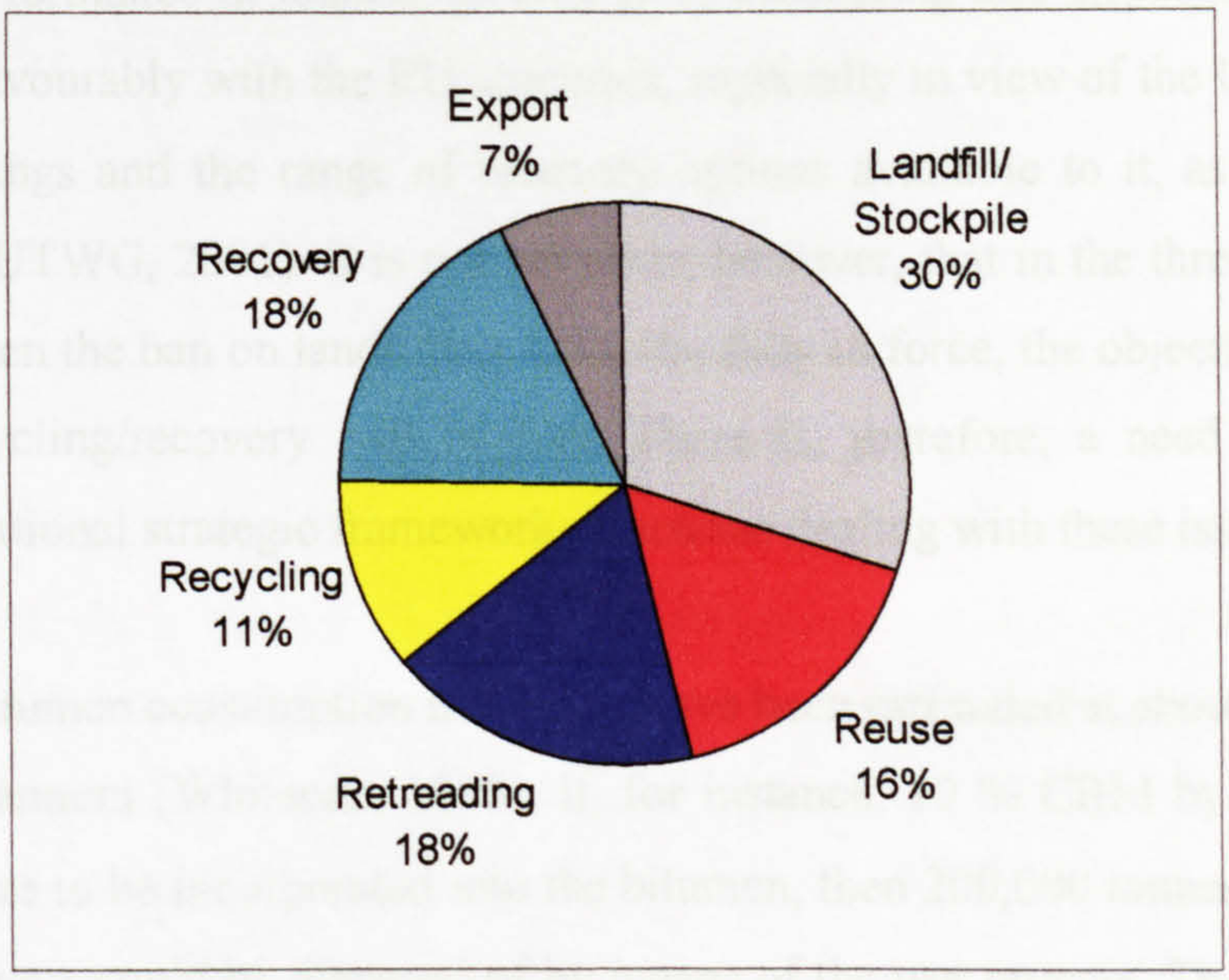

Figure 2.1 Disposal of used tyres in the UK

In the EU, the concept of 'sustainable development' and with regard to waste, the principle of waste hierarchy has been adopted. The waste management hierarchy dictates that the priority order for how to reduce the number of used tyres should be: reduction of consumption, reuse of the product, recycling of the material, energy recovery and, as the final option, disposal of the product.

The EU Landfill Directive (1999/31/EC), however, has prohibited the disposal to landfill of whole used tyres since July 2003 and will prohibit landfill of shredded tyres from July 2006. Thus, the UK will have to recover 100 % of used tyres when the landfill ban takes full effect. In order to achieve this, a substantial increase in the fields of material recycling and energy recovery will be needed to absorb the tyres previously landfilled.

Moreover, the End of Life Vehicle Directive (2000/53/EC) requires the reuse, recycling and recovery of vehicle components to be raised to 85 % by 2007. Tyres represent about 3.5 % of a vehicle's weight, so it is inevitable that, as one of the most recoverable parts of a car, tyres will provide an important contribution the overall recovery and recycling targets.

The UK performance in relation to used tyres processing and disposal generally compares favourably with the EU countries, especially in view of the UK's level of tyre arisings and the range of recovery options available to it, as shown in **Table 2.1** (UTWG, 2001). It is not yet clear, however, that in the three years up to 2006, when the ban on landfilling has to be fully in force, the objective of near 100 % recycling/recovery will be met. There is, therefore, a need for a co-ordinated national strategic framework of actions dealing with these issues.

Levels of bitumen consumption in the UK have been estimated at about 2 million tonnes per annum (Whiteoak, 1990). If, for instance, 10 % CRM by weight of bitumen were to be incorporated into the bitumen, then 200,000 tonnes of rubber from used tyres could be disposed of by means of the wet process. Thus, the wet process will be capable of using up all the tyres annually land-filled in the UK.

(Tonnes)	Arisings	Landfill	Export	Retreading	Recycling	Energy
Austria	50,000	20,000	5,000	4,500	500	20,000
Belgium	70,000	2,800	8,400	10,500	9,800	38,150
Denmark	37,500	0	4,500	1,125	26,250	5,625
Finland	30,000	0	3,000	1,800	24,000	0
France	370,000	74,000	18,500	74,000	55,500	29,600
Germany	650,000	32,500	110,500	117,000	78,000	279,500
Greece	58,500	46,800	0	1,755	1,585	4,095
Ireland	32,000	17,600	0	1,600	0	0
Italy	350,000	231,000	7,000	29,000	34,000	49,000
Luxembourg	2,750	0	2,613	137	0	0
Netherlands	67,000	0	12,060	1,340	20,100	33,500
Portugal	52,000	31,200	676	1,560	5,876	6,500
Spain	244,000	195,200	3,660	30,744	7,076	7,320
Sweden	60,000	1,200	3,600	7,200	18,600	20,400
UK	427,000	123,000	10,000	66,000	114,000	70,000
TOTAL	2,500,750	775,300	189,509	348,261	395,287	563,690

Table 2.1 Used tyres processing and disposal in the EU (after UTGW, 2001)

2.2 CRUMB RUBBER TECHNOLOGY

2.2.1 Crumb rubber

One of the principal ways in which used tyres can be recovered is by reducing the tyre to a granular form and then reprocessing. Rubber tyres are normally made out of vulcanised natural rubber (NR) and/or styrene butadiene rubber (SBR). The rubber has to be crosslinked, i.e. vulcanised, to become strong and elastic. Due to the chemical crosslinking, it is not possible to simply melt and reshape rubber materials. In order to reuse rubber tyres, special operations like grinding are needed.

Crumb rubber is produced using a process or a combination of processes which reduce the size of the raw materials. The feedstock may be whole or shredded tyres, or tyre buffings. Whole tyres require the least amount of pre-processing but are bulky and limit shipping capacity. Buffing waste, produced during the retreading process, is a source of good quality crumb because of their small size and high quality rubber. Shredded tyre rubber is, however, the primary form of raw material for producing crumb rubber.

Crumb rubber is generally specified in terms of physical and/or chemical properties. The most common specified properties include size/gradation, specific gravity, steel and fibre content, and rubber and carbon black content (Hicks et al., 1995).

2.2.2 Production methods

There are several methods for processing used tyres into crumb rubber but the primary aim of each is to reduce the size and separate the steel belting and fiber reinforcing from the rubber. Presently, there are four known methods for grinding used tyre rubber into crumb (Heiztman, 1992). A brief description of these methods is presented here:

- Crackermill process: This is the most common method for producing crumb rubber worldwide. The size of the rubber is reduced by forcing the material

through rotating corrugated steel drums. The tearing of the tyre rubber is controlled by the spacing between the drums and their differential speeds. The process is performed at ambient temperatures. The end product is usually an irregular shape particle with a large surface area, varying in size from 4.75 mm to 0.425 mm.

- Granulator process: This method uses revolving steel plates that pass at close tolerance to cut the tyre rubber. The resulting particles have a cubical and uniform shape with a low surface area. Particle sizes vary from 9.5 mm to 2 mm. The process is also performed at ambient temperatures.

- Micromill process: This process further reduces the rubber particles to a very fine size from 425 to 75 microns. It is an ambient and sometimes slurry process. In the slurry process, the rubber particles are mixed with water to make a slurrylike rubber. The slurry is then forced through a rotating abrasive disc to reduce the particle size. The processed slurry is then retrieved and dried to the final product.

- Cryogenic process: Cryogenic grinding is accomplished at extremely low temperatures (-198 ^{0}C to –87 ^{0}C) by submersing the used tyre rubber in liquid nitrogen. Below the glass transition temperature the rubber is very brittle and can be easily crushed in a hammer mill to the desire size. The resulting rubber particles have a lower surface area than the ones produced by ambient grinding.

Figure 2.2 illustrates schematically the ambient and cryogenic grinding processes.

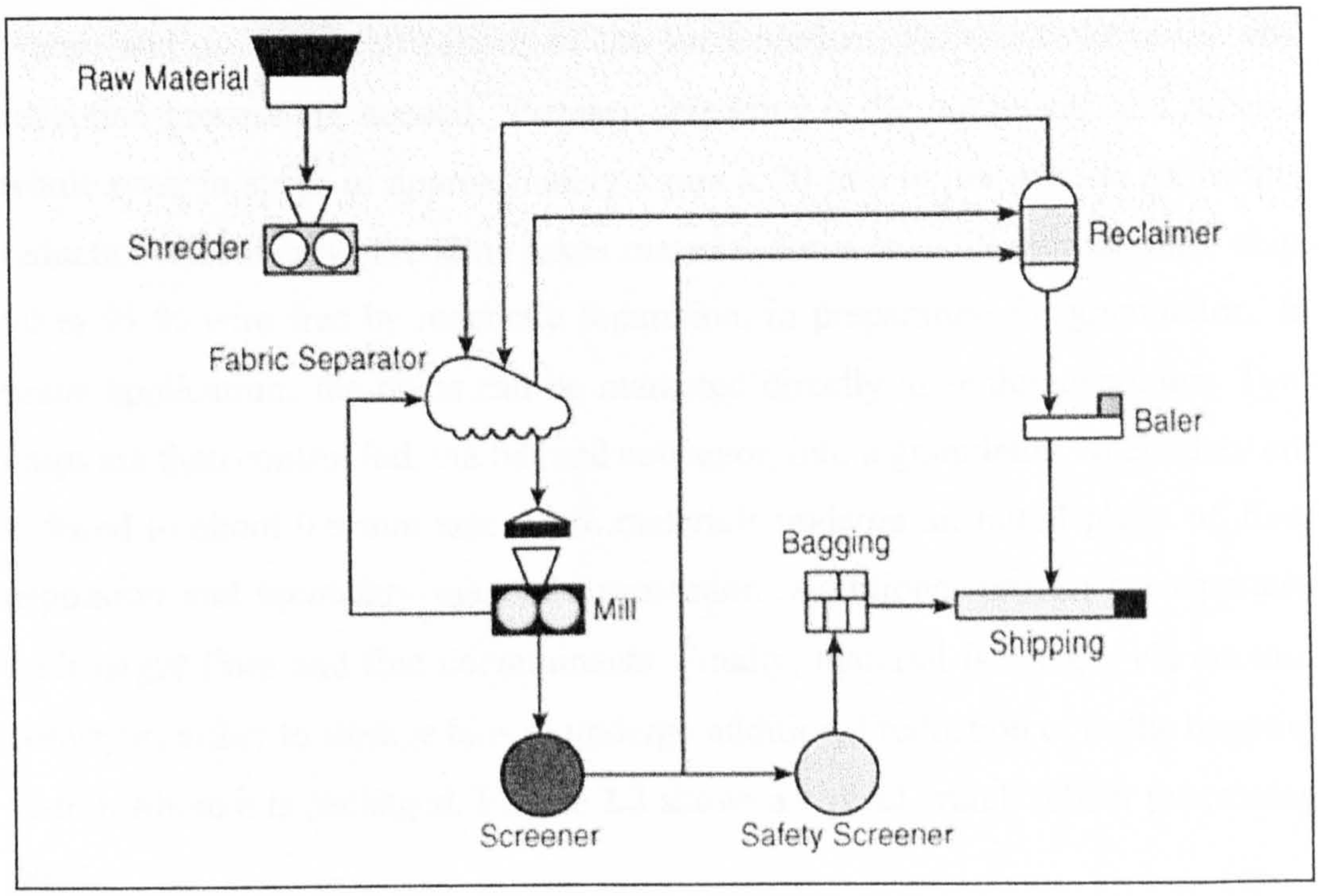

a) Ambient grinding

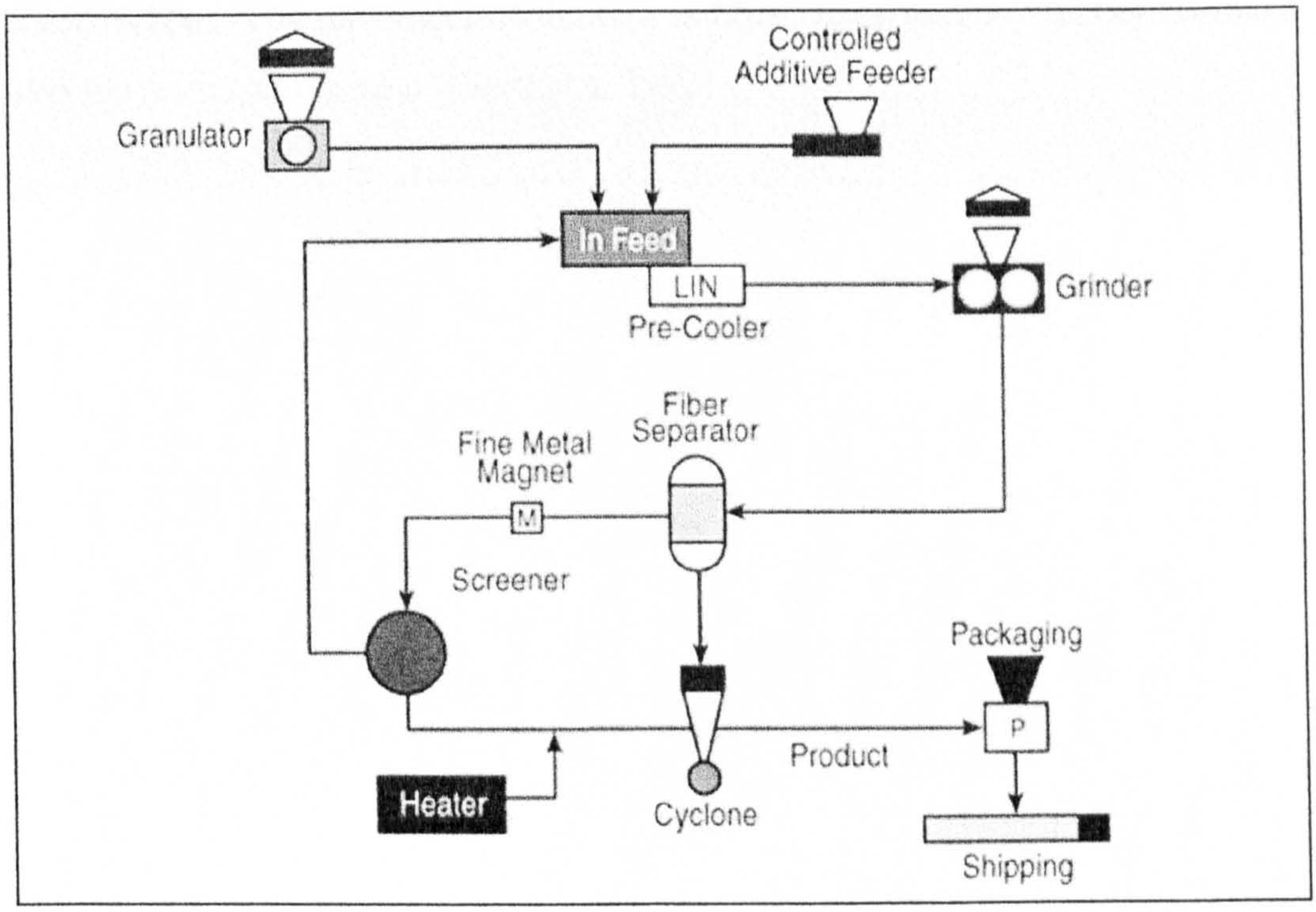

b) Cryogenic grinding

Figure 2.2 Crumb rubber grinding methods

Generally, depending on the raw material (whole or shredded tyres, or buffing waste) and on the specifications of the final product, various steps in the size reduction process are needed. Primary shredding is the initial step and reduces whole tyres to strips of approximately 5 mm x 20 mm in preparation for further reduction. Secondary shredding takes material down to a 1.9 mm nominal chip, 90 to 95 % wire free by magnetic separation, in preparation for granulation. In many applications the chips can be marketed directly after this operation. Tyre chips are then control fed, via bin and conveyor, into a granulator, where they are reduced to about 0.6 mm size. Here materials undergo an initial phase of fibre aspiration and secondary magnetic separation. Additional processing separates both larger fibre and fine contaminants. Finally, material is routed, via enclose conveyor, either to storage bins to undergo additional reduction or to the bagging station where it is packaged. **Figure 2.3** shows a typical crumb rubber processing plant.

In general, a used tyre weighing approximately 9 kg will produce 4.5 to 5.5 kg of crumb rubber. The remainder of the tyre is fibre, steel, and any rubber removed with the fibre and the steel (Heiztman, 1992).

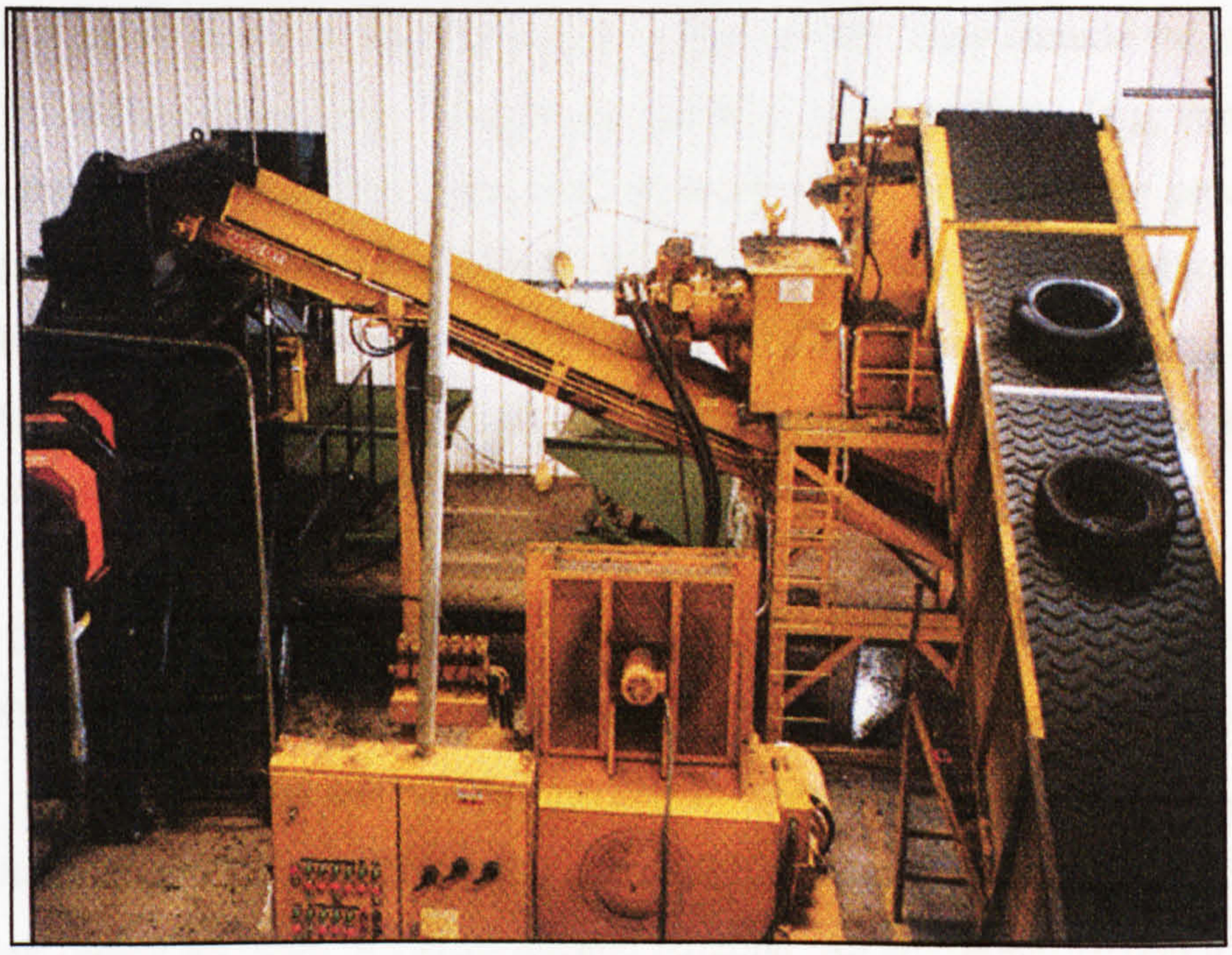

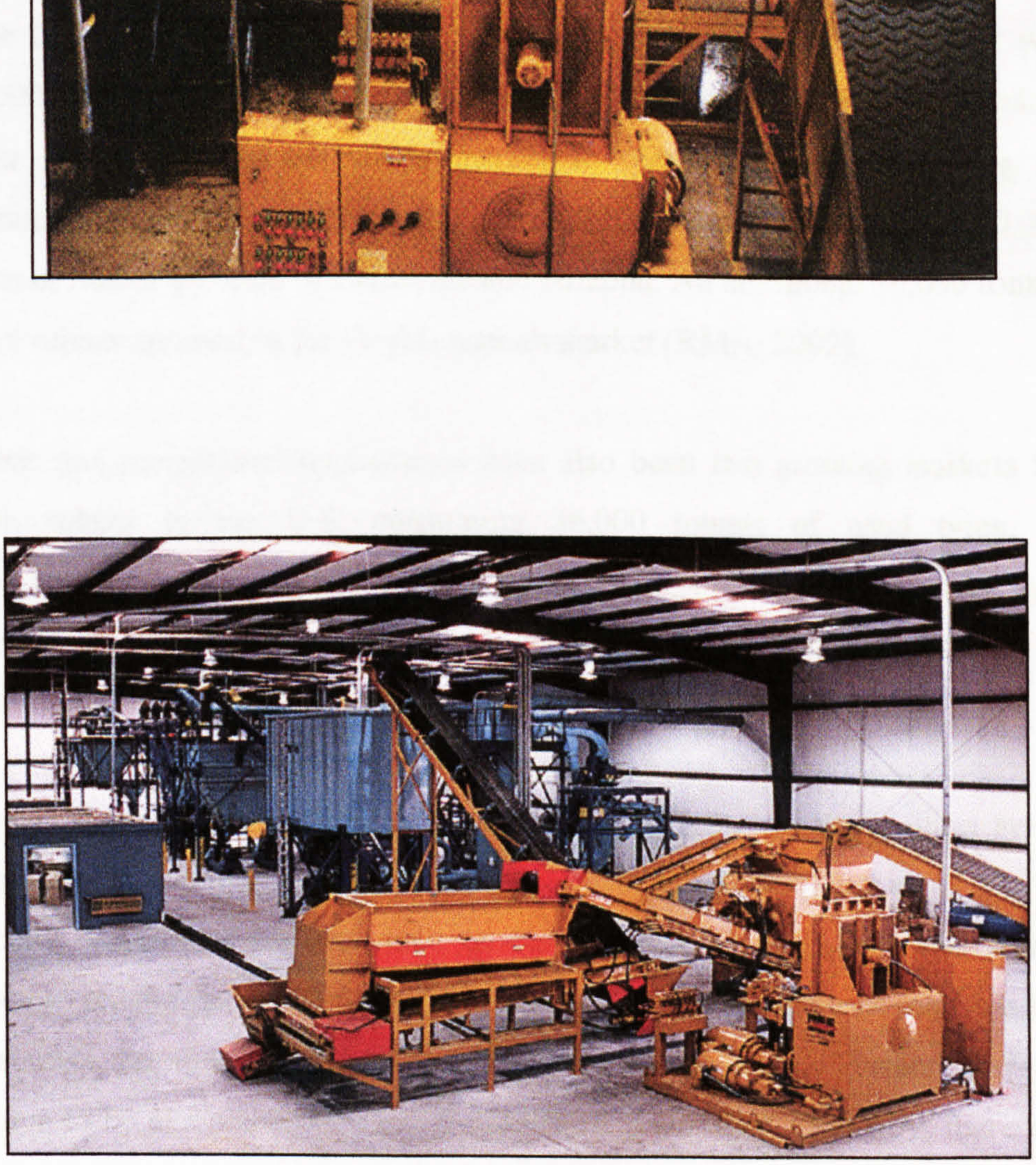

Figure 2.3 Crumb rubber processing plant

2.2.3 Applications

There is a large variety of applications for crumb rubber. They include the use of rubber in asphalt pavements, playground surfaces, sport surfaces (e.g. running tracks, grass-surfaced playing areas and equestrian mats), bound rubber products (e.g. carpet underlay, flooring material and dock bumpers), tyre manufacturing and moulded and extruded products. Crumb rubber is also used in some particular applications (bowling greens and golf courses) but the volumes of rubber are small compared with the main applications.

In the U.S, at the end of 2001, the total market volume of crumb rubber was 295,000 tonnes, which equates to approximately 33 million used tyres. Asphalt rubber remains the largest single market for crumb rubber, consuming an estimated 100,000 tonnes, or approximately 12 million tyres. Of note, 80,000 tonnes or rubber are used in California and Arizona. An additional 10,000 tonnes of tyre rubber are used in the Florida asphalt market (RMA, 2002).

Athletic and recreational applications have also been fast growing markets for crumb rubber in the U.S, consuming 36,000 tonnes of used tyres, or approximately 4 million tyres, in 2001. Other markets such us loose cover, tyre manufacturing and moulded/extruded products consumed about 60.000 tonnes of crumb rubber during the same year (RMA, 2002).

In the U.K, the number of tyres crumbed in 1998 reached 5.5 million tyres, resulting in approximately 48,000 tonnes of crumb rubber (Hird et al, 2001). Presently, traditional markets such us carpet underlay and sport and safety surfacings remain good, but the use of crumb rubber for equine uses (race tracks) has shown the most considerable growth in recent years. Further markets continue to be examined including crumb in road surfaces. Currently, there are two trial stretches of road in Battle, East Sussex, incorporating rubber crumb under evaluation. Funded focused research in this area, however, remains embryonic.

2.3 CRUMB RUBBER IN PAVING APPLICATIONS

2.3.1 History of developments

Crumb rubber modifier (CRM) has been used in road pavement applications for the last 40 years. CRM is a general term for used tyre rubber that is reduced in size and is used as a modifier in asphalt paving materials. Different methods have been developed for incorporating CRM in asphalt mixtures. In general, these methods can be classified under one of two categories, namely the 'wet process' and the 'dry process'.

In the 1960s Charles H. McDonald pioneered the US development of the wet process (McDonald, 1968). The wet process involves heating and reacting CRM particles with bitumen to produce a rubber modified bitumen (called asphalt rubber in the US). In 1968, the Arizona Department of Transportation (ADOT) placed its first stress absorbing membrane (SAM) using and asphalt rubber binder. Continued research and development led by 1972 to the development of a stress-absorbing membrane interlayer (SAMI), and in 1975 asphalt rubber binder was first used in an open-graded friction course. This process has continued to be developed and used since those early applications (Heitzman, 1992).

A different technology, known as the dry process, was also developed in the late 1960s in Europe. The dry process was originally developed in Sweden under the trade name Rubit (Björklund, 1979). The Swedish technology was then exported to the US and was patented in 1978 under the trade name PlusRide. In the dry process, crumb rubber is used as a replacement of mineral aggregate.

The wet and dry processes have been extensively used throughout the US and the use of CRM in paving applications has continued to increase. Furthermore, historically, the driving force behind the used of crumb rubber was the search for a cheap source of elastomeric materials to improve the engineering properties of the pavement by improving elasticity. In recent years, however, the interest shifted and is now strongly driven by environmental concerns as a recycling option for used tyres.

In 1991, the US Congress enacted the Intermodal Surface Transportation Efficiency Act (ISTEA), which contained a provision mandating the use of crumb rubber in a prescribed percentage of highways that were funded by the federal government. ISTEA required that, starting in 1993, 5 % of all federally funded highways needed to contain 9 kg of used tyre rubber per tonne of hot mix asphalt laid. ISTEA mandate further required that the rates be increased to 10 % by 1994, 15 % by 1995 and ultimately 20 % in 1996 and thereafter. Use of CRM in asphalt pavements, thus, increased substantially in the early 1990s due in large part to this mandate. A summary of the work done through 1993 has been reported by Epps (Epps, 1994).

Unfortunately, most state departments of transportation and the paving industry were opposed to this unfunded mandate due mainly to the additional cost of laying pavement with crumb rubber. Still, from 1992 through 1995 several states conducted asphalt rubber testing programs that led to an increase in activity. However, in 1995, the National Highway Safety Designation Act struck down the ISTEA mandate. In spite of this, various states and institutions continued to conduct research on the use of CRM in asphalt pavements. In the mid 90s, the majority of crumb rubber used in hot-mix asphalt was placed in the states of Arizona, California and Florida (Hicks et al., 1995). All three States made exclusive use of the wet process technology. CRM content by weight of bitumen varied from a minimum of 5 % in Florida to a maximum of 23 % in California, given between 0.3 and 2 % CRM content by weight of the total mix.

In Europe, the dry technology was first developed in Sweden under the trade name Rubit. In France, the Beugnet Group in association with Esso developed the Flexochape asphalt rubber binders in the early 1980s. These binders were first used in stress absorbing membranes (SAM) and stress absorbing membrane interlayer (SAMI) applications as an anti-reflective cracking surfacing (Eckmann and Plaindoux, 1983). Later, they were used in porous asphalt mixes to reduce traffic noise and improve durability (Sainton, 1990). In Holland and Belgium, both dense and open graded crumb rubber modified mixes produced by the wet and dry processes has been used successfully as wearing courses to reduce traffic noise and to improve durability (Heerkens, 1985 and Esso Belgium, 1984).

In the UK, the use of CRM in asphalt applications is much less known. In 1995, Sarco and Nottingham University developed a dry process rubber modified mix for use only on sports and safety surfaces. It was patented with the name of Sartek and its purpose was to provide flexibility and safety for users, as well as noise reduction. In 1998, Colas Ltd. laid a trial CRM surfacing, called Colsoft, at the Transport Research Laboratory with the objective of reducing traffic noise (Hargrave, 1998). Colsoft is a French import in which the dry process is used to incorporate rubber granulates into a traditional asphalt surfacing mix. The 1998 trial, however, was badly affected by fretting and started to fail within a month as a result of poor cohesion attributed to low laying temperatures. In 1999, a second trial was laid at 180 ^{0}C, after nine months, there was no indication of any lack of durability and the material was defect free (Child and Hicks, 2000).

2.3.2 Wet process

The wet process defines any method that adds the CRM to the bitumen before incorporating the binder into the aggregate blend. Hence, the method uses the rubber as a polymer modification of the bitumen. The first step is thus to blend the CRM and the bitumen to produce a rubber modified binder. CRM and bitumen are blended at high temperatures during which the rubber particles and the bitumen interact.

As regards interaction, Heitzman (1992) claims that the interaction between bitumen and CRM is a nonchemical reaction that does not result in a melting of the CRM into the bitumen. Instead, particles are swollen by absorption of the bitumen's oily phase at high temperatures to form a gel-like material. Furthermore, work by Bahia and Davies (1994) indicated that the interaction phenomena not only increases the effective volume of the rubber particles but also changes the nature of the liquid phase, thus, the bitumen.

Moreover, the interaction process is affected by a number of variables that can be classified as process variables and materials variables. Process variables include the temperature at which interaction occurs, the duration of the interaction and the amount of mechanical mixing energy. Materials variables, on the other hand,

include CRM content, size and origin (car or truck tyre), and bitumen type and chemical composition

2.3.3 Dry process

The dry process defines any method of adding CRM directly into the aggregate blend, typically pre-blending the CRM with the heated aggregate, before introducing the binder to the mixture. The dry process generates some reaction between the CRM and the bitumen, however, by limiting the time that the bitumen and CRM are maintained at mixing (reaction) temperatures, the CRM particles can retain their physical properties. This process is only applied to hot-mix asphalt applications.

The dry process originally developed in Sweden and patented under the trade name Plusride in the US, typically uses 3 to 4 % by weight relatively large (2 to 6 mm) rubber particles to replace some of the aggregates in a gap-graded aggregate structure. To provide space for the rubber particles, it is necessary to create a 'gap' in the gradation curve of the aggregates, primarily in the 3 to 6 mm size range. The rubber particles replace a portion of the mineral aggregate that normally occupy this size range. The patented specification requires a unique gap-graded aggregate gradation. Furthermore, the crumb rubber must also meet the required gradation specification (Takallou and Hicks, 1988).

A new generic dry process was developed by Takallou (Takallou and Hicks, 1988, and Takallou and Sainton, 1992) with the objective to incorporate CRM into conventional dense and gap-graded hot-mix materials. Unlike Plusride, which specifies a particular gradation for the aggregate, Takallou's technique considered the available generic gradation for the locality; hence the name, generic dry technology. In this process, the crumb rubber gradation is optimised per for each mix design. Typically, fine and coarse CRM are used. This causes some degree of binder modification as a result of the interaction between the fine CRM particles and the bitumen which would result in a higher viscosity binder in which the optimum reaction is achieved when the fine crumb rubber reaches maximum swelling. A pre-treatment with some swelling agent may be needed to

achieve the optimum particle swelling. The coarse CRM would act as an elastic aggregate, to improve elastic properties and to reduce temperature susceptibility.

The performance of bituminous mixtures containing CRM has varied greatly. Mixtures produced with asphalt-rubber binders (wet process) generally have better overall performance than those made with rubber asphalt (dry process) (Epps, 1994). Poor compaction, durability and resistance to permanent deformation have been generally associated with mixtures produced by the dry process.

In the dry process, however, up to 5 % CRM by weight of dry aggregate can be incorporated in to the mixture, whereas in the wet process up to 25 % CRM by weight of bitumen is blended with bitumen. Thus, for a typical bituminous mixture with a 5 % binder content by weight of the total mix, up to 4 times more rubber could be disposed of through the dry process as compared to the wet one. The dry process is, therefore, a better approach from the recycling point of view.

2.3.4 Polymer modified binders

The wet process, as defined earlier, involves interacting or blending CRM particles and bitumen. In this process, therefore, the rubber acts as a polymer modification of bitumen. There are, however, other polymers that have been used as bitumen modifiers aiming at improving the engineering properties of conventional binders.

Polymer modified binders (PMBs) are obtained by the incorporation of a polymer in the bitumen using mechanical mixing or chemical reaction. The aim of incorporating polymers to bituminous binders is to improve their mechanical properties and, consequently, to improve the performance of a pavement. Two classes of polymers are typically used in bitumen modification, elastomers and plastomers.

2.3.4.1 Elastomeric binders

Elastomeric polymers typically used in bitumen modification include Styrene-Butadiene-Styrene (SBS), Styrene-Butadiene Rubber (SBR), polybutadiene and others. SBS is a thermoplastic triblock copolymer with styrene end-blocks and a rubbery butadiene mid-block, whereas SBR is a randomly polymerised styrene-butadiene copolymer (Collins et al., 1991). Thermoplastic elastomers, such us SBS, commonly called thermoplastic rubbers, have proved to present the greatest potential when blended with bitumen (Bull and Vonk, 1987).

The use of SBS copolymers as bitumen modifiers was developed by Shell Chemical Company in the 1960s (Holden et al., 1969). When SBS is added to hot bitumen it absorbs maltenes from the bitumen and swell by up to nine times its initial volume, becoming the major component in the volume of the bitumen. As the bitumen cools, the polystyrene end-blocks form domains which become the physical crosslinking point for a three-dimensional network of polybutadiene. The polystyrene end-blocks impart strength to the structure and the polybutadiene mid-blocks gives the material its exceptional elasticity (Whiteoak, 1990).

Blends using SBS polymers usually contain between 4 and 6 % by mass of bitumen. Bitumen and polymer are blended at high temperatures, typically about 180 ^{0}C. Mixing temperatures should not exceed 185 ^{0}C, and the mixing time should be as short as possible, while allowing sufficient time to complete dissolve the polymer in the bitumen (Shell, 1991). Furthermore, the degree of mixing is influenced by a number of factors including the type and grade of the base bitumen. The time to complete a blend, therefore, varies with each base binder (Collins et al., 1991).

SBS modification has previously shown to increase the bitumen elasticity at high temperatures and improve the binder flexibility at low temperatures. Lu and Isacsson (1997) reported that temperature susceptibility of bitumens was reduced by SBS modification. Furthermore, Lu and Isacsson (2001) also indicated that characteristics and content of the polymer, and nature of the bitumen influence

the properties of these modified binders. Storage stability problems associated with bitumen-polymer phase separation as a result of gravitational fields have also been reported (Lu et al., 1999).

The enhanced properties of elastomeric binders have been manifested in improved mixture properties such us permanent deformation (Khosla and Zahran, 1989) and fatigue and low temperature cracking (Button et al., 1987 and Button, 1992).

2.3.4.2 Plastomeric binders

Thermoplastic polymers such us polystyrene and mainly Ethylene Vinyl Acetate (EVA) have also been used in modified road binders. EVA copolymers are thermoplastic materials with a random structure produced by the copolymerisation of Ethylene and Vinyl Acetate (Collins et al., 1991).

Plastomeric binders differ from elastomeric ones in that they form a stiffer, stronger mix with better resistance to rutting, but lack the flexibility and resilience offered by the latter. In the UK, EVA modified binders are used to enable 'cold weather working' as EVA tends to improve asphalt susceptibility to shear (Whiteoak, 1990)

2.3.5 Crumb rubber modified binders

2.3.5.1 Production of CRM binders

Rubber modified binders have evolved largely from original concepts developed by McDonald in the 1960s (McDonald, 1968). Different types of rubber, rubber sizes, rubber quantities, and reaction times and temperatures have been used to produce binders of varying properties.

Early rubber modified binders contained approximately 25 % CRM by weight of bitumen ranging from 0.6 to 3 mm nominal size approximately. Today's rubber binders generally contain a lower proportion of CRM, typically 5 to 20 % by weight of binder. Furthermore, in an attempt to improve the interaction between

the rubber particles and the bitumen smaller CRM sizes are used. Typically maximum size of the CRM used in wet process applications ranges from 2.36 to 0.18 mm. The State Highway Agency of Florida (US) uses 0.425 or 0.180 mm CRM nominal maximum size in hot-mix applications (Hicks et al., 1995). CRM specification is based primarily on gradation, though some chemical properties as well as a minimum percentage of natural rubber are some times required.

CRM produced by the ambient grinding method is preferentially used in rubber binders. This method appears to produce irregular rubber particles with large surface areas, which favour the interaction between CRM and bitumen.

Laboratory methods to produce CRM binders also vary. Typical CRM and bitumen blending or interaction temperatures vary between 150 and 190 ^{0}C for periods of time from 10 to 60 minutes to ensure adequate interaction between the CRM and the bitumen. There is not, however, widespread agreement as to the need for agitation, thus, initial, continuous or intermittent.

2.3.5.2 CRM binder properties

The use of CRM in bituminous binders requires an understanding of its effects on the physical, chemical and rheological properties of bitumen so that their performance in the field can be more accurately predicted. CRM binders have been generally characterised by the same techniques used for conventional binders, which have been based on both empirical and performance-related tests.

Primarily, the addition of CRM to bituminous binders increases the viscosity of the binder at high temperatures associated to mixing and construction conditions. Higher viscosities can make mix compaction more difficult which can lead to high void content and thus, high rates of oxidation. To overcome this problem an increase in mixing and laying temperatures are generally required when using CRM binders (Hicks et al., 1995).

Different studies have shown that CRM addition increases the binder's resistance to deformation at high service temperatures, which contributes significantly to the pavement ability to resist rutting. (Bahia and Davies, 1994 and Morrison and

Hesp, 1995). Low temperature performance of CRM binders, as related to pavement low temperature and thermal cracking, has also been investigated. Work by Morrison et al. (1995) indicated that the low temperature fracture resistance was enhanced by the incorporation of CRM.

Moreover, Kim et al. (2001) reported separation between crumb rubber and bitumen during storage. During storage at high temperature the rubber particles tended to settle as a result of gravitational forces. So, if separation occurs, agitation will be required to maintain homogeneity before the modified binder is used.

2.3.6 Crumb rubber modified mixtures

2.3.6.1 Design aspects

Marshall and Hveem mix design procedures have been used extensively for bituminous mixtures containing CRM binders (Epps, 1994 and Hicks et al., 1995). In general, CRM mixtures have shown lower stability and higher flow values than conventional ones. These design methods, however, are empirical and do not provide fundamental engineering properties of the material.

Optimum binder contents for CRM mixtures are generally higher than for conventional ones. Typically, CRM binder contents are 10 to 20 % higher than those used in conventional mixtures. Furthermore, the optimum binder content of a crumb-rubber modified mixture increases proportionally to the amount of CRM in the binder (Epps, 1994).

2.3.6.2 Rutting resistance

Rutting is a term used to describe the accumulation of permanent deformation in a bituminous paving material. Various studies have shown the greater resistance to rutting of CRM mixtures compared with unmodified ones (Troy et al., 1996 and Gowda et al., 1996). This higher resistance to rutting has been attributed to higher complex stiffness modulus associated with CRM binders. Gowda et al., (1996) noticed, however, that relatively higher levels of CRM in the binder could lead to a reduction in the rutting resistance of the mixtures.

2.3.6.3 Fatigue resistance

Fatigue cracking occurs when a pavement layer is subjected to repeated application of loads by the passage of traffic at a level which induces stresses generally below the tensile strength of the material. The use of CRM binders seems to enhance the fatigue resistance of pavement materials, as illustrated in a number of studies (Charantia et al., 1991, Rebala and Estakhri, 1995 and Raad and Saboundjian, 1998). The improved performance of CRM mixtures has been attributed to improved rheological properties of the crumb rubber binder (Bahia and Davies, 1994) and improved resistance to ageing (Sainton, 1990).

2.3.6.4 Thermal cracking

Thermal cracks in asphalt pavements are caused by cold temperatures, referred to as low-temperature cracking, or by thermal cycling, generally referred to as thermal fatigue cracking. These cracks are the result of thermally induced stresses in an asphalt pavement as the temperature drops or as a result of daily temperatures cycles.

The use of CRM in bituminous binders has shown a potential for reduced thermal cracking in pavements materials (Stroup-Gardiner et al., 1996). The improved resistance to low-temperature cracking attributed to CRM mixtures has been associated with lower binder stiffness at low temperature as a result of CRM modification (Bahia and Davies, 1994).

2.3.6.5 Durability

Durability refers to the resistance of a bituminous mixture to changes in its mechanical properties caused by environmental factors, principally water and air (oxygen). The entry of water into a mix may result in loss of adhesion between the binder and the mineral aggregate due to the displacement of the bitumen from the aggregate surface. On the other hand, the effect of ageing, as a result of bitumen oxidation, causes increased stiffness, viscosity and brittleness rendering the material susceptible to cracking.

Sensitivity of a bituminous mixture to moisture damage is generally assessed by subjecting a material specimen to a water-conditioning regime. The process consists of measuring some mechanical property, typically stiffness modulus or tensile strength, before and after the conditioning regime. Troy et al. (1996) measured the tensile strength of various CRM mixtures made in the laboratory before and after they were subjected to one cycle of freezing and thawing, and reported reductions in tensile strength around 30 %. Stroup-Gardiner et al. (1996), following the same procedure, reported reduction in tensile strength and stiffness modulus of around 30 and 50 %, respectively, for laboratory specimens. Rebala and Estakhri (1995), however, reported reduction in tensile strength and stiffness modulus of less than 10 %. Furthermore, some of the CRM mixtures investigated had stiffness modulus values significantly larger after moisture conditioning.

Oxidative aging of asphalt binders is a primary cause of binder-related long-term pavement failures. The effect of oxidative aging on the physical properties of CRM binders is still not fully understood. Furthermore, little information exists about the aging behaviour of crumb rubber modified mixtures.

Liang and Lee (1996) studied the short- and long-term aging behaviour of rubber modified asphalt mixtures by different laboratory aging procedures. Short-term aging by means of the thin film oven test (TFOT) showed higher oxidation levels for binders modified with CRM than for the unmodified ones. Comparisons between the short- and long-term aging behaviour of crumb-rubber modified and unmodified mixtures were, however, inconclusive.

Work by Chipps et al. (2001) indicated that the ageing characteristics of CRM binders are very dependant on the production conditions of time and temperature of blending. They suggested that CRM binders produced under high levels of mixing shear and temperature are less prone to ageing as the polymer chains freed by thermo-mechanical shear are integrated in the binder, shielding or retarding the oxidation of the binder.

2.3.7 Noise reduction

Traffic noise is generated primarily by the interaction of the tyres and pavement and by the internal combustion engine and the engine exhaust of the vehicle. Lefebvre (1993) classified the sources of traffic noise into two categories: road noise and engine noise. Rolling noise tends to predominate particularly on motorways and uncongested urban roads where the traffic speed exceeds 50 km/hr (Berengier et al., 1990).

Comparisons have been made of traffic noise level studies on wearing courses containing CRM binders (Epps, 1994). These studies indicated that a noise reduction between 50 to 90 %, or 3 to 10 dB, could be achieved when CRM binders are used in open-graded mixtures. In a recent study submitted to the Rubber Pavements Association (RPA, 2003), it was indicated that the use of rubber-modified binders in open-graded mixtures resulted in a net decrease in traffic noise levels of approximately 4 dB over that provided by conventional dense-graded mixtures. Furthermore, this reduction in traffic noise was attributed to a combination of the porosity and ductility of the rubberised road surface.

2.3.8 Recycling

In the last few years there has been growing concern about the reuse of bituminous materials that have been removed from the pavement structure as part of maintenance programmes. In the U.K, the material, known as reclaimed asphalt pavement (RAP), is permitted in hot-mix asphalt in accordance with the Specification of Highway Works Clause 902. Furthermore, a recent study by Woodside et al. (2000) has shown the benefits of using recycled materials in hot and cold bituminous mixtures. Currently, the U.K recycles about 300,000 m^2 a year and these figures are expected to increase gradually (Anon, 2000).

The ability to recycle asphalt pavements containing CRM is a critical issue. If these materials are to be fully accepted, they should be capable of being recycled. If not, their benefit will be substantially reduced and a new waste problem will be created. The main issues that need to be addressed as regards to recycling

CRM pavements are the reclaimed processes involved and the performance of the recycled material containing CRM.

Several field projects performed in the 1990s have recycled pavements containing CRM (Epps, 1994). The outcome of these projects showed that CRM pavements could be recycled using the same methods as for conventional pavements, i.e. in-situ (or surface) recycling and off-site (or hot mix) recycling. Furthermore, no major problems were reported during mix production and construction operations. There is still, however, little information about the performance of these recycled materials.

2.3.9 Environmental and health issues

Environmental risk assessment relative to the use of CRM binders in asphalt pavements is a complex issue. This complexity arises from the complicated chemical composition of the bitumen and the variability of the chemical components incorporated in the tyre rubber. Furthermore, hot-mix production facilities and air quality control systems differ and these differing systems create and measured different chemical compounds (Epps, 1994).

Bloomquist et al. (1993) summarised the environmental and health risk data of various field studies and concluded that there was no evidence that crumb rubber modified mixtures increases the threat to the environment or human health as compared to conventional mixtures. Later, work by Baker and Connolly (1995) indicated that, when using CRM, asphalt plant emissions of hydrocarbons, carbon monoxide and particulate emissions were within the emissions limit. Maupin (1996), however, reported that for some of the identified materials during asphalt plant emissions tests, the permissible exposure limits were not set. Furthermore, some chemical components, such us polynuclear aromatic hydrocarbons, sulphur heterocycles and benzene soluble fractions, were identified when paving with asphalt rubber mixtures.

2.3.10 Economic considerations

Bituminous mixtures containing CRM binders are generally considered to be an expensive option for highway surfacings. In 1993, in the US the initial average cost of either dense- or open-graded mixes containing CRM was 1.5 to 2 times higher than for conventional ones (Epps, 1994). Costs of CRM pavements, however, are expected to decrease in the future as a result of increased competition, supply and demand, and increased project volume.

The main reason for the increased cost is attributed to the initial cost of the rubber-modified binder, which consists of the cost of the CRM material plus the cost of producing or blending the CRM and the bitumen. The initial cost of the CRM depends on its size, thus the finer the CRM the higher the cost (see **Table 2.2**). Also, as the percentage of CRM in the bitumen increases, the cost of the rubber-modified binder will increase. Morris (1993) estimated that the cost of crumb rubber binders for either spray or hot mix applications is approximately 3 to 4 times the cost of conventional binders.

Hicks (1995), in a summary of practices in Arizona, California and Florida, the main users of CRM in asphalt pavements, reported costs of CRM binders around 2 to 4 times higher than conventional ones, as shown in **Table 2.3**. Also, the cost of the various crumb-rubber modified mixtures used in each of the three surveyed States is presented in **Table 2.4.**

Size (mm)	Mesh	Price ($/lbs)	Price (£/kg)
6.300	4	0.03	0.10
2.000	10	0.12	0.38
0.850	20	0.20	0.63
0.425	40	0.32	1.02
0.180	80	0.38	1.21

1 lb=0.45 kg 1 $=0.7 £

Table 2.2 Current average market prices for CRM (C.R.U.M.B., 2003)

State	Conventional Asphalt	Asphalt-rubber		
		5% 80 mesh	12% 40 mesh	17-22% 10 mesh
Arizona	$108/tonne	_	_	$245/tonne
California	$113/tonne	_	_	$336/tonne
Florida	$99/tonne	$211/tonne	$197/tonne	_

Table 2.3 Typical cost of asphalt rubber (after Hicks, 1995)

State	Type of mix	Cost ($/m^{2}mm)	
		Conventional mix	Rubber-modified mix
Arizona	Open-graded friction course	0.11	0.19
	Gap-graded mix	0.58	1.20
California	Dense-graded mix	0.91	1.22
	Gap-graded mix	–	1.44
	Open-graded mix	0.10	0.19
Florida	Dense-graded friction course	0.10	0.11
	Open-graded friction course	0.08	0.10

Table 2.4 Cost of various asphalt-rubber mixes (after Hicks, 1995)

Nowadays, cost comparisons indicate that CRM binders can be from up to twice as expensive as conventional bitumen. Furthermore, after incorporation into the HMA, the finished rubber modified product is generally from 25 to 75 percent more expensive for the gap-graded rubber mix than the typical dense-graded

HMA and 80 to 160 percent more expensive than the typical open-graded friction course (Way, 1998).

Work by Fager (1994) indicated that paving projects using the wet and dry processes were about 60 % (wet) and 20 % (dry) more expensive than those using conventional mixtures. Cost differences between the two processes were mainly due to the added cost of blending rubber and bitumen at high temperature (177 ^{0}C) for up to 90 minutes.

However, in spite of the higher initial costs associated with rubber modified materials, the advantages gained from their use can be significant. To evaluate the economic benefits of these materials, it is necessary to bring into consideration the associated costs of tyre disposal to landfill. Moreover, limited life cycle cost analysis studies (Emery, 1995, Jung et al., 2002 and Hicks and Epps, 2002) have indicated that there is a potential for considerable savings, on a life cycle cost basis, when using CRM materials. Further research, however, is needed to assess the long-term performance of these materials.

Chapter 3

RUBBER-BITUMEN INTERACTION

Chapter 3

RUBBER-BITUMEN INTERACTION

3.1 INTRODUCTION

The method of producing rubber-modified bitumen involves mixing the CRM particles and the bitumen under controlled conditions (wet process). When CRM is added to bitumen at elevated temperatures, the rubber particles interact with the bitumen and tend to swell. The extent and rate of swelling depend on factors like the nature of the rubbers, the bitumens' chemical composition and the processing parameters, e.g. time, temperature and degree of agitation.

Uncrosslinked rubbers may dissolve in bitumen and become molecularly dispersed. Vulcanised (crosslinked) rubbers are not soluble in bitumen, as they exist as networks. However, bitumen components will diffuse into and swell the rubber particles. So, the rubbers will absorb some bitumen components preferentially, according to their interaction parameters.

This chapter presents a study on the interactions that occur when bitumen and rubber from waste tyres are blended together at elevated temperatures. The study is based on the diffusion theory applied to solvent-polymer systems, which enables the determination of the kinetic parameter, diffusion coefficient, which is a major factor that controls the swelling mechanism.

3.2 SWELLING PHENOMENA

3.2.1 Swelling of polymers

Swelling is a property possessed by a wide range of polymers, both natural and synthetic. Polymers may be divided into those that are soluble in water (hydrophilic) and those that are soluble in organic solvents (hydrophobic). The first group includes polyethylene oxide and polyvinyl alcohol, while the second group consists of the rubbers, both natural and synthetic.

When polymer networks are exposed to low-molecular-weight liquids, the liquid molecules diffuse into and are absorbed within the polymer network. The small liquid molecules occupy positions among the polymer molecules forcing the macromolecules to move apart such that the polymer swells or expands. The increase of polymer chain separation as a result of swelling reduces the secondary intermolecular bonding forces, making the polymer softer and more ductile.

Uncrosslinked polymers will be swollen by and dissolve in liquids with suitable interaction parameters. For crosslinked polymers, solvents will be absorbed into and swell the network, but the network structure will prevent dissolution. Thus, swelling of rubbers by organic liquids may be considered to be a partial dissolution process in which there is only a limited solubility of the polymer in the solvent. On the other hand, dissolution occurs when the polymer is completely soluble and might be thought of as just a continuation of swelling.

In general, the best solvents or swelling agents for a given polymer are those whose chemical structure is closely related to that of the polymer. For example, hydrocarbon rubbers (natural rubber, SBR, polybutadiene) are readily soluble in hydrocarbon liquids (gasoline, benzene, etc), but insoluble in polar liquids such us acetone and alcohol.

In the case of rubber and bitumen, as the rubber is, by definition, above its glass transition temperature, the polymer chains have considerable mobility so the system is essentially that of two fluid phases in contact but one phase has a network structure of polymer chains. So, in principle, when rubber and bitumen are placed in contact, mobile components can diffuse between the two phases, processing oils and additives from the rubber into the bitumen, and components of the bitumen into the rubber.

3.2.2 Thermodynamic principles

3.2.2.1 Ideal and non-ideal solutions

In a solution, defined as a homogeneous mixture of two or more substances constituting a single phase, the thermodynamic condition, under constant temperature (T) and pressure (P), for formation of a two-component solution is given by:

$$\Delta G_m = \Delta H_m - T\Delta S_m < 0 \tag{3.1}$$

where ΔG_m is the Gibbs free energy of mixing, ΔH_m is the enthalpy of mixing and ΔS_m is the entropy of mixing.

For an ideal solution, considered as a mixture of molecules of component 1 and 2 that are identical in size with no interaction between them, ΔH_m=0, and simple lattice theory establishes that,

$$\Delta S_m = -R\left[n_1 \ln X_1 + n_2 \ln X_2\right] \tag{3.2}$$

Thus the free energy of mixing is,

$$\Delta G_m = RT\left[n_1 \ln X_1 + n_2 \ln X_2\right] \tag{3.3}$$

where N_1, N_2 are the numbers of molecules 1 and 2, $n_1 = N_1 / N_A$, $n_2 = N_2 / N_A$, are the numbers of moles, $X_1 = n_1/(n_1+n_2)$, $X_2 = n_2/(n_1+n_2)$ are the mol fractions; N_A and R are the Avogadro and the universal gas constant respectively.

For ideal solutions, ΔG_m is always negative and the components forming an ideal solution will always be completely miscible (spontaneous process).

Polymer solutions, however, show major deviations from ideal solution behaviour, attributed not only to the existence of a finite heat of mixing ($\Delta H_m \neq 0$) but also to the large difference in size between the polymer and solvent molecules. The failure of the simple lattice theory to predict the thermodynamic properties of polymer solutions arises from the assumption that the solvent and solute molecules are identical in size.

3.2.2.2 Flory-Huggins theory

The theory considered that the dissolution of a polymer in a solvent depends on the transfer of the polymer chain from a pure, perfectly ordered state to a state of disorder, which has the necessary freedom to allow the chain to be placed randomly on a lattice. The theory also considered the interactions of the polymer chains with the solvent molecules.

The Flory-Huggins theory established that,

$$\Delta S_m = -R\left[n_1 \ln \phi_1 + n_2 \ln \phi_2\right] \tag{3.4}$$

and,

$$\Delta H_m = RTn_1\phi_2\chi \tag{3.5}$$

Thus,

$$\Delta G_m = RT\left[n_1 \ln \phi_1 + n_2 \ln \phi_2 + n_1\phi_2\chi\right] \tag{3.6}$$

where V_1, V_2 are the volumes of components 1 and 2, and $\phi_1 = N_1V_1/(N_1V_1 + N_2V_2)$ and $\phi_2 = N_2V_2/(N_1V_1 + N_2V_2)$ are their volume fractions. The parameter χ is commonly known as the Flory-Huggins polymer-solvent interaction parameter and depends only on the properties of the particular polymer-liquid combination.

3.2.2.3 *Thermodynamics of swelling*

When a polymer is mixed with a suitable solvent, it disperses in the solvent and behaves as though it too is a liquid, a viscous liquid. If the *Gibbs free energy of dilution* ΔG_1, defined as the change in the free energy of the system due to the transfer of unit quantity (1 mol) of solvent (component 1) from the liquid phase to a large quantity of mixed phase (solvent + polymer), the condition of equilibrium with respect to the transfer of liquid is then,

$$\Delta G_1 = 0 \tag{3.7}$$

and,

$$\Delta G_1 = \Delta H_1 - T\Delta S_1 \tag{3.8}$$

where ΔH_1 and ΔS_1 are the changes in the enthalpy and entropy of the system per mole of liquid transferred from the liquid phase to the mixed phase.

In the case when only one component (the liquid) has an appreciable vapour pressure the free energy of dilution is given by,

$$\Delta G_1 = RT \ln(p / p_0) \tag{3.9}$$

where p is the vapour pressure of the liquid component in equilibrium with the mixture (swollen rubber) and p_0 is its saturation vapour pressure.

The enthalpy of dilution can be obtained as follows,

$$\Delta H_1 = \frac{\partial(\Delta G_1 / T)}{\partial(1/T)} = -RT^2 \frac{\partial \ln(p / p_0)}{\partial T} \tag{3.10}$$

Equations 3.9 and 3.10 enable ΔG_1 and ΔH_1 to be determined by experiment, the value of ΔS_1 is determined from Equation 3.8.

Treloar (1975) studied the swelling of unvulcanized natural rubber in benzene. From the relative magnitudes of ΔG_1, ΔH_1 and $T\Delta S_1$, it was shown that the term ΔH_1 was relatively small compared to $T\Delta S_1$, and opposed the process of swelling or solution. Treloar concluded that the driving force in the process of swelling or solution is the large increase in the entropy, the corresponding change in enthalpy (heat) being relatively unimportant.

Thermodynamically, this process is similar to the diffusion process, where, there is a large increase in the entropy of the system, there are no strong chemical intermolecular forces and the change in enthalpy is relatively small. Thus, swelling of rubbers can be regarded as a physical mixing or diffusion process in which the two components are chemically neutral.

Furthermore, the free energy of dilution ΔG_1 with respect to the liquid component can be obtained by differentiation of Equation 3.6 with respect to liquid content n_1 and it is given by,

$$\Delta G_1 = RT\left[\ln(1-\phi_2)+\phi_2+\phi_2^{\,2}\chi\right] \tag{3.11}$$

The importance of this result is that it includes only a single adjustable parameter χ, which depends only on the properties of the particular polymer-liquid combination. Furthermore, if $\chi<1/2$, ΔG_1 is negative for all values of ϕ_2, and the polymer and liquid are miscible in all proportions. On the other hand, if $\chi>1/2$, there is a particular value of ϕ_2 for which $\Delta G_1=0$, this represents the condition of equilibrium swelling.

In a cross-linked polymer, however, the interconnected network precludes the possibility of dilution. The total free energy of dilution must therefore be expressed as the sum of the free energy of dilution prior to cross-linking and the free energy associated to the elastic expansion of the network. The free energy due to elastic expansion can be obtained from the Gaussian network theory.

Therefore,

$$\Delta G_1 = RT\left[\ln(1-\phi_2)+\phi_2+\phi_2{}^2\chi+\frac{\rho V_1}{M_c}\phi_2{}^{1/3}\right] \qquad (3.12)$$

where ρ is the density of the polymer, V_1 is the molar volume of the swelling liquid and M_c is the molecular weight of the network chains. The condition for equilibrium swelling is given by $\Delta G_1 = 0$.

3.2.2.4 The solubility parameter

The solubility parameter was first developed by Hildebrand and Scott (1964) for calculating estimates of the enthalpy of mixing, ΔH_m, for mixtures of liquids. The equation used is,

$$\Delta H_m = V_m\phi_1\phi_2(\delta_1-\delta_2)^2 \qquad (3.13)$$

where V_m is the molar volume of the mixture and, δ_1 and δ_2 are the solubility parameters of components 1 and 2 respectively.

The solubility parameter is defined as the square root of the energy of vaporization per unit volume of material and is given by,

$$\delta = \left[(\Delta H_v - RT)/V\right]^{1/2} \qquad (3.14)$$

where ΔH_v is the molar enthalpy of vaporization and V is the molar volume. The quantity δ^2 is often called the cohesive energy density, which is defined as the energy required to separate all the molecules in a given material from one another.

According to Equation 3.13 the heat (enthalpy) of mixing is always positive, and $\Delta H_m = 0$ when $\delta_1 = \delta_2$. In the case of a polymer-liquid mixture, for a given

polymer swollen in different liquids, the swelling should be a maximum when the enthalpy of dilution is a minimum, thus when the solubility parameter of the liquid is equal to that of the polymer. However, because polymers are not volatile, the δ must be obtained indirectly. The method often used for cross-linked polymers is based on a maximum in swelling using series of solvents of varying and known solubility parameters. The δ value of the polymer is taken as being that of the solvent which gives the maximum degree of swelling.

3.2.3 Diffusion process

Diffusion is defined as the process by which matter is transported from one part of a system to another as a result of random molecular motions.

The mathematical theory of diffusion in isotropic substances (Crank, 1956) is based on the hypothesis that the rate of transfer of diffusing substance (J), defined as the mass diffusing through and perpendicular to a unit cross-sectional area per unit time, is proportional to the concentration gradient measured normal to the section, thus,

$$J = -D\frac{\partial C}{\partial x} \tag{3.15}$$

where:

J	=	diffusion flux
C	=	concentration of diffusing substance
x	=	space coordinate normal to the section
D	=	diffusion coefficient

The fundamental differential equation for diffusion is derived from Equation 3.15 considering the mass-balance of an element of volume. The resulting equation for one-dimensional diffusion, provided that D is a constant, is expressed as follows,

$$\frac{\partial C}{\partial t} = D\frac{\partial^2 C}{\partial x^2} \tag{3.16}$$

Equations 3.15 and 3.16 are commonly referred to as Fick's first and second laws of diffusion.

In many polymer systems, however, D depends on the concentration of diffusing substance C. In this case, the diffusion equation becomes,

$$\frac{\partial C}{\partial t} = \frac{\partial}{\partial x}\left(D\frac{\partial C}{\partial x}\right) \tag{3.17}$$

3.3 MATERIALS CONSIDERATIONS

3.3.1 Tyre rubber: natural and synthetic rubbers

Tyre rubber is primarily a composite of natural rubber and synthetic rubber. Historically, passenger car tyres contained approximately 20 % natural rubber and 26 % synthetic rubber, whereas truck tyres contained approximately 33 % natural rubber and 21% synthetic rubber. Nowadays passenger car tyres typically contain approximately 16 % natural rubber and 31 % synthetic rubber, whereas truck tyres contain approximately 31 % natural rubber and 16 % synthetic rubber (Hicks et al., 1995).

Natural rubber (NR) is obtained in the form of latex from the tree *Hevea Braziliensis* and it is essentially a hydrocarbon. Chemically, the rubber hydrocarbon is a polymer of isoprene (C_5H_8) built up in the form of a continuous chain. The succession of isoprene units in the chain is perfectly regular, with every fourth carbon atom in the chain carrying the methyl (CH_3) side-group. In natural rubber the single bonds lie on the same side of the double bond, forming the so-called cis-(1,4)configuration. Chemical structure of natural rubber is illustrated in **Figure 3.1**.

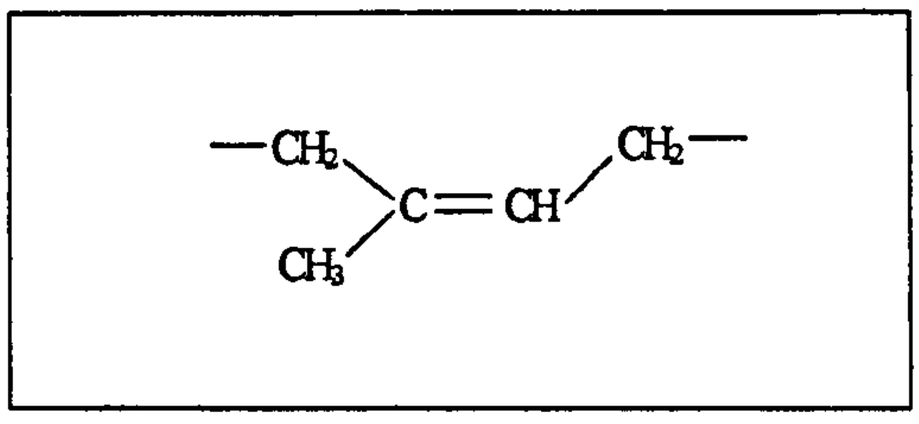

a) Natural rubber: cis-1,4 (polyisoprene)

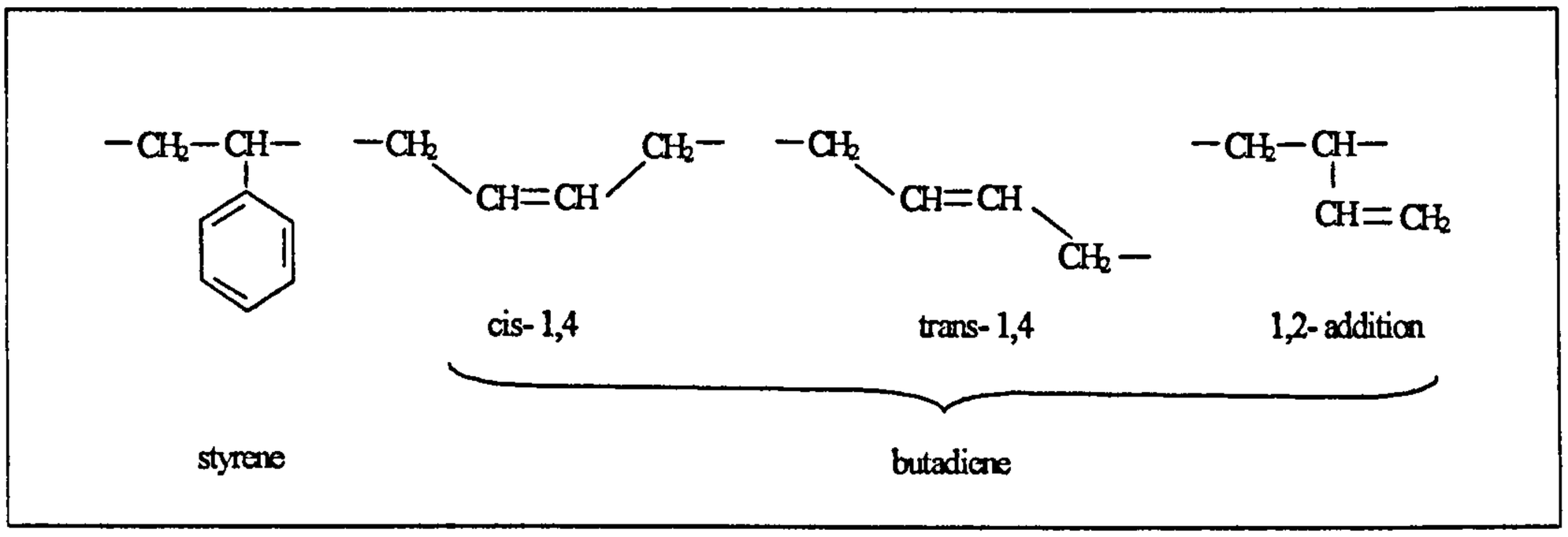

b) Synthetic rubber: styrene-butadiene statistical copolymer

Figure 3.1 Chemical structures of natural and styrene-butadiene rubber

Synthetic rubbers are produced by a chemical process known as *polymerisation.* The most common synthetic rubber used in tyre manufacturing is styrene-butadiene statistical copolymer (SBR). The simplest fundamental unit is formed of styrene (C_8H_8) and butadiene (C_4H_6). Butadiene units have all microstructures cis-1,4, trans-1,4, and 1,2- addition. Chemical structure of SBR is also presented in **Figure 3.1**.

To achieve elastomeric properties, most rubbers are required to be *vulcanised.* Vulcanization is the process of chemical crosslinking of the rubber polymer chains. The process most commonly used is sulphur vulcanisation. Sulphur is used at a level of 0.5 – 5 parts per hundred of rubber and the crosslinking reaction takes place upon heating at temperatures in the range 120 – 180 ^{0}C. This reaction is relatively slow and inefficient, thus it is usual to add and accelerator and an activator to increase the rate and improve the efficiency.

During tyre-rubber manufacture various additives are included to give desired characteristics to the end product. They include carbon black, pigments, softeners and others. Carbon black is an anti-abrasive and it is used to stiffen rubber. Pigments include zinc oxide and a number of organic dyes. Softeners usually consist of petroleum products, such us oils or waxes; pine tar; or fatty acids (Stern, 1967).

3.3.2 Bitumen constitution and structure

Petroleum bitumen is typically a high boiling vacuum distillation residue that is prepared from numerous petroleum stocks. The chemistry and physical properties, therefore, vary quite significantly from one another.

Bitumen is a complex mixture of organic molecules of predominantly hydrocarbon nature that vary widely in composition. These molecular structures also contain varying amounts of certain so-called heteroatoms, predominantly oxygen, nitrogen and sulphur, together with trace quantities of metals such us vanadium and nickel (Petersen, 1984).

Because the number of molecules in bitumen with different chemical structures is extremely large, a complete analysis of bitumen is generally considered impractical. However, it is possible to study bitumen composition by separation into broad chemical groups. Some separation methods include solvent extraction (Hoiberg and Garris, 1944), chemical precipitation (Rostler and White, 1962) and chromatographic techniques (Schweyer et al. 1955, and Corbett and Swarbrick, 1958).

This last technique has been most widely used to analyse bitumen chemical composition. The method is based on the polarity of the constituent compounds comprising the bitumen. The separated groups of compounds which progressively increase in their polarities are saturates, aromatics, resins and asphaltenes; also known as the SARA fractions.

The saturate fraction is characterised by the lack of polar chemical functional groups. It may contain saturated normal and branched-chain hydrocarbons, saturated cyclic hydrocarbons and a small amount of mono-ring aromatic hydrocarbons. Sulphur is often found incorporated in molecules of the saturate fraction (Petersen, 1984).

The aromatic fraction consist of non-polar carbon chains in which the unsaturated ring systems dominate. The molecules usually contain condensed non-aromatic and aromatic ring systems, and in addition to sulphur, oxygen and nitrogen may also be part of the molecule (Petersen, 1984).

The resins contain highly condensed aromatic ring systems and functional groups containing heteroatoms, similar to the asphaltenes (David and Petersen, 1967). The main feature of this fraction is the preponderance of molecules with highly condensed planar and polarizable aromatic ring systems together with a high concentration of polar, heteroatom-containing functional groups. Because of these features, molecules of this fraction are strongly attached to each other (Petersen, 1984).

The asphaltenes are separated first based on their insolubility in a non-polar paraffinic solvent. This removes the most polar and least soluble asphalt components and facilitates further separation. Asphaltenes are considered as highly polar and complex aromatic compounds containing, in addition to carbon and hydrogen, some nitrogen sulphur and oxygen. They are colloidally dispersed in a continuous medium of oils (saturates and aromatics) and this dispersion is stabilised by the absorption of resins on the peripheries of the asphaltenes (Dransfield et al., 1995). Asphaltenes have been shown to have a major influence on bitumen rheology as seen by the increase in viscosity with increasing asphaltene concentration (Lin et al., 1996).

Molecular weights of the bitumen fractions have been obtained by several methods. Among these methods, vapor pressure osmometry (VPO) (Moschopedis et al., 1976, Chung et al., 1979 and Yarranton and Masliyah,

1996) and gel permeation chromatography (GPC) (Nali and Manclossi, 1995 and Champagne et al., 1985) have been used extensively.

Peramanu and Pruden (1999) used VPO to measure the overall molecular weight of Athabasca and Cold Lake bitumens and their corresponding SARA fractions, while GPC was used to measure the molecular weight distributions. GPC results showed that the peaks become broader in the order of saturate, aromatic, resin and asphaltene fractions, and the asphaltene fraction was found to contain compounds of molecular weights ranging from 100 to more than 100000.

Bukka et al. (1991) studied the influence of chemical composition on bitumen viscosity. Two different Utah tar sand bitumens, Asphalt Ridge and Sunnyside were investigated. Molecular weights of the different fractions were obtained using vapor-phase osmometer. They found that molecular weights of the bitumen fractions increased gradually from saturates to asphaltenes.

3.4 SWELLING OF RUBBER BY SOLVENTS

3.4.1 Experimental procedure

In order to estimate the solubility parameters of truck and car-tyre rubbers, individual pieces of rubber cut from tyre tread were immersed in various solvents at room temperature. Rubber specimens were removed from the solvents after various immersion times, wiped dry with absorbent paper and re-weighed. Rubber samples with nominal dimensions of 15 x 10 x 1 mm approximately, were incorporated into 20 ml of solvent approximately.

Sovents used in this study included n-hexane and cyclohexane (aliphatic hydrocarbons), ethanol and butanol-1 (aliphatic alcohols), toluene (aromatic hydrocarbon), chloroform and chlorobenzene (chlorinated solvents), acetonitrile (nitrile), acetone (ketone) and tetrahydrofuran (cyclic ether). Densities and solubility parameters corresponding to these solvents are presented in **Table 3.1.**

Solvent	Density ($g\ cm^{-3}$)	Solubility parameter ($(cal\ cm^{-3})^{1/2}$)
n-Hexane	0.654	7.3
Cyclohexane	0.788	8.2
Toluene	0.866	8.8
Tetrahydrofuran	0.889	9.1
Chloroform	1.483	9.3
Chlorobenzene	1.105	9.5
Acetone	0.789	9.9
Butanol-1	0.809	11.4
Acetonitrile	0.785	11.9
Ethanol	0.789	12.7

Table 3.1 Densities and solubility parameters of solvents

The rubber samples were also immersed in bitumen (20 ml) at 180 ^{0}C. The samples were then removed from the bitumen after different immersion times, cleaned from excess bitumen by wiping with absorbent paper while hot and brushing for a few seconds with cold chlorobenzene.

Bitumens used were supplied by Shell Bitumen and included 50 and 100 penetration grades of Kuwaiti (KSR) and Venezuelan (VEN) origins. SARA fractions of the binders were provided by Shell Bitumen and are presented in **Table 3.2**.

Binder	Saturates (%)	Aromatics (%)	Resins (%)	Asphaltenes (%)
50 VEN	8.0	51.4	19.7	20.9
100 VEN	9.7	49.8	23.5	17.0
50 KSR	8.0	48.0	22.0	22.0
100 KSR	7.1	57.6	19.1	16.2

Table 3.2 SARA fractions of bitumens (data provided by Shell Bitumen)

3.4.2 Solubility parameters

The swelling of samples of rubber in a selection of solvents was examined in order to estimate the solubility parameters of the crosslinked rubbers. Specific volumes of solvent absorbed were obtained knowing the sample weight increase and the densities of the solvents. Specific volumes of solvent absorbed per gram of truck and car-tyre rubber were then determined as functions of immersion time in the solvent, and are presented in **Figure 3.2.**

Figures 3.2 show that greatest swellings were found with chlorinated solvents (chloroform and chlorobenzene), toluene and tetrahydrofuran, for both types of rubbers. The main difference between the two rubbers was the extent of swelling observed in cyclohexane and n-hexane. Aliphatic solvents such us cyclohexane and especially n-hexane swelled truck-tyre rubber far more than they did car-tyre rubber; the low equilibrium swelling of car-tyre rubber by n-hexane was achieved rapidly but the greater swelling of truck-tyre rubber was approached more slowly. Polar solvents such us alcohols (ethanol and butanol-1), acetone and acetonitrile did not swell the rubbers at all.

Solubility parameters of the rubbers were identified as the peaks in the plots of equilibrium specific volumes of solvent as functions of solubility parameters as shown in **Figure 3.3**. Both rubbers showed peaks at a solubility parameter of 9.3, approximately, where samples swell by about 200 % by volume. It is clear that the solubility parameters and the cohesive energy densities of the two rubbers are very similar.

It has been previously reported that solubility parameters for bitumens are in the range 8.4 to 9.2 (Ling et al., 1997). Thus, the similarity between the solubility parameters of bitumen and truck and car-tyre rubber indicates that bitumen is a swelling agent of both rubbers. Furthermore, polymers with solubility parameters outside the range corresponding to the bitumen have not shown good performance as binder modifiers (Curtis et al., 1995).

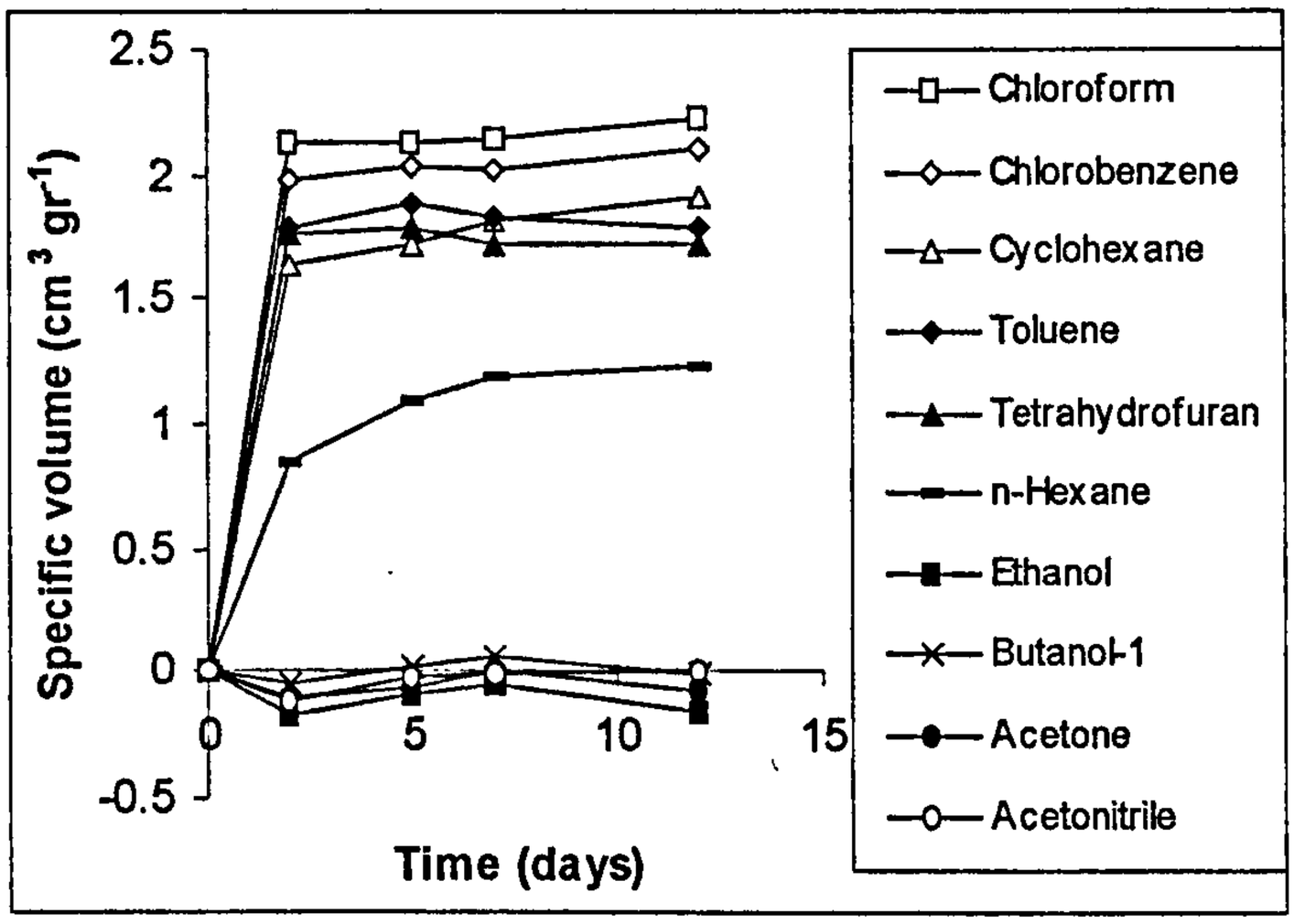

a) Swelling of truck-tyre rubber by solvents

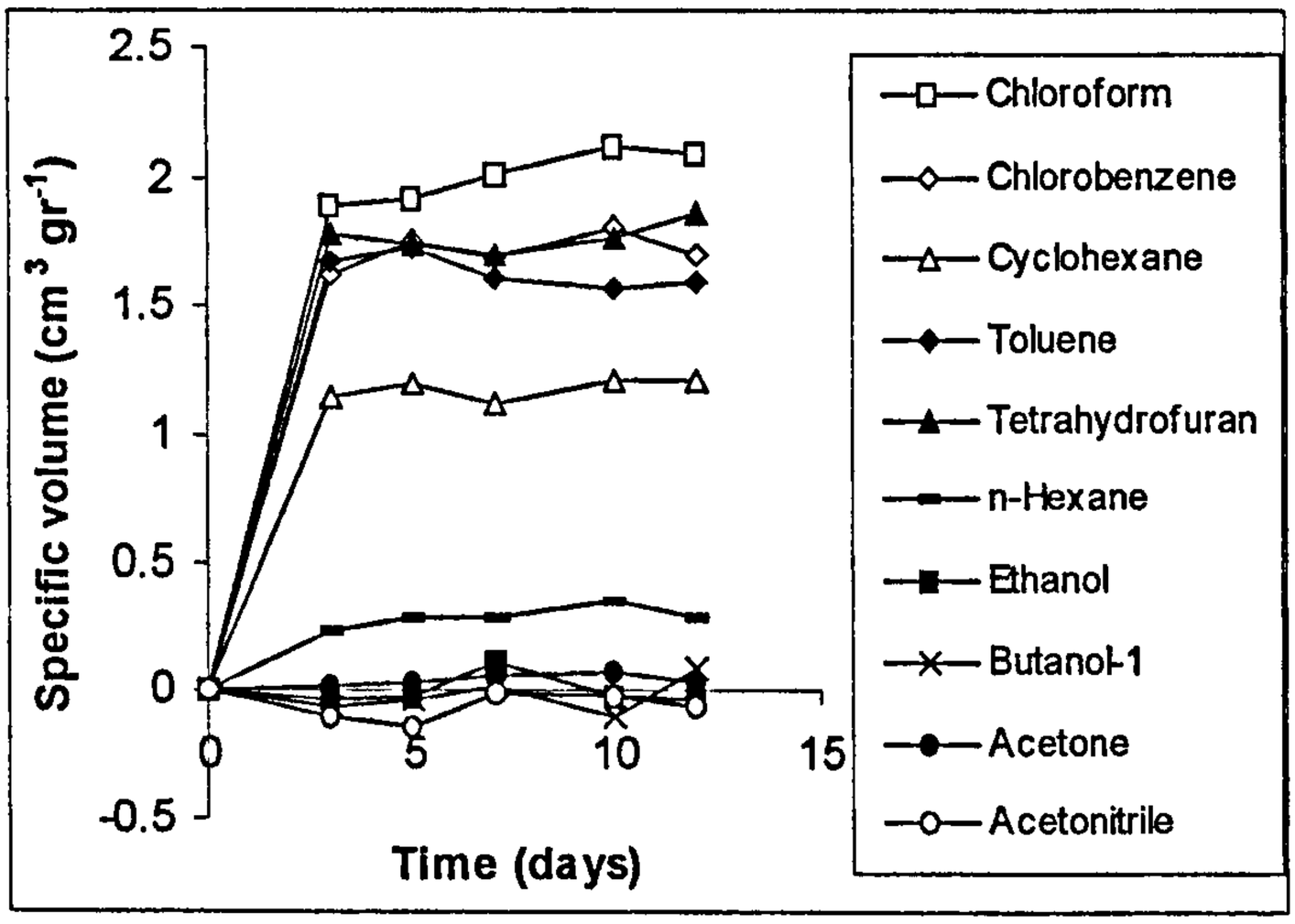

b) Swelling of car-tyre rubber by solvents

Figure 3.2 Swelling of rubber by solvents

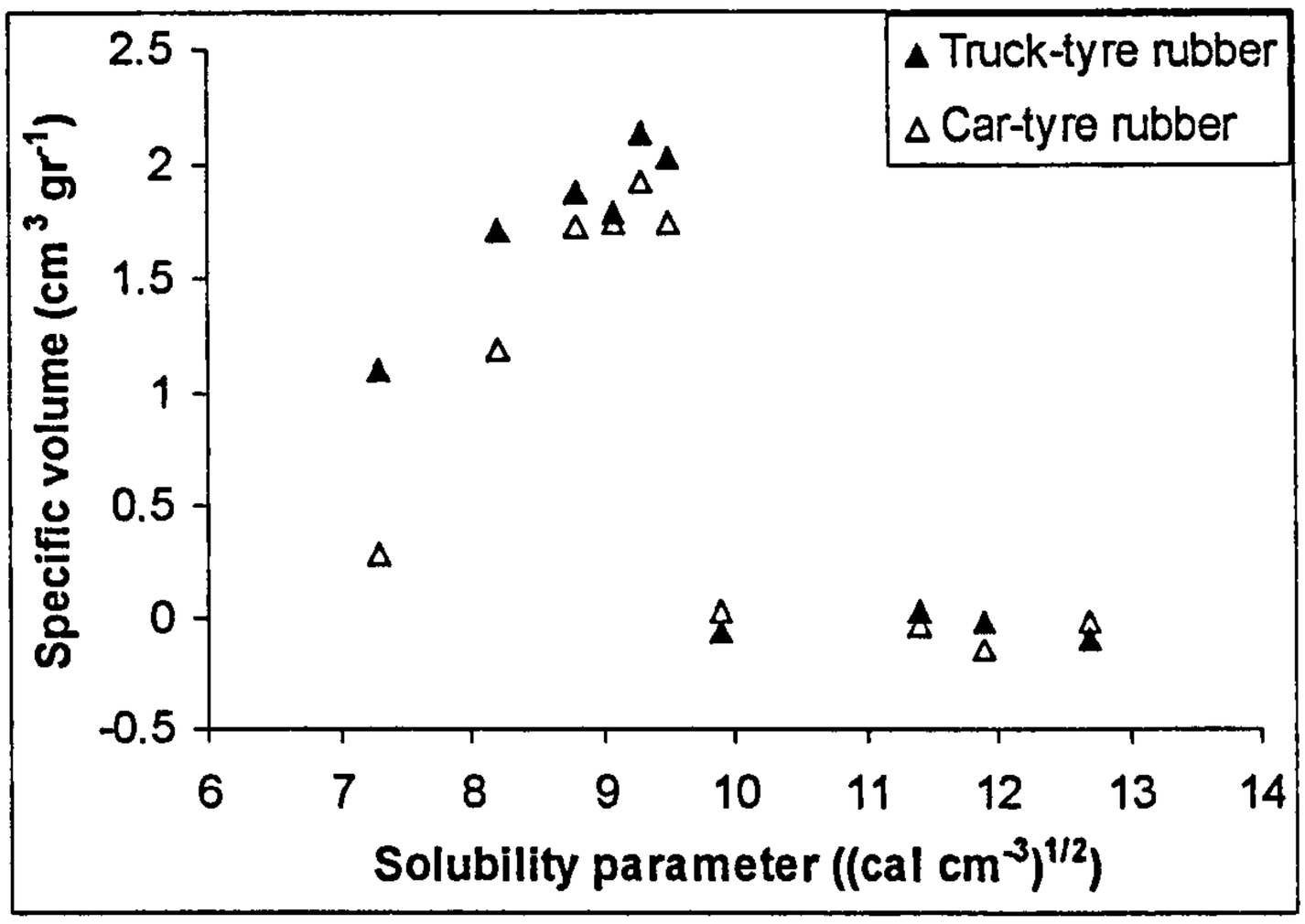

Figure 3.3 Determination of the solubility parameters of the rubbers

3.4.3 Solvent extraction

It was observed that during solvent swelling experiments coloured material was extracted from the rubbers after prolonged soaking in solvents. In general, those solvents which cause significant swelling extracted the most material while solvents which did not swell the rubbers extracted little material.

After evaporation of solvent, the residues extracted from the rubbers were examined by infrared spectroscopy. In the absence of specific information on the composition of components incorporated into tyres during manufactured, the 'finger-print' regions of the spectra were too complex to allow identification of substances extracted.

Nevertheless amounts of substances extracted were so small, in comparison with the large amount of bitumen absorbed, that it was considered that such processes would have negligible effects on the final properties of the modified rubber particles or of the bitumen phase. For similar reasons it was not possible to identify specific substances absorbed from the bitumen by the rubbers by solvent extraction and infrared analysis and the general nature of substances transferred

was inferred from solvent swelling of the rubbers and the overall composition of the bitumens as given by SARA analysis.

3.4.4 Discussion

Although most components of bitumen and rubber are hydrocarbons, solvent swelling data suggest that aromatic components of the bitumen will diffuse into the rubbers preferentially. Swelling data can also predict different swelling of the rubbers by bitumen because of the different relative swelling propensities by aliphatic hydrocarbons.

It is also established, from concepts of polymer-polymer miscibility that high-molecular-weight components of the bitumen, such us asphaltenes and resins, will not be miscible with the high-molecular-weight rubber (Olabisi et al., 1979). Furthermore, these bitumen fractions are highly polar and it has been shown that polar solvents do not diffuse (swell) into the rubbers. Aromatic components, on the other hand, will have a relatively high tendency to diffuse into the rubbers, compared with the aliphatic components but possibly moderated by the molecular weights of the components.

3.5 DIFFUSION OF BITUMEN INTO RUBBER

3.5.1 Experimental procedure

Diffusion of bitumen into rubber at high temperatures was investigated by immersing weighed rubber monoliths in bitumen at elevated temperature. Rubber samples with nominal dimensions of 15 x 10 x 1 mm approximately, were cut from truck and car tyre tread. Hot bitumen was poured into 20 ml glass beakers and kept in an oven at the desired temperature. Individual rubber samples were immersed in each of the glass beakers containing the bitumen. The individual rubber samples were then removed from the bitumen after different immersion times, cleaned from excess bitumen by wiping with absorbent paper while hot and brushing for a few seconds with cold chlorobenzene. Rubber samples were then reweighed and the mass uptake was obtained by difference between the initial weight and the weight after immersion in bitumen.

Diffusion studies were carried out at 150, 180 and 210 ^{0}C. Bitumens used and their SARA fractions were presented in **Table 3.2**.

3.5.2 Bitumen uptake data: sorption curves

Data collected from the diffusion experiments have been presented in the form of plots of percentage change in weight of the rubber samples, $(W_t\text{-}W_0)/W_0$ %, where W_t is the weight of the sample at time t and W_0 the initial weight, against $t^{1/2}/d$ where t is the immersion time of the rubber sample in bitumen and d is the thickness of the sample.

Figures 3.4 – 7 show the data obtained for the absorption of different bitumens into car and truck-tyre rubber at 180 ^{0}C.

The following general features have been observed:

1. At elevated temperatures (180 ^{0}C) bitumen was initially absorbed rapidly by the rubber and then approached equilibrium. For short times, up to about 3 hours approximately ($t^{1/2}/d \approx 100$ sec$^{1/2}$/mm), the sorption curves were initially linear. This linear region corresponded approximately to a weight increase up to about 50 % of the total weight increase.

2. For long times, equilibrium swelling was reached and was maintained until the rubber samples became mechanically weak and degraded physically on handling. For synthetic car-tyre rubber equilibrium swelling was established after about 1 day ($t^{1/2}/d \approx 300$ sec$^{1/2}$/mm) and was maintained for approximately 8 days ($t^{1/2}/d \approx 800$ sec$^{1/2}$/mm). After longer periods of immersion, rubber samples became very soft and tacky, and degraded physically on handling. In the case of truck-tyre (natural) rubber equilibrium was achieved after approximately 1 day, but it was more difficult to establish the equilibrium swelling accurately as physical degradation on handling become noticeable within 2 – 3 days ($t^{1/2}/d \approx 400 - 500$ sec$^{1/2}$/mm).

3. Equilibrium weight increase for truck-tyre rubber at 180 ^{0}C was greater than that for car-tyre rubber.

4. Bitumen uptake during the early stages of the diffusion process was faster for truck-tyre rubber than for car-tyre rubber as seen by the highest initial slope of the sorption curves.

3.5.3 Experimental error

Experimental scatter observed on the sorption data was mainly due to irregularities of the rubber samples as a result of cutting from the tyre treads. Rubber sample thickness was measured using a micrometer but some non-uniformity in sample thickness was observed. Due to the elastic character of the rubber, some error was also introduced when measuring the thickness of the samples.

Another cause of error could be introduced when cleaning the rubber samples after immersion in bitumen in order to obtain the weight increase. Rubber samples were cleaned first by wiping with absorbent paper and then by brushing with chlorobenzene. As seen before, chlorobenzene is a swelling agent of the rubbers, thus some chlorobenzene could have been absorbed into the rubber during the cleaning process. In order to check this, a weighed rubber sample was brushed with the solvent for a few seconds and then reweighed. It was found that rubber weight increase as a result of solvent absorption was negligible.

In general, handling of the rubber samples from truck-tyres (NR) was more difficult than from car-tyres (SBR). Truck-tyre rubber samples became very soft and tacky after immersion in bitumen making the handling and cleaning process more difficult.

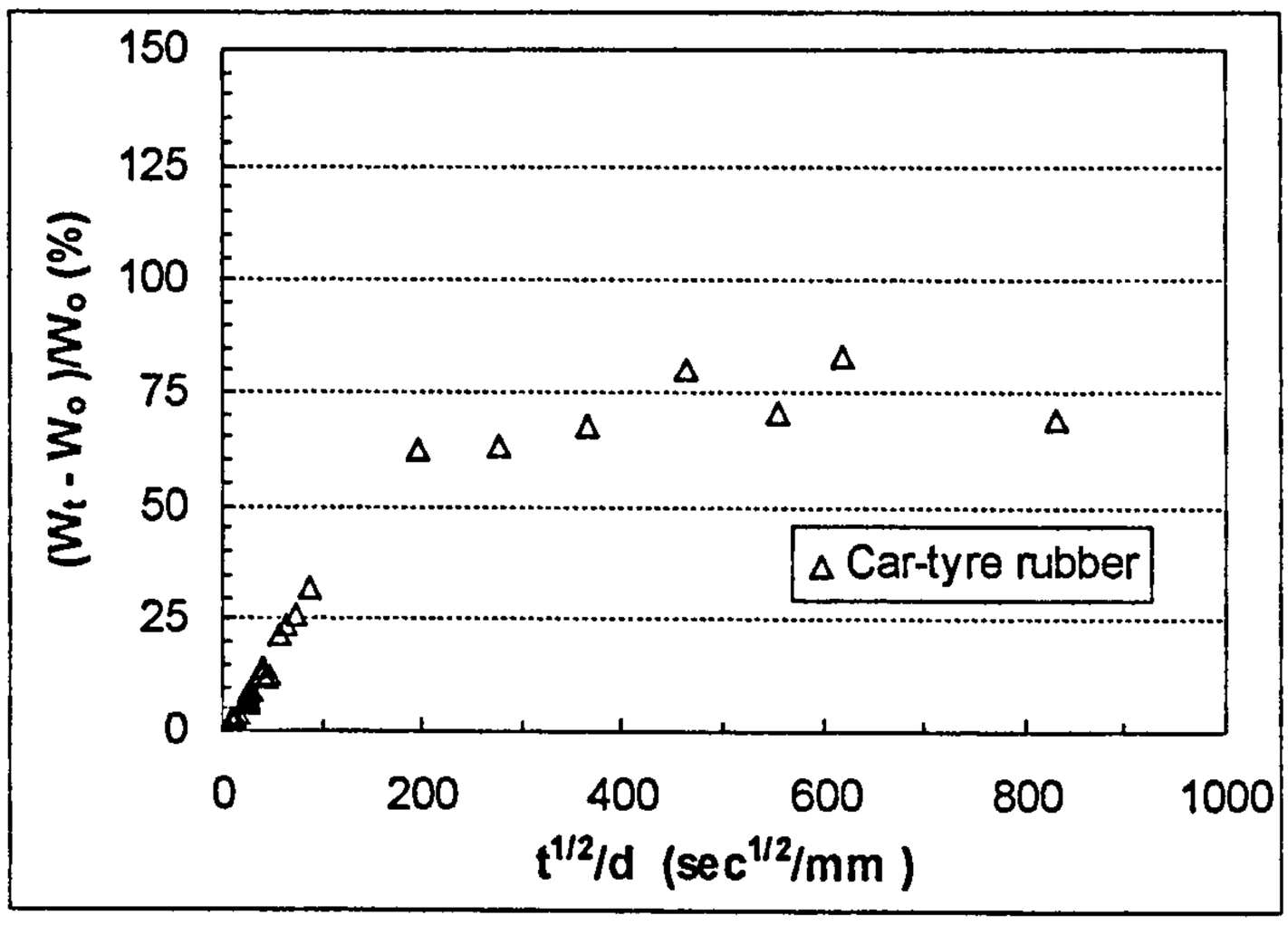

a) Car-tyre rubber

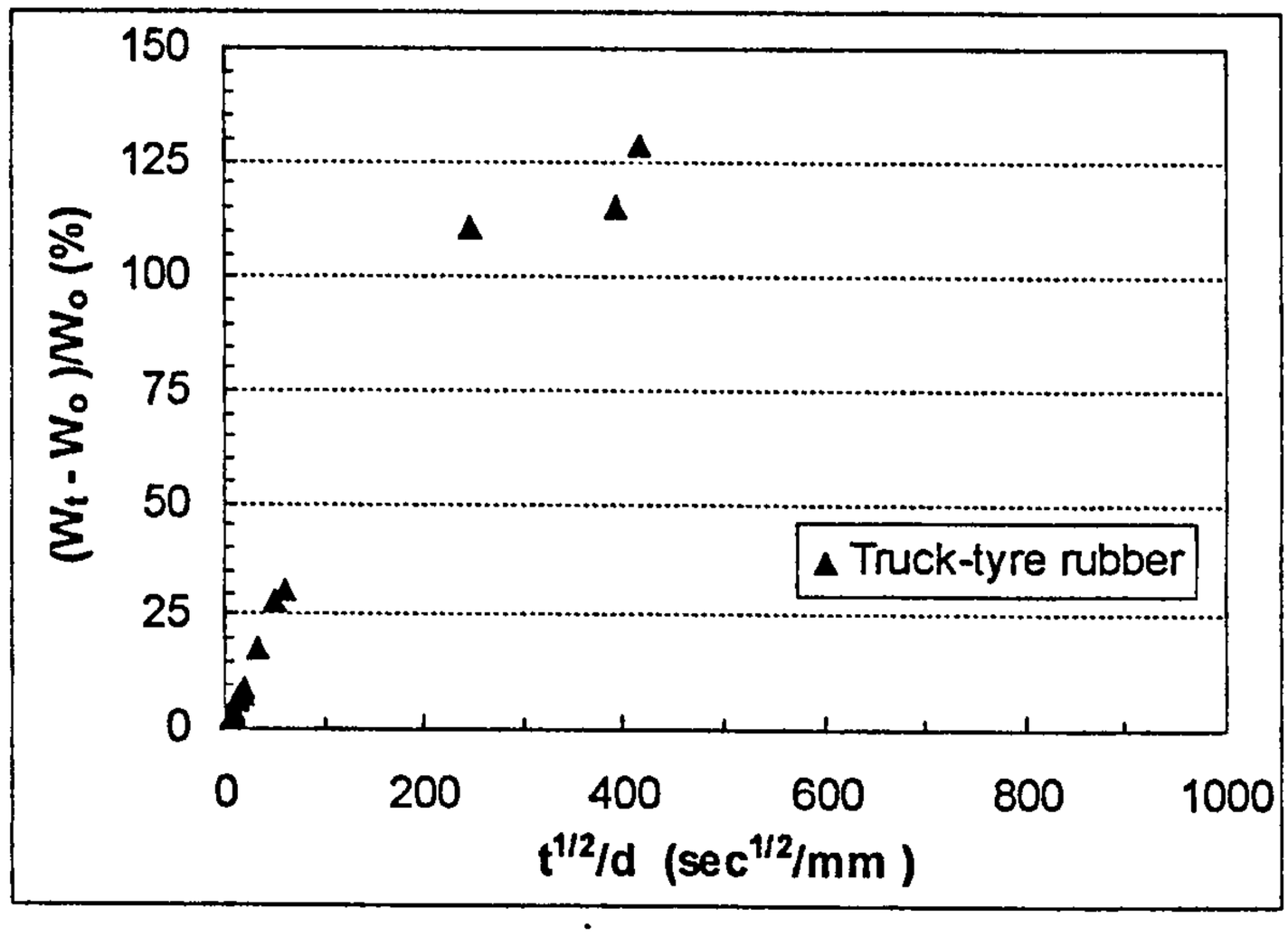

b) Truck-tyre rubber

Figure 3.4 Absorption of 100 KSR bitumen into rubber

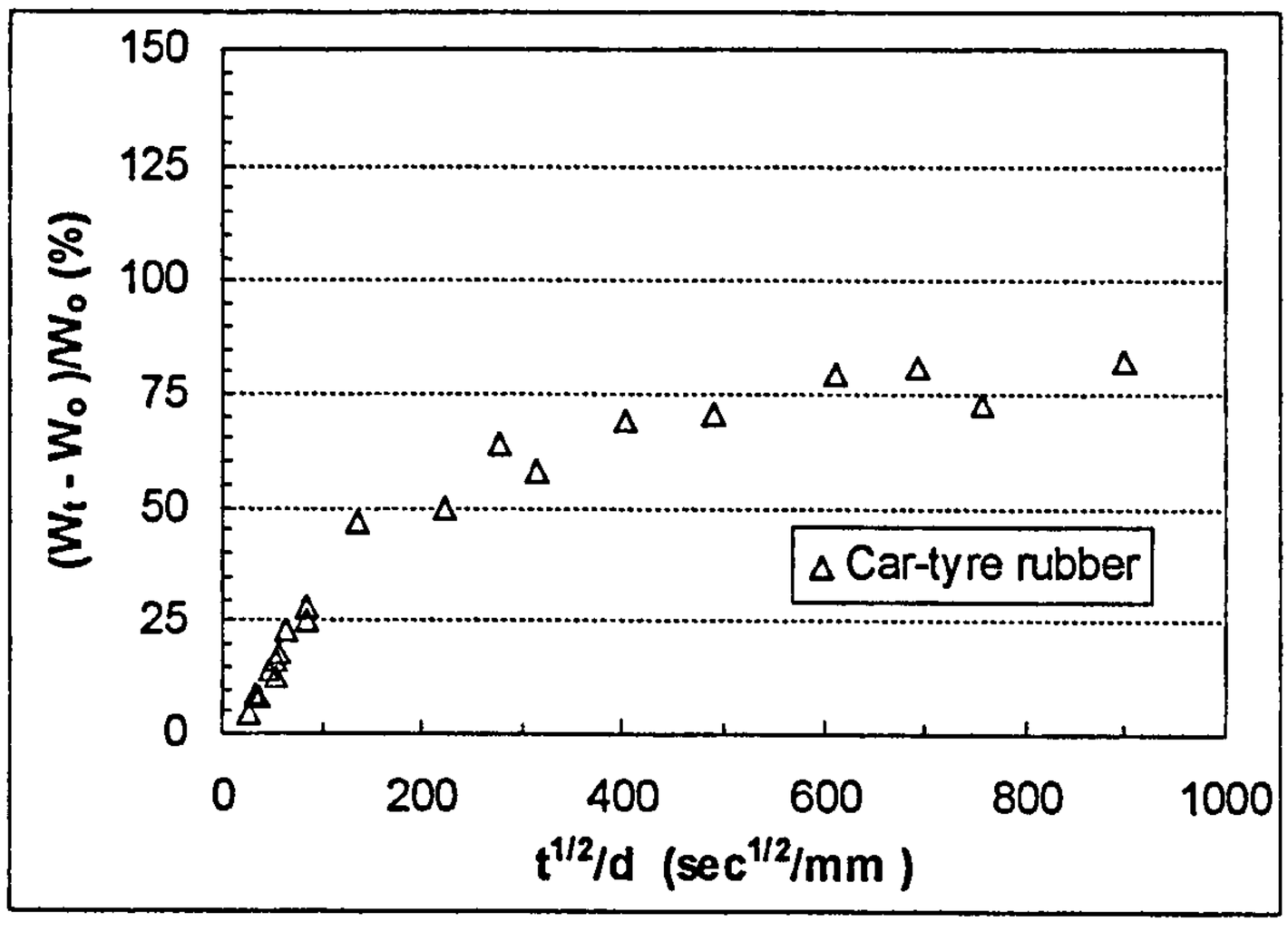

a) Car-tyre rubber

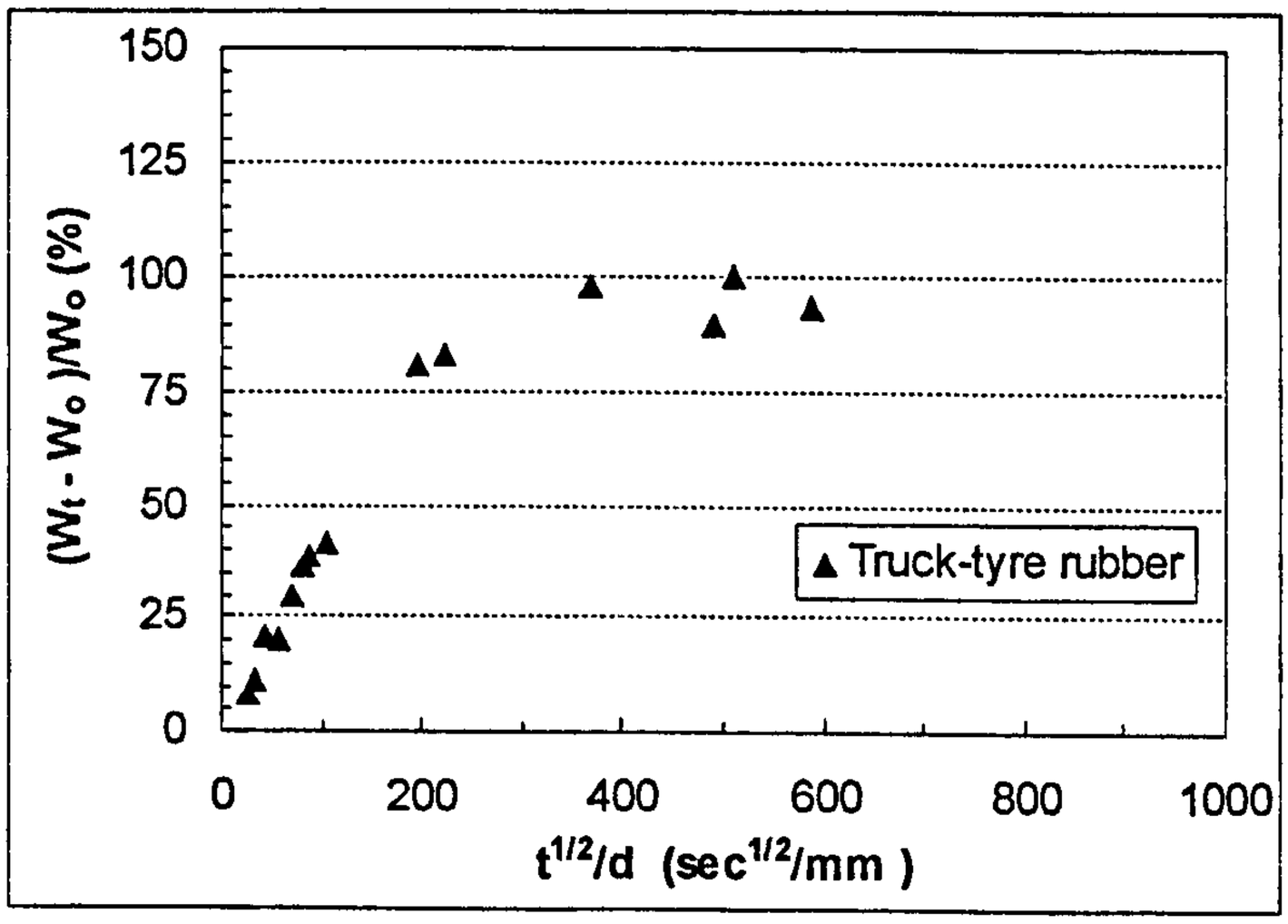

b) Truck-tyre rubber

Figure 3.5 Absorption of 50 KSR bitumen into rubber

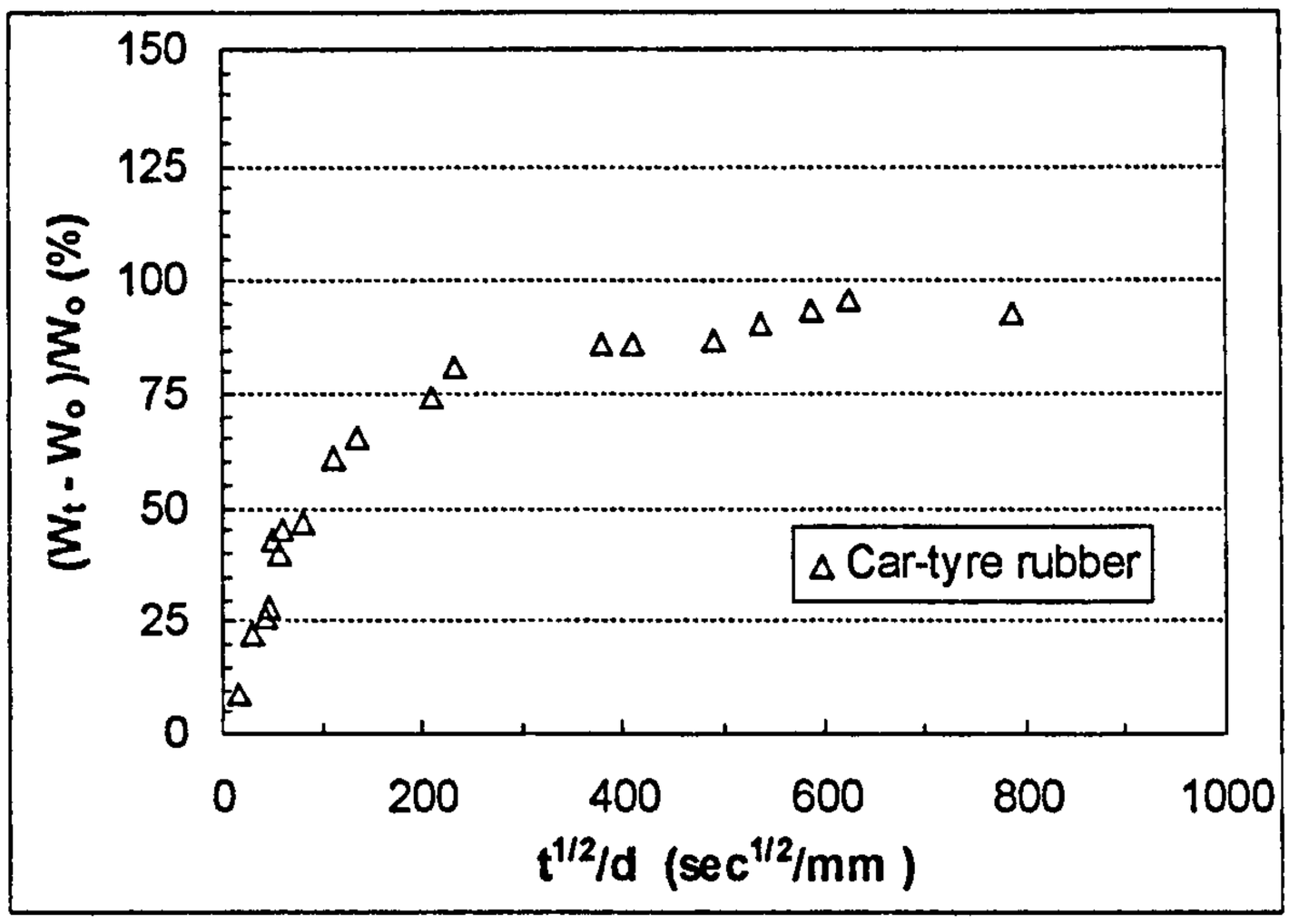

a) Car-tyre rubber

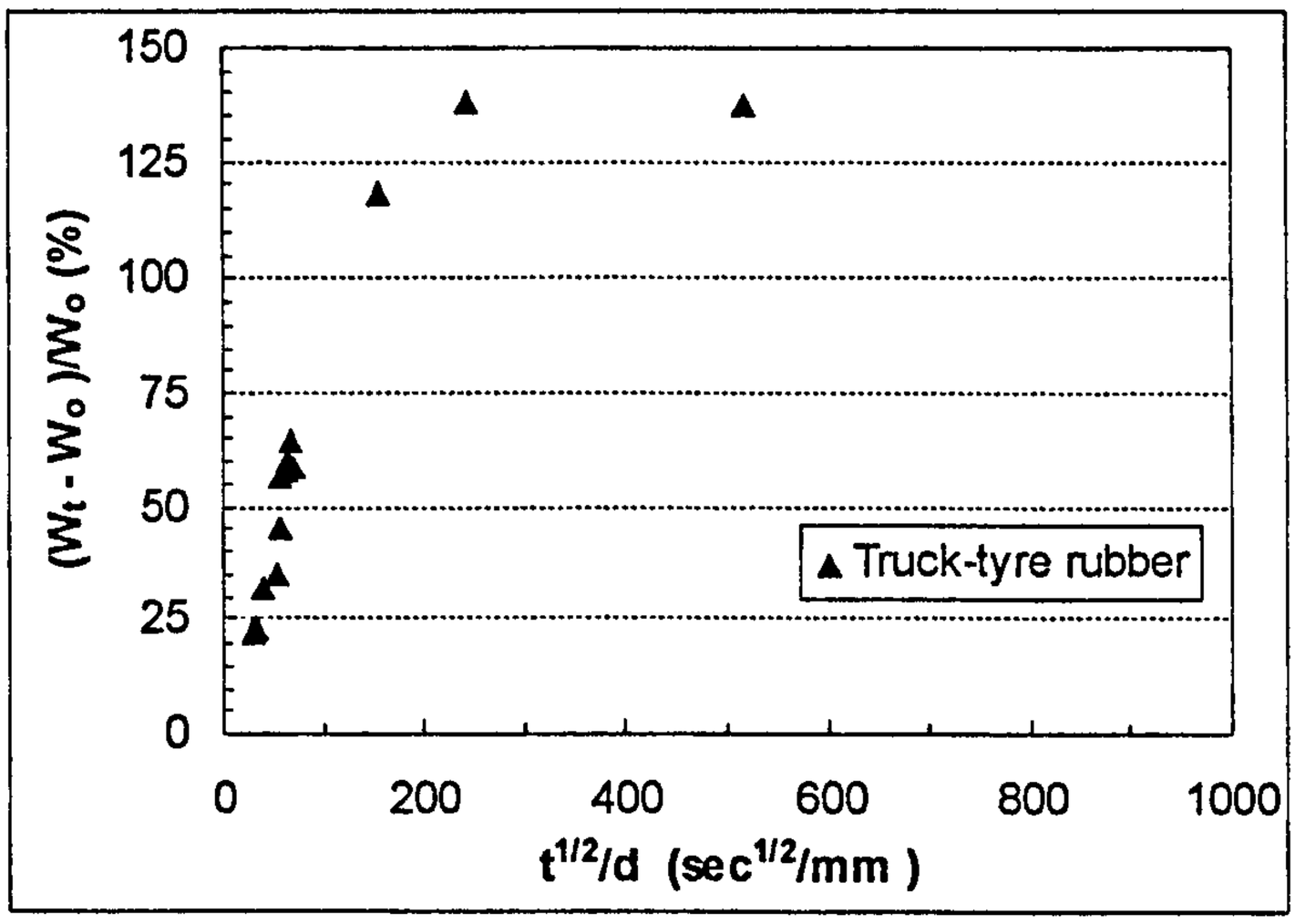

b) Truck-tyre rubber

Figure 3.6 Absorption of 100 VEN bitumen into rubber

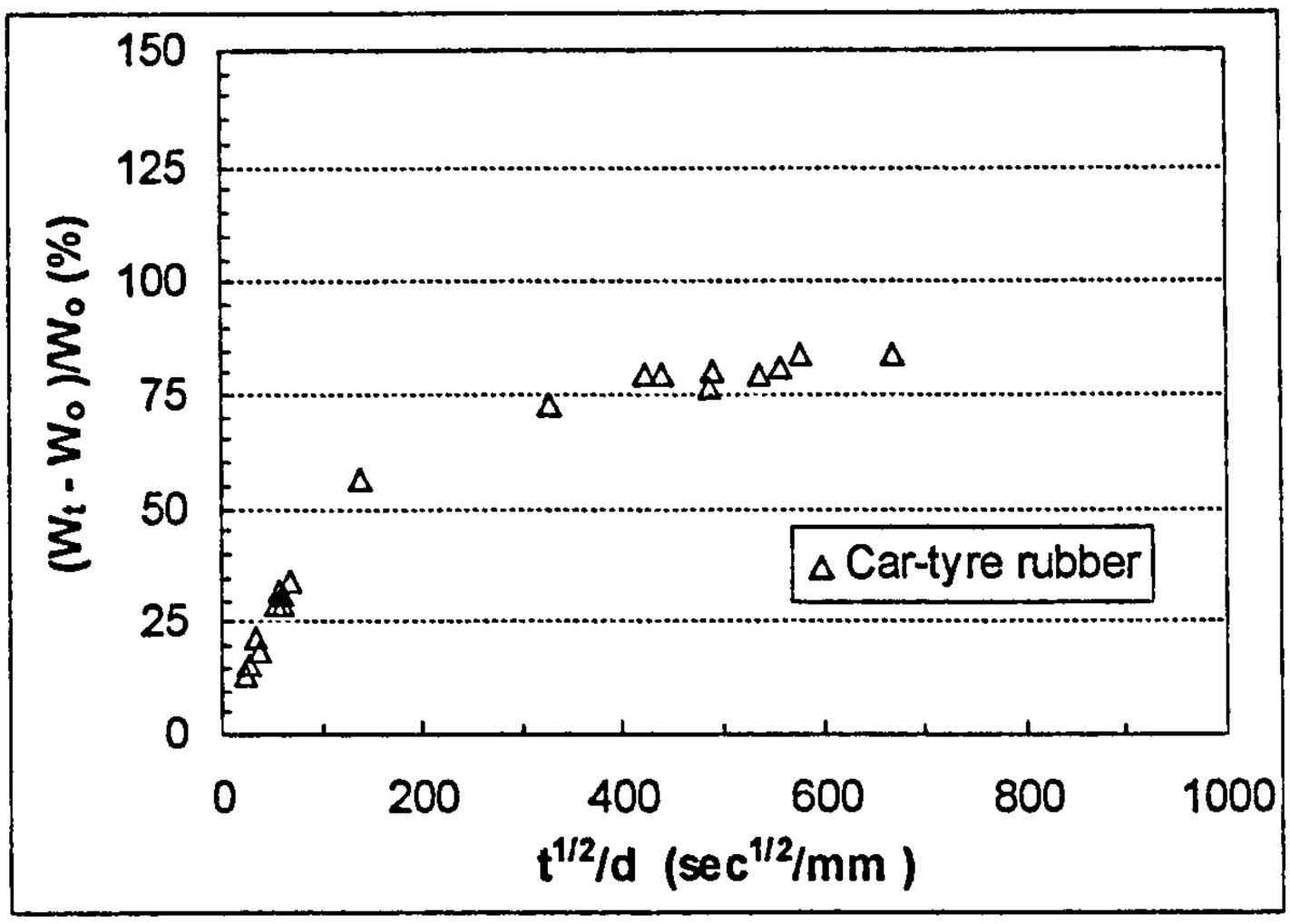

a) Car-tyre rubber

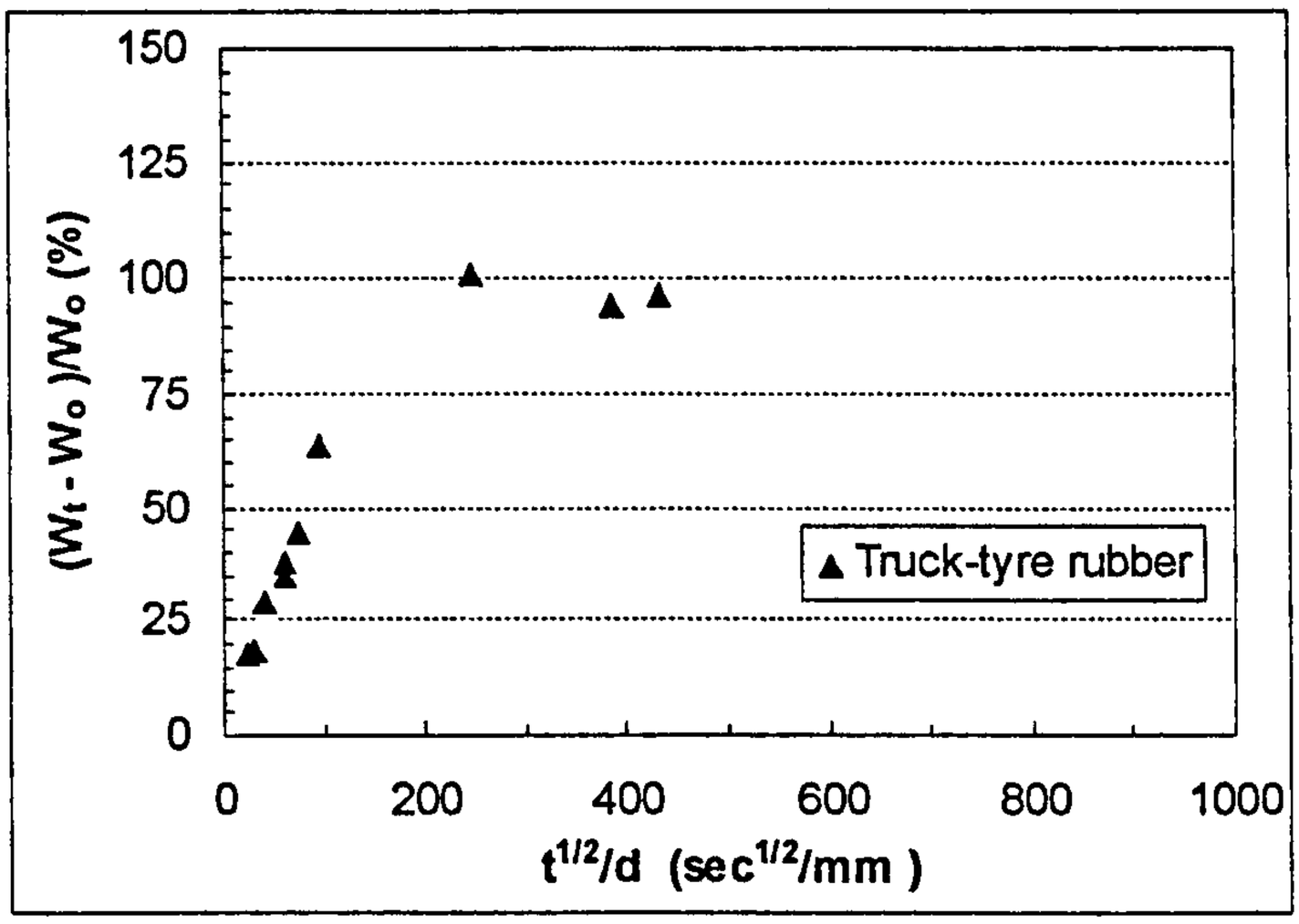

b) Truck-tyre rubber

Figure 3.7 Absorption of 50 VEN bitumen into rubber

3.5.4 Diffusion coefficients

3.5.4.1 Diffusion in a plane sheet

Consider a plane sheet of thickness d, whose surface is maintained at constant concentration C_0, and with no initial concentration of diffusing substance throughout the sheet. If the sheet occupies the region $-d/2 \le x \le d/2$, the boundary conditions may be written as follows:

$$\begin{aligned} C &= C_0, \; x = d/2, \; t \ge 0 \\ \frac{\partial C}{\partial x} &= 0, \; x = 0, \quad t \ge 0 \end{aligned} \tag{3.18}$$

The solution of Equation 3.16 for a semi-infinite film, $0 \le x \le d/2$, in an infinite bath, and assuming that equilibrium between the bath and the surface of the film was established instantaneously on immersion (Crank, 1956), is expressed as:

$$\frac{C}{C_0} = 1 - \frac{4}{\pi} \sum_{n=0}^{\infty} \frac{(-1)^n}{2n+1} \exp\left\{-D(2n+1)^2 \frac{\pi^2 t}{d^2}\right\} \cos \frac{(2n+1)\pi x}{d} \tag{3.19}$$

If M_t represents the total amount of diffusing substance which has penetrated the sheet at time t, and M_∞ the corresponding quantity after infinite time, then,

$$\frac{M_t}{M_\infty} = 1 - \sum_{n=0}^{\infty} \frac{8}{(2n+1)^2 \pi^2} \exp\left\{-D(2n+1)^2 \frac{\pi^2 t}{d^2}\right\} \tag{3.20}$$

For long times Equation 3.20 simplifies to,

$$\frac{M_t}{M_\infty} = 1 - \frac{8}{\pi^2} \exp\left\{-D \frac{\pi^2 t}{d^2}\right\} \tag{3.21}$$

and at short times Equation 3.20 may be approximated by,

$$\frac{M_t}{M_\infty} = \frac{4}{d}\left(\frac{Dt}{\pi}\right)^{1/2} = \frac{4D^{1/2}}{\pi^{1/2}}\left(\frac{t^{1/2}}{d}\right) \qquad (3.22)$$

Equation 3.22 indicates that a plot of M_t / M_∞ against $t^{1/2}/d$ should be initially linear. So, if the initial slope is obtained experimentally, the value of the diffusion coefficient, assumed constant, can be determined.

The diffusion theory, as developed for diffusion of vapours into and through polymer films where the concentration of penetrant is low, assumes that the thickness, *d*, of the sheet remains constant as sorption proceeds. In practice, however, the sheet frequently swells, so this effect has to be considered when determining the kinetic parameters.

3.5.4.2 Determination of diffusion coefficients

Absorption data presented in the previous section were normalised and plotted as the variation in M_t/M_∞ with $t^{1/2}/d$, where M_t and M_∞ are the mass % increase at time *t* and at equilibrium, *t* is the immersion time for the rubber in bitumen and *d* is the sample thickness. Values of the mass increase at equilibrium, M_∞, were estimated from the sorption curves presented in **Figures 3.4 - 7.**

Figure 3.8 shows the variation in M_t/M_∞ with $t^{1/2}/d$ for the absorption of 100 Pen KSR bitumen into car- and truck-tyre rubber at 180 ^{0}C. Plots show linear regions in the early stages of diffusion. For longer times, the relationship is no longer linear and M_t/M_∞ tends asymptotically to 1 as equilibrium swelling is reached. This behaviour is consistent with simple Fickian diffusion through a plane sheet of thickness *d*.

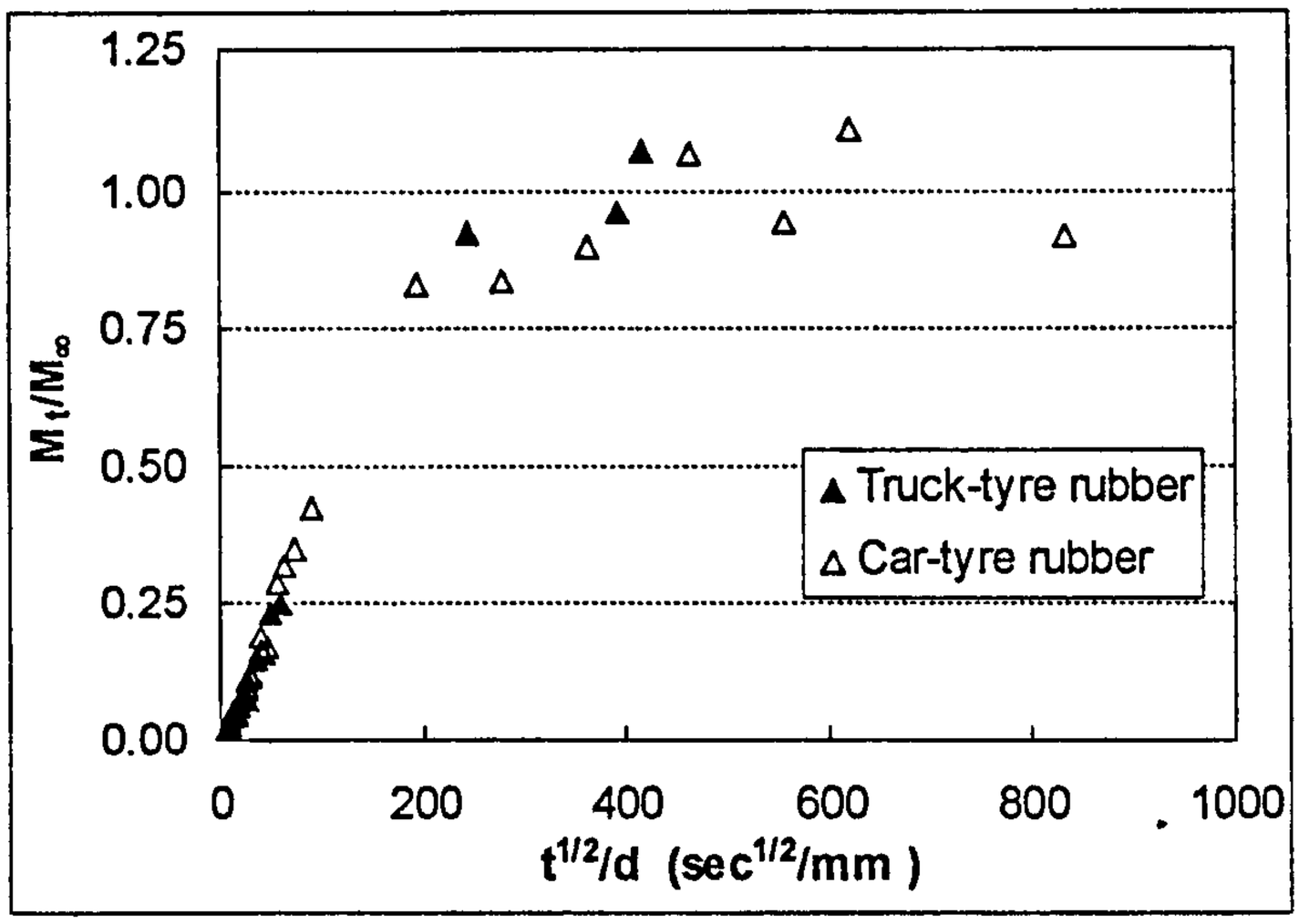

Figure 3.8 Variation in M_t/M_∞ with $t^{1/2}/d$ for the absorption of 100 Pen KSR bitumen into rubbers at 180 ^{0}C.

For one-dimensional diffusion through a plane sheet of thickness d in an infinite medium where the concentrations just within the surfaces are maintained constant and assuming that equilibrium between the bath and the surface of the sheet was established instantaneously on immersion, the value of the diffusion coefficient, D, which is assumed constant, can be deduced from the initial slope of a plot of M_t/M_∞ as a function of $(t^{1/2}/d)$.

From Equation 3.22, the slope of the linear region is given by,

$$m = \frac{4D^{1/2}}{\pi^{1/2}} \tag{3.23}$$

Thus,

$$D = \frac{\pi m^2}{16} \tag{3.24}$$

where m is the initial slope of a plot of M_t/M_∞ as a function of $(t^{1/2}/d)$, and D is the diffusion coefficient.

The slopes of the linear regions were estimated by fitting a straight line of the form $y = mx + n$ through the experimental data before attainment of 50 % equilibrium swelling, as seen in **Figure 3.9** for the diffusion of 100 Pen KSR bitumen into car and truck-tyre rubber.

Experimental constants, m and n, and regression coefficients, R^2, for the absorption of two penetration grade bitumens, 50 and 100 Pen, from Venezuelan (VEN) and Kuwaiti (KSR) origins into car and truck-tyre rubber at 180 ^{0}C are presented in **Table 3.3**.

So far, it has been assumed that the thickness or the rubber sheet, d, remains constant as sorption proceeds. However, significant swelling of the rubber samples was observed during sorption experiments. Hence, corrections to diffusion coefficients under swollen conditions were essential. This was done by calculating the intrinsic diffusion coefficient, D^*, from the volume fraction ϕ of the rubber in the swollen sample using the following relationship (Brown et al., 1973),

$$D^* = \frac{D}{\phi^{7/3}} \tag{3.25}$$

The volume fraction of the rubber can be obtained as follows,

$$\phi = \frac{\frac{m_R}{SG_R}}{\frac{m_R}{SG_R} + \frac{m_B}{SG_B}} \tag{3.26}$$

where m_R, m_B, SG_R and SG_B are the masses and the specific gravities of the rubber and the bitumen respectively.

Specific gravities of car and truck-tyre rubber have not been determined, however, typical values for vulcanised natural rubber and styrene-butadiene rubbers vary between 0.92 – 1.0 and between 0.94 – 1.0, respectively (Roff and Scott, 1971). On the other hand, specific gravity of the bitumen is mainly dependent on the grade of the bitumen and the temperature. Typical specific gravities at 180 ^{0}C vary between 0.91 – 0.96 (Whiteoak, 1990).

In order to estimate the volume fraction of the rubbers in the swollen condition (equilibrium swelling), the specific gravities of the rubbers and the bitumens were assumed to be the same. From Equation 3.26, the volume fraction of the rubber can now be estimated as follows,

$$\phi = \frac{1}{1+\frac{m_B}{m_R}} = \frac{1}{1+M_\infty} \tag{3.27}$$

Equilibrium swelling mass uptake (M_∞), volume fraction of the rubbers (ϕ) and diffusion coefficient values (D and D^*) at 180 ^{0}C were obtained and are presented in **Table 3.4**.

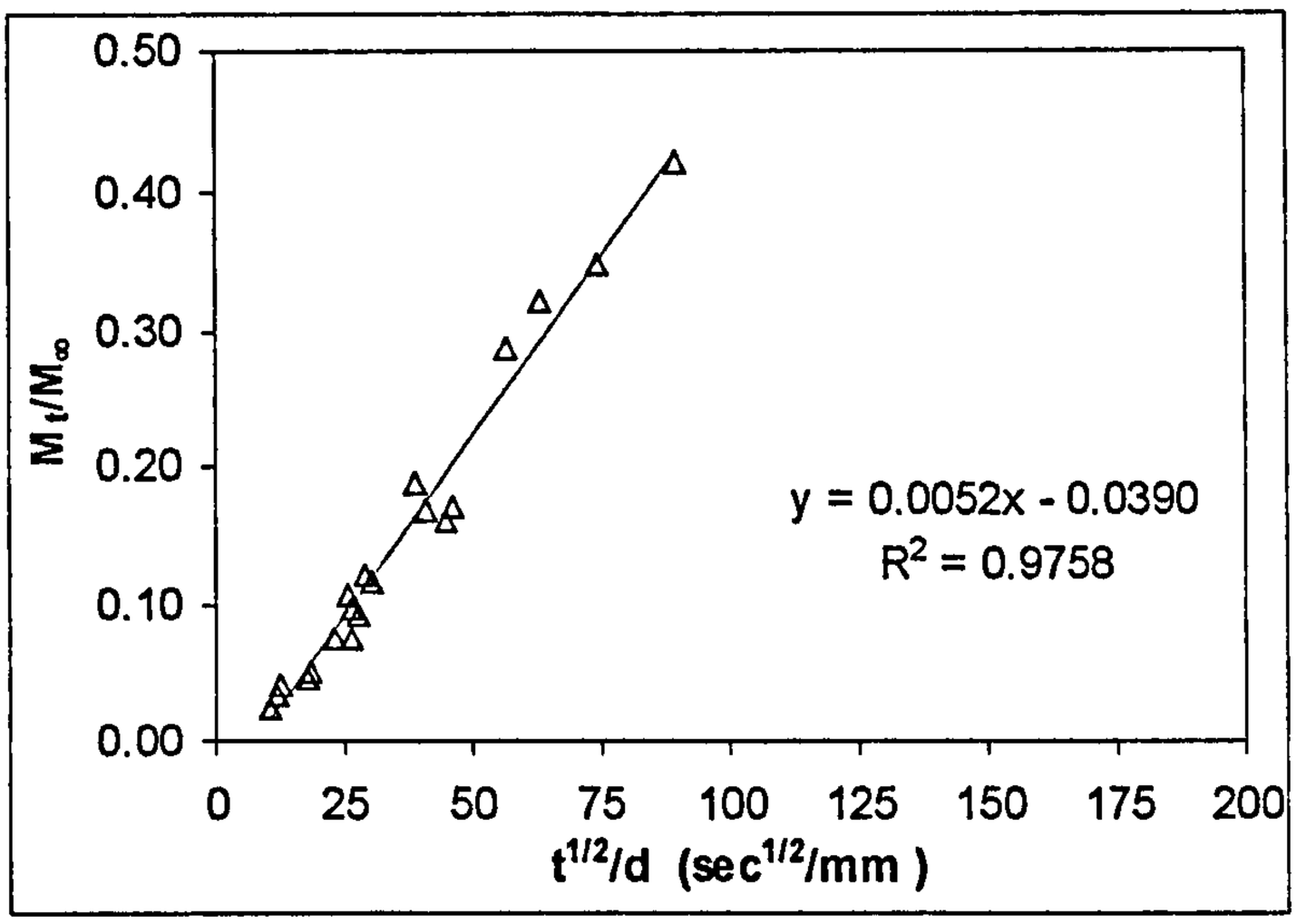

a) Car-tyre rubber

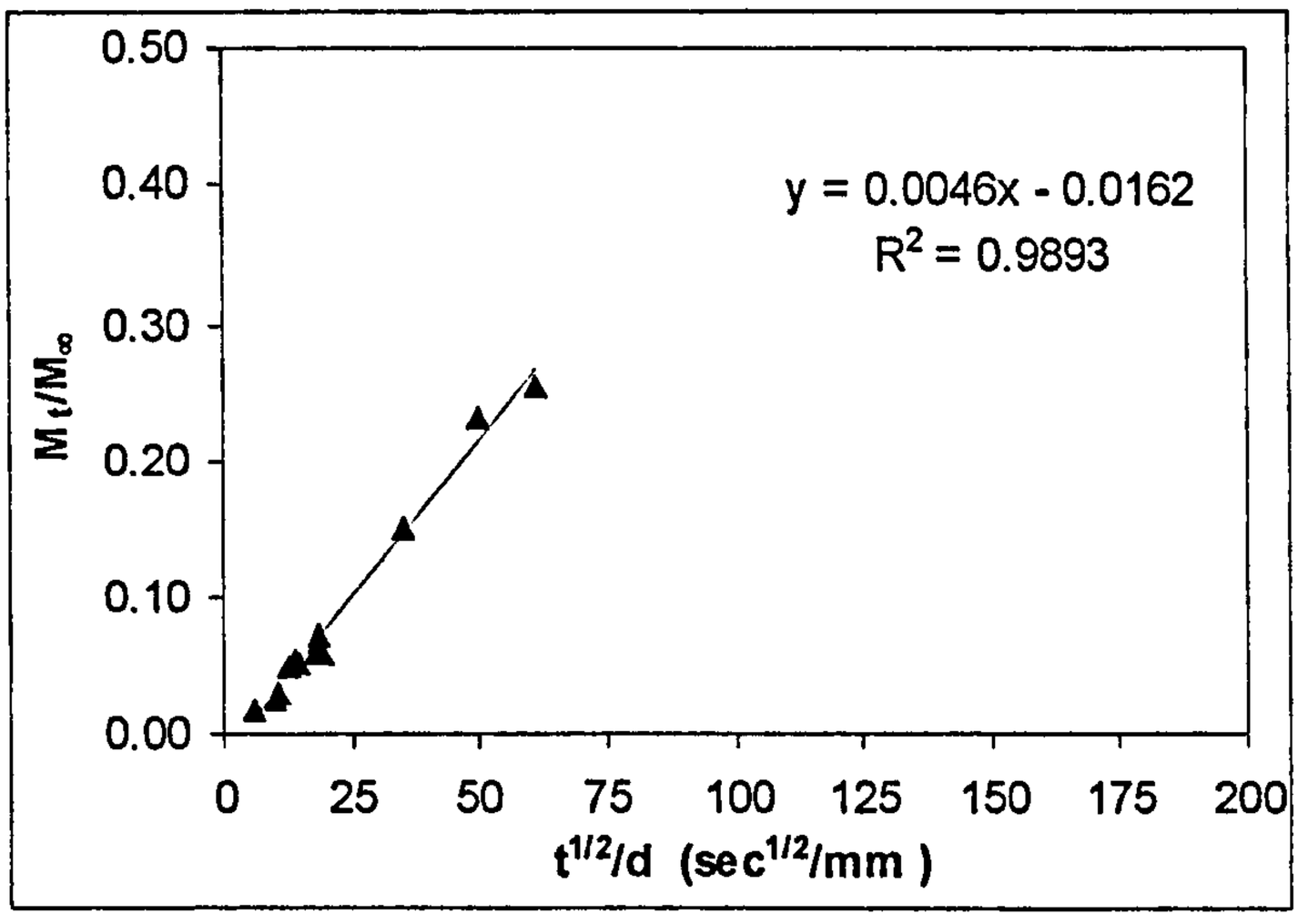

b) Truck-tyre rubber

Figure 3.9 Linear regions for the absorption of 100 Pen KSR bitumen into rubber

Binder	Rubber	*m*	*n*	R^2
100KSR	Car	0.0052	-0.0390	0.98
	Truck	0.0046	-0.0162	0.99
50KSR	Car	0.0052	-0.0700	0.95
	Truck	0.0048	-0.0343	0.96
100VEN	Car	0.0090	-0.0685	0.87
	Truck	0.0070	-0.0642	0.87
50VEN	Car	0.0066	0	0.95
	Truck	0.0064	0	0.94

Table 3.3 Experimental constants, *m* and *n*, and R^2 at 180 ^{0}C

Binder	Rubber	M_∞ (%)	D x10^{-6} ($mm^2\ s^{-1}$)	ϕ	D^* x10^{-6} ($mm^2\ s^{-1}$)
100KSR	Car	75	5.30	0.571	19.56
	Truck	120	4.15	0.455	26.12
50KSR	Car	75	5.30	0.571	19.56
	Truck	95	4.52	0.513	21.47
100VEN	Car	90	15.90	0.526	71.09
	Truck	140	9.62	0.417	74.19
50VEN	Car	80	8.55	0.556	33.70
	Truck	95	8.04	0.513	38.19

Table 3.4 Equilibrium swelling and diffusion coefficients at 180 ^{0}C

3.5.4.3 Discussion

Diffusion coefficients determined from the slopes of the linear regions were considered as apparent for several reasons. First, the equation for Fickian diffusion, used to estimate values of *D*, assumes that, the diffusion coefficient is constant, thus the nature of the matrix (bitumen) does not change as equilibrium is approached; and equilibrium between the matrix and the surface of the sheet is established instantaneously on immersion. Diffusion of large weight fractions of

bitumen into the rubbers markedly changes their physical properties as they soften and, inevitably, molecular mobility within them increases. Therefore, the diffusion coefficient cannot be expected to remain constant throughout. For a constant diffusion coefficient, the graph for a sorption experiment is a straight line for M_t/M_∞ as much as about 50%. If D is a function of concentration, which increases as penetrant concentration increases, the graph is linear over a larger increase in M_t/M_∞ (Crank and Park, 1968).

Second, bitumen is a complex material and different components might diffuse into the rubber at different relative rates as the rubber swells. Solvent swelling observations indicate that the lighter aromatic components might diffuse into both rubbers preferentially in the early stages and enhance diffusion of other components in the later stages as the environment within the swollen rubber changes. Aliphatic components might also diffuse into truck rubber in the early stages.

3.5.5 Dependence of sorption parameters on rubber type

Data presented in **Table 3.4** showed that equilibrium weight increase for truck-tyre rubber (NR) was greater than that for car-tyre rubber (SBR), independent of the bitumen grade and origin. Higher equilibrium swellings associated with truck-tyre rubber might reflect the greater solubility of bitumen aliphatic components in the truck tyre rubbers, as seen from solvent swelling data.

Moreover, chain flexibility of the rubbers, which determines the free volume available and, consequently the sorption parameters, is controlled by factors like the nature of the polymer chain, the number and distribution of crosslinks between rubber chains, the presence of fillers (carbon black) and the temperature.

The flexibility of a polymer depends on the ability of a polymer chain to rotate about the constituent chain bonds. Chain flexibility is related to the *glass transition temperature*, T_g, that is defined as the temperature at which the

polymer undergoes the transformation from the glass to the rubber-like state. A flexible chain has a low T_g whereas a rigid chain has a high T_g (Cowie, 1991).

Typical glass transition temperatures of polymer compounds in NR and SBR determined by Differential Scanning Calorimetry (DSC) are presented in **Table 3.5**. Glass transition temperature of cis–1,4 (polyisoprene) in NR is about –73 ^{0}C. A typical butadiene mixture as in SBR might have a glass transition temperature of approximately – 60 ^{0}C; the styrene units (T_g =100 ^{0}C) however, raise the glass transition temperature depending on the percentage styrene by weight in SBR.

Polymer	Microstructure	T_g (^{0}C)
Polyisoprene	cis -1,4	-73
	trans - 1,4	-53
Polybutadiene	cis -1,4	-108
	trans - 1,4	-18
	1, 2	20
Polystyrene	/	100

Table 3.5 Glass transition temperatures of rubber compounds

When crosslinks between polymer chains are introduced, the molecular motion is restricted and T_g rises. The presence of fillers in the rubbers, such us carbon black, also reduce molecular mobility as seen in the increase in T_g. The effect of crosslink density and filler content has not been evaluated in the current study due to the variability of these factors when using rubber from different wasted tyres.

3.5.6 Dependence of sorption parameters on bitumen composition

Comparisons between the equilibrium swellings for the bitumens from Venezuelan and Middle East origins (see **Table 3.4**) show that at equilibrium the rubbers absorb more bitumen components from the former than from the latter, as seen by the higher values of the equilibrium mass uptake, M_∞. Furthermore, these differences are more relevant when comparing the 100 Pen binders from the two origins than for the 50 Pen binders.

Moreover, diffusion coefficients for the Venezuelan binders are also higher than those for the Middle East, and again the differences are larger when comparing the 100 Pen binders from the two different origins as seen in **Table 3.4**.

The differences between the sorption parameters, M_∞ and D^*, of the bitumens might be attributed to differences in their molecular composition. SARA fractions of the binders presented in **Table 3.2** indicate that the binders with the highest asphaltene content, which corresponded to the low penetration grade binders, swell the rubbers less than those with lower asphaltene content, which corresponded to higher penetration grade bitumens. As discussed previously, asphaltenes have high molecular weight and are not likely to diffuse into the high-molecular weight rubbers, so, binders with high asphaltene content are less prone to swell the rubbers.

When comparing same penetration grade binders from different origins, the higher asphaltene content of the 50KSR binder is seen in the slightly decrease in the equilibrium swelling for the car-tyre rubber. However, the lower asphaltene content of the 100KSR in comparison with the 100VEN binder does not correspond to a higher equilibrium swelling. No relationship was found between the remaining SARA fractions, saturates, aromatics and resins, and the equilibrium swellings.

Bitumen viscosity, which depends on temperature and binder chemical composition and structure, is the other factor that controls the diffusion process. Binder viscosity measurements at different temperatures were carried out using a

Brookfield viscometer (see Chapter 4, Section 4.2.2) and are presented in **Figure 3.10**.

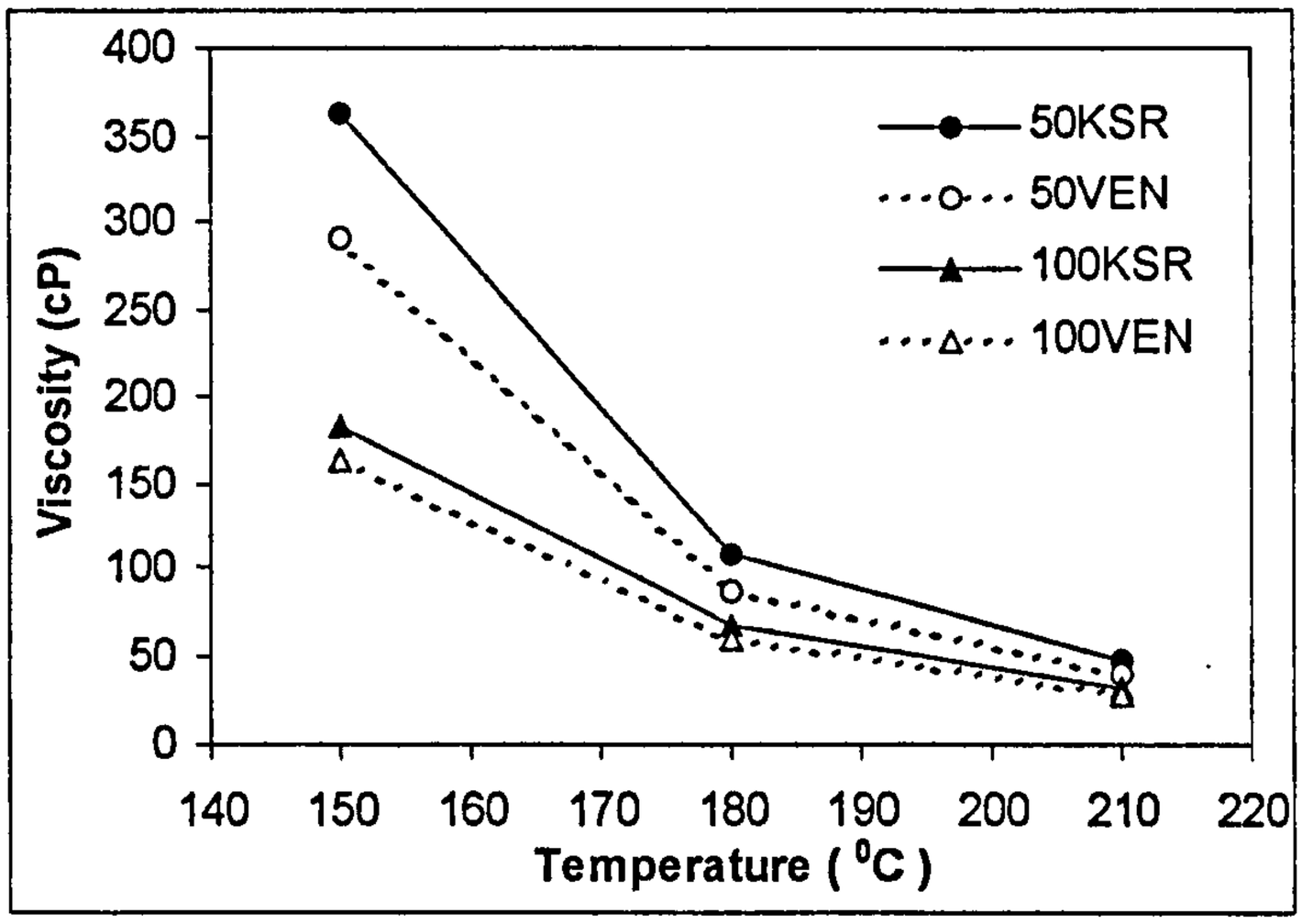

Figure 3.10 Brookfield viscosities of bitumens

Viscosity data at 180 ^{0}C showed as expected that the high penetration grade binders (100 Pen) had lower viscosities than the low penetration ones (50 Pen). Furthermore, for the same grade, the binders from Venezuelan origin (VEN) had lower viscosities than the ones from the Middle East (KSR).

The lowest viscosity associated to the 100VEN binder resulted in the highest values of the diffusion coefficients for both type of rubbers. The diffusion coefficients for the 50VEN binder were lower than the ones corresponding to the 100VEN as a result of its higher viscosity. Although there were differences in the viscosities of the KSR binders, these differences were not manifested in the diffusion coefficient values.

3.5.7 Effect of temperature on the diffusion process

In order to study the effect of temperature on the diffusion process, absorption of bitumen into rubber experiments were carried out at different temperatures, 150, 180 and 210 ^{0}C.

3.5.7.1 Sorption data

Absorption data have been presented, as before, in the form of plots of percentage change in weight of the rubber samples, $(W_t\text{-}W_0)/W_0$ %, where W_t was the weight of the sample at time t and W_0 the initial weight, against $t^{1/2}/d$ where t was the time that the rubber sample was immersed in the bitumen and d was the thickness of the sample.

Figures 3.11 and **3.12** show the data obtained for the absorption of 100 Pen KSR bitumen into car and truck-tyre rubber at 150 and 210 ^{0}C respectively. Data at 180 ^{0}C have already been presented in **Figure 3.4**.

Absorption data at 150 ^{0}C showed that for short times, up to about 6 hours approximately ($t^{1/2}/d \approx 150$ sec$^{1/2}$/mm), the sorption curves were initially linear. For long times, equilibrium swelling for car-tyre rubber was established after about 4 days ($t^{1/2}/d \approx 600$ sec$^{1/2}$/mm) and was maintained for the duration of the tests without appreciable physical degradation of the rubber on handling. Equilibrium swelling for car-tyre rubber corresponded to a mass increase of about 70 %. In the case of truck-tyre rubber equilibrium swelling was assumed to be achieve after approximately 4 days, which corresponded to the last data point of the test, and the equilibrium swelling uptake taken was 120 %. For longer times, the rubber degraded physically on handling.

At the highest temperature, 210 ^{0}C, the sorption curve for car-tyre rubber was initially linear up to about 1.5 hours ($t^{1/2}/d \approx 75$ sec$^{1/2}$/mm). For long times, equilibrium swelling was reached after about 11 hours ($t^{1/2}/d \approx 200$ sec$^{1/2}$/mm) and was maintained up to about 4 days ($t^{1/2}/d \approx 600$ sec$^{1/2}$/mm). Equilibrium swelling for car-tyre rubber resulted in mass increase of 70 % approximately. Furthermore, the linear part of the sorption curve represented up to about 70 % of

the total weight increase. In the case of truck-tyre rubber the absorption data showed quite large scatter as a result of the difficulties in handling the rubber samples, which became very soft and tacky in the early stages of the test. However, for short times, the sorption curve might still be considered as linear. Equilibrium swelling for truck-tyre rubber at this temperature could not be determined because the rubber samples degraded physically when removed from the bitumen and during the cleaning process.

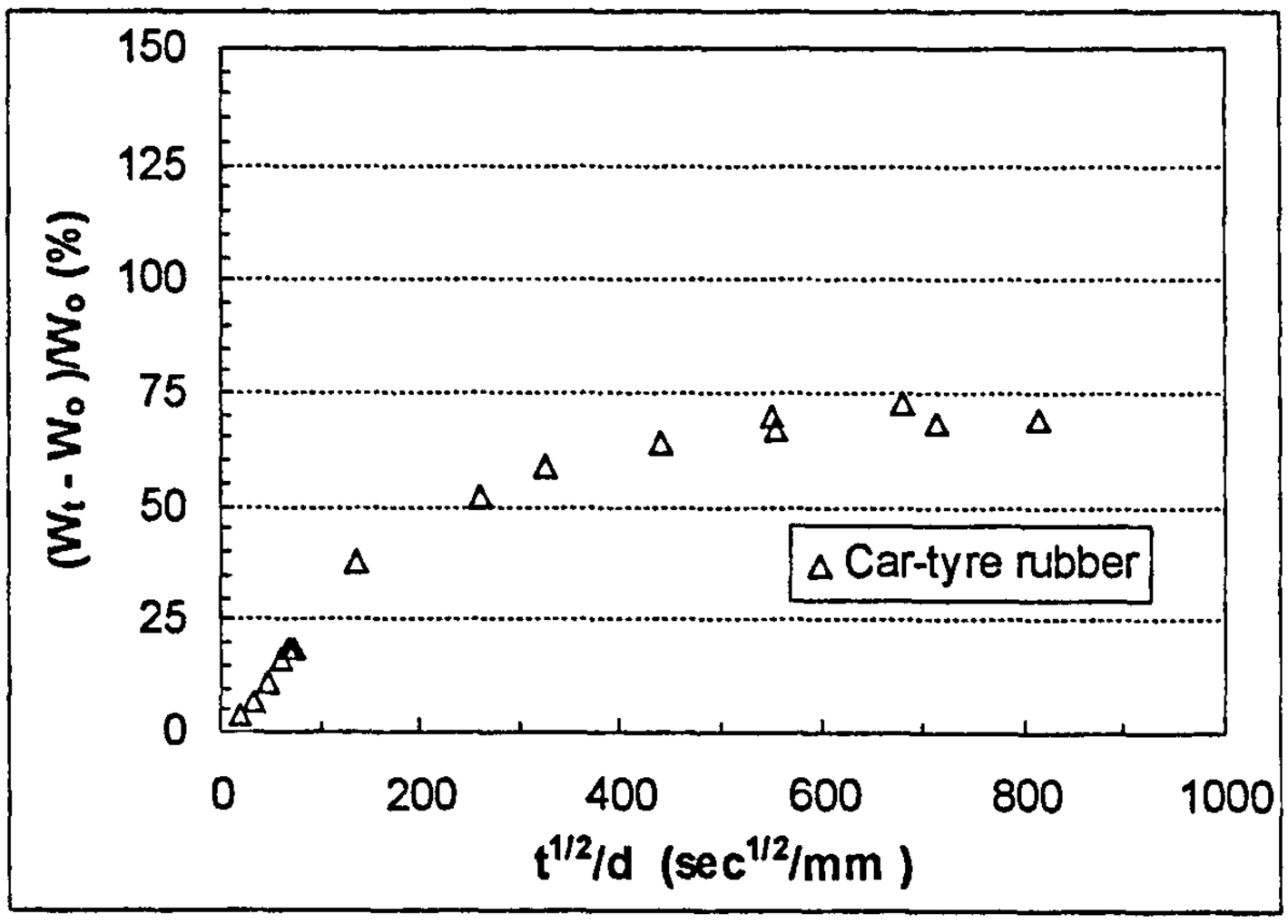

a) Car-tyre rubber

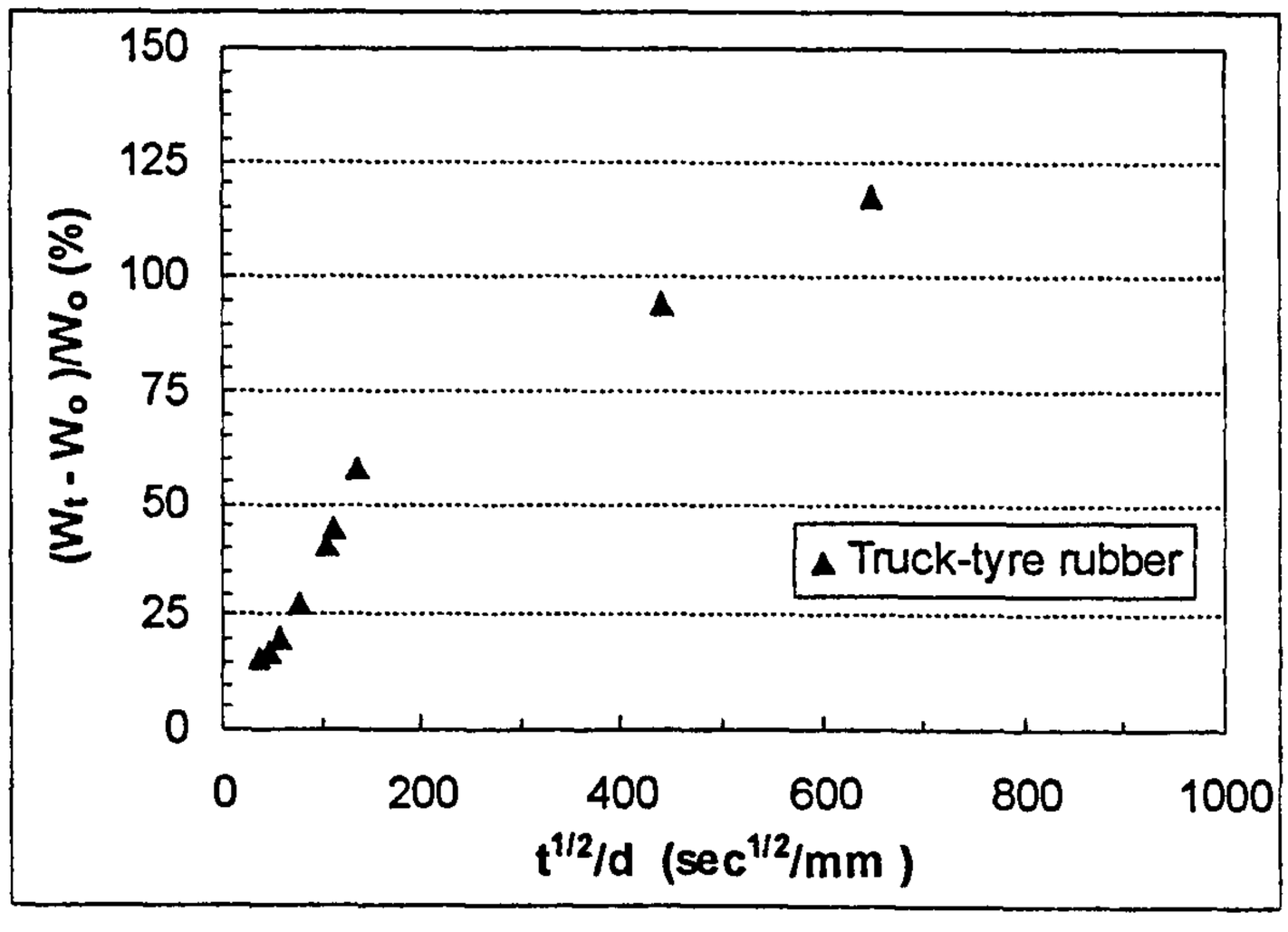

b) Truck-tyre rubber

Figure 3.11 Absorption of bitumen into rubber at 150 ^{0}C

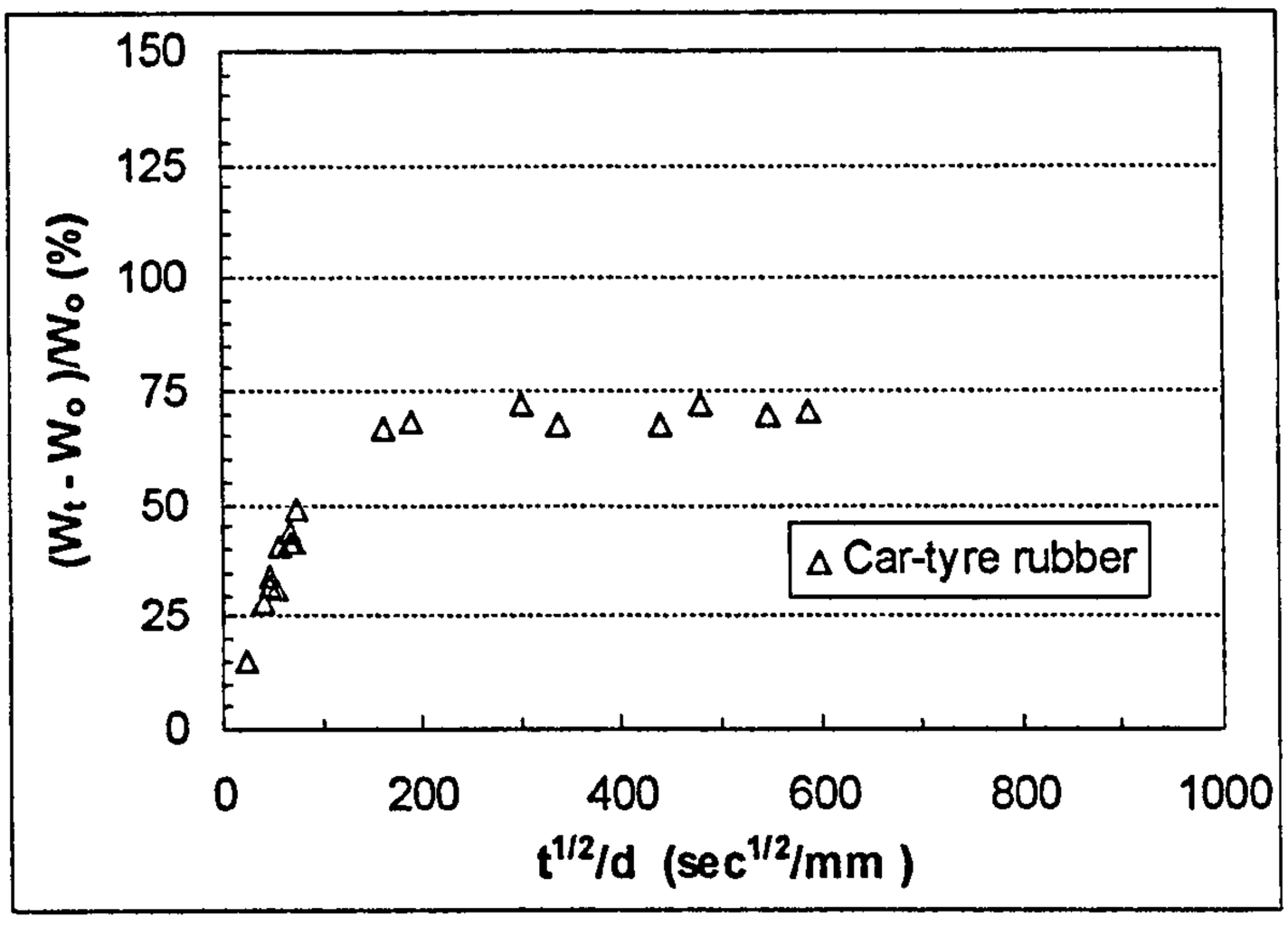

a) Car-tyre rubber

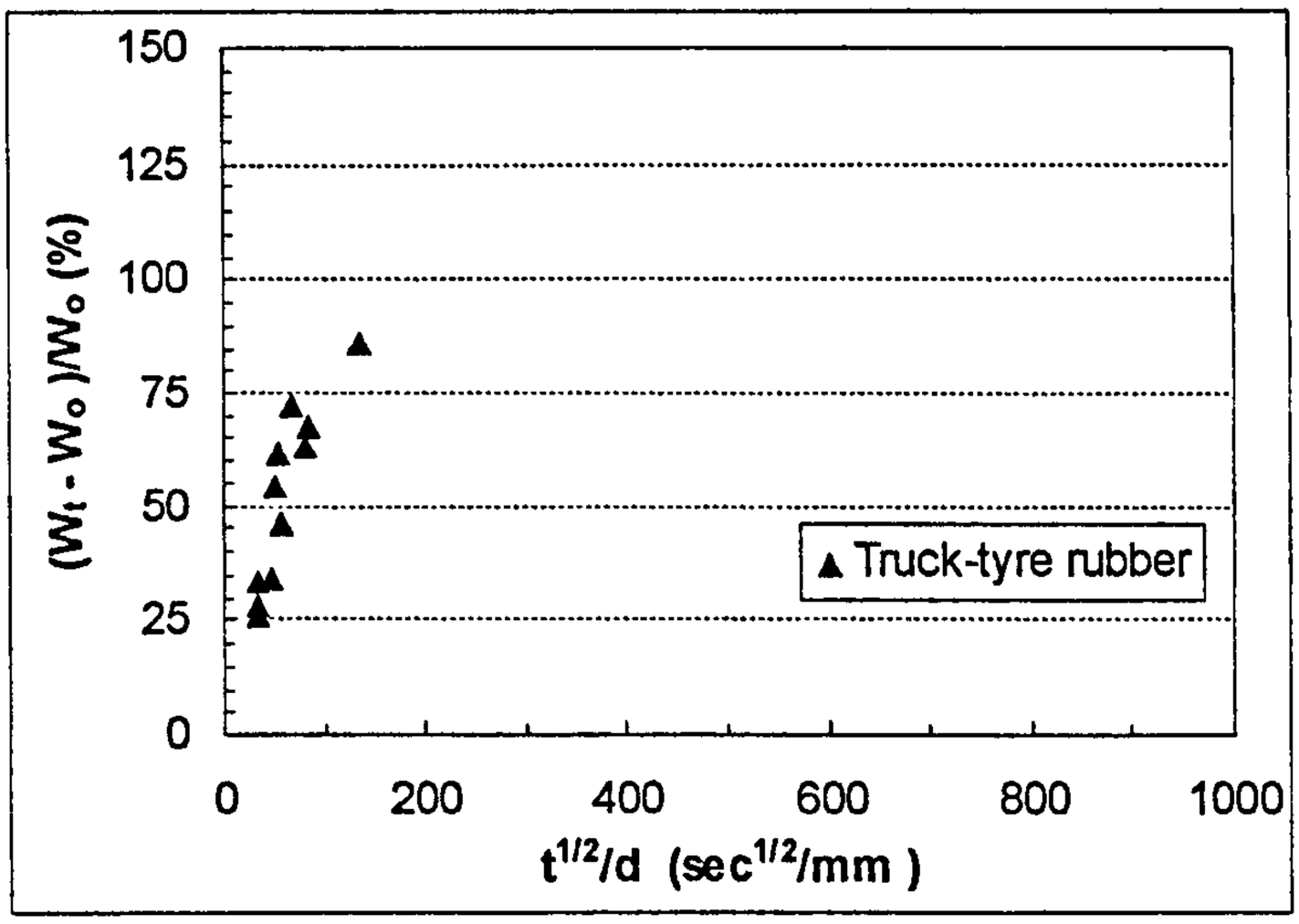

b) Truck-tyre rubber

Figure 3.12 Absorption of bitumen into rubber at 210 ^{0}C

3.5.7.2 Diffusion coefficients

Absorption data at different temperatures were normalised and plotted as the variation in M_t/M_∞ with $t^{1/2}/d$, where M_t and M_∞ are the mass % increase at time t and at equilibrium, t is the immersion time for the rubber in bitumen and d is the sample thickness of the rubber. Values of the mass increase at equilibrium, M_∞, were estimated from the sorption curves presented in **Figures 3.11** and **3.12** Equilibrium swelling uptake for truck-tyre rubber at 210 ^{0}C could not be determined but it was approximated to the value at 180 ^{0}C, thus 120 % in order to calculated the diffusion coefficient.

Values of the diffusion coefficient were deduced from the initial slopes of the plots of M_t/M_∞ as a function of $(t^{1/2}/d)$ using Equation 3.24. The slopes of the linear regions were estimated by fitting a straight line of the form $y = mx + n$ through the experimental data. Experimental constants, m and n, and regression coefficients, R^2, for the absorption of 100KSR bitumen into car and truck-tyre rubber at 150, 180 and 210 ^{0}C are presented in **Table 3.6.**

Temperature (^{0}C)	Rubber	m	n	R^2
150	Car	0.0044	-0.0481	0.99
	Truck	0.0037	-0.0328	0.98
180	Car	0.0052	-0.0390	0.98
	Truck	0.0046	-0.0162	0.99
210	Car	0.0093	0	0.93
	Truck	0.0074	0	0.77

Table 3.6 Experimental constants, m , n and R^2 at 150, 180 and 210 ^{0}C

Furthermore, due to extensive swelling of the rubber samples, diffusion coefficients were corrected using Equation 3.25. Finally, equilibrium swelling mass uptakes and diffusion coefficient values for the diffusion of 100 Pen KSR bitumen into car and truck-tyre rubber at different temperatures were calculated and are presented in **Table 3.7**.

Temperature (^{0}C)	Rubber	M_∞ (%)	D x10^{-6} ($mm^2\ s^{-1}$)	ϕ	D^* x10^{-6} ($mm^2\ s^{-1}$)
150	Car	70	3.80	0.588	13.11
	Truck	120	2.69	0.455	16.93
180	Car	75	5.30	0.571	19.56
	Truck	120	4.15	0.455	26.12
210	Car	70	16.98	0.588	58.57
	Truck	120	10.75	0.455	67.67

Table 3.7 Equilibrium swellings and diffusion coefficients at different temperatures

It is clear from the data that temperature affects the rate of diffusion. As the temperature increases the diffusion coefficient values for the two rubbers also increase.

The increase in the diffusion coefficient values with increasing temperature can be related to the viscosity of the bitumen at different temperatures (see **Figure 3.10**). As the temperature increases, the viscosity of the bitumen decreases increasing the rate of diffusion into the rubbers. **Figure 3.13** illustrates the relationship between bitumen viscosity and diffusion coefficients.

Moreover, as the temperature increases, the amplitude of segmental oscillations of polymer chains also increases. Greater segmental motion results in an increase in the size of free volume and subsequent increase in diffusivity as the temperature is increased (Peterlin, 1975).

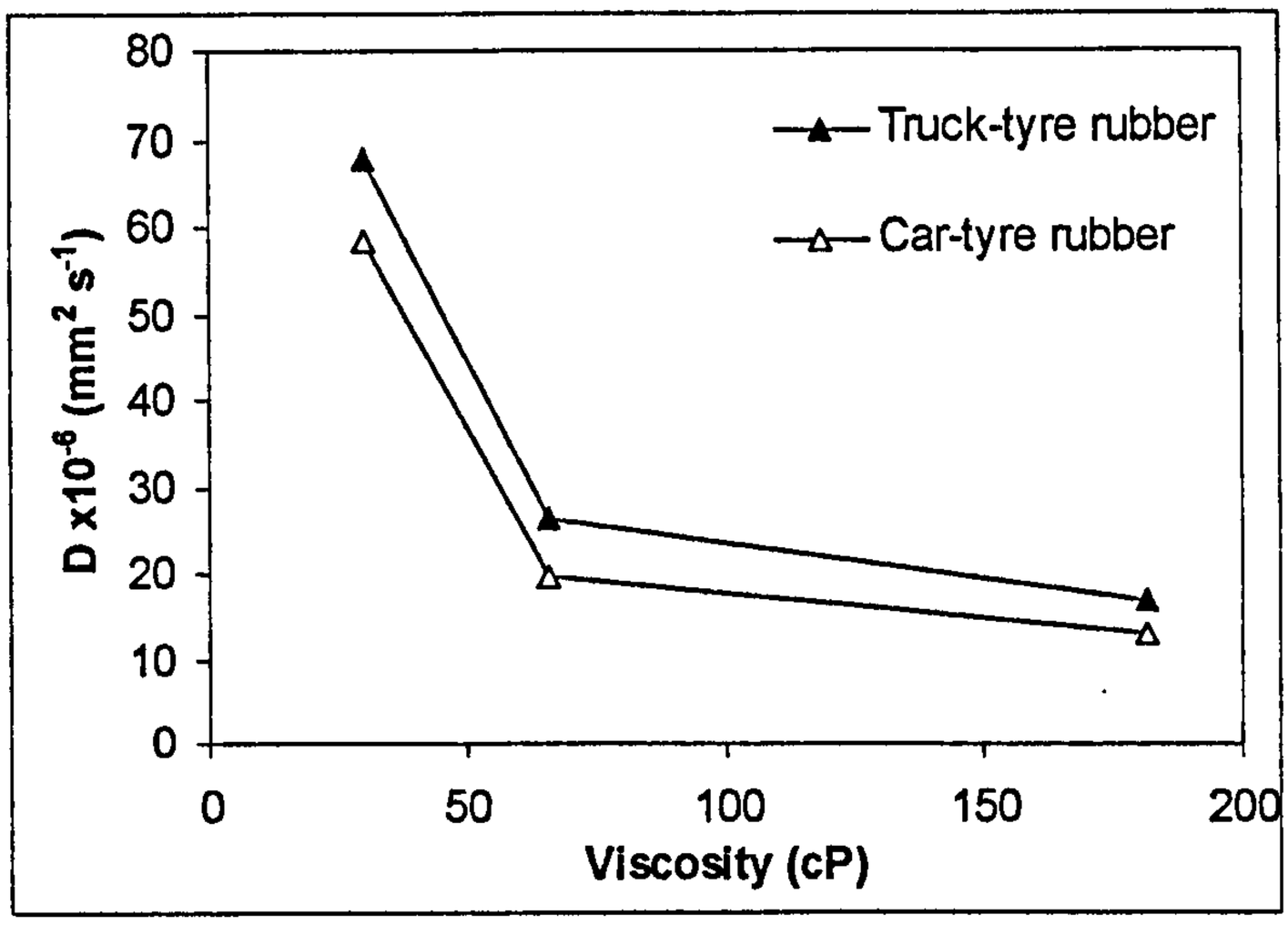

Figure 3.13 Relationship between bitumen viscosity and diffusion coefficient

3.5.7.3 Activation energy

The temperature dependence of the diffusion coefficient has been observed to follow an Arrhenius relationship, characteristic of an activated process (Crank and Park, 1968). Thus,

$$D = D_0 \exp(-E_D / RT) \tag{3.28}$$

where D_0 is a constant, E_D represents the activation energy, R the universal gas constant (R=8.31 JK^{-1} mol^{-1}) and T temperature in absolute scale (K). Typical Arrhenius plots of ln D against $1/T$ in linear scale, where T was the temperature in degrees Kelvin, are given in **Figure 3.14**.

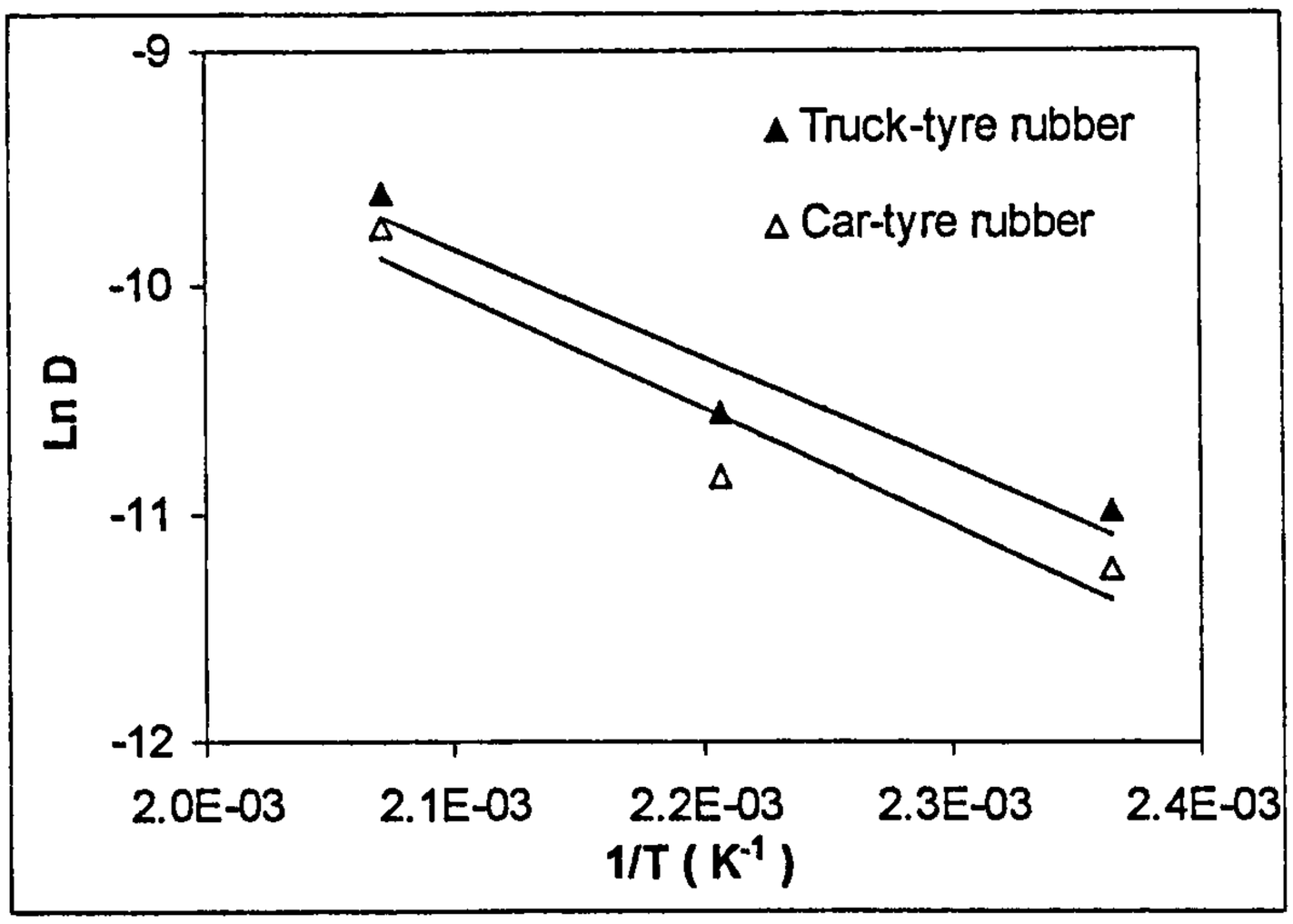

Figure 3.14 Arrhenius plots of ln *D* against 1/*T* for car and truck-tyre rubber in bitumen (100 Pen KSR)

From Equation 3.27, the slope of the lines in **Figure 3.14** may be given by $(-E_D / R)$ and hence, values of the activation energies, E_D, for the two rubbers under investigation were calculated. The slopes were estimated by fitting a straight line of the form $y = mx + n$ through the experimental data. Experimental constants, m and n, and regression coefficients, R^2, were found to be –5037.9 and –4672.2 K, 0.544 and –0.0357, and 0.92 and 0.94, for car and truck-tyre rubber respectively.

The activation energies were found to be 41.8 and 38.8 kJ/mol for car and truck-tyre rubber respectively. It can be seen that the activation energy for car-tyre rubber was greater than that of truck-tyre rubber, which indicates the higher temperature sensitivity of the car-tyre rubber.

For one component diffusion, E_D might be seen as the activation energy required to create an opening between polymer chains large enough to allow the penetrant molecule to pass. Thus, E_D is a function of the inter- and intrachain forces that must be overcome in order to create the space for a unit diffusional jump of the

penetrant. The activation energy value will be greater the larger the penetrant molecule, the stronger the polymer cohesive energy, and the more rigid the chains (Harogoppad and Aminabhavi, 1991).

3.5.8 Diffusion of bitumen into CRM

The preceding swelling and diffusion data were obtained on rubber monoliths, and absorption data were analysed based on the diffusion theory assuming plane-sheet geometry. However, CRM particles approximate more closely to spheres. It is therefore necessary to know the state of the rubber particles and estimate the kinetics of diffusion into those particles when bitumen and CRM are blended under production conditions.

3.5.8.1 Production of crumb rubber modified binders

Crumb rubber modified binders have been produced using a high-shear Silverson mixing machine (see **Figure 3.15**) under controlled conditions of temperature, time, and shear rate.

Approximate amounts of 600 g of bitumen contained in 1-litre flasks were preheated in an oven to the selected mixing temperature for about two hours. The flasks then were placed on an iso-mantle heater and covered with an insulation mantle also preheated to the required temperature. The hot bitumen was then stirred in the mixer for about 10 minutes at 1000 rpm after which the temperature of the bitumen remained constant as measured by a thermometer.

Specific quantities of CRM were weighed and added continuously to the hot bitumen, this process lasted about 5 minutes. Once all the CRM was added to the bitumen, which corresponded to the zero time, the shear rate was increased up to 2000 rpm and mixing was continued for various times, during which the temperature of the bitumen was monitored.

Mixing temperatures selected were 150, 180 and 210 ^{0}C, mixing time varied from 1 up to 24 hours, and the shear rate applied during mixing process was 2000 rpm.

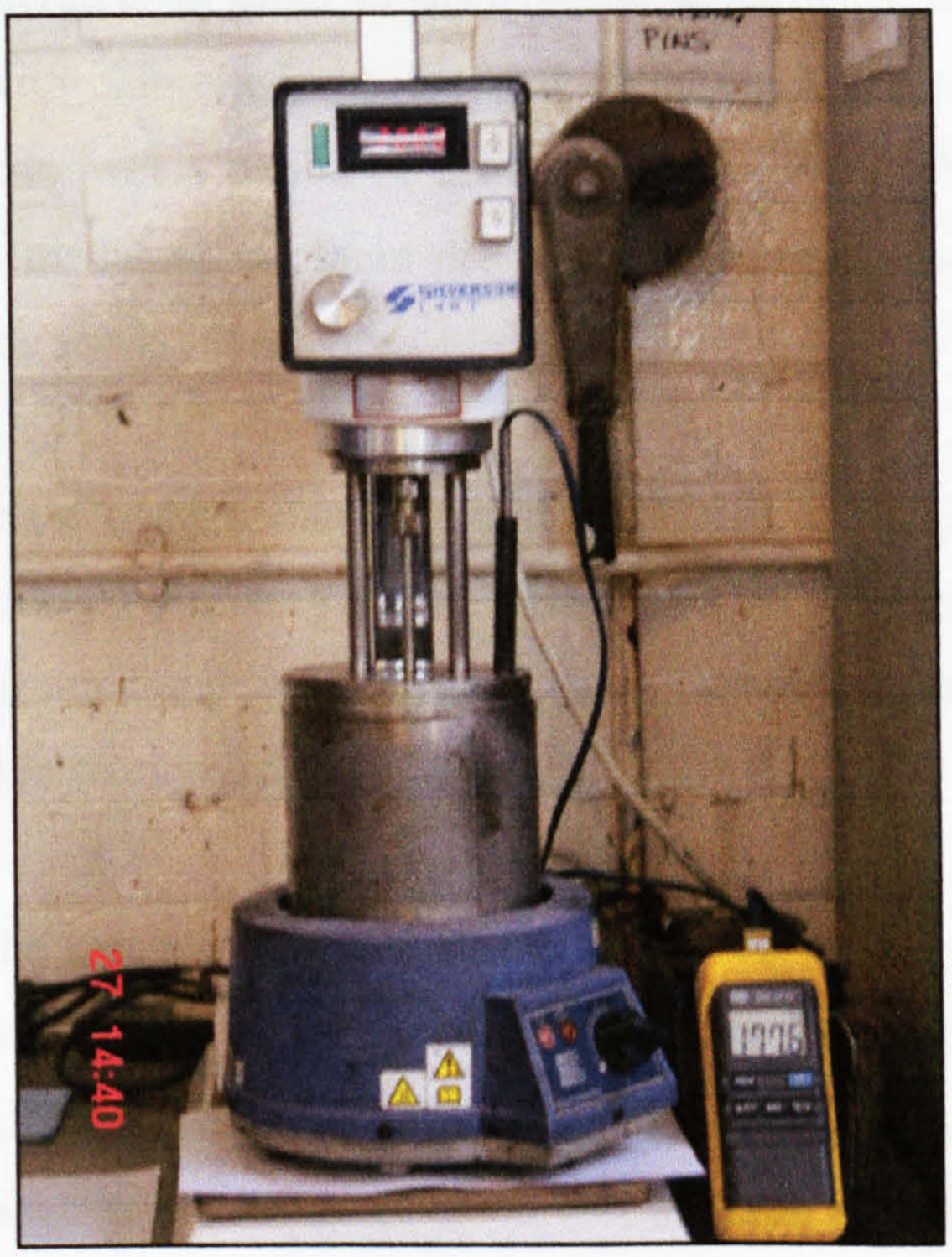

Figure 3.15 Silverson mixer arrangement

3.5.8.2 Isolation of components from rubber-bitumen blends

A procedure was developed to separate the bitumen and the rubber particles from rubber-bitumen blends produced as before. The procedure consisted of filtering 50 ml of rubber-modified bitumen through a polyester cloth filter of 50 μm sieve size while hot (180 ^{0}C). Following this method, it was possible to obtain samples of bitumen, after interaction with the rubber crumb, from the rubber-bitumen blends. However, it was not possible to remove all the bitumen from the crumb rubber.

Chlorobenzene was used to remove the excess bitumen from the surface of the crumb rubber. In attempts to minimise solvent effect, various procedures were tested. A convenient procedure was to filter off a sample of 50 ml of rubber-modified bitumen and then to add to the rubber particles and bitumen blend (100 ml) and equal volume of chlorobenzene. The resulting mixture was stirred for 10

minutes after which the sample was filtered again. The resulting particles were tacky and agglomerated. In order to disperse these particles, the samples were further washed with chlorobenzene. Several filtrations were carried out using fresh chlorobenzene over a period of about 2 hours. Finally, the crumb rubber was washed with methanol to obtain dry samples; contact time with methanol before filtering was about 30 minutes.

In order to isolate the components from crumb rubber-bitumen blends, modified binders were produced by mixing 100 Pen KSR and VEN binders with 10 % by weight CRM from truck and from car tyres from 1 up to 24 hours following the method explained in section 3.5.8.1.

Examination of the resulting isolated crumb rubber after various mixing times showed that, in comparison with original crumb, there had been a small change in particle size. Although particle size distribution of the isolated CRM particles could not be obtained due to the small amount of material recovered, the samples showed similar combination of large and small particles as seen in **Figure 3.16.** This was for CRM particles of 300 μm maximum size before and after interaction with bitumen for 6 hours at 180 ^{0}C. This suggested that, to a first approximation, there was insufficient chemical or physical degradation to cause major disintegration and dissolution of the crumb rubber particles.

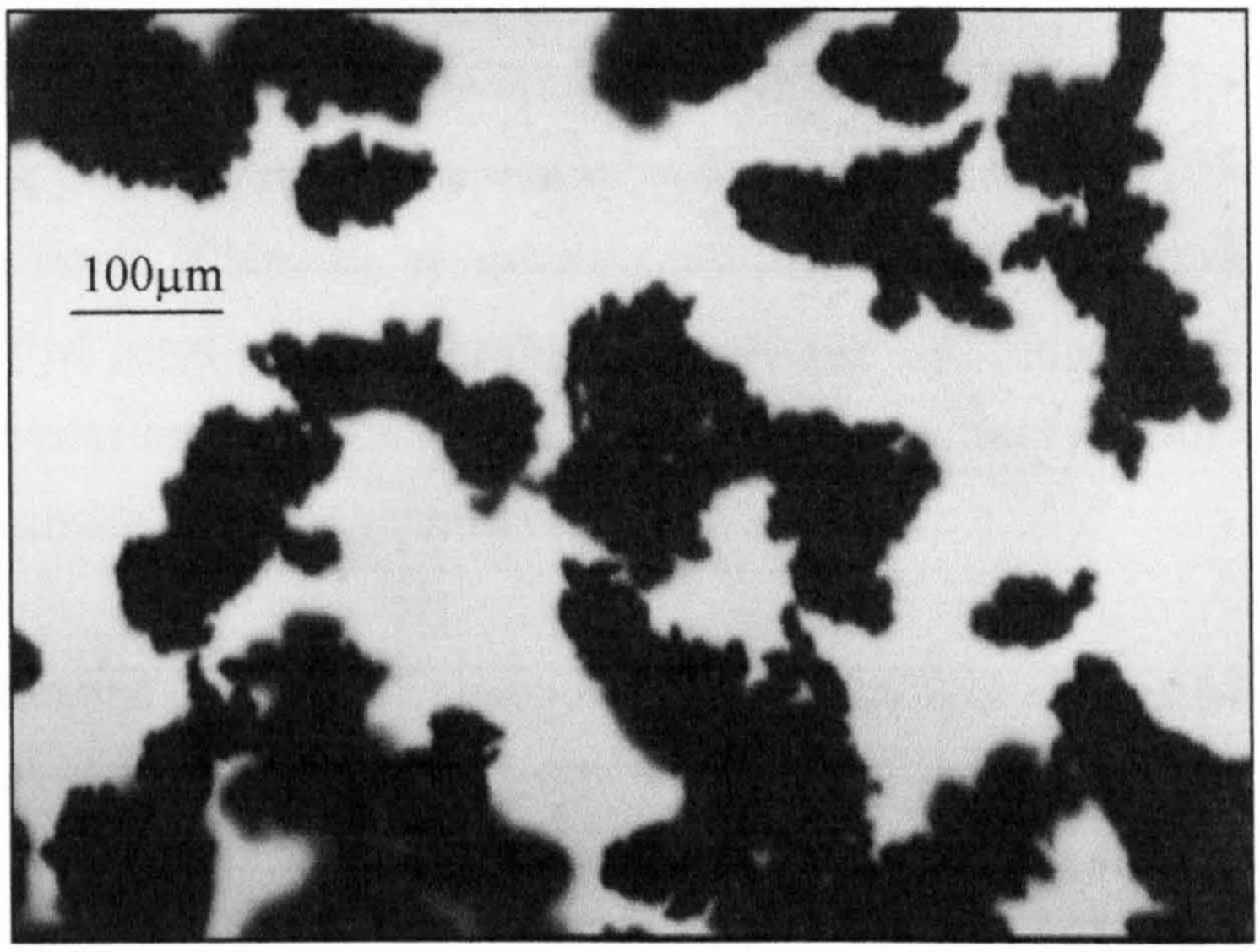

a) Before interaction with bitumen

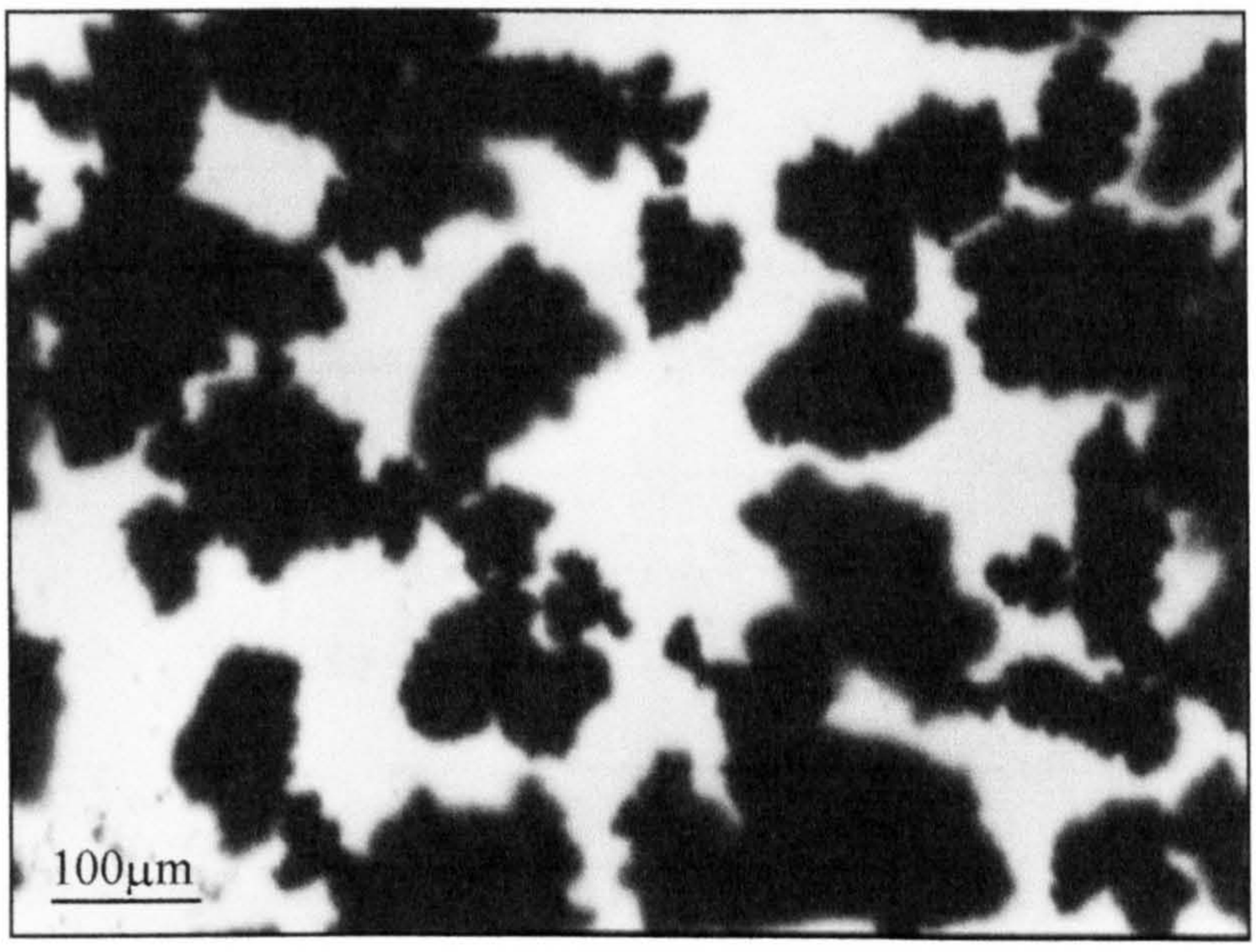

b) After interaction with bitumen for 6 hours at 180 ^{0}C

Figure 3.16 CRM 300 μm maximum size before and after interaction with bitumen for 6 hours at 180 ^{0}C

3.5.8.3 Diffusion in a sphere

As discussed previously, it was established that after digestion of CRM in bitumen the CRM particles remained intact though some swelling occurred as a result of diffusion of bitumen components, primarily aromatics, from the bitumen into the CRM particles. To estimate the kinetics of diffusion into those CRM particles, whose might be approximated to spheres, the theory of diffusion was applied assuming spherical geometry.

The fundamental differential equation when the diffusion is radial and the diffusion coefficient is constant is given by:

$$\frac{\partial u}{\partial t} = D\frac{\partial^2 u}{\partial r^2} \tag{3.29}$$

where: $u = Cr$, C is the concentration of diffusing substance, and r is the radial coordinate.

For a sphere of radius a, with no initial concentration of diffusing substance, and with a uniform concentration C_0 at the surface, the solution to Equation 3.29 (Crank, 1956) is expressed as:

$$\frac{C}{C_0} = 1 + \frac{2a}{\pi r}\sum_{n=1}^{\infty}\frac{(-1)^n}{n}\sin\frac{n\pi r}{a}\exp\left\{\frac{-Dn^2\pi^2 t}{a^2}\right\} \tag{3.30}$$

The total amount of diffusing substance entering or living the sphere is given by:

$$\frac{M_t}{M_\infty} = 1 - \frac{6}{\pi^2}\sum_{n=1}^{\infty}\frac{1}{n^2}\exp\left\{\frac{-Dn^2\pi^2 t}{a^2}\right\} \tag{3.31}$$

For long times Equation 3.31 simplifies to,

$$\frac{M_t}{M_\infty} = 1 - \frac{6}{\pi^2}\exp\left\{-D\frac{\pi^2 t}{a^2}\right\} \tag{3.32}$$

3.5.8.4 Equilibrium swelling

Assuming that crumb rubber is a homogeneous isotropic material, thus, the diffusion coefficient is the same in any direction, the diffusion coefficient values calculated for plane sheet geometry (one-dimensional diffusion) can be introduced in the equations for the diffusion in a sphere.

Equation 3.32 has been used to estimate equilibrium swelling times for such spherical particles. Crumb rubber maximum sizes used in this study were 300 (50 mesh) and 600 μm (30 mesh), considered as a spheres, the approximate radius are 150 and 300 μm. Equilibrium swelling times were approximated by the values at 99.99% equilibrium swelling (M_t/M_∞=0.9999).

Table 3.8 shows the estimated equilibrium swelling times for 100 Pen KSR bitumen into car and truck-tyre rubber particles (spheres) of different sizes and at different temperatures. It can be seen that equilibrium swelling times decreased as the temperature increased. Furthermore, swelling times for truck–tyre rubber were shorter than for car-tyre rubber. Also, the smallest particles reached equilibrium after a shorter period of time in comparison with the largest particles. The shortest swelling time, 4.9 minutes, corresponded to truck-tyre rubber particle of 300 μm at a temperature of 210 ^{0}C; and the longest one, 101 minutes, corresponded to car-tyre rubber particle of 600 μm at a temperature of 150 ^{0}C.

Moreover, crumb rubber particles are not true spheres but have larger surface areas as a result of protrusions on the surfaces of the rough abraded particles as seen in **Figure 3.16**. As a result, diffusion will be probably faster than the predicted for spheres and consequently swelling times will be shorter.

Based on the diffusion studies, it can be concluded that rubbers with a high proportion of NR, such as truck-tyre rubber, will swell more and at faster rate than those with a low proportion of NR, such as car-tyre rubber. Furthermore, high penetration grade bitumens with a relatively low asphaltene content will also be more prone to interact and swell the rubber particles.

Temperature (^{0}C)	Rubber Type	Diffusion coefficient x10^{-6} ($mm^2 s^{-1}$)	Rubber size (diameter) (μm)	Equillibrium swelling time (min)
150	Car	13.1	300	25.3
			600	101.0
	Truck	16.9	300	19.5
			600	78.2
180	Car	19.6	300	16.9
			600	67.7
	Truck	26.1	300	12.7
			600	50.7
210	Car	58.6	300	5.7
			600	22.6
	Truck	67.7	300	4.9
			600	19.6

Table 3.8 Diffusion coefficients and equilibrium swelling times for rubber spherical particles

It should be noted that conclusions made here concerning interaction feasibility between bitumens from different crude oil and rubber from different origins are based solely on obtained results. Different materials, not used in this work, may interact differently and, thus, may produce findings that are independent of the ones arrived at herein.

Chapter 4

RHEOLOGY

Chapter 4

RHEOLOGY

This chapter presents the results of an investigation into the effects of CRM on the rheological properties of bituminous binders. Crumb-rubber modified binders were characterised in terms of their viscosities at high temperatures and their dynamic viscoelastic properties over a wide range of service temperatures. Furthermore, the effects of material variables and production conditions of temperature and time were also investigated.

4.1 INTRODUCTION

Rheology is the study of materials flow and deformation characteristics and is used to describe the mechanical properties of bituminous binders. Thus rheology, considers the flow properties of bitumen, which include their dynamic viscoelastic properties as well as their flow and creep properties.

Bituminous binders are considered as viscoelastic materials and their mechanical behaviour is dependent on both temperature and duration of loading. At high temperatures and long loading times their stiffness is low and they behave as viscous liquids. At low temperatures and short loading times their stiffness is high and they behave as elastic solids. At intermediate temperatures and loading times bitumens exhibit both elastic and viscous behaviour, and the term "viscoelastic " is used.

During mixing and compaction of bituminous mixtures, bitumen properties can be considered in terms of viscosity. During mixing, the bitumen must be able to coat the dried aggregate in a relatively short period of time (typically 30 to 90 seconds), which determines the lowest mixing temperature. At the other end, very high mixing temperatures are not recommended, as the bitumen will oxidise. Bituminous mixtures must also be sufficiently workable to enable satisfactory compaction. If the viscosity is high the material will be probably too

stiff to allow any further compaction. If, however, the viscosity is too low the material will probably too mobile to compact.

During service conditions bitumens behave visco-elastically and their properties are dependent on both loading time and temperature. The critical conditions for the performance of bituminous mixtures are generally associated with high service temperatures (permanent deformation), and low service temperatures (fatigue and low temperature cracking).

4.2 VISCOSITY

4.2.1 Newtonian and non-Newtonian fluids

Viscosity is a measure of the internal friction of a fluid. The application of a force to a liquid is relieved by the flow of molecules past one another into new positions in the system. A liquid, forced to flow in this way by a shearing force σ, experiences a viscous resistance expressed by,

$$\eta = \frac{\sigma}{\dot{\gamma}} \tag{4.1}$$

where $\dot{\gamma}$ is the shear rate and η is the viscosity of the liquid.

A liquid is said to exhibit Newtonian flow if η is independent of $\dot{\gamma}$ but materials which show deviations from this flow pattern, with either decreasing or increasing $\sigma/\dot{\gamma}$ ratios, are termed non-Newtonian. The viscosity of such fluids will, therefore, change as the shear rate is varied.

There are several types of non-Newtonian flow behaviour, characterized by the way a fluid's viscosity changes in response to variations in shear rate (see **Figure 4.1**). The most common types of non-Newtonian flow behaviour include, 'shear-thinning', 'shear-thickening' and 'plastic flow'. Shear-thinning occurs when the fluid's viscosity decreases with increasing shear rate, shear-thickening is characterised by an increase in viscosity with increasing shear rate, and for

plastic flow a certain amount of force, called yield value, must be applied to the fluid before any flow is induced.

Some fluids also display a change in viscosity with time under conditions of constant shear rate, as illustrated in **Figure 4.1**. A thixotropic fluid undergoes a decrease in viscosity with time, while it is subjected to constant shearing. On the other hand, for a rheopectic fluid the viscosity increase with time as it is sheared at constant rate. Both thixotropy and rheopexy may occur in combination with any of the previously discussed flow behaviours, or only at certain shear rates.

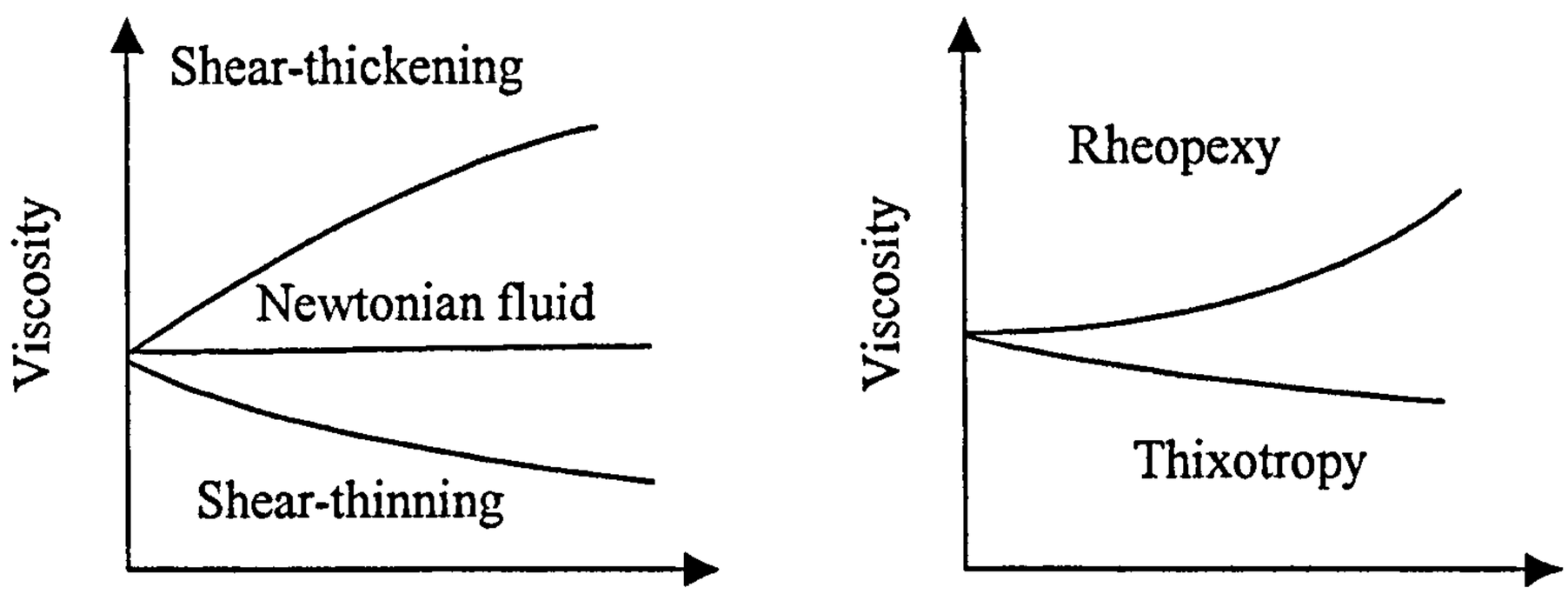

Figure 4.1 Newtonian and non-Newtonian fluids

4.2.2 Brookfield viscometer

The Brookfield Viscometer (Model LVDV-I+) has been used to measured binder viscosity at high temperatures associated with application conditions of mixing, laying and compaction. The Brookfield Viscometer is illustrated in **Figure 4.2**.

The principle of operation of the viscometer is to drive a spindle, which is immersed in the test fluid, through a calibrated spring. The viscous drag of the fluid against the spindle is measured by the spring deflection. Spring deflection is measured with a rotary transducer. The shear rate in a given measurement is determined by the rotational speed of the spindle, its shape and size, the size and shape of the container the spindle is rotating in, and the distance between the container wall and the spindle surface.

Figure 4.2 The Brookfield Viscometer

The following equations, included in the Brookfield Viscometer manual, are used to determine the viscosity of the fluid considering coaxial-cylinder geometry,

$$\dot{\gamma} = \frac{2R_c^{\,2}\omega}{R_c^{\,2} - R_b^{\,2}} \tag{4.2}$$

$$\sigma = \frac{M}{2\pi R_b^{\,2} L} \tag{4.3}$$

where,

ω = angular velocity of spindle

R_c = radius of container

R_b = radius of spindle

L = length of spindle

M = torque input

The viscosity, η, is then obtained using Equation 4.1.

For viscosity measurements of small samples at high temperature, the viscometer includes the Thermosel System, which consists of a special coaxial-cylinder and sample chamber, an electric heater apparatus and a digital temperature controller. The temperature controller covers the temperature range 15 – 300 ^{0}C with a resolution of 0.1 ^{0}C and a reading accuracy of ± 1.0 ^{0}C up to 150 ^{0}C and ± 2.0 ^{0}C from 150 up to 300 ^{0}C.

Viscosity measurements were carried out with a spindle (SC-31) of 11.76 mm diameter and 25.15 mm side length in a sample chamber (SC-13R) of 19.05 mm diameter, which allows viscosity measurements between 30 and 100,000 cP. For this spindle/chamber geometry the recommended sample size is 10 ml. Speeds used varied from 2.5 up to 100 rpm depending on the base binder, CRM content and temperature.

4.2.3 Viscosity measurements

4.2.3.1 Procedure

Viscosities of unmodified and crumb-rubber modified binders were obtained using the Brookfield rotational viscometer, measured at temperatures between 110 and 170 ^{0}C. Shear rates varied from 2.5 to 100 rpm depending on temperature and CRM content.

Crumb rubber binders were produced following the procedure explained in Chapter 3, section 3.5.8.1. Two 100 Penetration Grade binders from two origins, Venezuela (VEN) and the Middle East (KSR) were modified by adding various percentages of CRM by weight of binder from two different sources, truck and car tyres. CRM maximum nominal sizes used were 600 (30 mesh) and 300 μm (50 mesh) referred to as coarse and fine CRM respectively. For all the modified binders, CRM and bitumen were mixed at 180 ^{0}C for 1 hour under high shear (2000 rpm).

The procedure followed for viscosity measurements can be summarised as follows. Approximately, 12 g of binder was collected from a 1-litre flask heated at a temperature of 120 ^{0}C, and placed on release paper. Once cold, the binder

(semi-solid) was introduced in the viscometer sample container and heated to the first test temperature. When the temperature of the binder was stabilised, the spindle, heated to the same temperature, was lowered into the fluid and the first reading was taken after 15 minutes. Thereafter, viscosity readings were taken 15 minutes after the temperature of the binder reached each selected temperature. In order to obtain accurate viscosity readings (torque range between 10 – 100 %) the shear rate had to be increased, by increasing the angular velocity of spindle (ω), when the temperature was raised for all the binders investigated.

4.2.3.2 Results and discussions

Figures 4.3 – 5 show the Brookfield viscosities of the unmodified and crumb-rubber modified binders investigated. The initial aim was to achieve a basic understanding of the net effect that the quantity of CRM has on the binder with regard to mixing and construction conditions. It is widely accepted that mixing and compaction viscosities should lay around 0.2 Pa.s (200 cP) for mixing and between 2 to 20 Pa.s for compaction (Whiteoak, 1990).

Figures 4.3 – 5 show that increasing the percentage of CRM increases the viscosity of the binders. Furthermore, mixing viscosities are achieved at temperatures around 145 ^{0}C for the unmodified binders. For the CRM binders this viscosity was achieved at temperatures of about 160, 180 and in excess of 190 ^{0}C when the neat binders were modified with 5, 10 and 15 % CRM respectively. Thus, at CRM contents greater than 10 %, mixing temperatures in excess of 180 ^{0}C would be required to achieve a suitable binder viscosity for mixing with aggregates. However, in routine paving operations such conditions are not practicable, so it is recommended to limit the CRM content to no more than 10 % by weight of binder.

The SHRP binder specification (Anderson and Kennedy, 1993), developed primarily for neat (unmodified) binders, allows for binders with a maximum viscosity of 3 Pa.s (3000 cP) at 135 ^{0}C, at a recommended rate of 20 rpm. All the binders investigated, except the ones modified with 15 % CRM by weight of binder, complied with this specification.

CRM binder viscosity is also affected by factors such us the origin of the binder, and the size and source of CRM. **Figure 4.3** shows the effect of the origin of the base binder on viscosity after modification with CRM. It can be seen that CRM binders produced with KSR bitumen had higher viscosities than the ones produced with the VEN bitumen. These differences can be attributed to differences in the chemical composition of the two binders, which affect the interaction between bitumen and CRM particles and, consequently, their resulting viscosities.

The effect of CRM size on binder viscosity is presented in **Figure 4.4**. It can be seen that the binders modified with fine CRM had higher viscosities that the ones modified with coarse CRM, at the same CRM content by weight of binder. Enlarging the surface area of the CRM particles by reducing their size increases the interaction between CRM and bitumen, increasing the viscosities of the binders. This effect was more pronounced at higher CRM concentrations. However, the effects of CRM concentration appeared to be more important than the size of CRM. Similar findings have been reported by others (Billiter et al., 1997a, Liang and Lee, 1996 and Kim et al., 2001).

CRM binders' viscosity is also dependent on CRM source, truck tyres or car tyres. Data presented in **Figure 4.5** shows that bitumen modified with CRM from truck tyres developed higher viscosities than those modified with CRM from car tyres. As seen in Chapter 3, truck-tyre rubber, with its higher percentage of natural rubber, is more compatible with bitumen and has a greater tendency to swell. This higher tendency to swell may be represented by increased viscosities (Stroup-Gardiner et al., 1993).

4.2.3.3 Non-Newtonian behaviour

Most bituminous binders show Newtonian behaviour at high temperatures, thus, viscosity is independent of shear rate. However, the behaviour of some polymer-modified binders is shear dependent, hence, non-Newtonian (Bahia et al., 1997).

Stroup-Gardiner et al. (1993) and Kim et al. (2001) found that crumb-rubber modified binders showed non-Newtonian behaviour as seen by the decrease in viscosity with increasing shear rate (shear-thinning). They also found that non-Newtonian behaviour increased with increasing CRM concentration.

Crumb-rubber modified binders have been reported to develop a slight tendency towards thixotropy at high CRM concentrations, hence, change in viscosity with time under constant shear rate conditions (Stroup-Gardiner et al., 1993). In the present study, thixotropy was observed during viscosity measurements, however, for comparison purposes, thixotropic effects were limited by taking viscosity measurements after a fixed period of time (15 minutes).

Non-Newtonian behaviour was not investigated in the current study as the shear rate had to be increased with increasing temperature and CRM content to obtain accurate viscosity measurements (torque range between 10 – 100 %).

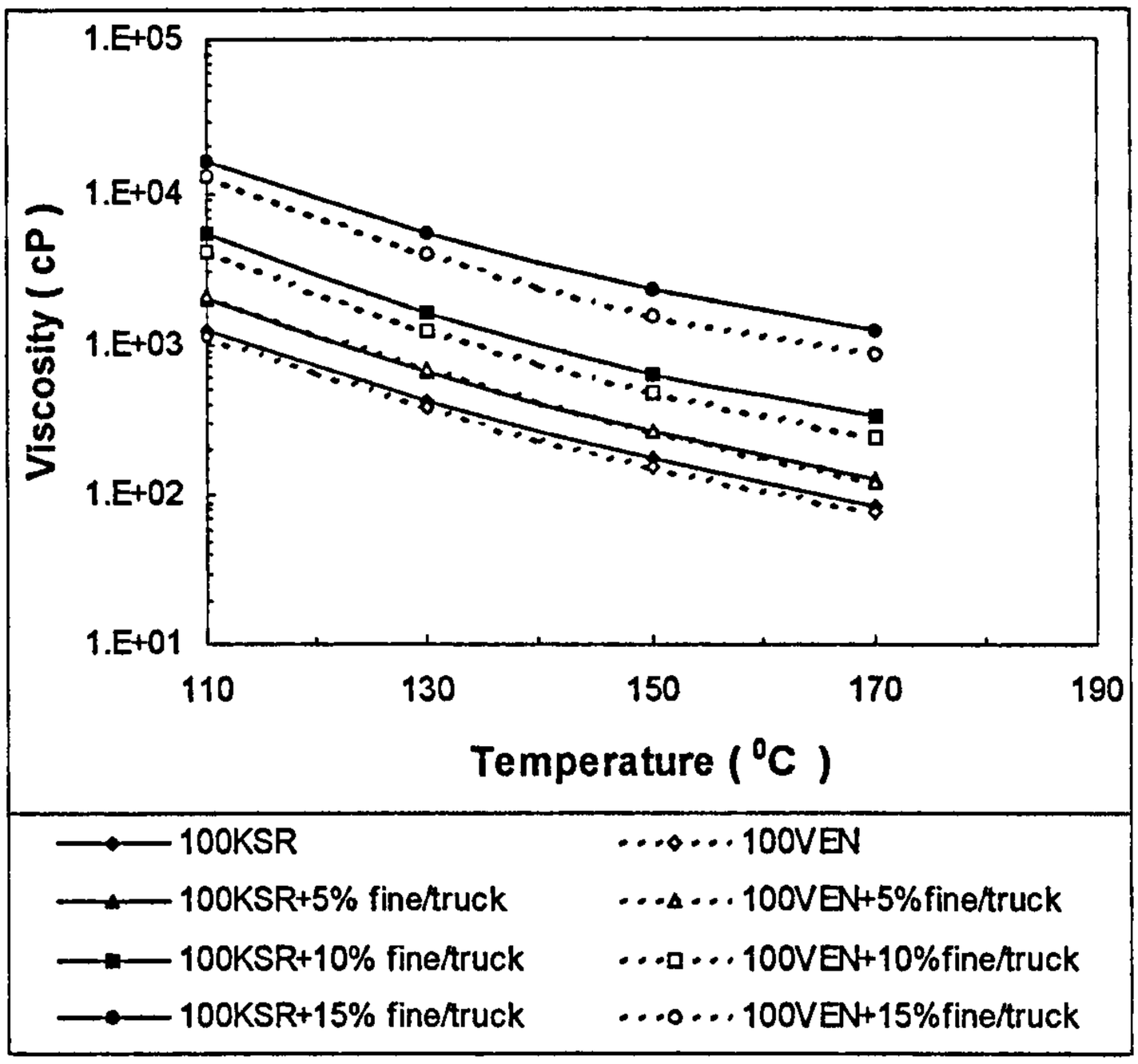

Figure 4.3 Effect of bitumen origin on CRM binder viscosity

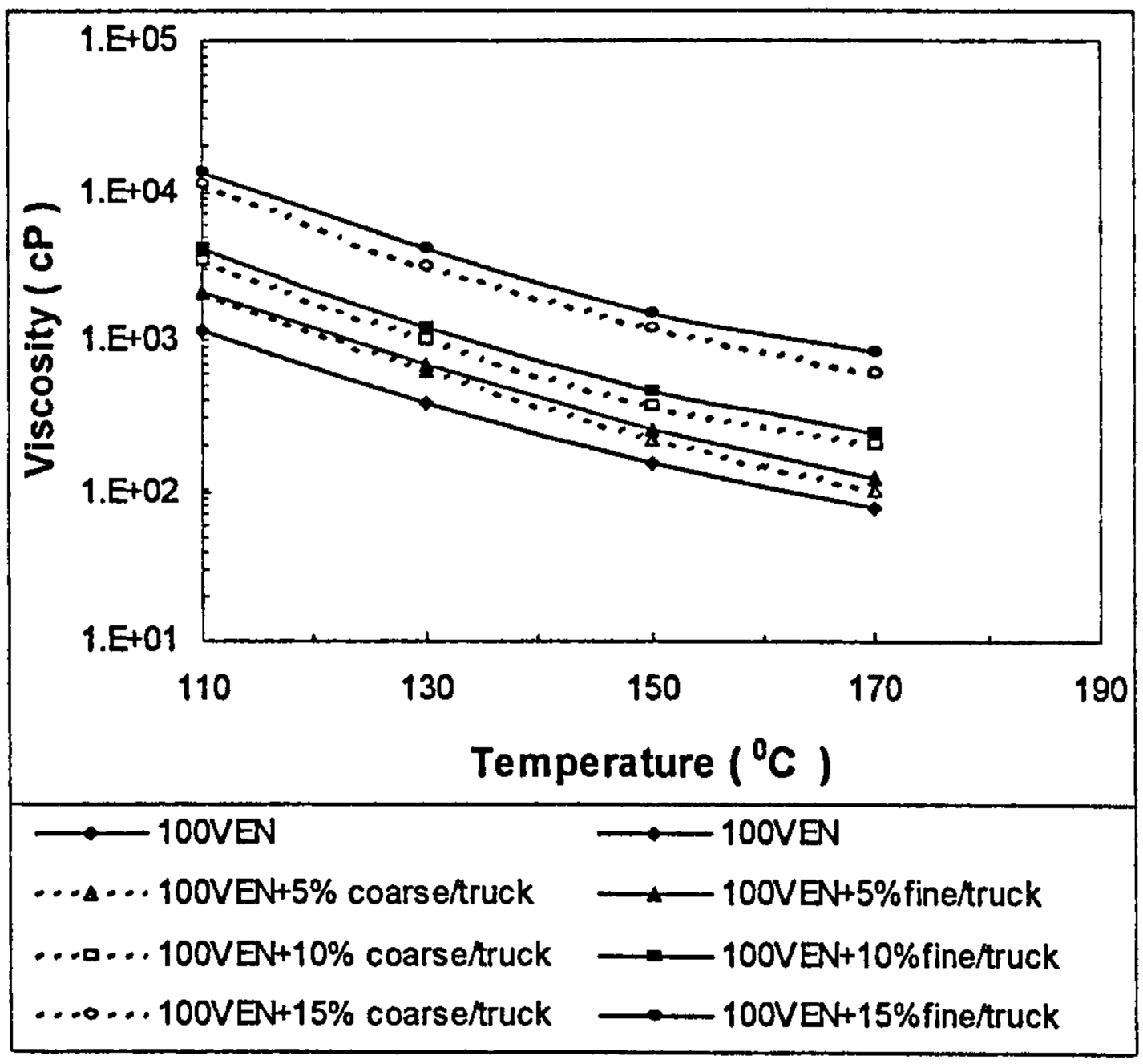

Figure 4.4 Effect of CRM size on CRM binder viscosity

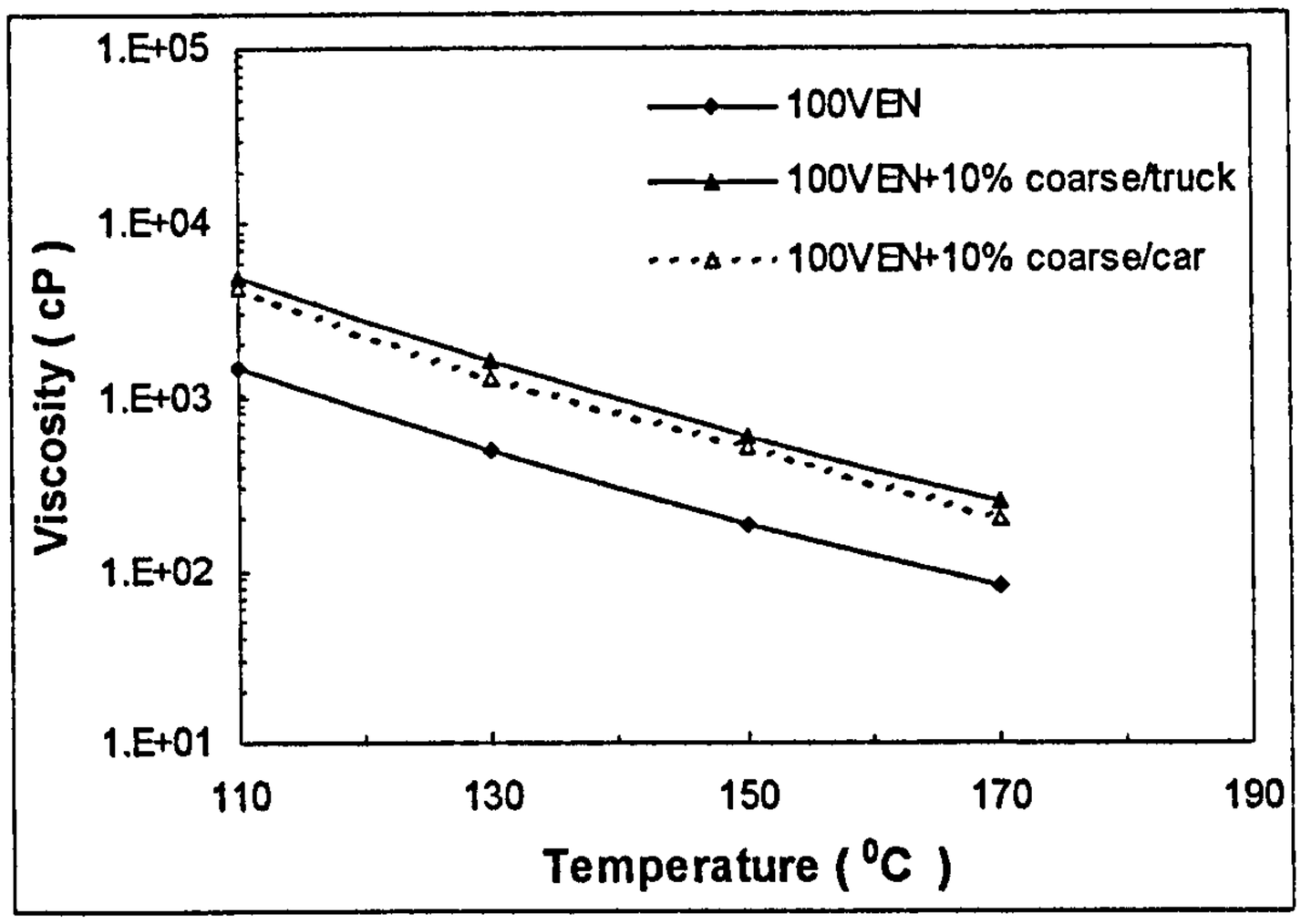

Figure 4.5 Effect of CRM source on CRM binder viscosity

4.3 DYNAMIC MECHANICAL ANALYSIS

4.3.1 Dynamic viscoelastic functions

Dynamic mechanical tests involve the application of a periodically varying strain or stress to a material sample. In dynamic tests, a shear stress is usually applied as a sinusoidal varying stress of constant amplitude and fixed frequency. The deformation, given by the shear strain, also varies sinusoidally with the same frequency as the applied shear stress, but the shear strain response lags behind the applied stress as illustrated in **Figure 4.6**. This lag is termed the 'phase angle (δ)'.

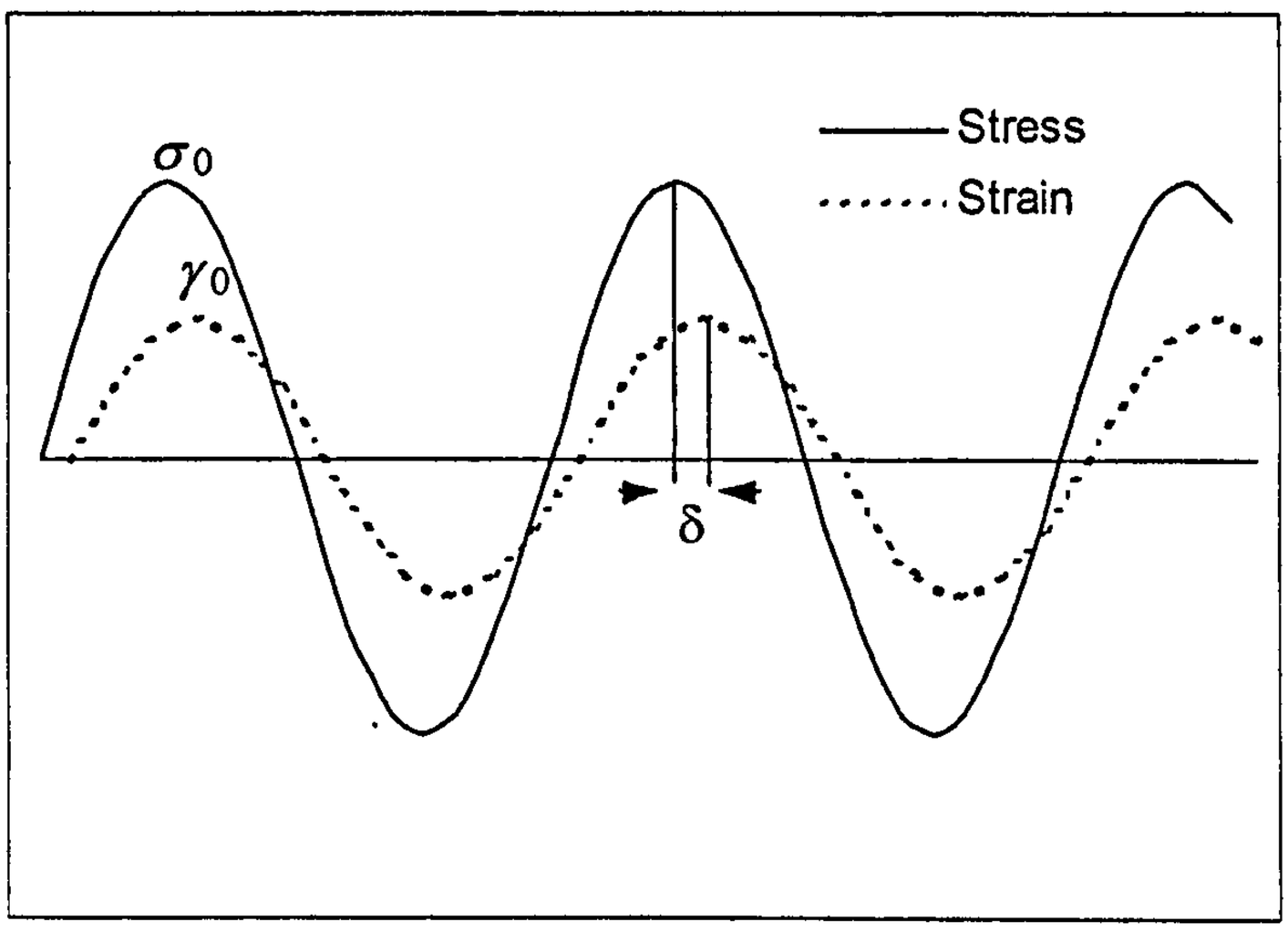

Figure 4.6 Shear stress and strain waveforms in a dynamic oscillatory test

The phase angle is a measure of the viscoelastic character of a material. A perfectly elastic material would exhibit a phase angle equal to zero, whereas a viscous material would exhibit and angle of 90^0. For a visco-elastic material the phase angle varies between 0^0 and 90^0, depending on the test conditions of temperature and loading time or frequency.

A sinusoidal varying shear strain, as shown in **Figure 4.6**, may be expressed as

$$\gamma = \gamma_0 \sin \omega t \tag{4.4}$$

and the resulting shear stress

$$\sigma = \sigma_0 \sin(\omega t + \delta) \tag{4.5}$$

where σ_0 and γ_0 are the stress and strain amplitudes respectively, ω is the angular frequency (rad/sec) of the oscillation, and t is the time (sec).

It is convenient to express the sinusoidal varying stress and strain as complex quantities, thus,

$$\gamma^* = \gamma_0 e^{i(\omega t)} \tag{4.6}$$

$$\sigma^* = \sigma_0 e^{i(\omega t + \delta)} \tag{4.7}$$

where σ^* and γ^* are the complex stress and strain respectively, and $i = \sqrt{-1}$.

The complex shear modulus is then given by (Ferry, 1970):

$$G^* = \frac{\sigma^*}{\gamma^*} \tag{4.8}$$

Substituting Equations 4.6 and 4.7 in 4.8

$$G^* = \frac{\sigma_0 e^{i(\omega t + \delta)}}{\gamma_0 e^{i(\omega t)}} = \frac{\sigma_0}{\gamma_0} e^{i\delta} \tag{4.9}$$

Making use of the following relationship:

$$e^{i\delta} = \cos\delta + i\sin\delta$$

Equation 4.9 can be written as:

$$G^* = \frac{\sigma_0}{\gamma_0}(\cos\delta + i\sin\delta) \tag{4.10}$$

The norm of the complex modulus, or simply complex modulus, is given by:

$$\left|G^*\right| = \frac{\sigma_0}{\gamma_0} \tag{4.11}$$

and is defined as the ratio of the stress amplitude to strain amplitude.

Equation 4.10 can now be written as:

$$G^* = \left|G^*\right|\cos\delta + i\left|G^*\right|\sin\delta \tag{4.12}$$

The in-phase component of G^* is referred to as the storage modulus, G', and the out-of-phase component as the loss modulus, G'', thus,

$$G' = \left|G^*\right|\cos\delta = \frac{\sigma_0\cos\delta}{\gamma_0}$$

$$G'' = \left|G^*\right|\sin\delta = \frac{\sigma_0\sin\delta}{\gamma_0}$$

The storage modulus, G', is defined as the ratio of the amplitude of the in-phase component of stress to the strain amplitude, and describes the amount of energy stored and released elastically in each oscillation, thus it is also called the elastic modulus. The loss modulus, G'', is defined as the ratio of the amplitude of the out-of-phase stress component to the strain amplitude, and describes the average

energy-dissipation rate associated with viscous effects, thus, is sometimes called viscous modulus (Lu and Isacsson, 1997).

Hence Equation 4.12 can now be expressed as:

$$G^* = G' + iG'' \tag{4.13}$$

4.3.2 Dynamic Shear Rheometer

Dynamic mechanical analysis (DMA) was performed using a Bohlin Dynamic Shear Rheometer (DSR-II). The DSR was used to measure the dynamic properties of conventional and crumb rubber modified binders. The device is capable of measuring these properties under a wide variety of temperatures and loading frequencies. A computer, via an interface box, governs the execution and control of the test. Compressed air is required to facilitate frictionless movement of the working parts whilst a Temperature Control Unit (TCU) regulates the thermal conditions during testing.

Controlled-strain mode of testing was performed in the DSR by applying a sinusoidal varying strain to the test specimen and measuring the magnitude and phase of the resulting stress.

The principle of oscillatory testing in the DSR is illustrated in **Figure 4.7**. A sample of bitumen is placed between two parallel circular plates. The bottom plate is fixed and the top plate is oscillating by a computer-controlled electronic motor. The angular rotation (θ) and applied torque (M) are measured and the shear strain (γ_0) and stress (σ_0) are calculated using the following equations (Kennedy et al., 1994):

$$\gamma_0 = \frac{\theta r}{h} \tag{4.14}$$

and,

$$\sigma_0 = \frac{2M}{\pi r^3} \tag{4.15}$$

where r and h are the radius of the plate and the gap between plates respectively. The complex modulus, G^*, is then calculated using Equation 4.11.

The phase angle, δ (radians), is determined from the time lag between the induced shear strain (angular rotation) and the required shear stress (torque) using the following equation:

$$\delta = 2\pi \frac{\Delta t}{t} \tag{4.16}$$

where Δt and t are the time shift and the cycle time respectively.

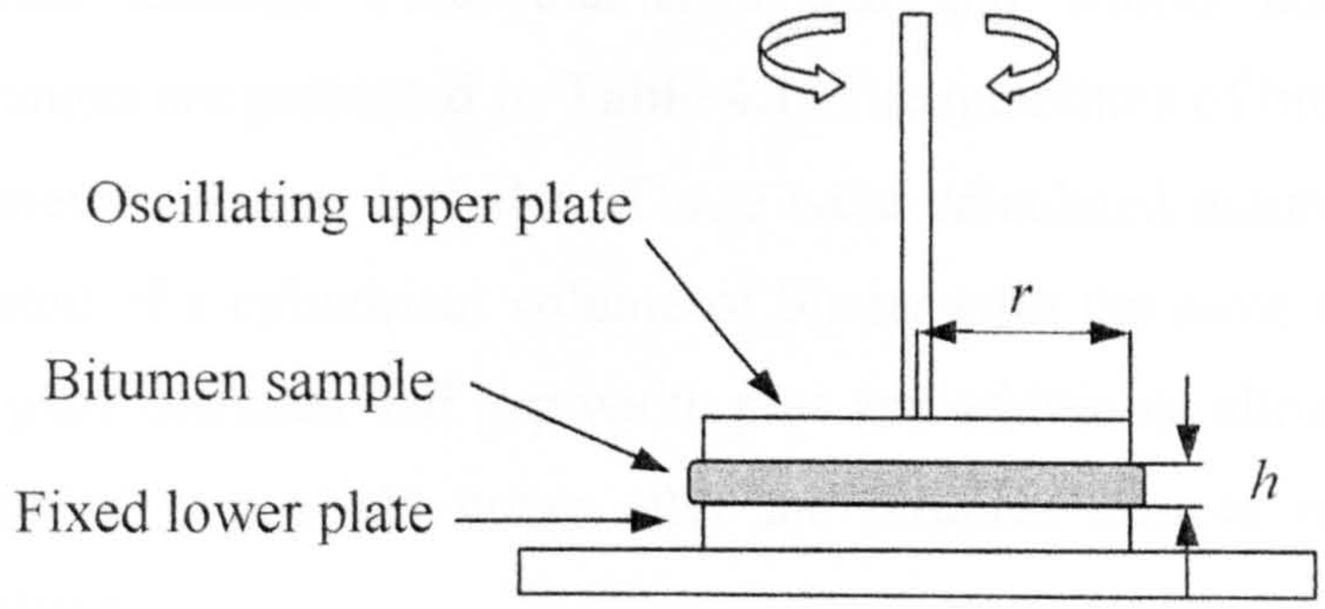

Figure 4.7 Principle of oscillatory testing in the DSR

4.3.3 Testing conditions

4.3.3.1 Temperature

Bituminous materials properties' are very sensitive to small variations in temperature. Accurate temperature control is, therefore, essential for rheological testing of asphalt binders. This is achieved in the DSR by encompassing the binder sample in circulating fluid, which is pumped from the TCU. The high thermal conductivity of the fluid in contact with the sample ensures that thermal equilibrium is achieved in a very short time.

Testing temperatures selected varied from –5 ^{0}C to 55 ^{0}C in 10 ^{0}C increments, which covers a wide range of service temperatures in UK pavements. At each temperature, a minimum delay of ten minutes was adopted before testing commenced to ensure thermal equilibrium through the sample. Temperature control to ± 0.1 ^{0}C was achieved during testing.

Different geometries had to be used in order to maximise accuracy over the range of temperatures selected. Plate diameters and gap widths across various temperature ranges are presented in **Table 4.1**. The quantities of binder required for each geometry are also included. These were calculated assuming that the sample consisted of a cylindrical volume of binder with the same diameter and height as the plate diameter and gap width plus and additional allowance. These quantities resulted in a slight bulge after the bitumen sample was squeezed between the plates.

Temperature range (^{0}C)	Plate diameter (mm)	Gap width (mm)	Bitumen mass (g)
from -5 to 15	8	2	0.104
from 15 to 35	8	1	0.052
from 25 to 55	25	1	0.505

Table 4.1 DSR test geometries and quantities of binder required

Prior to testing, accurate DSR gap setting and sample preparation was essential in order to obtain reliable and repeatable results. The method of sample preparation developed for this investigation is presented in **Appendix A**.

Furthermore, gap width (h) between the parallel plates is one of the geometrical variables used in the calculation of the viscoelatic functions as seen in Equation 4.14. During testing over a wide temperature range thermal expansion and contraction of the plates is inevitable. However, this is overcome in the DSR by means of the Automatic Expansion Compensation facility, which ensured that the gap width remained constant as the temperature changed.

4.3.3.2 Rate of loading

The effect of loading times on the dynamic properties of the binders was investigated via frequency sweeps. Frequency sweeps initially selected varied from 0.1 to 100 Hz, which included ten points equally spaced on a logarithmic scale. However, it was found later that plate slip at the highest frequencies (50 and 100 Hz) occurred as a result of high stiffness of the binders at these high frequencies. Therefore, the final frequency range selected was from 0.1 to 23.1 Hz.

Frequency of oscillation in the DSR is related to loading time associated with moving traffic at different speeds. However, there is no direct relationship between these two parameters. Work by Ferry (1970) quoted the following equivalent sinusoidal frequency, f (Hz) for a viscoelastic material subjected to a square pulse load of t_0 seconds duration,

$$f = \frac{1}{2\pi t_0} \tag{4.17}$$

Assuming load durations of 1 and 0.01 seconds for 'slow' and 'fast' moving traffic (Sisko and Brunstrum, 1969) the corresponding frequencies for these traffic speeds are 0.16 and 16 Hz respectively. Furthermore, SHRP recommends testing at a single frequency of 1.6 Hz (Anderson et al., 1994). Hence, the range

of frequencies selected in this project can be considered to cover all normal range of traffic speeds.

4.3.3.3 Linear Viscoelastic Region (LVER)

The dynamic mechanical functions presented in section 4.3.1, which define the fundamental linear viscoelastic material properties and their relationship to one another, are based on the validity of the linearity principle. Whenever the time-dependent stress response is directly proportional to the strain, the behaviour is termed linear viscoelastic. This situation arises whenever the magnitude of the deformation is small enough or the rate of deformation is slow enough relative to the material relaxation time. This is to ensure that the statistical distribution function characterizing the microstructure of the fluid is only slightly perturbed from equilibrium (Ferry, 1970).

Within the linear region, G^* is independent of stress or strain. This independency can be ascertained by applying a strain sweep to the sample and observing the resulting value of G^*. Anderson et al. (1994) defined the limit of the LVER as the point beyond which the measured value of G^* decreased to 95 % of its original value.

Marasteanu and Anderson (2000) indicated that a material must obey two simultaneous conditions to be linear viscoelastic: the homogeneity (proportionality) condition and the linear superposition principle (Boltzman superposition principle). The first condition is checked as before. The method for checking the second condition is to conduct a multiwave experiment in which the applied stress (or strain) is composed of several stress (or strain) signals applied simultaneously. If the material is linear, the response due to the multiwave signal should be equal to the sum of the responses to the individual waves composing the multiwave signal.

The procedure followed in this study was to determine the LVER by applying strain sweeps at the extremes of the temperature and frequency ranges. The magnitude of the stress applied to the sample was gradually increased and the

resulting strain, G^* and δ were monitored. **Figure 4.8** shows the amplitude sweep outputs at the extremes of the temperature and frequency ranges for the 100 Pen VEN binder modified with 10 % CRM from truck tyres. It can be seen that although the magnitudes of G^* and δ varied with temperature and frequency of oscillation, they were not affected by the strain level, indicating linear viscoelastic response.

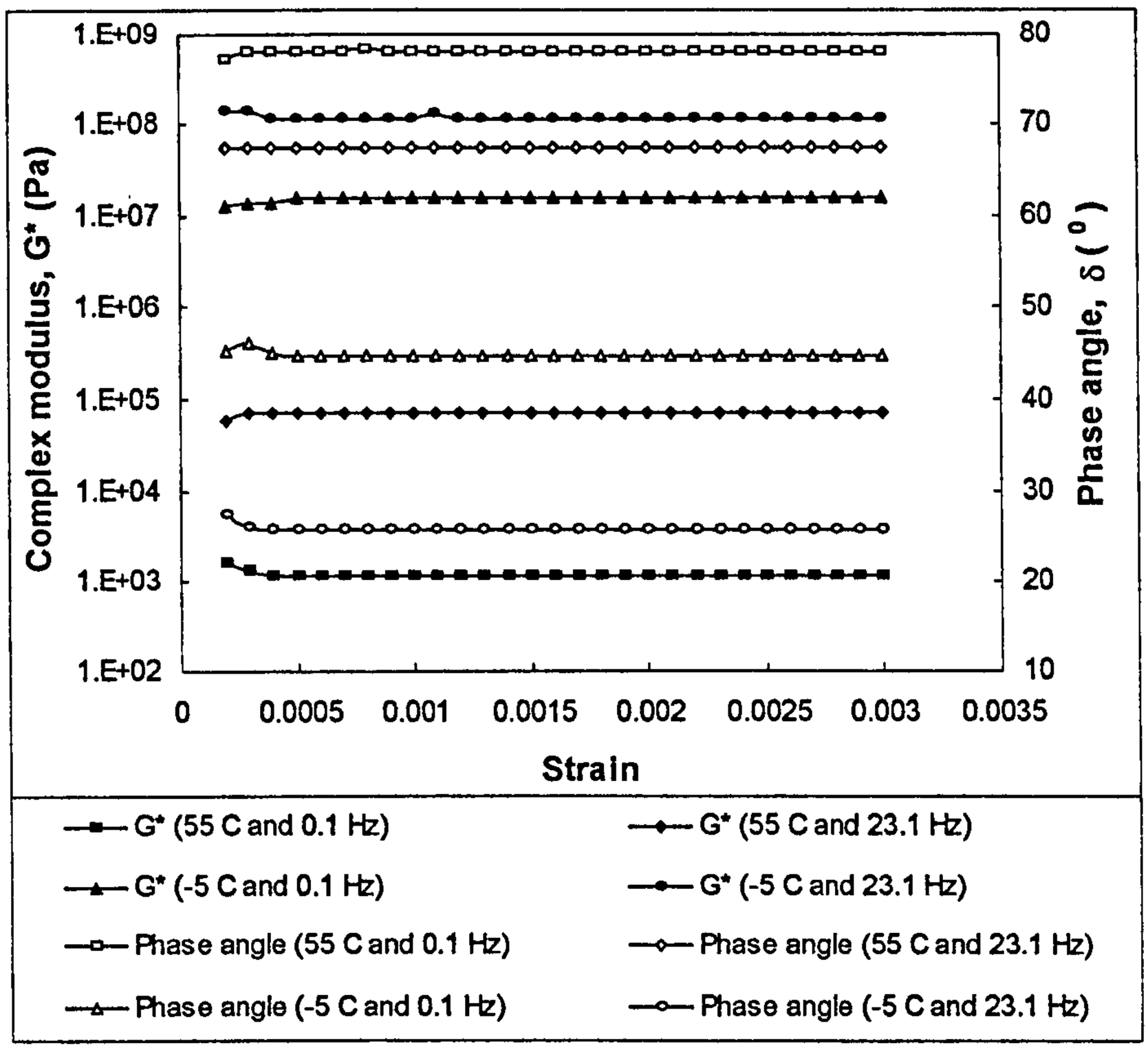

Figure 4.8 LVER for a 100 Pen VEN binder modified with 10 % CRM from truck tyres

The strain level selected for testing conventional and crumb-rubber modified binders was 0.001 (0.1 %) that was found to satisfy the condition of linearity for all the materials investigated.

Controlled strain mode of testing in the DSR was controlled by the AutoStress facility in the Bohlin software, which adjusted the applied stress until the resulting strain within the binder was 0.001 within 1 % tolerance.

4.3.4 Data representation

4.3.4.1 Black diagrams

A Black diagram is a plot of the phase angle, δ, against the complex stiffness modulus, G^*, obtained from a dynamic test. Thus, dynamic data at various temperatures and frequencies can be represented by means of a single curve. Data plotted in Black space approaches a horizontal asymptote at high temperatures, when asphalt binders tend to behave as Newtonian fluids. As the temperature decreases, the behaviour of the material becomes elastic in nature as the phase angle decreases and the complex stiffness modulus increases.

The Black diagram provides a simple tool for identifying potential problems with DSR test data. A smooth, single curve should result when the phase angle is plotted against the complex stiffness modulus if the material is linear viscoelastic, thermodynamically simple, and if there are no testing errors (Marasteanu and Anderson, 2001). Unlike other methods, the production of Black diagrams does not require any data transformation and is valid for unmodified and polymer modified bitumens (Buisine et al., 1993 and Planche et al., 1996).

Figure 4.9 shows the Black diagram corresponding to a 100 Pen VEN binder. It can be seen that at high temperatures the material exhibits predominantly viscous behaviour as evidenced by a high phase angle and a low complex stiffness modulus. As the temperature decreases the behaviour of the material tends towards an elastic nature as the phase angle decreases and the complex stiffness modulus increases.

Furthermore, **Figure 4.9** also shows test data at the same temperature but using different geometries. At 35 and 15 ^{0}C, the two geometries used yielded similar results and both data sets overlapped. At 25 ^{0}C, however, tests run with different

geometries did not yield the same result. When using a 25 mm plate with a 1 mm gap setting the stiffness exhibited by the sample diverted drastically from the trend line suggested by the rest of the data due to strain (compliance) effects within the instrument itself. Decreasing the plate diameter from 25 mm to 8 mm increased the response of the sample and eliminated the strain (compliance) effects.

Figure 4.10 illustrates the Black diagram for a 100 Pen VEN binder modified by adding 10 % CRM (600 μm nominal size) from truck tyres and produced by blending CRM and bitumen at 180 ^{0}C for 1 hour under high shear. Data presented here corresponded to the test geometries selected at each test temperature. As for the base bitumen, the crumb-rubber modified binder showed viscoelastic behaviour. Furthermore, the modified binder showed a plateau around a G^* value of 10^5 Pa, which is characteristic for elastomeric binders, and it is not found in unmodified bitumen (Philipps, 1997).

In this project Black diagrams corresponding to all the materials investigated were initially plotted in order to identify testing errors and machine compliance effects.

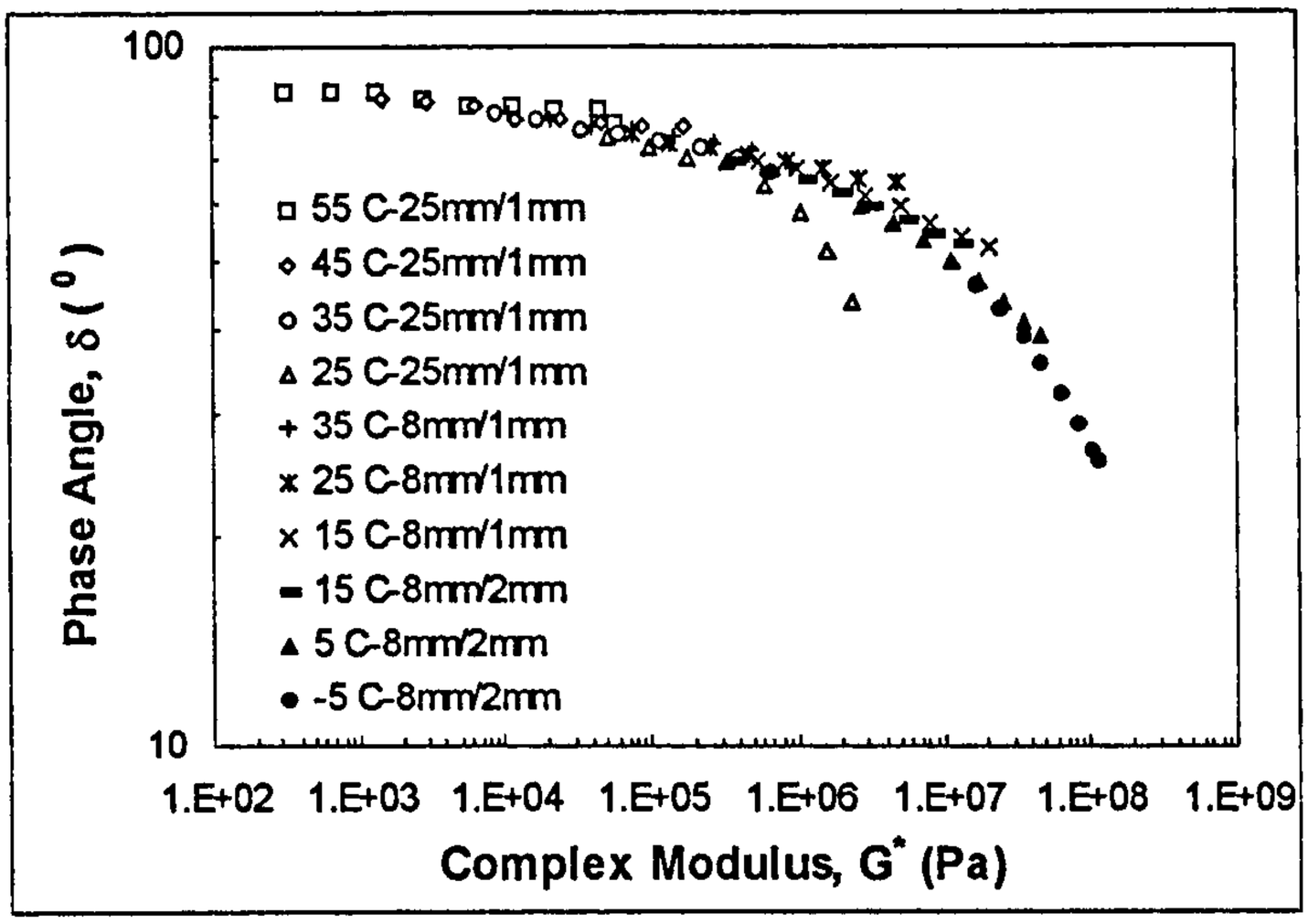

Figure 4.9 Black diagram for 100 Pen VEN

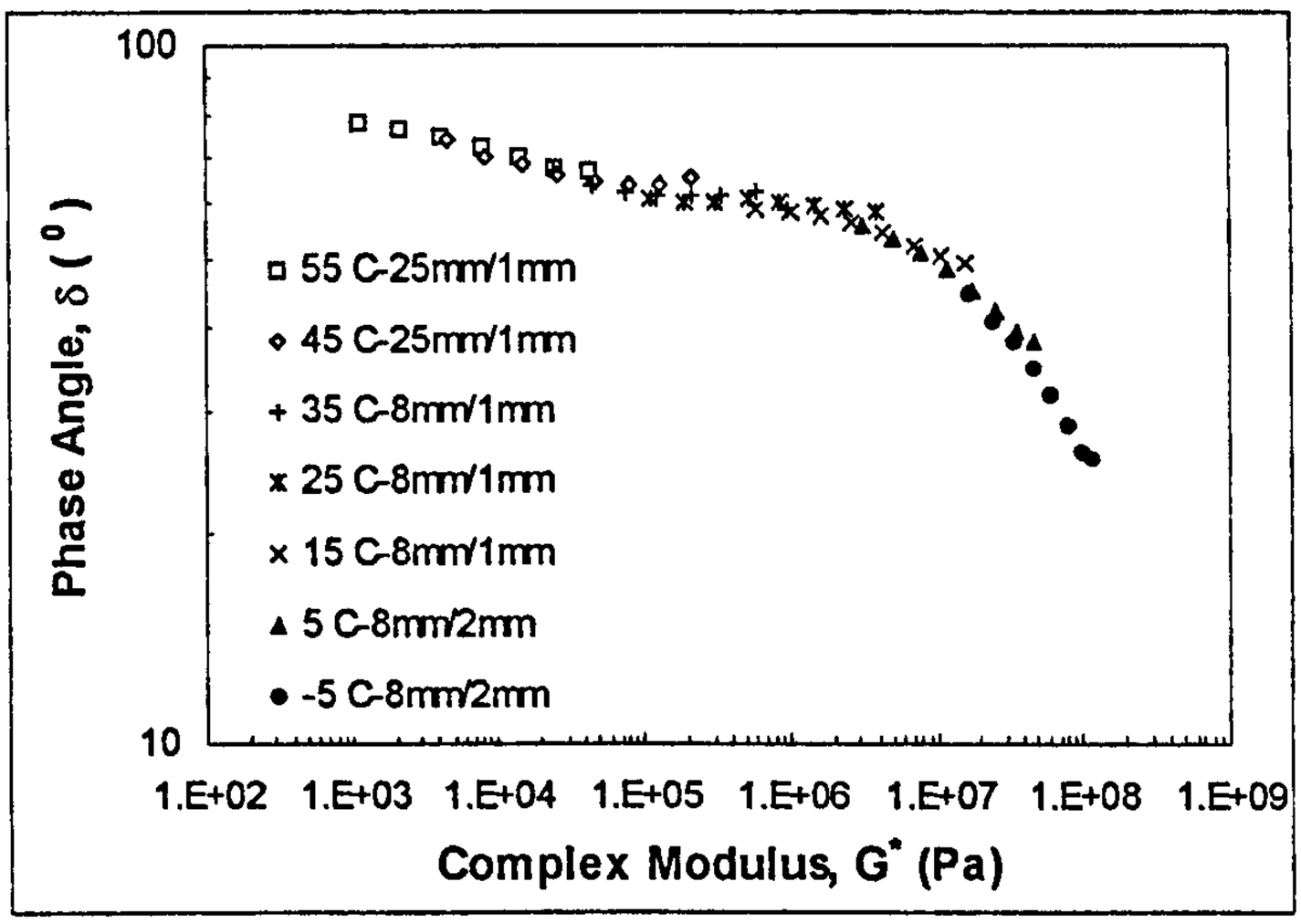

Figure 4.10 Black diagram for a 100 Pen VEN modified with 10 % CRM (coarse/truck)

4.3.4.2 Master curves

Most bituminous materials obey the principle of time-temperature superposition, hence, they are said to be thermo-rheologically simple. This implies that in a dynamic test, the effect of a change in temperature is to shift the position of the isotherms of the viscoelastic functions along the time (frequency) axis without changing their shapes.

The procedure for time-temperature superposition consists of shifting laterally the isotherms at various temperatures to overlap and form a continuous curve, known as the master curve, at a constant reference temperature. The horizontal translation of data through which one isotherm is shifted to overlap another isotherm at the reference temperature is described by a shift factor (a_T). **Figure 4.11** shows how isotherms at different temperatures can be shifted laterally to overlap and form a continuous curve at a constant reference temperature (T_{REF} = 25 ^{0}C). The shift factors applied to the isotherms in **Figure 4.11** are plotted as a function of temperature in **Figure 4.12**. Both figures relate to the data corresponded to a 100 Pen VEN binder modified with 10 % CRM (coarse/truck) also presented in the Black diagram of **Figure 4.10**.

The principle of time-temperature superposition permits separation of the time and temperature dependence of bituminous materials. The time (frequency) dependency is reflected in the position and shape of the master curve whilst the change of a_T with temperature reflects the temperature dependency. The principle also extends the scope of the frequency axis beyond the range that was measurable in the laboratory, as seen in **Figure 4.11**.

Time-temperature superposition criteria establish that the same values of a_T must be used for all the viscoelastic functions of a particular material. In this study, curve shifting was carried out using the IRIS 5 software package. In constructing the master curves, the dynamic mechanical data were shifted on the basis of the complex modulus (G^*). In general, this shift resulted in a fairly smooth curve for the phase angle (δ), which was also investigated. The a_T

values obtained in this way were used to construct G^* and δ master curves at a reference temperature of 25 ^{0}C.

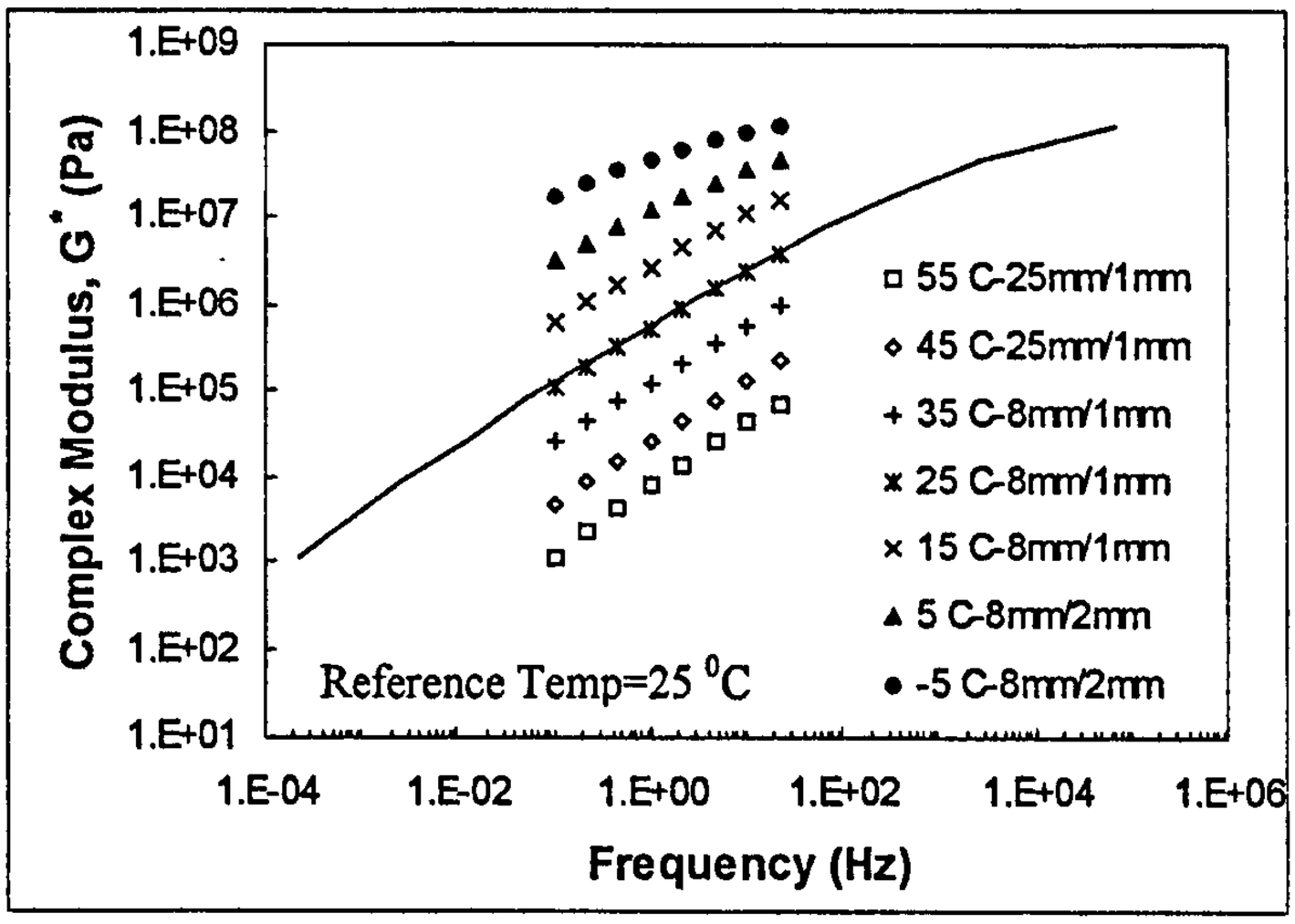

Figure 4.11 G^* master curve for 100 Pen VEN binder modified with 10 % CRM (coarse/truck)

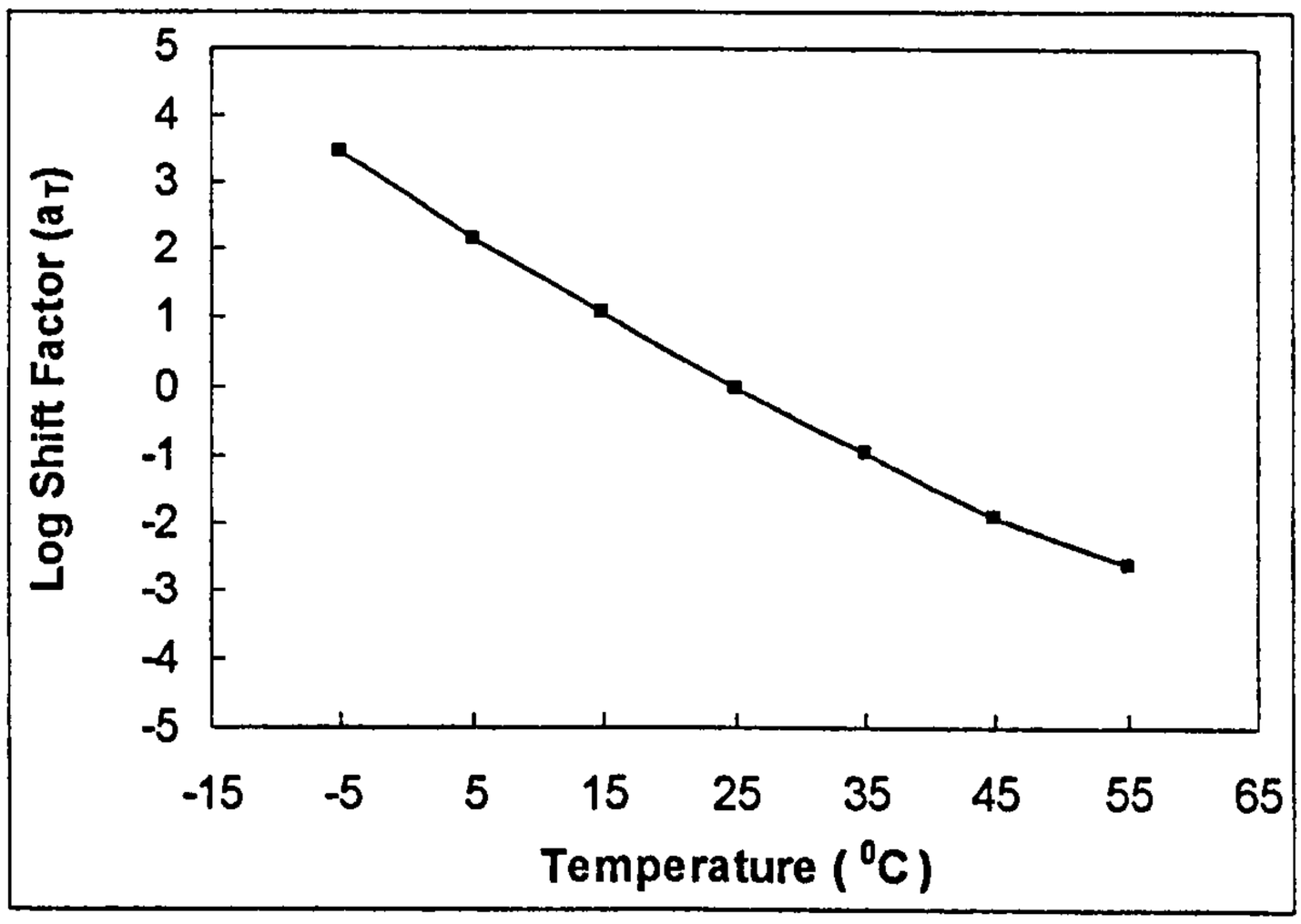

Figure 4.12 Variation of shift factor (a_T) with temperature used to produce the master curve in Figure 4.11

4.3.4.3 Results and discussions

Master curves, at a reference temperature of 25 ^{0}C, are presented in **Figures 4.13 - 16**. For presentation purposes, the number of points in these figures has been drastically reduced.

The G^* and δ master curves for the materials investigated followed similar trends. As the frequency decreased (temperature increased) the stiffness of the binders decreased and the phase angle tended towards 90^0, indicating viscous behaviour. On the other hand, as the frequency increased (temperature decreased) the stiffness of the binders increased and the phase angle decreased to a value between 20 and 30^0 approximately.

However, differences were found between the G^* and δ master curves of the base binders and the same binders after modification with CRM. Furthermore, these differences depended on the origin of the base binder, which determines its chemical composition, the CRM content by weight of binder, and the CRM size and source.

Figure 4.13 shows the G^* master curves for 100 Pen KSR binder modified with CRM (fine/truck) at various contents. It can be seen that at the low frequency end (high temperature) the stiffness increases with increasing CRM content. At the high frequency end (low temperature), however, the effect of CRM is reversed, hence, the stiffness is reduced as the CRM content increases, though these differences are less pronounced that at the low frequency end. Hence, the overall effect of CRM modification is to reduce the gradient of the master curves, which leads to a reduction in the sensitivity of the complex modulus to the loading frequency (Leech and Nunn, 1997).

The phase angle master curves corresponding to the above binders are presented in **Figure 4.14**. It can be seen that CRM modification reduces the phase angle of the base binder (100 Pen KSR) over the whole frequency range. Furthermore, the reduction in the phase angle increases with increasing CRM content.

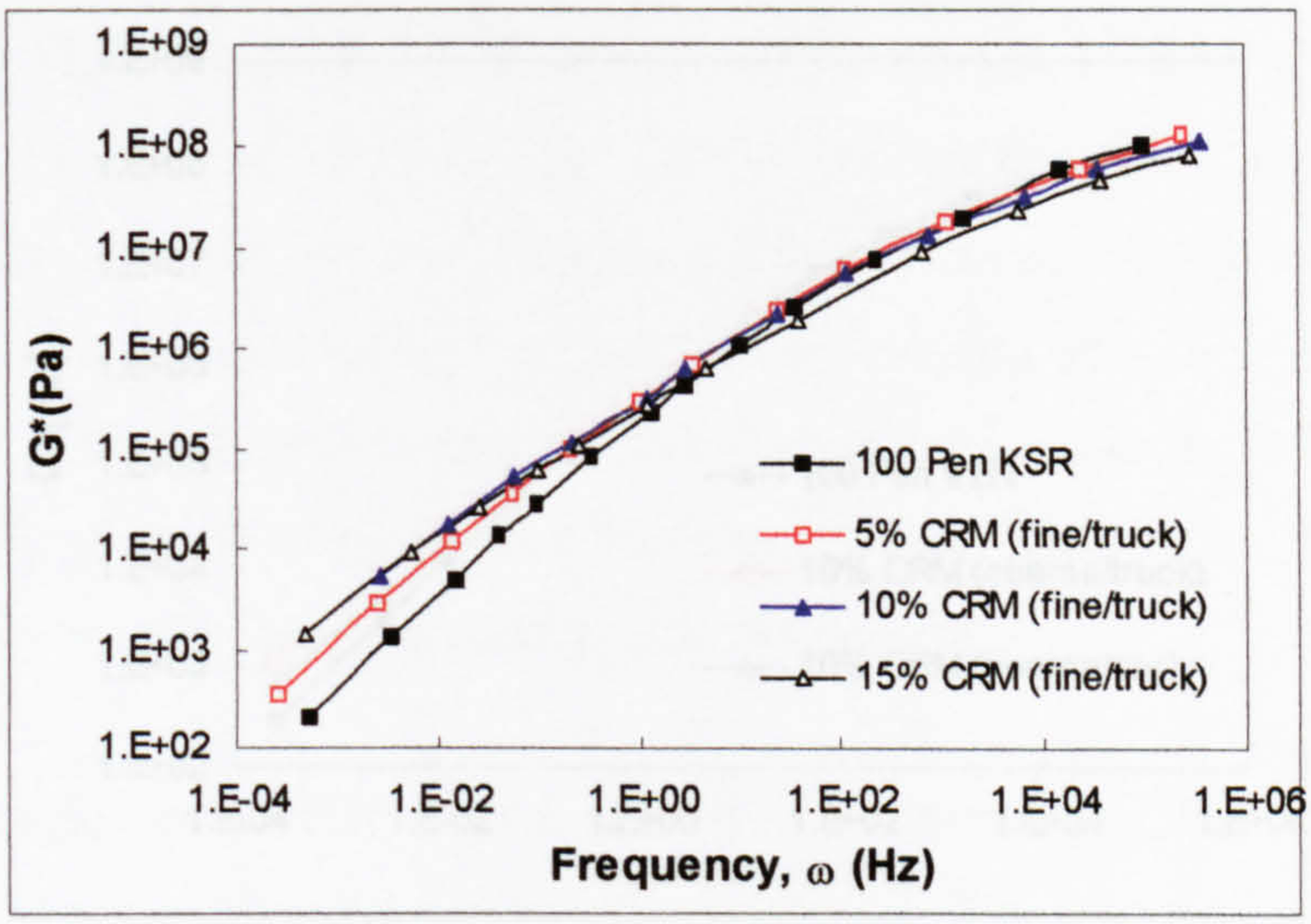

Figure 4.13 G* master curves for 100 Pen KSR modified with CRM (fine/truck) at various contents

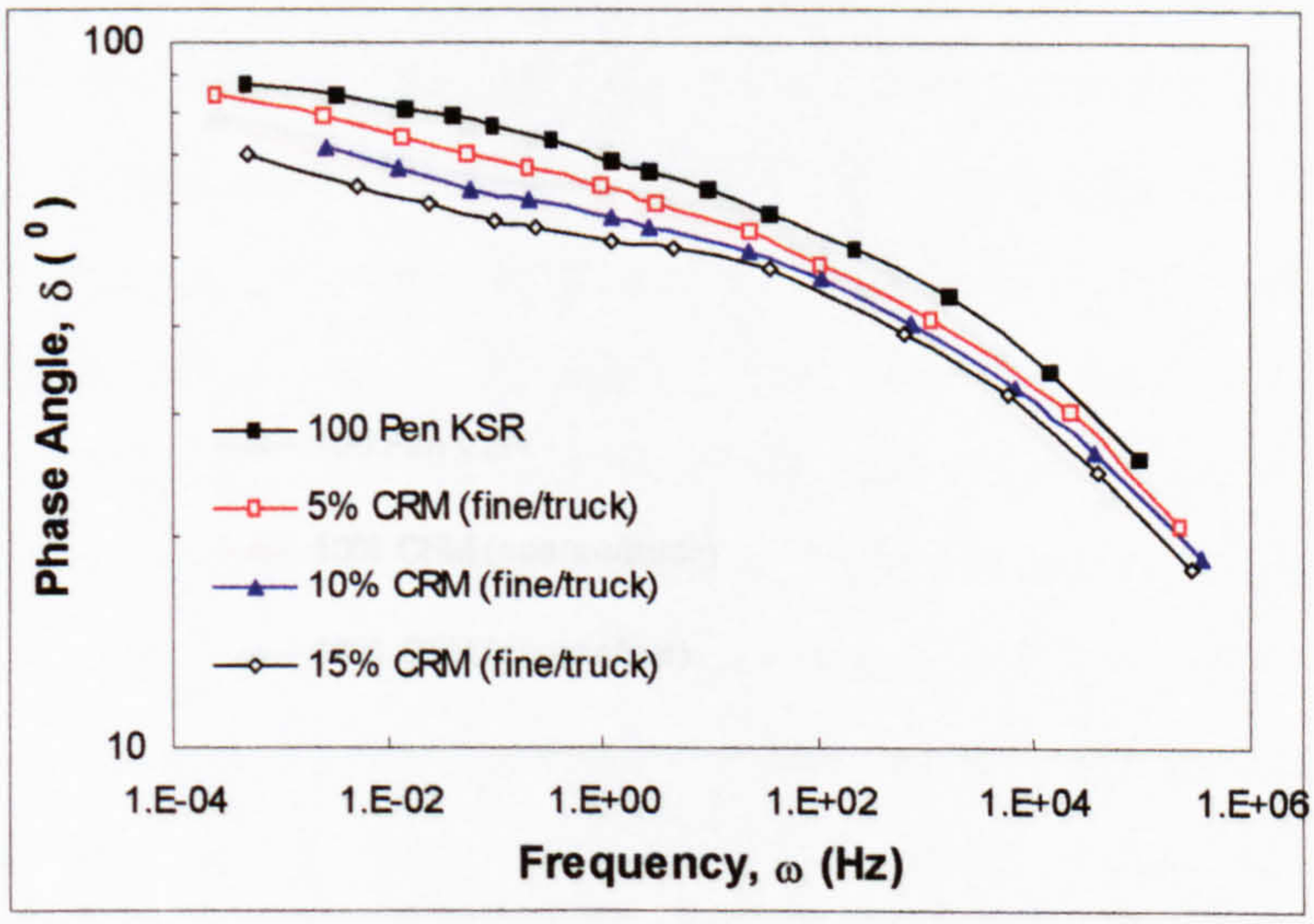

Figure 4.14 δ master curves for 100 Pen KSR modified with CRM (fine/truck) at various contents

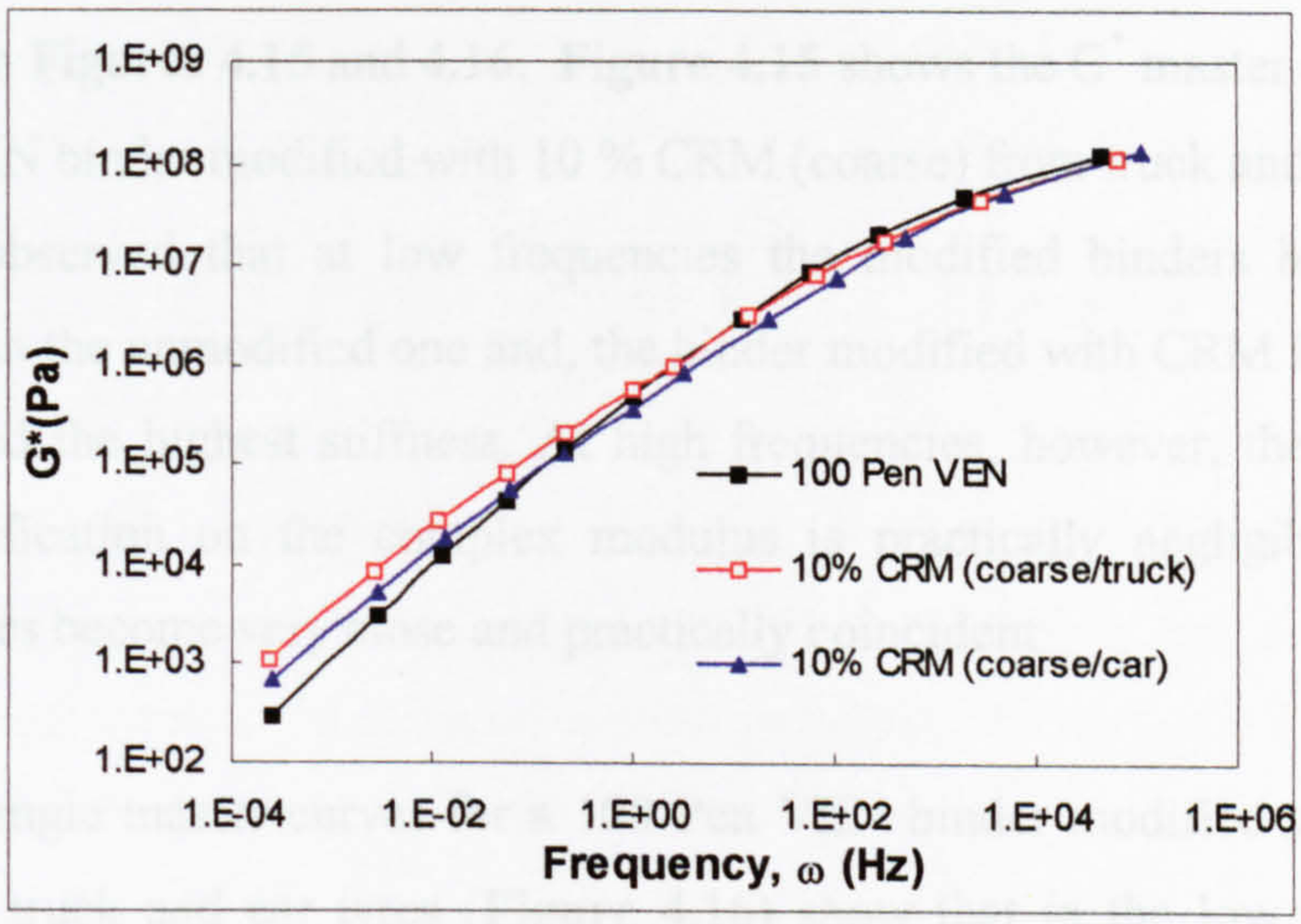

Figure 4.15 G* master curves for 100 Pen VEN modified with 10 % CRM (coarse) from truck and car-tyre rubber

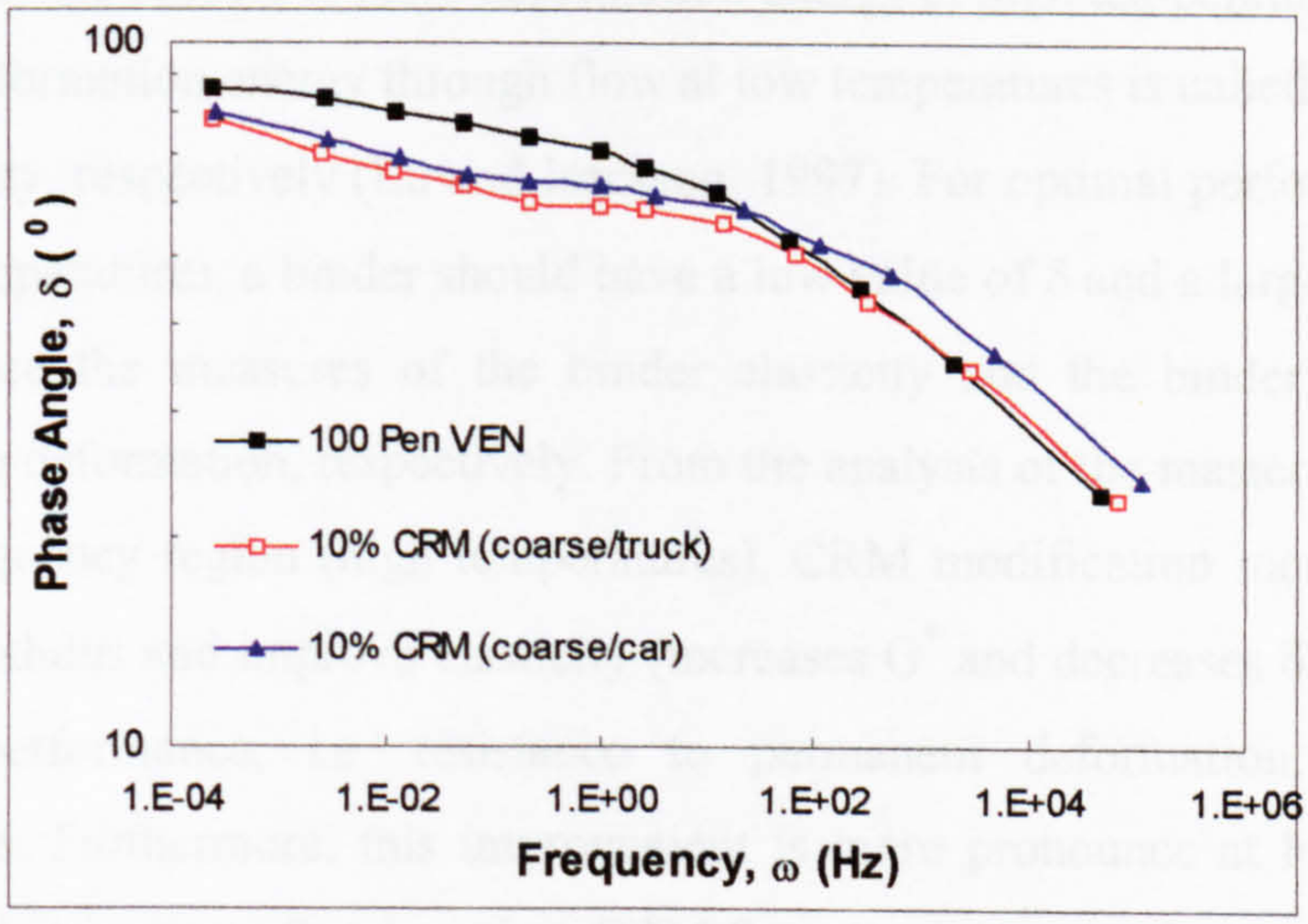

Figure 4.16 δ master curves for 100 Pen VEN modified with 10 % CRM (coarse) from truck and car-tyre rubber

The effect of CRM source, i.e. truck or car tyre, on the G^* and δ master curves is illustrated in **Figures 4.15** and **4.16**. **Figure 4.15** shows the G^* master curves for 100 Pen VEN binder modified with 10 % CRM (coarse) from truck and car tyres. It can be observed that at low frequencies the modified binders had higher stiffness than the unmodified one and, the binder modified with CRM from truck tyres showed the highest stiffness. At high frequencies, however, the effect of CRM modification on the complex modulus is practically negligible as the master curves become very close and practically coincident.

The phase angle master curves for a 100 Pen VEN binder modified with 10 % CRM from truck and car tyres (**Figure 4.16**) show that in the low frequency region the phase angle is reduced by the incorporation of CRM, and this reduction is more pronounced when using CRM from truck tyres. In the high frequency region, however, the unmodified binder exhibited the lowest phase angle.

The ability of the binders to store deformation energy at high temperatures and to dissipate deformation energy through flow at low temperatures is called elasticity and flexibility, respectively (Lu and Isacsson, 1997). For optimal performance at elevated temperatures, a binder should have a low value of δ and a large value of G^* which are the measures of the binder elasticity and the binder's overall resistance to deformation, respectively. From the analysis of the master curves in the low frequency region (high temperatures), CRM modification increases the complex modulus and improve elasticity (increases G^* and decreases δ). Thus, it improves performance, i.e. resistance to permanent deformation, at high temperatures. Furthermore, this improvement is more pronounce at high CRM contents and, it is more effective when CRM from truck- tyre rubber is used.

At low temperatures (high frequencies), CRM binders have a slightly lower complex modulus than the base bitumens. This will probably contribute to an increase in the binder flexibility at low temperatures, which might have a beneficial effect on fatigue and low temperature cracking resistance. However,

the effectiveness of CRM at low temperatures is much less than at high temperatures.

4.4 RHEOLOGICAL STUDY OF THE INTERACTION OF BITUMEN WITH CRM

4.4.1 Interaction processes

The method of producing crumb-rubber modified binders by the wet process involves blending the CRM particles and the bitumen under controlled conditions of time, temperature and shear. When CRM and bitumen are blended at elevated temperatures the rubber particles interact with the bitumen and swell. Furthermore, degradation of the rubber particles might also occur. The extent of these two processes, swelling and degradation, depends on factors like the nature of the rubbers, the bitumens' chemical composition and the interaction process variables, time, temperature and degree of agitation. In addition, these processes will determine the final properties of the crumb-rubber modified binders.

During interaction with bitumen at high temperatures, rubber particles are swollen by absorption of predominantly bitumen's aromatic components. The rate and extent of swelling are controlled by factors such us temperature and time, as discussed in Chapter 3. Once equilibrium swelling is reached and depending on these factors, the rubber particles may suffer some form of degradation.

The mechanism of rubber degradation as a result of interaction with bitumen at high temperatures has not been fully characterized. Heiztman (1992) claimed that the interaction between CRM and bitumen is a nonchemical reaction and the CRM does not dissolve into the bitumen phase. Billiter et al., (1997**b** and 1997**c**) showed that by utilizing high mixing temperatures and high shear, along with extended interaction times, the rubber particles could be devulcanized and depolymerized into the bitumen to produce a binder that is both homogeneous and truly elastic. Zanzotto and Kennepohl (1996) also showed that by applying high temperatures and shear rates, CRM could be partially devulcanized and depolymerised in the bitumen medium.

Devulcanization is defined as the process by which sulphur-sulphur or carbon-sulphur bonds that are formed by the vulcanisation process during tyre manufacturing are broken. Depolymerization, on the other hand, is defined as the breaking of the backbone of the main polymer chain. In the studies mentioned above, however, the two concepts were not clearly distinguished.

4.4.2 Materials and production conditions

In previous sections, the rheological properties of CRM binders produced under the same conditions of time (1 hour), temperature (180 ^{0}C) and shear rate (2000 rpm) were investigated.

In this section the effect of the process variables, blending time and temperature, on the properties of the CRM binders is investigated. Furthermore, the two main interaction mechanisms, swelling and degradation, are related to the changes in these rheological properties.

To study the effects of the process variables, two binders, 100 Pen KSR and 100 Pen VEN were modified by adding 10 % CRM by weight of binder under different conditions of mixing time and temperature. Coarse CRM (600 μm maximum nominal size) from both truck and car tyres were used to modify the base binders.

In order to investigate the effects of interaction time, CRM and bitumen were blended at 180 ^{0}C under high shear (2000 rpm) from 1 up to 24 hours, following the procedure explained in Chapter 3, section 3.5.8.1. Furthermore, bitumen samples isolated from the CRM-bitumen blends were obtained by filtering through cloth filters (see Chapter 3, Section 3.5.8.2) after 1, 6, 12 and 24 hours interaction with CRM at 180 ^{0}C. The base binders were also stirred at a rate of 1000 rpm in the Silverson mixer and at a temperature of 180 ^{0}C for up to 24 hours with the absence of any rubber modifier.

To study the effects of interaction temperature, CRM binders were produced by blending CRM and bitumen at various temperatures say, 150, 180 and 210 ^{0}C, for 1 up to 6 hours and at a shear rate of 2000 rpm.

Dynamic as well as creep and creep recovery tests were used to investigate the effects of the process variables on the rheological properties of the CRM binders produced as above.

4.4.3 Dynamic testing

The dynamic viscoelastic functions complex modulus (G^*) and phase angle (δ) defined in Section 4.3.1 and measured by the DSR were used to investigate the effects of the process variables on the properties of the crumb-rubber modified binders.

Oscillatory testing in the DSR was carried out at temperatures of 45 and 55 ^{0}C, using a 25 mm plate diameter and 1 mm gap width. From the analysis of the G^* and δ master curves presented in section 4.3.4.3, it was found that these relatively high temperatures (low frequencies) testing conditions were suitable to differentiate measured properties, G^* and δ corresponding to unmodified and crumb-rubber modified binders. Data presented in the subsequent sections were obtained at 45 ^{0}C and at a loading frequency of 10 Hz.

4.4.3.1 Influence of interaction time

The changes of the binders properties, complex modulus, G^*, and phase angle, δ, with interaction time at 180 ^{0}C corresponding to the materials investigated are presented in **Figures 4.17 – 20**.

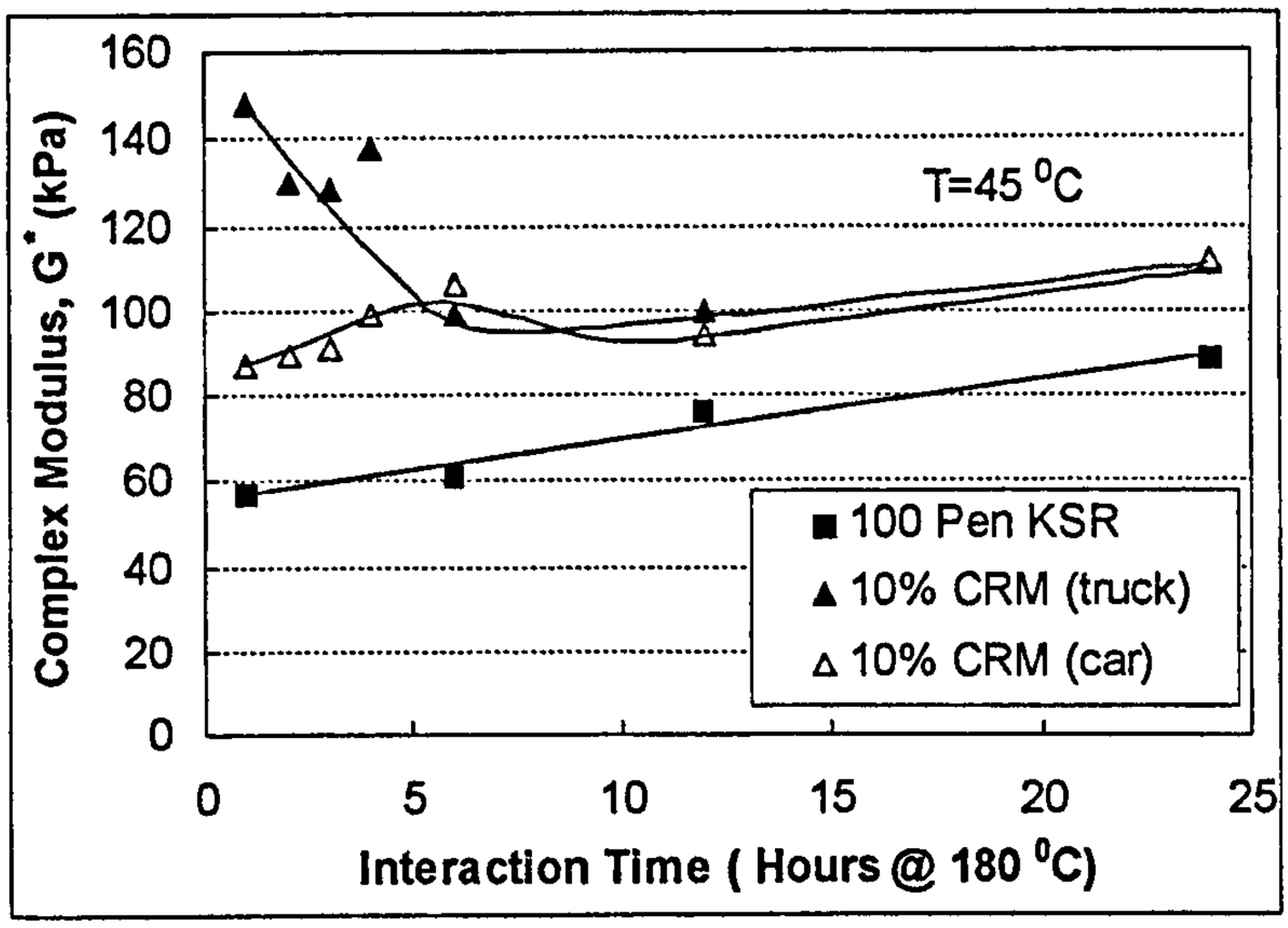

Figure 4.17 Evolution of G^* with interaction time for 100 Pen KSR binder modified with 10 % CRM from truck and car tyres

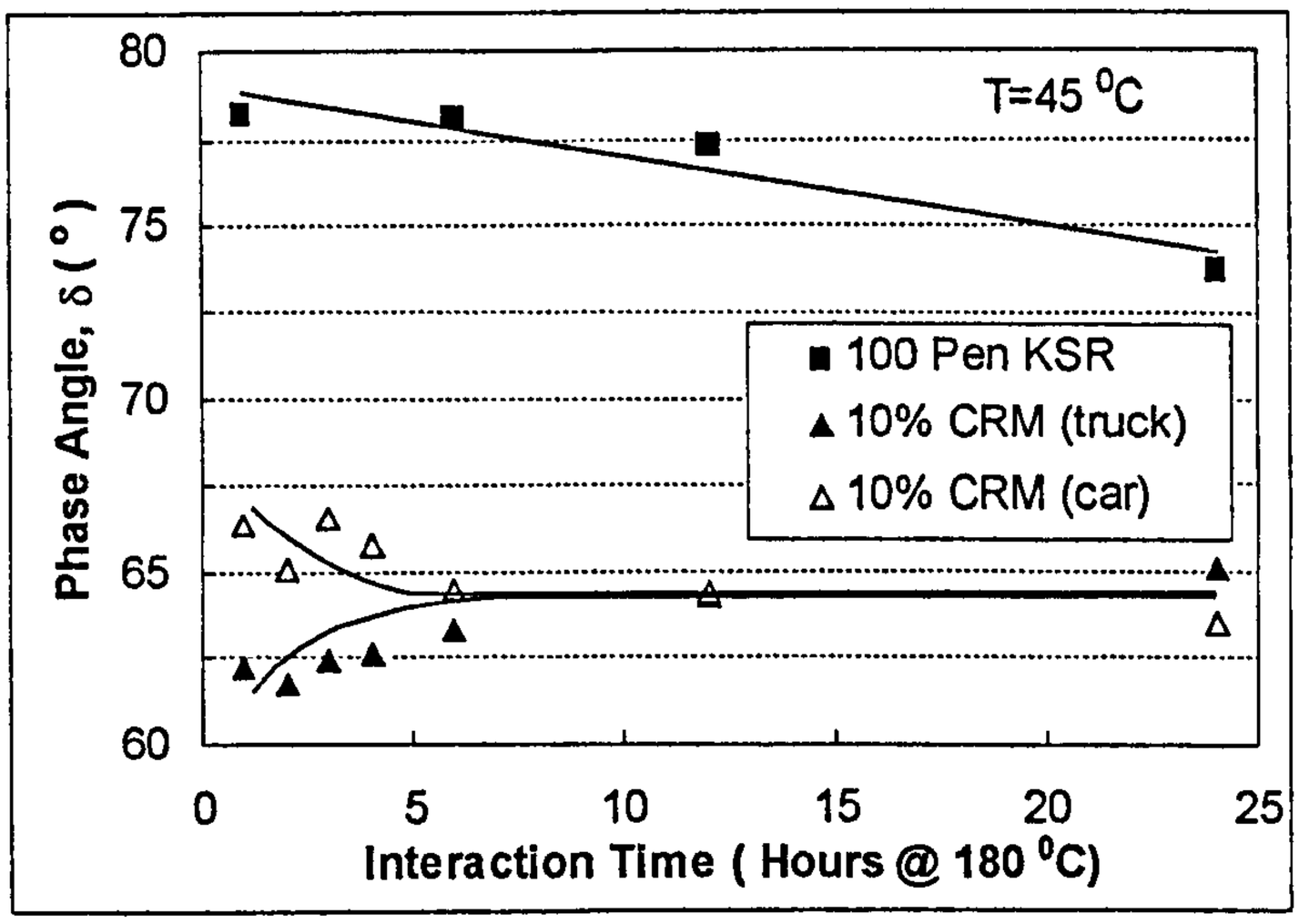

Figure 4.18 Evolution of δ with interaction time for 100 Pen KSR binder modified with 10 % CRM from truck and car tyres

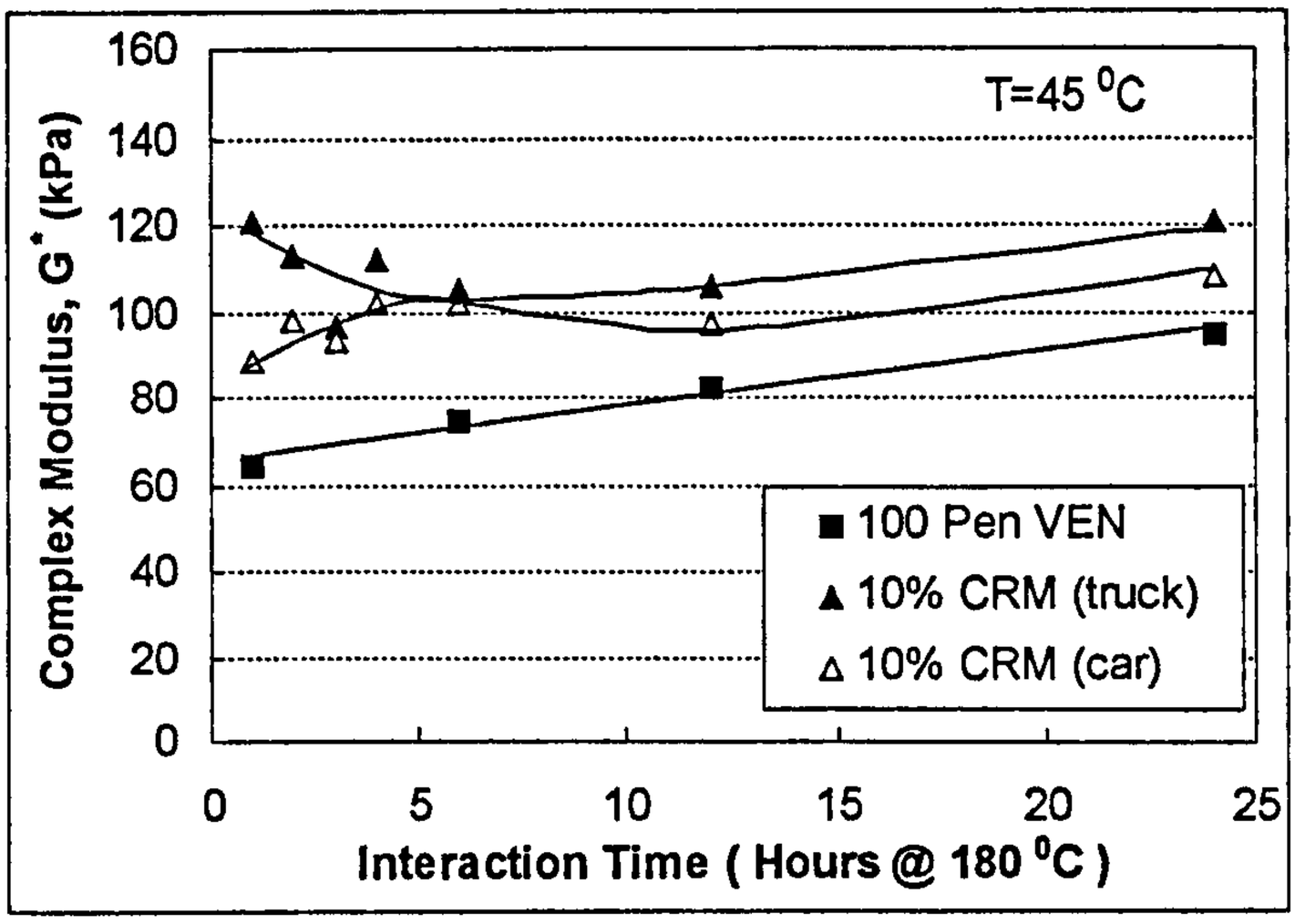

Figure 4.19 Evolution of G^* with interaction time for 100 Pen VEN binder modified with 10 % CRM from truck and car tyres

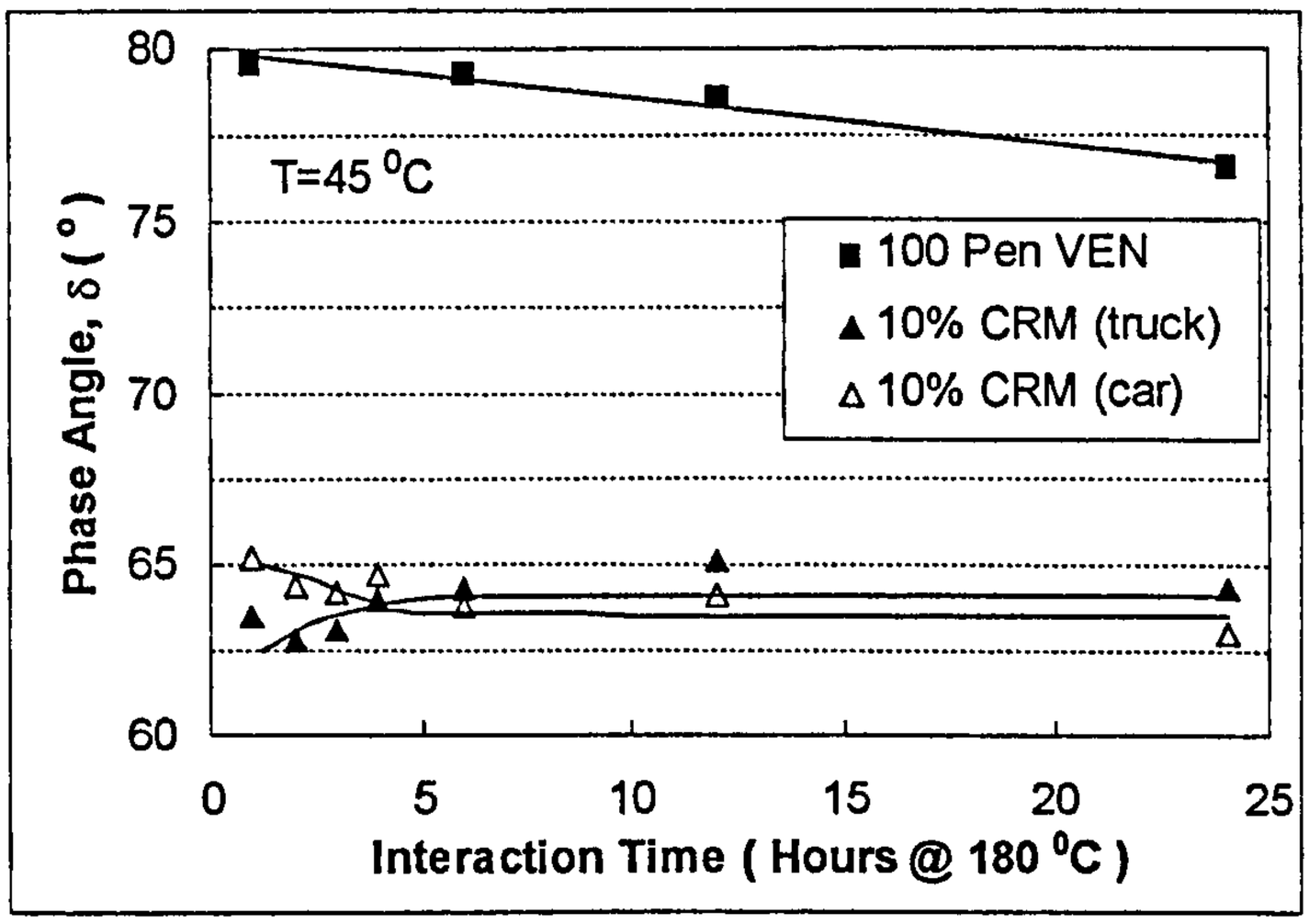

Figure 4.20 Evolution of δ with interaction time for 100 Pen VEN binder modified with 10 % CRM from truck and car tyres

Data showed that CRM binders exhibited higher G^* and lower δ than the base binders at all interaction times. Thus, the binders became stiffer and more elastic by the addition of CRM under the mixing conditions of time and temperature investigated.

When heating the base binders at 180 ^{0}C for prolonged times, G^* increased and δ decreased with time. This effect was indicative of bitumen oxidation (ageing) at high temperatures. The evolution of G^* and δ with interaction time for the CRM binders was, however, more complex and depended on the source of CRM, and to some extent on the origin of the base binder.

Binders modified with CRM from truck tyres developed their highest G^* after one hour mixing at 180 ^{0}C. This initial high stiffness was attributed to swelling of rubber particles, reducing the inter-particle distance, and the stiffening of the bitumen matrix by diffusion of light components into the rubber particles. Starting at a high value, G^* then decreased continuously up to about 6 hours interaction time. This decrease in G^* might suggest some degree of degradation, devulcanization and/or depolymerization, of the rubber particles. For longer interaction times, G^* increased at a similar rate to the unmodified binder suggesting, thus, hardening as a result of binder oxidation. The effect of interaction time on the modification of phase angle was seen as a slight increase in δ during the first 6 hours. For longer interaction times, δ stabilised, indicating no phase angle modification.

Binders modified with CRM from car tyres showed different behaviour. Initially, G^* after 1 hour interaction time increased with respect to the base binders, as a result of CRM modification. Then, G^* continued to increase with interaction time up to about 6 hours, probably as a result of binder oxidation. Between 6 and 12 hours a small decrease in G^* was observed, suggesting some degree of degradation of the CRM particles from car tyres. For longer interaction times, times G^* increased indicating again hardening by oxidation. The effect of interaction time on phase angle was seen as a slight decrease in δ during the first

6 hours, confirming the ageing of the modified binders. For longer interaction times, δ stabilised, indicating no phase angle modification.

Comparison of data for the binders modified by CRM from truck and car tyres showed that after one-hour interaction/mixing time, binders modified with CRM from truck tyres were stiffer than the ones modified with CRM from car tyres. This was attributed to differences in the chemical composition of both types of rubbers. Furthermore, this enhanced stiffness confirmed the greater swelling of the truck rubber particles (natural rubber) in comparison with the car rubber particles (synthetic rubber), as discussed in Chapter 3, Section 3.5.5.

G^* and δ data corresponding to the base binders and the residual binders isolated (filtered) from the rubber-bitumen blends, after interaction at 180 ^{0}C with 10 % CRM from truck and from car tyres are presented in **Figures 4.21 – 24**.

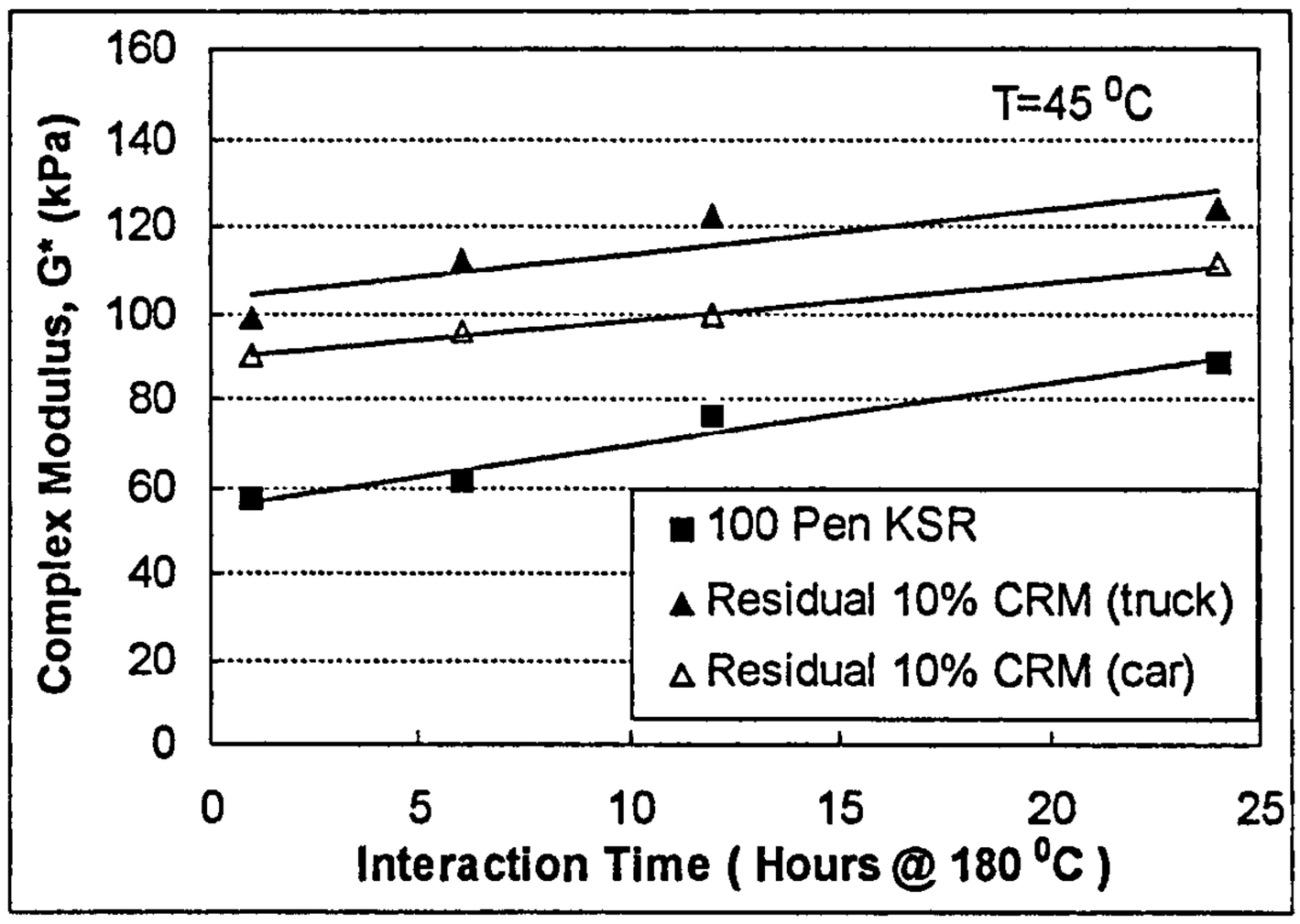

Figure 4.21 Evolution of G^* with interaction time for residual 100 Pen KSR binder modified with 10 % CRM from truck and car tyres

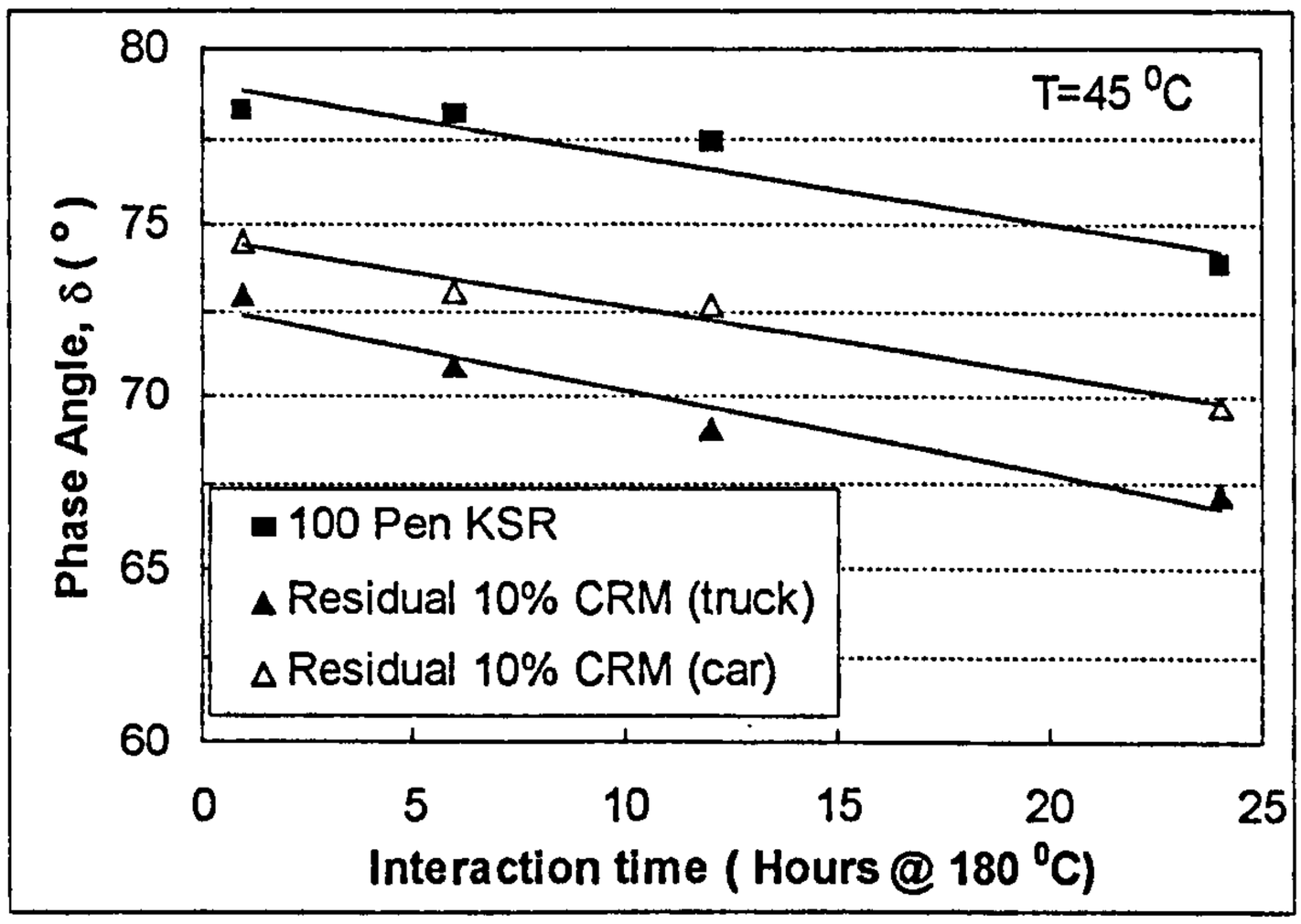

Figure 4.22 Evolution of δ with interaction time for residual 100 Pen KSR binder modified with 10 % CRM from truck and car tyres

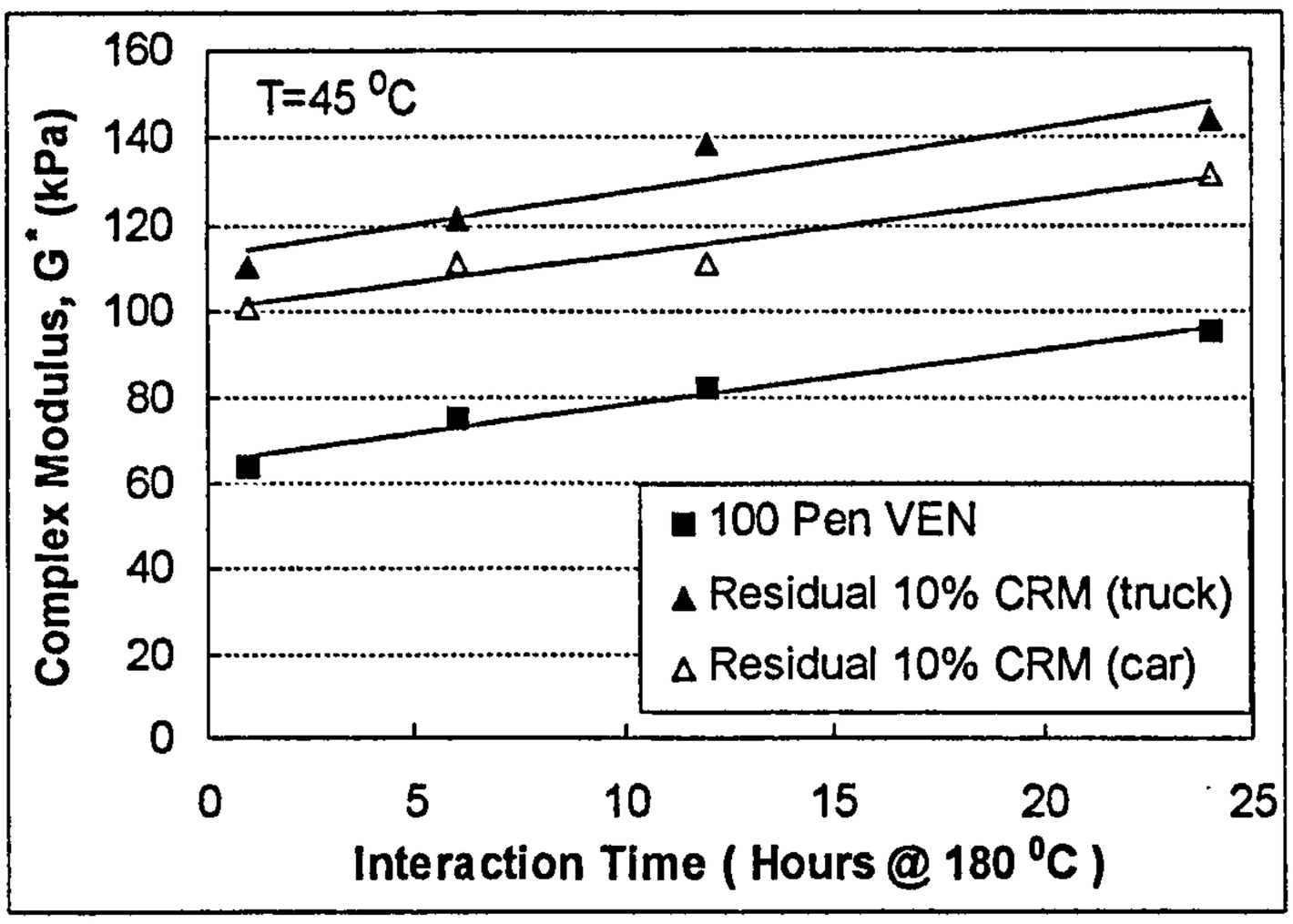

Figure 4.23 Evolution of G^* with interaction time for residual 100 Pen VEN binder modified with 10 % CRM from truck and car tyres

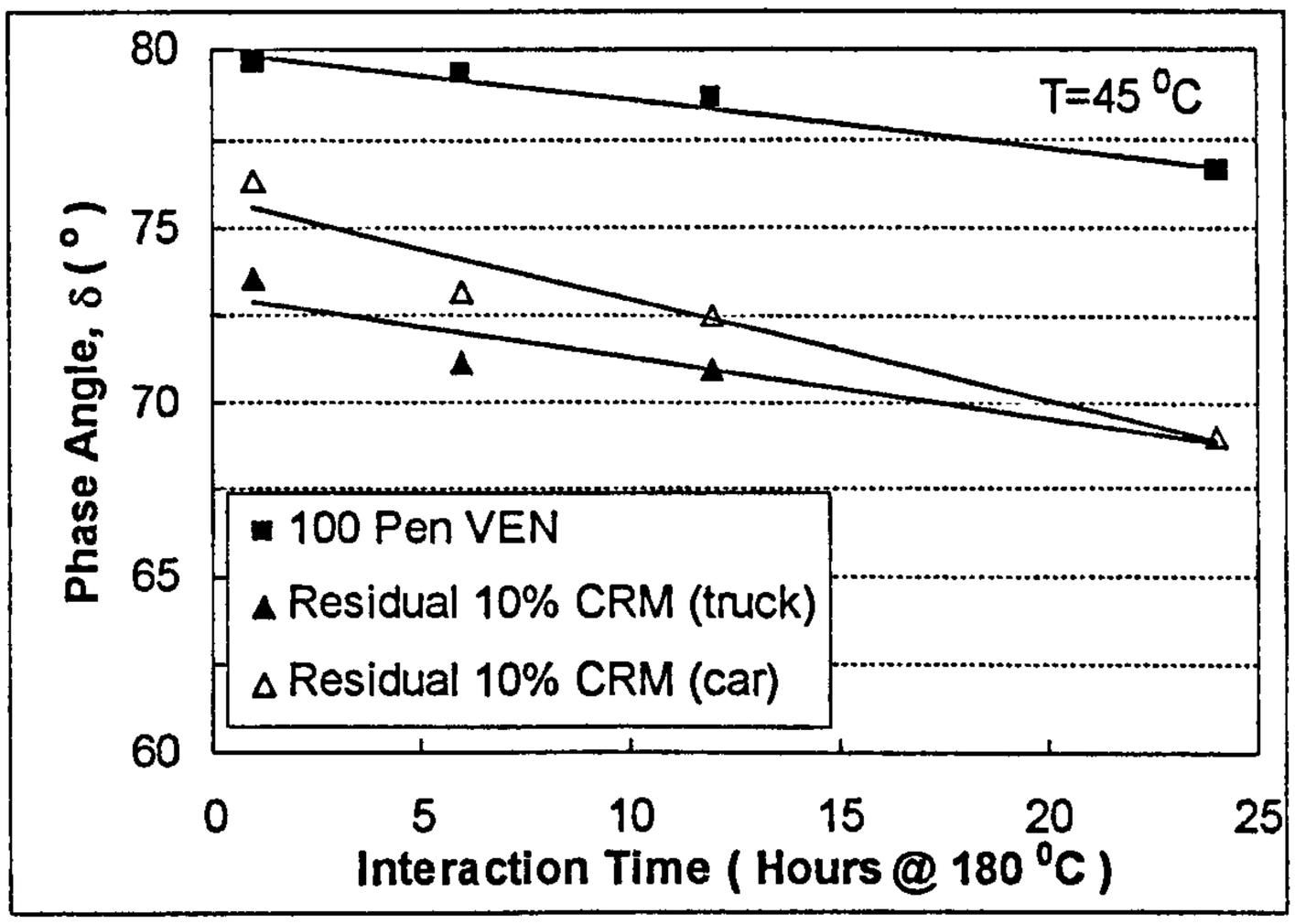

Figure 4.24 Evolution of δ with interaction time for residual 100 Pen VEN binder modified with 10 % CRM from truck and car tyres

Data showed that the residual binders, after interaction with the rubber particles, had increased stiffness, as seen by the higher values of G^*. Thus, it is concluded that CRM and bitumen interaction at high temperature hardens the bitumen matrix. Furthermore, this increase in stiffness is consistent with diffusion of mobile components from the bitumen into the rubber particles and responsible for the swelling of the rubber.

Comparison between G^* for the isolated binders showed that the stiffness of the residual binders after interaction with truck-tyre rubber was higher than those after interaction with car-tyre rubber. This was attributed to higher swelling of the truck rubber (NR) particles. Furthermore, this is consistent with the swelling data presented in Chapter 3, Section 3.5.2, where it was found that truck-tyre rubber, with its higher proportion of natural rubber, absorbed more bitumen components than car-tyre rubber did.

Figures 4.21 and **4.22** also show that the increase in G^* of the residual binders followed a similar trend to those of the base bitumens. This suggests that diffusion of bitumen components into the rubber and consequently swelling occurred during the early stages of the interaction process, thus, before one-hour interaction time at 180 ^{0}C. This is confirmed by the diffusion data presented in Chapter 3, section 3.5.8.4, where it was found that for a 100 Pen KSR bitumen, equilibrium swelling times at 180 ^{0}C for truck and car-tyre rubber were 50 and 67 minutes respectively, assuming spherical particles. For CRM particles, which are not truly spheres but have protrusions on the surfaces, however, swelling times were expected to be shorter.

Comparison between the two base binders, KSR and VEN, showed that the residual VEN binders, after interaction with the rubber, had higher stiffness than the residual KSR binders after interaction with the same amount and type of CRM. This effect was due to an initial higher stiffness of the VEN bitumen. It might also be due to a higher absorption of bitumen components from the VEN binder in comparison with the KSR binder, as showed in Chapter 3, section 3.5.2, which increases the stiffness of the residual binders.

The changes in the phase angle of the base binders and the residual ones are presented in **Figures 4.22** and **4.24**. The figures showed that the isolated bitumens have lower phase angles than the neat binders, indicating a more elastic response of the residual binders. Furthermore, the phase angles corresponding to the isolated bitumens after interaction with truck-tyre rubber were lower than the values corresponding to the isolated bitumens after interaction with car-tyre rubber. This is attributed, as for G^*, to differences in the absorption of bitumen into the different types of rubber.

4.4.3.2 Influence of interaction temperature

The changes of binder properties, complex modulus, G^*, and phase angle, δ, with interaction time and at interaction temperatures of 150, 180 and 210 ^{0}C are presented in **Figures 4.25 – 30**.

Figures 4.25 and **4.26** show G^* and δ data at the low interaction temperature, 150 ^{0}C. It can be seen that G^* practically did not change during the period of time investigated, though a small increase in G^* was observed in some of the binders. The slight increase in G* was accompanied by a reduction in δ. This reduction in δ with interaction time was more pronounced for the binders modified with CRM from car tyre. The evolution of the properties G^* and δ suggested, thus, some small degree of oxidation of the binders.

The evolution of G^* and δ at the intermediate temperature, 180 ^{0}C, is presented in **Figures 4.27** and **4.28**. Data show differences between the binders modified with CRM from truck tyres and from car tyres. G^* corresponding to the binders modified with truck-tyre rubber decreased with interaction time while δ increased. This suggests some form of partial degradation, devulcanization and/or depolymerization of the swollen rubber particles at high temperatures. On the other hand, G^* for the binders modified with car-tyre rubber increased with interaction time while δ decreased, which could indicate hardening of the binders as a result of oxidation (ageing).

The different behaviour of the binders modified with CRM from truck and car tyres at 180 ^{0}C might be attributed to differences in the oxidative stabilities of the two types of rubber at high temperatures, car-tyre rubber (synthetic rubber) being more stable than truck-tyre rubber (natural rubber).

The evolution of G^* and δ at the high temperature, 210 ^{0}C, is presented in **Figures 4.29** and **4.30**. It is shown that G^* decreased while δ increased with interaction time, indicating continuous partial degradation of both types of rubbers during mixing with bitumen at this high temperature.

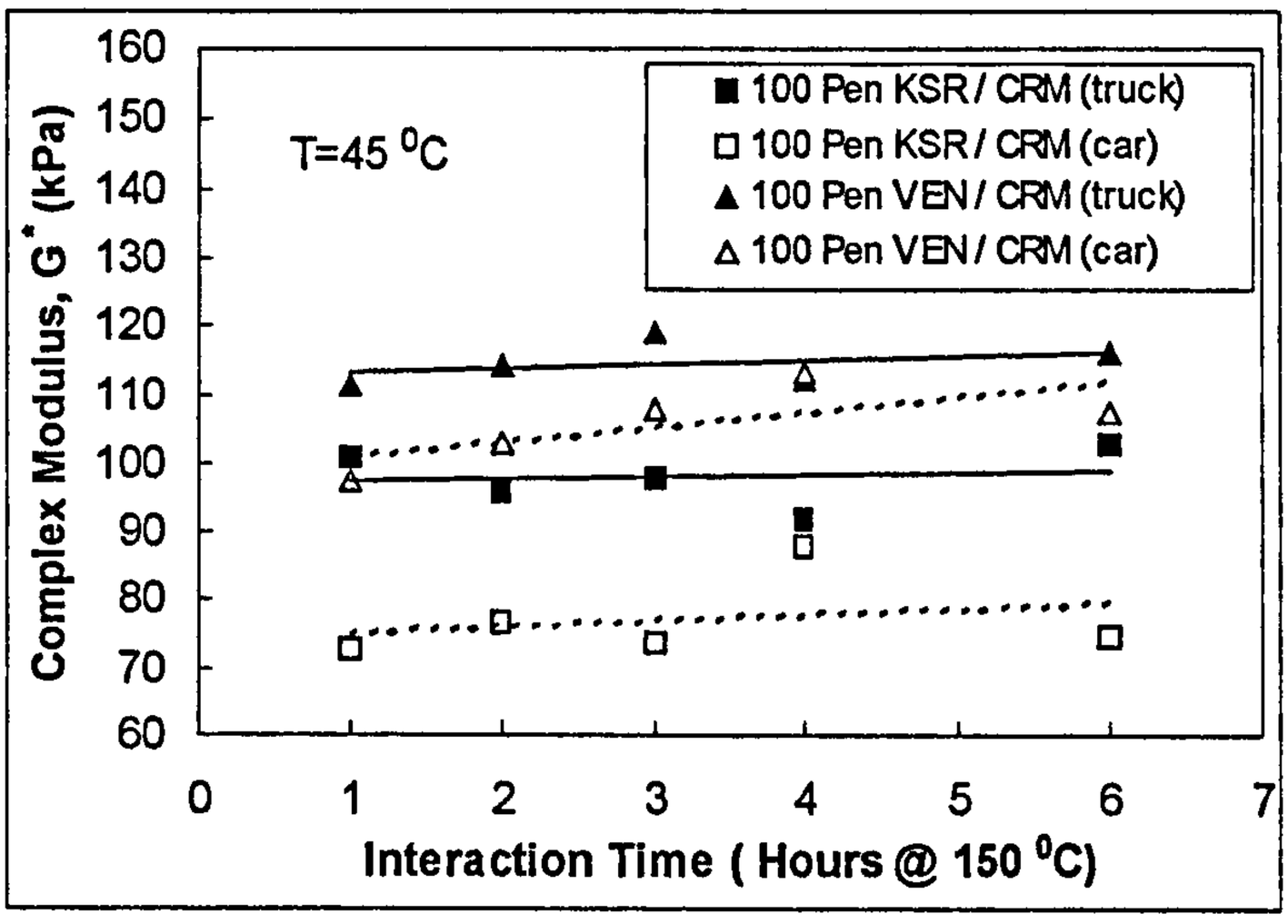

Figure 4.25 Evolution of G^* with interaction time at 150 °C

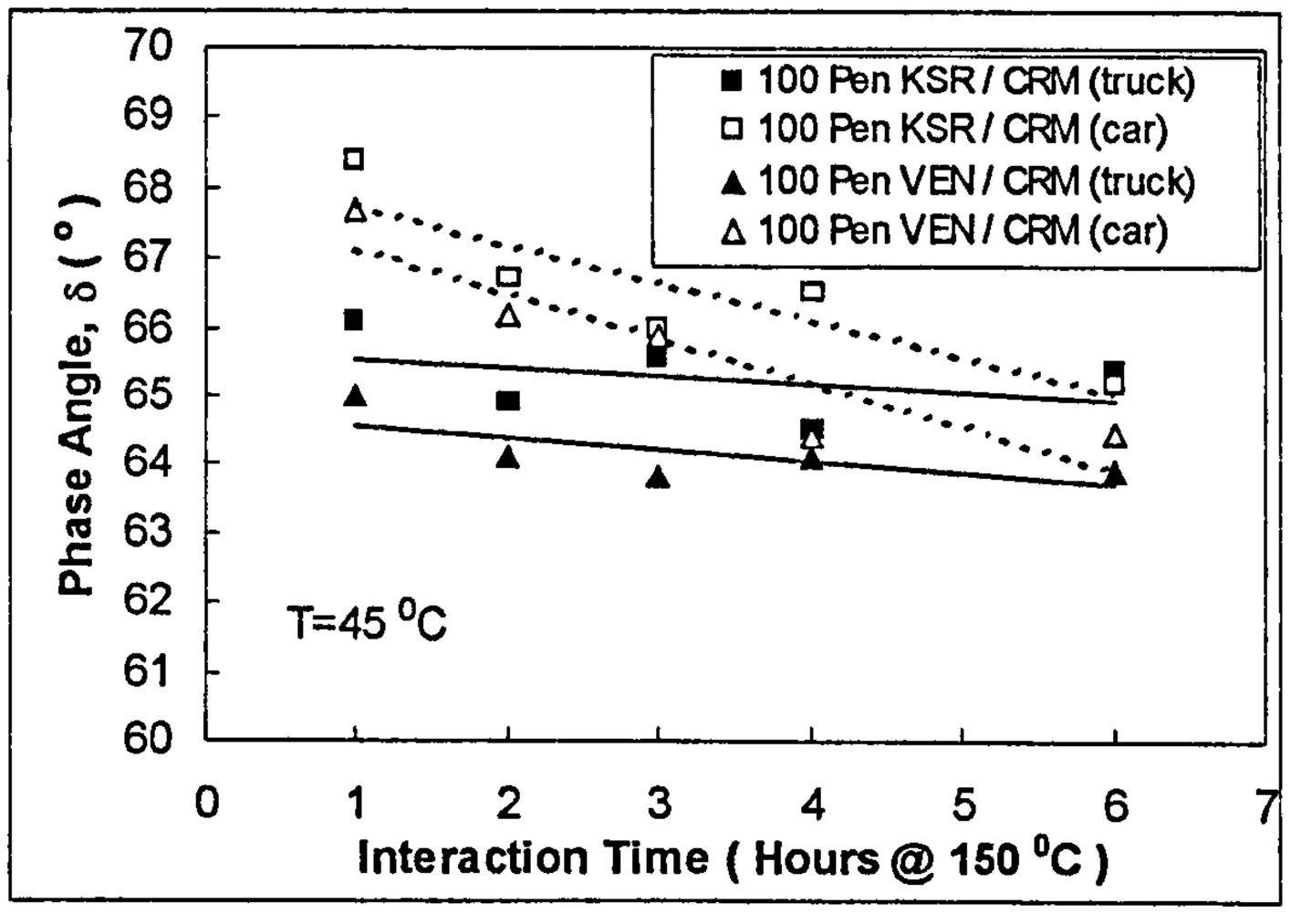

Figure 4.26 Evolution of δ with interaction time at 150 °C

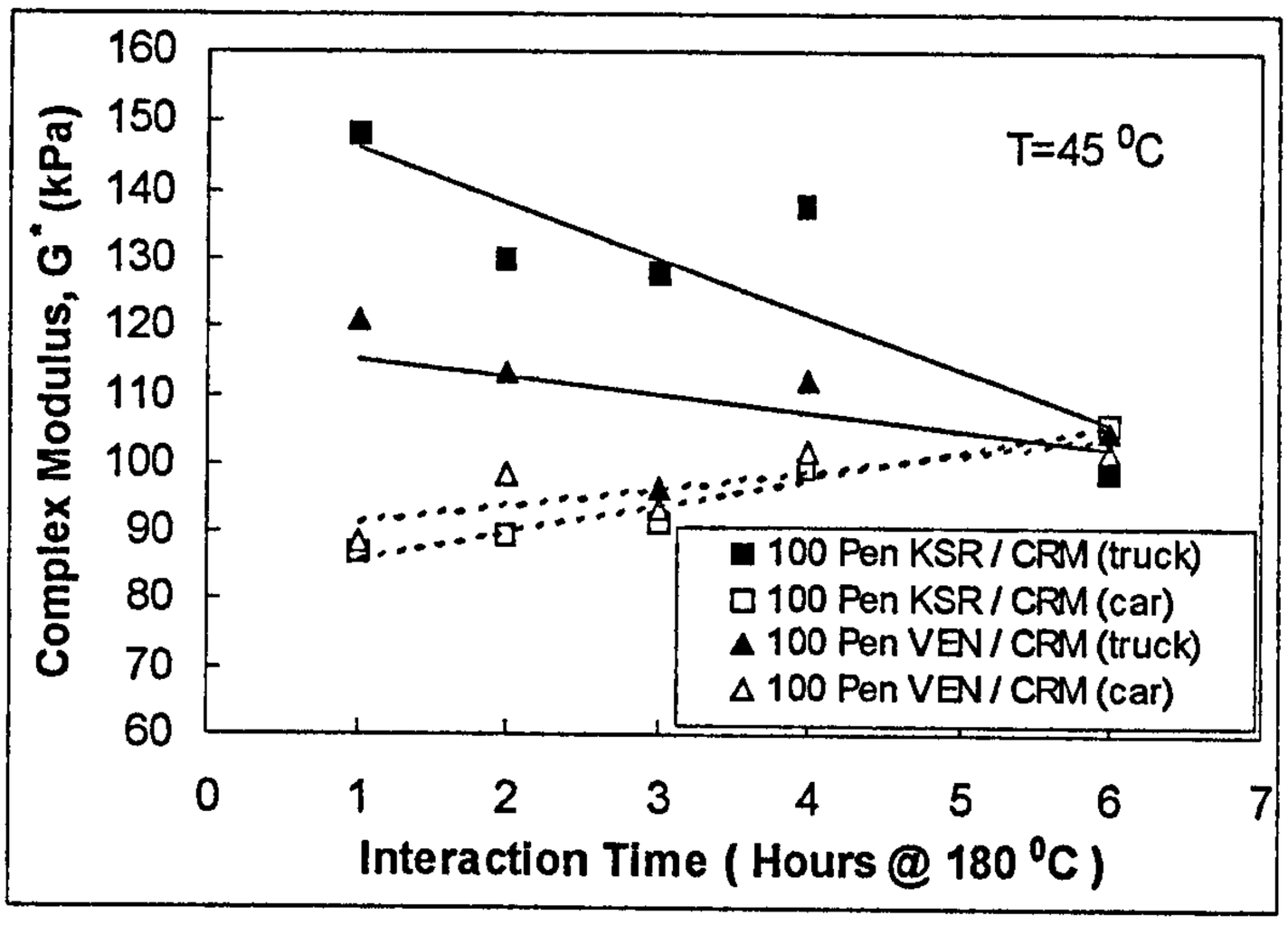

Figure 4.27 Evolution of G^* with interaction time at 180 °C

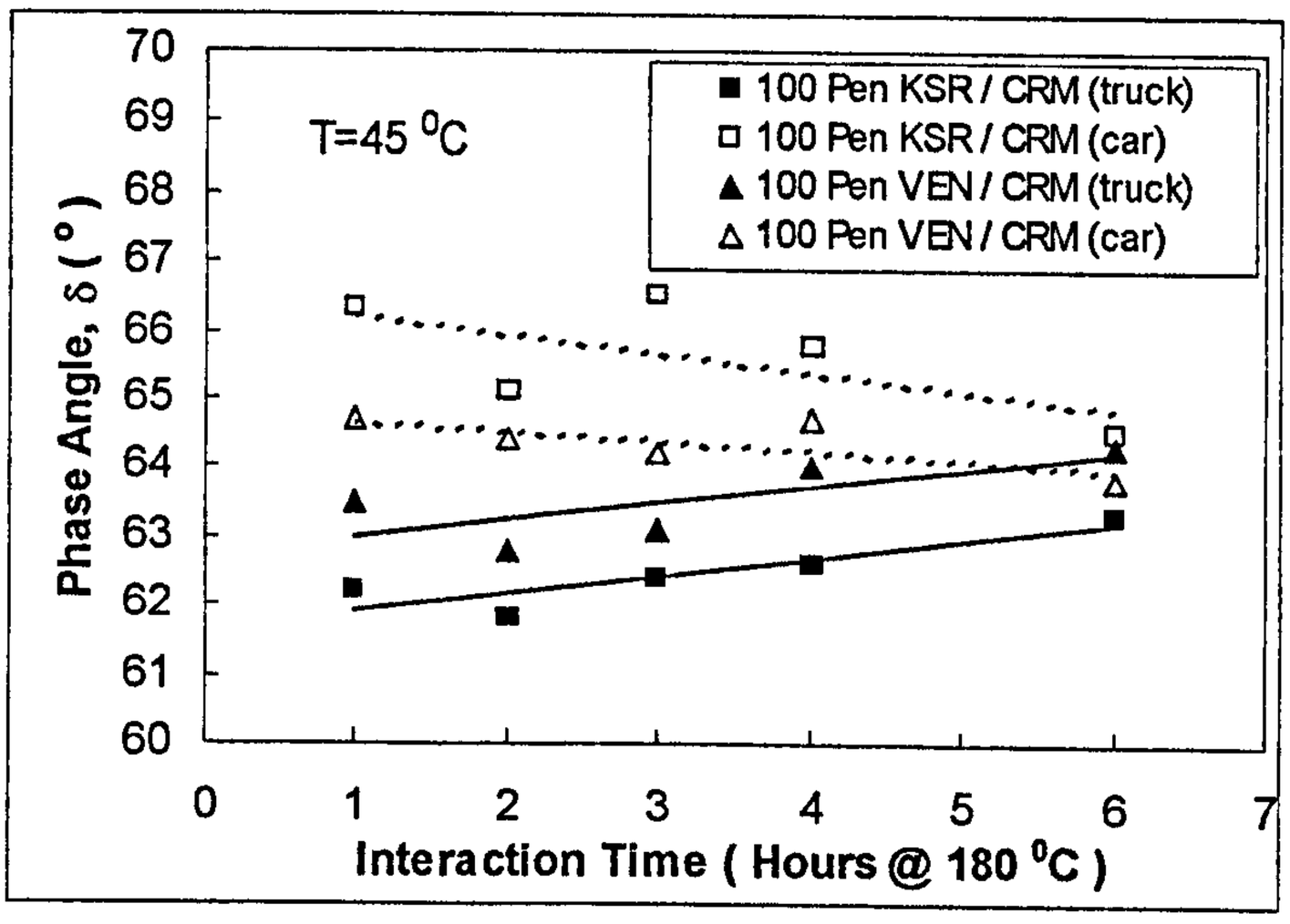

Figure 4.28 Evolution of δ with interaction time at 180 °C

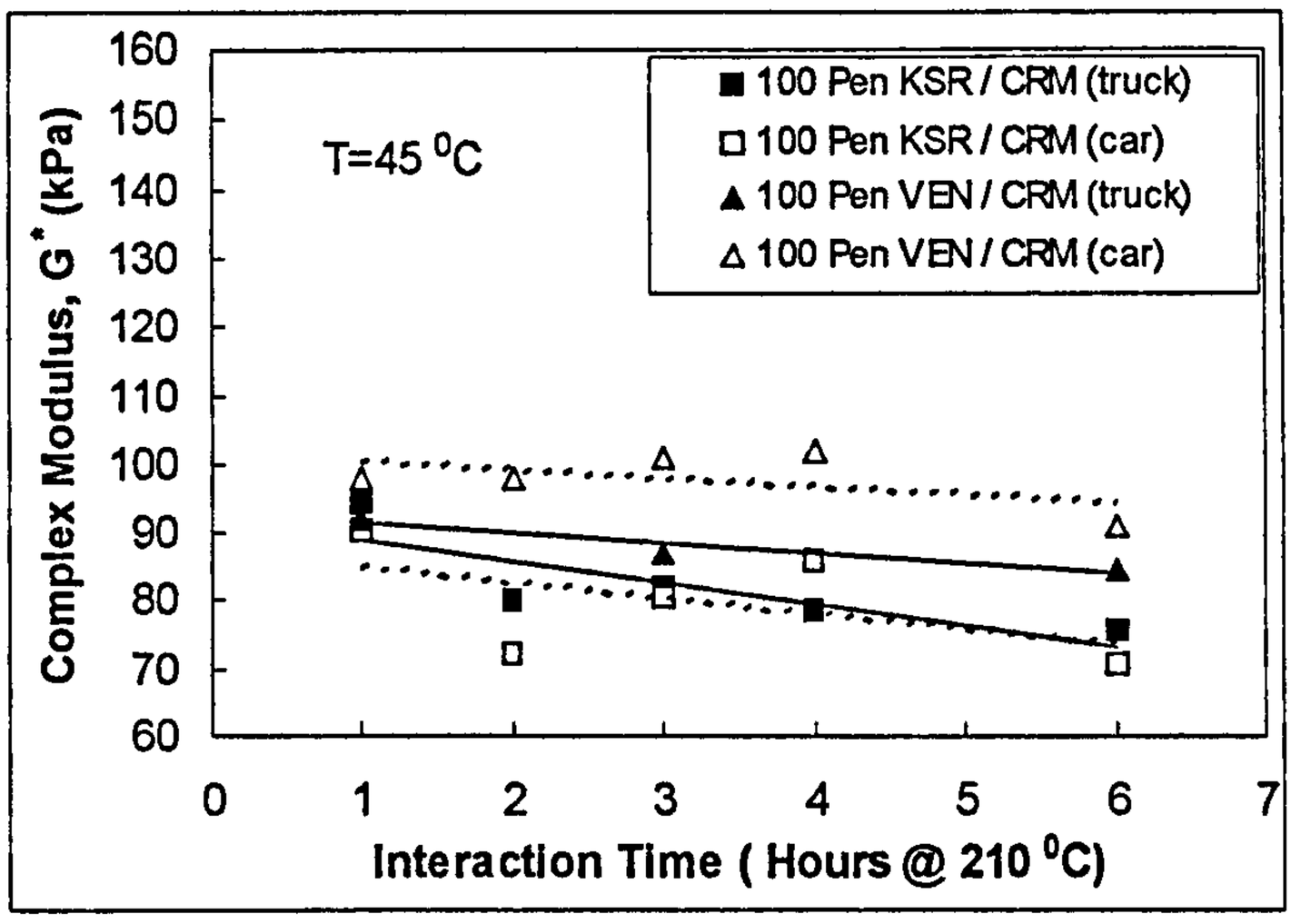

Figure 4.29 Evolution of G^* with interaction time at 210 °C

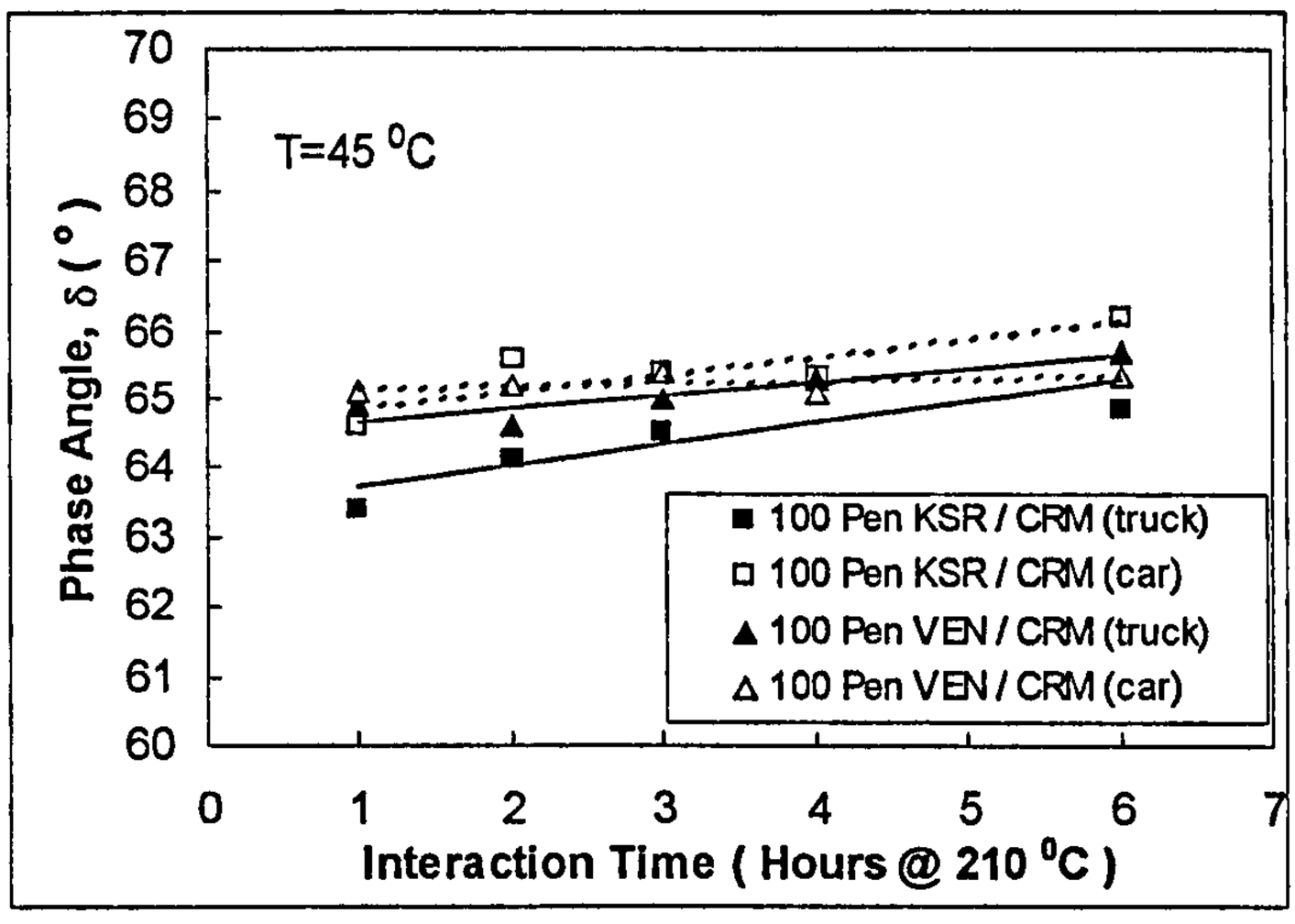

Figure 4.30 Evolution of δ with interaction time at 210 °C

4.4.4 Creep and creep recovery testing

The effects of the process variables on the properties of the CRM binders have so far been described in terms of the dynamic viscoelastic functions, complex stiffness modulus (G^*) and phase angle (δ). Creep and creep recovery tests performed in the DSR can also be used to characterise CRM binders produced under different conditions of temperature and time.

4.4.4.1 Theory and definitions

In a creep test a sample is subjected to a step in shear stress, σ, which is held constant for a specific time, t_c. The resulting shear strain, $\gamma(t)$, is then monitored by the DSR as a function of time, t, and the material's creep behaviour is characterised in terms of its compliance, $J(t)$ which is defined as the ratio of the strain to the imposed stress, thus,

$$J(t) = \frac{\gamma(t)}{\sigma} \tag{4.18}$$

The creep behaviour of a viscoelastic material can be modelled by the following general expression for times t less or equal to the creep time t_c,

$$J(t) = J_g + J_d \cdot \varphi(t) + t/\eta \tag{4.19}$$

where:

J_g is the instantaneous glassy or elastic compliance

J_d is the delayed elastic compliance

$\varphi(t)$ is the retardation function which satisfies,

$\varphi(t=0) = 0$ and $\varphi(t \to \infty) = 1$

t/η is the term representing the steady-state viscous flow

The behaviour of typical viscoelastic materials in a creep test is thus described by three components representing elastic, delayed elastic and viscous response respectively. In general, the short time behaviour is governed by the elastic terms whereas at long times the material exhibits steady viscous flow. For long times, where the steady-state viscous flow prevails, the viscosity can thus be estimated from the slope of the compliance curve.

When the applied stress, σ, is removed at some time t_c elastic recoil or creep recovery takes place. Using the superposition principle, the following expression for the compliance $J(t)$ at times t greater than the creep time t_c is given,

$$J(t) = J_d \cdot \left(\varphi(t) - \varphi(t - t_c)\right) + t_c/\eta \qquad (4.20)$$

For convenience, the compliance during recovery $J_R(t)$ is defined by:

$$J_R(t) = J(t + t_c) \qquad (4.21)$$

The recoverable compliance is given by,

$$J_0 = J_R(0) - J_R(\infty) \qquad (4.22)$$

Substituting Equations 4.19, 4.20 and 4.21 in 4.22,

$$J_0 = J_g + J_d \cdot \varphi(t_c) \qquad (4.23)$$

If the creep test is run for a sufficient time t_c, where the steady-state viscous flow prevails, then $\varphi(t_c) \to 1$ and the limiting recoverable compliance is $J_0 = J_g + J_d$.

The principle of a creep and creep recovery test is shown in **Figure 4.31**. It can be noted that the limiting recoverable compliance can be estimated either by running a creep test until steady viscous flow dominates and extrapolating back along the creep curve; or by following the creep test within a recovery one.

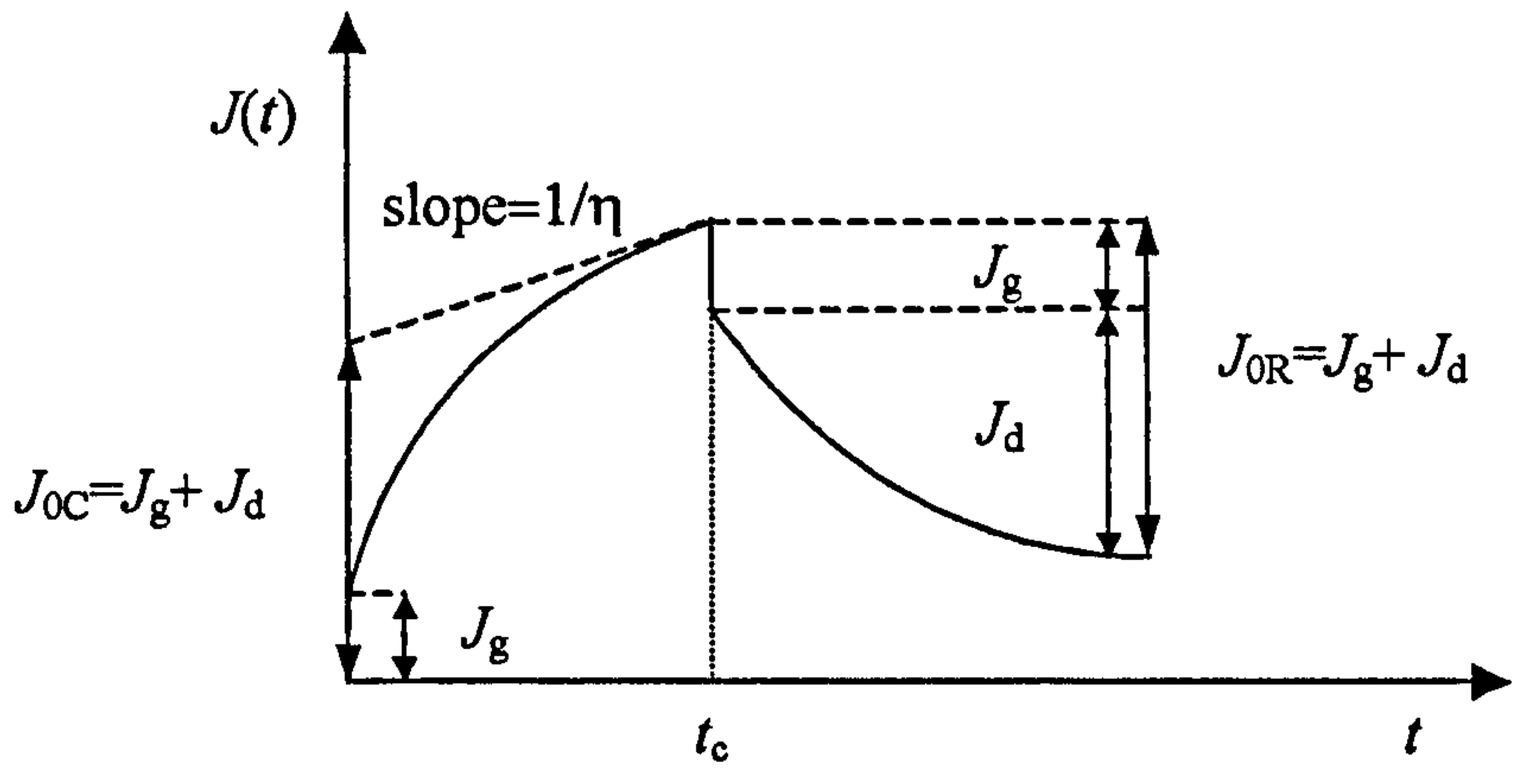

Figure 4.31 The principle of a creep and creep recovery test

4.4.4.2 Data processing

The creep and creep recovery models used in the Bohlin Rheology Data Processing Software are the multiple creep and multiple creep recovery.

The multiple creep model consists of a Maxwell element in series with 9 Kelvin elements arranged in series. This model has the following creep compliance function,

$$J(t) = J_g + \sum_{i=1}^{9} J_{di}(1 - e^{t/t_{ri}}) + t/\eta_0 \qquad (4.24)$$

where J_g is the glassy compliance, J_d represents the delayed compliances and η_0 is the zero shear viscosity, which is defined as the viscosity value in the lower shear rate range, known as the first Newtonian region (Barnes et al., 1989).

The multiple creep recovery model consists of a Maxwell element with 10 Kelvin elements in series and has the following recoverable compliance,

$$J_R(0) - J_R(t) = J_g + \sum_{i=1}^{10} J_{di}(1 - e^{t/t_{ri}}) \qquad (4.25)$$

where J_g and J_d are defined as before.

The retardation times, t_r in Equations 4.24 and 4.25 are generated automatically within the software and form a geometric progression spanning the time for the experiment. The software imposes the additional constraint that all the delayed compliances (J_d) are positive in the least squares algorithm.

During a creep/creep recovery test in the DSR the following parameters were recorded: temperature, creep time, creep angle, creep compliance, recovery time, recovery angle and recovery compliance. Furthermore, the rheological models used by the software permitted calculation of the creep shear rate ($\dot{\gamma}$), creep viscosity (η_0), the approach to steady flow, $\left(\frac{dLn(J)}{dLn(t)}\right)$, the recoverable compliance measured in creep (J_{0C}) and the recoverable compliance measured in the creep recovery test (J_{0R}).

4.4.4.3 Test parameters

As for dynamic tests, creep tests have to be conducted within the linear region wherein the binders' molecular structure is only slightly perturbed from its equilibrium state. Phillips and Robertus (1996) performed creep and recovery tests at 40 ^{0}C on conventional and polymer modified binders and found that linear behaviour was observed across a shear stress range from 30 to 100 Pa, whilst de L. Costello (1997) adopted a range of 50 to 100 Pa when testing conventional and elastomeric modified binders.

In this study, determination of the linear region was effected by overlapping creep compliance curves at successive increasing shear rates until divergence occurred. At a test temperature of 40 ^{0}C, a shear stress of 50 Pa was found to satisfy the requirements of linearity for all the materials investigated. Using the

test geometry of 25 mm parallel plates and 1 mm gap width, creep loading was applied for 600 seconds after which the load was removed and creep recovery was measured for another 600 seconds.

Steady-state viscous flow was reached within 600 seconds, considering a 5 % tolerance on the steady state condition, as seen by the values of $\frac{dLn(J)}{dLn(t)}$ which varied between 0.95 and 1 for all the materials investigated (see **Table 4.2** and **4.3**). Phillips and Robertus (1995) also reported that, for unmodified binders and incompatible bitumen/modifier combinations, a steady state is usually reached within minutes.

4.4.4.4 Results and discussions

Creep and creep recovery data for 100 Pen KSR and VEN binders modified with 10 % CRM from truck and car tyres under different interaction conditions of time and temperature are presented in **Tables 4.2** and **4.3**. Creep and creep recovery curves are also illustrated in **Figures 4.32 – 34**.

Viscosity values obtained from the slopes of the creep curves, once the steady state was reached, showed that the addition of CRM increased the viscosity of the binders. Furthermore, the 100 Pen KSR binder resulted in lower viscosities than the 100 Pen VEN after modification with CRM, in spite of its higher viscosity before modification. Also, shear rates decreased, as expected, as the viscosity of the binders increased on addition of CRM.

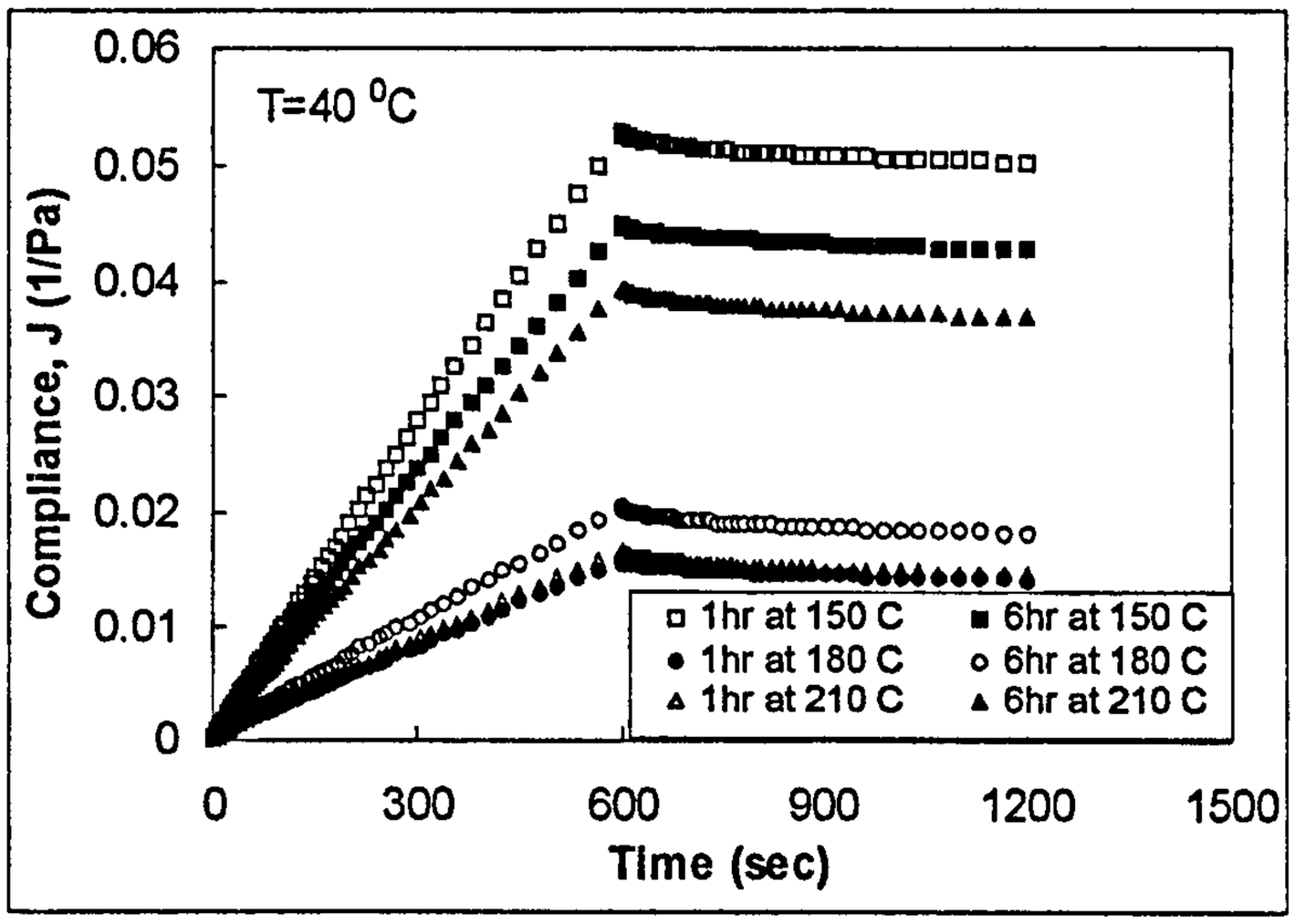

Figure 4.32 Creep and recovery for 100 Pen KSR modified with 10 % CRM from truck tyres

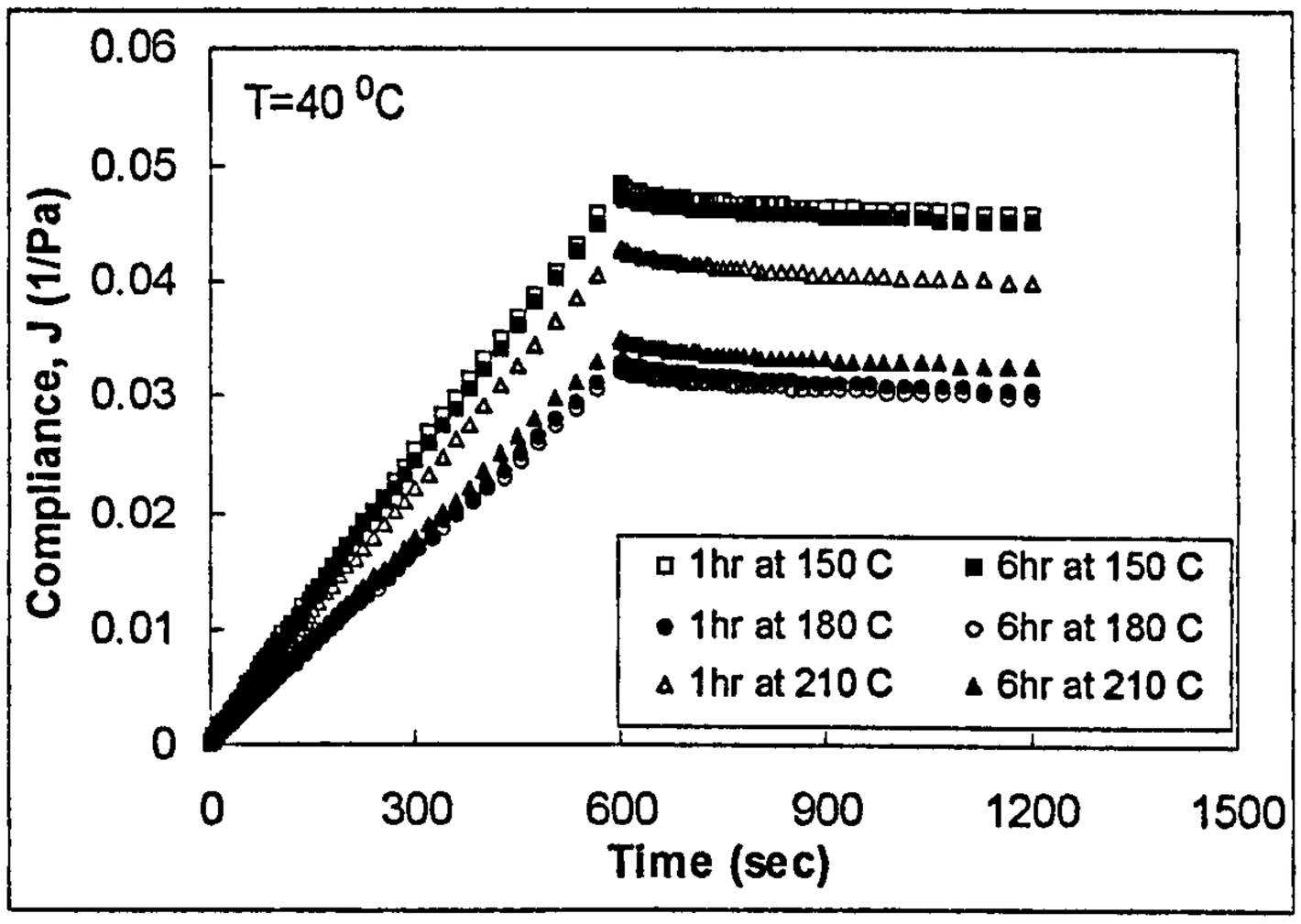

Figure 4.33 Creep and recovery for 100 Pen KSR modified with 10 % CRM from car tyres

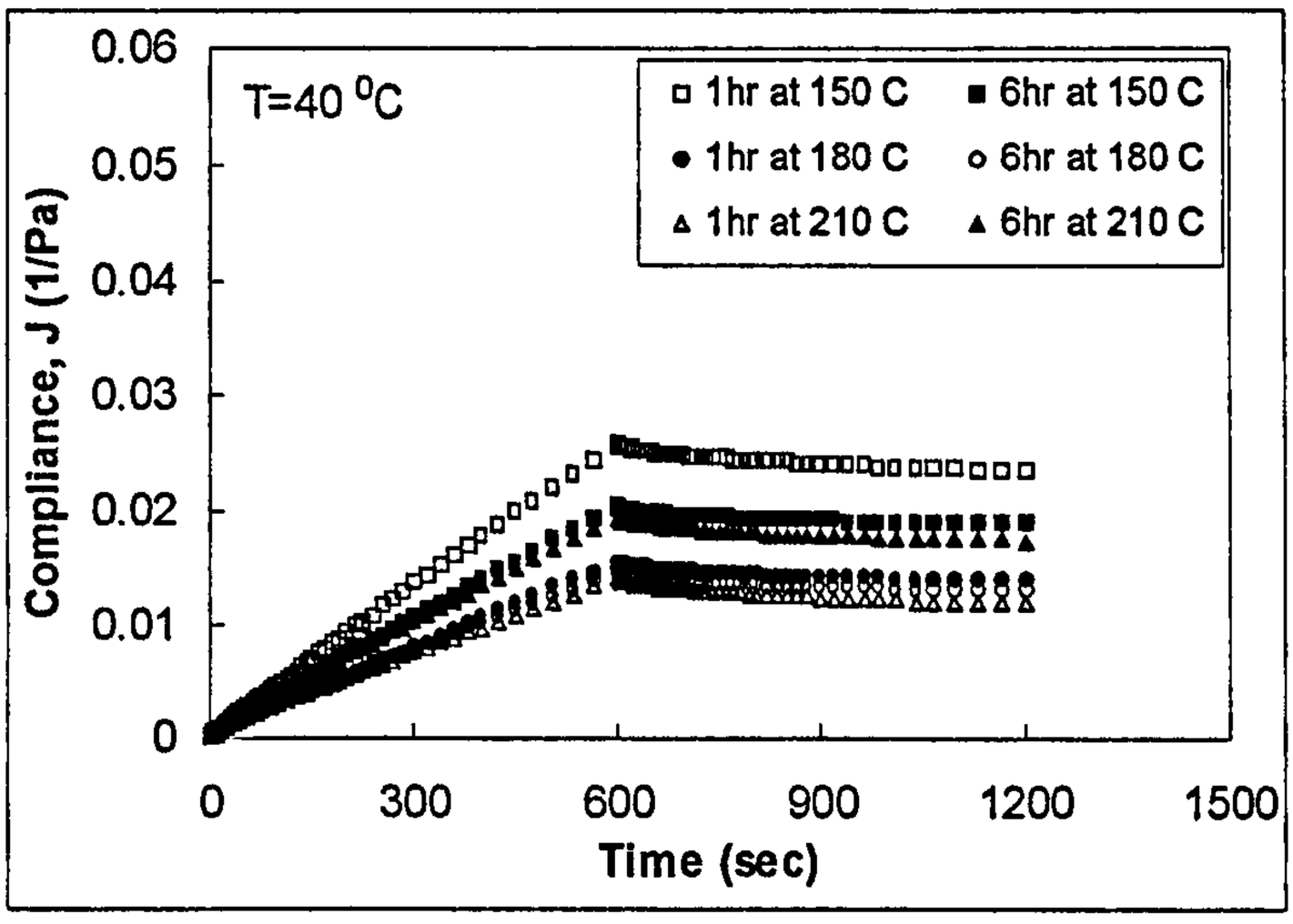

Figure 4.34 Creep and recovery for 100 Pen VEN modified with 10 % CRM from truck tyres

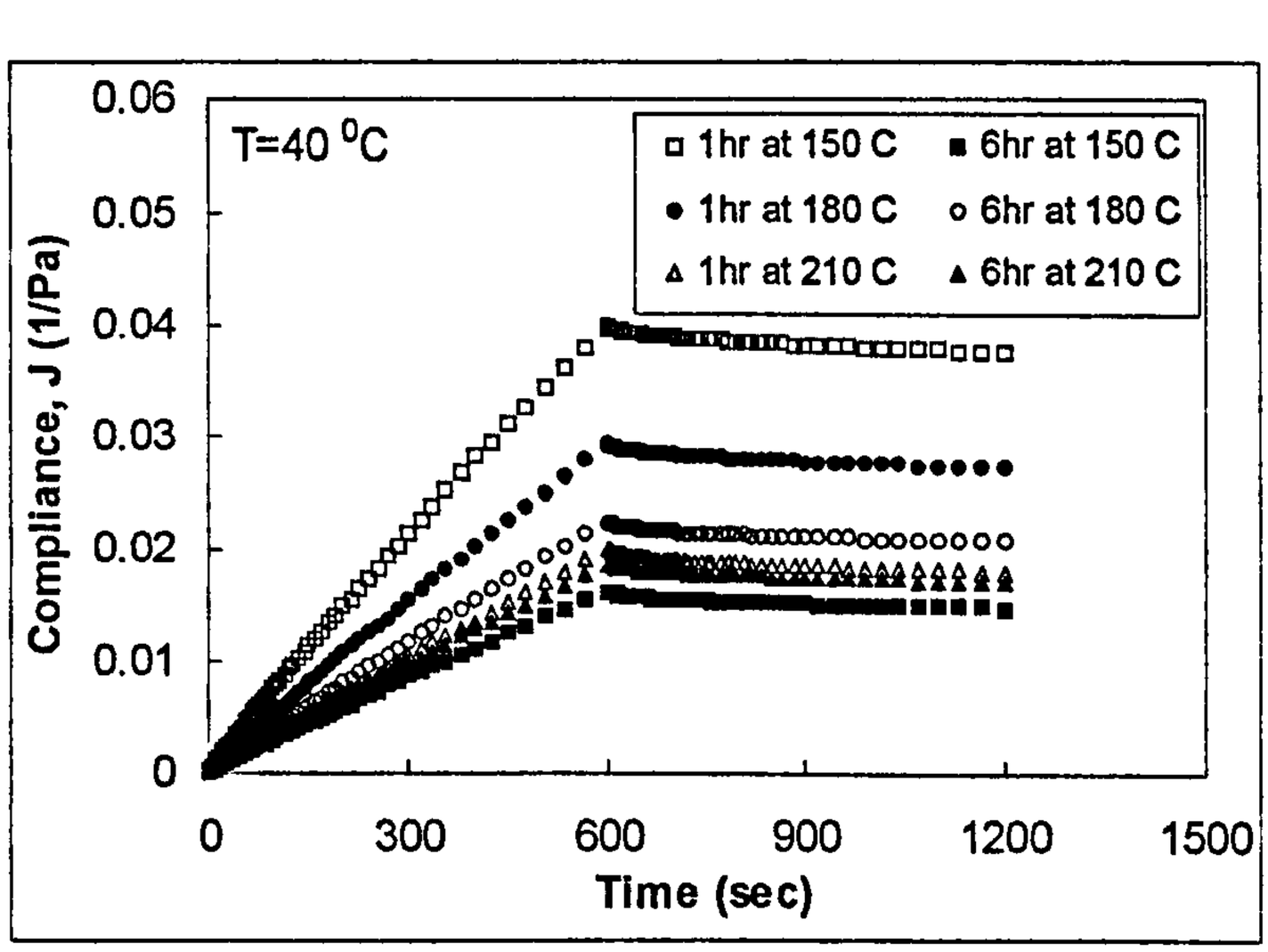

Figure 4.35 Creep and recovery for 100 Pen VEN modified with 10 % CRM from car tyres

Creep and creep recovery curves presented in **Figures 4.32 – 35** showed that creep compliances at 600 seconds loading (J_0) for the CRM binders produced at 150 ^{0}C were the highest, except for the VEN binder modified with CRM from car tyres after 6 h interaction. This indicated that the stiffness modulus ($S(t)$) of these binders was the lowest ($S(t)=1/J(t)$). Furthermore, J_0 decreased (S increased) when the mixing time was increased from 1 to 6 hours, as also observed during oscillatory testing.

CRM binders produced at 180 ^{0}C showed different behaviour depending on the type of CRM. The KSR binder modified with CRM from truck tyres exhibited an increase in J_0 with increasing mixing time from 1 to 6 hours, whilst the same binder modified with CRM from car tyres did not show appreciable differences. The VEN binder, on the other hand, showed that after modification with CRM from truck tyres J_0 remained practically the same, though a small decrease was observed for longer interaction times. For the same base binder but now modified with CRM from car tyres, J_0 clearly decreased for longer interaction times.

Modified binders produced at 210 ^{0}C showed that J_0 increased with mixing time when both base binders were modified by CRM from truck tyres, thus indicating a decrease in stiffness for longer interaction times at this high temperature. However, the opposite effect, i.e. a decrease in J_0, was found when they were modified by CRM from car tyres.

Of special interest, however, is not the compliance when a load is applied nor when delayed elastic deformation is still occurring, but the recoverable compliance after the applied load has been removed. This recoverable compliance is a measure of the elasticity in a material.

The recoverable compliance (J_0), as explained earlier, can be obtained from creep tests or from creep followed by recovery tests. The recoverable compliance in a creep test is calculated by extrapolating back along the creep curve when in steady viscous flow and it is denoted as J_{0C}. This method is fine for estimating

J_0 but is prone to error since it generally involves extrapolating back from a large number to obtain a small number. A far better method of obtaining J_0 is to measure it directly by the creep recovery test. After the steady-state viscous flow is reached and the stress is removed the material will recoil due only to elasticity. By directly measuring this recoil, the recoverable compliance, J_{0R}, can be determined. Ideally, J_{0C} and J_{0R} should be the same but J_{0R} is, in general, more accurate.

Recoverable compliances calculated from creep tests, J_{0C}, from recovery tests, J_{0R}, and creep recovery values (%) obtained from creep recovery tests are presented in **Tables 4.2** and **4.3**. The first point to notice is that the conventional binders showed practically no recovery. CRM binders, however, showed between 4 and 16 % recovery depending on materials and production conditions.

In general, binders modified with CRM from car tyres showed less recovery than those modified with CRM from truck tyres, when produced under the same conditions of temperature and time. This indicates the greater elasticity of the latter binders. Furthermore, modified binders based on the VEN bitumen exhibited higher recovery than the ones based on the KSR bitumen. This might be attributed to the higher level of interaction between the VEN binder and the rubber particles, which enhances the cross-linking between the rubber and the bitumen, resulting in a more elastic binder.

The effect of interaction temperature on recovery is seen as an increase in recovery with increasing interaction temperature when comparing binders after mixing for one hour. The effect of interaction time on recovery is, however, dependent on the interaction temperature. For all the binders investigated, recovery decreased after 6 hours interaction at the highest interaction temperature (210 ^{0}C). At interaction temperatures of 150 and 180 ^{0}C, the modified binders did not show much change in recovery with interaction time, except for the VEN binder modified with car-tyre rubber at 150 ^{0}C.

CRM source	Mixing temp. (^{0}C)	Mixing time (h)	Steady flow	Viscosity (Pa.s)	Shear rate (s^{-1})	J_C (1/Pa)	J_{OC} (1/Pa)	J_R (1/Pa)	J_{OR} (1/Pa)	Recovery (%)
Neat binder			1.03	6.13E+03	8.16E-03	9.49E-02	-3.22E-03	9.41E-02	7.90E-04	**0.83**
Truck	150	1	0.95	1.19E+04	4.19E-03	5.29E-02	2.74E-04	5.04E-02	2.51E-03	**4.75**
Truck	150	6	0.94	1.43E+04	3.57E-03	4.50E-02	2.82E-04	4.29E-02	2.09E-03	**4.64**
Truck	180	1	0.96	3.93E+04	1.27E-03	1.58E-02	6.39E-04	1.42E-02	1.60E-03	**10.12**
Truck	180	6				2.05E-02		1.83E-02		**10.57**
Truck	210	1	0.95	3.79E+04	1.32E-03	1.67E-02	9.21E-04	1.47E-02	2.01E-03	**12.07**
Truck	210	6	0.97	1.56E+04	3.20E-03	3.95E-02	1.27E-04	3.71E-02	2.50E-03	**6.32**
Car	150	1	0.95	1.39E+04	3.80E-03	4.85E-02	2.57E-04	4.60E-02	2.49E-03	**5.14**
Car	150	6	0.97	1.33E+04	3.84E-03	4.75E-02	1.63E-04	4.53E-02	2.22E-03	**4.66**
Car	180	1	0.98	1.84E+04	2.07E-03	3.31E-02	5.08E-04	3.07E-02	2.40E-03	**7.25**
Car	180	6	0.98	1.89E+04	2.64E-03	3.24E-02	6.93E-04	3.02E-02	2.20E-03	**6.79**
Car	210	1	0.95	2.33E+04	2.14E-03	2.71E-02	1.38E-04	2.47E-02	2.45E-03	**9.03**
Car	210	6	0.96	2.09E+04	2.39E-03	3.00E-02	1.37E-04	2.78E-02	2.16E-03	**7.21**

Table 4.2 Creep and recovery data for 100 Pen KSR modified with CRM

CRM source	Mixing temp. (^{0}C)	Mixing time (h)	Steady flow	Viscosity (Pa.s)	Shear rate (s^{-1})	J_C (1/Pa)	J_{OC} (1/Pa)	J_R (1/Pa)	J_{OR} (1/Pa)	Recovery (%)
Neat binder			1.01	5.22E+03	9.96E-03	1.18E-01	-1.36E-04	1.17E-01	7.60E-04	**0.64**
Truck	150	1	0.96	2.48E+04	2.02E-03	2.58E-02	1.65E-04	2.35E-02	2.26E-03	**8.78**
Truck	150	6	0.96	3.14E+04	1.59E-03	2.04E-02	1.36E-04	1.90E-02	1.46E-03	**7.13**
Truck	180	1	0.95	4.01E+04	1.25E-03	1.57E-02	7.74E-04	1.40E-02	1.62E-03	**10.34**
Truck	180	6	0.97	4.43E+04	1.13E-03	1.49E-02	1.29E-04	1.32E-02	1.67E-03	**11.25**
Truck	210	1	0.95	4.49E+04	1.11E-03	1.41E-02	8.15E-04	1.19E-02	2.23E-03	**15.74**
Truck	210	6	0.95	3.25E+04	1.56E-03	1.95E-02	1.10E-04	1.75E-02	2.08E-03	**10.30**
Car	150	1	0.96	1.64E+04	3.05E-03	4.00E-02	3.53E-04	3.77E-02	2.34E-03	**6.85**
Car	150	6	0.95	3.88E+04	1.28E-03	1.63E-02	8.88E-04	1.48E-02	1.48E-03	**9.10**
Car	180	1	0.95	2.15E+04	2.32E-03	2.94E-02	1.57E-04	2.73E-02	2.11E-03	**7.18**
Car	180	6	0.95	2.84E+04	1.76E-03	2.25E-02	1.46E-04	2.08E-02	1.78E-03	**7.56**
Car	210	1	0.97	3.80E+04	1.62E-03	2.01E-02	6.10E-04	1.80E-02	2.07E-03	**10.33**
Car	210	6	0.95	3.44E+04	1.45E-03	1.86E-02	1.19E-04	1.71E-02	1.56E-03	**8.38**

Table 4.3 Creep and recovery data for 100 Pen VEN modified with CRM

Chapter 5

MIX DESIGN AND EVALUATION

Chapter 5

MIX DESIGN AND EVALUATION

This chapter presents a rational method for the design and assessment of bituminous mixtures. A volumetric mix design approach, based on the volumetric control of the internal void structure of dry aggregate blends, has been used for the design of close-graded wearing courses. The selected mixes, which include a conventional and two crumb-rubber modified mixtures, have been evaluated in terms of stiffness, moisture sensitivity, permanent deformation and surface characteristics.

5.1 MIX DESIGN PROCEDURES

5.1.1 Mix requirements

The objective of mix design is to produce an economical material, making used of local resources that meet the required level of pavement performance. Pavement performance is commonly assessed in terms of permanent deformation, fatigue cracking, and low-temperature cracking. Furthermore, performance requirements are dictated by factors such us the volume of traffic, the climate and the structural section of the pavement.

Thus, bituminous mixes have to fulfil a wide range of requirements for today's traffic. These requirements can be summarised as in **Table 5.1**.

5.1.2 Recipe specifications

Recipe specifications provide a description of a particular bituminous mix in terms of the aggregate type and grading, and the composition of each of the components, together with the method of production, laying and compaction. Recipe specifications are relatively simple to use and are applicable to all types of mixes. They are based on experience of known compositions, which have performed successfully in practice.

The recipe approach to mix design is still the basis of most specifications, particularly in the UK. The vast majority of British Standard Specifications for bituminous mixes are of the recipe type and apply nationwide.

Recipe specifications have, however, a number of limitations, as follows:

- The conditions of traffic, climate, and so on, to which the mix is to be subjected, may not be the same as those existing when the experience, on which the recipe is based, was obtained.

- Component materials may have different properties. These differences may require modifications to the recipe but there is no means of assessing what these modifications should be.

- The aggregate grading curve that is the basis of recipe specifications does not take into account the aggregate properties, shape, texture and packing characteristics.

- Recipe specifications are restrictive towards new materials, since they cannot be used until experience has been sufficient to allow a specification to be written.

Mix requirement	Related property	Aggregate		Bitumen	
		Grading	Shape	Grade	Content
Stability	Permanent deformation	Dense	Harsh	Hard	Low
Flexibility	Fatigue cracking	Dense	/	Soft	High
	Low-temperature cracking				
Durability	Moisture damage	Dense	/	/	High
	Aging				
Workability	Mix viscosity	/	Smooth	Soft	High
Safety	Skid resistance	/	Harsh	/	Low
	Fretting and ravelling		/	Soft	High
Impermeability	Void content	Dense	/	/	High
Structural strength	Stiffness	Dense	/	Hard	Low

Table 5.1 Summary of mix requirements and compositions required

5.1.3 The Asphalt Institute design method (TAI, 1988)

The Asphalt Institute method is the most widely used procedure for the design of continuously graded mixes and makes use of the Marshall test (BSI, 1990**a**) as a design criterion.

The aim is to produce a dense mix by selecting and appropriate aggregate grading. The gradings used for continuously graded mixtures are based on maximising the density of the aggregate structure by following a gradation curve developed by Fuller and Thompson (1907), as follows:

$$P = 100\left(\frac{d}{D}\right)^n \tag{5.1}$$

where:

P = percentage passing a sieve size d

d = sieve size

D = maximum aggregate size

n = grading exponent ($0 < n < 1$)

Nijboer (1948) showed that the densest mixes were obtained with n between 0.4 and 0.5. The grading exponent is usually about 0.45 for maximum density but for many values of D, the filler contents given by Equation 5.1 are generally impractical.

Cooper et al. (1985) proposed a modified version of the Fuller curve, given by:

$$P = \frac{(100 - F)(d^n - 0.075^n)}{(D^n - 0.075^n)} + F \tag{5.2}$$

where:

F = filler content

When the values of the grading exponent, n, are between 0.5 and 0.7, the grading will normally result in a dense aggregate blend with an acceptable void content.

Some limitations of the Marshall method of mix design can be associated to the test conditions, temperature (60 ^{0}C) and loading rate (50 mm/min) which do not represent real in-situ conditions. Furthermore, the method attempts to relate material performance with empirical properties, such us Marshall stability and flow, but the method cannot ensure that the designed mix will meet the specific requirements.

5.1.4 The Superpave mix design method

The Superpave (Superior Performing Pavement) mix design method was developed as part of the Strategic Highway Research Program (SHRP) during 1987-1993. The Superpave Mix Design Manual for New Constructions and Overlays (Cominsky et al., 1994) facilitates selecting and combining asphalt binder, aggregate, and any necessary modifier to achieve the required level of pavement performance.

The main features of the Superpave mix design method can be summarised as follows:

- The criteria for selection of a mix design are based upon performance-based (directly related to performance) and performance-related (indirectly related to performance) properties.

- Performance-based specifications are based on the predicted performance of the pavement built within the paving mix under design.

- The method explicitly considers the interaction of pavement structure, climate and traffic with the paving mix.

- It directly addresses the reduction and control of permanent deformation, fatigue cracking, and low-temperature cracking.

- It considers the effects of aging and moisture sensitivity.

The selection of the aggregate structure is based on mixture volumetric properties, predominately voids in mineral aggregate (*VMA*) and the Superpave gradation specification. As an example, for a 12.5 mm nominal maximum size, minimum *VMA* is 14 % and target void content is 4 %. The Superpave gradation specification, control points and boundaries of aggregate restricted zone, are given in **Figure 5.1**. Any trial blend gradation has to pass between the control points established on the five sieves. In addition, it has to be outside of the area bounded by the limits set for the restricted zone.

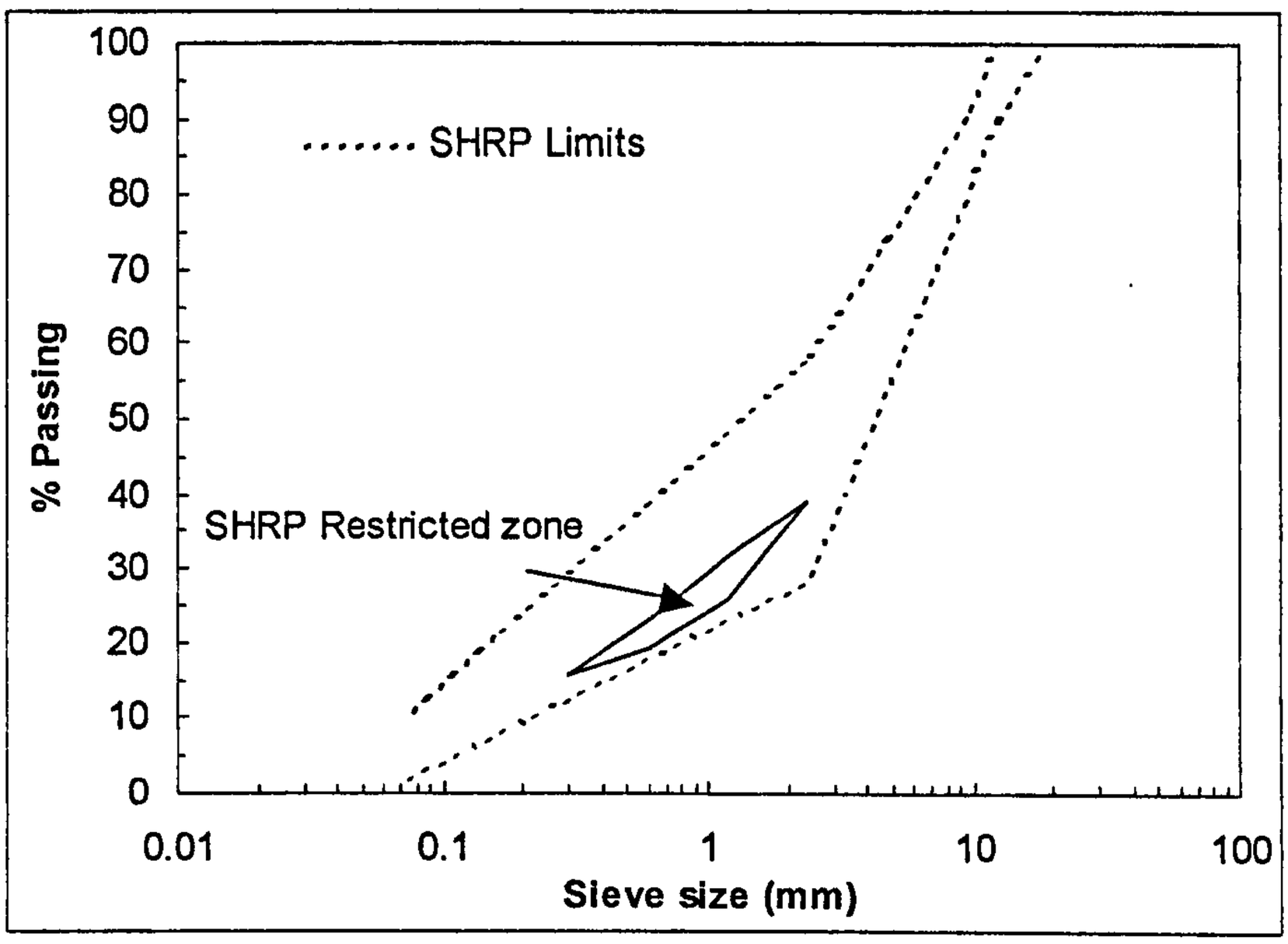

Figure 5.1 Superpave aggregate specification 12.5 mm nominal size

The Superpave mix design method uses gyratory compaction as compaction method, and a set of performance-based test methods for paving mixes. The methods and procedures, the equipment required and their related property or distress are presented in **Table 5.2.**

Test Equipment	Method or Procedure	Related Property / Distress
SHRP gyratory compactor	Gyratory compaction	Void content
Environmental conditioning system	Moisture sensitivity	Durability
Forced draft oven	Short and long-term aging	Aging
Shear test	Frequency sweep at constant height	Permanent deformation and fatigue cracking
Shear test	Simple shear at constant height	Permanent deformation and fatigue cracking
Shear test	Uniaxial strain	Permanent deformation
Shear test	Volumetric (hydrostatic)	Permanent deformation
Shear test	Repeated shear at constant stress ratio	Permanent deformation
Indirect tensile test	Indirect tensile creep	Low-temperature cracking
Indirect tensile test	Indirect tensile strength	Low-temperature cracking and fatigue cracking

Table 5.2 Superpave mix design tests

5.2 VOLUMETRIC APPROACH TO THE DESIGN OF CLOSE-GRADED WEARING COURSES

5.2.1 Close-graded mixtures

Continuously-graded materials in the UK are normally termed coated macadams and their composition is specified in BS 4987, Part 1 (BSI, 2001). They are commonly used for roadbases and basecourses and for wearing courses in minor roads.

Increasing the mass proportion of finer fractions (< 2.36 mm) within a continuously-grade bituminous macadam reduces the voids within the aggregate structure and, therefore, closes up the mixture. These materials are called close-graded mixtures. More continuous gradings are obtained reducing furthermore the coarse aggregate fraction and increasing the fine aggregate and filler proportion, which results in denser mixtures. Close-graded wearing course materials used in the UK are specified in BS 4987, Part 1 (BSI, 2001). Typical materials include 14 and 10 mm size close-graded wearing courses, formerly known as dense wearing course macadams.

5.2.2 Aggregate grading design

Aggregate gradings currently used, are mainly based on specifications, such us BS 4987 and Superpave grading specifications, which do not deal with the packing characteristics of the aggregates. The aggregate grading curve that is the basis of recipe specifications does not take into account aggregate properties, shape and texture that will affect the packing behaviour of the aggregate blend. Thus, materials with the same or similar grading curves may result in different volumetric mix proportions, which will affect their engineering properties and in-situ performance.

When designing a continuously graded aggregate structure the aim is to produce blends that give maximum density or minimum void content. These can be done by selecting a gradation curve developed by Fuller and Thompson (1907), using Equation 5.1 or its modified version (Cooper et al., 1985), using Equation 5.2.

More recently, an analytical mix design procedure based on a volumetric approach has been developed by the Belgian Road Research Centre (Francken et al., 2003). The procedure is aided by a software package called PRADO (PRogramme for Asphalt mix Design and Optimisation) and was initially developed for continuously graded materials though it has been generalised for a wide variety of bituminous mixtures.

The method proposed here for the design of close-graded bituminous mixtures is based on the examination of the compacted aggregate structure. Work by Lees (1970) demonstrated how dense gradings could be developed by sequentially blending binary aggregate combinations to design a material that would offer high performance characteristics when in service. The method determined the require binder content through the assessment of the aggregate packing characteristics.

When two aggregate of different sizes are blended, there is an optimum proportion of the two components, which result in minimum voids in the aggregate blend and this minimum value is lower than the voids of the respective single components (Furnas, 1931). If a finer fraction is added incrementally to a coarser fraction, the voids are reduced up to a point where the finer fraction no longer finds room in the void spaces of the larger aggregate fraction. If the amount of the fine fraction increases further, the void content of the finer fraction becomes dominant.

In the design of a multi-component aggregate blend the first step is to determine the proportions of the binary blend of the coarsest fractions to achieve minimum voids. For the next step, the blend at the proportions corresponding to minimum voids is selected as the new coarse component into which the next smaller fraction is added incrementally to result in minimum voids. This sequence continues for all the coarse aggregate fractions. Finally, the finer fraction is added incrementally to the new coarse fraction obtained as before. This method enables the selection of aggregate gradings with any desired voids when the void content in the coarse aggregate matrix is at its minimum (Cabrera and Hamzah, 1996). Furthermore, the method is applicable to the design of close-graded

aggregate structures where the finer fraction fills some of the voids in a dense coarse aggregate skeleton closing-up the aggregate blend.

5.2.3 Constituent materials

5.2.3.1 · Aggregates

Aggregates are classified in three categories depending upon the size fraction. The fraction retained on 2.36 mm, passing 2.36 mm retained 75 μm and passing 75 μm sieves are generally referred to as coarse aggregate, fine aggregate and filler respectively. Most aggregates are natural, either crushed rock or gravel for coarse aggregate and either crush rock fines or natural sand for fine aggregate, but artificial aggregates are sometimes used. Commonly used fillers include limestone dust, Portland cement and hydrated lime.

The aggregates used in this study were supplied by Tarmac and were sourced from Bayston Hill Quarry in Shropshire. The aggregate type was gritstone, sandstone with coarse and usually angular grains including fragmental volcanic rocks. The filler was limestone, a sedimentary rock consisting predominantly of calcium carbonate. Aggregate sizes used in the study were 14, 10 and 6 mm (coarse), 3 mm to dust (fine), and filler. Specific gravities were 2.710 for the coarse aggregates, 2.696 for the fine aggregates and 2.721 for the filler.

5.2.3.2 Binders

The binder used in the mix design was a 100 Pen from Venezuelan origin supplied by Shell Bitumen. This binder was modified by adding 10% by weight Crumb Rubber Modifier (CRM) from two sources, truck tyres and car tyres. The CRM was supplied by J. Allcock & Sons LTD (Manchester) and was produced by ambient grinding. CRM maximum size was 600 μm.

Crumb-rubber modified binders were manufactured in the laboratory using a Silverson mixer under controlled temperature, mixing time and shear rate conditions. Mixing conditions selected were: temperature 180 ^{0}C, mixing time 1 hour and shear rate 2000 rpm. Two different modified binders, namely CRM binder 1 and CRM binder 2, were manufactured in this way. CRM binder 1 was

produced by adding 10 %wt CRM from truck tyres whereas CRM binder 2 was produced by adding the same percentage of CRM but from car tyres. Differences between these two crumb-rubber modified binders were discussed previously (see Chapters 3 and 4).

The relevant properties of the binders used in the mix design are presented in **Table 5.2**. They include Penetration, Softening Point and Brookfield viscosity values.

Property		Binder		
		100 Pen	**CRM binder 1**	**CRM binder 2**
Penetration (dmm) - BSI, 2000a		87	62	74
Softening Point (^{0}C) - BSI, 2000b		42.5	49.5	49.5
Brookfield viscosity (Poise)	130 ^{0}C	4.95	16.02	12.60
	150 ^{0}C	1.86	6.04	5.20
	170 ^{0}C	0.84	2.52	2.00

Table 5.3 Properties of the binders used in mix design

5.2.4 Volumetric design procedure: an overview

The first step in the mix design procedure is the selection of the aggregate grading by determining the voidage profile using the aggregate sources and sizes proposed for a mixture design. A voidage profile is the graphic representation of the change in void content when an aggregate fraction size is added to a different aggregate fraction size. When blending two different aggregate fraction sizes, the smaller fraction size will fit within the void spaces within the skeleton of the larger fraction size. The limit to the blend proportion of the smaller fraction size able to fit within the void space of the larger fraction is defined as the pessimum point. This point represents the densest aggregate blend or minimum void content.

From the voidage profile different aggregate blends are then selected based on the voids in the dry aggregate blend and on the proportions of coarse and fine

aggregates. After estimation of the bitumen content for a target mixture void content, bitumen-aggregate trials on the selected aggregate blends are conducted, and the mix design parameters are determined. Mix design parameters include compacted density of the mix (*CDM*), voids in mineral aggregate (*VMA*), voids in the mix (*VIM*) and mix stiffness (*ITSM*). Finally, binder content and bitumen-aggregate mix are selected based on the mix design parameters.

For the design of a 14 mm close-graded mixture the methodology adopted can be summarised as follows:

1. Determination of the voidage profile when the 10 mm fraction size is added to the 14 mm fraction size, and selection of the blend proportions at the pessimum.

2. Determination of the voidage profile when the 6 mm fraction size is added to the 14/10 mm fraction size at the pessimum, and selection of the blend proportions at the pessimum.

3. Determination of the voidage profile when the 3 mm fraction size is added to the 14/10/6 mm fraction size at the pessimum.

4. Preliminary blend selection (four blends).

5. Determination of voidage profiles for the selected aggregate blends after filler at different proportions is added.

6. Blend selection (two blends).

7. Estimation of binder demand.

8. Bitumen-aggregate mixes trials on selected aggregate blends.

9. Determination of the mix design parameters, *CDM*, *VMA*, *VIM* and *ITSM*.

10. Optimum binder content and mix selection.

5.2.5 Dry aggregate voidage profiles

5.2.5.1 Test procedure

The method for the determination of the void content in an aggregate blend is based on the knowledge of the compacted density of the aggregate blend and its specific gravity. Cylindrical moulds were used to determine the compacted density of the mixed aggregates. Aggregate blends of different proportions were prepared and placed in moulds. The blends were then compacted by a vibrating hammer. Finally, the compacted density of the mixed aggregate was obtained knowing the weight of the blend and the volume after compaction. **Appendix B** illustrates the full procedure for the determination of the void content in a dry aggregate blend.

5.2.5.2 Compaction of dry aggregate blends

To evaluate the degree of compaction a test sample of 14/10 mm aggregate blend was compacted for different times, and the dry density (*CDMA*) was calculated following the procedure explained in the previous section. **Figure 5.2** shows that, initially, the dry density increased rapidly up to about 20 seconds approximately. For longer compaction times, the dry density continued to increase but at a slower rate.

Aggregate crushing during compaction was assessed by sieving test samples of size 14/10 mm aggregate through a 2.36 mm sieve after different compaction times and determining the amount of material which passes as percentage of the original mass of the sample (BSI, 1990b). **Figure 5.2** shows the percentage passing 2.36 mm sieve after different compaction times. Sieve analysis results are presented in **Appendix C**. It was observed that crushing increased rapidly during the early stages of compaction, and then continued to increase but at a lower constant rate.

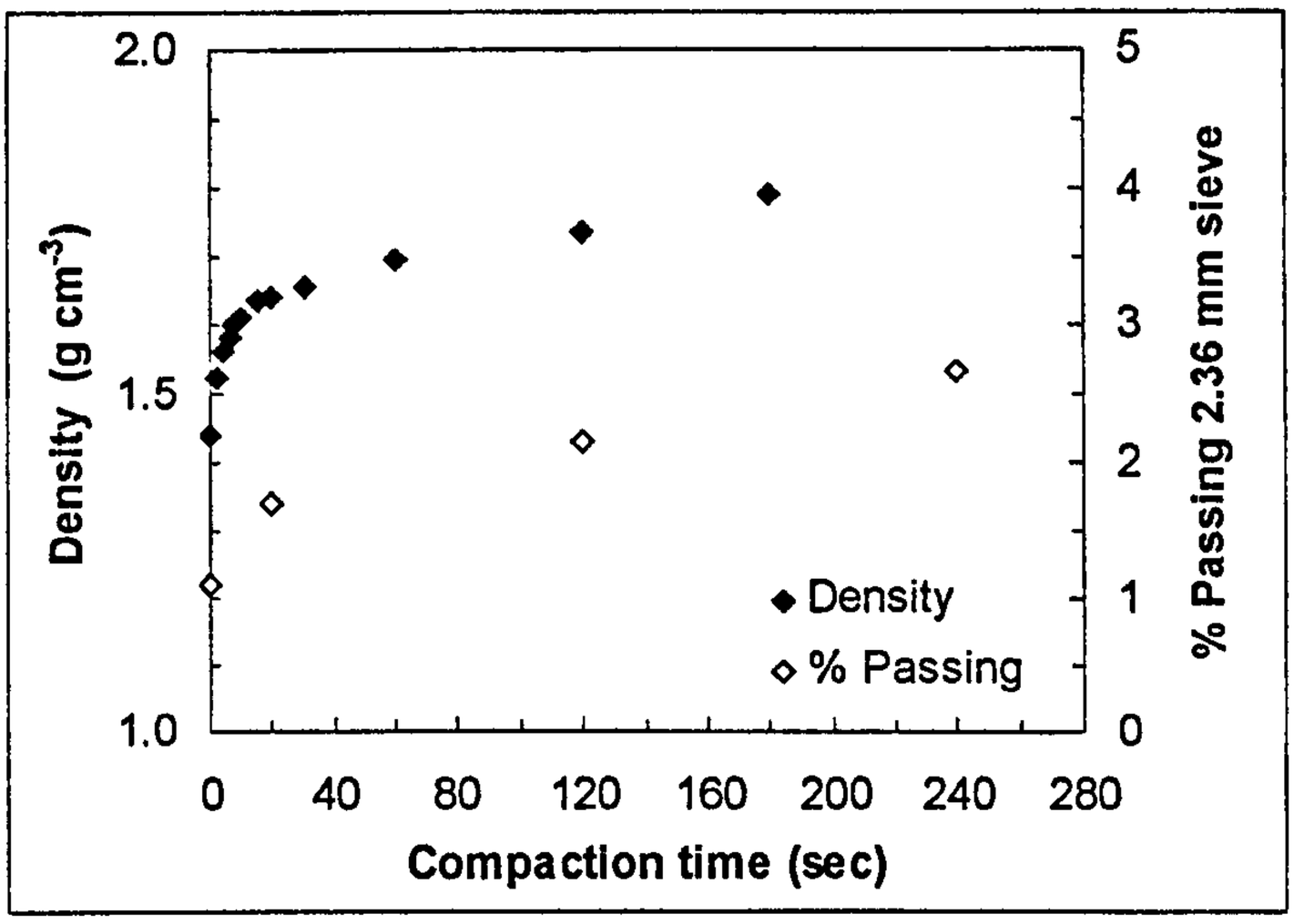

Figure 5.2 Influence of compaction time on aggregate density and crushing

The selection of the compaction time was based upon two factors, optimum packing of the aggregates, hence, maximum dry density or minimum voids, and avoidance of excessive crushing. Thus, the choice of 20 seconds as compaction time gave a compromise between the above-mentioned factors.

5.2.5.3 Measured voidage profiles

First obtained was the voidage profile for a blend of 14 mm and 10 mm aggregate sizes, as seen in **Figure 5.3**. The volume of voids within the single size 14 mm was measured as 41 % by volume and the volume of voids within the single size 10 mm was measured as 39 % by volume. The pessimum, or minimum voids, was found around a 14 and 10 mm blend proportion of 40/60, giving approximately 38 % voids.

Next, the voidage profile for a blend of 14 mm and 10 mm at the pessimum (40/60) and 6 mm aggregate sizes was determined, as shown in **Figure 5.4**. The volume of voids within the single size 6 mm was measured as around 39 % by volume. The pessimum was found around a 14/10 mm and 6 mm blend proportion of 55/45, giving approximately 36 % voids.

Then, the voidage profile for a blend of 14, 10, 6 mm at the pessimum (55/45) and 3 mm to dust aggregate sizes was calculated, as seen in **Figure 5.5**. The volume of voids within the single size 3 mm was measured as around 23 % by volume. The pessimum was found around a 14/10/6 mm and 3 mm to dust blend proportion of 40/60, giving approximately 19 % voids.

From the voidage profile shown previously (**Figure 5.5**), four aggregate blends were initially selected. These were, blend 1 (70 % coarse / 30 % fine), blend 2 (60 % coarse / 40 % fine), blend 3 (50 % coarse / 50 % fine) and blend 4 (40 % coarse / 60 % fine). Coarse corresponded to the 14, 10, 6 mm aggregate sizes, and fine was the 3 mm to dust aggregate sizes.

The next step was to add filler to the above blends at three different proportions of the total blend, 2, 4 and 6 %. The voidage profiles of these blends are presented in **Figure 5.6.** Initially, blends with 2 % added filler were considered adequate. The volume of voids when 2 % filler was added varied between 20 % for blend 1 and 17 % for blend 4.

Void measurements corresponding to the different aggregate blends are presented in **Appendix D**.

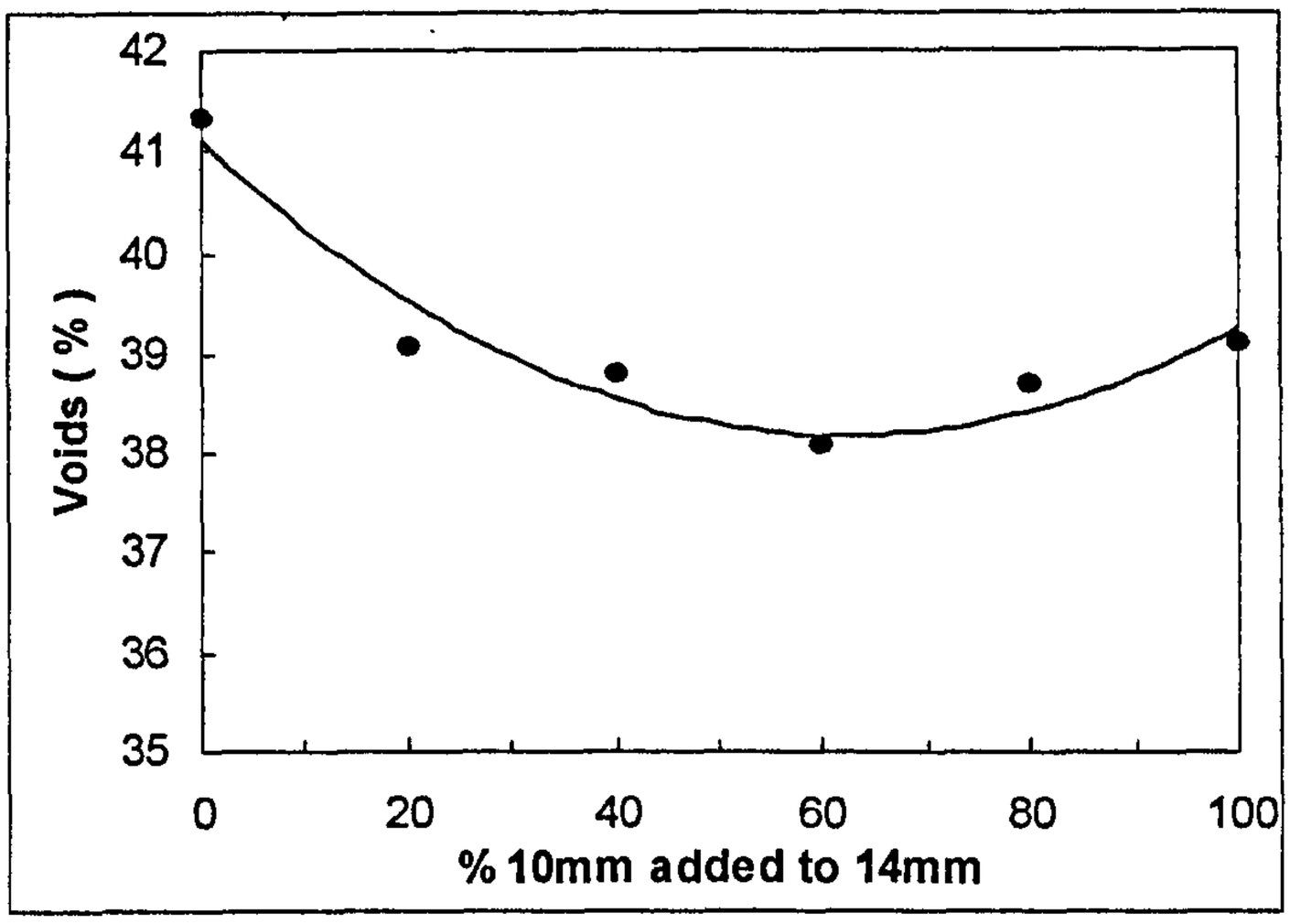

Figure 5.3 Voidage profile of the 10 mm added to the 14 mm size

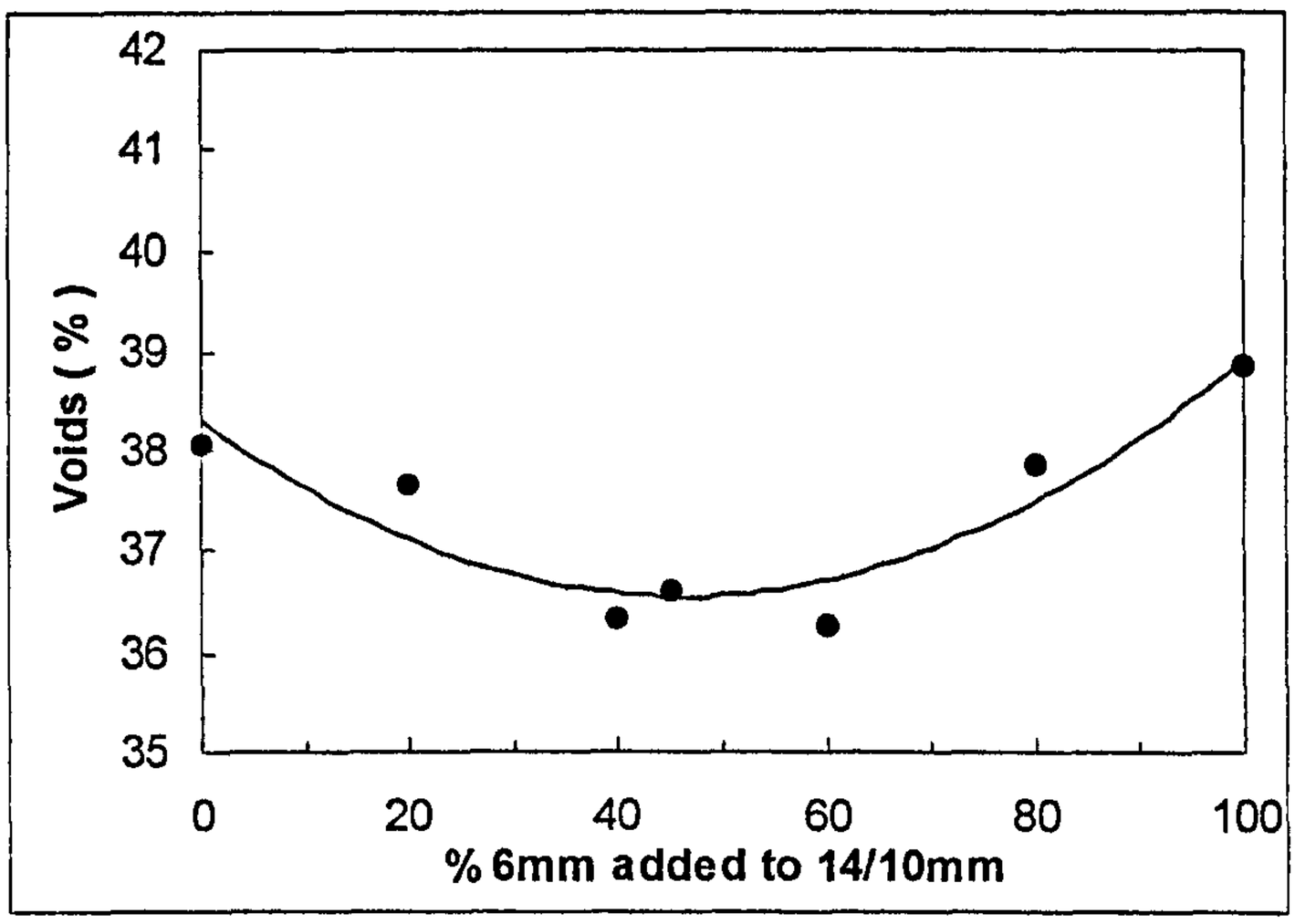

Figure 5.4 Voidage profile of the 6 mm added to the 14/10 mm sizes

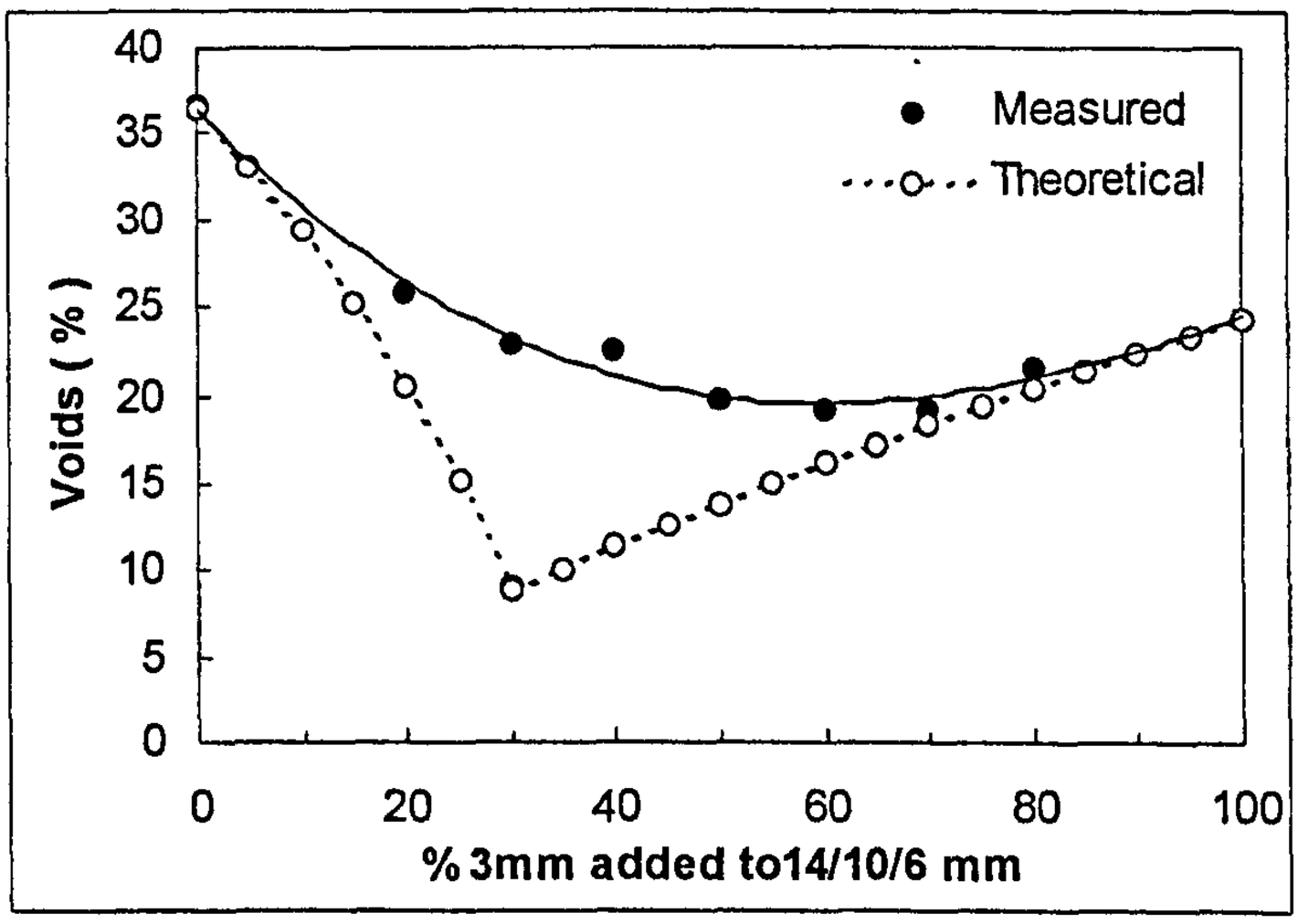

Figure 5.5 Voidage profile of the 3 mm added to the 14/10/6 mm sizes

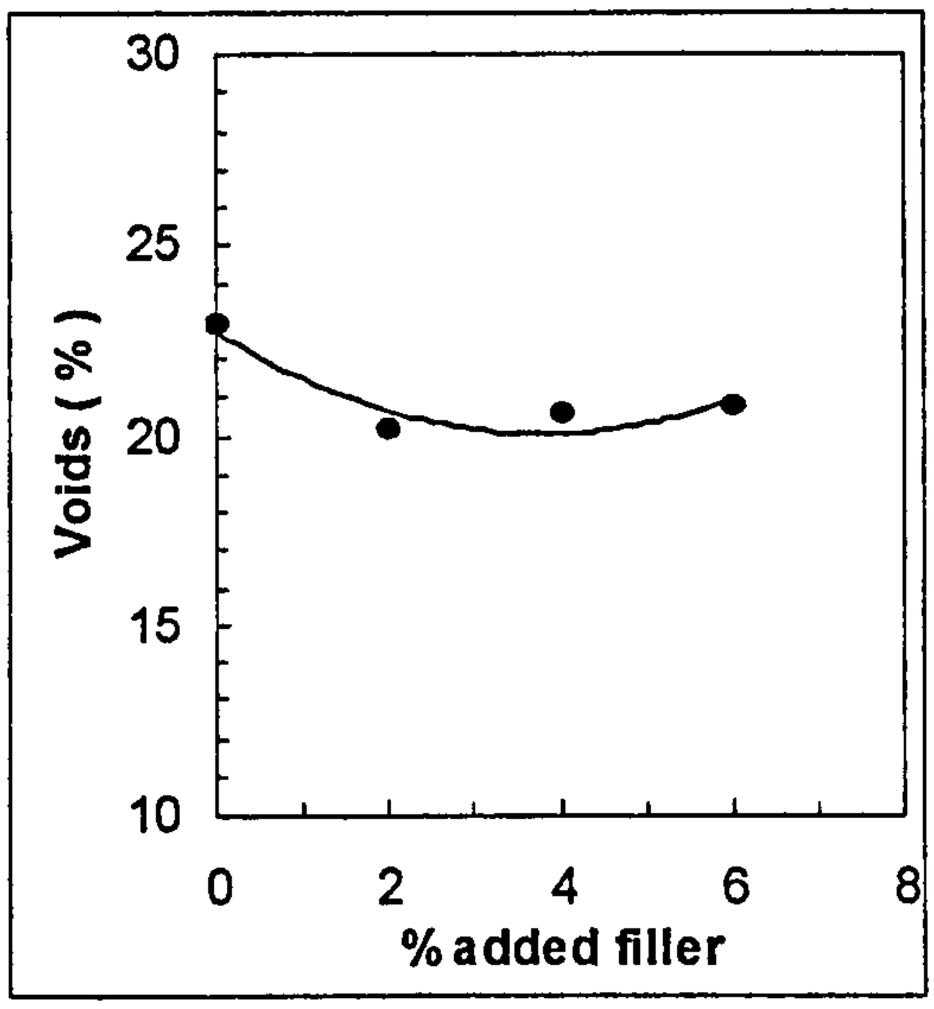

a) Blend 1 (70/30)

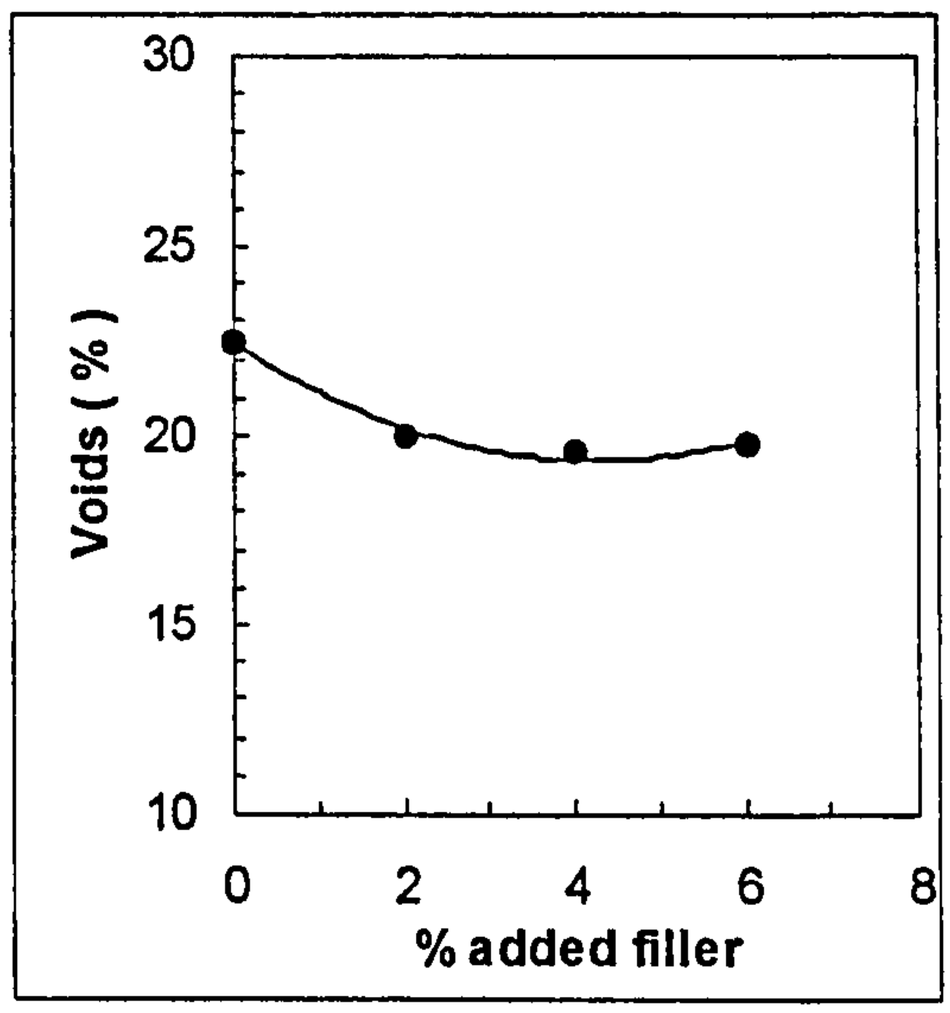

b) Blend 2 (60/40)

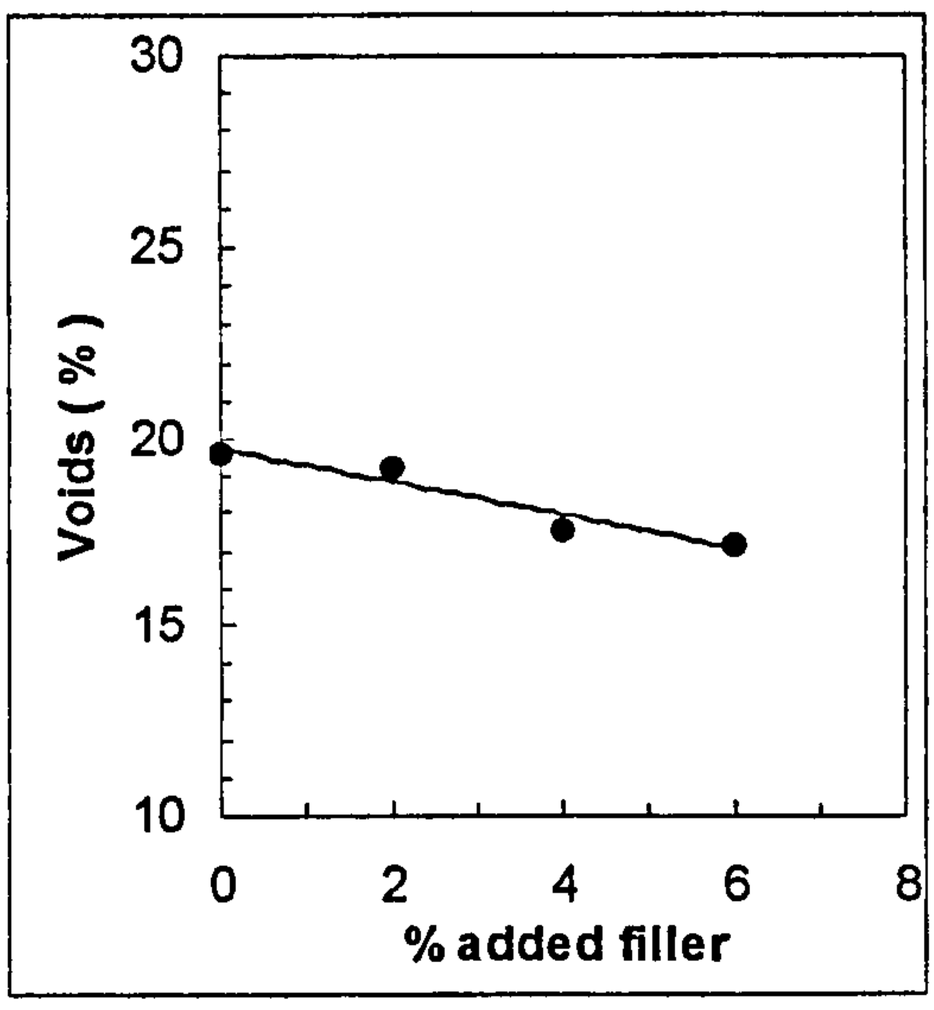

c) Blend 3 (50/50)

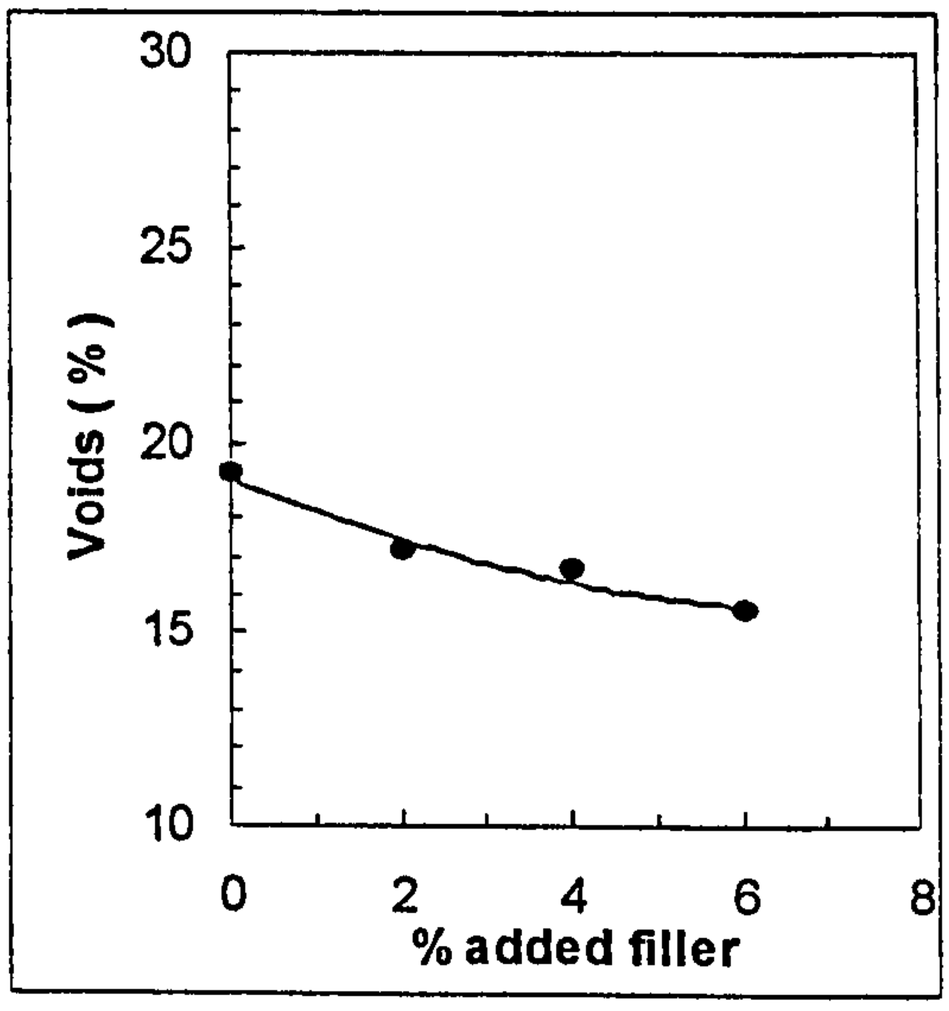

d) Blend 4 (40/60)

Figure 5.6 Voidage profile as filler is added to blends 1, 2, 3 and 4

5.2.5.4 Theoretical voidage profile

Voidage profiles of aggregate blends can also be calculated theoretically (Khalid, 2000). Two different methods are used depending on which side of the voidage profile, coarse side or fine side, is being considered. Distinct assumptions are made for each side of the profile based on how the void content would progressively change by the addition of the other component.

At the coarse side of the voidage profile, where the starting point is 100 % coarse aggregate, when the smaller aggregate fraction size, or fine aggregate, is added, the fine aggregate will be progressively filling the voids created by the coarse aggregate. As the fine aggregate proportion increases, the volume of the aggregate blend will begin to decrease, increasing the density of the blend and reducing the voids, as more fine aggregate will replace the coarse aggregate.

The equation used to calculate the theoretical voids at the coarse side of the voidage profile is given by,

$$VMA_{ca}(\%) = \left[1 - \frac{\frac{100}{P_{ca}/\rho_{ca}}}{SGMA}\right] \times 100 \qquad (5.3)$$

where:

$$SGMA = \frac{100}{\frac{P_{ca}}{SG_{ca}} + \frac{P_{fa}}{SG_{fa}}}$$

P_{ca} = % by weight of the total blend of coarse aggregate

P_{fa} = % by weight of the total blend of fine aggregate

SG_{ca} = Specific gravity of coarse aggregate

SG_{fa} = Specific gravity of fine aggregate

$$\rho_{ca} = SG_{ca}\left[1-\frac{VMA^{*}_{ca}}{100}\right]$$

VMA^{*}_{ca} = measured voids in coarse aggregate (%)

At the other side, where the starting point is 100 % fine aggregate, when the larger fraction size is blended with the smaller fraction size, the former will exist within the smaller fraction size as discrete particles, increasing the bulk volume but not the void content. As there is no interlock, the aggregate packing will result in an increase in density. This will continue until aggregate interlock occurs at high stone content.

The equation used to calculate the theoretical voids at the fine side of the voidage profile is given by,

$$VMA_{fa}(\%) = \left[1-\frac{\dfrac{100}{P_{fa}/\rho_{fa} + P_{ca}/SG_{ca}}}{SGMA}\right]\times 100 \qquad (5.4)$$

where,

$$\rho_{fa} = SG_{fa}\left[1-\frac{VMA^{*}_{fa}}{100}\right]$$

VMA^{*}_{fa} = measured voids in fine aggregate (%)

Derivations of Equations 5.3 and 5.4 are presented in **Appendix E**.

It should be notice that the starting points at both sides of the voidage profile (100 % coarse aggregate and 100 % fine aggregate) are entirely dependent on the measured bulk density of the dominant size and is a function of aggregate size, shape, distribution and compaction features.

The two theoretical curves obtained are entirely different. The curve corresponding to the coarse side of the profile is much steeper than the one corresponding to the fine side of the profile. Where these curves meet can be regarded as the minimum theoretical void content of the aggregate blend. The theoretical voidage profile for a blend of fine aggregate, 3 mm to dust, within a blend of coarse aggregate, 14, 10 and 6 mm, is presented in **Figure 5.5**.

5.2.5.5 Discussion

Comparisons between the experimental and theoretical voids for a blend of fine aggregate within a blend of coarse aggregate shows that the latter are lower than the former as seen in **Figure 5.5.** At the coarse side of the profile, the fine aggregate fraction is filling the voids in the coarse aggregate fraction, but doing so, the theoretical model assumes that there are no voids in the fine aggregate fraction, as a result the theoretical voids are lower than the experimental ones. At the fine side of the profile, the coarse aggregates are added as discrete particles introducing internal boundaries effects, which create zones of locally higher voids in the vicinity of the larger particles (Lees, 1969). This effect results in higher voids than the predicted from the theoretical model. Both situations are illustrated in **Figure 5.7**.

Moreover, external boundaries, i.e. the walls of containers, exert and influence on the packing and hence voids in aggregate blends. Hughes (1962) observed that the measured voids of a given granular material increased as the size of the container in which the determination was made was reduced and that increasing the size of the aggregate in a given container produced a similar effect. Different attempts have been carried out to derive a correction for container-wall effect. Lees (1969) suggested that, for the design of an aggregate grading, there may be no alternative to making the voids determination in a container of the size and shape in which it is intended the aggregate should ultimately be placed. In the current study, corrections due to boundary effects have not been considered.

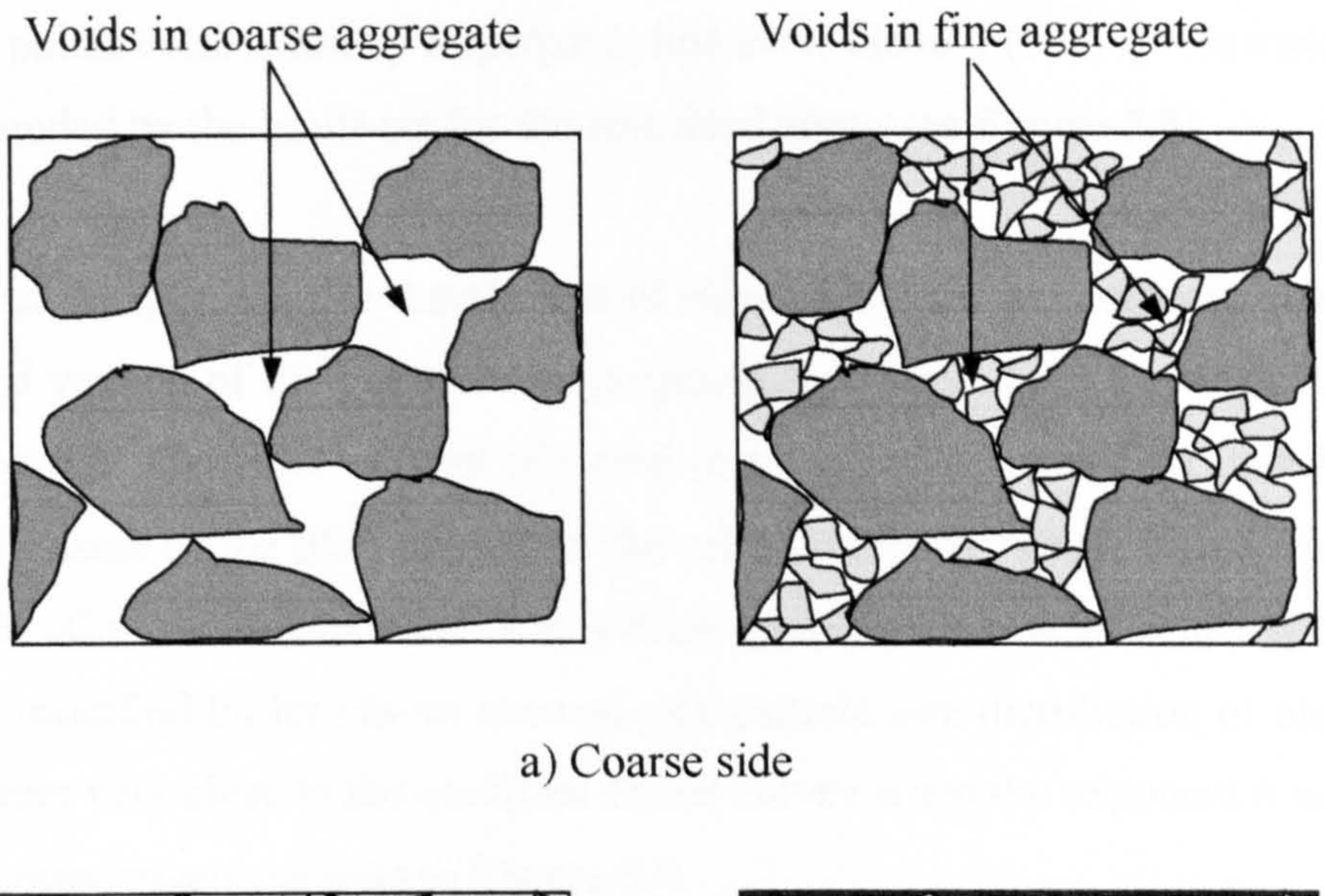

a) Coarse side

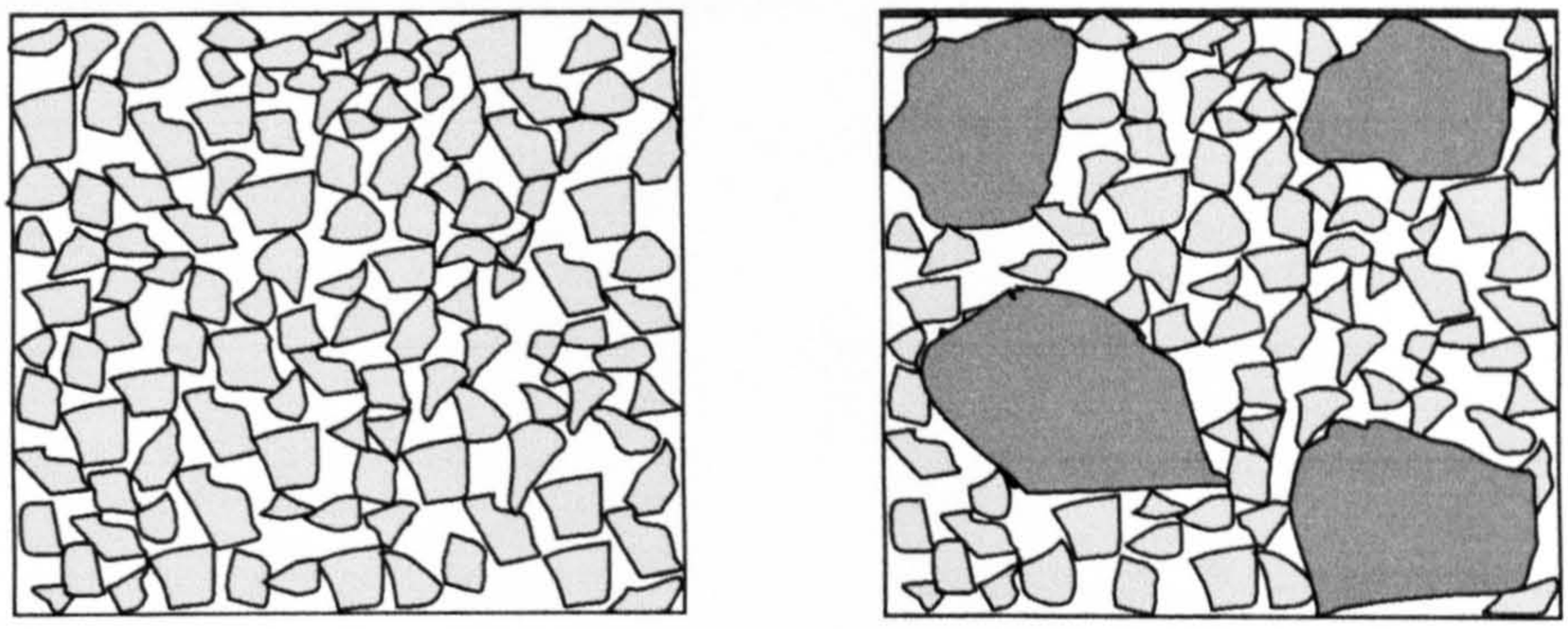

b) Fine side

Figure 5.7 Packing of aggregates

5.2.6 Particle size distribution of selected aggregate blends

Particle size distribution of selected aggregate blends, blend 1 (70/30), blend 2 (60/40), blend 3 (50/50) and blend 4 (40/60) with 2 % added filler were determined and are illustrated in **Figure 5.8.** Sieve analysis results for these blends are presented in **Appendix F**.

Particle size distribution of selected blends were plotted in conjunction with the grading envelope for a 14 mm close graded wearing course as per BS 4987 and the Superpave aggregate specification. It was found that blend 1 (70/30) and blend 2 (60/40) were inside the BS grading envelope, and blend 3 (50/50) and blend 4 (40/60) were not. Furthermore, all the aggregate blends pass between the

control points established by Superpave, however, blend 3 (50/50) was inside the area bounded by the limits set for the restricted zone (see **Figure 5.8**).

Moreover, the particle size distribution of selected blends was compared with the modified version of the Fuller curve proposed by Cooper et al. (1985) given by Equation 5.2. The filler content (F) used in Equation 5.2 was 5 %, which was about the same as the filler content of the selected blends, which varied from 4.9 to 5.6 %. Comparison between the particle size distribution of selected blends and the modified Fuller curves showed that particle size distribution of blends 1 and 2 were very close to the modified Fuller curves when the exponent n was 0.7 and 0.6 respectively, as seen in **Figure 5.9**.

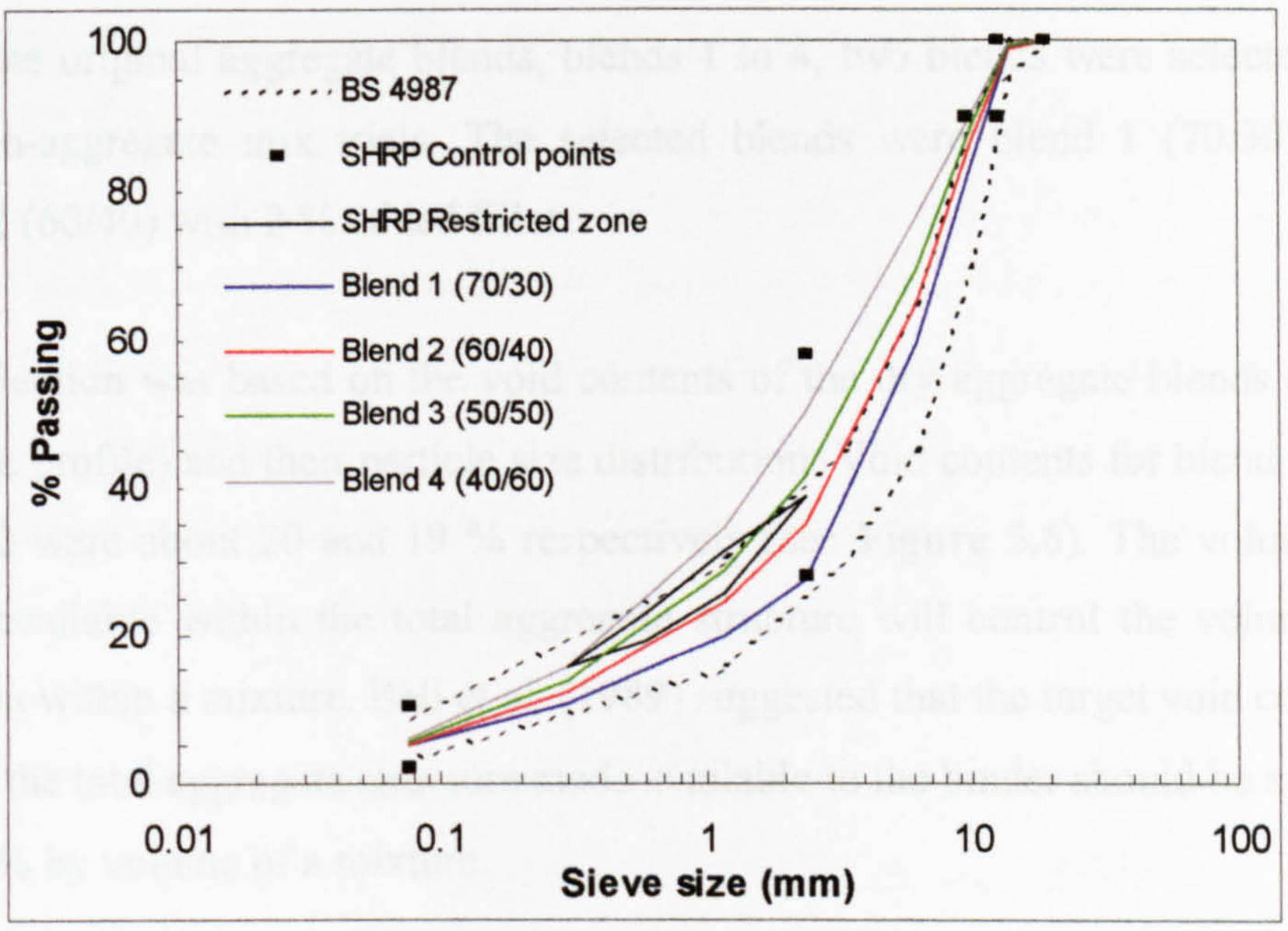

Figure 5.8 Particle size distribution of selected blends with 2 % added filler

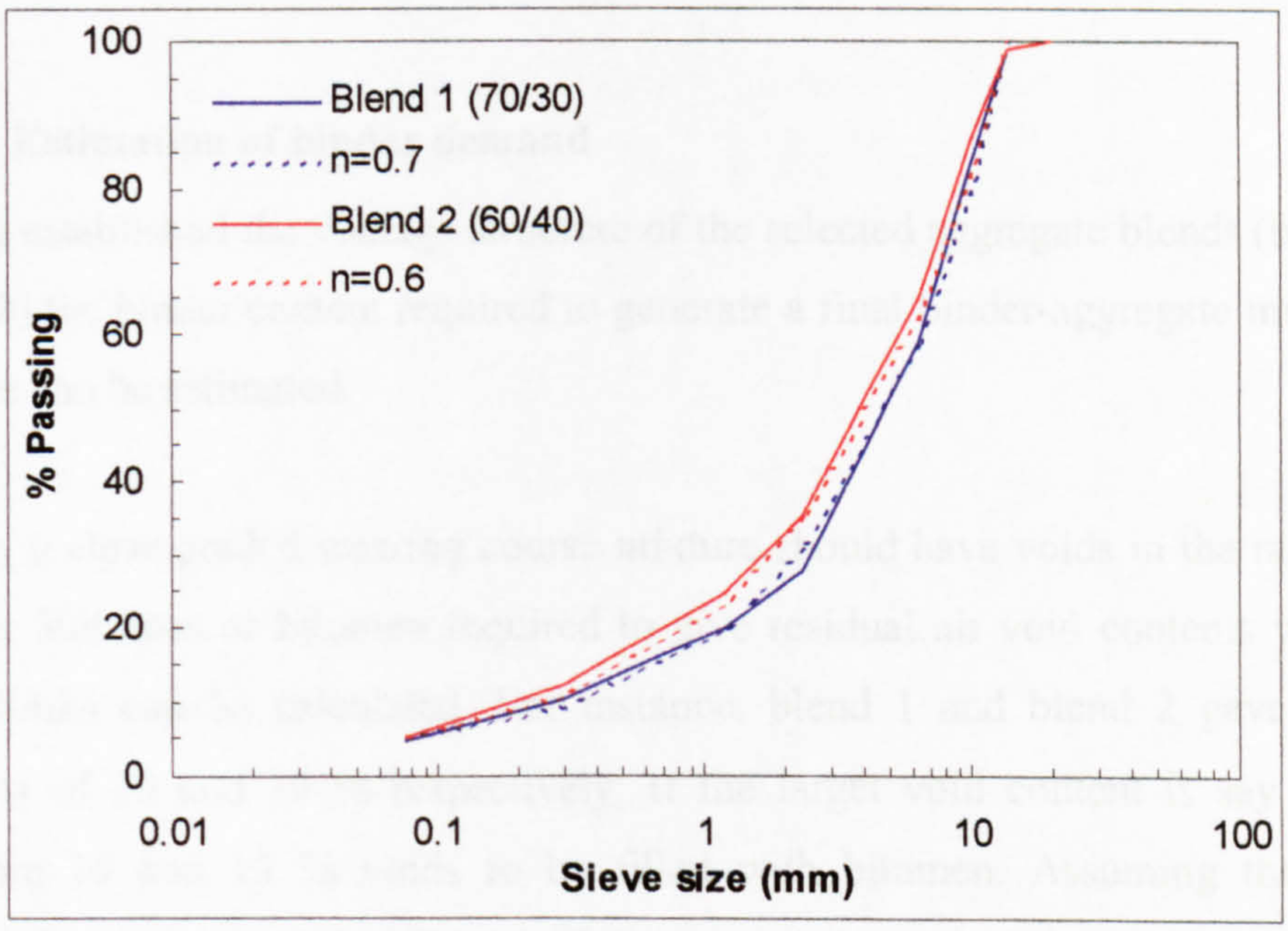

Figure 5.9 Comparison between the particle size distribution of the selected blends and the modified Fuller curves.

5.2.7 Selection of aggregate blends

From the original aggregate blends, blends 1 to 4, two blends were selected for bitumen-aggregate mix trials. The selected blends were blend 1 (70/30) and blend 2 (60/40) with 2 % added filler.

The selection was based on the void contents of the dry aggregate blends (from voidage profile) and their particle size distribution. Void contents for blend 1 and blend 2 were about 20 and 19 % respectively (see **Figure 5.6**). The volume of voids available within the total aggregate structure will control the volume of bitumen within a mixture. Bell et al. (1989) suggested that the target void content within the total aggregate structure made available to the binder should be around 15-17 % by volume of a mixture.

Particle size distribution of blends 1 and 2 showed that the percentage of coarse aggregates (>2.36 mm) were about 72 and 65 % of the total blend respectively. Ferguson et al. (1999) suggested a target coarse aggregate content of around 70 % for stone mastic mixtures and around 65 % for continuously graded mixtures.

5.2.8 Estimation of binder demand

Having established the voidage structure of the selected aggregate blends (blends 1 and 2) the binder content required to generate a final binder-aggregate mixture voidage can be estimated.

Ideally, a close-graded wearing course mixture should have voids in the range 3 to 5 %. Volumes of bitumen required to give residual air void contents within these limits can be calculated. For instance, blend 1 and blend 2 gave void contents of 20 and 19 % respectively; if the target void content is say 4 %, therefore 16 and 15 % voids to be filled with bitumen. Assuming that the bitumen has a density of 1.03 gm/ml, then the percentage by weight of bitumen required to fill 16 and 15 % voids to result in a mix of an estimated density of say 2.4 gm/ml is 6.8 and 6.4 % respectively. Thus the range of binder contents to be selected will be around these values.

It has been found, however, that the addition of bitumen into the mix reduces the void content in the mineral aggregate structure due mainly to the lubricant effect of the bitumen, which eases the packing of the aggregates. Furthermore, measured dry aggregate voids were determined using cylindrical moulds much smaller than the moulds used for the binder-aggregate mixtures and, as seen before, the measured voids in an aggregate blend increase when the dimensions of the mould decrease due to boundary or wall effects. Because of these two factors, the range of binder contents selected were about 1 % lower than the predicted, say around 6 % for blend 1 and around 5.5 % for blend 2.

5.3 BINDER-AGGREGATE MIXTURE TRIALS

Trial binder-aggregate mixtures are required to be manufactured in the laboratory with binder contents around the target value to define the design binder content and to select the binder-aggregate mixture.

5.3.1 Specimen preparation

Specimen preparation consisted of aggregate and binder proportioning and weighing, mixing, compaction and coring. Slabs were manufactured in the laboratory and cylindrical specimens were cored from the slabs, as seen in **Figure 5.10.** The full method for preparing mixture specimens is provided in **Appendix G**.

The binder contents selected varied between 5 and 6 % for blend 1 and between 4.5 and 5.5 % for blend 2. The binder used was a 100 Pen from Venezuelan origin. The specimens manufactured in this way were used throughout the different stages of the mix design procedure.

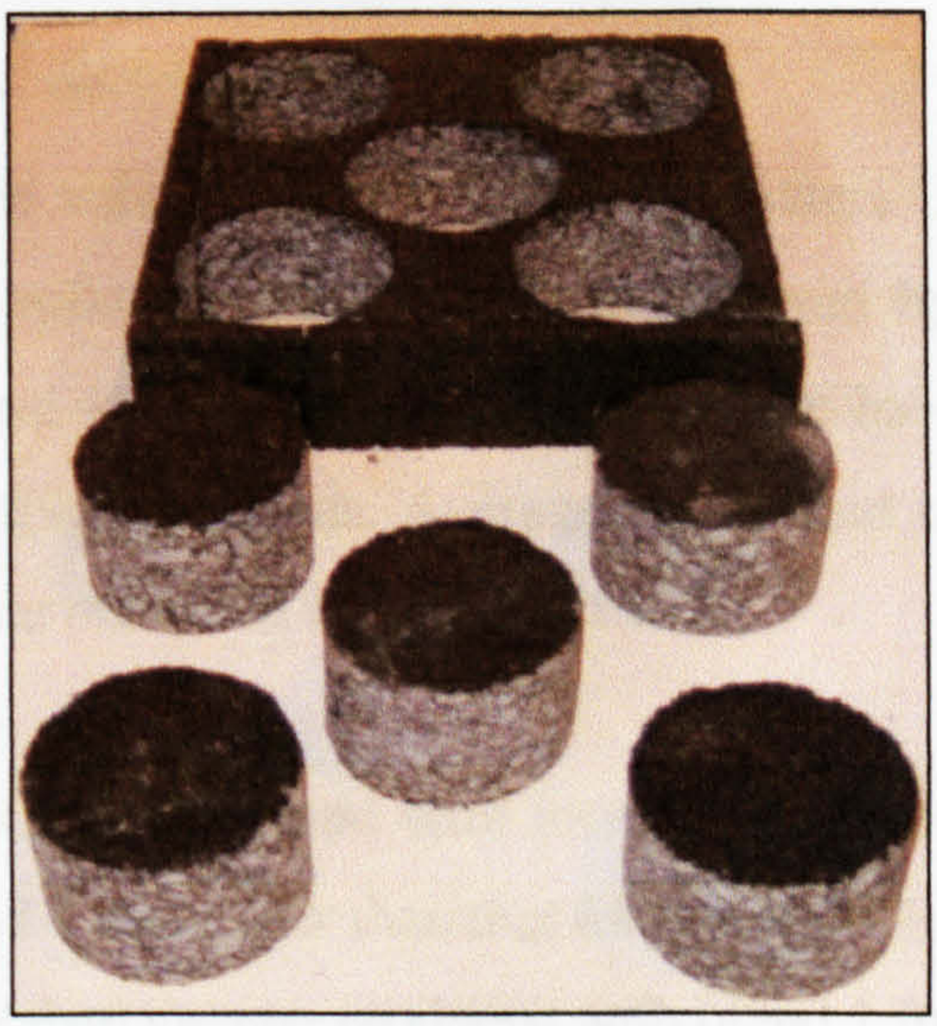

Figure 5.10 Cored specimens

5.3.2 Volumetric measurements

Once the specimens have been produced they were weighed in air and in water. From the two weights, the Compacted Density of the Mix (*CDM*) can be calculated.

A problem arises when specimens with pores connecting the surface to their interior are submerged in water. Water enters and fills air voids within the specimen distorting subsequent calculations. This problem is usually overcome by dipping the specimens in melted paraffin wax, which seals the surface from the ingress of water. However, this method is time consuming and messy.

Del Valle (1985) proposed an alternative solution by using a type of "cling-film" called Parafilm^{TM}. The cling-film seals the specimen from the ingress of water and can be quickly applied and removed. This method was adopted in this study.

After the measurement of the *CDM* the following parameters are calculated: Compacted Density of Mixed Aggregate (*CDMA*), theoretical Specific Gravity of Mix (*SGM*), Voids in Mixed Aggregate (*VMA*), and theoretical Voids in Mix (*VIM*). The equations used for the determination of the above parameters are presented in **Appendix H**.

5.3.2.1 Results and discussions

Figure 5.11 shows the volumetric mix design parameters *CDM*, *VMA* and *VIM* corresponding to the mixtures initially investigated and base on two different aggregate blends, blend 1 and blend 2. The results are based upon the average value obtained from five specimens. Average values and standard deviation of these measurements are presented in **Appendix I**.

Results showed that *CDM* increased with increasing binder content, and *CDM* corresponding to blend 1 was lower than that for blend 2. Thus, the mix produced with blend 2 is denser than the one produced with blend 1 for the range of binder contents selected.

VMA values for blend 1 were higher than those for blend 2, as also found from the voidage profile of the dry aggregate blends. However, the values obtained from the measurements of the coated aggregate blends, between 18 – 17 % for blend 1 and between 17 – 16 % are around 2 % lower than the values obtained from the voidage profile, around 20 and 19 % for blend 1 and 2 respectively. These differences might be attributed to the lubricant effect of the bitumen, boundary effects when measuring voids in aggregate blends, and the different compaction method.

As expected, the air void contents of the two mixtures decreased with increasing binder content. For the binder contents selected, the void contents varied from about 3 % up to about 6.5 %. Furthermore, at the same binder content, the void content for blend 1 was more than 1 % higher than the one corresponding to blend 2, as a result of higher voids in the mineral aggregate.

5.3.3 Mix stiffness

Although bituminous mixtures are viscoelastic materials, at typical traffic speeds and road temperatures their behaviour is practically elastic (Nunn, 1997). The elastic stiffness modulus of a bituminous mixture is an indicator of its load spreading ability. It also controls the level of tensile strain induced in the underlying layers. Thus, a material with a high elastic stiffness modulus will have a good load spreading ability which will reduce the deflections due to the passing traffic reducing at the same time the tensile strains in the underlying layers.

The Indirect Tensile Stiffness Modulus (ITSM) test is the most commonly test method used for the determination of the stiffness modulus of a bituminous material. Details of the ITSM test can be found in **Appendix J**.

The stiffness of a particular mix at any temperature and time of loading can also be estimated through the use of a series of nomographs developed by Shell (SIPC, 1989). The inputs required for these nomographs are the penetration (dmm) and the softening point (^{0}C) of the binder, which enable the determination of the stiffness modulus of the binder, and the volume (%) of binder and mineral aggregate. These nomographs, however, can only be used when the stiffness of the binder exceeds $5x10^6$ Pa.

5.3.3.1 Results and discussions

Figure 5.11 shows the results from ITSM test corresponding to the mixtures initially investigated and base on two different aggregate blends, blend 1 and blend 2. The results are based upon the average values obtained from five specimens. Average values and standard deviation of these measurements are presented in **Appendix I**.

At the test conditions of temperature and loading, mix stiffness modulus is mainly dependent on the stiffness modulus of the binder and the volumetric composition of the mix. As the same binder has been used in both mixtures (100 Pen VEN), differences in stiffness values are attributed the volumetric

proportions of both mixtures. In general, mix stiffness modulus is higher as the volume of aggregates is increased.

For the two mixtures initially studied, the stiffness modulus decreased with increasing binder content for the range of binder contents investigated. At low binder content, the higher stiffness of the mixes is attributed to stone to stone contact by friction and interlock, and the bond supplied by the binder. As the binder content increases, the thicker binder films on the surface of the aggregates reduces the contribution of the friction effects to the stiffness modulus. As a result, the stiffness decreased as the binder content was increased.

5.3.4 Binder content and mixture selection

The design parameters used for mix selection and optimum binder content included *CDM*, *VMA*, *VIM* and *ITSM*. Mix design parameters for the two mixtures initially studied, blend 1 and blend 2, are presented in **Figure 5.11**.

It has been found that optimum binder contents for blend 1 and 2 were around 5.5 and 5 % respectively. These binder contents gave air voids of about 4.5 % for both mixes. Furthermore, the *ITSM* at 5.5 % binder content (blend 1) and at 5 % binder content (blend 2) were 960 and 1300 MPa, respectively. The *ITSM* for blend 1 at the optimum binder content was considered low, and this blend was rejected in favour of blend 2.

Finally, the optimum binder content selected for blend 2 was 4.8 %. The selection of the binder content was based on the mix design parameters and on economic considerations, thus, cheaper mixes at lower binder contents. The selected binder proportion gave a void content of 5.6 %, and *ITSM* value of 1416 MPa. These parameters were considered adequate for this type of bituminous mixture, thus a close-graded material made with a medium/soft bitumen grade (100 Pen). Furthermore, mix stiffness at the optimum binder content and at the same conditions as the *ITSM* test, i.e. t=0.124 sec and T=20 ^{0}C, could not be estimated using the Shell nomographs as the stiffness of the binder was lower than $5x10^{6}$ Pa.

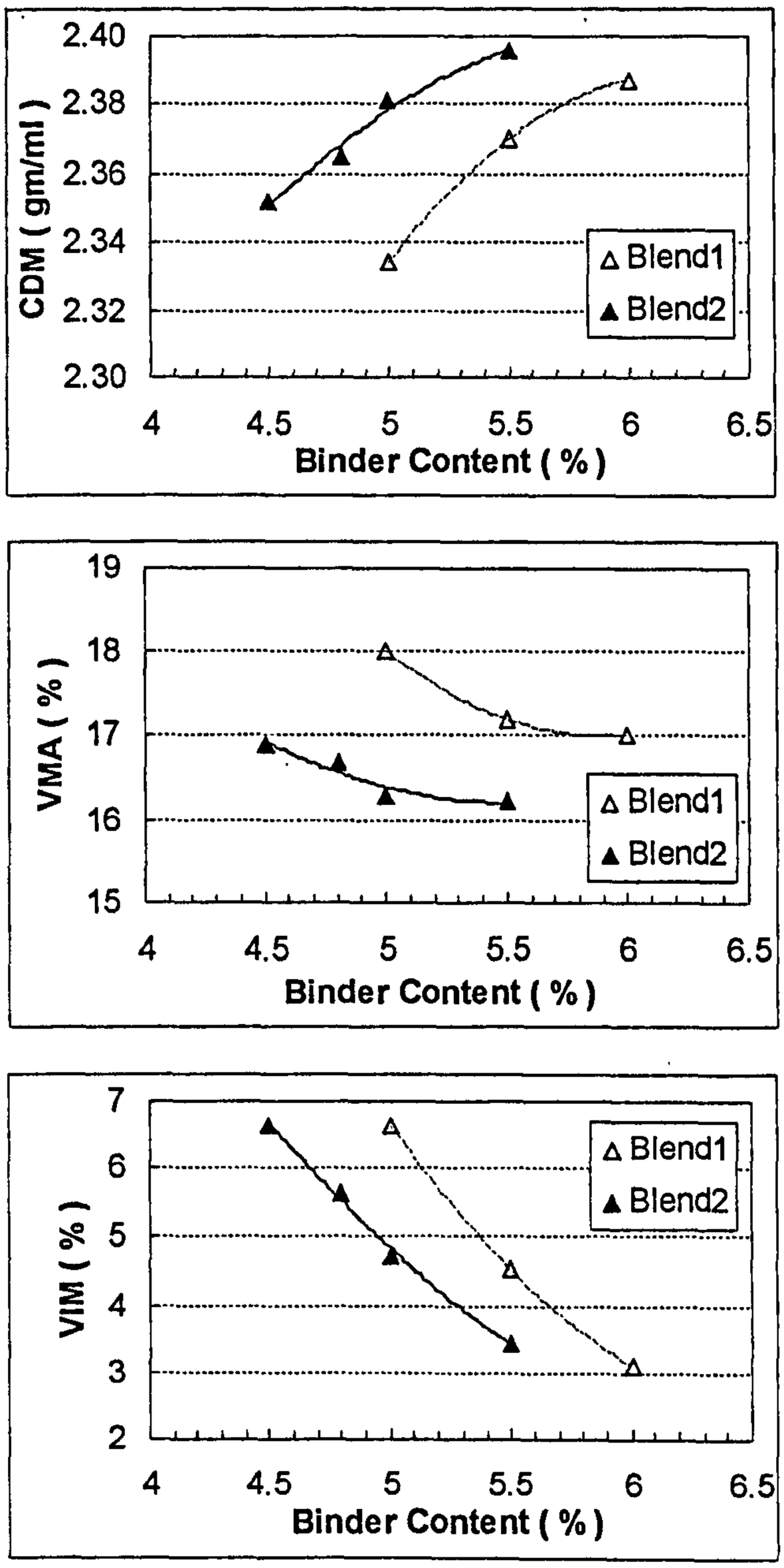

Figure 5.11 Mix design parameters for blend 1 and 2

5.4 DESIGN OF CRUMB-RUBBER MODIFIED MIXTURES

5.4.1 Introduction

In the previous section two conventional mixtures were designed based on the mix design parameters, *CDM*, *VMA*, *VIM* and *ITSM*. From the two mixtures, the mixture produced with the aggregate grading represented by blend 2 was considered the preferred one. Based on the same aggregate proportions as per the preferred conventional mix (blend 2), two crumb-rubber modified mixtures have been designed.

5.4.2 Specimen preparation

The procedure followed was the same as for the conventional mixtures, thus slabs 306 x 306 x 64 mm^3 were manufactured in the laboratory and cylindrical specimens, 99 mm diameter and 64 mm height were cored from the slabs for further analysis. The full method for preparing crumb-rubber modified mixtures is also provided in **Appendix G**.

Two modified mixtures, namely CRM mix 1 and CRM mix 2, were produced with a 100 Pen binder modified with 10 % wt CRM from truck tyres (CRM mix 1) and with 10 % wt CRM from car tyres (CRM mix 2). The binder contents selected varied between 5 and 6 % for both mixtures. One slab per binder content was made and five cylindrical specimens were obtained from each slab.

5.4.3 Volumetric measurements

Volumetric mix design parameters, *CDM*, *CDMA*, *SGM*, *VIM* and *VMA* were calculated using the equations presented in **Appendix H**.

5.4.3.1 Results and discussions

Figure 5.12 shows the volumetric mix design parameters *CDM*, *VMA* and *VIM* corresponding to the two crumb-rubber modified mixtures, CRM mix 1 and CRM mix 2, in conjunction with the values for the conventional mix, Control mix (blend 2). The results are based upon the average value obtained from five

specimens. Average values and standard deviation of these measurements are presented in **Appendix I.**

Results showed that *CDM* increased with increasing binder content, and *CDM* corresponding to CRM mix 2 was slightly lower than that for CRM mix 1. Furthermore, the conventional mix (Control mix) was denser than the modified mixes for the range of binder contents selected.

Only small differences between the *VMA* values for CRM mix 1 and CRM mix 2 were found. However, these values were higher than the ones corresponding to the Control mix. Moreover, void content for the crumb-rubber modified mixtures decreased with increasing binder proportion. Also the differences in void content between the two mixtures were considered negligible.

It is interesting to note that at the same binder proportion, the void contents of the modified mixtures were higher than that of the conventional mix. Thus, to produce mixtures with the same void content more modified binder is needed. For instance, to produce mixtures with 5 % voids, around 5 % binder content is required if the conventional binder is used, and around 5.5 % if the modified binders are used. This is easily explained knowing that at 5.5 % binder content for binders modified with 10 % CRM, around 5 % represents the amount of neat bitumen and the other 0.5 % corresponds to the CRM.

5.4.4 Mix stiffness

The Indirect Tensile Stiffness Modulus (ITSM) test was used for the determination of the stiffness modulus of the crumb-rubber modified mixtures.

5.4.4.1 Results and discussions

Figure 5.12 shows the results from ITSM test corresponding to the crumb-rubber modified mixtures, CRM mix 1 and CRM mix 2. The results are based upon the average values obtained from five specimens. Average values and standard deviation of these measurements are presented in **Appendix I.**

For the two modified mixtures studied, CRM mix 1 and CRM mix 2, the stiffness modulus decreased with increasing binder content for the range of binder contents investigated. Furthermore, mix stiffness corresponding to the mix modified with CRM from truck tyres was slightly higher than that for the mix modified with CRM from car tyres. This higher mix stiffness was attributed to higher binder stiffness associated with the binder modified with CRM from truck tyres in comparison with the binder modified with CRM from car tyres, as showed in Chapter 4.

Comparison between the crumb-rubber modified mixtures and the conventional one showed that ITSM values for the conventional mix were lower than those for the modified mixtures. The higher stiffness of the modified mixtures was associated to higher binder stiffness as a result of binder modification with CRM, as showed in Chapter 4.

5.4.5 Mix design parameters: design binder content

Mix design parameters for the two modified mixtures studied, CRM mix 1 and CRM mix 2 are presented in **Figure 5.12**. It has been found that optimum binder content for the crumb-rubber modified mixtures had to be increased to compensate for the reduced amount of bitumen in the CRM binders and to restore the mobility of the binder to coat aggregates. As a result, the design binder content selected, based on the mix design parameters presented in **Figure 5.12**, was 5.8 % by weight, which resulted in 3.5 % void contents for both modified mixtures.

Furthermore, *ITSM* values at the optimum binder content were 1860 and 1810 MPa for CRM mix 1 and CRM mix 2, respectively. Moreover, mix stiffness from Shell monographs corresponded to CRM mix 1 was 1360 MPa, which was about 27 % lower than the stiffness determined from the ITSM test. Furthermore, mix stiffness for CRM mix 2 could not be determined as the stiffness of the binder was lower than $5x10^6$ Pa.

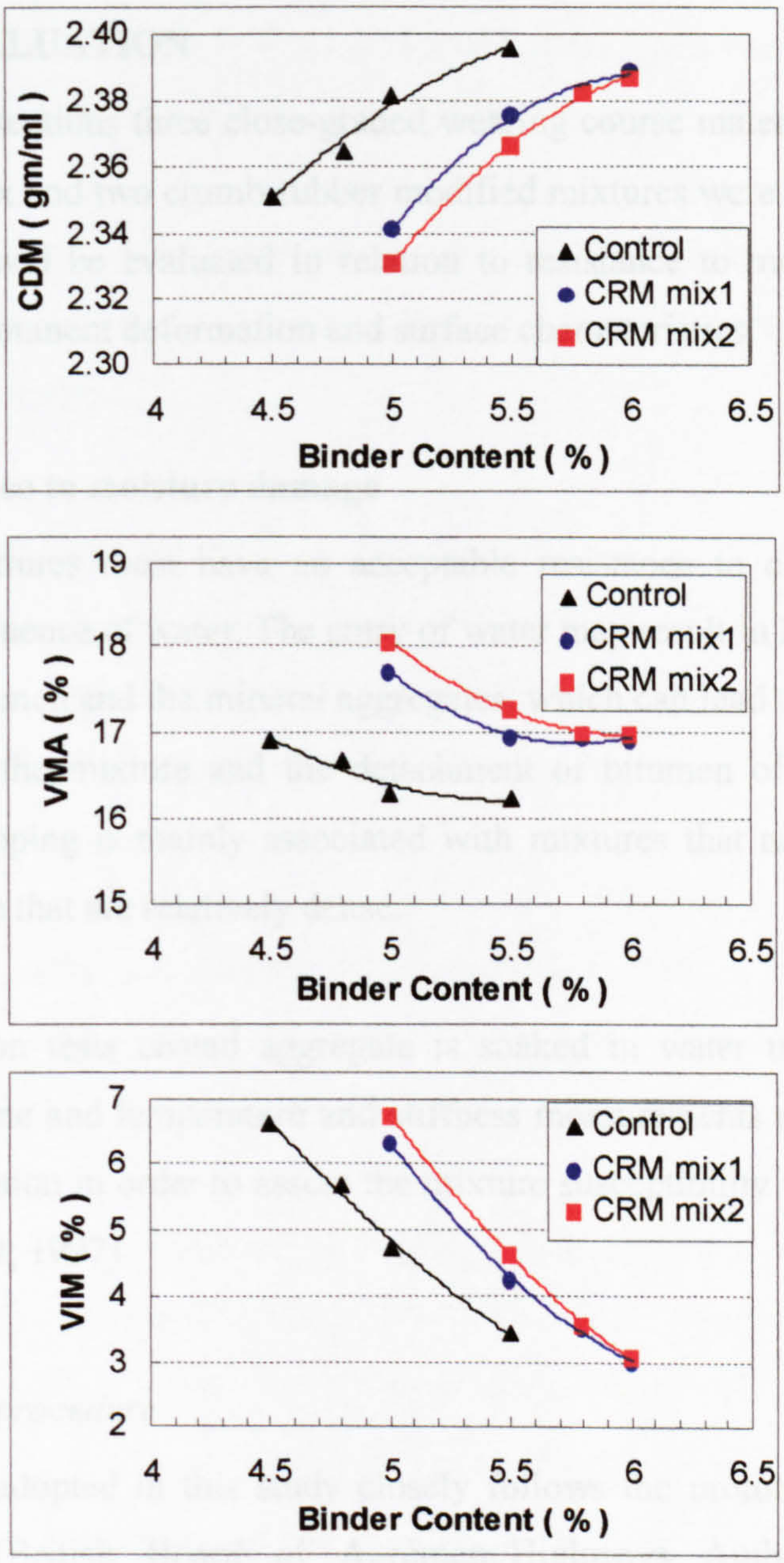

Figure 5.12 Mix design parameters for CRM mix 1 and CRM mix 2

5.5 MIX EVALUATION

In the previous sections three close-graded wearing course materials including a conventional mix and two crumb-rubber modified mixtures were designed. Now, these mixtures will be evaluated in relation to resistance to moisture damage, resistance to permanent deformation and surface characteristics.

5.5.1 Resistance to moisture damage

Bituminous mixtures must have an acceptable resistance to changes brought about by the influence of water. The entry of water may result in loss of adhesion between the bitumen and the mineral aggregates, which can lead to a reduction in the strength of the mixture and the detachment of bitumen off the aggregate (stripping). Stripping is mainly associated with mixtures that are permeable to water even those that are relatively dense.

In most adhesion tests coated aggregate is soaked in water under controlled conditions of time and temperature and stiffness measurements are taken before and after immersion in order to assess the mixture susceptibility to water ingress (Heslop and Catt, 1997).

5.5.1.1 Test procedure

The procedure adopted in this study closely follows the protocol described in BBA/HAPAS (British Board of Agrèment/Highways Authorities Product Approval Scheme) for thin surfacings (BBA, 1998). This protocol describes a method for the determination of the water sensitivity by measuring the retained stiffness after water conditioning.

The test procedure used in this study can be summarised as follows. First the stiffness of the unconditioned specimens was determined. The specimens were placed in the vacuum desiccator at 20 ^{0}C, and a partial vacuum of 500 mm Hg was applied for 30 minutes. The specimens were then removed from the desiccator and placed in a water bath at 60 ^{0}C for 6 h, and then immediately placed in a cold water bath at 5 ^{0}C for 16 ± 1 h. This thermal conditioning cycle,

6 h at 60 ^{0}C and 16 ± 1 h at 5 ^{0}C, was repeated three times one after the other. After the last cycle, the specimens were removed from the cold-water bath and immediately placed in a water bath at 20 ^{0}C for 2 h. The specimens were then removed from the bath and allowed to stand for 2 h at 20 ^{0}C, surface dry. Finally, the specimens were conditioned inside the NAT for a further 2 h, and their stiffness was determined.

5.5.1.2 Discussion of results

Figure 5.13 shows the percentages of the mix stiffness that were retained after conditioning. The results are based upon the average values obtained from three specimens. Average values and standard deviation of these measurements are presented in **Appendix I**.

The effects of water are widely acknowledged to reduce the strength of bituminous materials, however the opposite effect was found in some of the mixtures studied.

It has been found that the mixtures with greater binder contents retained a larger proportion of their stiffness after conditioning. This is the result of thicker binder films coating the mineral aggregates and preventing the ingress of water.

5.5.2 Resistance to permanent deformation

Permanent deformation of the selected mixtures was assessed using the Repeated Load Axial (RLA) test, which is currently a British Standard Draft for Development (BSI, 1996).

5.5.2.1 The RLA test

During the RLA test the specimen is subjected to repeated load pulses with rest periods and the relation between the number of load pulses and the axial strain is recorded. Axial strains are measured by means of LVDTs. The test applies a one second square pulse load of 100 kPa followed by one second rest period. Initially, a conditioning stress of 10 kPa is applied to the specimen for 120 s. The

number of applied cycles is 1800 and the total duration of the test is 1 h. The temperature selected for the RLA test was 40 ^{0}C.

5.5.2.2 Discussion of results

Figure 5.14 shows the RLA test results for the three mixtures studied. The results are based on the average value obtained from two specimens.

The results showed that for the Control mix (unmodified), the permanent deformation, given by the percentage axial strain, did not change significantly with binder content. At the lowest binder content, the permanent deformation was the highest, due maybe to the high void content, around 6.6 %. For the rest of binder contents used, the permanent deformation of the specimens tested remained practically constant, indicating the relatively small effect of the unmodified binder on the permanent deformation of the mixture.

RLA test values for the crumb-rubber modified mixtures showed different behaviour. Initially, the permanent deformation increased with increased binder content, due to lower stiffness at higher binder contents. After a maximum, the permanent deformation decreased probably because of the recovery effect (see Chapter 4) of the crumb-rubber modified binders at these relatively high binder contents.

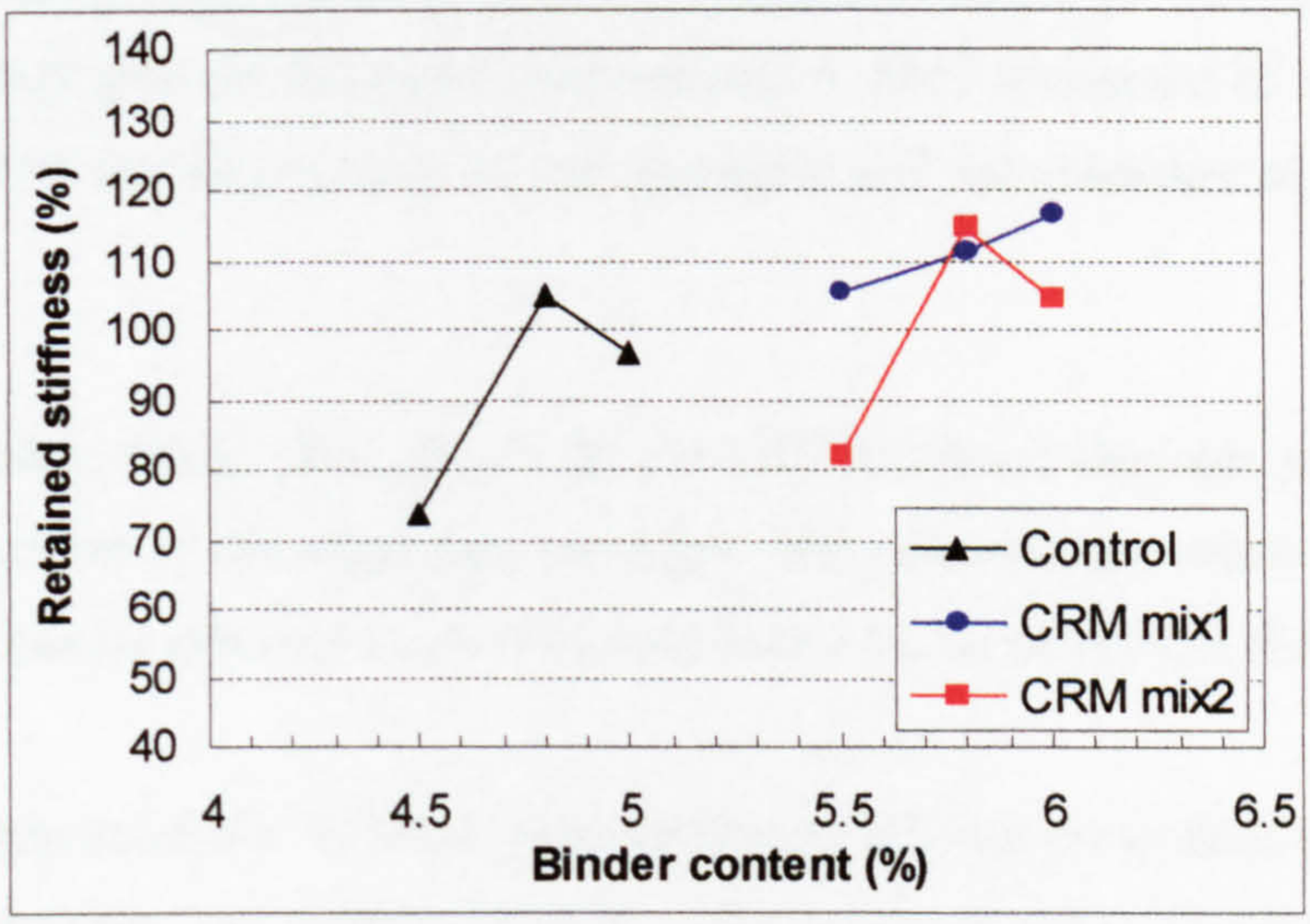

Figure 5.13 Retained ITSM values after conditioning

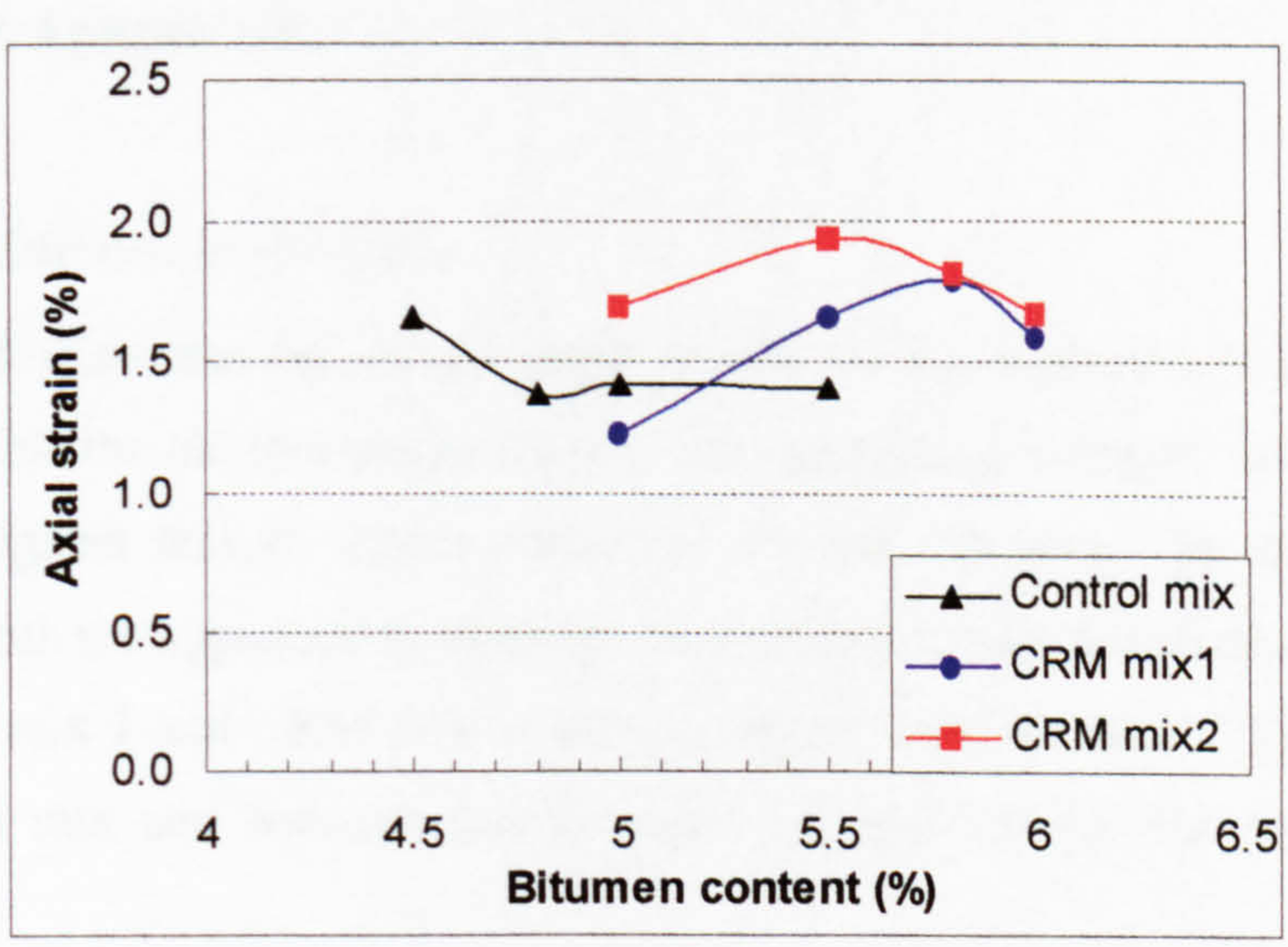

Figure 5.14 RLA test results

5.5.3 Surface properties

When bituminous mixtures are used as wearing courses an added requirement is that they must provide adequate skid resistance. Skid resistance of a surface is determined by the microtexture of the aggregate and macrotexture of the surface itself.

At low speeds, below about 50 km/h, the skid resistance depends primarily on the microtexture of the aggregate particles. The microtexture characteristics of aggregates can be assessed by the Polished Stone Value (PSV) test (BSI, 1989).

At higher speeds, above 50 km/h, skid resistance depends on an additional factor, the macrotexture or surface texture. The macrotexture characteristics of aggregates can be assessed by the Aggregate Abrasion Value (AAV) test (BSI, 1990**c**). Macrotexture is required in order to provide drainage channels for the water to be dispersed. The macrotexture of a road surface is measured using the sand patch test (BSI, 1990**d**). A brief description of the sand patch test is presented in **Appendix K**.

5.5.3.1 Discussion of results

Figure 5.15 illustrates the texture depth results for the mixtures investigated. It was found that the mixture produced with the aggregate grading given by blend 1 gave the highest texture depths, between 2.6 and 2.8 mm. For the mixtures produced with the aggregate grading given by blend 2, which include the Control mix, CRM mix 1 and CRM mix 2, texture depths vary between 1.5 and 1.9 for the Control mix and between and between 1.2 and 1.6 for the crumb-rubber mixtures.

Typical texture depths of newly-laid bituminous surfacings vary between 0.6 – 1.2 mm for dense bitumen macadam and between 1.3 – 2.5 mm for hot rolled asphalt (heavily chipped). Thus, texture depths of the designed mixtures at the design binder content were considered adequate for use as wearing courses.

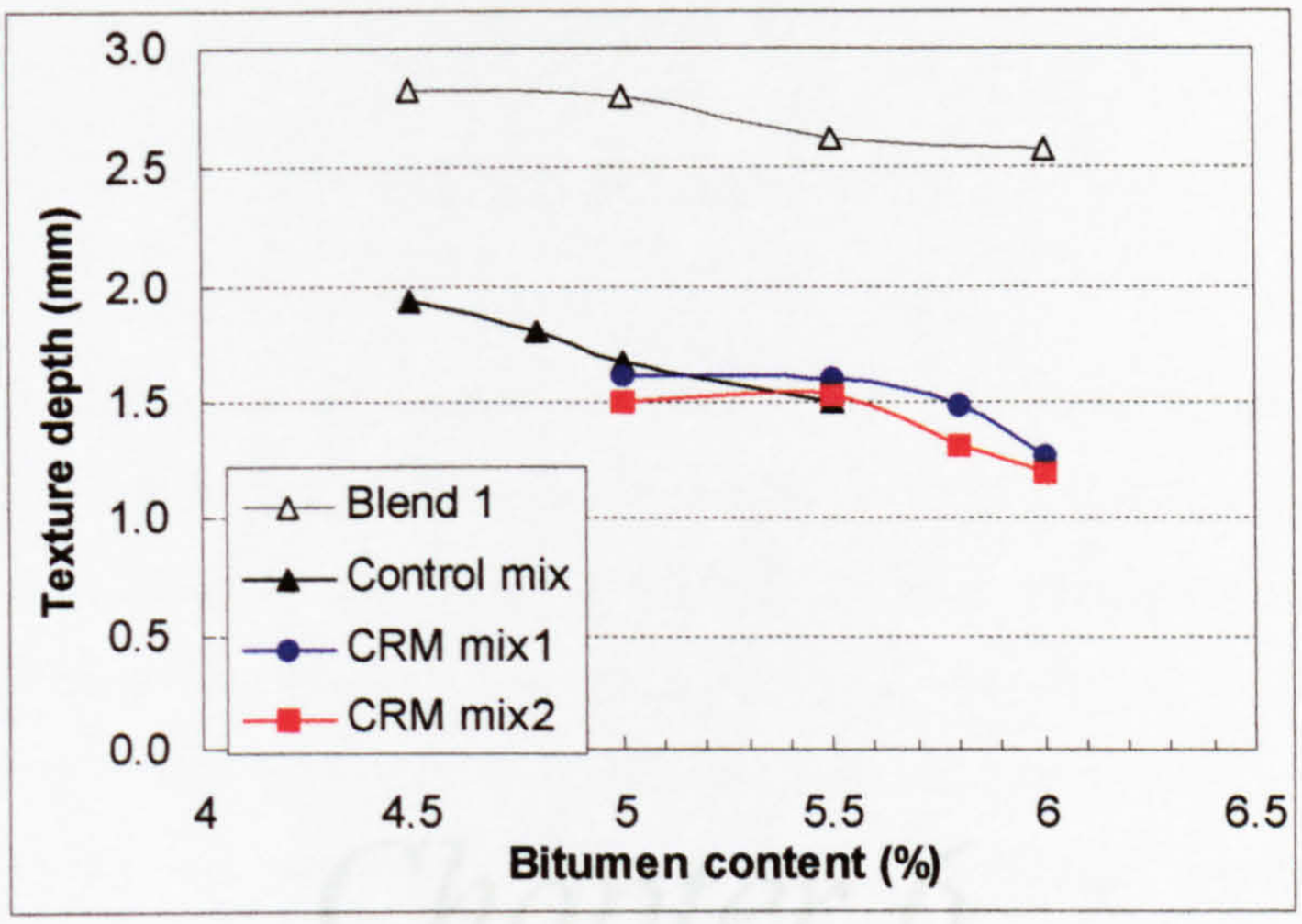

Figure 5.15 Relationship between texture depth and binder content

For continuously graded mixtures, the actual texture depth achieved will depend on the nominal size and grading of the aggregate. Thus, the higher texture depths associated to the mixtures produce with blend 1 (70 % coarse / 30 % fine) can be attributed to a higher proportion of coarse aggregate when comparing with the mixtures produced with blend 2 (60 % coarse / 40 % fine). Furthermore, for all the mixtures investigated, the texture depths decreased with increasing binder content, presumably as external voids were filled with bitumen.

Chapter 6

FATIGUE RESISTANCE

Chapter 6

FATIGUE RESISTANCE

This chapter presents and analyses the fatigue test results obtained from four-point bending beam test. Three close-graded wearing courses, including a conventional and two crumb rubber modified mixtures have been investigated. Fatigue lives have been presented in terms of the number of cycles to failure and to macro-crack formation. A fatigue damage parameter was introduced and the damage accumulation rate was used to characterise the fatigue resistance of the mixtures.

6.1 FATIGUE OF BITUMINOUS MIXTURES

Fatigue strength of bituminous materials is defined as the ability of the material to resist cracking after repeated wheel load applications. Fatigue cracking is one of the major load-related distress modes experienced in asphalt pavements, and occurs when a bituminous layer is subjected to repeated loading under the passing traffic.

6.1.1 Fatigue test configurations

Fatigue characteristics of bituminous mixtures have been studied with different test configurations, as illustrated in **Figure 6.1**. These can be divided into two main categories: the homogeneous and the non-homogeneous tests (Di Benedetto et al., 1996).

In a homogenous test the strains and stresses are uniform across the cross sectional area, and the measurements of the loads (stresses) and deflections (strains) directly provide the physical properties of the material. Homogeneous tests include Uniaxial, Triaxial and Shear Tests. The uniaxial test configuration is illustrated in **Figure 6.1**. In this test an axial force in tension/compression is applied to the specimen.

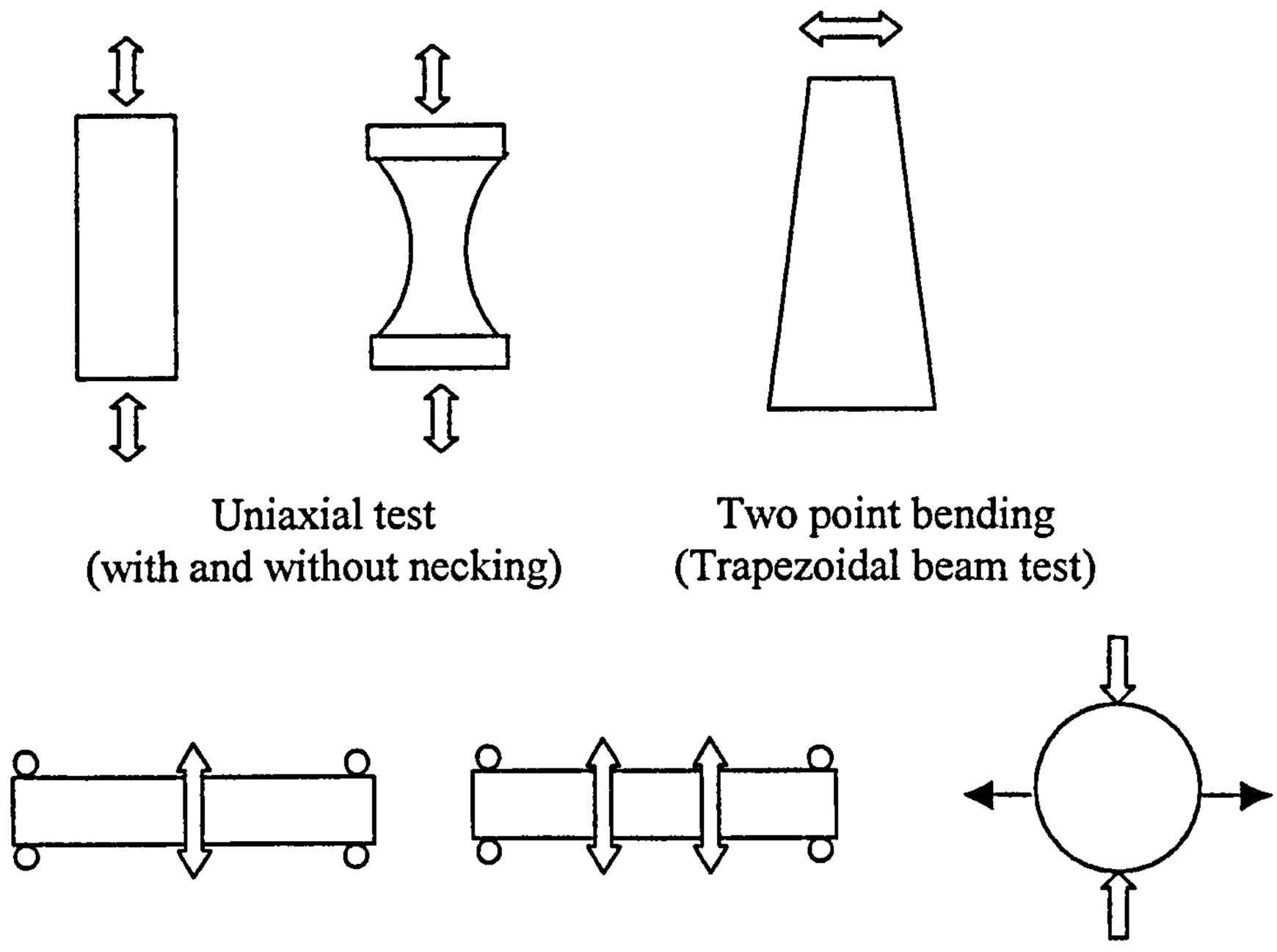

Figure 6.1 Tests for measuring fatigue properties

In a non-homogeneous test, the strains and stresses are different at different points across the cross sectional area. The interpretation of the fatigue data for a non-homogeneous test is only possible if we assume elastic or viscoelastic behaviour. These conditions are only complied with when the deformation levels (strains) are small.

Three configurations are mainly employed, Two-Point Bending and Three or Four-Point Bending Tests, as also shown in **Figure 6.1**. The Two Point Bending Test uses a trapezoidal shaped cantilever beam specimen that is fixed at the base with the top of beam being cyclically loaded. The Three and Four Point Bending Tests use prismoidal shaped beam specimens that are held horizontally and dynamically loaded. Another non-homogeneous test is the Indirect Tensile Fatigue Test (ITFT), also illustrated in **Figure 6.1**. In this test, a cylindrical specimen is loaded along the vertical diametral plane, resulting in tensile stresses perpendicular to the direction of the applied load.

6.1.2 Testing mode

Fatigue tests are carried out in two modes, "controlled strain" and "controlled stress". In controlled strain mode, the strain is kept constant by decreasing the stress during the test. In a controlled stress test, on the other hand, the stress is maintained constant and the strain increases during the test.

In general, controlled stress testing has been related to relatively thick pavement construction where high stiffness is the fundamental parameter to assess the fatigue life. On the other hand, controlled strain testing has been associated with thin conventional flexible pavements where the elastic properties of the material have a fundamental impact on its fatigue life (Pell, 1973).

6.1.3 Definition of failure

Fatigue test data in controlled strain or stress mode tests has been used to derive a relationship between strain, ε, or stress, σ, and fatigue life, N_f. Monismith and Deacon (1969) proposed the following equations based on simple flexural beam tests:

$$N_f = C_1\left(\frac{1}{\varepsilon}\right)^m \tag{6.1}$$

and

$$N_f = C_2\left(\frac{1}{\sigma}\right)^n \tag{6.2}$$

where:

N_f	=	number of load applications to failure
ε	=	tensile strain
σ	=	tensile stress
C_1, C_2, m, n	=	material regression coefficients

More recently, the stiffness of the asphalt mixture was introduced into the fatigue relation to account for the variation in load frequency and temperature (Monimisth et al., 1985), as follows:

$$N_f = C_1\left(\frac{1}{\varepsilon}\right)^m\left(\frac{1}{S_{mix}}\right)^d \tag{6.3}$$

where:

S_{mix} = initial stiffness

d = experimental coefficient

Fatigue failure has been defined in different ways depending on the mode of testing. Failure in constant strain has been widely defined as 50% reduction in the initial stiffness (Pronk and Hopman, 1990, Tayebaly et al., 1992**a** and Tayebaly et al., 1993). For controlled stress testing, fatigue failure is reached when either the specimen has fractured (Pell and Cooper, 1975), or when the stiffness is at 10% of its original value (van Dijk and Visser, 1977).

6.1.4 Dissipated energy

6.1.4.1 Dissipated energy concept

When a load is applied to a material, the resulting stress will induce a strain. The area under the strain–stress curve represents the energy being input into the material. After the load is removed, the stress is removed and the strain is recovered.

When a perfectly elastic material undergoes cyclic deformation under loading, all the energy stored in the material during loading is recovered during unloading, and the loading and unloading curves coincide. In contrast, for a viscoelastic material, not all the energy is recovered after unloading, and the two curves do not coincide. This energy difference, or dissipated energy, is lost in the material in the form of mechanical work, heat generation or damage. This phenomenon is

commonly known as "Hysteresis" and the dissipated energy is the area within the loop.

The dissipated energy can be obtained from the knowledge of the load and deflection, and the phase lag between the applied load and the response of the material. If the load and deflection are expressed in terms of stress and strain, the dissipated energy per loading cycle is obtained as follows:

$$w_i = \pi \sigma_i \varepsilon_i \sin \phi_i \tag{6.4}$$

where:

w_i = dissipated energy at cycle i

σ_i = stress amplitude at cycle i

ε_i = strain amplitude at cycle i

ϕ_i = phase lag between stress and strain at cycle i

During fatigue testing, the dissipated energy changes with number of load cycles. For controlled stress tests the dissipated energy per loading cycle increases whereas for controlled strain the dissipated energy decreases.

The cumulative dissipated energy is defined as the sum of the dissipated energies in each loading cycle, as follows:

$$W_n = \sum_{i=0}^{i=n} w_i = \pi \sum_{i=0}^{i=n} \sigma_i \varepsilon_i \sin \phi_i \tag{6.5}$$

In an earlier work by Chomton and Valayer (1972) and van Dijk et al. (1972) fatigue life was related to the total cumulative dissipated energy to failure as follows:

$$W_N = A \cdot N^z \tag{6.6}$$

where:

N = number of cycles to failure

A, z = experimental coefficients

Van Dijk (1975) suggested that the relation in Equation 6.6 was independent of test method and testing conditions. However, in later work (SHRP-A-404, 1994) this relation was found to be dependent on test temperature and mode of loading.

6.1.4.2 Definition of failure based on Energy Ratio

Traditionally, fatigue failure has been defined differently depending on the mode of loading. In general, the fatigue life obtained from constant stress testing is shorter than that obtained from constant strain testing for similar initial conditions. This might be due to the nature of the way damage is being done to the material. Damage is done faster in controlled stress testing where the same stress is applied to the material, whereas the stress decreases during controlled strain testing.

Hopman et al. (1989) proposed the use of an "Energy Ratio" to define the number of cycles (N_1) in a controlled strain fatigue test to a point where cracks are considered to initiate. The Energy Ratio, R_i, introduced by Hopman et al. is defined as follows:

$$R_i = \frac{n \cdot w_0}{w_i} \tag{6.7}$$

where:

n = number of load cycles

w_0 = dissipated energy at the first cycle

w_i = dissipated energy at the i-cycle

Hopman et al. found that when R_i is plotted against the number of load cycles in a controlled strain test, there is a clear change in behaviour at N_1 represented by

the change of the slope at this point. This generally happened when the reduction of the material's complex modulus, E^*, was around 40 %.

Rowe (1993) simplified the equation proposed by Hopman et al. to define the number of cycles N_1 where cracks are considered to initiate, and defined this point as the coalescence of micro-cracks to form a sharp crack, which then propagates. For a controlled strain test, the simplified equation for the energy ratio can be written as:

$$R_i^{\varepsilon} \cong \frac{n}{E_i^*} \tag{6.8}$$

where E_i^* is the complex modulus at the *i*-cycle.

N_1 in a controlled strain test is defined as the point at which the slope of the simplified energy ratio against the number of load cycles deviates from a straight line.

For a controlled stress test, the same approach was used resulting in the following simplified equation for the energy ratio,

$$R_i^{\sigma} \cong n \cdot E_i^* \tag{6.9}$$

N_1 in controlled stress testing corresponds to the peak value when the simplified energy ratio is plotted against the number of load cycles.

For controlled strain and controlled stress fatigue testing, N_1 represents the material in the same state of damage corresponding to "crack initiation" (Rowe 1993). The N_1 criterion, however, is more difficult and subjective to define for controlled strain than for controlled stress tests. To overcome this problem, Rowe and Bouldin (2000) applied the same analysis used for controlled stress tests to controlled strain tests. For a controlled strain test, when the energy ratio $n \cdot E^*$ for a controlled stress test was plotted against the number of cycles n a distinct

maximum appeared. This maximum corresponded to the N_1 point for a controlled strain test.

Pronk (1997) used a similar energy ratio to the one defined by Hopman et al. to define failure in fatigue testing. He used the following equation:

$$R_n = \frac{W_n}{w_n} = \frac{\sum_{i=1}^{n} w_i}{w_n} \qquad (6.10)$$

where:

W_n = cumulative dissipated energy up to the n cycle

w_n = dissipated energy at the n cycle

In order to obtain the N_1 point, the ratio between the cumulative dissipated energy up to cycle n and the dissipated energy at cycle n is plotted against the number of load cycles.

6.1.5 Interpretation of fatigue data

6.1.5.1 Phases in a fatigue process

Traditionally, fatigue data has been analysed by plotting the reduction in stiffness against the number of load cycles using logarithmic scales. Tayebali et al. (1992b) recommended plotting the stiffness reduction against the number of load cycles in logarithmic scales and fitting an exponential relationship to the data. However, there is no experimental evidence or theoretical basis for a power-law relationship (Rowe and Bouldin, 2000).

Di Benedetto et al. (1996) analysed fatigue data from triaxial tension/compression tests using linear scales and identified the existence of three phases during a fatigue test.

Phase I is characterised by a rapid reduction of stiffness modulus with number of load applications. Di Benedetto suggested that this effect is mainly due to internal heating of the sample. Due to their viscous properties, bituminous materials dissipate energy after each load cycle. This energy is transformed into heat, which first increases the temperature of the specimen and, then, it diffuses through the surface. This increase in temperature leads to a reduction of the stiffness modulus. Di Benedetto reported a temperature increase of 1.3 ^{0}C during this phase for one of the fatigue tests. For bituminous mixtures, this increase in temperature might lead to a decrease in modulus of more than 15%. Considering the 50% stiffness reduction as the failure criterion, more than 30% of the classical characterisation of fatigue might be due to heating.

Phase II is characterised by an approximate linear reduction in the stiffness modulus with number of cycles. After the initial rapid decrease in modulus during phase I, the variation of the stiffness modulus with number of load cycles becomes linear.

Phase III is characterised by rapid drop in stiffness modulus with loading cycles. This rapid degradation might be attributed to coalescence of micro-cracks to form a sharp crack.

The rapid decrease in the stiffness modulus observed during Phase I is still not fully understood. Pronk et al. (1996) used a theoretical model to predict the temperature distribution of an asphalt beam in a four-point bending test. They also compared the theoretical values with the measured values during a fatigue test under controlled displacement mode with relatively high strain amplitude of 200 μm/m. The maximum temperature increase obtained was about 2 ^{0}C and a good correlation was found between predicted and measured temperatures. However, the increase in temperature can only explain a very small part of the decrease in stiffness modulus at the beginning of the tests, or, Phase I.

Choi et al. (2002) also found temperature rises of about 1 ^{0}C during the early stages of the test under controlled stress conditions using a uniaxial

tension/compression fatigue device. They compared the behaviour of asphalt and fibre-reinforced concrete, which is a non-temperature sensitive material, and concluded that the increase in temperature during the test cannot be the main factor resulting in the rapid drop in stiffness.

Thom et al. (2002) considered a model of a two-particle system surrounded by bitumen to explain the reduction in stiffness in the early stages during a trapezoidal fatigue test. They suggested that low adhesion between stone and bitumen and the development of micro-cracks within the bitumen, commencing at particle contacts, are the mechanisms responsible for the decrease in stiffness modulus during the first phase of fatigue testing.

Neifar and Di Benedetto (2002) suggested that, considering a bituminous mixture as a heterogeneous material, combined with the effect of bitumen thixotropy, heating due to dissipated energy might be responsible for the initial decrease in stiffness modulus.

6.1.5.2 Fatigue damage and rate of damage accumulation

Pavement materials are subjected not only to individual cyclic stresses, as in fatigue testing, but also to varying cyclic stress amplitudes. A simple criterion for predicting the extent of fatigue damage considering compound loading is provided by Miner's Rule (Miner, 1954). This linear damage rule can be written as follows:

$$\sum_{i=1}^{m} \frac{n_i}{N_i} = 1 \qquad (6.11)$$

where:

n_i = number of load cycles corresponding to the ith level of stress

N_i = number of load cycles to failure corresponding to the ith level of stress

m = number of load levels

The relative contribution to the damage for a single load level can obtained as follows:

$$D_i = \frac{n_i}{N_i} \tag{6.12}$$

Assuming that the cumulative dissipated energy determines the damage in the fatigue process, Hopman et al (1989) defined the damage as the ratio of the cumulative dissipated energy up to load cycle n and the total amount of dissipated energy at the end of the test, at load cycle N. Based on this, they proposed a modified Miner's rule, as follows:

$$D_i = \left(\frac{n_i}{N_i}\right)^x \tag{6.13}$$

where:

x = experimental value

Hopman et al (1989) defined three stages in a fatigue process. Stage 1 is characterised by the formation of hairline cracks. In stage 2 the hairline cracks grow and a network of cracks is formed. Stage 3 is characterised by crack formation up to failure. The average values of x obtained from four point bending tests for two different mixes at different temperatures varied between 0.82 and 0.92 for stage 1, 0.04 and 0.28 for stage 2, and 1 for the third stage.

Di Benedetto et al. (1996) analysed fatigue data from triaxial tension/compression tests and identified the existence of three phases during a fatigue test. Phase I is characterised by a rapid reduction of stiffness modulus and corresponds to a phase where heating and fatigue occur, but heating is the predominant effect. In phase II, the temperature stabilises. This phase is characterised by an approximate linear reduction in the stiffness modulus with number of cycles. Phase III is characterised by rapid drop in stiffness modulus with loading cycles up to failure.

Di Benedetto et al. (1996) stated that the fatigue damage law could be isolated and characterised only during the second phase. The proposed damage law introduces an isotropic damage parameter, D (Lemaitre, 1996), defined at any number of cycles, N, by the following expression:

$$D(N) = \frac{E_{0\theta_N} - |E^*(N)|}{E_{0\theta_N}} \qquad 0 \le D \le 1 \tag{6.14}$$

where:

$E^*(N)$ = complex modulus of the damaged material at cycle N

$E_{0\theta_N}$ = norm of the initial complex modulus , which would be obtained at the temperature of the considered cycle, θ_N

The damage parameter, D, ranges from 0 (undamaged) to 1 (fully damaged).

The damage rate at each cycle can be obtained by derivation of Equation 6.14, as follows:

$$\frac{dD}{dN} = -\frac{1}{E_{0\theta_N}} \frac{d|E^*|}{dN} \tag{6.15}$$

The modulus $E_{0\theta_N}$ is unknown. A good approximation of this value can be obtained from the intercept, E_{00}, by linear extrapolation of the E^* against number of cycles N in phase II. This extrapolation is introduced to eliminate the heating effects taking place during phase I.

The resulting damage rate can then be written as follows:

$$\frac{dD}{dN} = -\frac{1}{E_{00}} \frac{d|E^*|}{dN} = -a_T \tag{6.16}$$

where:

a_T = slope of the linear regression of the curve E^*/E_{00} versus N

In order to compare the rate of damage for controlled strain and controlled stress tests, the influence of the thermal effects occurring during phase II must be considered. As stated earlier, during controlled strain fatigue testing the dissipated energy decreases with number of cycles, and increases during controlled stress tests. This produces changes on the temperature that generates variations in the stiffness modulus.

To evaluate the temperature effects on the slope a_T, Di Benedetto et al. (1997) decomposed the slope a_T into two terms, as follows:

$$a_T = a_\theta + a_F \tag{6.17}$$

where:

a_F = is the fatigue slope at constant temperature and corresponds to the one obtained on the road and,

a_θ = is the slope related to the variation of the modulus due to temperature change during phase II. It is positive for controlled stress tests and negative for controlled strain tests.

To obtain a_θ, Di Benedetto et al. (1997) assumed that the change in modulus due to temperature variations is proportional to the dissipated energy. The proposed relation to obtain a_θ is as follows:

$$a_\theta = -a_W \frac{E_0 - E_{00}}{E_{00}} \tag{6.18}$$

where:

E_0 = norm of the initial complex modulus during the first cycle

and,

$$a_W = \frac{1}{W_{00}} \frac{dW}{dN} \tag{6.19}$$

where:

a_W = slope of the linear regression calculated from the dissipated energy per cycle divided by W_{00}

W_{00} = intercept of the linear regression calculated from the dissipated energy per cycle

Finally, the corrected rate of damage can be written as follows:

$$\frac{dD_{corr}}{dN} = -a_F = -\left(a_T + a_W \frac{E_0 - E_{00}}{E_{00}} \right) \tag{6.20}$$

The proposed fatigue law is totally known if the relation between the rate of damage a_F and the strain amplitude, ε_0, is experimentally obtained. For simplicity, Di Benedetto et al. (1996) proposed a linear expression as follows:

$$\frac{dD_{corr}}{dN} = -a_F = m\varepsilon_0 + n \tag{6.21}$$

where m and n are experimental values.

In a similar manner, Choi et al. (2002) applied continuum damage mechanics in a simple way to model fatigue of asphalt mixtures. They performed uniaxial and trapezoidal fatigue tests under controlled stress at different temperatures. From the test data, the stiffness modulus was plotted as a function of load cycles. The evolution of the stiffness modulus was divided in three stages. The first stage was characterised by a rapid drop in stiffness. During the second stage, the reduction in stiffness modulus was approximately linear. This stage accounted for most of the fatigue life. Finally, the third stage was characterised by a sudden drop in

stiffness up to total failure. As seen before, Di Benedetto et al. (1996) also reported the same stages or phases in a fatigue test.

The state of the material was characterised by a dimensionless value known as damage, D^*, which varies from 0, undamaged to 1, fully damaged. The proposed damage can be written as follows:

$$D^* = \frac{S_0 - S}{S_0} \tag{6.22}$$

where S is the stiffness modulus; and S_0 is the modulus of the intact material.

Choi et al. (2002) modelled the second stage, fitting a straight line to the stiffness data. The Y-axis intercept was defined as the imaginary initial stiffness modulus, S_0. The slope of the fitting line was used to calculate the constant rate of damage accumulation, dD^*/dN.

It should be notice here that, the damage parameter and the rate of damage accumulation introduced by Di Benedetto et al. (1996) and by Choi et al. (2002) are equivalent, knowing that $S_0 = E_{00}$, and the slope of the fitting line corresponds to slope of the linear regression of the curve E^* versus N.

The rate of damage accumulation was then plotted as a function of the applied stress, and the following relation was obtained:

$$\frac{dD^*}{dN} = A\sigma_0^n \tag{6.23}$$

where σ_0 is the applied stress; and A and n are material constants.

Furthermore, controlled stress fatigue results were expressed in terms of the initial applied strain, ε_0, calculated using the imaginary stiffness modulus, S_0, as follows:

$$\varepsilon_0 = \frac{\sigma_0}{S_0} \tag{6.24}$$

and,

$$\frac{dD^*}{dN} = B\varepsilon_0^m \tag{6.25}$$

where B and m are material constants.

6.2 FATIGUE TEST PROCEDURES

6.2.1 Theory of the four-point bending test

The differential equation that governs the deflection due to bending in a four point bending test of a rectangular beam that is vertically loaded is given by:

$$E \cdot I \cdot \frac{\partial^4 V_b(x,t)}{\partial x^4} + \rho \cdot b \cdot h \cdot V_b(x,t) = Q(x,t) \tag{6.26}$$

where:

E	=	Young's modulus
I	=	Inertia moment of the beam ($bh^3/12$)
$V_b(x,t)$	=	Deflection due to bending
ρ	=	Density
b	=	Width of the beam
h	=	Height of the beam
$Q(x,t)$	=	Force distribution along the beam

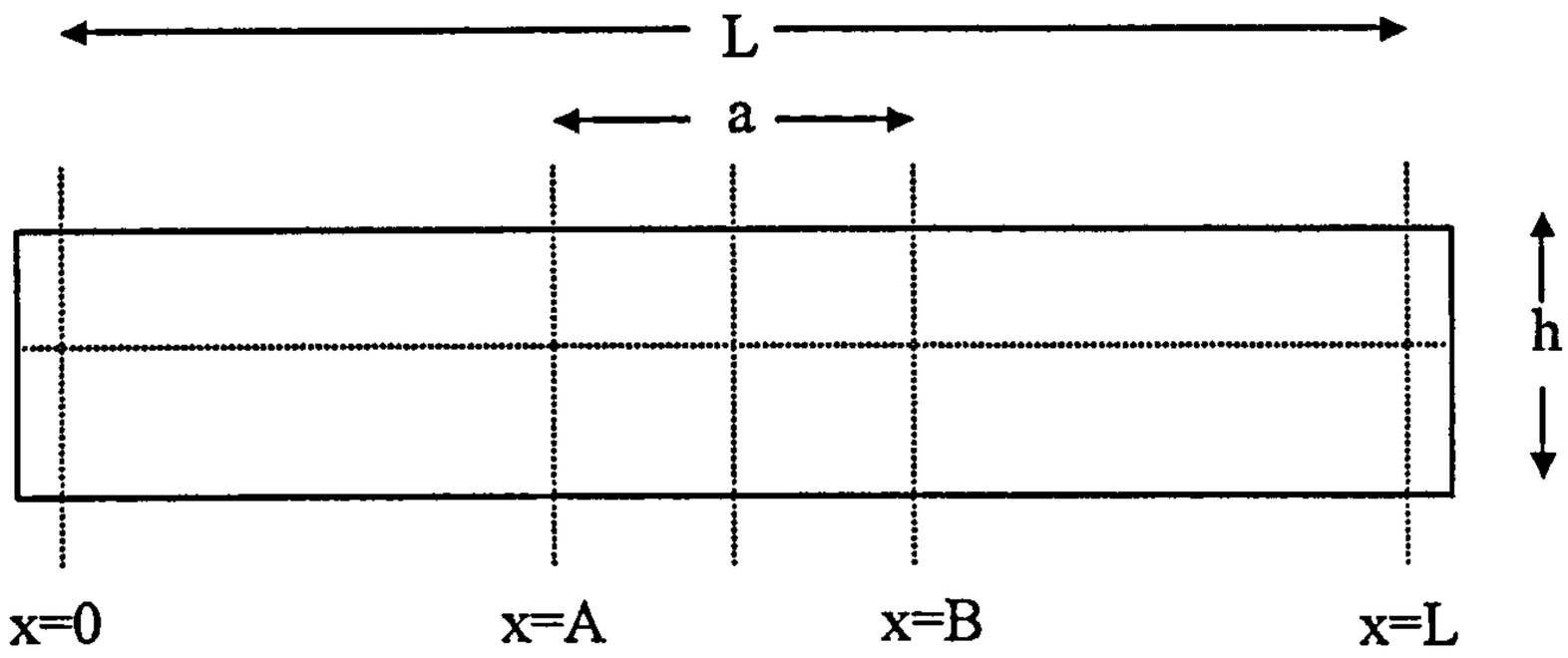

Figure 6.2 Four point coordinate system

For static bending, the fourth order differential equation is given by:

$$E \cdot I \cdot \frac{d^4 V_b(x)}{dx^4} = Q(x) \tag{6.27}$$

The load along the beam, $Q(x)$, consists of two applied point loads, F_a and F_b ($F_a = F_b = F_0/2$) at the clamps at x=A and x=B, and two reaction loads ($-F_0/2$) at the clamps at x=0 and x=L (see **Figure 6.2**).

The resulting second order differential equation and boundary conditions are given by:

$$-E \cdot I \cdot \frac{d^2 V_b(x)}{dx^2} = M(x) \tag{6.28}$$

$$\text{Region I: } A \le x \le \frac{L}{2}, \quad M(x) = \frac{F_0}{2} \cdot A \tag{6.29}$$

$$\text{Region II: } 0 \le x \le A, \quad M(x) = \frac{F_0}{2} \cdot x \tag{6.30}$$

and,

$$x=0:\quad V_b=0;\quad x=L/2:\quad \frac{dV_b(x)}{dx}=0 \tag{6.31}$$

$$x=A:\quad \frac{dV_b(x)}{dx}\quad \text{and}\quad V_b(x)\quad \text{are continuous} \tag{6.32}$$

Finally, the deflection along the beam is given by:

$$\text{Region I}: A\le x\le \frac{L}{2};$$
$$V(x)=\frac{8F_0L^3}{96EI}\cdot\frac{A}{L}\cdot\left(3\frac{x}{L}-3\frac{x^2}{L^2}-\frac{A^2}{L^2}\right) \tag{6.33}$$

$$\text{Region II}: 0\le x\le A;$$
$$V(x)=\frac{8F_0L^3}{96EI}\cdot\frac{x}{L}\cdot\left(3\frac{A}{L}-3\frac{A^2}{L^2}-\frac{x^2}{L^2}\right) \tag{6.34}$$

Therefore the deflection in the centre of the beam, V_{max}, can be written as:

$$V_{\max}=\frac{2F_0A}{96EI}\cdot\left[3L^2-4A^2\right] \tag{6.35}$$

knowing that

$$a=L-2A \tag{6.36}$$

hence

$$V_{\max}=\frac{F_0(L-a)}{96EI}\cdot\left[2L^2+2aL-a^2\right] \tag{6.37}$$

The following general relation exist between the horizontal strain in the beam and the deflection:

$$\varepsilon(x,y)=-\frac{M(x)y}{EI} \tag{6.38}$$

The maximum strain in the centre of the beam is given by:

$$\varepsilon_{\max} = -\frac{F_0 A h}{4EI} \tag{6.39}$$

Combining Equation 6.35 and 6.39:

$$\varepsilon_{\max} = \frac{12hV_{\max}}{3L^2 - 4A^2} \tag{6.40}$$

The maximum bending stress is then given by:

$$\sigma_{\max} = E \cdot \varepsilon_{\max} = \frac{3F_0 A}{bh^2} \tag{6.41}$$

The expression for the stiffness modulus of the beam is given by:

$$E = \frac{\sigma_{\max}}{\varepsilon_{\max}} = \frac{AF_0(3L^2 - 4A^3)}{4bh^3} \tag{6.42}$$

6.2.2 Four-point bending test apparatus

Fatigue testing was performed in a four-point bending test apparatus, shown schematically in **Figure 6.3**. The test equipment consists of a servo-hydraulic actuator connected to a 2.5 kN load cell mounted above the fatigue frame, shown in **Figure 6.4**. The load is applied through the actuator that is connected to the fatigue frame trough a steel shaft. Once inserted, the specimen is clamped in position at the four points of the fatigue frame by means of torque motors located underneath the four supports.

The vertical deflection at the centre of the specimen, δ, is measured using a Linear Variable Differential Transducer (LVDT) situated at the bottom of the beam. The transducer is pushed into contact with the specimen by means of a pneumatically controlled trigger mechanism prior to start of the test.

The vertical deflection was used to calculate the tensile strains. Maximum stress, strain and stiffness were computed by using the following relationships:

$$\sigma = \frac{3aP}{wh^2} \tag{6.43}$$

$$\varepsilon = \frac{12h\delta}{3L^2 - 4a^2} \tag{6.44}$$

$$S = \frac{\sigma}{\varepsilon} = \frac{aP\left(3L^2 - 4a^2\right)}{4\delta w h^3} \tag{6.45}$$

where:

σ	=	peak-to-peak stress
ε	=	peak-to-peak strain
P	=	applied peak-to-peak load
S	=	stiffness
L	=	beam span (L=270 mm)
w	=	width of beam (w=50 mm)
h	=	height of beam (h=50 mm)
δ	=	beam deflection at neutral axis
a	=	distance between inner clamps (a=L/3=90 mm)

The energy dissipated per cycle was computed as the area within the stress-strain hyteresis loop, using Equation 6.4.

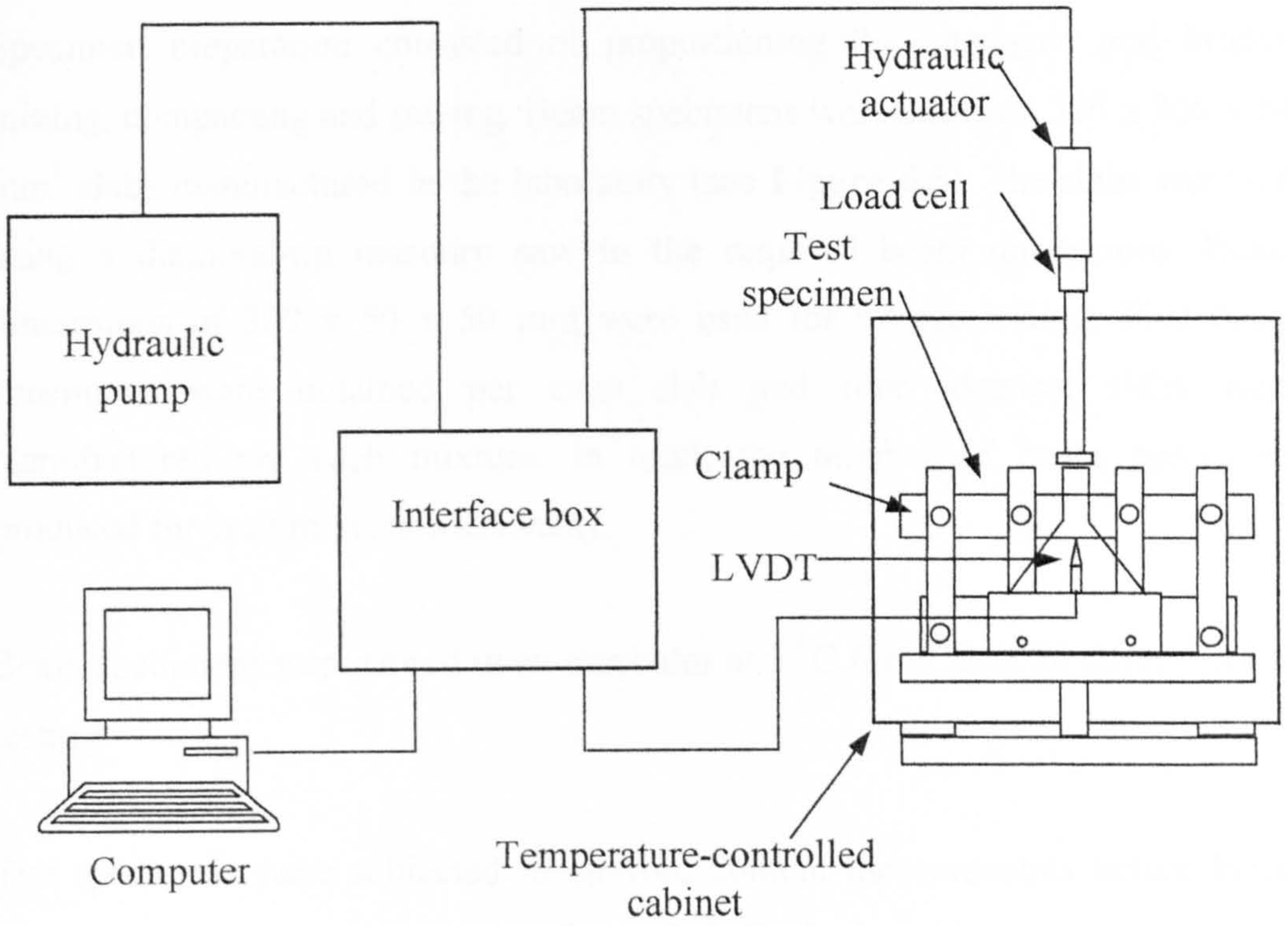

Figure 6.3 Four-point bending test apparatus

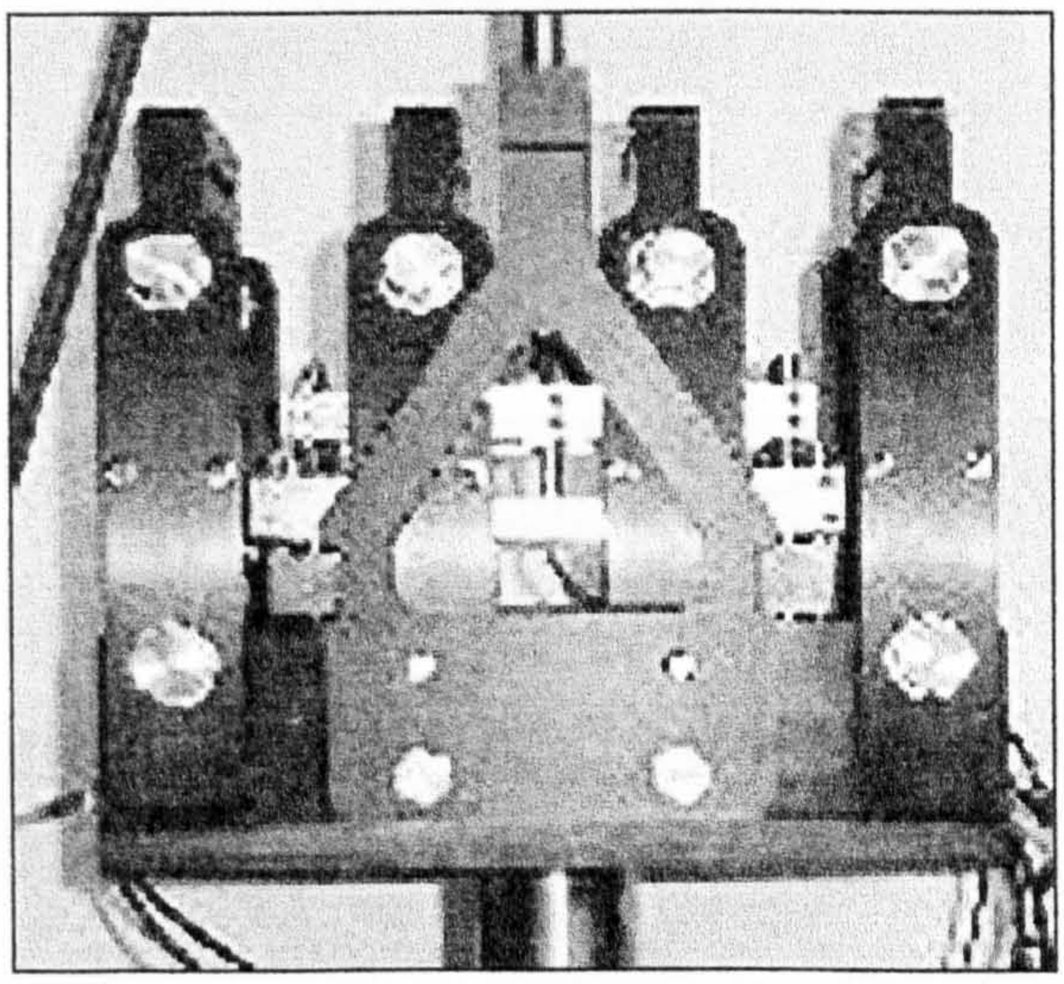

Figure 6.4 Four point fatigue frame

6.2.3 Specimen preparation

Specimen preparation consisted of proportioning the aggregate and binder, mixing, compacting and sawing. Beam specimens were cut from 306 x 306 x 64 mm^3 slabs manufactured in the laboratory (see **Figure 6.5**). The slabs were cut using a diamond-tip masonry saw to the required beam dimensions. Beam dimensions of 300 x 50 x 50 mm were used for fatigue testing. Five beam specimens were obtained per each slab and four identical slabs were manufactured per each mixture. In total, the number of beam specimens produced for each mixture was twenty.

Beam specimens were stored in an incubator at 5 ^{0}C for at least 20 days, prior to testing.

The specimens were subjected to air-void content measurements before being tested. The volumetric parameters for each individual specimen are presented in **Appendix L.**

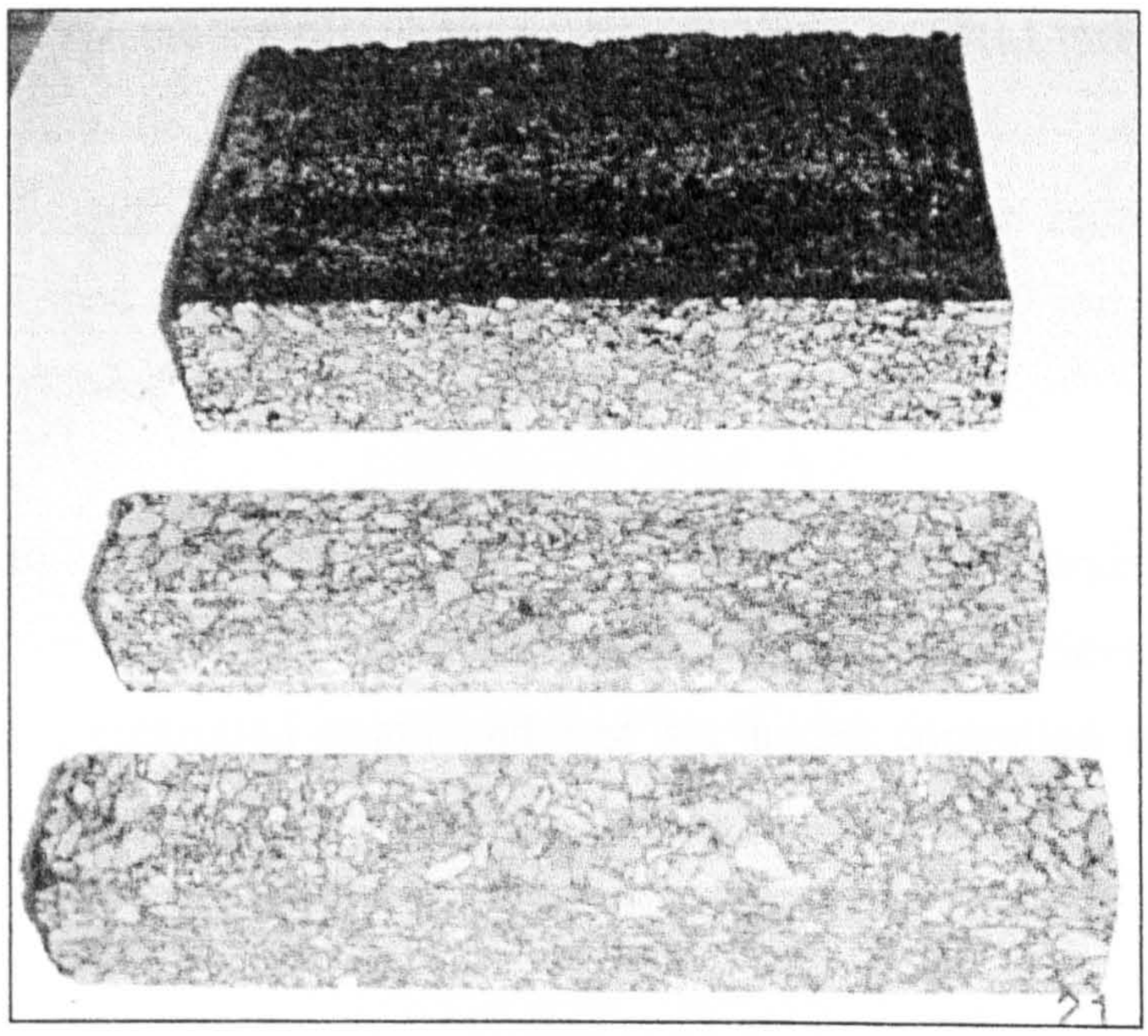

Figure 6.5 Fatigue specimens

6.2.4 Specimen testing

Specimens ready for testing were conditioned inside the fatigue temperature-controlled cabinet for at least 4 hours. All the specimens in this study were tested at 10 ^{0}C.

In order to check the behaviour of the fatigue apparatus a PVC beam (300 x 50 x 50 mm) was tested just before every asphalt specimen. The PVC beam was tested for a few hundred loading cycles, and the stiffness value obtained was compared with the known value of 3.7 GPa for this elastic material. A typical test is presented in **Appendix M**.

Fatigue testing was carried out under controlled strain and controlled stress conditions. All tests were conducted at a frequency of 10 Hz under sinusoidal loading with no rest periods.

For controlled strain testing, peak-to-peak strain levels selected varied between 250 and 350 μm/m for the unmodified mixture (Control mix), and between 300 and 400 μm/m for the crumb-rubber modified mixtures (CRM mix 1 and CRM mix 2). For controlled stress testing, peak-to-peak stress levels selected varied between 2000 and 3000 kPa for the unmodified mixture and the mixture modified with car-tyre rubber (CRM mix 2), and between 2500 and 3500 kPa for the mixture modified with truck-tyre rubber (CRM mix 1).

For each mixture, nine specimens were tested under controlled strain and another nine under controlled stress, except for the control mix, where eleven specimens were tested on controlled strain and just six under controlled stress. Three specimens were tested for each strain or stress level selected.

6.2.5 Fatigue test data

A computer programme created by Cooper Research Ltd was used to compute the stress and strain amplitudes and mean values; stiffness modulus and percentage reduction in stiffness; phase angle and dissipated energy per cycle as functions of the number of load cycles. Cumulative dissipated energy to a given load cycle was also computed.

Data was captured every 50 cycles and the test finished when the initial stiffness was reduced by 50 percent, for both controlled strain and stress modes.

Due to the large amount of data, a macro was written in Visual Basic to facilitate fatigue data reduction (see **Appendix N**). This program enabled the number of data points to be reduced by 1/10 or by 1/100, depending on the total number of data points. When the data was reduced by 1/10 the cycles sequence was 500, 1000, 1500 etc; and when the data was reduced by 1/100 the cycles sequence was 5000, 10000, 15000 etc. **Appendix O** contains a typical fatigue data file after data reduction.

Furthermore, the initial values of strain and stress amplitudes, stiffness and phase angle were calculated by linear regression of the first 500 cycles. The initial values selected were the values at 100 cycles. This regression method was used because of the variability of the data in some of the tests during the first few cycles.

Figures 6.6 and **6.7** show strain and stress amplitudes and mean values for the two modes of loading. It can be seen that for controlled strain testing (**Figure 6.6**) the strain amplitude remains constant and the stress amplitude decreases with number of load applications. On the other hand, for controlled stress mode (**Figure 6.7**) the stress amplitude remains constant and the strain amplitude increases with the number of cycles. Also shown are the mean values that are, in general, very close to 0.

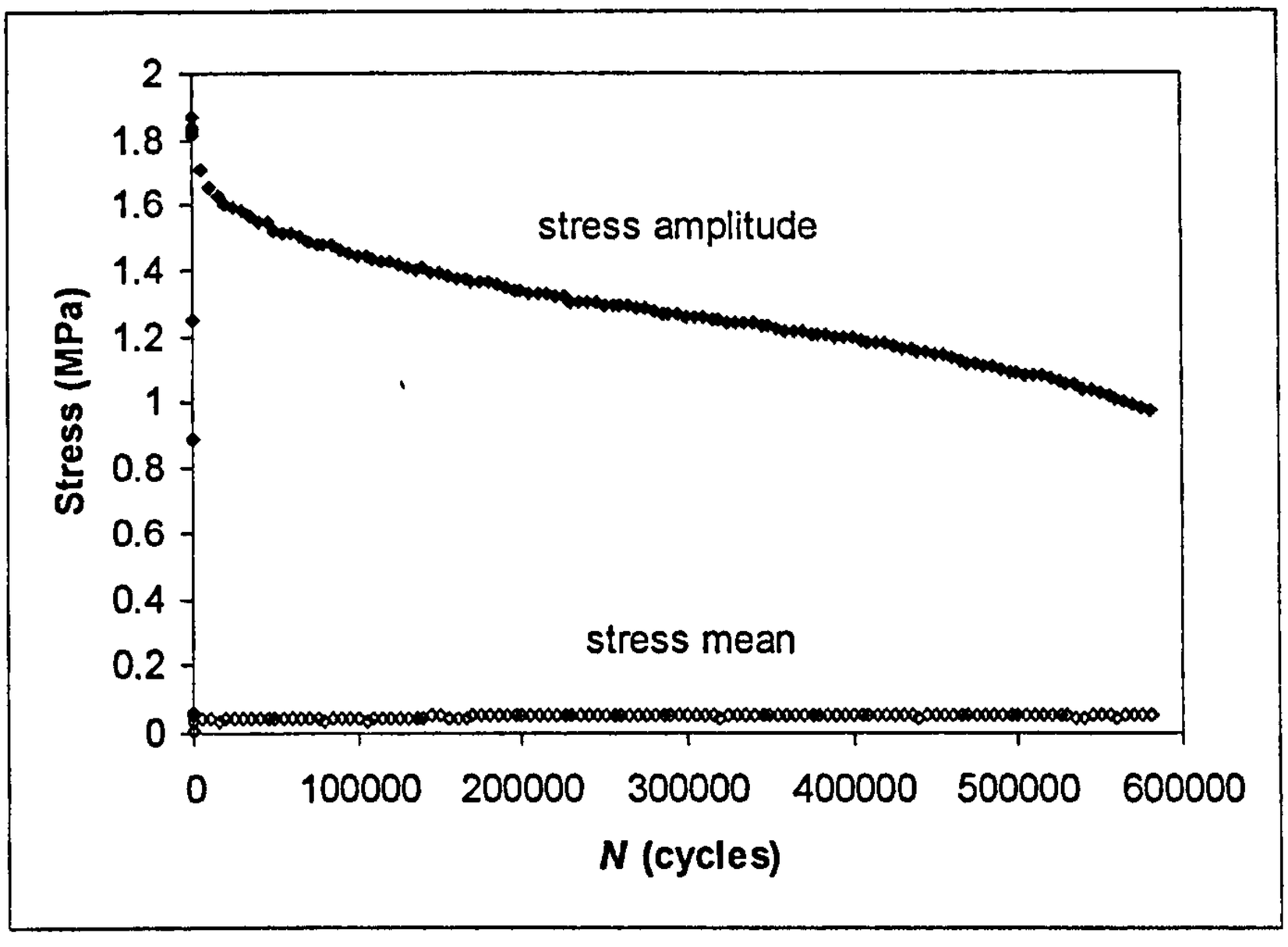

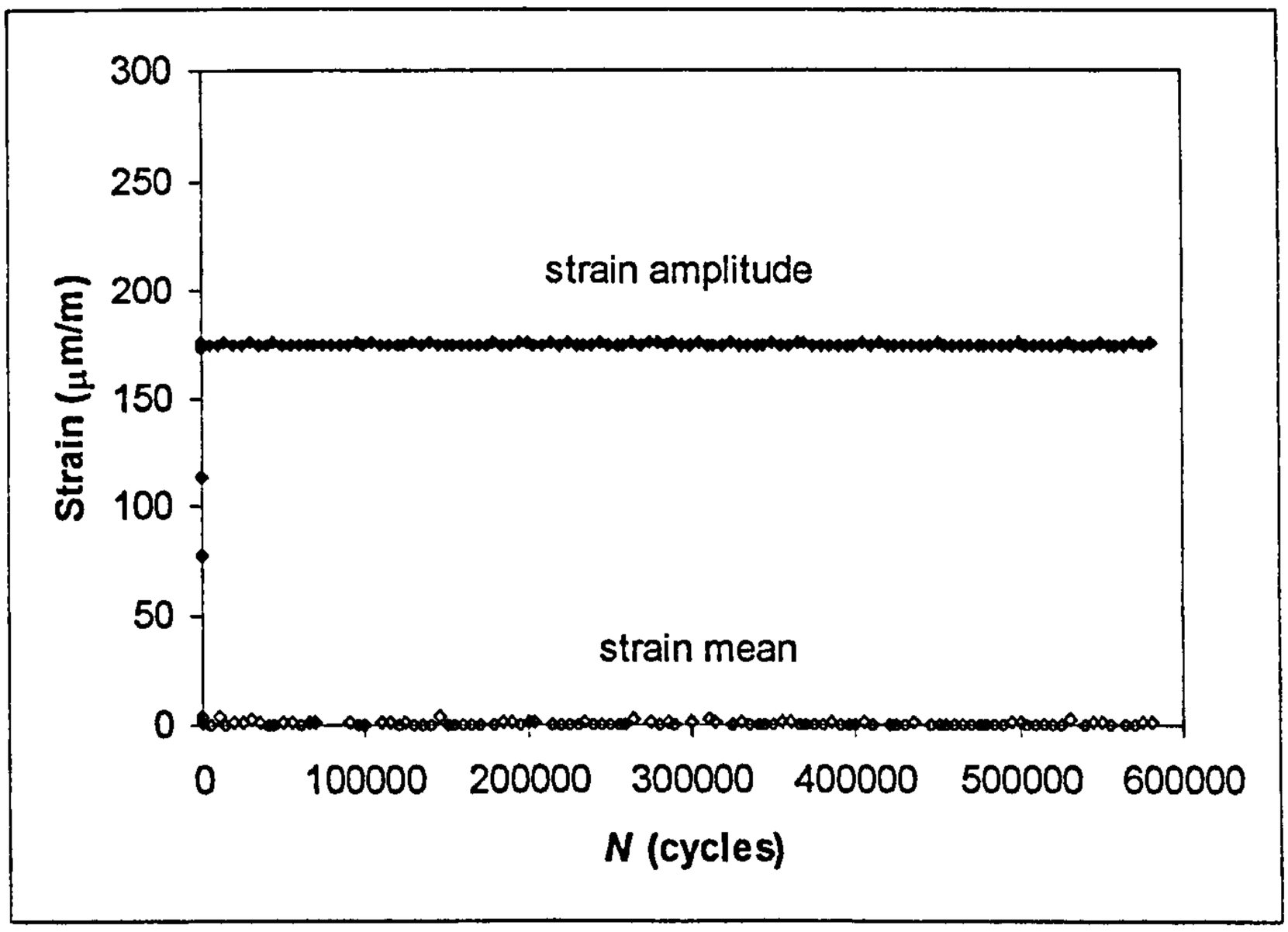

Figure 6.6 Stress and strain amplitudes and means in a controlled strain test

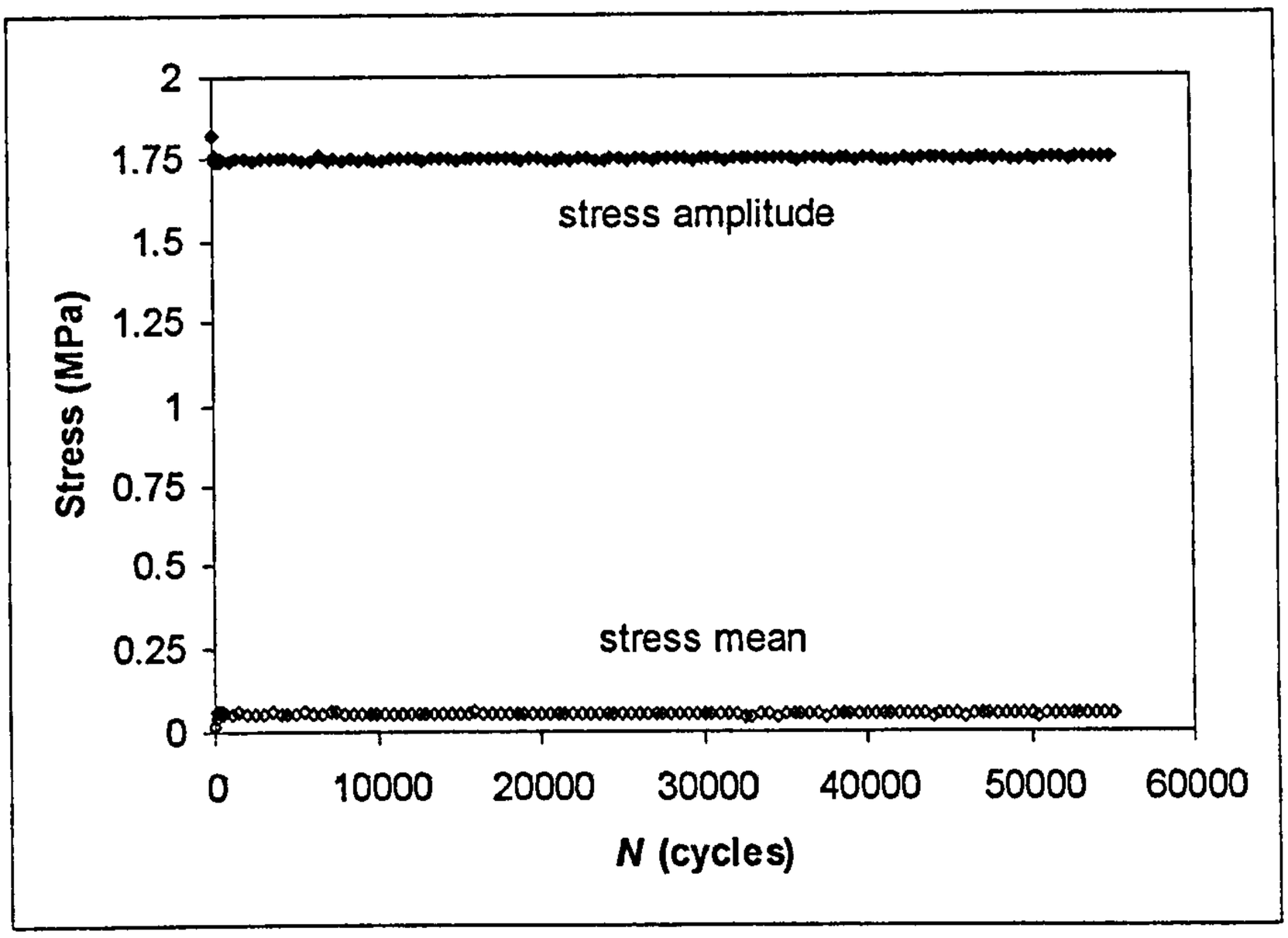

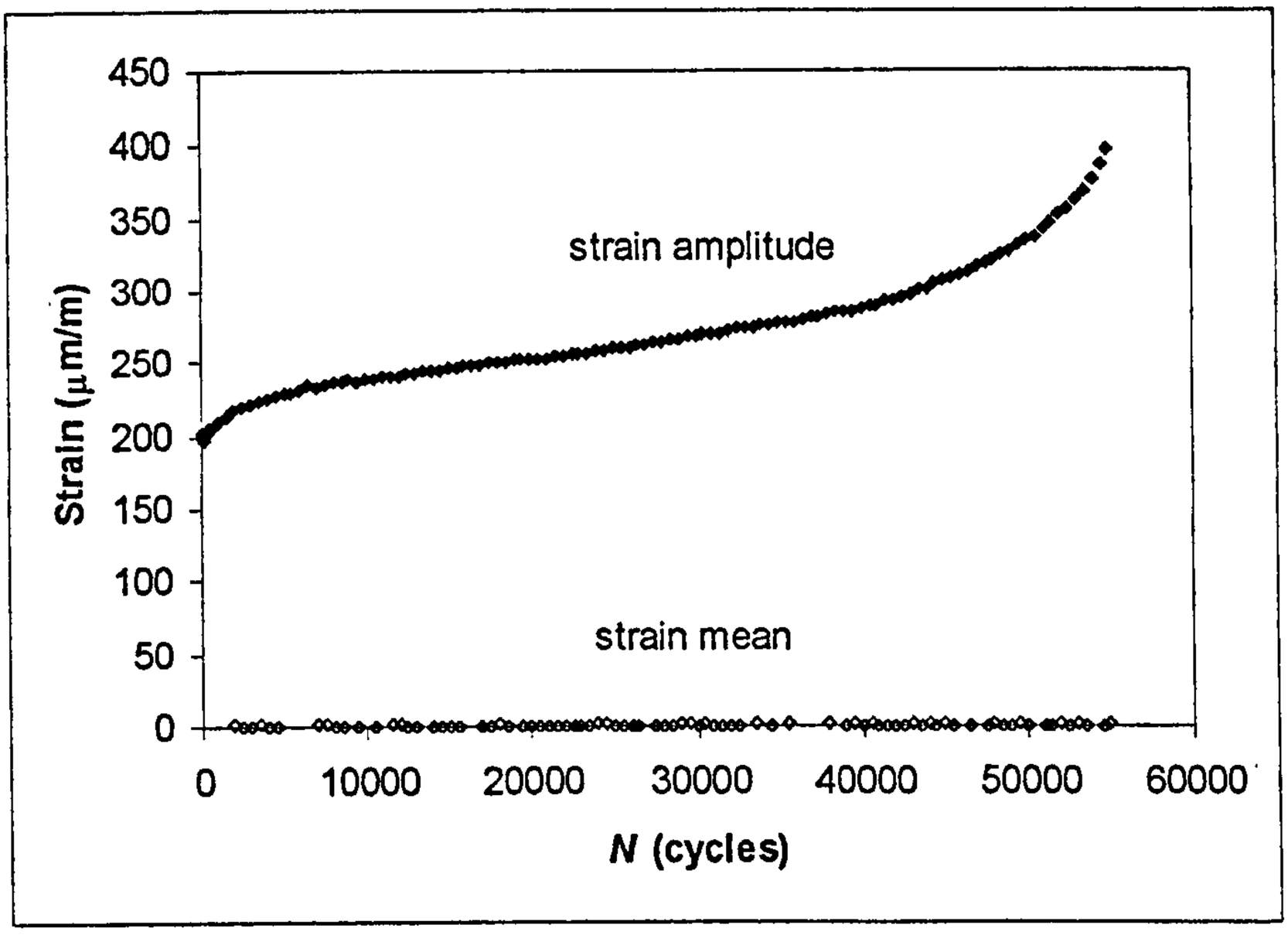

Figure 6.7 Stress and strain amplitudes and means in a controlled stress test

6.3 ANALYSIS OF FATIGUE TESTS RESULTS

6.3.1 Fatigue failure and crack initiation

Failure has been defined as 50 % reduction in the initial stiffness for both, controlled stress and strain conditions. N_f corresponds to the number of cycles at which the stiffness is reduced by 50 percent, as shown in **Figures 6.8** and **6.9** for controlled strain and stress tests respectively.

The Energy Ratio defined in Equation 6.10 has been used to define the number of cycles (N_1) in a controlled strain fatigue test to a point where cracks are considered to initiate. When the Energy Ratio is plotted against the number of load cycles in a controlled strain test, there is a clear change in behaviour at N_1 represented by the change of the slope at this point, as shown in **Figure 6.8**.

In controlled stress testing the stress amplitude remains constant and after crack initiation the stress at the crack tip increases rapidly. Consequently, N_1 corresponds to the peak value when the energy ratio is plotted against the number of load cycles, as shown in **Figure 6.9**.

For controlled strain and controlled stress fatigue testing, N_1 represents the material in the same state of damage corresponding to "crack initiation" (Rowe 1993).

Experimental fatigue data corresponding to the three materials tested is presented in **Table 6.1** (Control mix), **Table 6.2** (CRM mix 1) and **Table 6.3** (CRM mix 2). These include initial values (100 cycles) of strain, stress, stiffness modulus and phase angle, and the number of cycles to failure N_f and to crack initiation N_1.

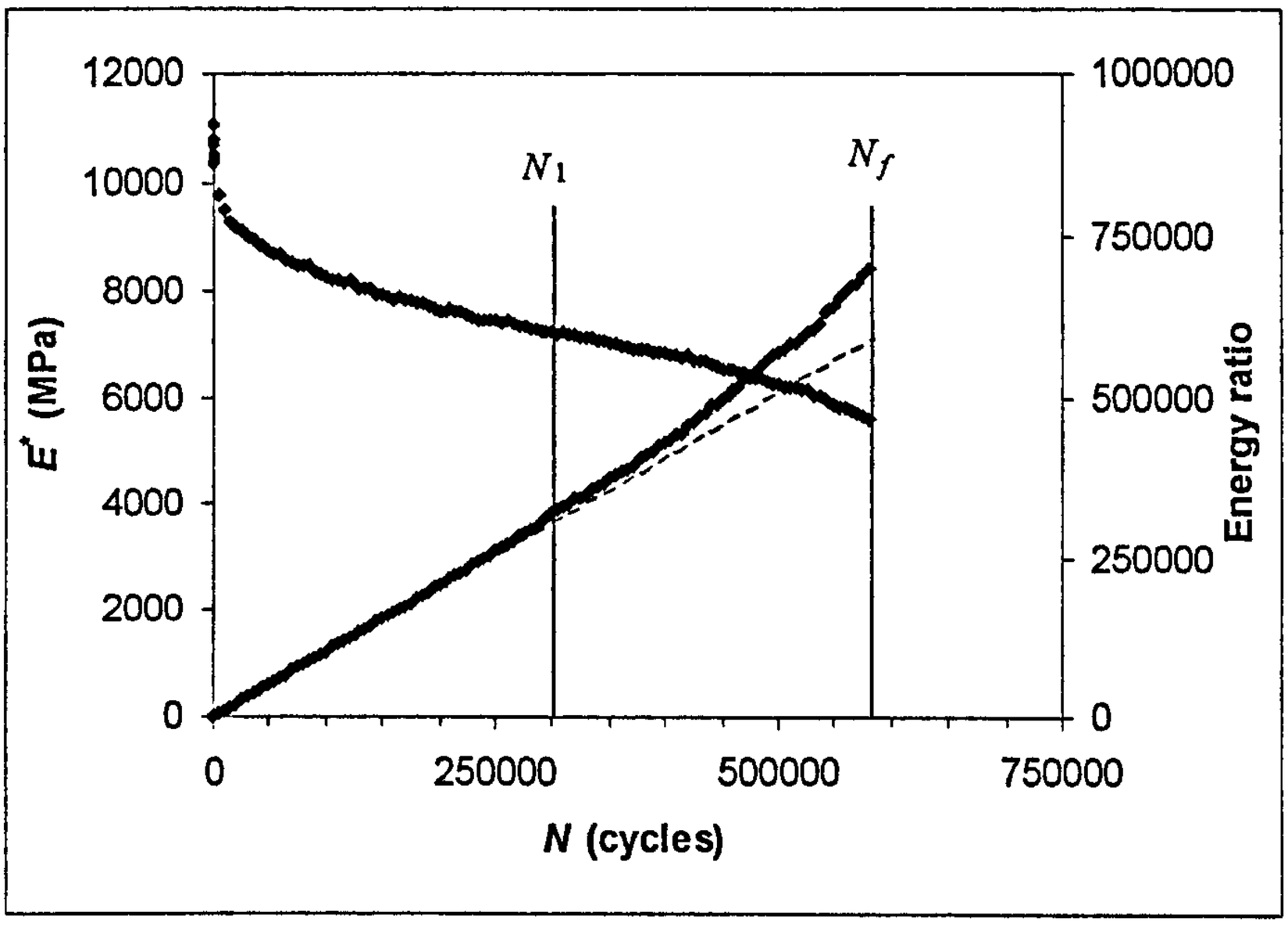

Figure 6.8 Definition of failure, N_1 and N_f in controlled strain tests

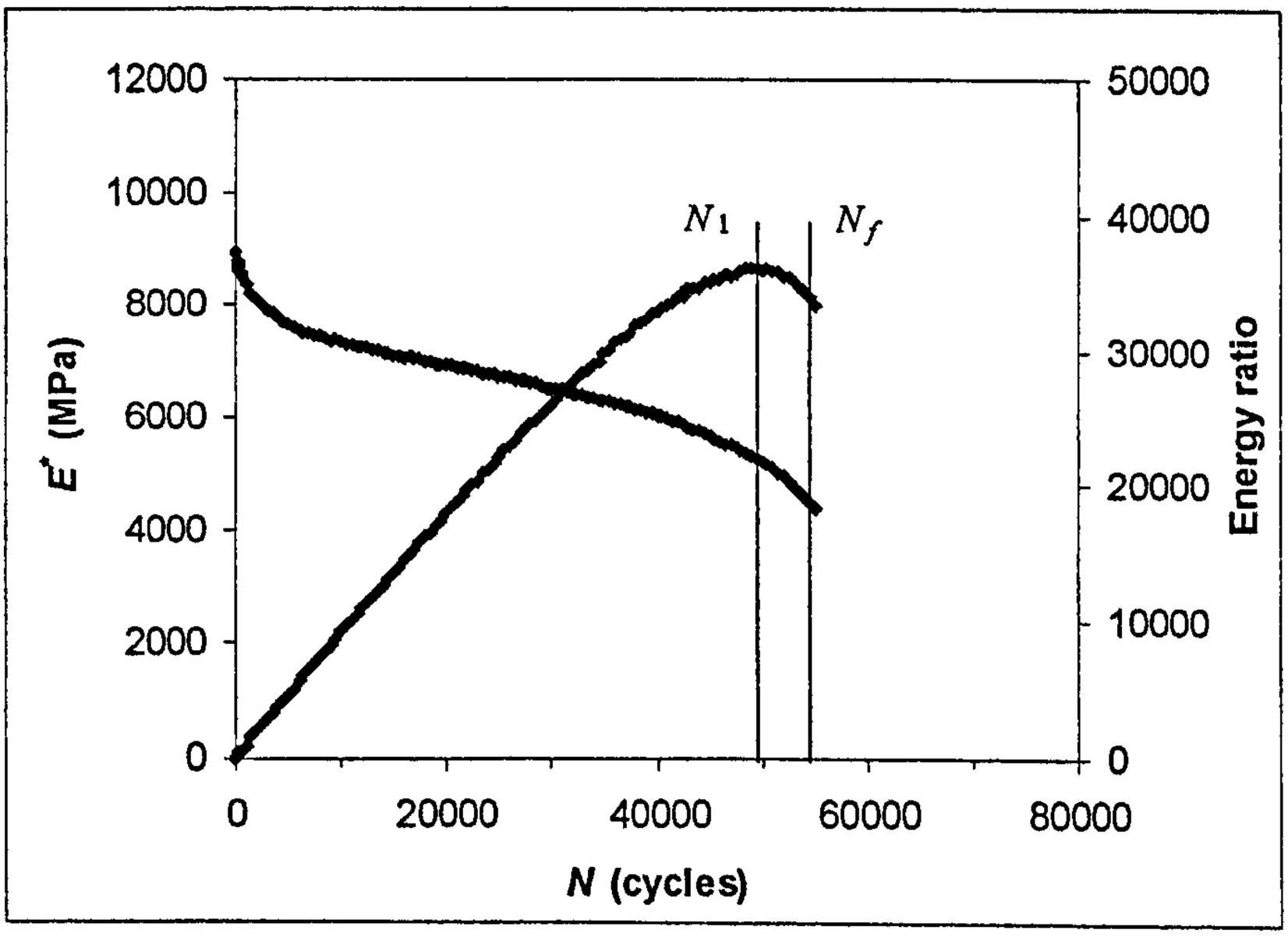

Figure 6.9 Definition of failure, N_1 and N_f in controlled stress tests

Sample	Type	ε_0 (με)	σ_0 (MPa)	E_0 (MPa)	φ_0 (^{0})	N_1 (cycles)	N_f (cycles)
C1	Strain	153	1.55	10108	20.1	190000	325000
C2	Strain	151.1	1.39	9160	21.1	250000	420000
C3	Strain	150.7	1.53	10080	20.5	170000	240000
C8	Strain	137.5	1.26	9200	22.6	550000	945000
C7	Strain	135.2	1.16	8911	20.6	300000	560000
C9	Strain	135	1.15	9387	19.2	350000	765000
C10	Strain	125.4	1.18	9400	21.8	700000	1460000
C11	Strain	126.8	0.97	8145	24.4	850000	2170000
C12	Strain	123.8	1.20	9775	21.8	750000	1540000
C13	Strain	176.6	1.69	10035	22.5	80000	220000
C14	Strain	175.5	1.60	9399	21.6	120000	255000
C16	Stress	144.9	1.50	10345	21.2	215000	240000
C17	Stress	152.2	1.50	9866	21.5	139500	152000
C6	Stress	161.5	1.50	9250	21.3	70000	78000
C18	Stress	136.7	1.25	9140	22.3	400000	435000
C19	Stress	133.7	1.25	9339	21	595000	660000
C20	Stress	117.5	1.00	8502	22.6	825000	875000
Average				**9414**	**21.5**		
STD				**565**	**1.1**		

Table 6.1 Fatigue tests results: Control mix

Sample	Type	ε_0 (με)	σ_0 (MPa)	E_0 (MPa)	φ_0 (^{0})	N_1 (cycles)	N_f (cycles)
RT1	Strain	150.2	1.69	11231	18.3	1250000	2295000
RT2	Strain	150.7	1.43	9518	21	750000	1405000
RT4	Strain	150.4	1.37	9149	20.4	900000	1810000
RT5	Strain	173.7	1.86	10872	19.3	300000	580000
RT6	Strain	174.8	1.91	10966	18.5	250000	445000
RT3	Strain	175.4	1.82	10409	19.6	600000	1055000
RT7	Strain	200.3	2.00	10144	19.4	130000	280000
RT8	Strain	201.3	1.70	8608	23	160000	405000
RT9	Strain	200	1.75	8871	21.6	170000	395000
RT10	Stress	143.3	1.50	10443	18.4	355000	385000
RT11	Stress	130.7	1.50	11453	16.6	285000	320000
RT12	Stress	137.2	1.50	10901	17.3	345000	385000
RT14	Stress	124	1.25	10064	19.7	700000	765000
RT16	Stress	106.3	1.25	11728	14.9	740000	825000
RT15	Stress	116.3	1.25	10765	17.4	1065000	1170000
RT17	Stress	174.5	1.75	10011	18.8	153000	167000
RT18	Stress	159.7	1.74	10938	17.2	110000	121000
RT19	Stress	197.6	1.75	8863	20.6	50500	55000
Average				**10274**	**19.0**		
STD				**911**	**1.9**		

Table 6.2 Fatigue tests results: CRM mix 1

Sample	Type	ε_0 (με)	σ_0 (MPa)	E_0 (MPa)	φ_0 (^{0})	N_1 (cycles)	N_f (cycles)
RC1	Strain	150.5	1.49	9969	17.8	550000	1060000
RC2	Strain	150.3	1.41	9419	19.7	900000	1670000
RC3	Strain	149.6	1.40	9423	18.4	800000	1830000
RC4	Strain	175.4	1.44	8326	17.6	260000	525000
RC5	Strain	174.7	1.66	9623	19.5	500000	865000
RC6	Strain	175.1	1.66	9618	18.5	100000	270000
RC20	Strain	199.6	2.11	10788	19.7	80000	164000
RC19	Strain	199.4	2.19	11176	19	80000	163000
RC9	Strain	200.9	1.47	7407	23.3	180000	380000
RC10	Stress	147.1	1.50	10196	18.3	169000	183500
RC11	Stress	139.9	1.50	10699	18	180000	197000
RC12	Stress	137.4	1.50	10886	18	123000	137500
RC13	Stress	130.2	1.25	9606	18.6	380000	420000
RC14	Stress	125.2	1.25	9963	17.8	490000	545000
RC15	Stress	122	1.25	10243	18.3	530000	590000
RC16	Stress	86.2	1.00	11588	17.1	2160000	2430000
RC17	Stress	103.2	1.15	11157	17.2	830000	880000
RC18	Stress	105.9	1.15	10806	17.7	720000	795000
Average				**10050**	**18.6**		
STD				**1043**	**1.4**		

Table 6.3 Fatigue tests results: CRM mix2

6.3.2 Relationship between strain/stress and fatigue life

Fatigue test data in controlled strain and stress mode tests has been used to derive a relationship between the initial strain, ε_0, and the applied stress, σ_0, and fatigue life.

As previously discussed, fatigue lives are presented in terms of N_1 and N_f, corresponding to crack initiation and failure. **Figures 6.10** and **6.11** illustrate the relationship between the number of cycles to crack initiation N_1 and the initial strain and stress amplitudes for controlled strain and stress tests respectively.

Initial strains or stresses, and the corresponding fatigue lives were plotted on logarithmic scales, and a power equation was fitted through the experimental data points in order to obtain a relationship between strain and stress and fatigue life.

For controlled strain and stress tests, the following relationships have been obtained:

$$N_1 = A_1 \varepsilon_0^{m_1} \tag{6.46}$$

and,

$$N_1 = B_1 \sigma_0^{n_1} \tag{6.47}$$

Material's constants, A_1 and m_1, B_1 and n_1, and regression coefficients values R^2 corresponding to the three materials tested are presented in **Table 6.4**.

Figures 6.12 and **6.13** illustrate the relationships between the number of cycles to failure N_f and the initial strain and initial applied stress. The following relationships have been obtained:

$$N_f = A_f \varepsilon_0^{m_f} \tag{6.48}$$

and,

$$N_f = B_f \sigma_0^{n_f} \tag{6.49}$$

Material's constants, A_f and m_f, B_f and n_f, and regression coefficients values R^2 corresponding to the three materials tested are presented in **Table 6.5**.

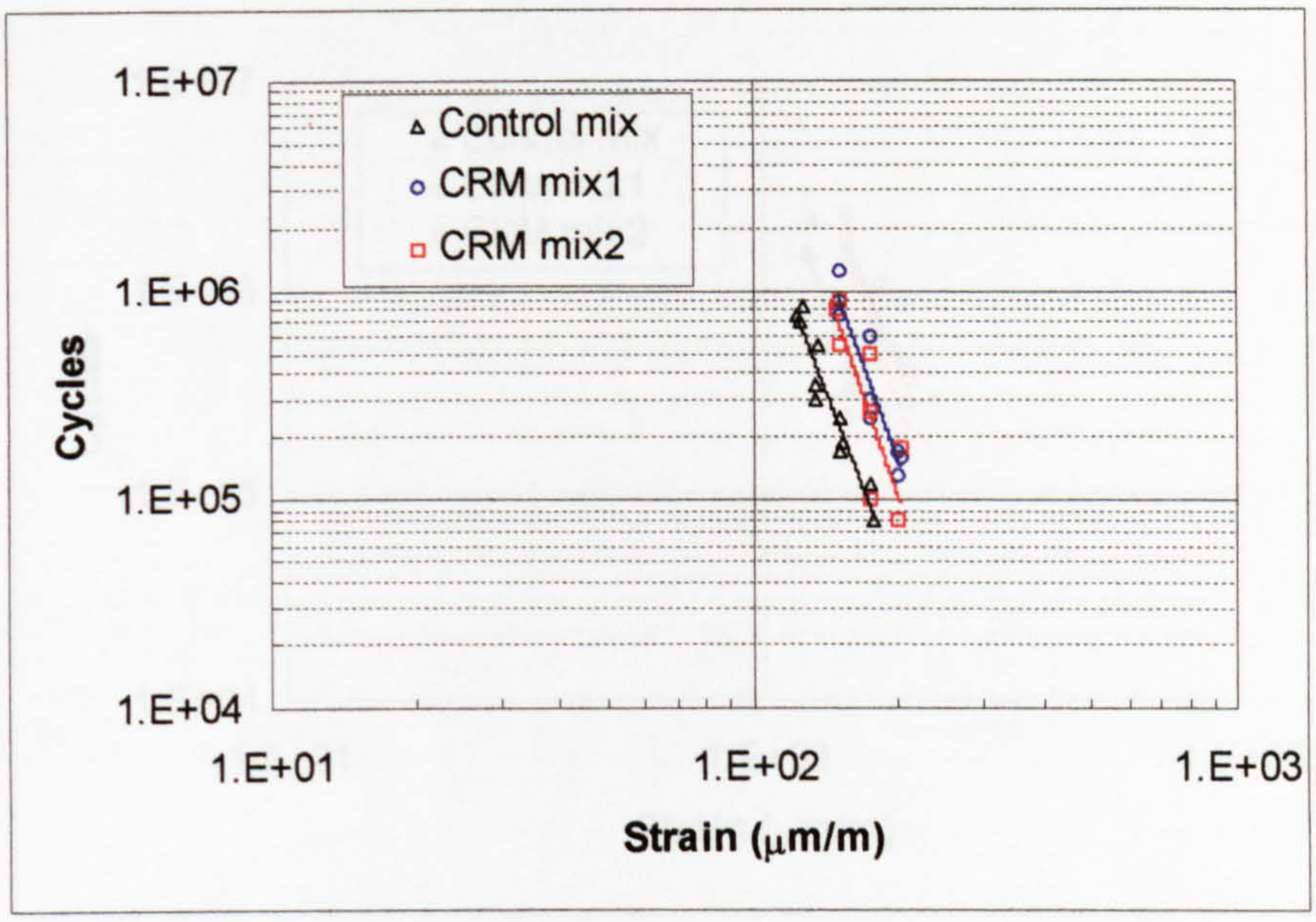

Figure 6.10 Relationship between fatigue life, N_1, and strain

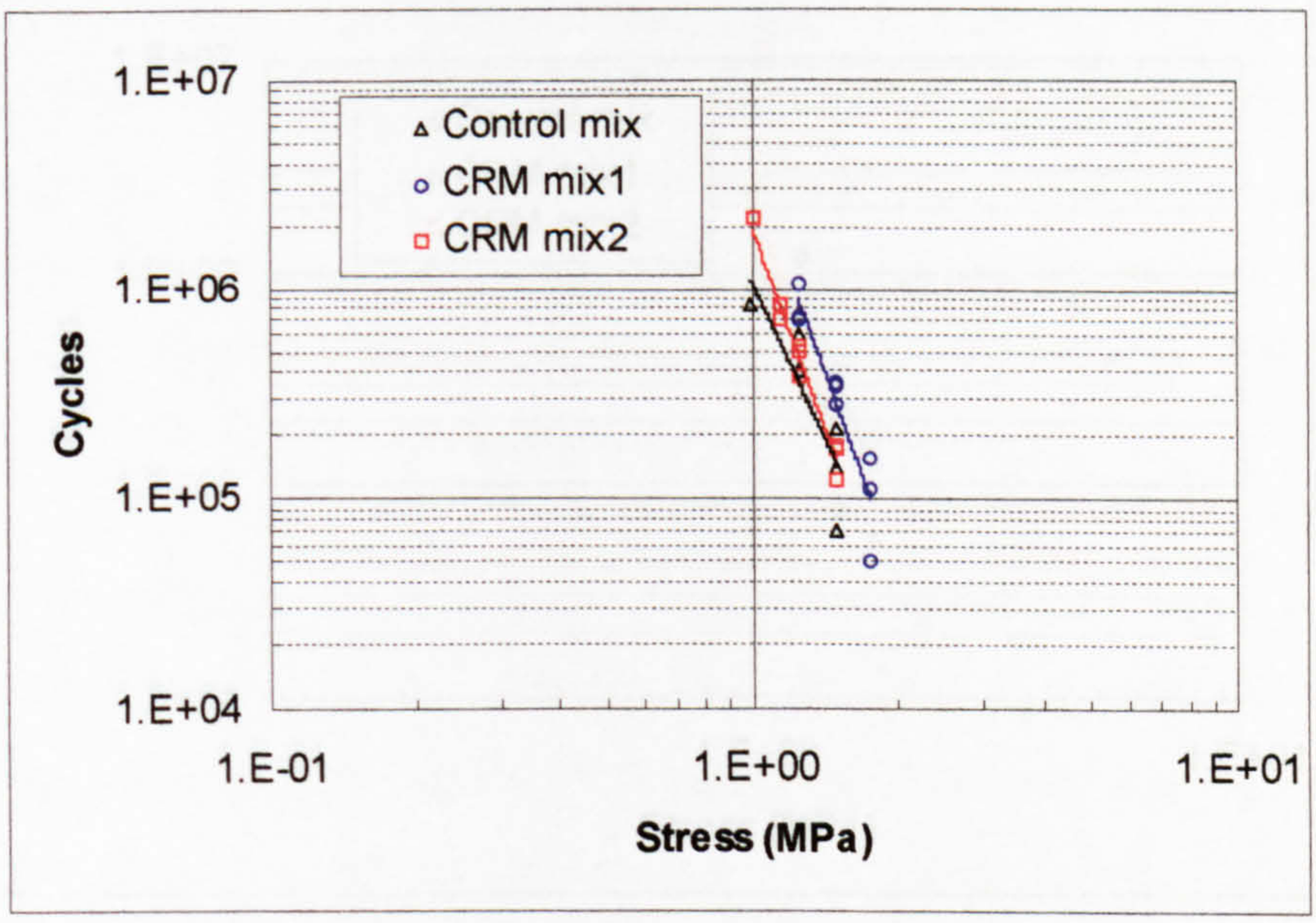

Figure 6.11 Relationship between fatigue life, N_1, and stress

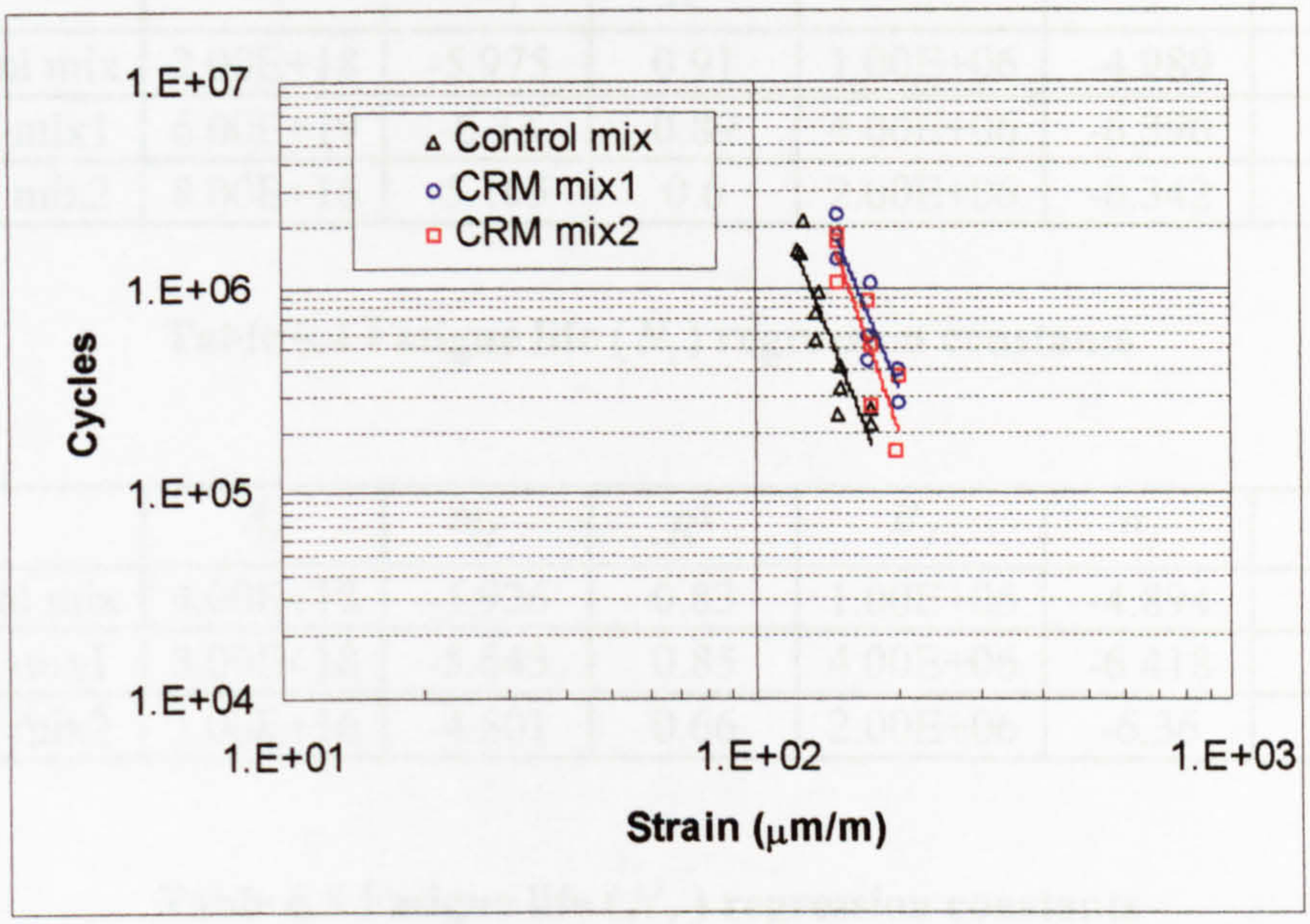

Figure 6.12 Relationship between fatigue life, N_f, and strain

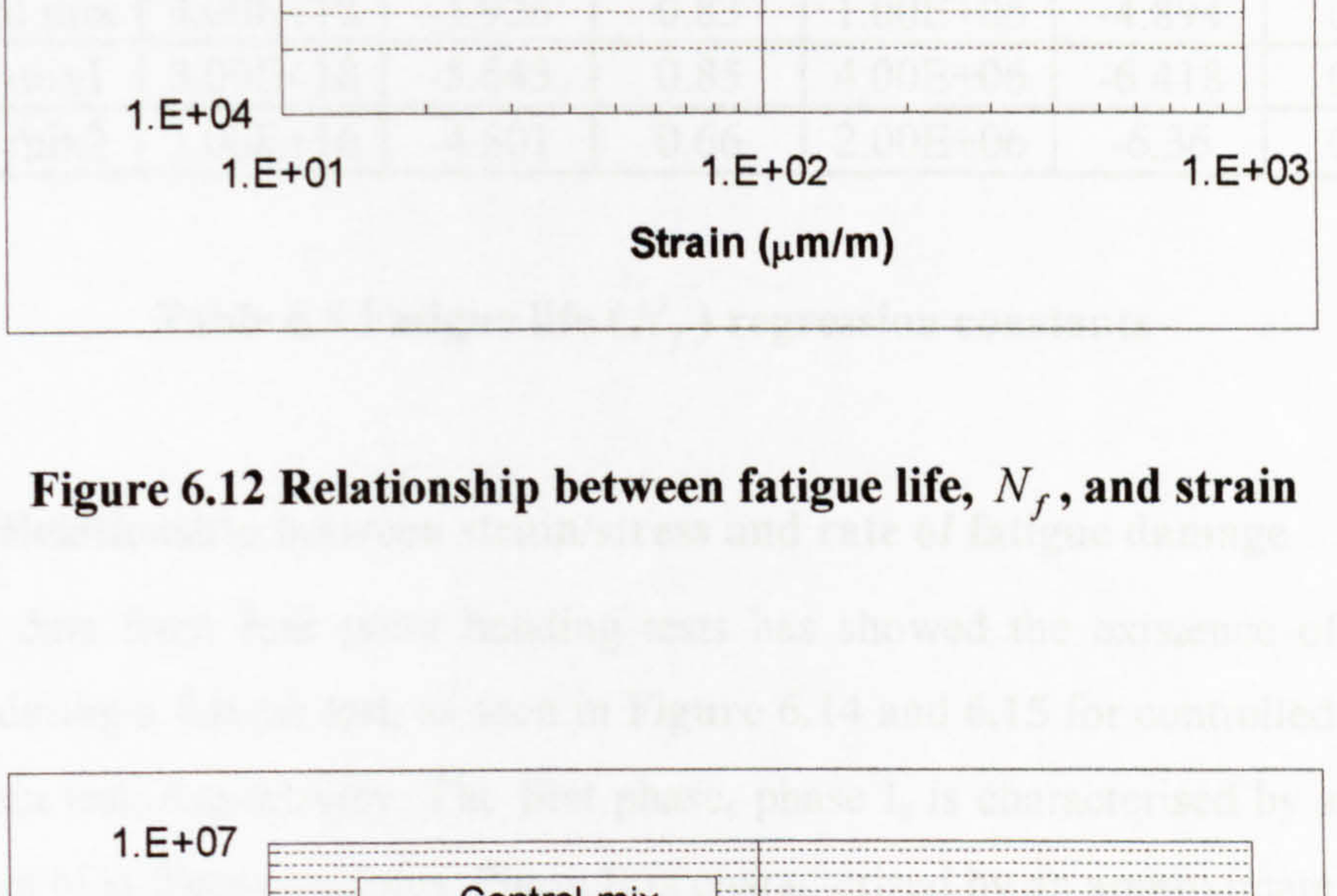

Figure 6.13 Relationship between fatigue life, N_f, and stress

	A_1	m_1	R^2	B_1	n_1	R^2
Control mix	2.00E+18	-5.975	0.91	1.00E+06	-4.989	0.76
CRM mix1	6.00E+19	-6.33	0.89	4.00E+06	-6.396	0.89
CRM mix2	8.00E+16	-5.105	0.6	2.00E+06	-6.342	0.97

Table 6.4 Fatigue life (N_1) regression constants

	A_f	m_f	R^2	B_f	n_f	R^2
Control mix	4.00E+18	-5.926	0.83	1.00E+06	-4.894	0.75
CRM mix1	3.00E+18	-5.643	0.85	4.00E+06	-6.418	0.89
CRM mix2	1.00E+16	-4.601	0.66	2.00E+06	-6.36	0.97

Table 6.5 Fatigue life (N_f) regression constants

6.3.3 Relationship between strain/stress and rate of fatigue damage

Fatigue data from four point bending tests has showed the existence of three phases during a fatigue test, as seen in **Figure 6.14** and **6.15** for controlled stress and strain test, respectively. The first phase, phase I, is characterised by a rapid reduction of stiffness modulus. Phase II is characterised by an approximate linear reduction in the stiffness modulus with number of cycles. Finally, phase III is characterised by a drop in stiffness modulus with loading cycles up to failure. Same behaviour during a fatigue test was observed by Di Benedetto et al. (1996) and Choi et al. (2002), and was explain in section 6.1.5.1.

The rate of damage accumulation was calculated using Equation 6.16. To obtain the rate of damage, dD/dN, a straight line was fitted to the stiffness data in phase II (see **Figures 6.14a** and **6.15a**). The point where the extrapolated fitted line intercepts the stiffness axis corresponded to E_{00}, and the slope of this line was dE^*/dN.

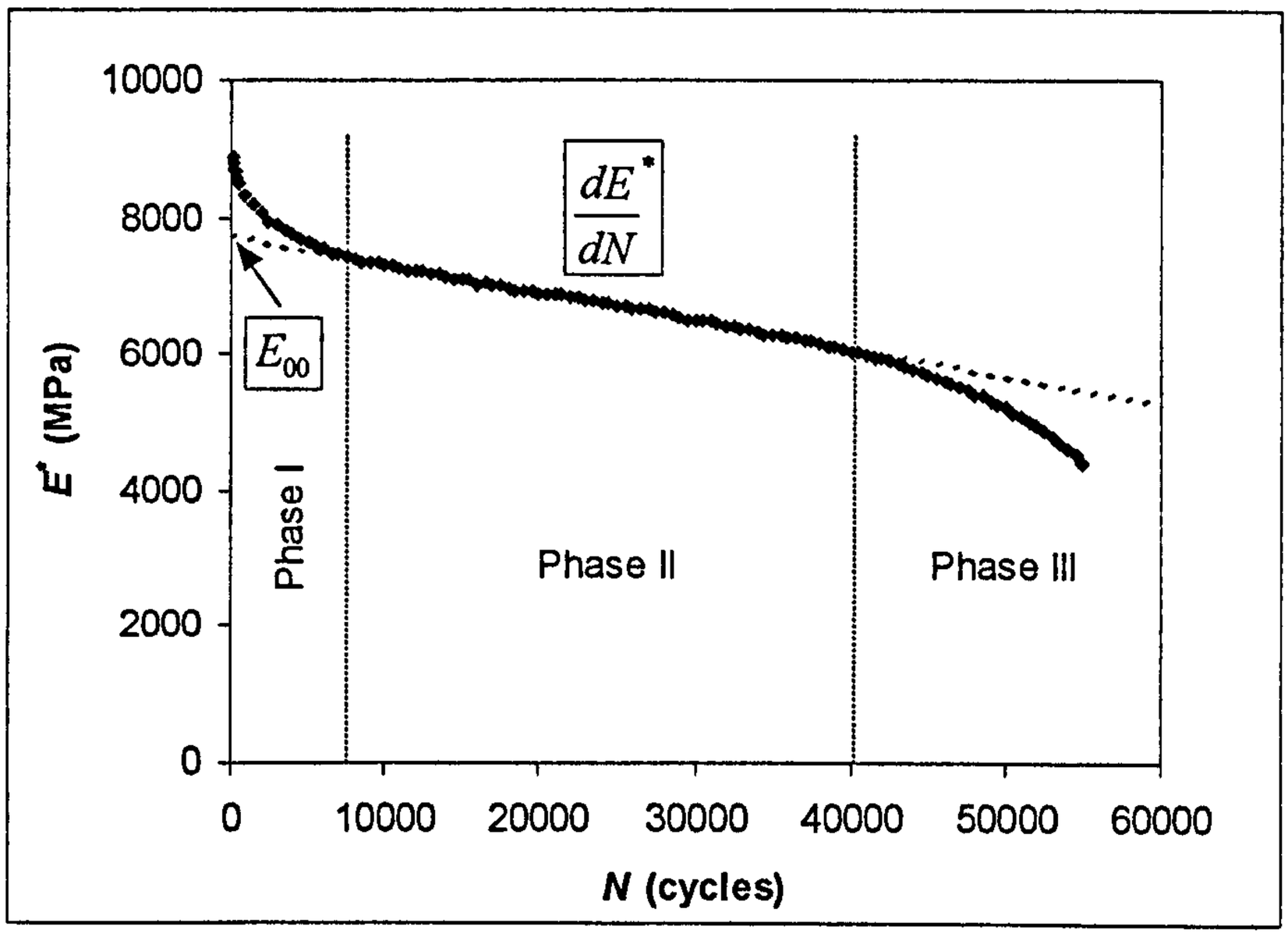

a) Evolution of the stiffness modulus

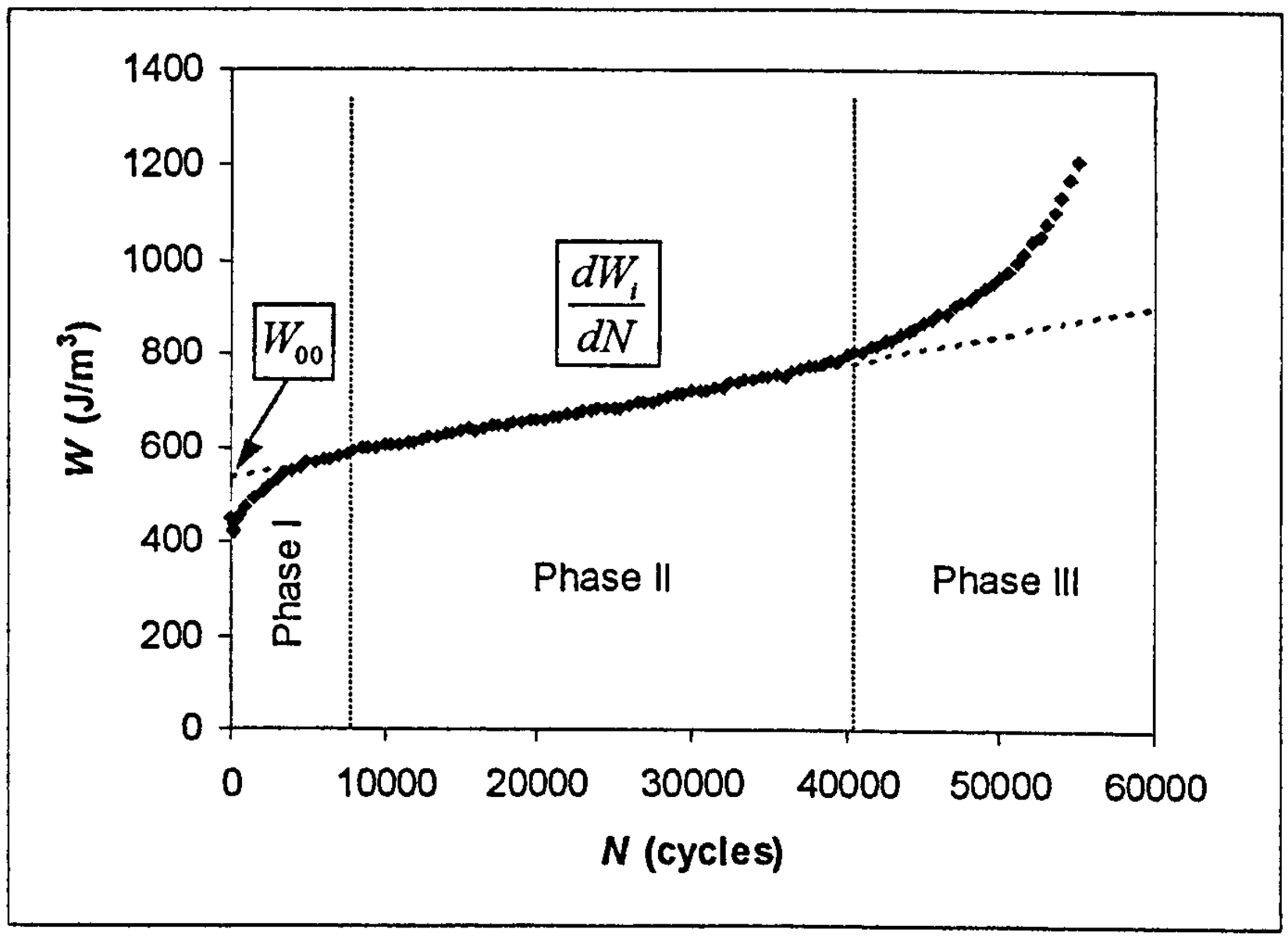

b) Evolution of the dissipated energy

Figure 6.14 Fatigue phases in a controlled stress test

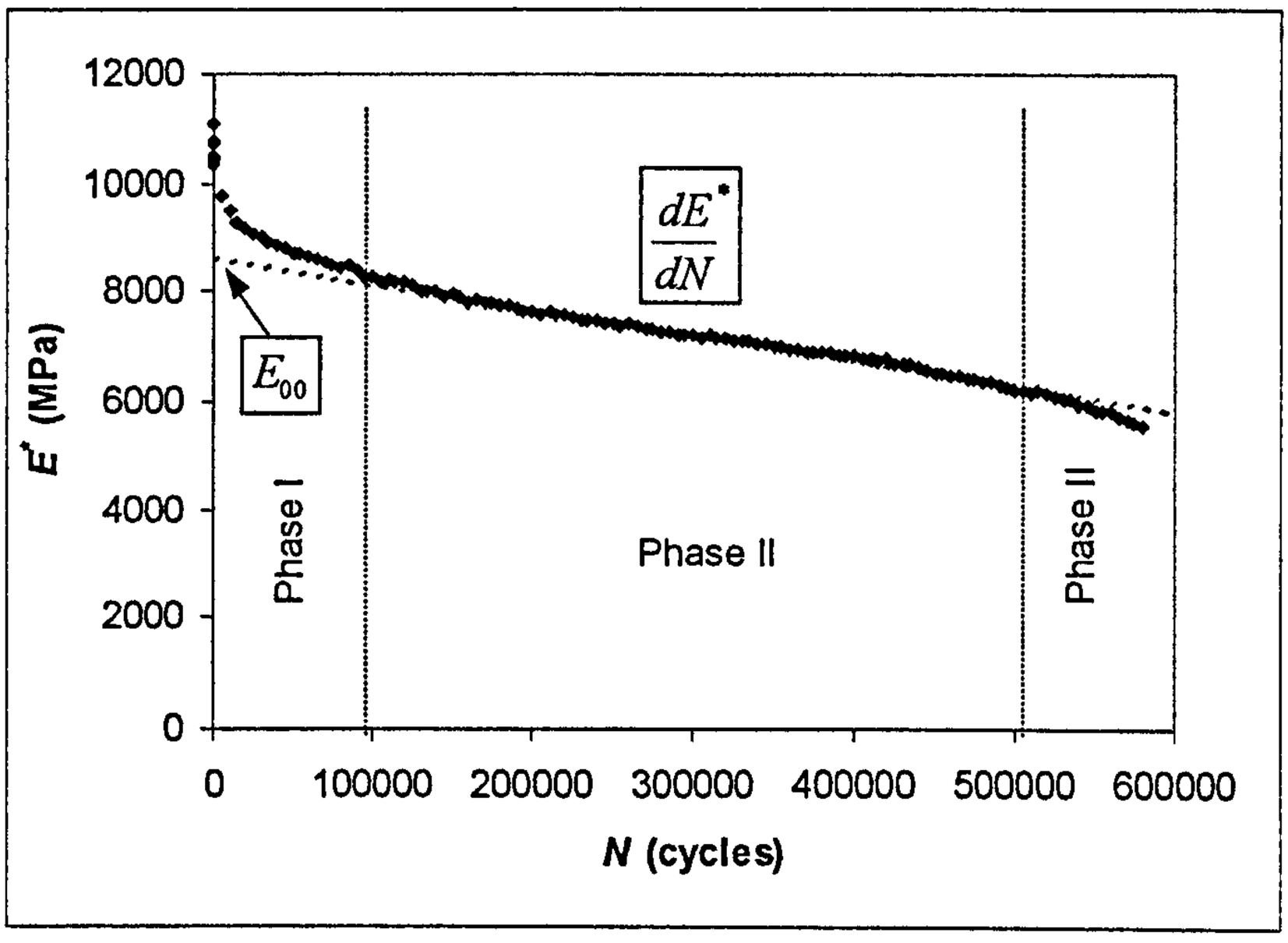

a) Evolution of the stiffness modulus

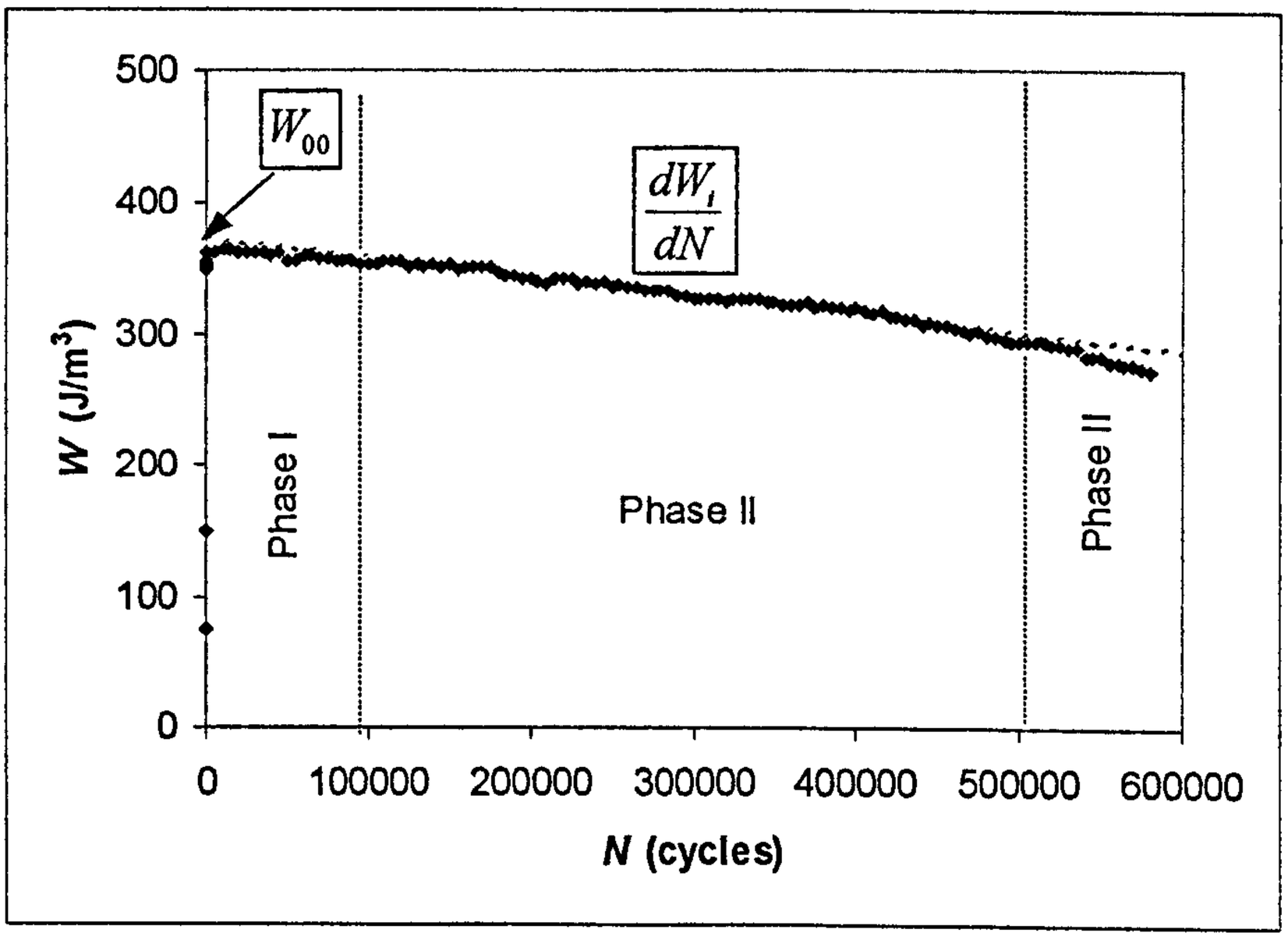

b) Evolution of the dissipated energy

Figure 6.15 Fatigue phases in a controlled strain test

For controlled strain conditions, the change in the damage parameter with number of load applications, or rate of damage, obtained using Equation 6.16, has been plotted as a function of the initial strain on log-log scales, as shown in **Figure 6.16**. It can be seen that data can be fitted by a straight line, indicating that the dependence of the rate of damage on initial strain is as follows:

$$\frac{dD}{dN} = -a_T = A_T \varepsilon_0^{m_T} \tag{6.50}$$

where:

ε_0 = initial strain

A_T , m_T = material constants

In the same way, the rate of damage for controlled stress testing has been plotted as a function of the applied stress on log-log scales, as shown in **Figure 6.17**. It can be seen again that the data can be fitted by a straight line, indicating that the dependence of the rate of damage with applied stress can be expressed as:

$$\frac{dD}{dN} = -a_T = B_T \sigma_0^{n_T} \tag{6.51}$$

where:

σ_0 = applied stress

B_T , n_T = material constants

Material's constants, A_T and m_T, B_T and n_T, and regression coefficients values R^2 corresponding to the three materials tested are presented in **Table 6.6**.

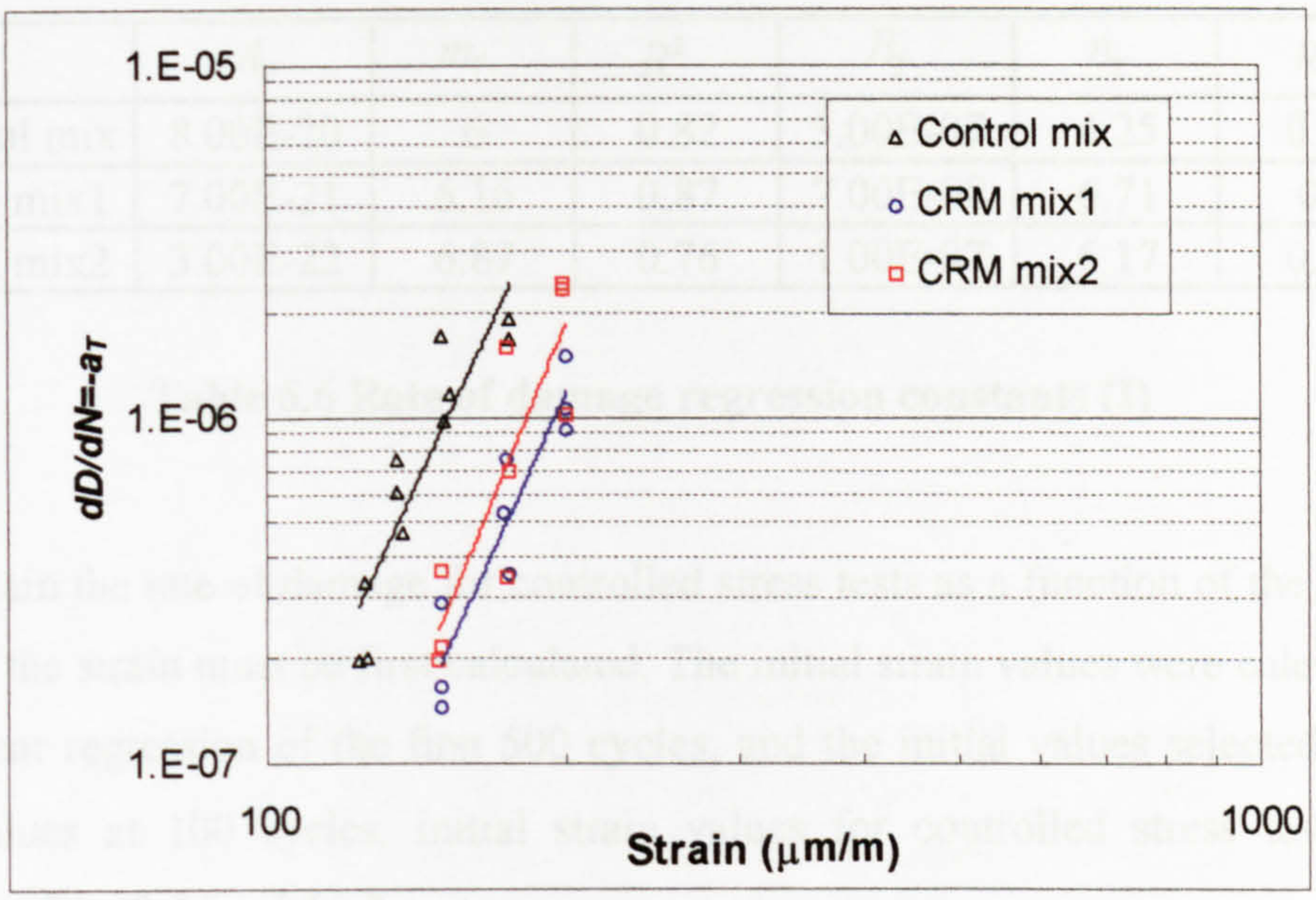

Figure 6.16 Relationship between the rate of damage, dD/dN , and the initial strain

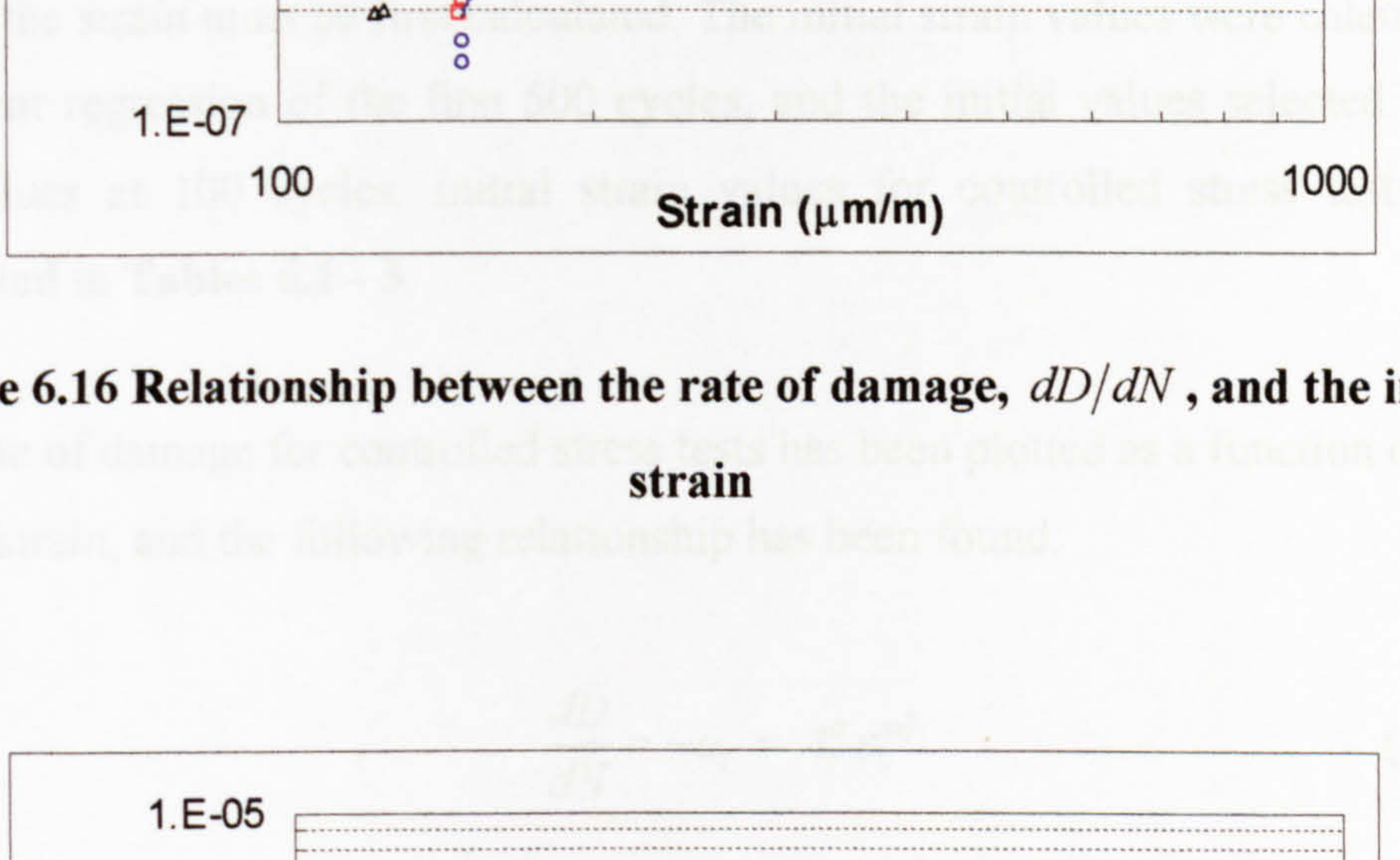

Figure 6.17 Relationship between the rate of damage, dD/dN , and the applied stress

	A_T	m_T	R^2	B_T	n_T	R^2
Control mix	8.00E-20	6	0.82	3.00E-07	4.25	0.75
CRM mix1	7.00E-21	6.16	0.87	7.00E-08	6.71	0.9
CRM mix2	3.00E-22	6.87	0.76	1.00E-07	6.17	0.98

Table 6.6 Rate of damage regression constants (I)

To obtain the rate of damage for controlled stress tests as a function of the initial strain, the strain must be first calculated. The initial strain values were calculated by linear regression of the first 500 cycles, and the initial values selected were the values at 100 cycles. Initial strain values for controlled stress tests are presented in **Tables 6.1 - 3**.

The rate of damage for controlled stress tests has been plotted as a function of the initial strain, and the following relationship has been found:

$$\frac{dD}{dN} = -a_T = A_T^{\sigma} \varepsilon_0^{m_T^{\sigma}} \tag{6.52}$$

where:

ε_0 = initial applied strain

$A_T^{\sigma}, m_T^{\sigma}$ = material constants

Figure 6.18 illustrates the rate of damage as a function of the initial strain for controlled strain and stress tests for the three materials tested.

Material's constant, A_T and m_T, A_T^{σ} and m_T^{σ}, and regression coefficients values R^2 corresponding to the three materials are presented in **Table 6.7**.

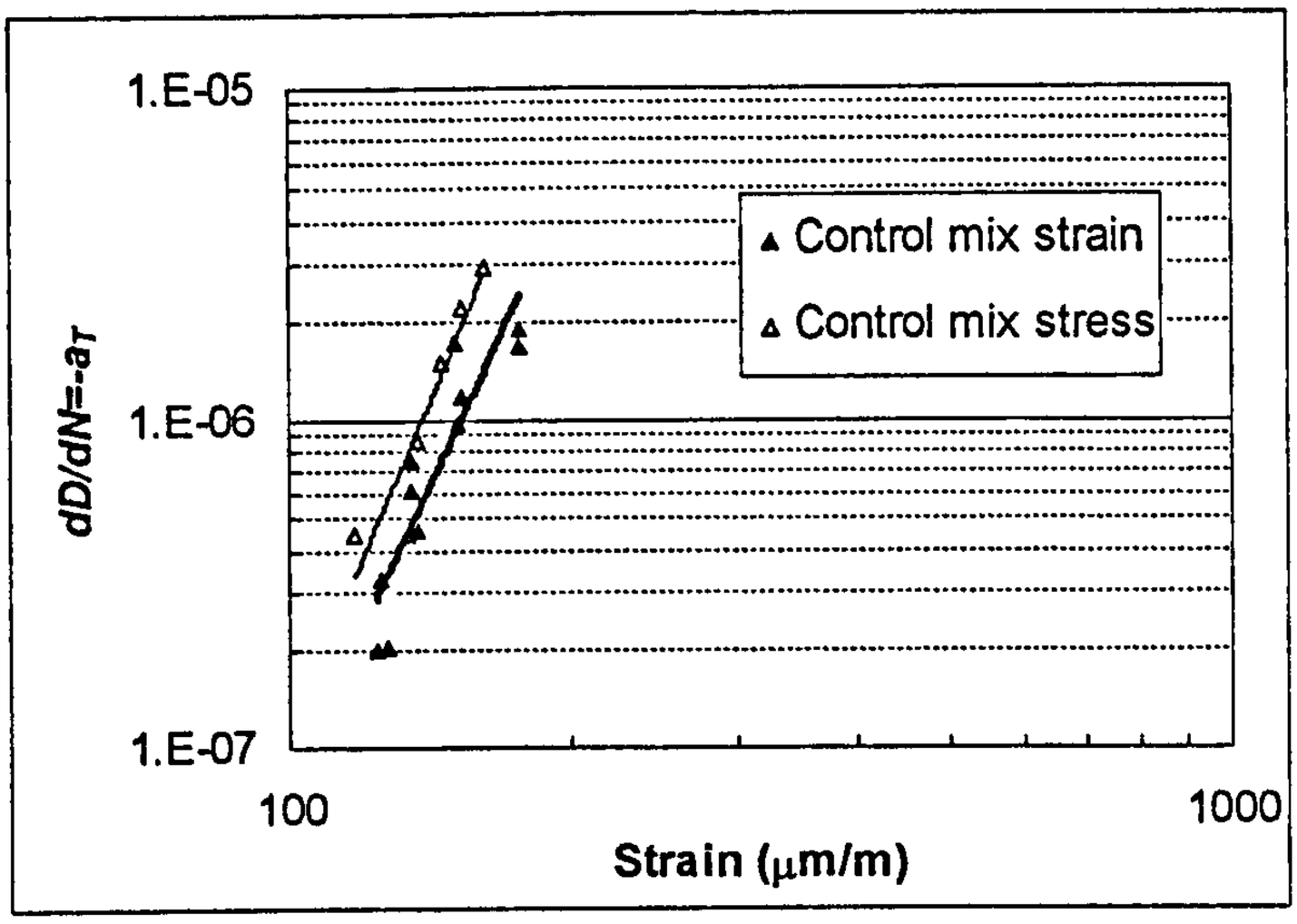

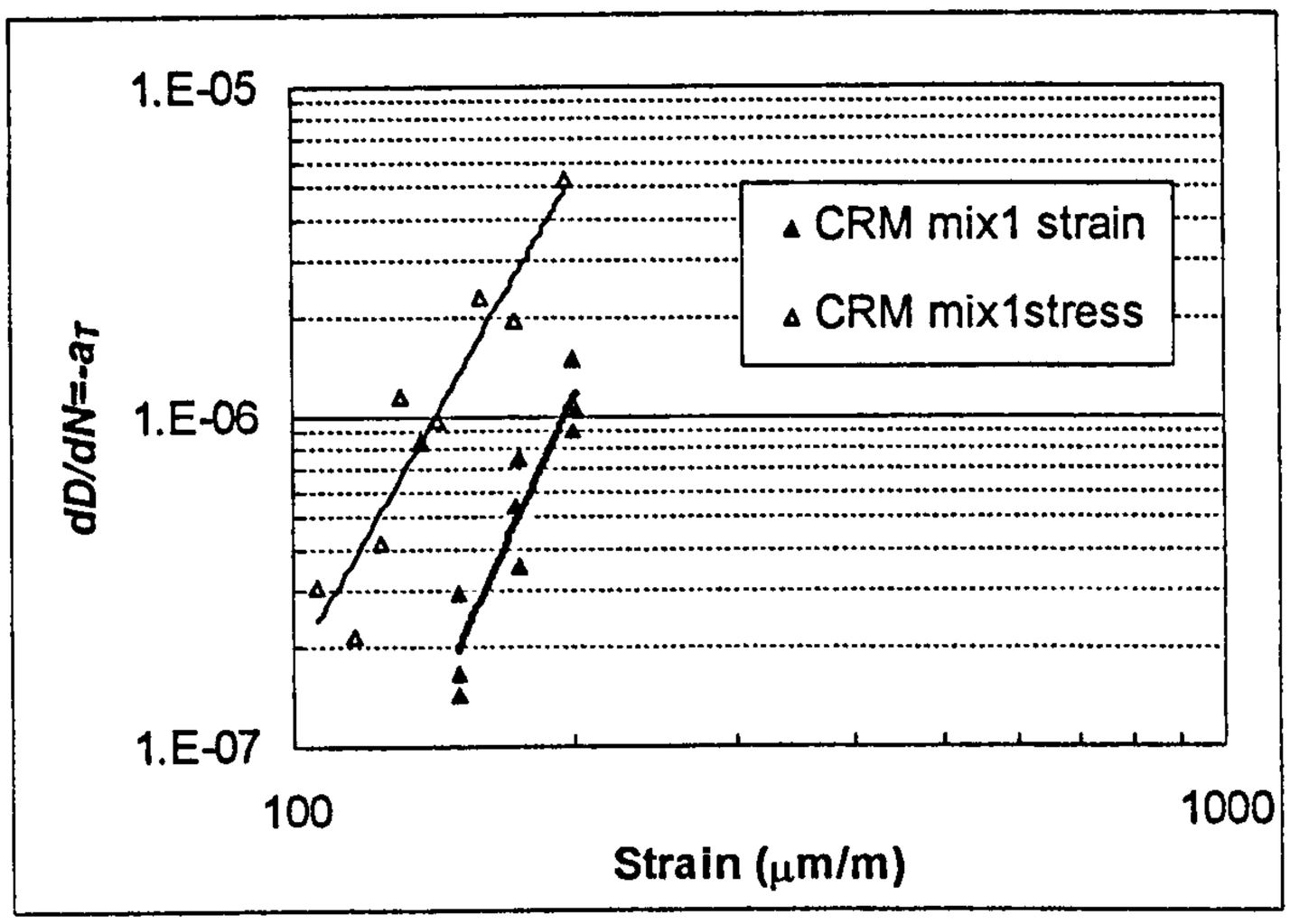

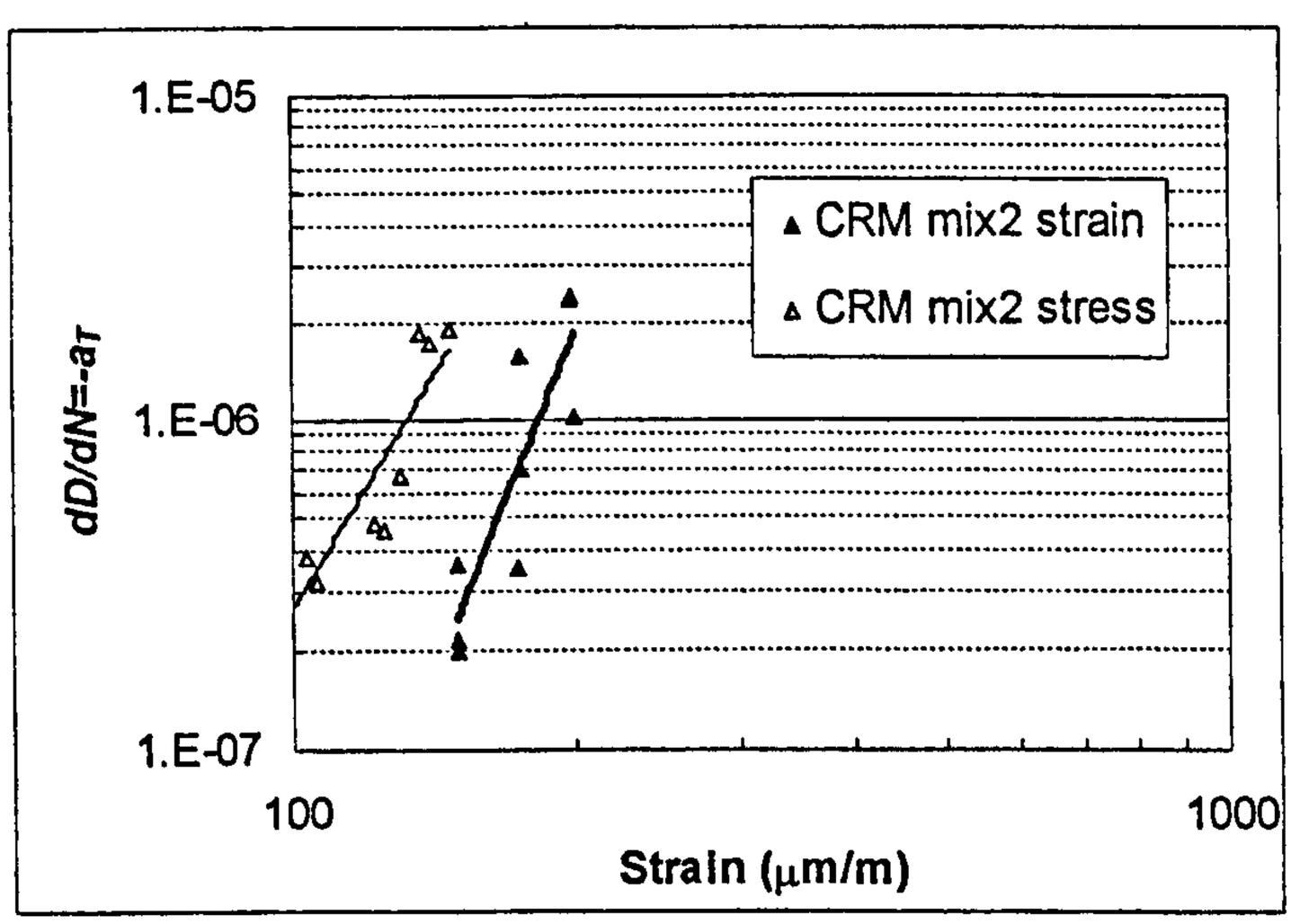

Figure 6.18 Relationship between the rate of damage and the initial strain for controlled strain and stress tests

	A_T	m_T	R^2	A_T^σ	m_T^σ	R^2
Control mix	8.00E-20	6	0.82	6.00E-21	6.63	0.86
CRM mix1	7.00E-21	6.16	0.87	3.00E-17	4.9	0.89
CRM mix2	3.00E-22	6.87	0.76	1.00E-16	4.71	0.86

Table 6.7 Rate of damage regression constants (II)

In order to compare the rate of damage for controlled strain and controlled stress tests, the influence of the dissipated energy effects occurring during phase II must be considered. As state earlier, during controlled strain fatigue testing the dissipated energy decreases with number of cycles, and increases during controlled stress tests, as shown in **Figures 6.14b** and **6.15b**.

The corrected damage rate introduced in Equation 6.20 can be rewritten as follows:

$$\frac{dD_{corr}}{dN} = -a_F = -a_T - Ca_W\left(\frac{E_0 - E_{00}}{E_{00}}\right) \tag{6.53}$$

where :

$a_T < 0$ for controlled strain and stress tests

$a_W > 0$ for controlled stress tests

$a_W < 0$ for controlled strain tests

The constant C is introduced to superimpose strain and stress data and depends on the material.

For controlled strain data, absolute values of a_W obtained using Equation 6.19 have been plotted as a function of the initial strain on log-log scales, as shown in **Figure 6.19**, and the following relationship has been found:

$$|a_W| = A_W \varepsilon_0^{m_W} \tag{6.54}$$

where:

ε_0 = initial strain

A_W, m_W = material constants

In the same way, absolute values of a_W for controlled stress testing have been plotted as a function of the applied stress on log-log scales, as shown in **Figure 6.20**. The following relationship has been found:

$$| a_W | = B_W \sigma_0^{n_W} \tag{6.55}$$

where:

σ_0 = applied stress

B_W, n_W = material constants

Material's constants, A_W and m_W, B_W and n_W, and regression coefficients values R^2 corresponding to the three materials tested are presented in **Table 6.8**.

	A_W	m_W	R^2	B_W	n_W	R^2
Control mix	1.00E-19	5.89	0.88	8.00E-07	4.05	0.68
CRM mix1	2.00E-21	6.31	0.87	2.00E-07	6.93	0.93
CRM mix2	1.00E-23	7.45	0.78	3.00E-07	6.15	0.89

Table 6.8 Parameter a_W regression constants (I)

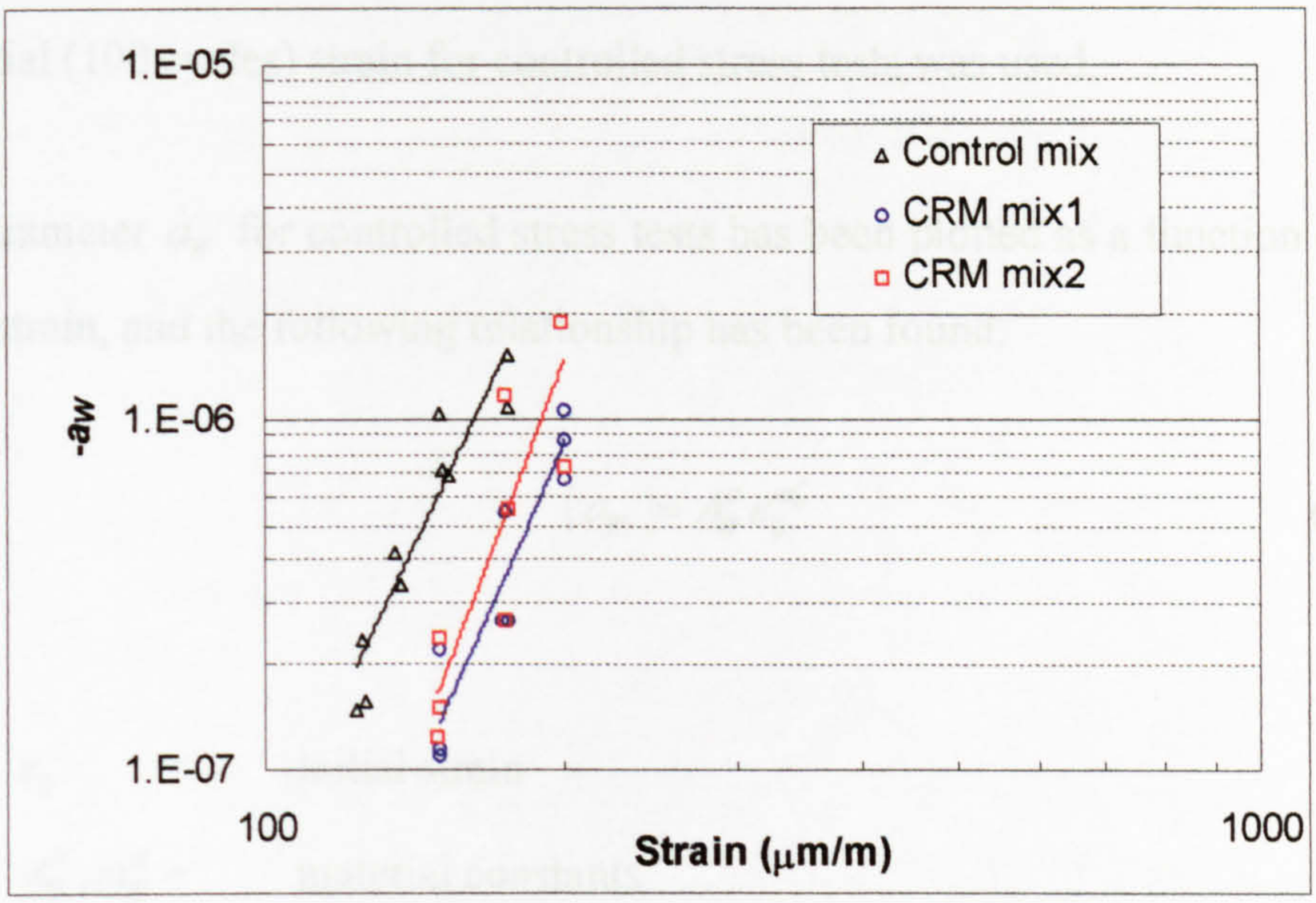

Figure 6.19 Relationship between the parameter a_W and the initial strain

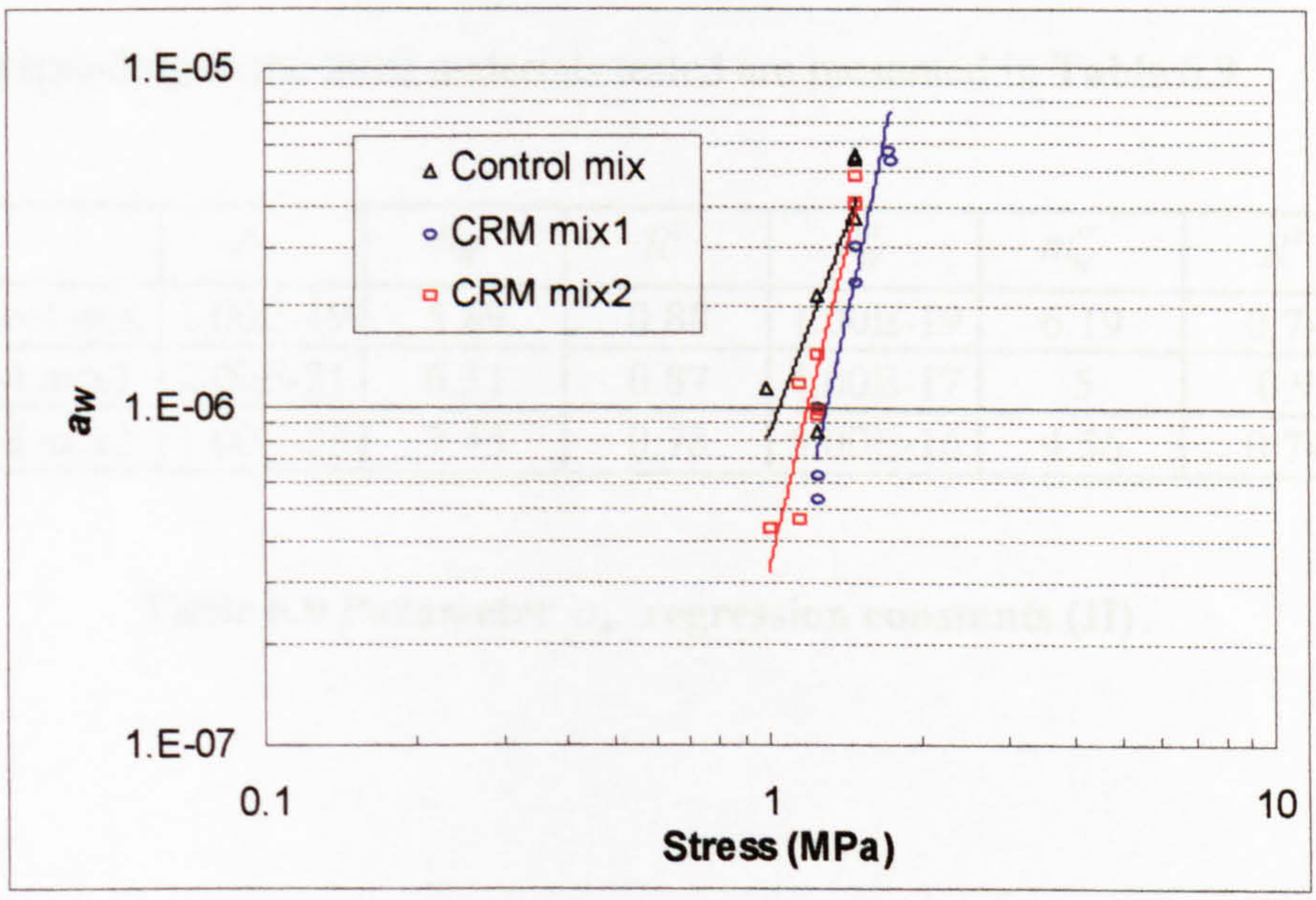

Figure 6.20 Relationship between the parameter a_W and the applied stress

To compare the parameter a_W from controlled strain and controlled stress tests, the initial (100 cycles) strain for controlled stress tests was used.

The parameter a_W for controlled stress tests has been plotted as a function of the initial strain, and the following relationship has been found:

$$| a_W | = A_W^{\sigma} \varepsilon_0^{m_W^{\sigma}} \tag{6.56}$$

where:

ε_0 = initial strain

$A_W^{\sigma}, m_W^{\sigma}$ = material constants

Figure 6.21 illustrates $|a_w|$ as a function of the initial strain from controlled strain and stress data, for the three materials tested.

Material's constants, A_W and m_W, A_W^{σ} and m_W^{σ}, and regression coefficients values R^2 corresponding to the three materials tested are presented in **Table 6.9**.

	A_W	m_W	R^2	A_W^{σ}	m_W^{σ}	R^2
Control mix	1.00E-19	5.89	0.88	1.00E-19	6.19	0.74
CRM mix1	2.00E-21	6.31	0.87	4.00E-17	5	0.9
CRM mix2	1.00E-23	7.45	0.78	5.00E-16	4.56	0.74

Table 6.9 Parameter a_W regression constants (II)

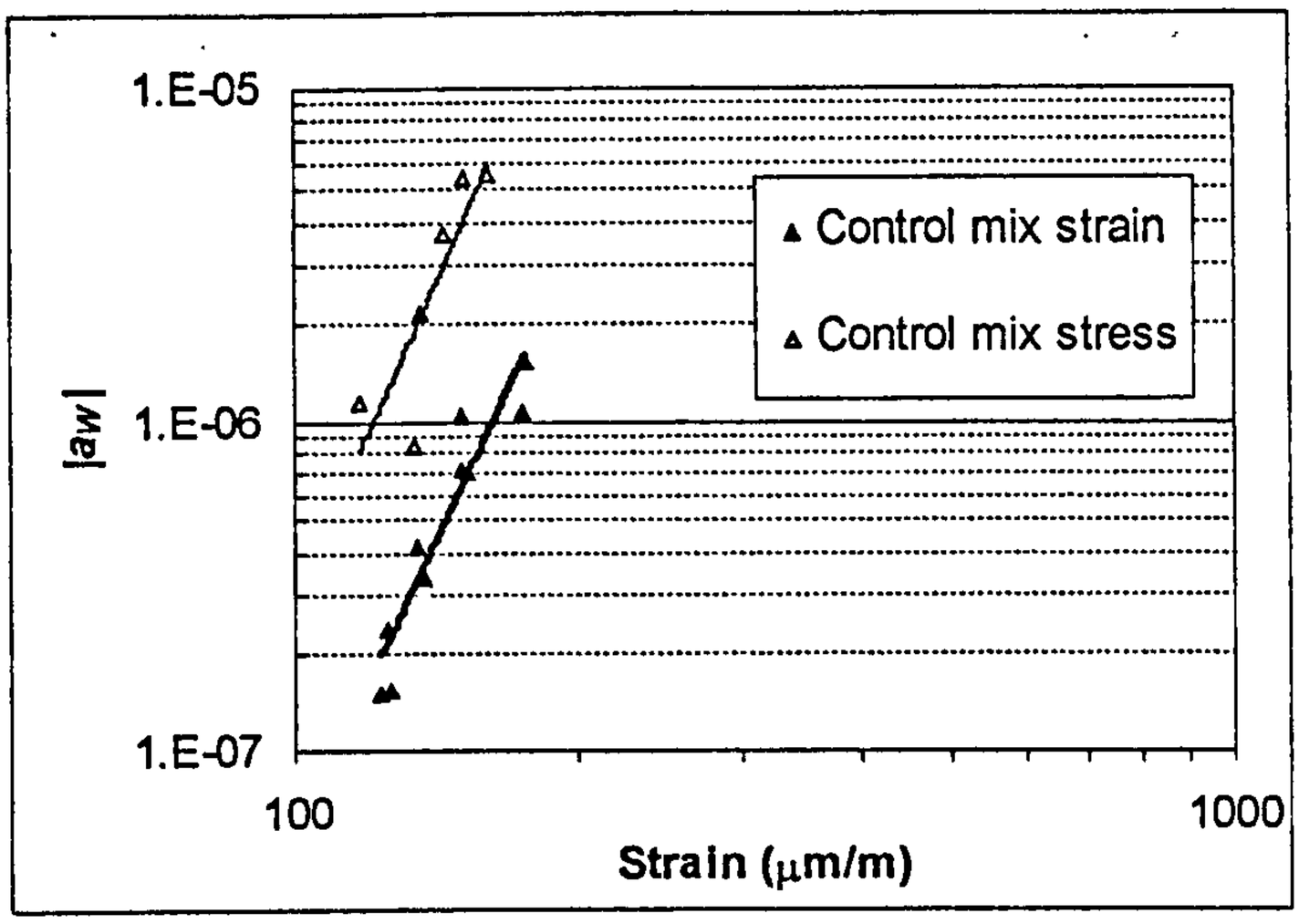

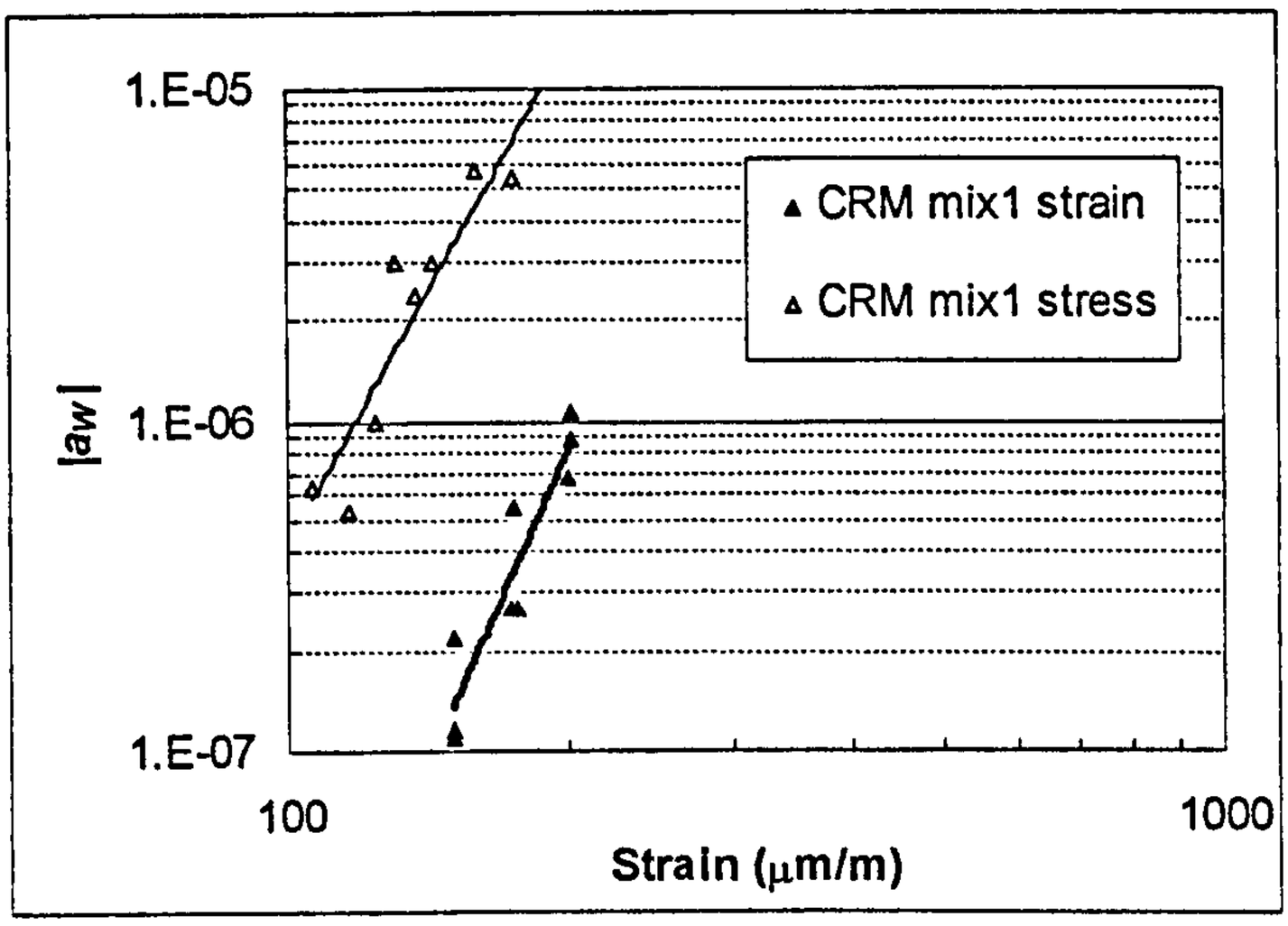

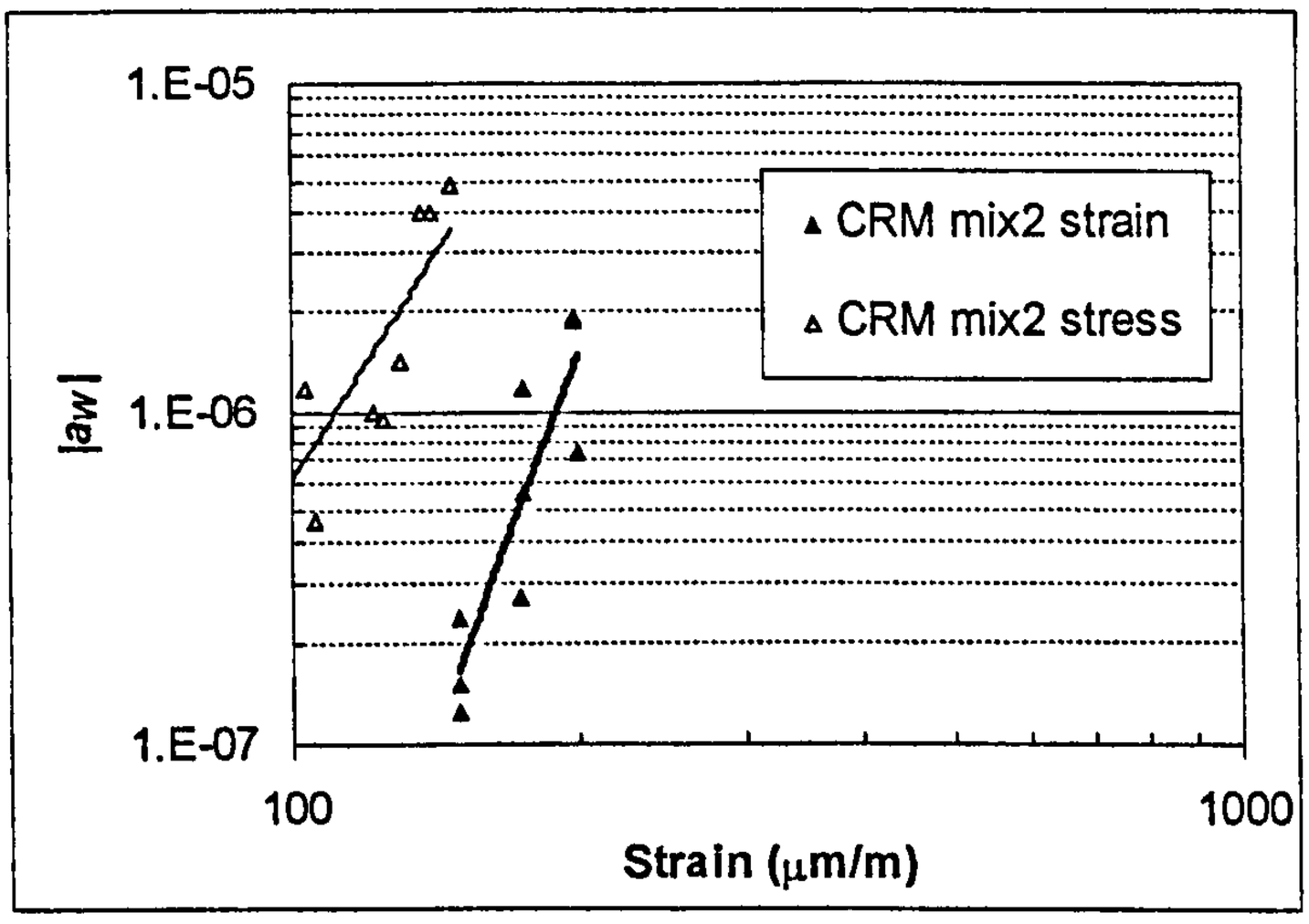

Figure 6.21 Relationship between the parameter a_w and the initial strain for controlled strain and stress tests

Finally, the corrected damage rates obtained from Equation 6.53 for controlled strain and stress tests were plotted as function of the initial strain and the following relationship was found:

$$\frac{dD_{corr}}{dN} = -a_F = A_F \varepsilon_0^{m_F} \tag{6.57}$$

where A_F and m_F are experimental material constants.

The value of the constant C has been calculated using a simple iterative technique, which aims at achieving the highest regression coefficient R^2 from Equation 6.57. **Figure 6.22** illustrates the method to find out the value of the constant C for one of the materials (CRM mix1). The values obtained were 1.95, 2.70 and 3.05 for the Control mix, CRM mix 1 and CRM mix 2 respectively.

Figures 6.23 illustrates the corrected rate of damage as a function of the initial strain for controlled strain and stress testing corresponding to the three materials studied.

Material's constants, A_F and m_F, and regression coefficients values R^2 corresponding to the three materials tested are presented in **Table 6.10**.

	A_F	m_F	R^2
Control mix	5.00E-19	5.66	0.81
CRM mix1	1.00E-15	3.91	0.75
CRM mix2	3.00E-17	4.68	0.84

Table 6.10 Corrected rate of damage regression constants

Fatigue parameters a_T, a_W and a_F for each individual fatigue specimen are presented in **Appendix P.**

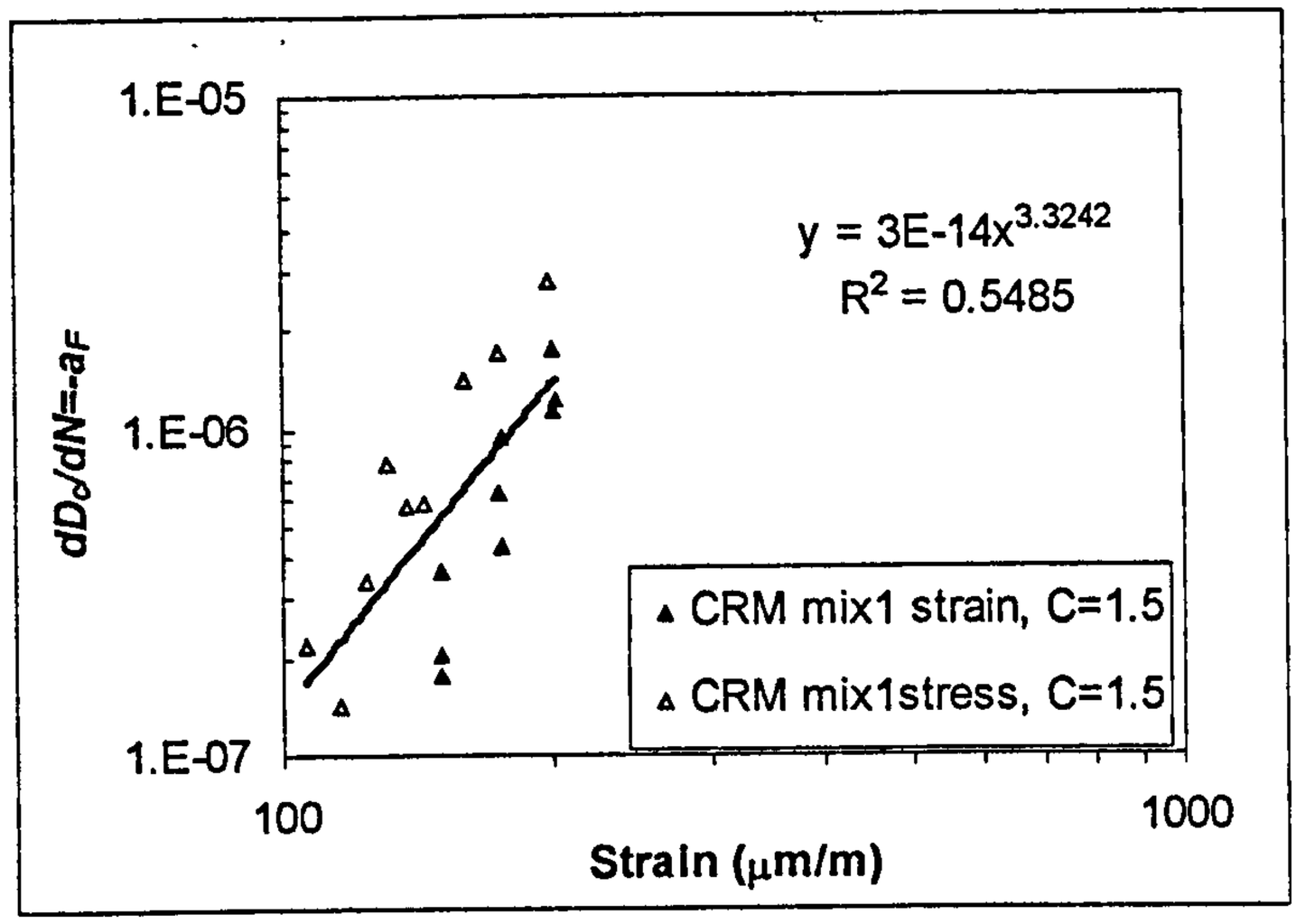

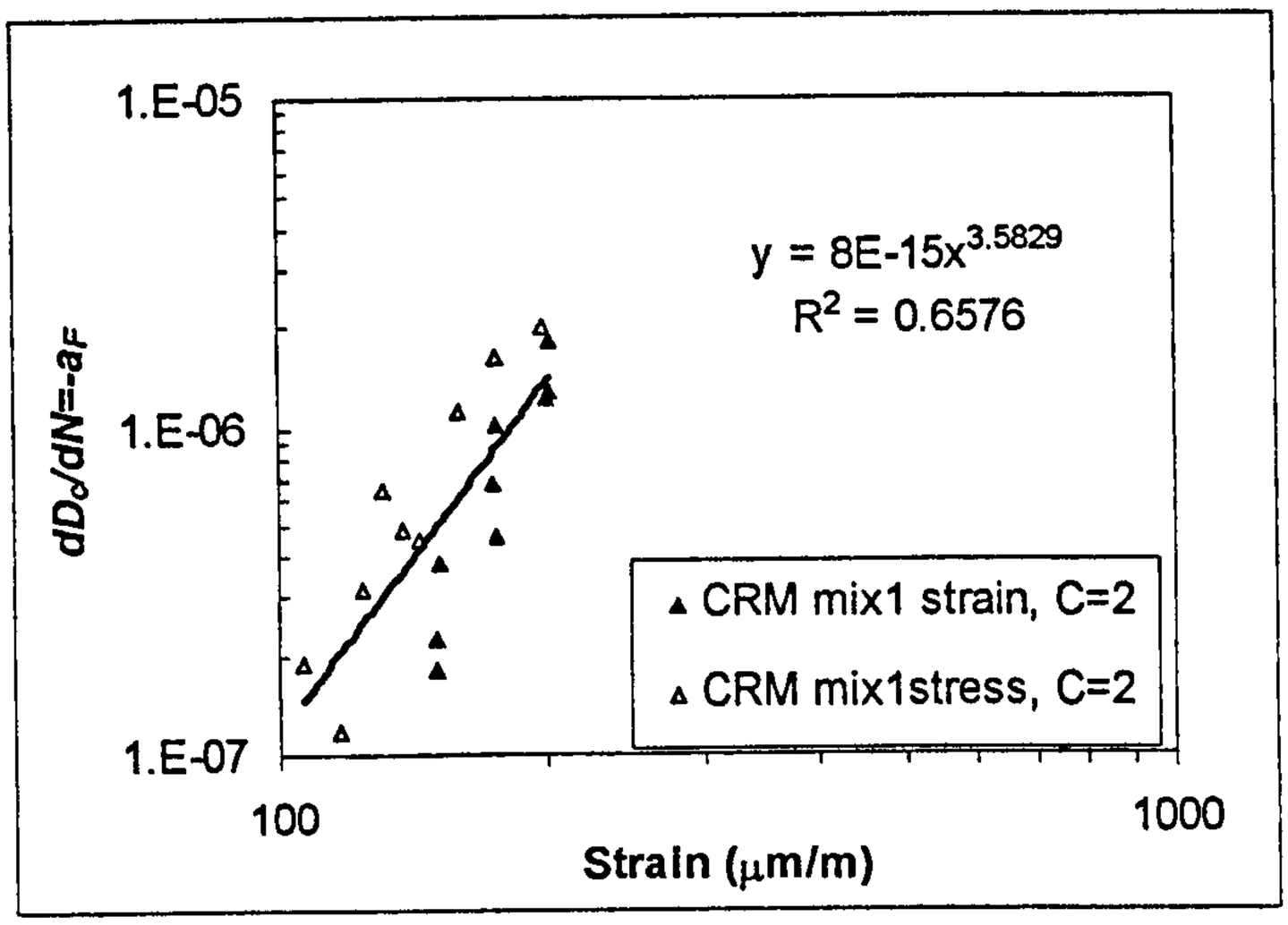

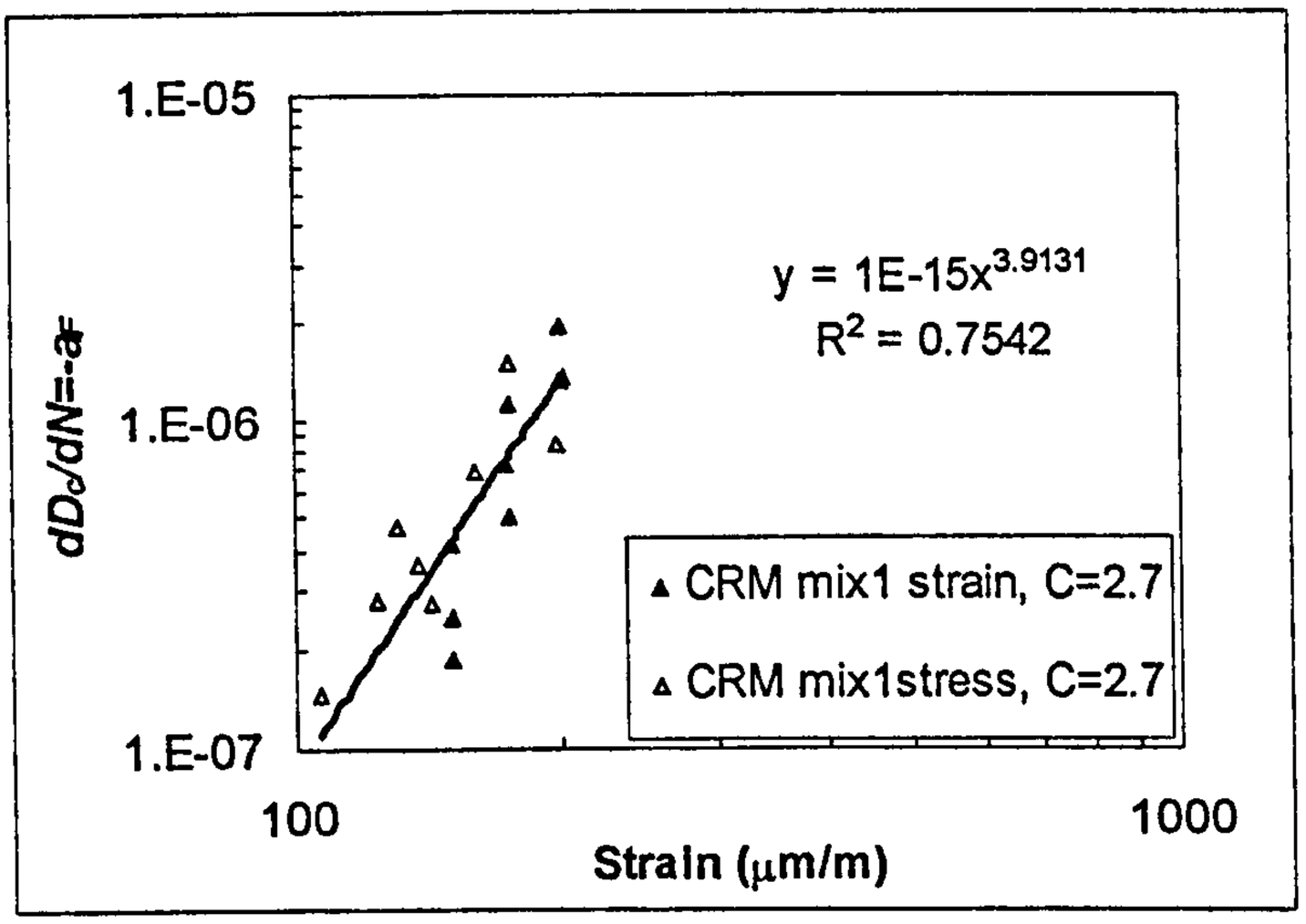

Figure 6.22 Method to calculate the value of the constant C

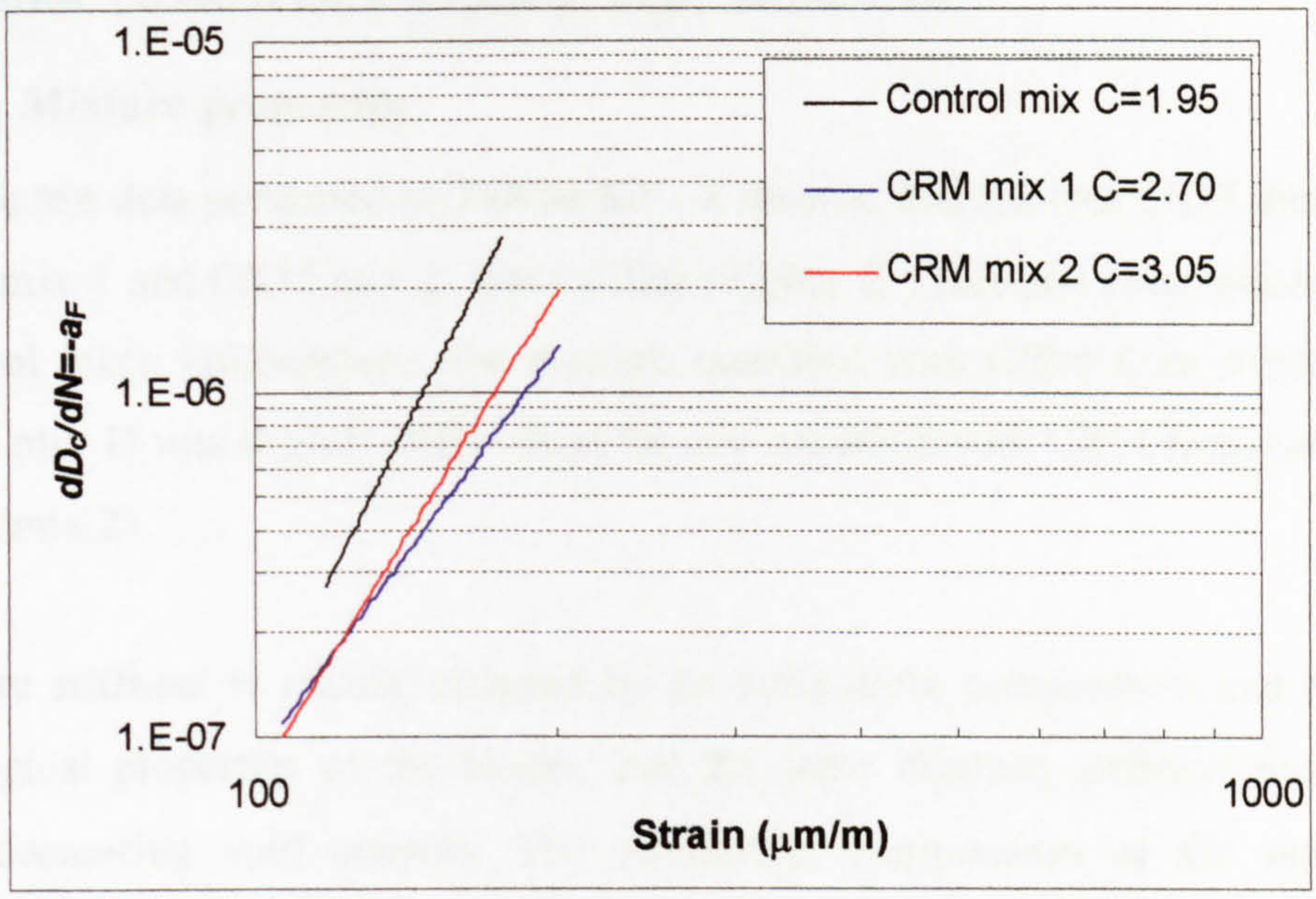

Figure 6.23 Relationship between the corrected rate of damage and the initial strain from strain and stress tests

6.4 DISCUSSION OF FATIGUE TEST RESULTS

6.4.1 Mixture properties

Fatigue test data presented in **Tables 6.1 - 3** showed that the two CRM mixtures, CRM mix 1 and CRM mix 2, were stiffer (higher E^*) than the conventional one (Control mix). Furthermore, the mixture modified with CRM from truck tyres (CRM mix 1) was slightly stiffer than the one modified with CRM from car tyres (CRM mix 2).

Mixture stiffness is mainly affected by its volumetric composition and by the rheological properties of the binder. For the same mixture, stiffness increases with decreasing void content. The volumetric composition of the mixtures presented in **Appendix L** showed that void contents of the rubber-modified mixtures were lower than that of the unmodified one. Lower voids resulted from higher binder contents used in the design of the modified mixtures. Mixture stiffness can also be related to binder properties since it is significantly affected by the binder stiffness.

Also presented in **Tables 6.1 - 3** are the phase angles for the materials tested. It can be seen that the initial phase angle corresponding to the conventional mixture, 21.5 ^{0}, is slightly higher than the phase angles for the rubber-modified mixtures, 19 and 18.6 ^{0}. Differences between the phase angles for the mix modified with CRM from truck tyres, 19 ^{0}, and the mix modified with CRM from car tyres, 18.6 ^{0}, are considered negligible. Lower phase angles indicate that the rubber mixtures behave more elastically than the conventional one. Elastic properties of these materials are mainly associated with binder properties.

6.4.2 Fatigue life

Fatigue lives have been presented in terms of N_1 and N_f, corresponding to macro-crack formation and failure. It has been found that the two CRM mixtures have longer fatigue lives than the conventional one, in both, controlled strain and stress conditions. Furthermore, fatigue life for the mix modified with CRM from truck tyres, was longer than for the mix modified CRM from car tyres (see

Figures 6.10 - 13). For instance, for controlled strain mode, the strain values at 10^6 cycles (ε_6) were 134, 163 and 149 μm/m for the Control mix, CRM mix 1 and CRM mix 2, respectively.

Fatigue life is mainly dependant on the air-void content of the mixture and the rheological properties of binder. Air-void content significantly influences fatigue life in that fatigue life is longer for mixtures with low voids than for those with high voids. Fatigue life also improves when binders with enhanced elastic properties are used.

Hence, the longer fatigue lives obtained with the rubber-modified mixtures can be attributed to their lower air-void contents and to the incorporation of CRM. It was not possible, however, to study the effects of these two variables separately as the mixtures containing the rubber-modified binders required larger binder contents, as discussed in Chapter 5, Section 5.4.5.

6.4.3 Relationship between mixture and binder properties

In order to relate mixture properties to binder properties, mixture properties obtained from fatigue tests carried out at 10 ^{0}C and 10 Hz were compared with binder rheology data obtained in the DSR at the same temperature and frequency.

Table 6.11 presents mixtures' properties, stiffness modulus (E^*) and phase angle (ϕ) corresponding to the three materials studied. Although these properties were measured throughout the fatigue test, only the initial values (100th cycle) are presented here. Furthermore, these values are the average values for all the individual fatigue tests (see **Tables 6.1 - 3**). Also presented in **Table 6.11** are the binders' rheological data, complex shear modulus (G^*), phase angle (δ), storage modulus ($G' = G^* \cos\delta$) and loss modulus ($G'' = G^* \sin\delta$) at 10 ^{0}C and 10 Hz.

	Binder				Mixture				
	G^* (MPa)	δ (^{0})	G' (MPa)	G'' (MPa)	E^* (MPa)	ϕ (^{0})	E' (MPa)	E'' (MPa)	$\log N_f$
Control mix	27	46.8	18.5	19.7	9414	21.5	8759	3450	5.376
CRM mix1	20.8	44.3	14.9	14.5	10274	19	9714	3345	5.841
CRM mix2	19.9	48.2	12.9	14.5	10050	18.6	9525	3206	5.743

Table 6.11 Mixture and binder properties at 10 ^{0}C and 10 Hz

Figure 6.24 shows the relationship between mixture stiffness (E^*) and binder complex modulus (G^*). The figure shows that for the CRM mixtures, mix stiffness increases with increasing binder complex modulus considering that both mixtures have the same air void level. It can also be seen that although the unmodified binder is stiffer than the modified ones, mixture stiffness is lower. This lower stiffness might be attributed to a higher void content for the unmodified mixture in comparison with the modified ones, which could mask the effect of binder stiffness.

Moreover, fatigue life has also been related to binder properties. For comparison purposes, fatigue life, N_f, was defined as the number of load cycles corresponding to a reduction in stiffness of 50 percent, in controlled strain fatigue tests, and at a strain amplitude of 175 μm/m.

Figure 6.25 illustrates the relationship between binder complex modulus and fatigue life ($\log N_f$). For the modified mixtures, fatigue life increased with increasing binder stiffness (G^*). Thus, the longer life corresponding to the mixture modified with CRM from truck tyres might be attributed to higher binder complex modulus as a result of binder modification with CRM from truck tyres in comparison with binder modification with CRM from car tyres. Furthermore, the elastic component of the complex modulus (G') for the binder modified with truck-tyre rubber is higher than that for the binder modified with car-tyre rubber (see **Table 6.11**).

Figure 6.25 also shows that although the complex modulus of the neat binder is higher than the one corresponding to the modified mixtures, the fatigue life is shorter. Shorter fatigue life might be attributed again to a higher void content for the unmodified mixture in comparison with the modified ones.

The asphalt binder specification criterion for fatigue performance introduced by the Strategic Highway Research Program (SHRP) is the loss modulus ($G^{"} = G^{*} \sin\delta$) at 10 rad/sec (1.6 Hz) and at a temperature equal to the average pavement temperature in the location of interest (Petersen et al, 1994). The specification calls for binders to be aged in the pressure aging vessel (PAV), before first testing to simulate long-term aging. The criterion establishes that the lower the binder loss modulus the longer the fatigue life of the mixture.

Binders' loss modulus ($G^{"}$) at 10 ^{0}C and 10 Hz presented in **Table 6.11** have been plotted as a function of fatigue life ($\log N_f$), as seen in **Figure 6.26**. It is shown that the SHRP criterion is followed when comparing unmodified and modified mixtures. Thus, the lower loss modulus for the CRM binders resulted in longer fatigue lives. However, the criterion did not discriminate between the fatigue lives of the two modified mixtures.

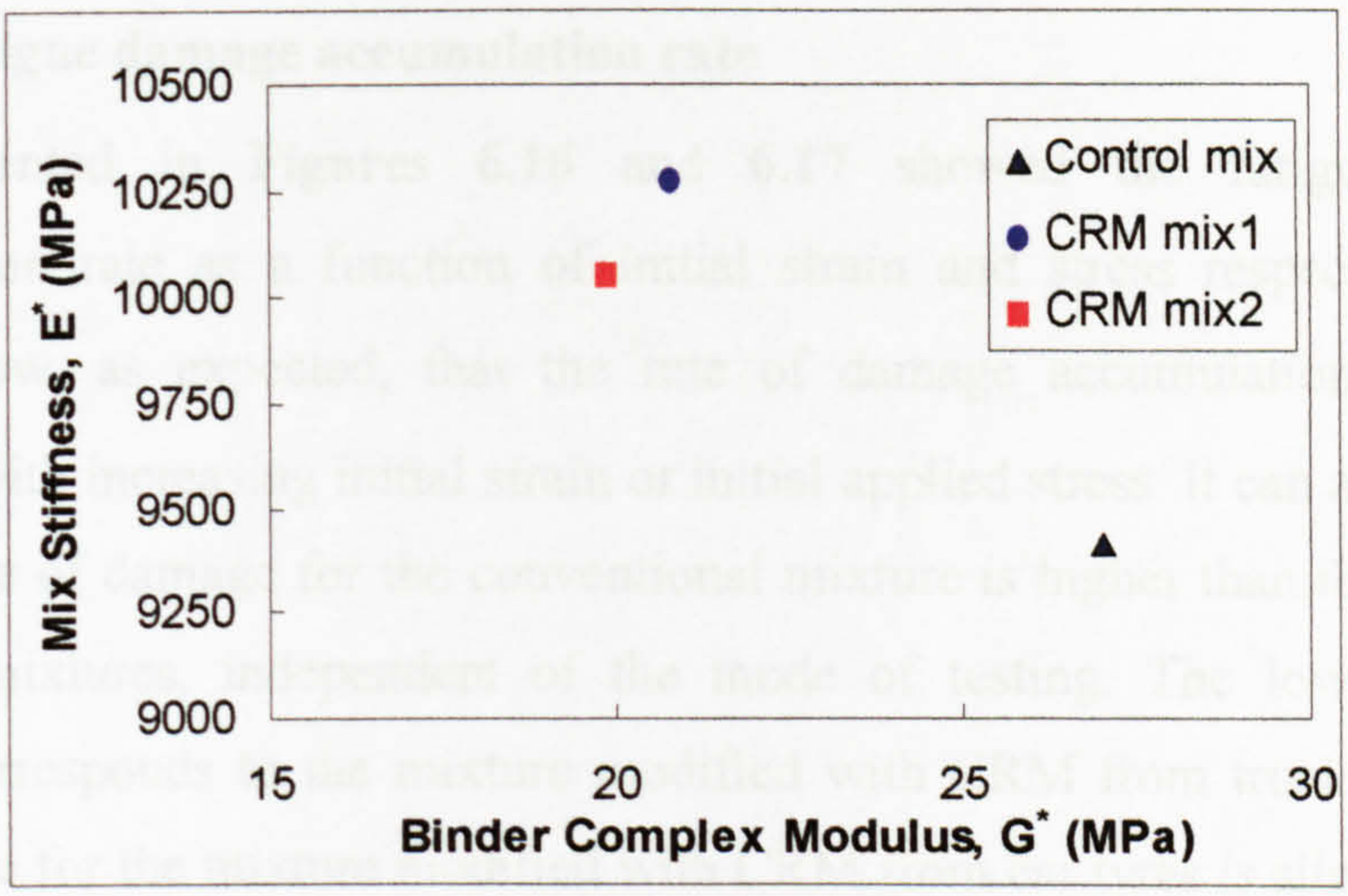

Figure 6.24 Relationship between binder complex modulus and mix stiffness

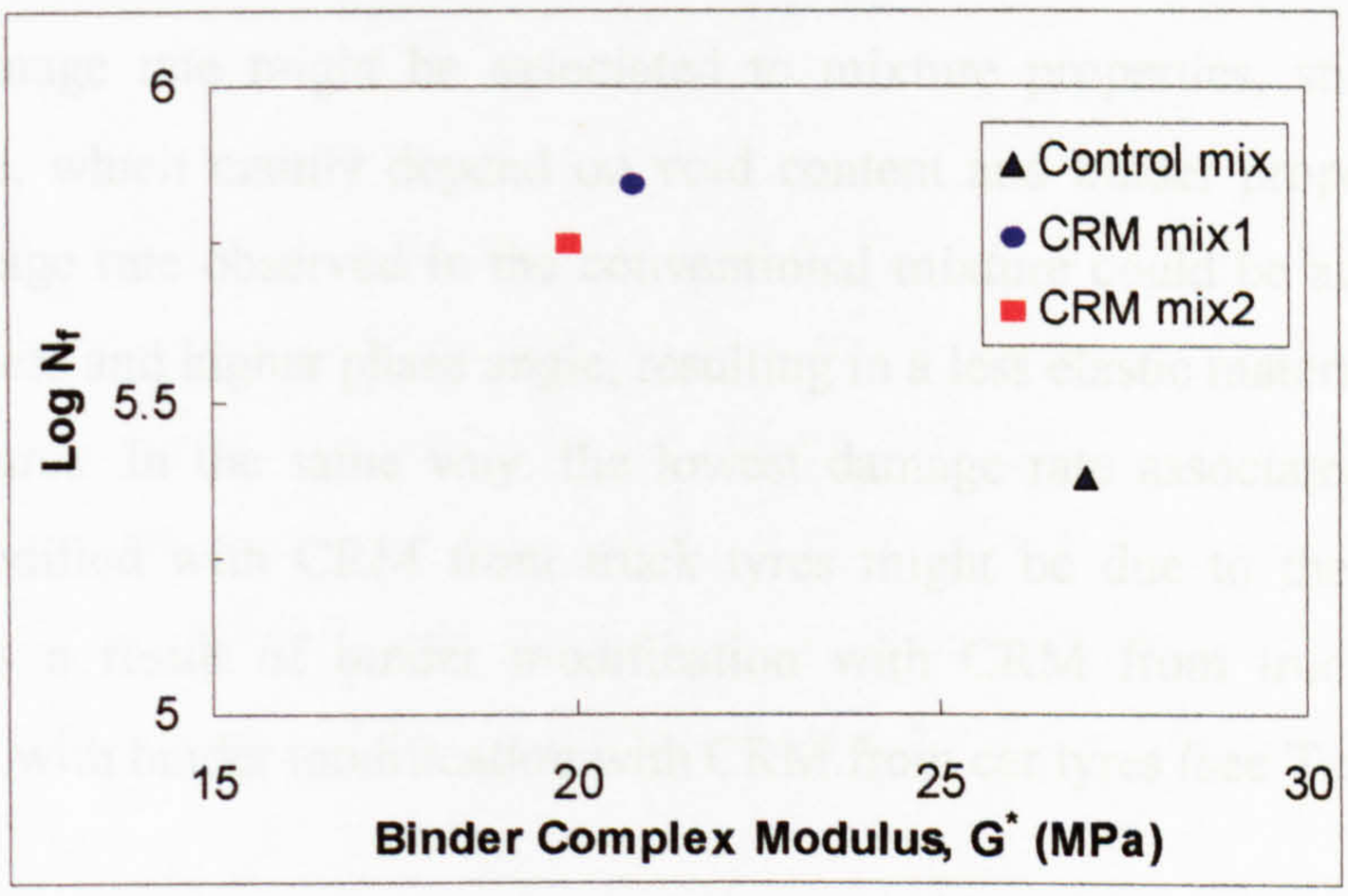

Figure 6.25 Relationship between binder complex modulus and fatigue life

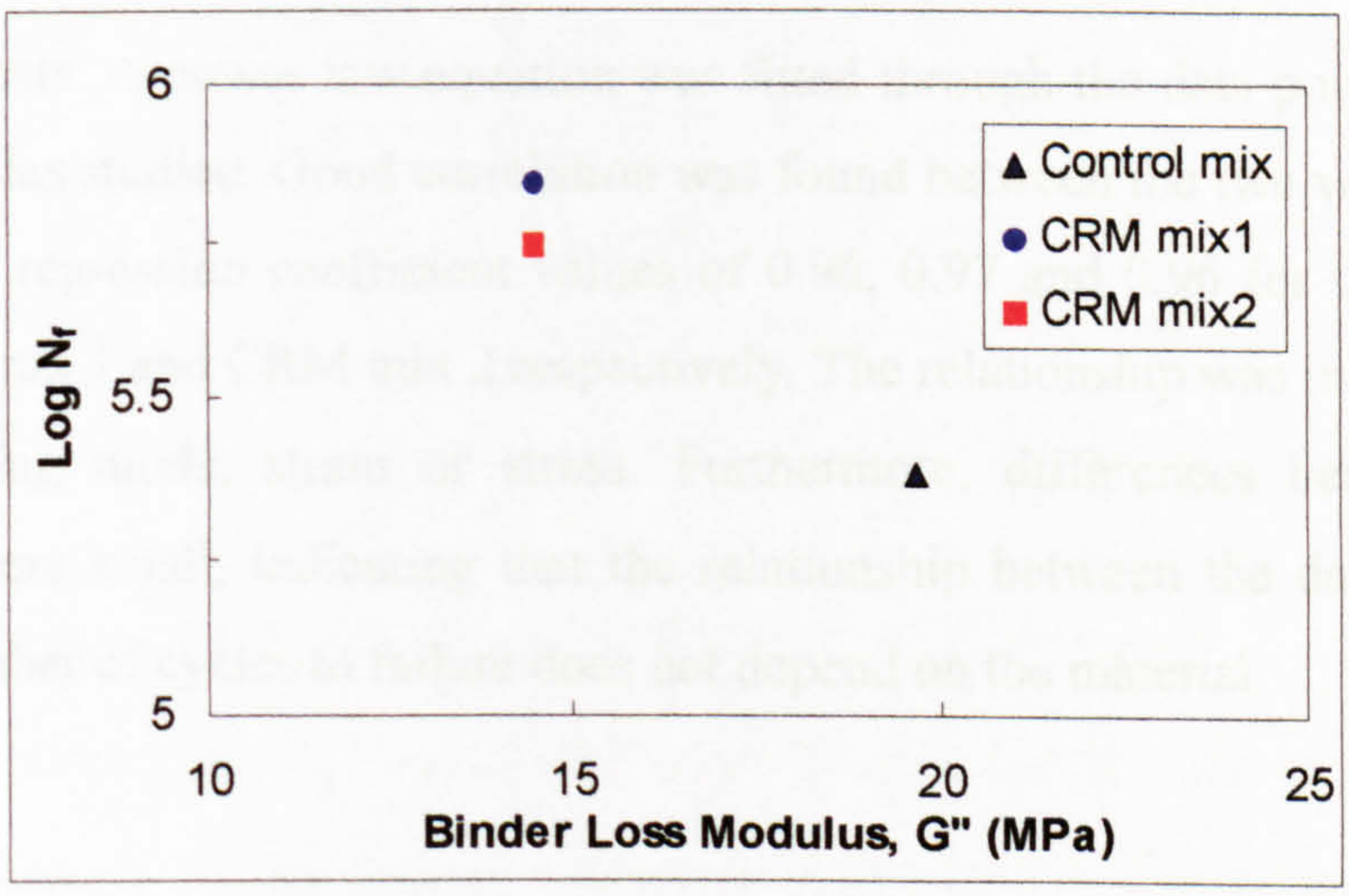

Figure 6.26 Relationship between binder loss modulus and fatigue life

6.4.4 Fatigue damage accumulation rate

Data presented in **Figures 6.16** and **6.17** showed the fatigue damage accumulation rate as a function of initial strain and stress respectively. The figures show, as expected, that the rate of damage accumulation (dD/dN) increases with increasing initial strain or initial applied stress. It can also be seen that the rate of damage for the conventional mixture is higher than those for the modified mixtures, independent of the mode of testing. The lowest rate of damage corresponds to the mixture modified with CRM from truck tyres. The damage rate for the mixture modified with CRM from car tyres is slightly higher than the one modified with CRM from truck tyres.

Fatigue damage rate might be associated to mixture properties, stiffness and phase angle, which mainly depend on void content and binder properties. The higher damage rate observed in the conventional mixture could be attributed to lower stiffness and higher phase angle, resulting in a less elastic material than the CRM mixtures. In the same way, the lowest damage rate associated with the mixture modified with CRM from truck tyres might be due to the enhanced elasticity as a result of binder modification with CRM from truck tyres in comparison with binder modification with CRM from car tyres (see **Table 6.11**).

Moreover, a relationship has been observed between the fatigue damage rate and the number of cycles to failure (N_f), as seen in **Figure 6.27**, for controlled strain and stress tests. A power law equation was fitted through the data points for the three materilas studied. Good correlation was found between the two variables as seen by the regression coefficient values of 0.96, 0.97 and 0.96 for the control mix, CRM mix 1 and CRM mix 2 respectively. The relationship was independent of the testing mode, strain or stress. Furthermore, differences between the materials were small, indicating that the relationship between the damage rate and the number of cycles to failure does not depend on the material.

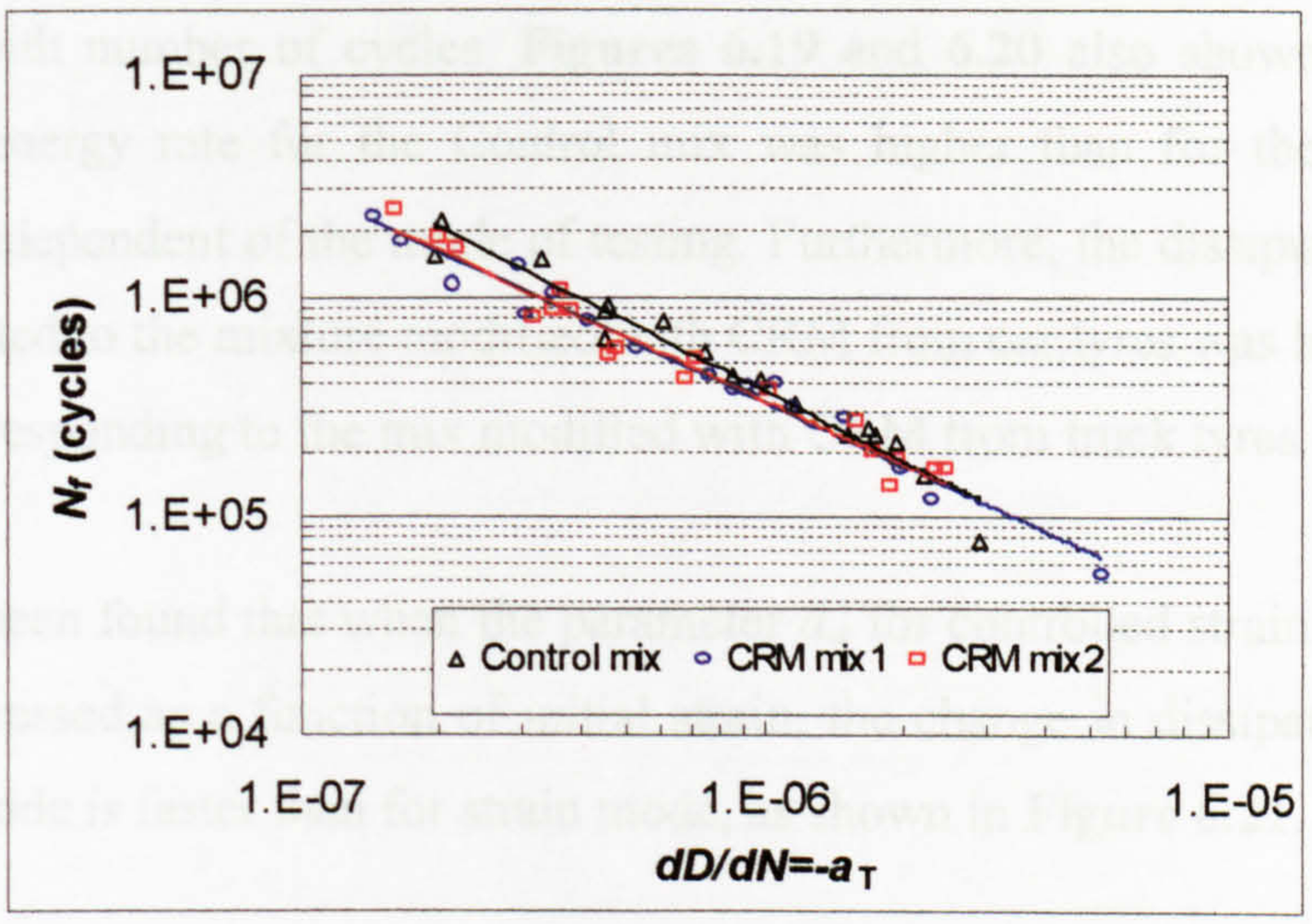

Figure 6.27 Relationship between damage rate, dD/dN , and fatigue life, N_f

It has also been observed that when the rate of damage for controlled strain and stress tests is expressed as a function of initial strain, the rate of damage for stress mode is higher than for strain mode for the three materials tested, as shown in **Figure 6.18**. This increased rate has been attributed to the influence of the dissipated energy effects. During controlled strain fatigue testing the dissipated energy decreased with number of cycles whereas during controlled stress testing the dissipated energy increased.

If fatigue characterization is an intrinsic property of a material, thus, independent of loading mode, the rate of damage at a particular strain level should be the same in controlled strain or stress mode. Based on this concept, a corrected damage rate was introduced. This corrected damage rate takes into account the dissipated energy effects during testing by introducing the parameter a_W , which represents the change in dissipated energy with number of loading cycles.

Data presented in **Figures 6.19** and **6.20** showed the parameter a_W as a function of initial strain and stress respectively. It can be seen first that the parameter a_W , which represents the dissipated energy rate, is negative for controlled strain testing, indicating that the dissipated energy decreases with loading cycles; and positive for controlled stress testing, indicating that the dissipated energy

increases with number of cycles. **Figures 6.19** and **6.20** also showed that the dissipated energy rate for the Control mix was higher than for the modified mixtures, independent of the mode of testing. Furthermore, the dissipated energy rate associated to the mixture modified with CRM from car tyres was higher than the one corresponding to the mix modified with CRM from truck tyres.

It has also been found that when the parameter a_w for controlled strain and stress tests is expressed as a function of initial strain, the change in dissipated energy for stress mode is faster than for strain mode, as shown in **Figure 6.21**.

Figures 6.23 presented the corrected damage rates as a function of the initial strain for both, controlled strain and stress tests. It has been found that the rate of fatigue damage accumulation for the conventional mixture was higher than for the CRM mixtures. Furthermore, the rate of fatigue damage accumulation corresponding to the mixture modified with CRM from truck tyres was the lowest.

6.4.5 Applicability to pavement design

Fatigue relationships obtained from laboratory testing have been used to assess their impact on the design life of the pavement structure. The common parameter adopted in the analytical design of flexible pavements is the horizontal strain at the bottom of the bituminous bound layers. This parameter safeguards against fatigue cracking of the pavement.

A pavement model proposed by Khalid (2000) was adopted. The pavement model used for the evaluation of the conventional and rubber-modified wearing course mixtures is presented in **Appendix Q**. The BISAR Program developed by Shell (SIPC, 1995) was used to determine the maximum tensile strains under the bituminous layers arising from loading the pavement model containing the different mixtures.

Maximum horizontal tensile strains under the bituminous bound layers occurred at the line of symmetry between the wheels. Furthermore, it was found that the

tensile strain generated by the conventional mixture was slightly larger than those of the rubber-modified mixtures. By applying these maximum tensile strains to the fatigue relationships presented in **Figure 6.12**, the estimated fatigue lives for each mixture was computed. These values are presented in **Table 6.12**.

	Maximum tensile strain (μm/m)	Fatigue life, N_f (cycles)
Control mix	185	1.47E+05
CRM mix1	184	4.97E+05
CRM mix2	184	3.80E+05

Table 6.12 Fatigue life of the pavement structure

It can be concluded that the design life of the pavement structure is improved when using rubber-modified wearing courses of the same thickness as the conventional material, i.e. 40 mm. Moreover, equivalent design lives were obtained when the thickness of the modified mixtures were reduced to 13 mm (CRM mix 1) and 14 mm (CRM mix 2). Hence, for the same design life, thinner wearing course layers could be used with rubber-modified materials. This will consequently have a beneficial impact on the initial cost of the pavement.

Chapter 7

FRACTURE AND LOW TEMPERATURE CRACKING

Chapter 7

FRACTURE AND LOW TEMPERATURE CRACKING

This chapter presents the low temperature fracture characteristics of a conventional and two crumb-rubber modified mixtures. Fracture resistance has been evaluated based on linear elastic fracture mechanics approach (LEFM), which leads to the determination of the critical stress intensity factor, also called fracture toughness; and on the elastic-plastic fracture mechanics (EPFM) concept that leads to the determination of the critical strain energy release, also known as the critical value of the J-integral.

7.1 THERMAL CRACKING IN BITUMINOUS MIXTURES

7.1.1 Definitions and approach

Thermal cracking due to low temperatures and temperature cycling is one of the most severe types of distress in asphalt pavement structures. Thermal cracks permit the ingress of water weakening the pavement structure and reducing its life. Ride quality is also badly affected by the presence of such cracks.

Thermal cracking results from the stresses created by different rates of thermal contraction in a pavement structure. Thermal stresses are caused by differential expansion and contraction of pavement layers, each having different coefficients of thermal expansion and thermal conductivity, under cyclic temperature change. When the tensile stress exceeds the tensile strength of the material a micro crack develops at the surface of the pavement. As microcracks, they have little effect on pavement performance. However, with repeated thermal and loading cycles many of these microcracks grow and propagate through the depth of the bituminous layer. The cracks formed in this way are transverse to the direction of traffic.

Bituminous mixtures are considered as viscoelastic materials. Consequently, at intermediate temperatures, the thermal tensile stresses originated when the

temperature decreases are dissipated through stress relaxation. However, at low temperatures a bituminous mixture behaves as an elastic material and the thermal stresses cannot dissipate. At this point cracking may occur if the tensile stresses exceed the tensile strength of the material, and the temperature at which failure occurs is referred as the fracture temperature.

Several approaches have been used to predict the induced thermal stresses in pavements layers. Hills and Brien (1966) proposed an approximate solution for the calculation of the thermal stresses associated with an infinite, completely restrained strip of asphalt material, based on the following equation:

$$\sigma(\dot{T}) = \alpha \sum_{T_0}^{T_f} S(t,T)\Delta T \qquad (7.1)$$

where:

$\sigma(\dot{T})$ = accumulated thermal stress for a particular cooling rate $\dot{T}$

α = coefficient of thermal contraction

T_0 = initial temperature

T_f = final temperature

$S(t,T)$ = mix stiffness (time and temperature dependent)

ΔT = temperature increment

Providing that the input parameters, coefficient of thermal contraction and mix stiffness, are correctly measured or assumed, Equation 7.1 may yield reasonable values. This equation indicates the fundamental fact that the thermal stresses responsible for low temperature cracking are directly related to the stiffness of the mix. Several authors have used Equation 7.1 to calculate thermal stresses and to predict fracture temperature (Burgess et al., 1971, Christison et al., 1972 and Haas and Phang, 1988).

A number of experimental tests methods have also been used to characterise the low temperature properties of pavement materials. These methods are presented in the next section.

7.1.2 Test methods

7.1.2.1 Thermal Stress Restrained Specimen

The thermal stress restrained specimen test (TSRST) was first proposed by Monismith et al. (1965), who suggested that thermal stresses in an asphalt beam could be obtained by measuring the stress required to maintain a specimen at constant length under a specific rate of cooling. Faab (1974) and Janoo (1989) used different versions of the apparatus employed by Monismith et al. Arand (1987) improved the test apparatus by inserting a closed-displacement feedback loop, which ensured that the stresses in the specimen would not relax because the specimen length was continuously corrected during the test.

A modified version of the TSRST system has been developed by Jung and Vinson (1994), and it is shown in **Figure 7.1**. In this system, the chamber and the specimen are cooled with vaporized liquid nitrogen. As the specimen contracts, linear variable differential transducers (LVDTs) sense the movement which causes the screw jack to maintain the specimen at its original length. The process continues till the specimen fails. A typical result from a TSRST test is presented in **Figure 7.2**. The thermal stresses increase as temperature decrease, until the specimen fractures. At this point the stress reaches its maximum value, which is referred to as the fracture strength, with a corresponding fracture temperature.

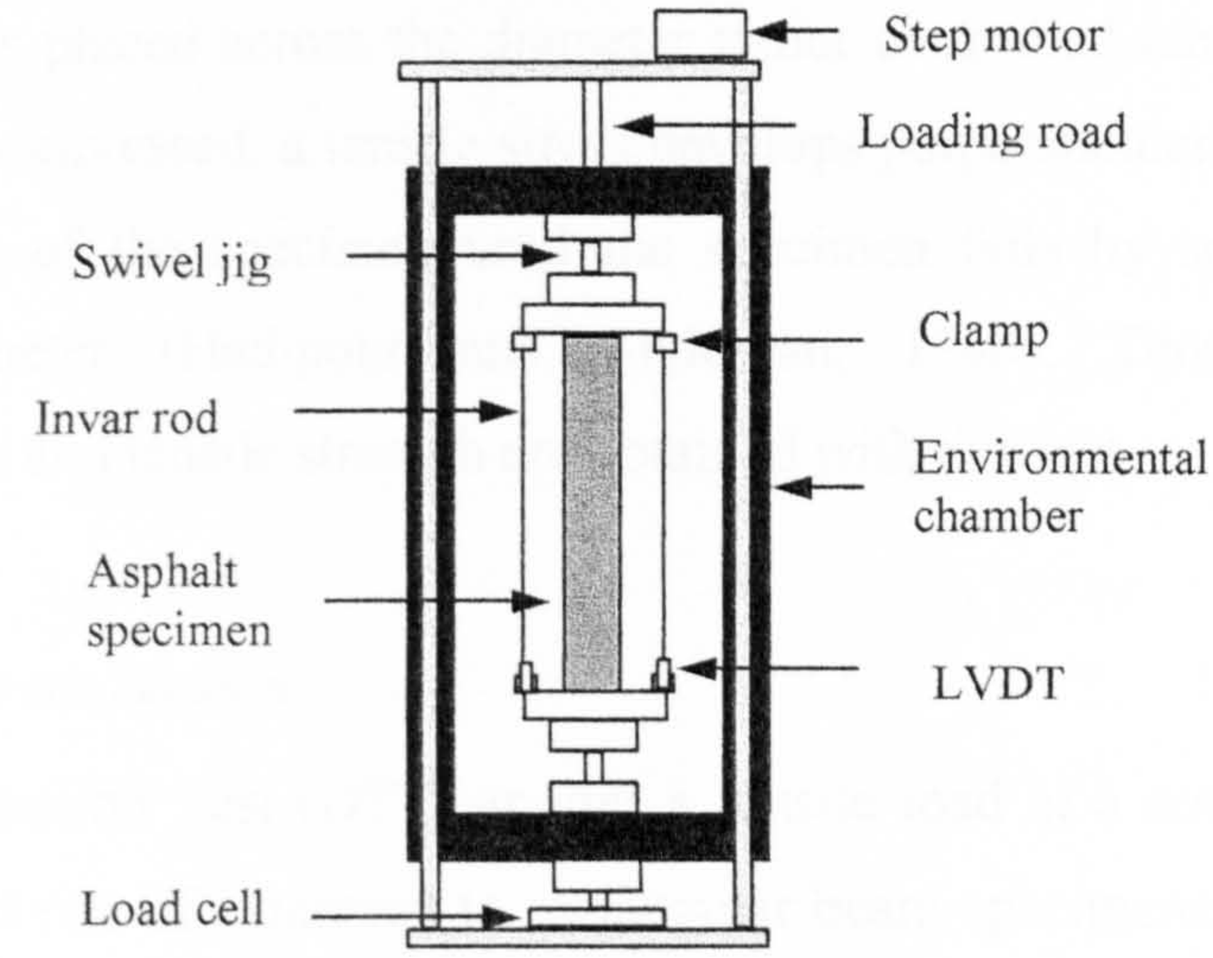

Figure 7.1 TSRST apparatus (after Jung and Vinson, 1994)

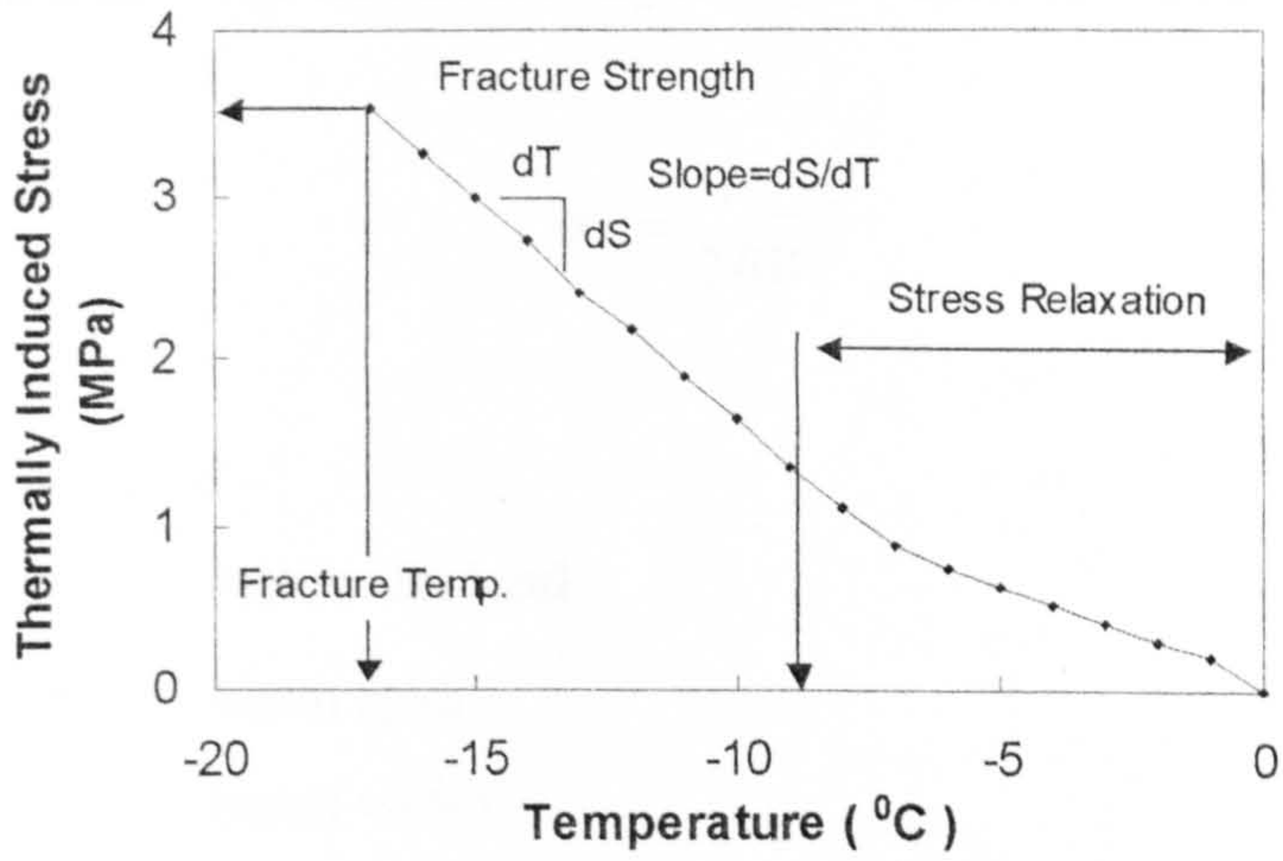

Figure 7.2 Typical TSRST results (after Kliever et al., 1996)

7.1.2.2 Indirect Tension

The Indirect Tension Test (ITT) is conducted in cylindrical specimens through loading stripes placed across the diameter under controlled temperature. As the specimen is compressed, a tensile stress develops perpendicular to and along the vertical plane of the specimen until the specimen fails by splitting along its vertical diameter (Hadipour and Anderson, 1988). Tensile stress/strain characteristics and tensile strength are obtained with this test.

7.1.2.3 Direct Tension

The Direct Tension Test (DTT) applies a tensile load at a control temperature and a constant rate of extension to rectangular beam specimens. During the test, extension of the specimen, temperature, load and time are recorded. The properties measured include tensile strain/stress characteristics and the tensile strength.

7.1.2.4 Flexural Bending

Three-point bending tests have been used to measure the tensile strength of bituminous materials. The flexural strength may be determined as follows:

$$\sigma_f = \frac{3F_{\max}L}{2BW^2} \tag{7.2}$$

where:

$F_{\max}$ = maximum load

L = beam span

B = beam width

W = beam depth

Tests are carried out under load control or displacement control. Relatively slow rates of loading, or deformation, are usually chosen to approach thermally induced stresses rather than traffic related stresses.

7.2 FRACTURE MECHANICS

7.2.1 Introduction

Engineering materials contain defects or flaws that are microstructural in origin, introduced during fabrication or induced during in-service loading. These flaws act as stress concentrators and may have a significant effect on the fracture properties of the material. It has been found that material fracture strengths are well below the theoretical values because of the presence of such flaws. This has led to the development of theories, which seek to analyse mathematically the state of stresses in areas where flaws exist. The above theoretical work is termed fracture mechanics and its aim is to identify fracture criteria.

Two of the most important fracture criteria are the energy criterion and the stress-intensity factor criterion. The energy criterion (Griffith, 1920) is based on a balance between the decrease in potential energy, which is related to the release of strain energy and the external load, and the increase in surface energy resulting from the presence of a crack. The stress intensity factor criterion (Irwin, 1957) introduces the parameter K (stress intensity factor) that defines uniquely the stress field around a sharp crack. The criterion states that fracture will occur when K reaches some critical value, say, K_C.

7.2.2 Energy criterion

An analysis of the critical stress to cause crack propagation in elastic materials was proposed by Griffith (1920) who obtained the following relationships for plain stress and plain strain conditions:

$$\sigma_c = \sqrt{\frac{2\gamma E}{\pi a}} \qquad \text{for plain stress} \qquad (7.3)$$

$$\sigma_c = \sqrt{\frac{2\gamma E}{\pi a(1-\nu^2)}} \qquad \text{for plain strain} \qquad (7.4)$$

where:

σ_c	=	critical stress for fracture
γ	=	specific surface energy
ν	=	Poisson's ratio
E	=	elastic modulus
a	=	one-half the crack length.

Equation 7.4 is generally written in the following form:

$$\sigma_c = \sqrt{\frac{2(\gamma + \gamma_p)E}{\pi a}} = \sqrt{\frac{G_c E}{\pi a}} \tag{7.5}$$

where γ_p is the work done in plastic deformation per unit area of crack extension, and $G_c = 2\left(\gamma + \gamma_p\right)$ is a fundamental property of a material and is termed the *toughness*, or critical strain energy release rate.

7.2.3 Stress-intensity factor criterion

Irwin (1970) obtained solutions for crack-tip stress distributions associated to the three major modes of loading shown in **Figure 7.3**. In mode I, i.e. opening or tensile mode, the crack surfaces move directly apart. In mode II, i.e. sliding mode, the crack surfaces slide over one another in a direction normal to the crack front. Finally, in mode III, i.e. tearing mode, the crack surfaces move parallel to the crack front and remain in the crack plane. Mode I loading is the most commonly encountered and it is associated with a local displacement in which the crack surfaces move directly apart.

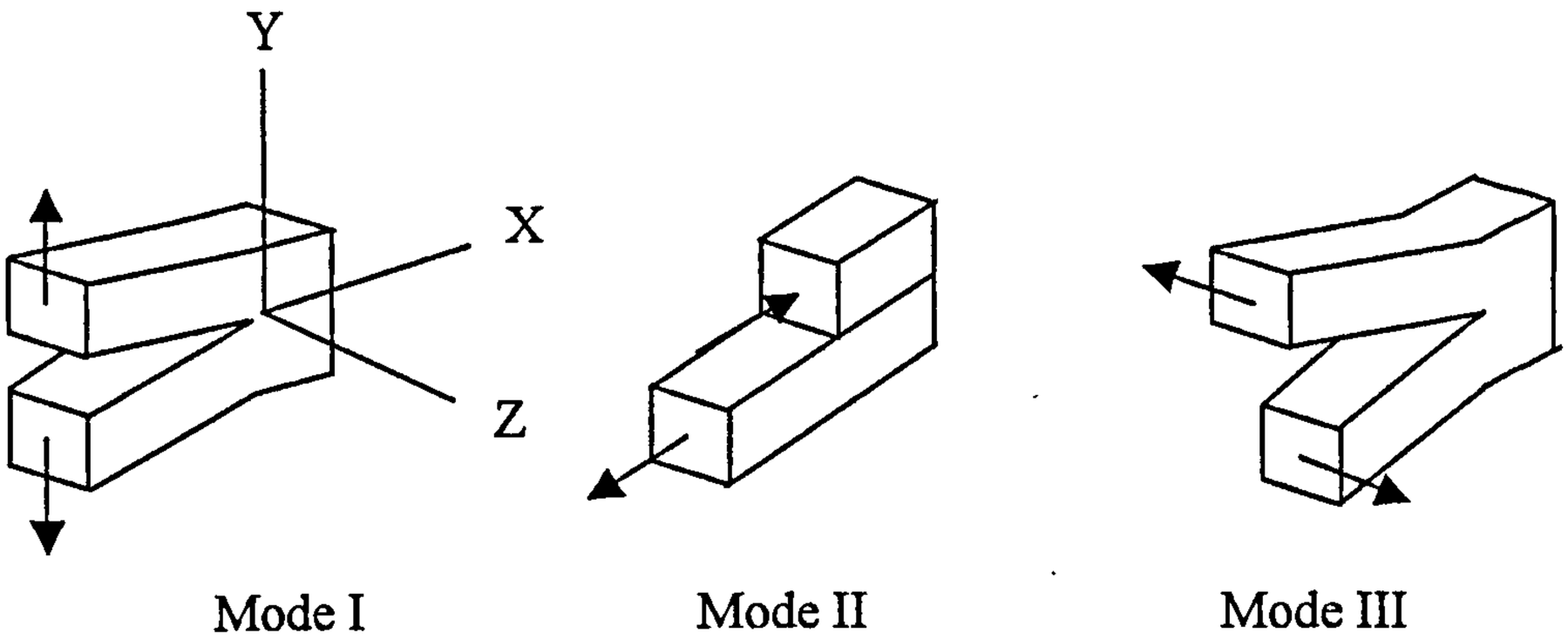

Figure 7.3 Modes of loading

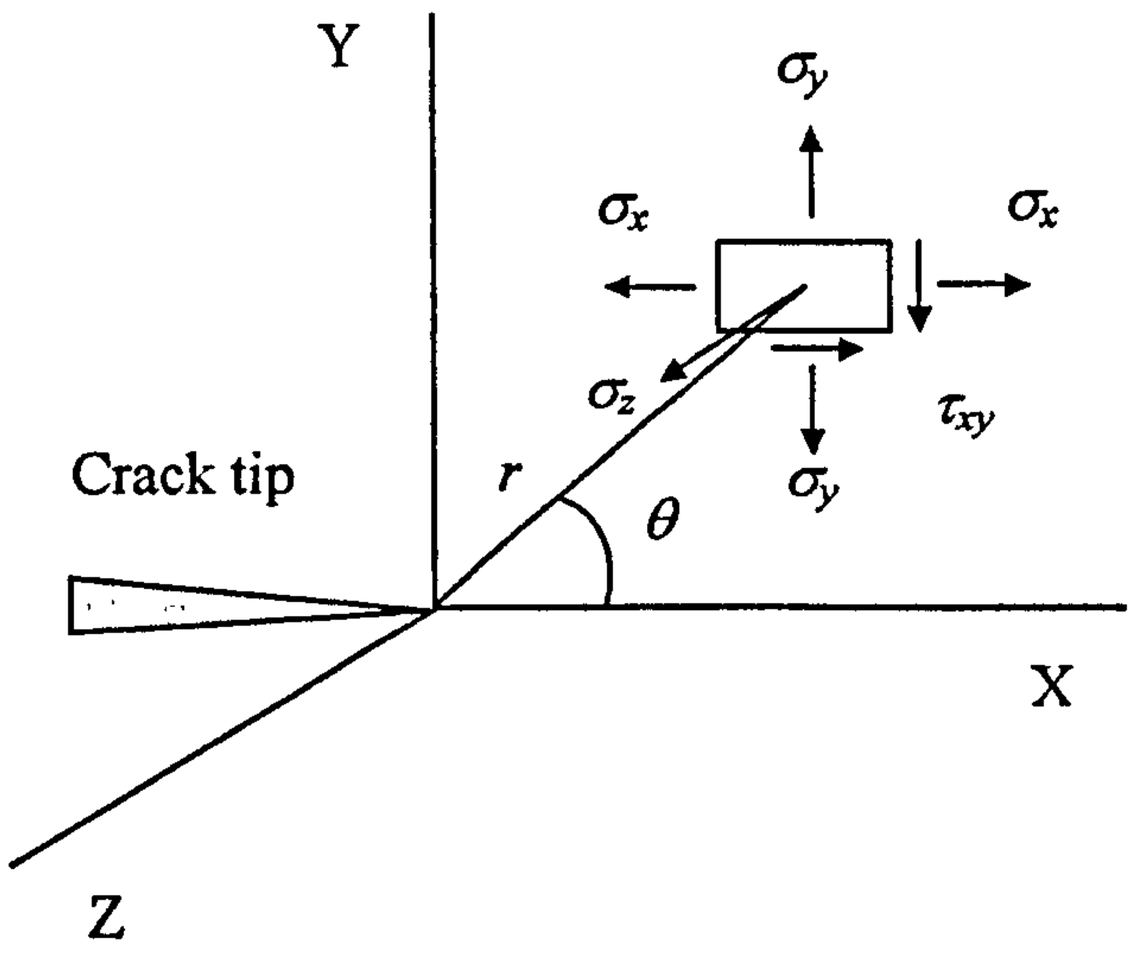

Figure 7.4 Distribution of stresses in vicinity of crack tip

Based on concepts of elastic theory, if a crack is subjected to a tensile stress, σ, the stresses at the crack-tip, for the notation shown in **Figure 7.4**, are found to be

$$\sigma_x = \frac{K_I}{\sqrt{2\pi r}}\cos\frac{\theta}{2}\left(1-\sin\frac{\theta}{2}\sin\frac{3\theta}{2}\right)$$
$$\sigma_y = \frac{K_I}{\sqrt{2\pi r}}\cos\frac{\theta}{2}\left(1+\sin\frac{\theta}{2}\sin\frac{3\theta}{2}\right) \qquad (7.6)$$
$$\sigma_z = \nu(\sigma_x+\sigma_y) \quad \text{(for plane strain)}$$
$$\sigma_z = 0 \quad \text{(for plane stress)}$$

and,

$$\tau_{xy} = \frac{K_I}{\sqrt{2\pi r}}\cos\frac{\theta}{2}\left(\sin\frac{\theta}{2}\cos\frac{3\theta}{2}\right)$$
$$\tau_{xz} = 0 \qquad (7.7)$$
$$\tau_{yz} = 0$$

where Equations 7.6 and 7.7 represent the normal and shear stresses respectively.

In the above equations, r and θ are the polar coordinates at the crack tip, ν is the Poisson's ratio and K_I is the stress intensity factor. It is apparent from Equation 7.6 that the stresses in the vicinity of the crack tip could increase to extremely high values as r approaches zero.

For tensile mode, or Mode I, (see **Figure 7.3**), since there can be no stress normal to a free surface, σ_z must be zero at both surfaces but may be relatively large at the mid-thickness plane. For a relatively thin specimen, where σ_z cannot increase appreciably in the thickness direction, a condition of plane-stress dominates, so $\sigma_z \approx 0$. However, for thick specimens, a σ_z stress is developed which restricts straining in the z direction. Thus a condition of plain-strain dominates, so $\varepsilon_z \approx 0$.

The stress intensity factor depends on the configuration of the cracked component, or geometry, and on the manner in which the loads are applied. In general, stress intensity factors may be written in the following form:

$$K_I = Y\sigma\sqrt{a} \tag{7.8}$$

where σ is the applied stress, Y is a geometry factor and a is the crack length. Stress intensity factors have been determined by analytical and numerical techniques for both typical cracked component configurations and standard laboratory test sample shapes.

The stress intensity factor, K_I, uniquely defines the stress field at the crack tip. Once it is known, it is then possible to determine the maximum stress intensity factor that would cause failure. This critical value, K_{IC}, is known as the *fracture toughness* of the material. Therefore, the failure criteria may be expressed in the following form:

$$K_I \geq K_{IC} \tag{7.9}$$

7.2.4 Relation between energy rate and stress intensity factor

The two approaches used to characterise the fracture properties of materials can be related combining Equations 7.3 and 7.5. For an elliptical shaped crack in a plate of infinite size ($Y = \pi^{1/2}$) the following expressions are obtained:

$$K_I = \sqrt{EG_I} \quad \text{(plain stress)} \tag{7.10}$$

and,

$$K_I = \sqrt{\frac{EG_I}{(1-\nu^2)}} \quad \text{(plain strain)} \tag{7.11}$$

7.2.5 Elastic-plastic analysis: The *J*-integral

An alternative parameter has been developed for assessing the fracture behaviour of a material experiencing both elastic and plastic deformation. The method, developed by Rice (1968a), is based on the determination of an energy term that expresses the change in potential energy with changing crack length. Rice (1968a) solved two-dimensional crack problems and demonstrated that the change in potential energy could be replaced by a path-independent line integral around the crack tip.

The form of this line integral, the J integral (Rice, 1968b), is given by the following equation:

$$J = \int_C \left(W dy - \mathrm{T} \frac{\partial \mathrm{u}}{\partial x} ds \right) \tag{7.12}$$

where:

x, y	=	coordinates normal to the crack front
ds	=	increment along contour C
T	=	stress vector acting on the contour
u	=	displacement vector
W	=	strain energy density

Rice (1968a and 1968b) also presented an equivalent experimental method of evaluating *J*. **Figure 7.5** shows non-linear loading curves corresponding to two identical specimens with crack lengths a and $(a+\Delta a)$. The change in strain energy per unit thickness ΔU associated with a change in crack length Δa is equal to $J\Delta$a or,

$$J = \frac{\Delta U}{\Delta a} \tag{7.13}$$

where U is the strain energy (area under the loading curve) per unit thickness and a is the crack length.

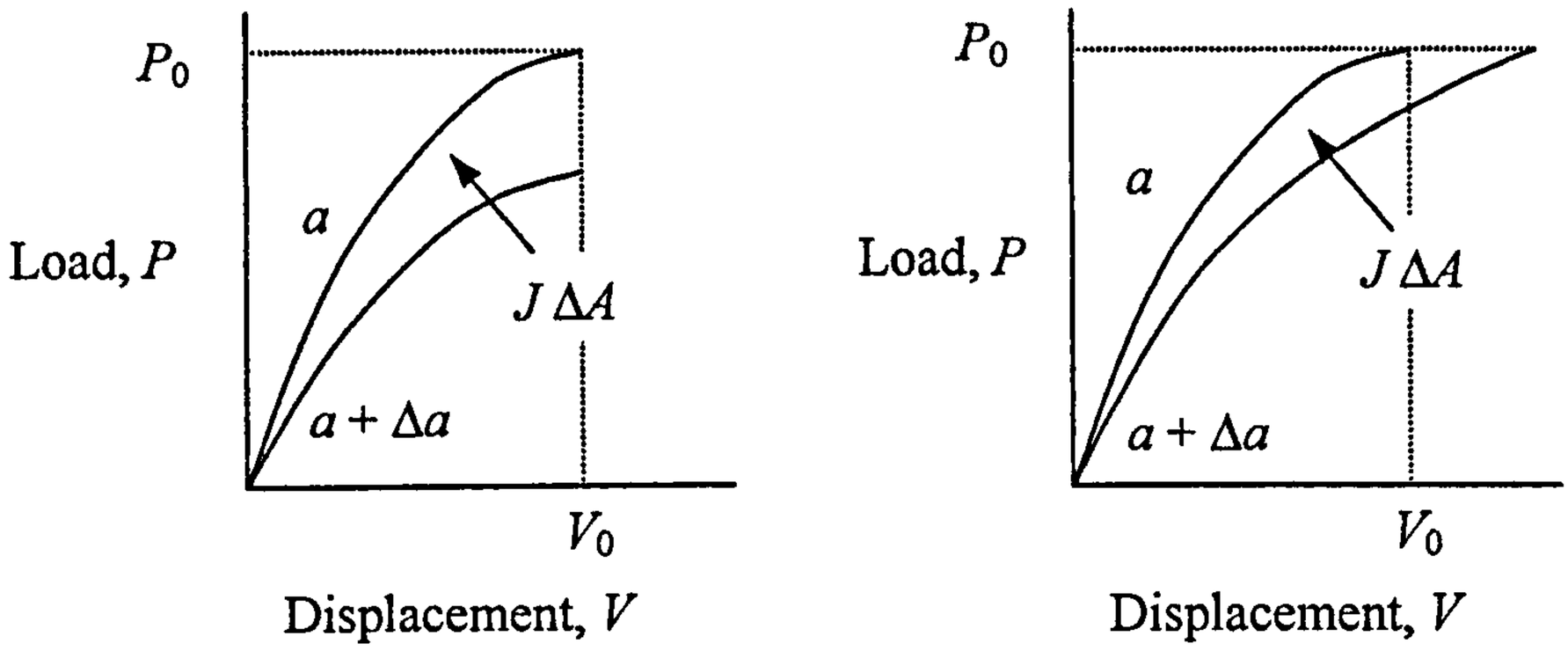

Figure 7.5 Determination of the *J*-integral

For linear and non-linear elastic conditions, J represents the energy made available at the crack tip, or the crack driving force, and corresponds to the energy release rate G for elastic conditions. Therefore,

$$J = G = \frac{K^2}{E'} \tag{7.14}$$

where:

$E' = E =$ Elastic modulus (plane stress)

$E' = \dfrac{E}{(1-\nu^2)}$ (plane strain)

On the other hand, for elastic-plastic conditions, J no longer represents the energy made available at the crack tip because some energy is dissipated irreversibly during plastic flow. However, J can be defined in the same manner for non-linear elastic and elastic-plastic conditions so long as the stress-strain curves are the same.

Experiments in which J has been measured in two different specimen geometries, such as beam and compact specimens, have shown that a constant value, J_{IC}, characterises fracture in both geometries (Begley and Landes, 1972). There is,

then, evidence that a critical parameter, J_{IC}, adequately characterises the toughness of a material near the outset of crack extension. Furthermore, the values of J_{IC} appear to extrapolate well from those of G_{IC} determined from plane-strain fracture toughness. For this condition,

$$J_{IC} = G_{IC} = \frac{K_{IC}^2}{E}(1-\nu^2) \tag{7.15}$$

where E and ν are the elastic modulus and Poisson's ratio respectively.

7.2.6 Fatigue crack propagation

In many practical applications, catastrophic failures can occur if initially small flaws grow to critical lengths during in-service loading by mechanisms such us fatigue.

A fracture mechanics approach to characterise fatigue crack propagation was first proposed by Paris and Erdogan, (1963). They found that the rate of crack propagation was a function of the stress intensity factor K, as follows:

$$\frac{da}{dN} = A(\Delta K)^m \tag{7.16}$$

where:

$\frac{da}{dN}$ = fatigue crack growth rate

ΔK = stress intensity factor range $\left(\Delta K = K_{\max} - K_{\min}\right)$

A, m = material constants

As the crack propagates in an elastic material, the stress field at the crack tip increases until a stage is reached where rapid unstable crack growth and the critical condition of K_{IC} takes place.

7.2.7 Application of fracture mechanics to bituminous materials

Traditionally, low-temperature fracture behaviour of bituminous mixtures has been characterised by comparing the calculated thermal stresses with the tensile strength of the material. This method assumes the tensile strength as the fracture criteria, thus the higher the tensile strength the higher the resistance to fracture.

Fracture mechanics theory, however, establishes that high strength materials can be very susceptible to fracture in the presence of cracks. These cracks act as stress concentrators and have a fundamental effect on the fracture strength. If a flaw (micro crack) exists or is formed in a bituminous pavement layer, the pavement will fail at very much lower level of stress than it can sustain without the flaw.

Fracture mechanics theory was first applied to bituminous materials in the late 1960s. Moavenzadeh (1967) and Bahgat and Herrin (1968) used fracture mechanics theory to evaluate brittle fracture in asphalt materials, and showed that at low temperatures the Griffith theory of brittle fracture could be applied to characterise fracture behaviour. Majidzadeh et al. (1969 and 1971) also used fracture mechanics to analyse fatigue and fracture of asphalt mixtures.

The critical stress intensity factor, K_{IC}, or fracture toughness, has been used as a failure criterion of bituminous materials (Aglan and Figueroa, 1993). More recently, Kim and El Hussein (1997) utilized a newly developed K_{IC} formula to reflect the non-linear load-deflection behaviour prior to the attainment of the peak load of quasi-brittle materials. The method, known as the effective crack model (ECM), is a direct method for laboratory determination of fracture toughness of a single-edge notched asphalt beam tested in a three-point bending setup.

The critical strain energy release rate, also called the critical value of the J integral, J_{IC}, has also been used to study the fracture characteristics of bituminous materials. Abdulshafi and Majidzadeh (1985) applied the J_{IC} criteria to asphalt mixtures. Notched Marshall specimens with various initial crack lengths were

tested in load control mode, and the load versus displacement curves were obtained. The areas under the load-displacement curves were found at different displacements and were used to find the relationship between the strain energy per unit thickness and the initial crack length. The slope of these curves is found to be the J integral value.

Dongre et al. (1989) employed the critical strain energy rate, J_{IC}, and the critical stress intensity factor, K_{IC}, as a fracture criterion of asphalt mixtures. Notched beams with notch to beam depth ratios between 0.5 and 0.7 were tested under three-point bending at different temperatures. Two methods were used to evaluate the J integral. In the first method, J_{IC} was obtained by calculating the area under the load displacement curves up to failure for different notch depths. The second method required only one specimen and one crack length, and was only applicable for length-to-depth ratio equal to 4 and notch-to-depth ratios between 0.5 and 0.7 (Sumpter and Turner, 1976). The outcome of this study showed that the critical value of the J-integral, J_{IC}, as a fracture characterization parameter, is sensitive to binder and mix properties; and the critical stress intensity factor, K_{IC}, as a fracture parameter is not sensitive to binder grade or source.

Mahboub (1990) studied the fracture properties of plasticized sulphur paving mixtures. Notched beams under three-point bending were tested to determine the critical value of the J integral, J_{IC}. To accommodate special fracture characteristics of bituminous materials, modifications to the ASTM E813-89 standard for J_{IC}, (ASTM, 1993a) were proposed and discussed. J_Q values, which are a provisional representation of J_{IC} were obtained from multiple loadings and unloadings of a single chevron notched specimen tested in displacement control mode. In this study, the value of J_Q was defined to be the Y-intercept of the J-integral versus crack extension plot, which is commonly referred to as the J_R-curve. According to ASTM E813-89, it is required to construct a blunting line on the plot of J-integral versus crack extension. The intersection of this blunting line and the J_R-curve, represented by a linear slope, is defined as J_{IC}. However, the J_{IC} value is often not very different from the J_Q value defined in this study, as shown in **Figure 7.6**.

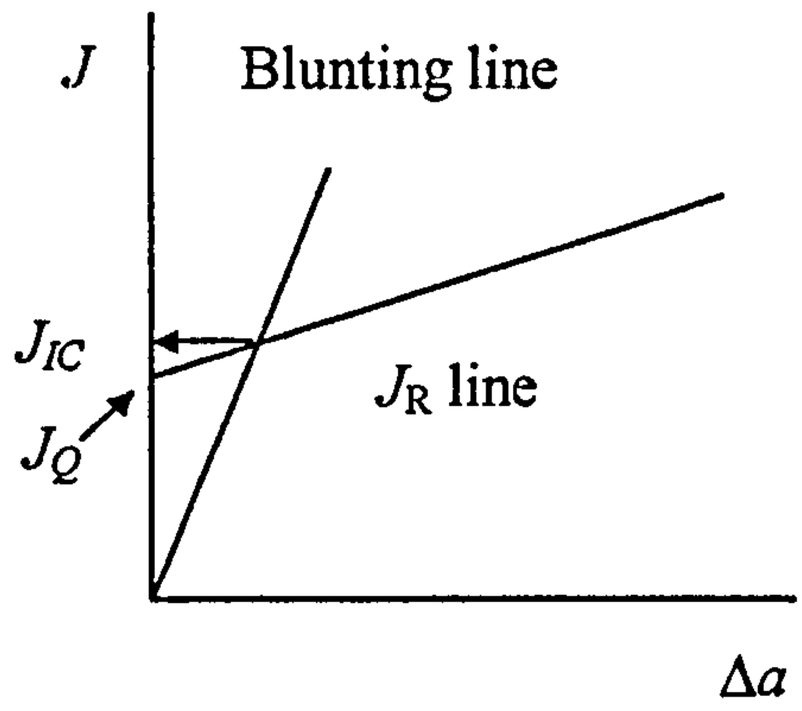

Figure 7.6 Definition of J_{IC} according to ASTM E813-89

Sulaiman and Stock (1995) applied fracture mechanics to assess a series of mixes in which the variable was the quantity of reclaimed asphalt. The study examined conditions under which linear elastic and elastic-plastic fracture data could be obtained. In particular, plane strain fracture toughness, K_{IC}, was determined on notched beams under three point bending. The results were considered to give valid K_{IC} values if they met the criteria set by ASTM E399-90 (ASTM, 1993**b**).

7.3 EXPERIMENTAL PROCEDURE

7.3.1 Fracture specimens

Fracture beam specimens were cut from 306 x 306 x 64 mm^3 slabs manufactured in the laboratory. The slabs were cut using diamond-tip masonry saw to the required beam dimensions. Beam dimensions selected were 300 mm length (L), 70 mm depth (W) and 50 mm width (B).

Beam specimens were notched at the midpoint using a diamond-tip saw. Notch width was approximately 3 mm and notch depth (a_0) to beam depth (W) ratios (a_0/W) selected were 0.3, 0.4 and 0.5. Typical notch depths used were 21, 28 and 35 mm. **Figure 7.7** illustrates the specimen geometry, and a typical fracture specimen is presented in **Figure 7.8.**

Fracture specimens were subjected to air-void content measurements before being tested. The volumetric parameters for each individual specimen are presented in **Appendix R.**

7.3.2 Test conditions

Fracture tests were conducted at three different temperatures. Specimens were conditioned at the test temperature in a temperature-control cabinet for a period of 24 hours. Specimen temperature was monitored during the test to observe if any significant changes were to occur. Temperature monitoring was carried out by means of a thermocouple situated just inside the crack tip. A dummy specimen was used for this purpose. The dummy specimen was place inside the temperature-controlled cabinet set at a temperature of 1 or 0.5 ^{0}C below the required test temperature. The dummy specimen was then removed from the cabinet and placed immediately on the three-point bend frame. Finally, the change in temperature with time from the moment that the specimen was removed from the cabinet up to about 10 minutes was recorded. **Figure 7.9** represents the temperature evolution corresponding to the dummy fracture specimen.

To control specimen temperature during testing, the time from the moment the specimen was removed from the temperature-control cabinet until the test was finished was recorded. This time was about 2 minutes for each individual test. During this time, the temperature of the specimens was +/-0.5 ^{0}C off the required test temperature.

Test temperatures selected were –5, 5 and 15 ^{0}C. Three specimens, with different notch depths, per mix were tested at each temperature. Three mixtures, namely Control mix, CRM mix 1 and CRM mix 2, designed in Chapter 5, were investigated. In total, the number of fracture tests carried out was twenty-seven.

The mode of testing was set at controlled displacement to produce a stable crack growth during loading. The loading rate selected was 60 mm/min (Sulaiman and Stock, 1995).

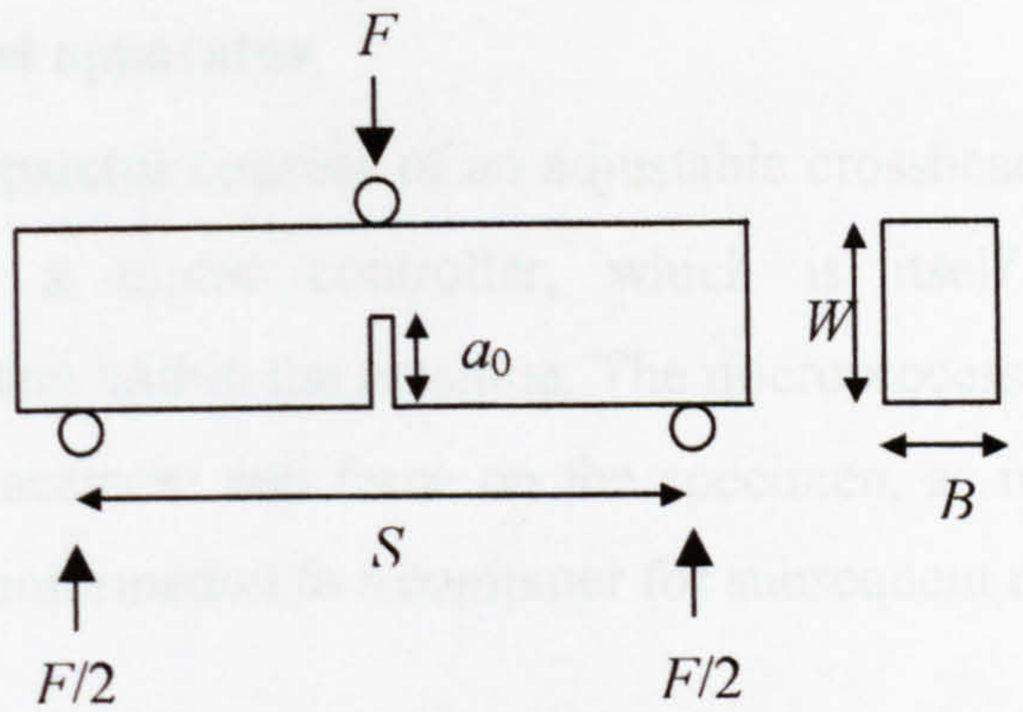

Figure 7.7 Fracture specimen geometry

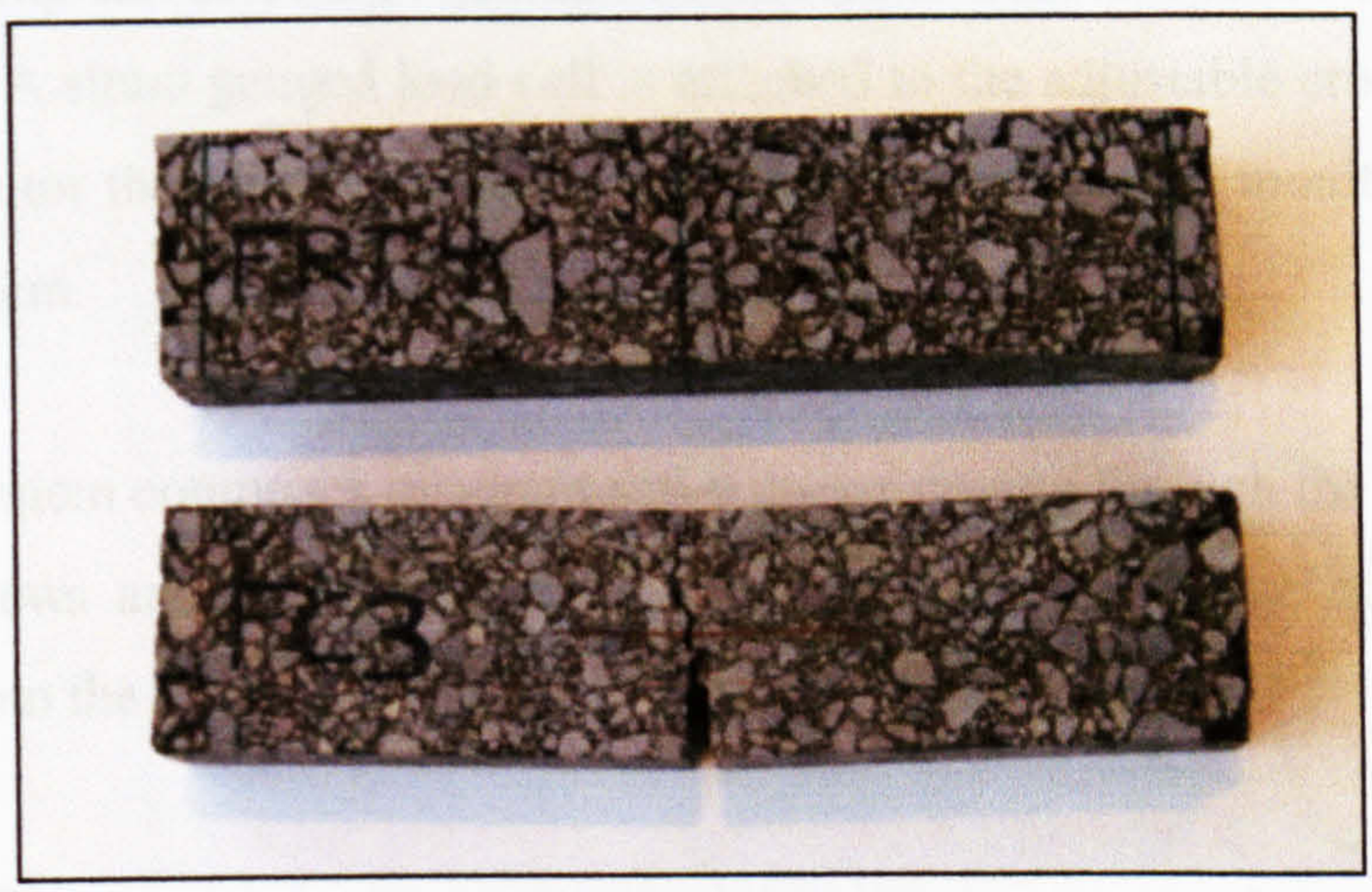

Figure 7.8 Typical fracture specimen

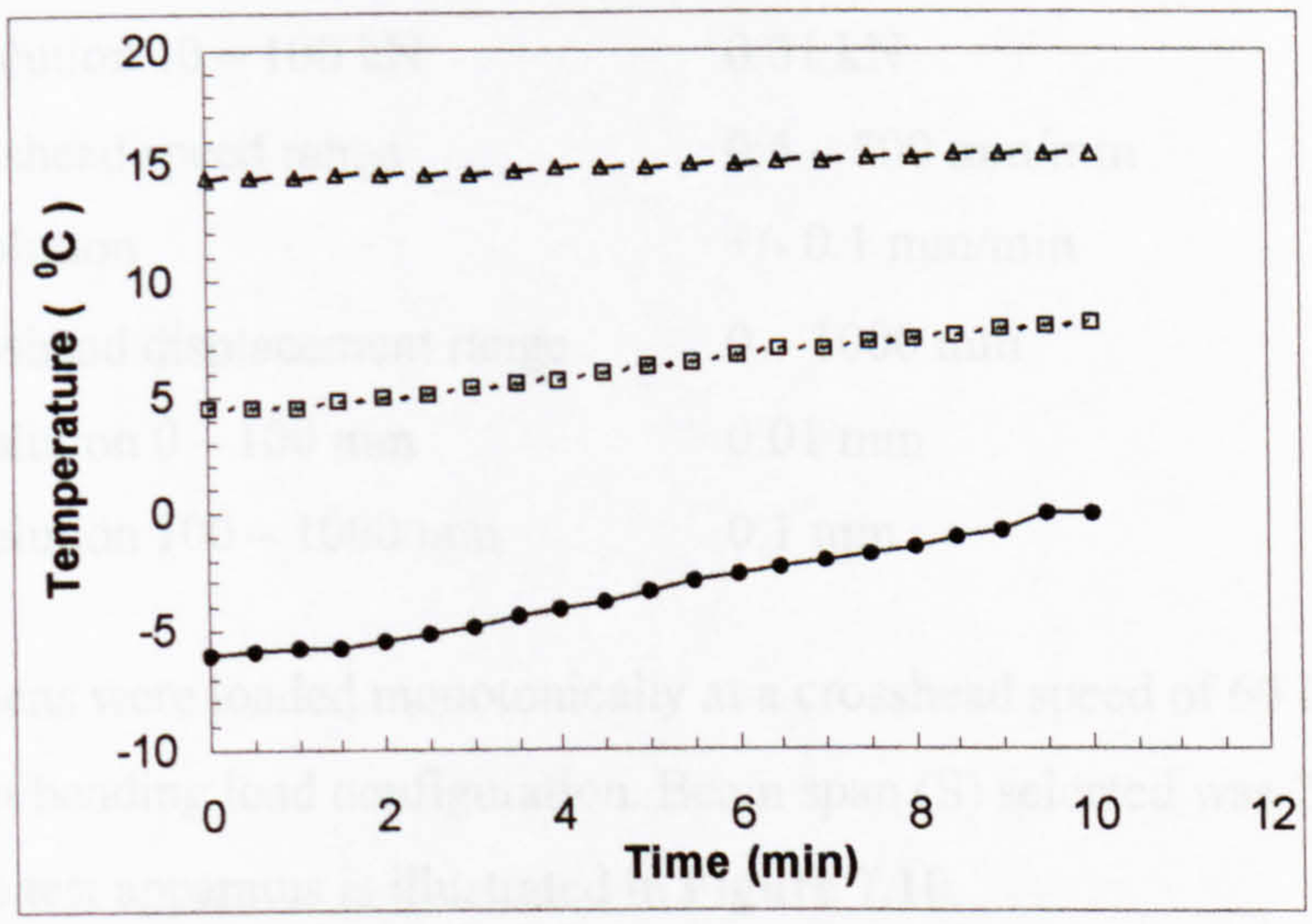

Figure 7.9 Temperature evolution for a fracture specimen

7.3.3 Fracture test apparatus

The fracture test apparatus consists of an adjustable crosshead that is driven at a rate governed by a motor controller, which is itself controlled by a microprocessor system within the machine. The microprocessor system monitors the crosshead displacement and force on the specimen, as measured by a load cell, and sends this information to a computer for subsequent data processing.

The adjustable crosshead within the frame can be traversed up or down by means of recirculating ball screws. A gearbox connected to a motor system drives these ball screws. A strain gauged load cell is attached to the adjustable crosshead and used to monitor the load. The position of the crosshead is also monitored by an encoder system.

The drive system comprises quadrant servo motor driving through the gearbox to the ball screws and hence moves the crosshead. A wide range of speeds is available from the motor system.

Specifications:

• Load range	0 – 100 kN
Resolution 0 – 10 kN	0.001 kN
Resolution 10 – 100 kN	0.01 kN
• Crosshead speed range	0.5 – 500 mm/min
Resolution	+/- 0.1 mm/min
• Crosshead displacement range	0 – 1000 mm
Resolution 0 – 100 mm	0.01 mm
Resolution 100 – 1000 mm	0.1 mm

Test specimens were loaded monotonically at a crosshead speed of 60 mm/min in a three-point bending load configuration. Beam span (S) selected was 280 mm. The fracture test apparatus is illustrated in **Figure 7.10.**

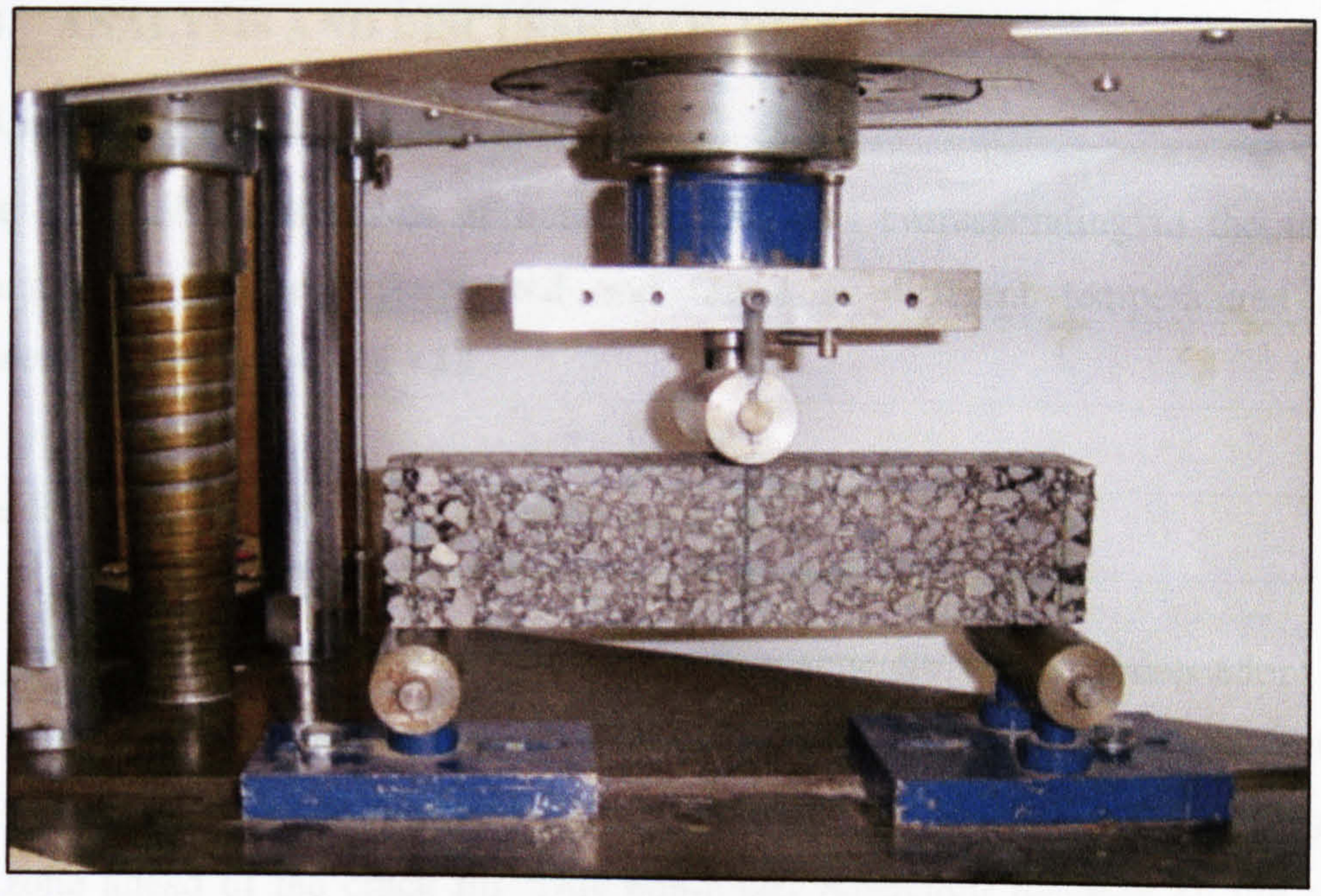

Figure 7.10 Fracture test apparatus

7.4 ANALYSIS AND DISCUSSION OF RESULTS

7.4.1 Load-deflection behaviour

The load-deflection curves of notched specimens corresponding to the three bituminous mixtures investigated and tested at different temperatures are presented in **Figures 7.11 - 13**.

The following general features can be observed:

1. Initially, the load-deflection response is practically linear, independent of notch depth, temperature or material. Before the maximum load is reached, a non-linear response is observed as a result of the development of a plastic zone ahead of the crack tip. This non-linear behaviour depends on the test temperature and on the material. Once the maximum load is reached, the crack then propagates, as seen by the slow decay, until the specimen fails. Failure occurs in Mode I, tensile or opening mode, where the crack surfaces move directly apart.

2. As the notch depth decreases, the maximum load sustained by the specimen increases, and the deflection corresponding to this load also increases slightly. This is simply because the effective cross section of the specimen is increased when the crack length is reduced.

3. As the temperature increases, the maximum load sustained by the specimen decreases and the corresponding deflection increases. This occurs as a result of the reduction in stiffness with increasing temperature.

4. The maximum loads sustained by the crumb rubber mixtures are higher than those for the control mix, independent on temperature or notch depth. Also, the mixture modified with truck-tyre rubber (CRM mix 1) shows slightly higher peak loads than the mixture modified with car-tyre rubber (CRM mix 2) at any temperature or notch depth.

5. As the temperature increases, the non-linearity response of the material before the maximum load is reached is more pronounced. This is the result of the increase in size of the plastic zone ahead of the crack tip with increasing temperature. Furthermore, this effect is more prominent for the unmodified mix than for the crumb rubber modified mixtures.

Dimensions, maximum loads and the corresponding deflections of each individual fracture specimen are presented in **Table 7.1.**

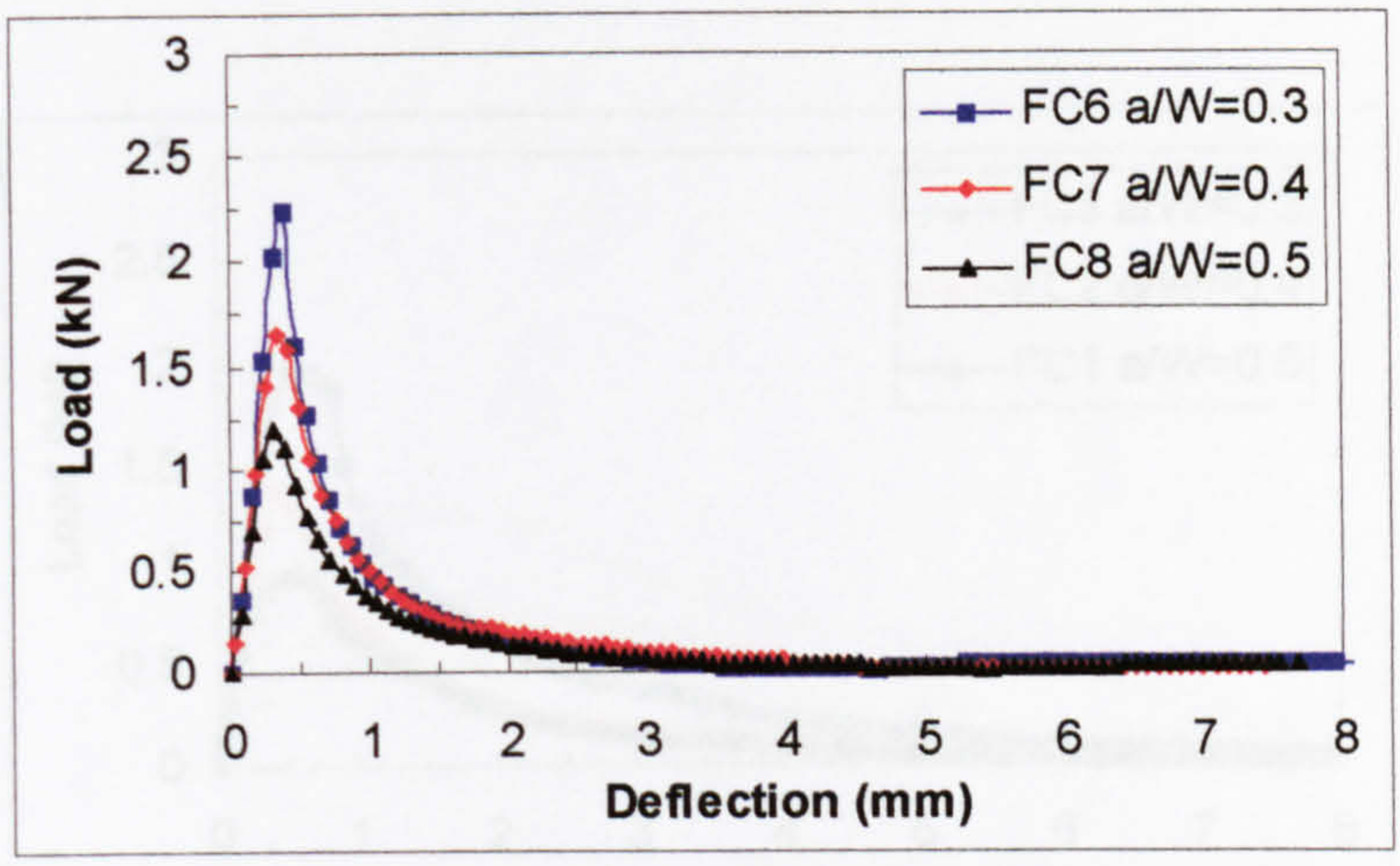

a) Control mix

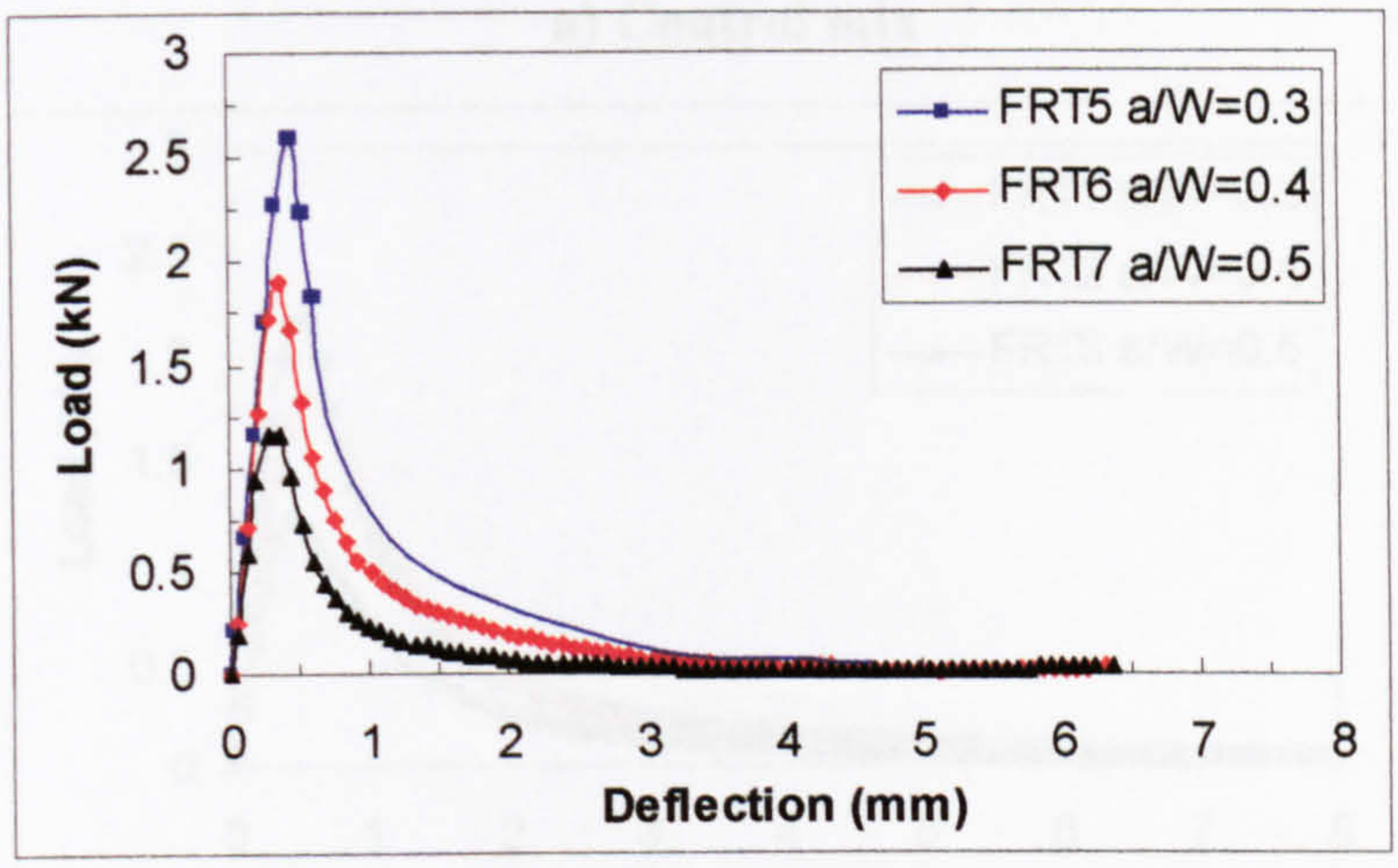

b) CRM mix 1

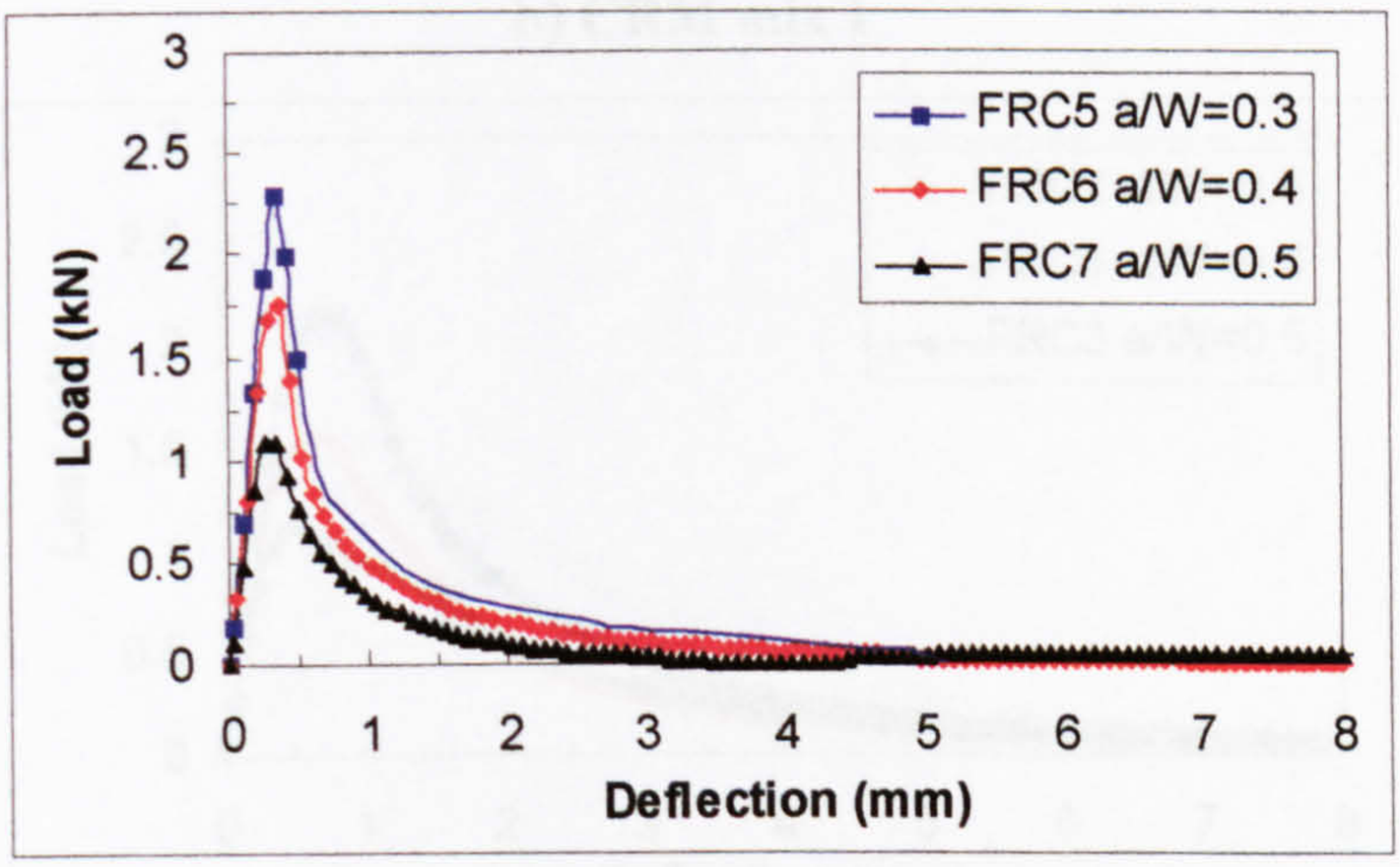

c) CRM mix 2

Figure 7.11 Load-deflection curves at -5 ^{0}C

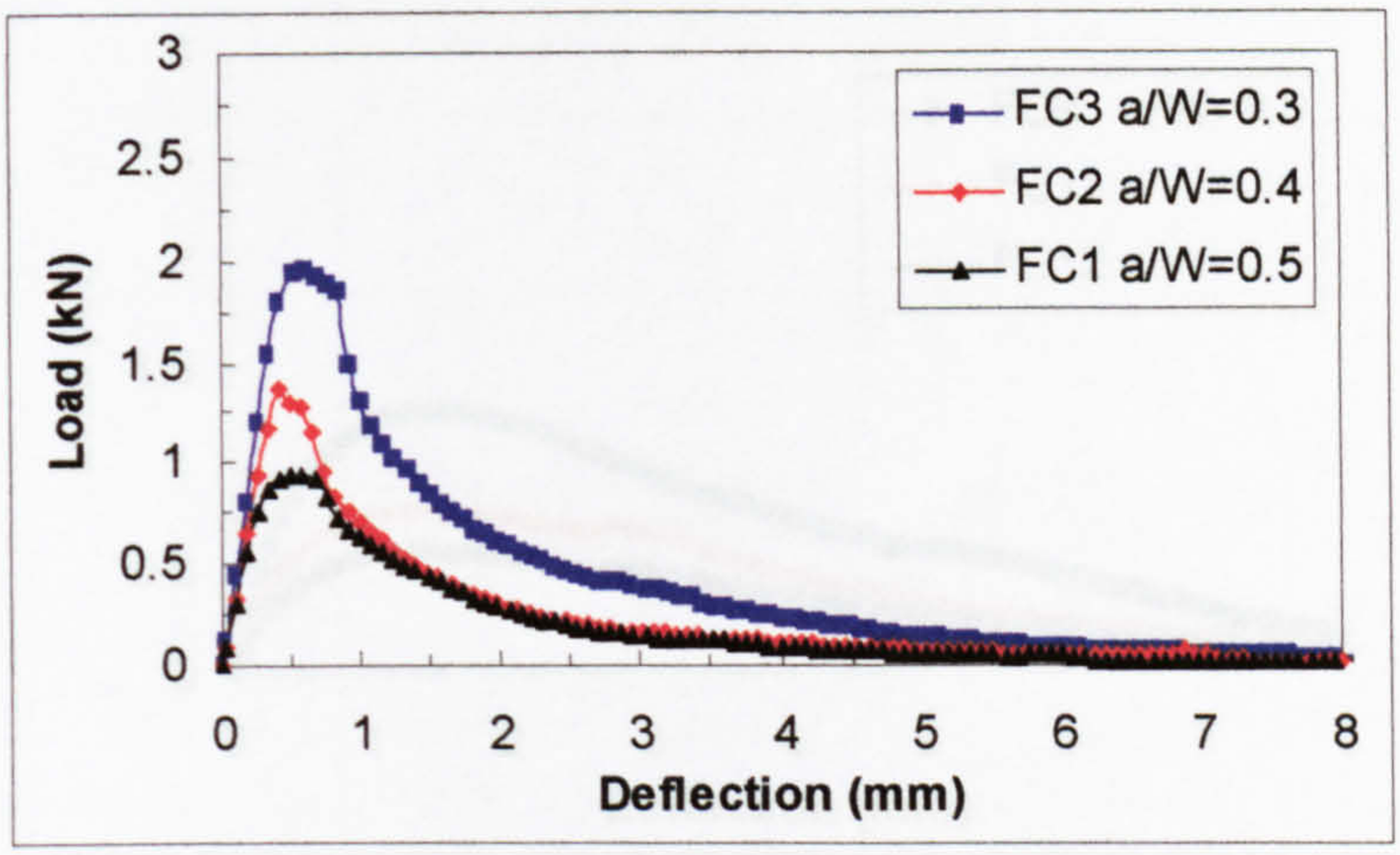

a) Control mix

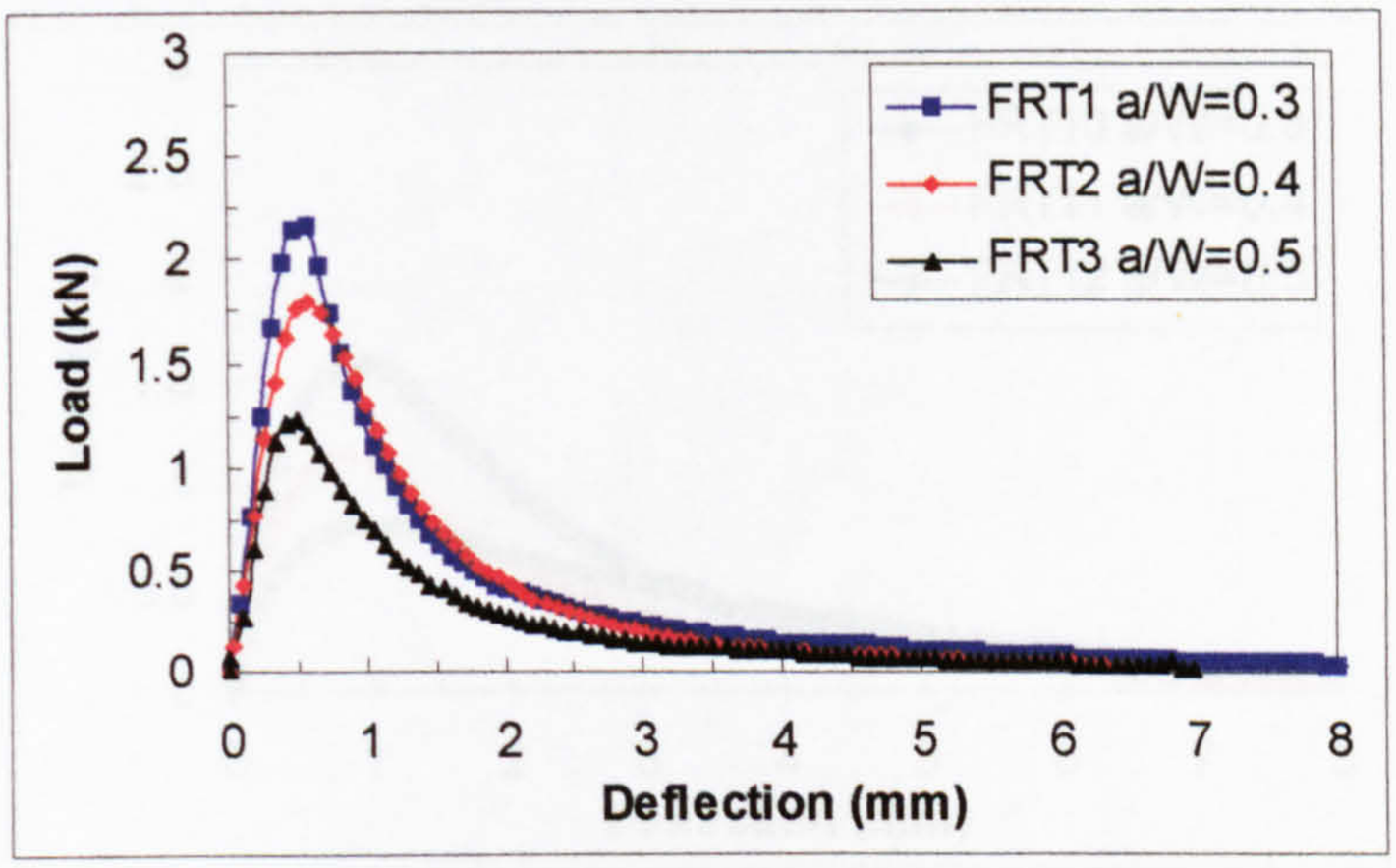

b) CRM mix 1

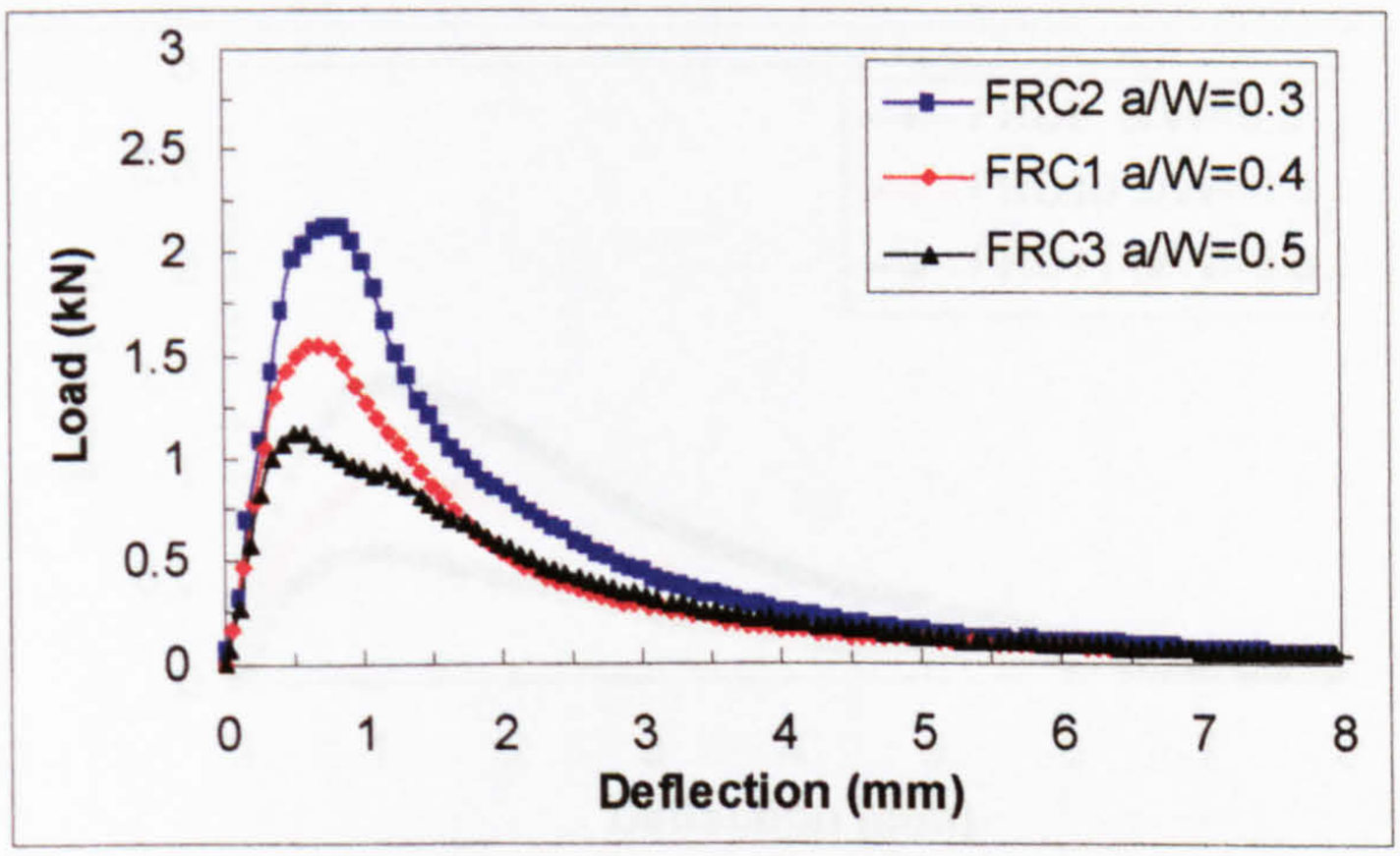

c) CRM mix 2

Figure 7.12 Load-deflection curves at 5 ^{0}C

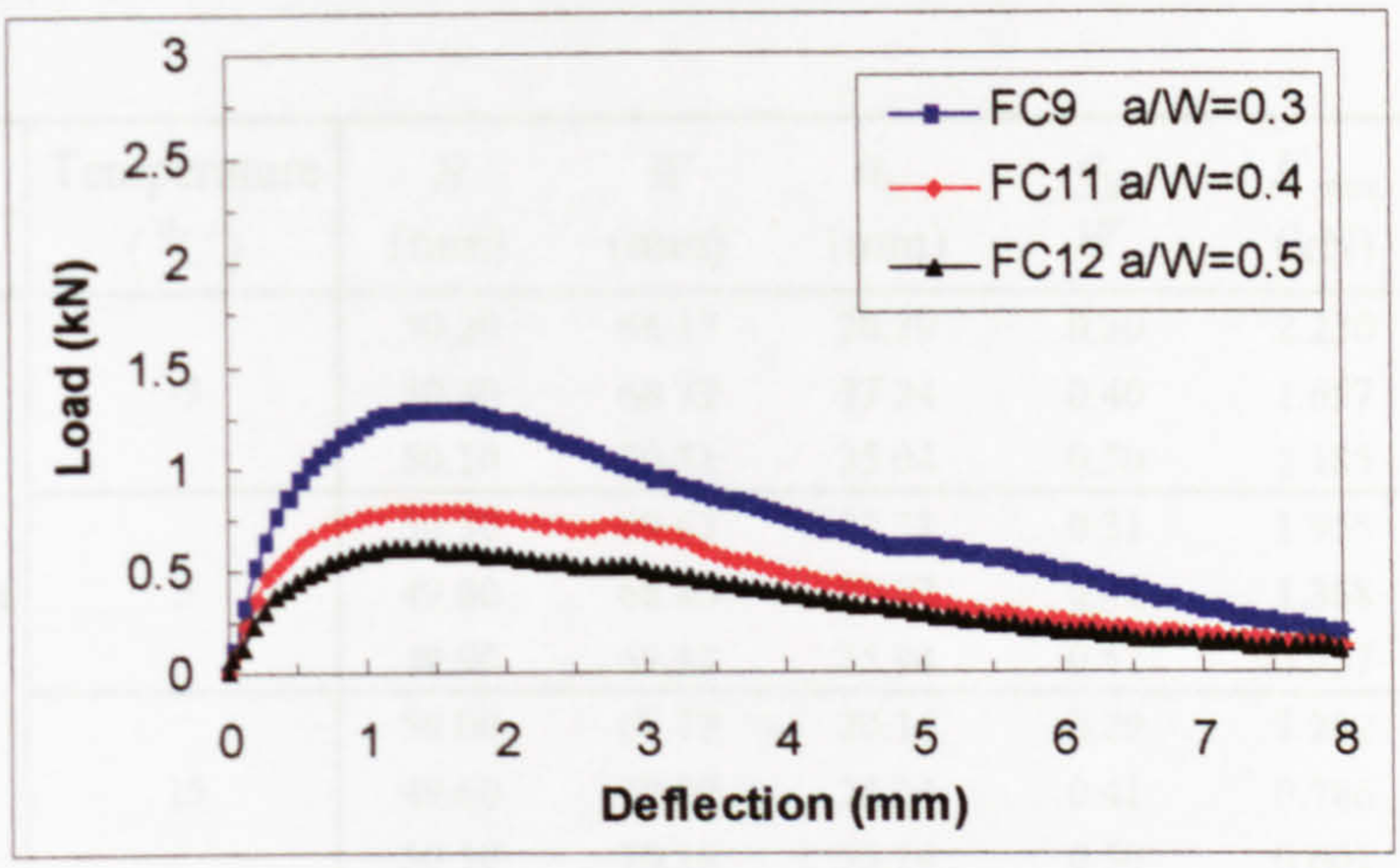

a) Control mix

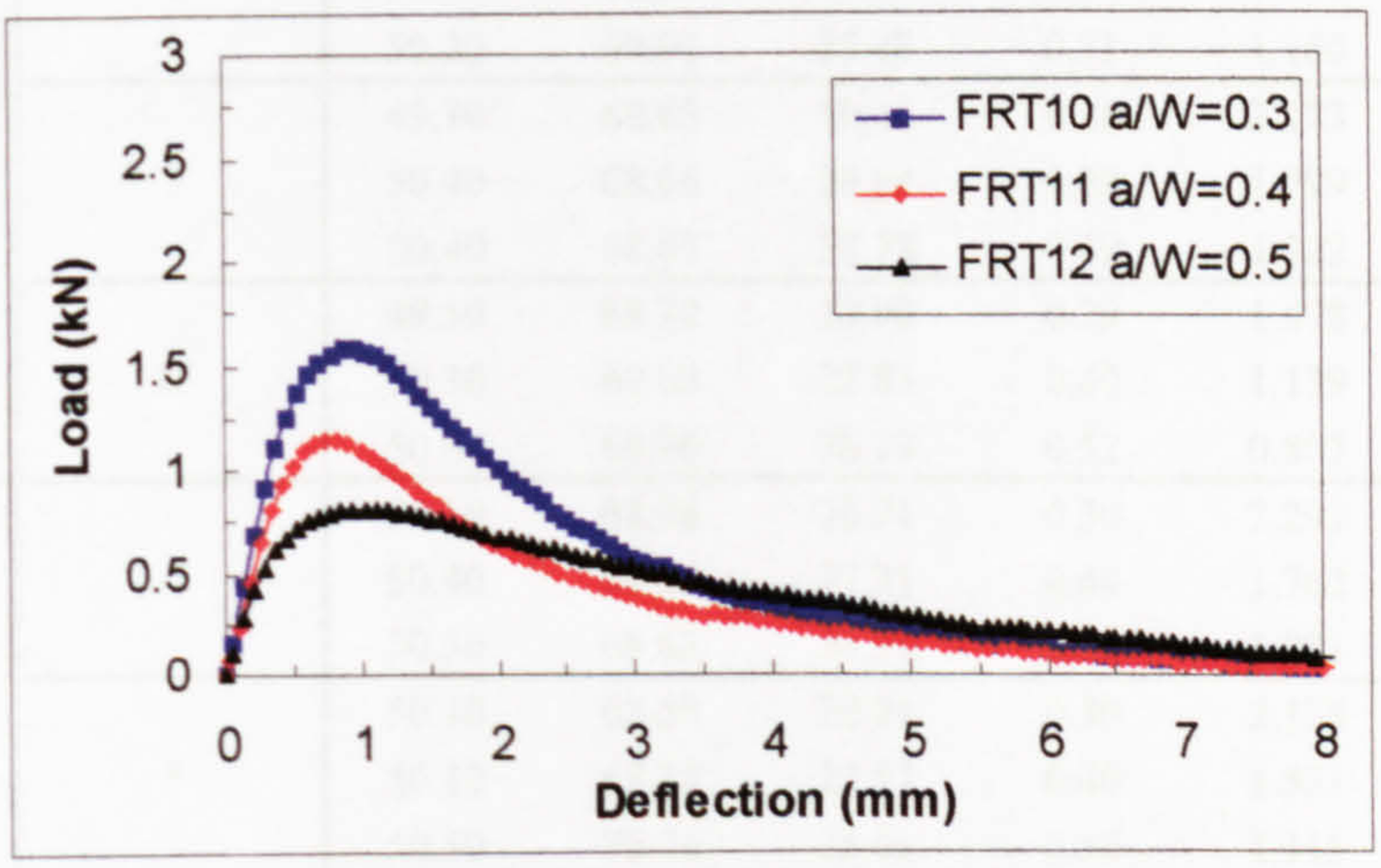

b) CRM mix1

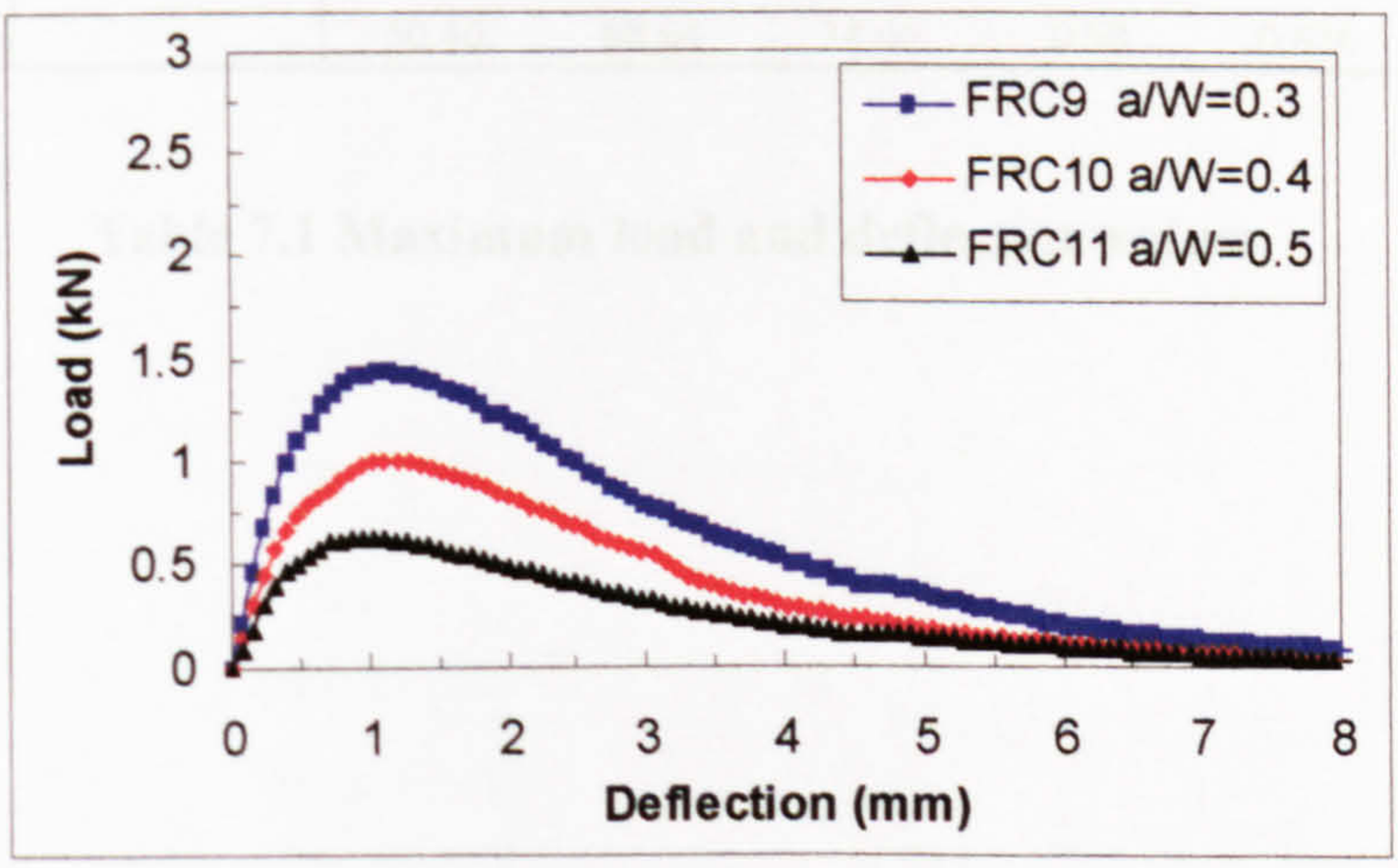

c) CRM mix2

Figure 7.13 Load-deflection curves at 15 ^{0}C

Mixture	Temperature (^{0}C)	B (mm)	W (mm)	a_0 (mm)	$\frac{a_0}{W}$	F_{max} (kN)	δ_{max} (mm)
Control mix	-5	50.20	68.17	20.39	0.30	2.230	0.40
		50.30	68.72	27.24	0.40	1.657	0.35
		50.10	70.31	35.04	0.50	1.185	0.32
	5	50.30	69.63	21.31	0.31	1.955	0.60
		49.60	68.86	29.02	0.42	1.368	0.42
		49.90	69.43	35.94	0.52	0.937	0.59
	15	50.00	68.73	20.16	0.29	1.282	1.57
		49.60	68.29	28.04	0.41	0.786	1.51
		50.10	70.28	35.14	0.50	0.601	1.30
CRM mix1	-5	50.10	68.11	20.04	0.29	2.584	0.44
		50.70	68.97	27.96	0.41	1.908	0.37
		50.30	69.91	35.48	0.51	1.160	0.28
	5	49.70	68.85	19.44	0.28	2.173	0.57
		50.40	68.66	26.94	0.39	1.799	0.59
		50.40	68.67	33.78	0.49	1.222	0.50
	15	49.50	68.22	19.90	0.29	1.578	0.95
		50.30	69.03	27.83	0.40	1.139	0.83
		50.00	69.90	36.13	0.52	0.807	0.94
CRM mix2	-5	50.10	68.98	20.91	0.30	2.291	0.35
		50.40	68.25	27.31	0.40	1.762	0.38
		50.50	68.63	34.31	0.50	1.081	0.26
	5	50.10	68.59	20.31	0.30	2.138	0.74
		50.10	68.38	27.57	0.40	1.551	0.69
		50.50	70.29	35.01	0.50	1.115	0.59
	15	50.60	68.57	21.16	0.31	1.434	1.14
		50.10	68.93	28.30	0.41	0.998	1.21
		50.40	68.64	34.40	0.50	0.626	0.95

Table 7.1 Maximum load and deflection values

7.4.2 Linear elastic analysis: Plain-strain fracture toughness

Plane stress fracture toughness, K_{IC}, is a measured of a material's resistance to crack extension when the stress state near the crack tip is predominantly plane strain, plastic deformation is limited, and opening mode monotonic loading is applied.

Plain-strain fracture toughness values have been calculated from load versus displacement curves obtained from three-point bending tests as showed previously. Because no standard exists for bituminous materials, the metallic materials standard BS 7448-1:1991 (BSI, 1991) has been used as a guide.

The stress intensity factor for a notched beam specimen based on The Boundary Collocation Method (Murakami, 1987) is given by the following equation:

$$K = \frac{FS}{BW^{\frac{3}{2}}} \times f\left(\frac{a_0}{W}\right) \tag{7.17}$$

where:

$$f\left(\frac{a_0}{W}\right) = \frac{3\left(\frac{a_0}{W}\right)^{\frac{1}{2}}\left[1.99 - \left(\frac{a_0}{W}\right)\left(1 - \frac{a_0}{W}\right)\left(2.15 - \frac{3.93a_0}{W} + \frac{2.7{a_0}^2}{W^2}\right)\right]}{2\left(1 + \frac{2a_0}{W}\right)\left(1 - \frac{a_0}{W}\right)^{\frac{3}{2}}} \tag{7.18}$$

and

K	=	stress intensity factor	[Nmm$^{-3/2}$]
F	=	load	[N]
S	=	beam span	[mm]
B	=	beam width	[mm]
W	=	beam depth	[mm]
a_0	=	crack length	[mm]

To calculate the value of the plane strain fracture toughness, K_{IC}, the following approximation has been used,

$$K_{IC} = K_{max} = \frac{F_{max} S}{B W^{\frac{3}{2}}} \times f\left(\frac{a_0}{W}\right) \tag{7.19}$$

where F_{max} is the maximum load sustained by the specimen.

This approximation is valid when the response of the material is linear up to nearly the peak load and the non-linear region before the attainment of the peak is limited.

Equation 7.19 was used to calculate K_{max} for each individual fracture specimen. K_{max} values for each mixture at various temperatures were obtained by averaging the results corresponding to different notch-to-depth ratios. These results are presented in **Table 7.2.**

Flexural strength has also been calculated using Equation 7.2 for three-point bending tests based on elastic solutions for the deflection of a beam with a centre crack. In this equation, the value of the specimen depth, W, is substituted by the effective specimen depth for a notched specimen given by (W-a_0), where a_0 is the notch depth (Kim and El. Hussein, 1997). Flexural strength results for the materials investigated are also presented in **Table 7.2.**

Mixture	Temp. (^{0}C)	$\frac{a_0}{W}$	$f\left(\frac{a_0}{W}\right)$	K_{max} (Nmm$^{-3/2}$)	Mean (Nmm$^{-3/2}$)	Std.Dev (Nmm$^{-3/2}$)	σ_f (MPa)	Mean (MPa)	Std.Dev (MPa)
Control mix	-5	0.30	1.518	33.54	31.69	1.90	8.17	8.07	0.09
		0.40	1.962	31.77			8.04		
		0.50	2.649	29.75			7.99		
	5	0.31	1.545	28.93	27.66	1.79	6.99	7.11	0.17
		0.42	2.104	28.44			7.30		
		0.52	2.818	25.61			7.03		
	15	0.29	1.495	18.84	16.69	1.91	4.56	4.25	0.27
		0.41	2.041	16.05			4.11		
		0.50	2.663	15.18			4.08		
CRM mix1	-5	0.29	1.499	38.51	35.22	4.47	9.37	8.98	0.70
		0.41	2.012	37.01			9.40		
		0.51	2.727	30.13			8.17		
	5	0.28	1.454	31.16	32.07	1.75	7.52	8.17	0.57
		0.39	1.941	34.09			8.61		
		0.49	2.596	30.96			8.37		
	15	0.29	1.489	23.59	22.48	0.98	5.73	5.76	0.17
		0.40	1.999	22.10			5.60		
		0.52	2.811	21.74			5.94		
CRM mix2	-5	0.30	1.533	34.27	32.25	3.63	8.31	8.23	0.57
		0.40	1.983	34.42			8.76		
		0.50	2.662	28.06			7.63		
	5	0.30	1.506	31.68	30.03	2.03	7.68	7.64	0.18
		0.40	1.999	30.65			7.80		
		0.50	2.646	27.76			7.45		
	15	0.31	1.555	21.73	19.32	2.74	5.30	4.94	0.44
		0.41	2.041	19.89			5.07		
		0.50	2.672	16.34			4.45		

Table 7.2 Fracture toughness and flexural strength results

7.4.2.1 Discussion of results

Analysis of the load-deflection curves showed that at -5 ^{0}C the materials' response during loading was linear-elastic until the maximum load was reached (within the resolution of the apparatus). Thus, linear-elastic approach was applicable and the value, K_{max}, obtained corresponded to the fracture toughness of the material, K_{IC}.

At this temperature, -5 ^{0}C, linear-elastic behaviour has been observed on the three materials investigated. Furthermore, fracture toughness values for the crumb-rubber modified mixtures were higher than that of the conventional mix and, fracture toughness for the mix modified with truck-tyre (CRM mix 1) rubber was higher than that of the mix modified with car-tyre rubber (CRM mix 2).

As the temperature increases, a plastic zone develops just ahead of the crack tip as seen by the non-linear behaviour of the load-deflection curves at 5 ^{0}C just before the peak load is reached. This non-linear region is more prominent for the conventional mix (Control mix) and the mix modified with car-tyre rubber (CRM mix 2) than for the mix modified with truck-tyre rubber (CRM mix 1), as seen in **Figure 7.12**. However, the size of the plastic zone, which is related to non-linearity, is still very small and the linear-elastic fracture mechanics approach is still applicable. Thus, the stress intensity factor corresponding to the maximum load sustained by the specimens, K_{max}, is a good approximation of the fracture toughness of the material at this temperature.

Fracture toughness values at 5 ^{0}C corresponding to the crumb-rubber mixtures were, again, higher than the one corresponding to the conventional mix. Also, fracture toughness for the mix modified with truck-tyre rubber was higher than that of the mix modified with car-tyre rubber.

As the temperature increases further, the materials' response is no longer linear as observed on the load-deflection curves at 15 ^{0}C. The size of the plastic zone surrounding the crack tip becomes larger and linear-elastic theory is no longer

applicable. As a result, K_{max} values at 15 ^{0}C cannot be considered as the fracture toughness values.

However, for comparison purposes, K_{max} values at 15 ^{0}C have been calculated and showed that, as for the data at –5 and 5 ^{0}C, K_{max} values for the rubber modified mixtures were higher than that for the conventional mix and, K_{max} for the mix modified with truck-tyre rubber was higher than that of the mix modified with car-tyre rubber.

K_{max} values corresponding to the three materials investigated at three different temperatures, -5, 5 and 15 ^{0}C are illustrated in **Figure 7.14.** It can be seen that, firstly, K_{max} decreases with increasing temperature and, secondly, K_{max} values for the crumb-rubber mixtures are higher than for the conventional one. Furthermore, K_{max} values for the mixture modified with truck-tyre rubber are higher than that modified with car-tyre rubber.

Flexural strength, σ_f, for three-point bending tests has also been calculated. **Figure 7.15** illustrates the flexural strength values for the mixtures studied. It can be seen that flexural strength decreases with increasing temperature. Furthermore, the crumb-rubber mixtures had higher σ_f than the conventional mix, and the mixture modified with truck-tyre rubber showed the highest σ_f.

Comparison of **Figures 7.14** and **7.15** shows the same changing pattern of fracture toughness, K_{max}, and flexural strength, σ_f, with temperature. Correlation of the two properties has been carried out by regression analysis, as shown in **Figure 7.16**. Good linear relations were found for all mixtures. Furthermore, the regression lines for the three mixtures practically coincide. Even though the magnitude of defectiveness is a factor affecting K_{max}, increasing flexural strength resulted in an increased K_{max} for all mixtures.

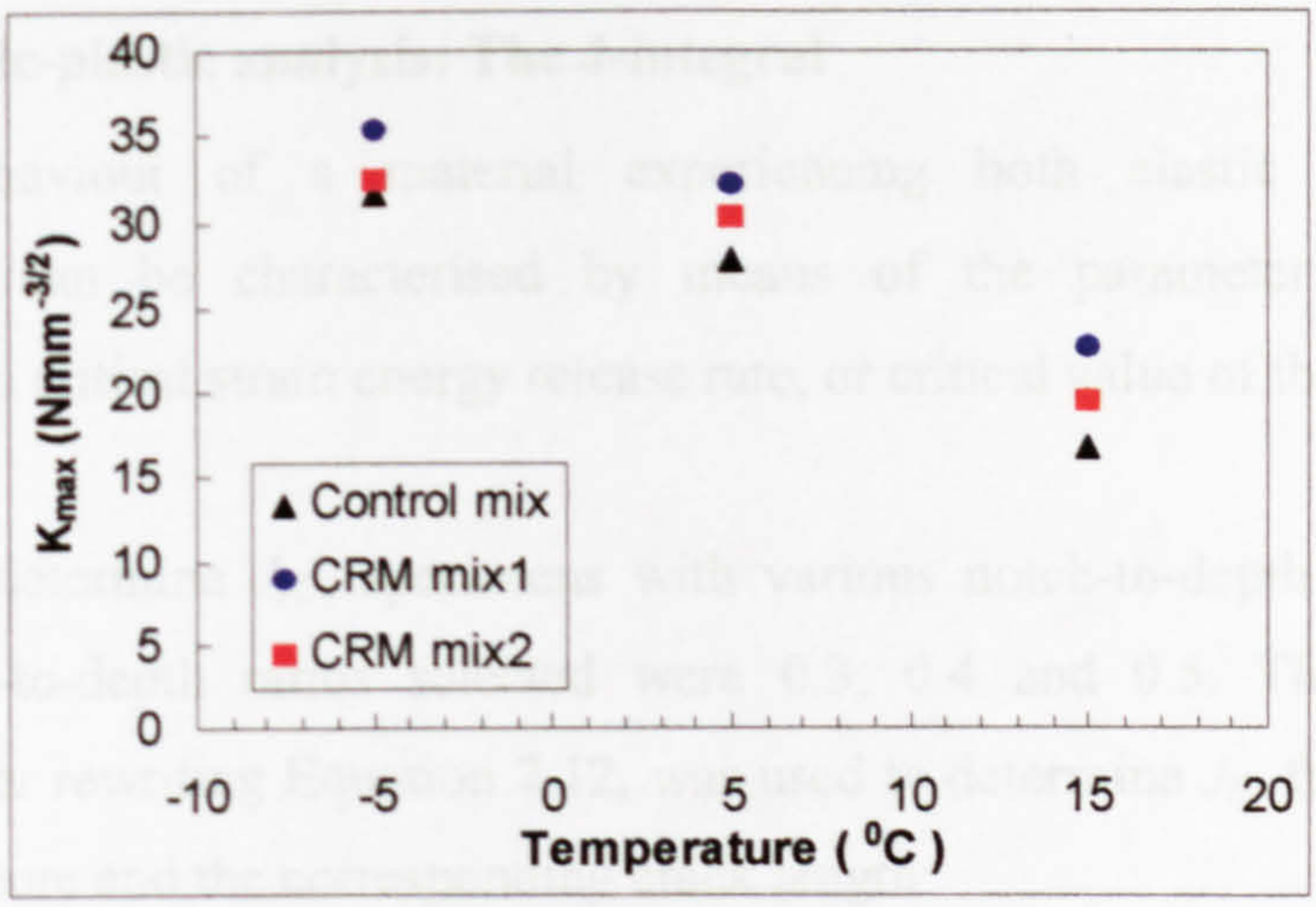

Figure 7.14 Change in fracture toughness with temperature

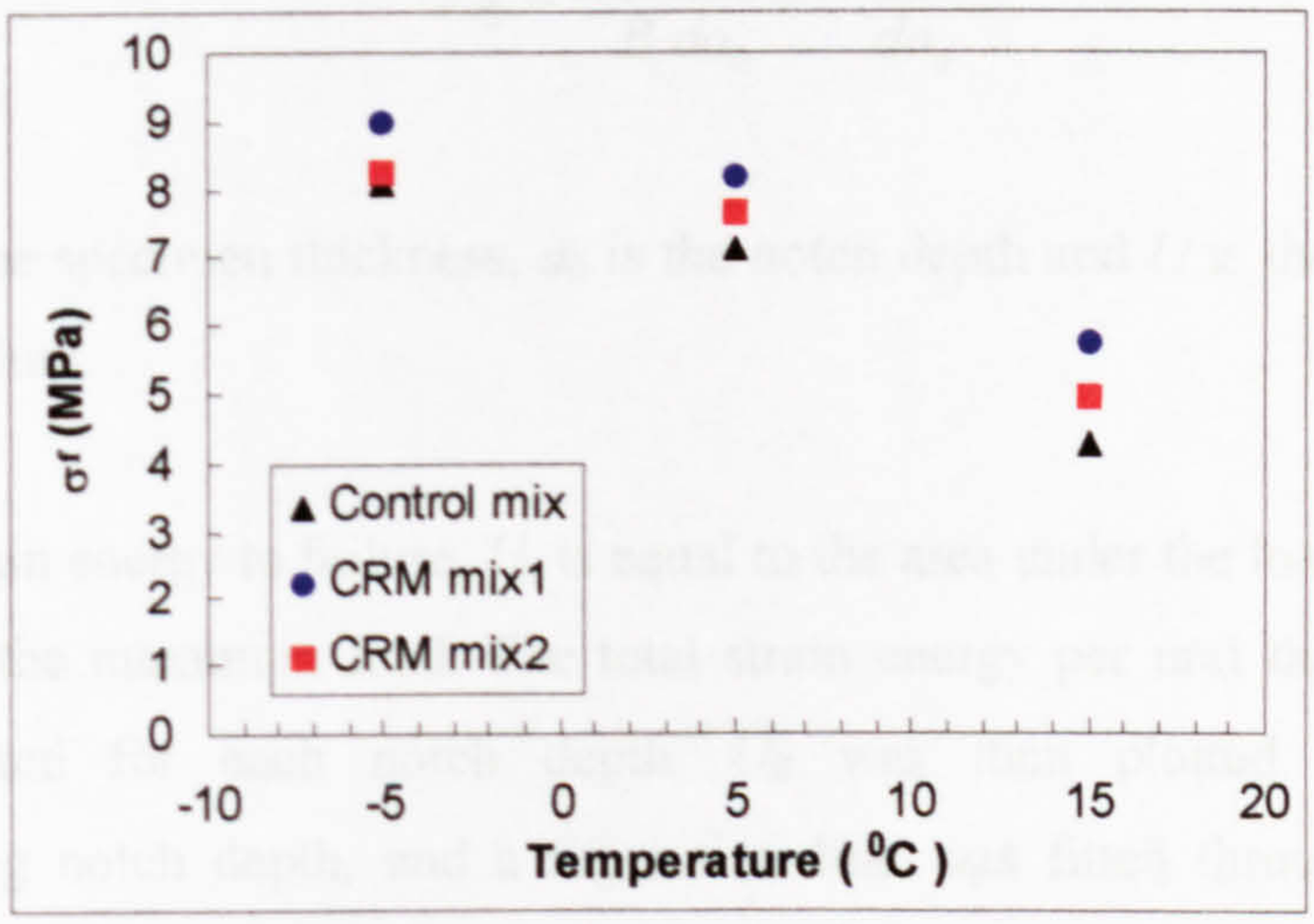

Figure 7.15 Change in flexural strength with temperature

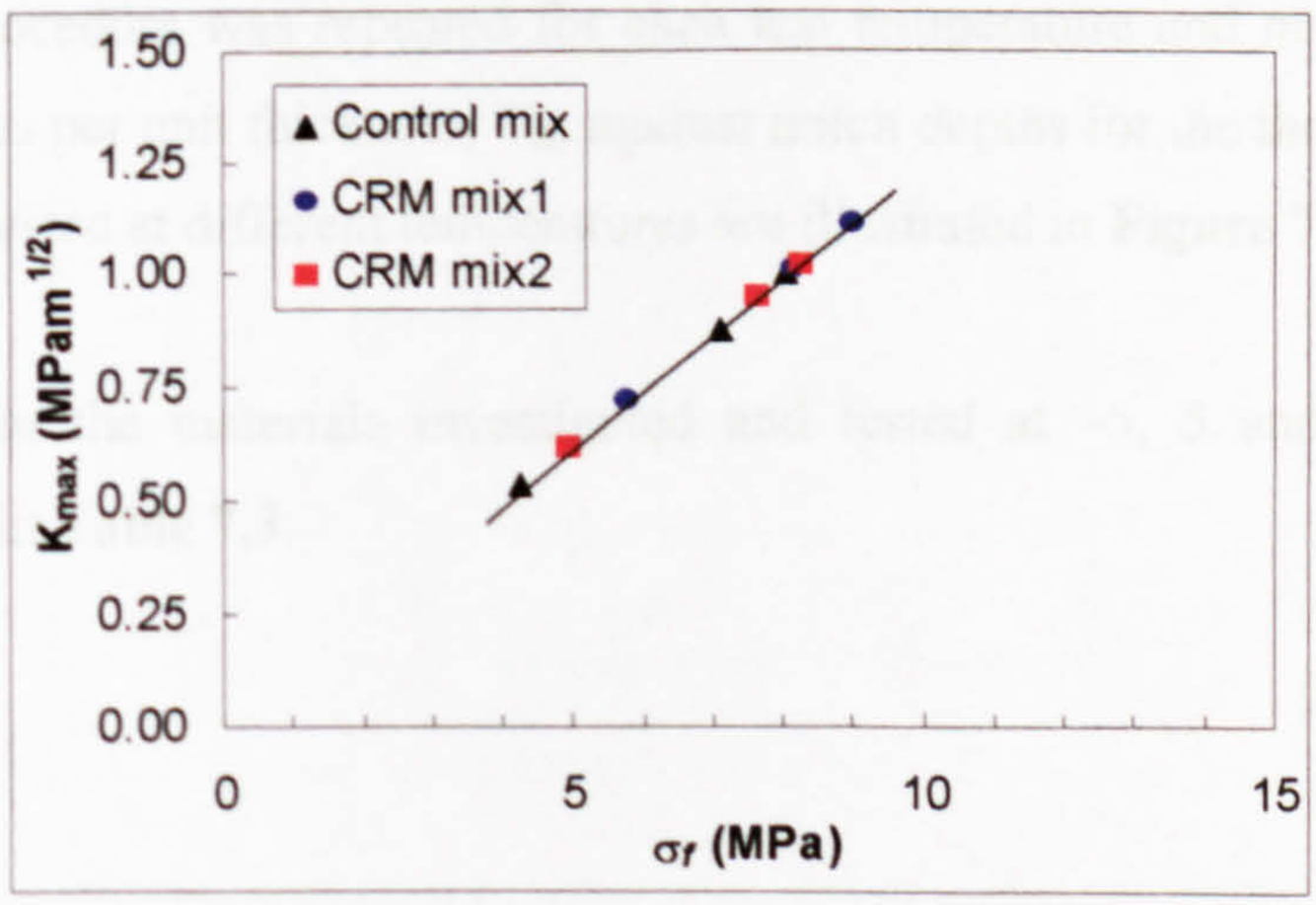

Figure 7.16 Relation of flexural strength with fracture toughness

7.4.3 Elastic-plastic analysis: The J-integral

Fracture behaviour of a material experiencing both elastic and plastic deformation can be characterised by means of the parameter J_{IC}, which represents the critical strain energy release rate, or critical value of the J integral.

In order to determine J_{IC}, specimens with various notch-to-depth ratios were used. Notch-to-depth ratios selected were 0.3, 0.4 and 0.5. The following equation, after rewriting Equation 7.12, was used to determine J_{IC} from the total energy to failure and the corresponding crack length:

$$J_{IC} = -\frac{1}{B}\frac{dU}{da_0} = -\frac{dU_B}{da_0} \tag{7.20}$$

where B is the specimen thickness, a_0 is the notch depth and U is the total strain energy to failure.

The total strain energy to failure, U, is equal to the area under the load-deflection curve up to the maximum load. The total strain energy per unit thickness, U_B, was calculated for each notch depth. U_B was then plotted against the corresponding notch depth, and a regression line was fitted through the data points. The slope of this line represented the critical J integral, J_{IC}.

The same procedure was repeated for each test temperature and mixture. Total strain energies per unit thickness, U_B, against notch depths for the three materials studied and tested at different temperatures are illustrated in **Figure 7.17**.

J_{IC} results for the materials investigated and tested at –5, 5 and 15 ^{0}C are summarised in **Table 7.3**.

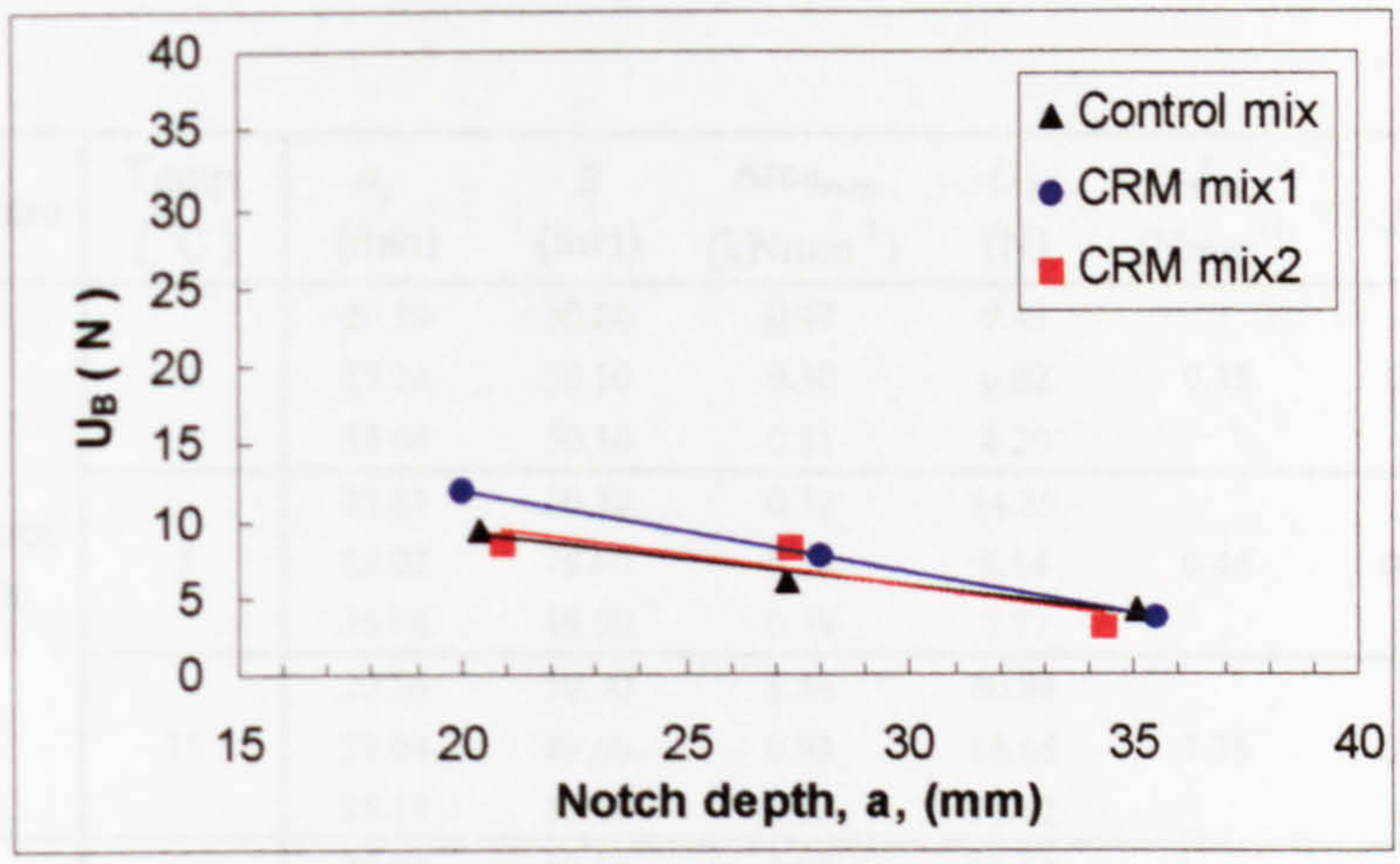

a) Tested at –5 ^{0}C

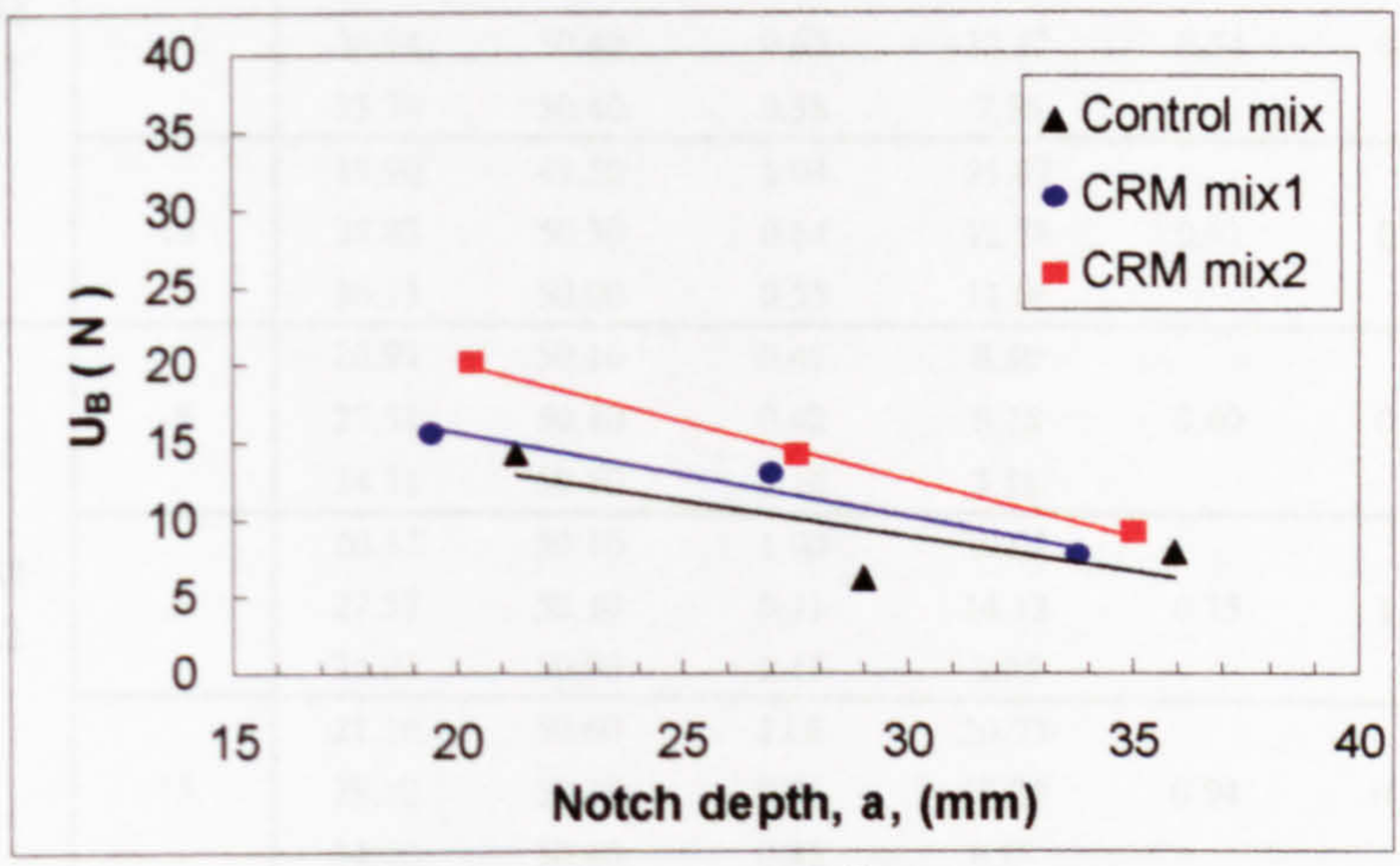

b) Tested at 5 ^{0}C

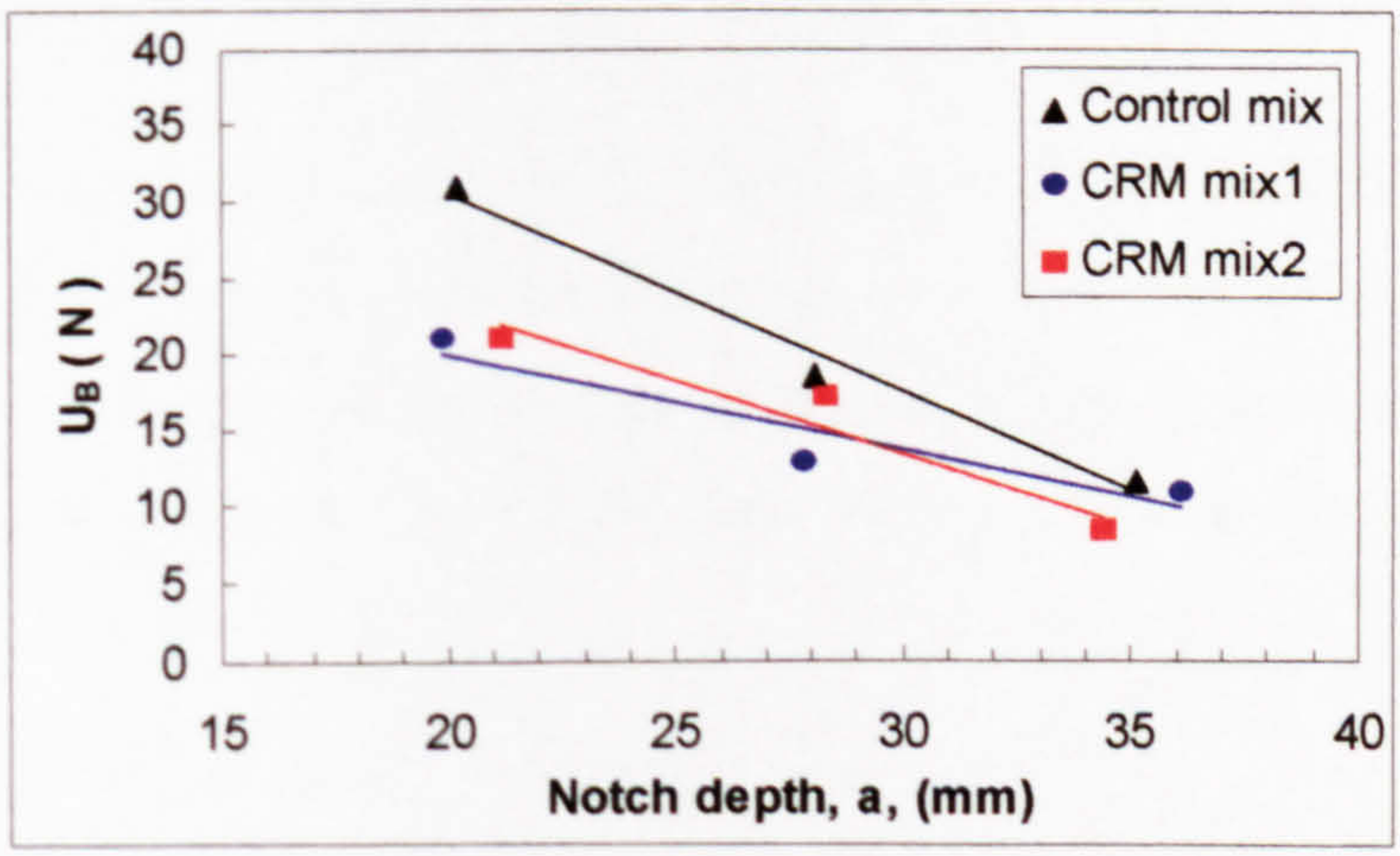

c) Tested at 15 ^{0}C

Figure 7.17 Fracture energy per unit thickness as a function of notch depth

Mixture	Temp. (^{0}C)	a_0 (mm)	B (mm)	Area$_{max}$ (kNmm^{-1})	U_B (N)	J_{IC} (Nmm^{-1})	R^2
Control mix	-5	20.39	50.20	0.47	9.41	0.35	0.96
		27.24	50.30	0.30	6.02		
		35.04	50.10	0.21	4.20		
	5	21.31	50.30	0.72	14.39	0.46	0.61
		29.02	49.60	0.30	6.14		
		35.94	49.90	0.39	7.77		
	15	20.16	50.00	1.54	30.84	1.28	0.98
		28.04	49.60	0.93	18.65		
		35.14	50.10	0.58	11.62		
CRM mix1	-5	20.04	50.10	0.60	11.97	0.53	1.00
		27.96	50.70	0.40	7.86		
		35.48	50.30	0.19	3.79		
	5	19.44	49.70	0.76	15.37	0.54	0.95
		26.94	50.40	0.65	12.82		
		33.78	50.40	0.38	7.56		
	15	19.90	49.50	1.04	21.07	0.61	0.87
		27.83	50.30	0.64	12.78		
		36.13	50.00	0.55	11.06		
CRM mix2	-5	20.91	50.10	0.43	8.50	0.40	0.80
		27.31	50.40	0.42	8.28		
		34.31	50.50	0.16	3.16		
	5	20.31	50.10	1.00	20.02	0.75	1.00
		27.57	50.10	0.71	14.12		
		35.01	50.50	0.45	8.95		
	15	21.16	50.60	1.06	20.93	0.94	0.92
		28.30	50.10	0.86	17.25		
		34.40	50.40	0.42	8.23		

Table 7.3 J_{IC} results

7.4.3.1 Discussion of results

Critical values of the *J* integral have been calculated from the slopes of the total strain energy to failure as a function of notch depth. As can be seen from the linear regression coefficients in **Table 7.3**, the relation between these two parameters is practically linear for all three mixtures studied and tested at different temperatures.

Critical *J* integral values for the three materials investigated showed that at the lowest temperature, -5 ^{0}C, the fracture resistance of the rubber-modified mixtures was better than that of the conventional mix (Control mix). Also, the mix modified with truck-tyre rubber (CRM mix1) showed better fracture resistance than the one modified with car-tyre rubber (CRM mix2).

At 5 ^{0}C, the rubber-modified mixtures had again better fracture resistance than the conventional mix. However, at this temperature, the fracture resistance of the mix modified with car-tyre rubber exceeded that of the mix modified with truck-tyre rubber.

As the temperature increases up to 15 ^{0}C, the crumb rubber modified mixtures showed lower fracture resistance than the conventional mix, and the lowest J_{IC} value corresponded to the mix modified with truck-tyre rubber.

Critical *J* integral values, J_{IC}, for the three materials investigated have been plotted as a function of temperature, and a regression line of the form $J_{IC} = Ae^{BT}$ has been fitted through the data points, as seen in **Figure 7.18.** Values of *A*, *B* and regression coefficients R^2 for the three materials studied are presented in **Table 7.4.**

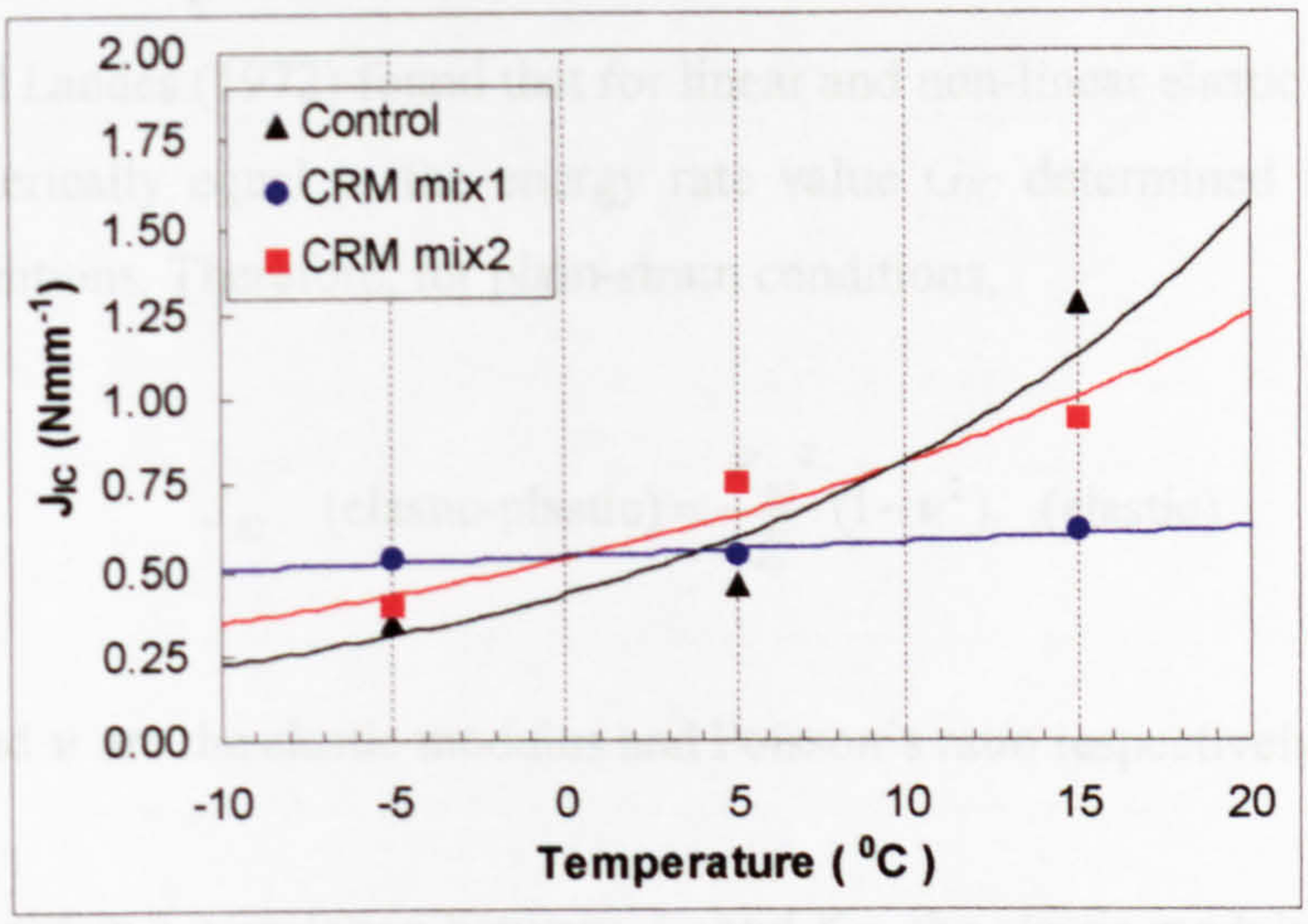

Figure 7.18 Experimental J_{IC} values as a function of temperature

Mixture	A	B	R^2
Control mix	0.43	0.06	0.90
CRM mix1	0.54	0.01	0.85
CRM mix2	0.53	0.04	0.93

Table 7.4 J_{IC} regression coefficients

Figure 7.18 shows the change in fracture resistance, represented by J_{IC}, with changing temperature. It can be seen that the fracture resistance for the conventional mix is more sensitive to temperature changes, as seen by the higher value of the regression parameter B (B=0.06), in comparison to the mix modified with car-tyre rubber (B=0.04) and with truck-tyre rubber (B=0.01).

The above curves also give an indication of the transition temperatures from elastic to plastic behaviour. This transition will occur at higher temperatures for the modified mixtures compared to the conventional mix. This phenomenon can also be observed on the load-deflection curves presented in **Figures 7.11 - 13**.

7.4.4 Relationship between K_{IC} and J_{IC}

Begley and Landes (1972) found that for linear and non-linear elastic conditions, J_{IC} is numerically equal to the energy rate value G_{IC} determined from linear elastic conditions. Therefore, for plain-strain conditions,

$$J_{IC} \quad \text{(elastic-plastic)} = \frac{K_{IC}^{\,2}}{E}(1-\nu^2) \quad \text{(elastic)} \tag{7.21}$$

where E and ν are the elastic modulus and Poisson's ratio respectively.

In order to obtain a correlation between J_{IC} and K_{IC}, the elastic modulus had to be determined. Merkle et al. (1975) proposed the following expression based on elastic solutions for the deflection of a beam with a centre crack,

$$E = \frac{PS^2}{\delta B(W-a)^2} \tag{7.22}$$

where:

E	=	elastic modulus
P	=	load
S	=	beam span
δ	=	beam deflection
B	=	beam width
W	=	beam depth
a	=	crack depth

Elastic modulus for each individual fracture specimen obtained using Equation 7.22, and average values at each temperature are presented in **Table 7.5**. Poisson's ratio was assumed to be 0.35 for the three mixtures studied. J_{IC} values calculated from Equation 7.21, J_{IC} (th), are also presented in this table in conjunction with the experimental values obtained previously, J_{IC} (exp).

Mixture	Temp. (^{0}C)	$\frac{a_0}{W}$	E (MPa)	Mean (MPa)	Std.Dev (MPa)	J_{IC} (th) (Nmm^{-1})	J_{IC} (exp) (Nmm^{-1})
Control mix	-5	0.30	3813.86	4253.65	423.35	0.21	0.35
		0.40	4288.69				
		0.50	4658.39				
	5	0.31	2175.15	2547.83	603.10	0.26	0.46
		0.42	3243.64				
		0.52	2224.71				
	15	0.29	542.75	545.50	39.08	0.45	1.28
		0.41	507.86				
		0.50	585.88				
CRM mix1	-5	0.29	3977.13	4721.91	735.23	0.23	0.53
		0.41	4741.38				
		0.51	5447.21				
	5	0.28	2463.29	2770.48	332.24	0.33	0.54
		0.39	2725.06				
		0.49	3123.09				
	15	0.29	1126.78	1189.09	67.07	0.37	0.61
		0.40	1260.08				
		0.52	1180.40				
CRM mix2	-5	0.30	4432.89	4738.77	645.20	0.19	0.40
		0.40	4303.40				
		0.50	5480.02				
	5	0.30	1939.63	2136.29	209.82	0.37	0.75
		0.40	2112.07				
		0.50	2357.17				
	15	0.31	867.10	841.09	51.42	0.39	0.94
		0.41	781.86				
		0.50	874.32				

Table 7.5 Experimental and theoretical J_{IC} values

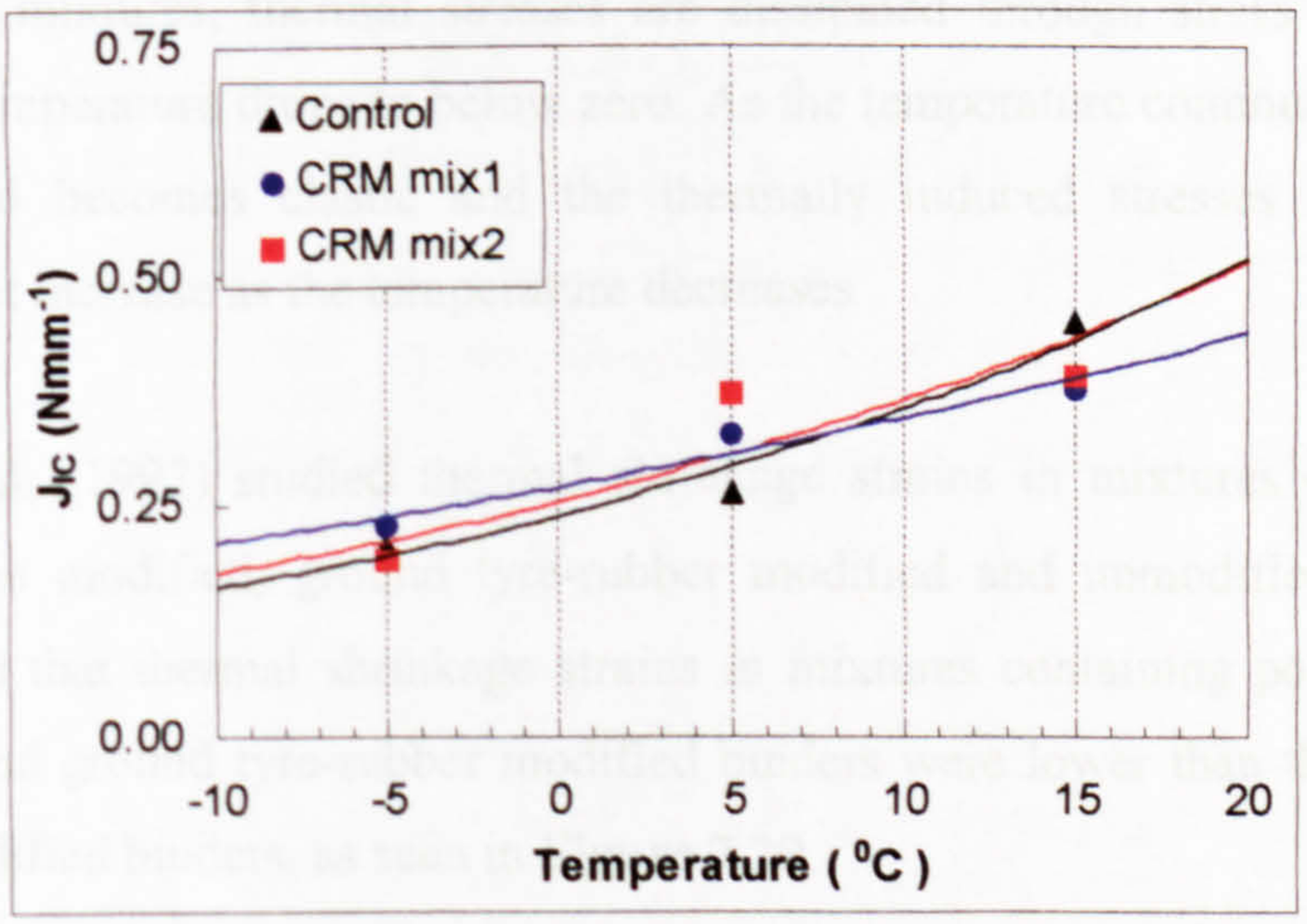

Figure 7.19 Theoretical J_{IC} values as a function of temperature

Theoretical J_{IC} values have been plotted as a function of temperature, as seen in **Figure 7.19**. Similar behaviour as for the experimental J_{IC} values has been observed. However, it has been found that theoretical J_{IC} values are about half the experimental ones. Two factors might be responsible for these differences. Firstly, fracture toughness values, K_{IC}, in Equation 7.21 were approximated by K_{max} values, which are a good approximation of K_{IC} at very low temperatures, when the behaviour of the material is practically linear. As the temperature increases, however, the material's behaviour is no longer linear and K_{max} does not represent the fracture toughness since the K_{IC} parameter is defined only for linear elastic conditions. Secondly, the other parameter affecting Equation 7.21, the elastic modulus, has been again calculated assuming elastic conditions, which is not always the case as seen previously.

The differences between the theoretical and experimental J_{IC} values indicate that plastic deformations processes affecting fracture of bituminous materials are significant enough to question the validity of linear elastic fracture parameters when applied to asphalt mixtures.

7.4.5 Effect of crumb rubber on low temperature cracking

Low-temperature cracking of pavement materials is attributed to thermally induced tensile stresses that develop in the material as the temperature drops. For bituminous mixtures, thermal stresses are dissipated through stress relaxation when the temperature drops to below zero. As the temperature continues to drop, the material becomes elastic and the thermally induced stresses no longer dissipate but increase as the temperature decreases.

Joseph et al. (1992) studied thermal shrinkage strains in mixtures containing polyethylene modified, ground tyre-rubber modified and unmodified binders. They found that thermal shrinkage strains in mixtures containing polyethylene modified and ground tyre-rubber modified binders were lower than those made with unmodified binders, as seen in **Figure 7.20**.

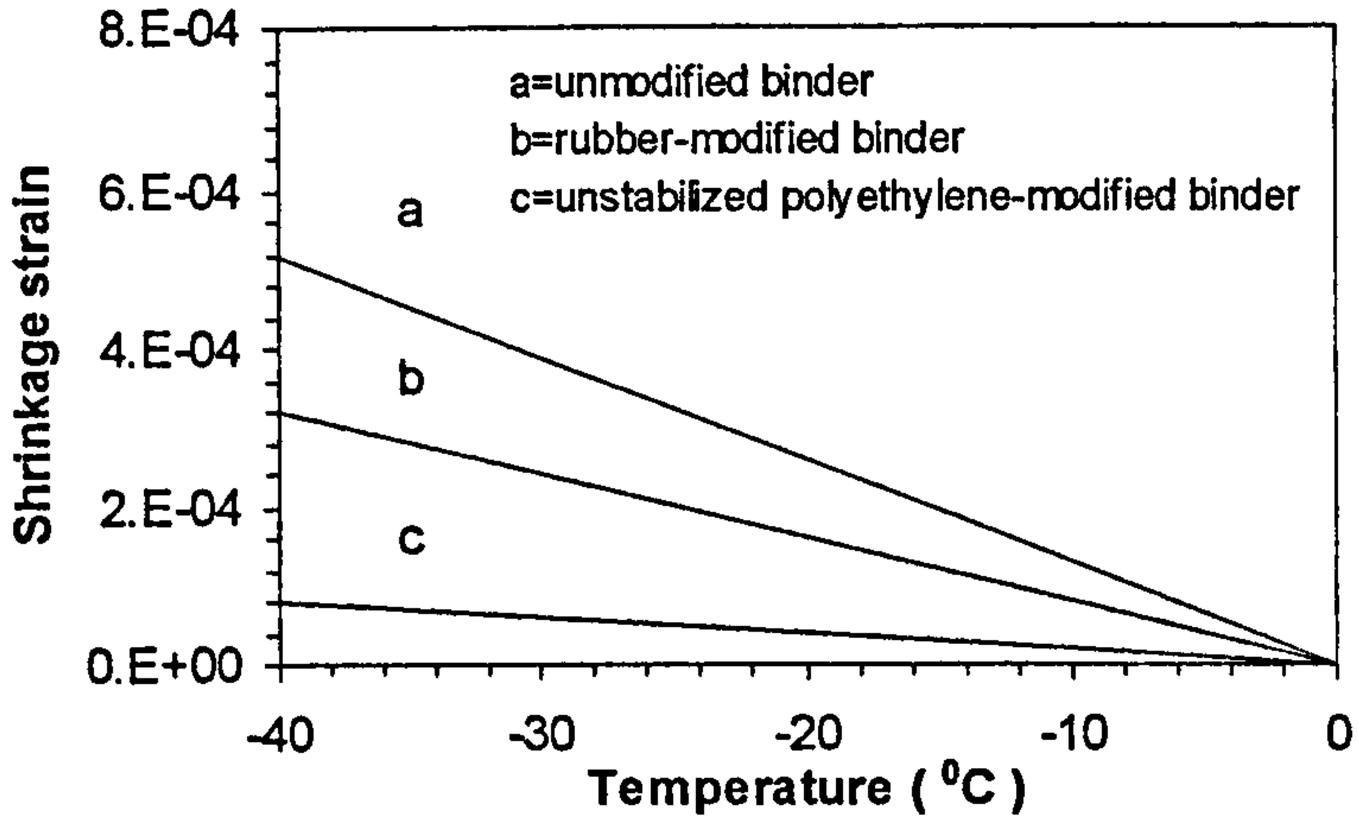

Figure 7.20 Unrestrained shrinkage strain in various asphalt-aggregate mixes (after Joseph et al., 1992)

Using the Thermal Stress Restrained Specimen Test (TSRST), Jung and Vinson (1993) showed that the low-temperature performance of the mix is influenced by the thermal and mechanical properties of the binder. When performed with polymer-modified binders, these tests confirmed that the addition of polymers often improves the low temperature performance of given bitumen.

Data presented in section 7.4.2 showed that when linear elastic fracture mechanics was applicable (approximately at temperatures equal or below 5 ^{0}C), fracture toughness of the two crumb-rubber modified mixtures was superior to that of the conventional mix. Also, the mixture modified with truck-tyre rubber showed higher fracture toughness than the one modified with car-tyre rubber. Moreover, the critical J integral, J_{IC}, of the crumb-rubber modified mixtures was also higher than that of the conventional mix at temperatures equal and below 5 ^{0}C. However, at temperatures above 5 ^{0}C, the conventional mix showed better resistance to fracture (see section 7.4.3).

It can, thus, be concluded that low temperature fracture resistance of the two crumb-rubber modified mixtures exceeds that of the unmodified one, and at temperatures below freezing the mixture modified with truck-tyre rubber presents the best fracture resistance.

Factors affecting low temperature cracking of pavement materials may be divided into material, environmental and pavement structure geometry factors. Materials' factors include bituminous binder properties, aggregate type and gradation, binder content and air void content.

For the three materials investigated, the same aggregate type and gradation have been used. Binder contents selected were 4.8 and 5.8 %, and air voids were about 5.5 and 3.5 % for the conventional and the crumb-rubber mixtures respectively. Binder content does not have a significant influence on low temperature properties of the mixture. Since the thermal crack propagates through the binder matrix, no big difference on the thermal cracking resistance should appear when considering varying binder contents (Vinson et al., 1989).

The single most important factor affecting low temperature performance of pavement mixtures is the viscoelastic behaviour of the bituminous binder, in particular the temperature-stiffness relationship, or temperature susceptibility. Thus, the improved fracture resistance observed on the crumb-rubber mixtures studied must be attributed to the enhanced properties of the crumb-rubber modified binders at low temperatures.

Hui et al. (1994) investigated low-temperature fracture toughness of rubber modified asphalt binders in notched, three-point bending beam fracture tests at – 20 ^{0}C. They found an increase in toughness for binder modification with 4 to 10 wt percent 30-, 40- and 80-mesh rubber particles.

In a similar way, Anderson et al. (2001) found a significant improvement in low-temperature fracture, as measured by K_{IC}, when elastomers were added to a base binder. They also found that the ranking afforded by fracture toughness was different from the ranking afforded by the properties determined from either the Bending Beam Rheometer (BBR) or the Direct Tension Test (DTT). Further, the ranking according to the K_{IC} values agreed with field experience wherein elastomers typically enhance resistance to low temperature cracking.

Chapter 8

CONCLUSIONS AND RECOMMENDATIONS

Chapter 8

CONCLUSIONS AND RECOMMENDATIONS

8.1 CONCLUSIONS

This thesis presents a comprehensive study of the effects of Crumb Rubber Modifier (CRM) from used tyres on the viscoelastic properties of bituminous binders. Moreover, performance-related properties associated with asphalt mixtures containing these rubber-modified binders are also presented and evaluated. This work was instigated by the lack of existing UK research in this area, the outcomes of which, could help alleviate the problem of used tyre disposal.

8.1.1 Structure and properties of CRM binders

From the surveyed literature, supported by the findings of this investigation, CRM binders are considered heterogeneous 2-phase systems of swollen rubber particles dispersed within a bitumen matrix. Absorption of bitumen components by the rubber depletes the bitumen of the absorbed components and modified the properties of both, the rubber and the bitumen phases.

From the results of swelling experiments, the following conclusions can be drawn:

- Aromatic solvents markedly swelled car- and truck-tyre rubbers but aliphatic solvents swelled truck-tyre rubber far more strongly than car-tyre rubber. It was concluded that the same pattern of solubility applied to absorption of bitumen components by the rubbers.

- Solubility parameters of both rubbers were estimated at 9.3 $(\text{cal cm}^{-3})^{1/2}$ where the rubbers swelled by 200 % by volume approximately.

- Truck-tyre rubber absorbed more bitumen than car-tyre rubber. For instance, for the 100 Pen KSR bitumen at 180 ^{0}C, equilibrium swelling mass % increase for truck- and car-tyre rubber was 120 and 75 %, respectively. This was attributed to the greater solubility of bitumens' aliphatic components in truck-tyre rubber as well as the higher polymer chain flexibility associated with natural rubber in truck-tyre rubber.

- Equilibrium swelling mass uptake depended on bitumen origin and grade, hence, on chemical composition. In general, bitumens with high asphaltene content were less prone to swell the rubbers.

- From the analysis of the sorption curves, the absorption of bitumen into rubber monoliths was consistent with simple Fickian diffusion for plane sheet geometry. This allowed a kinetic parameter, the diffusion coefficient (D), to be determined from the slopes of the linear regions in the early stages of swelling.

- The kinetics of swelling, as given by D, indicated a faster rate of bitumen absorption by truck-tyre rubber than by car-tyre rubber. Furthermore, D was very dependent on temperature, as the temperature increased D also increased, and to a lesser degree on bitumen chemical composition.

- Based on the assumption that CRM particles were spherical, it was found that, for the materials and conditions examined, the shortest equilibrium swelling time of 4.9 minutes corresponded to truck-tyre rubber particle of 300 μm nominal size at a temperature of 210 ^{0}C. The longest time of 101 minutes corresponded to car-tyre rubber particle of 600 μm nominal size at a temperature of 150 ^{0}C.

From dynamic and creep/creep recovery tests performed in the DSR, the following conclusions can be drawn:

- Interaction of CRM with bitumen stiffened the bitumen phase, i.e. increased the complex stiffness modulus (G^{*}) and lowered and phase angle (δ). Furthermore, truck-tyre rubber hardened the bitumen matrix appreciably more

than car-tyre rubber. This hardening effect, due to absorption of bitumen components by the rubbers, occurred during the early stages of interaction (within an hour), as confirmed from the diffusion studies.

- Changes in viscoelastic properties with blending (interaction) time due to interaction temperature were not straightforward as a number of processes occurred simultaneously, thereby, complicating the nature of the outcome.

- Creep and creep recovery tests showed that steady-state viscous flow for all the materials investigated was attained within the applied loading time of 600 seconds, with a 5 % tolerance.

- Creep recovery values indicated that conventional binders showed practically no recovery. CRM binders, however, showed between 4 and 16 % recovery depending on materials and production conditions.

- Binders modified with CRM from truck tyres exhibited more recovery than those modified with CRM from car tyres, when they were produced at 180 and 210 ^{0}C. Also, CRM binders based on the VEN bitumen showed the highest recovery.

- For one hour blending time, recovery increased when the interaction temperature was increased. For instance, for the 100 Pen VEN bitumen modified with 10 % CRM from truck tyres, recovery increased from 9 to 16 % when the interaction temperature was increased from 150 to 210 ^{0}C. The effect of interaction time on recovery is, however, dependent on interaction temperature.

- Master curves showed that, in the low frequency region (high temperatures), CRM modification increases the binder's overall resistance to deformation and improves elasticity, i.e. increases G^* and decreases δ. This effect increases with increase in CRM content. The level of this change in properties is larger with CRM from truck-tyre rubber.

- Master curves also indicated that, at high frequencies (low temperatures), CRM modification slightly reduced G^*. This would probably contribute to an increase in the binder flexibility at low temperatures. The effectiveness of CRM modification at low temperatures is, however, much less than at high temperatures.

Brookfield viscosities measurements of selected CRM binders have shown that:

- Increasing CRM content increased the viscosities of the binders. Binder viscosity was also affected by the origin of the bitumen, and the size and source of the CRM. However, the effect of these variables was not as significant as the CRM content.

- Viscosities representative of mixing conditions could only be achieved at temperatures of 160, 180 and in excess of 190 ^{0}C when the neat binders were modified with 5, 10 and 15 % CRM, respectively.

8.1.2 Design and assessment of CRM mixtures

Based on the mix design method adopted in this study, the following conclusions can be drawn:

- Differences were found between void measurements of dry and coated aggregates. For the selected aggregate blend (Blend 2), void content in dry aggregate was 19 %, whereas void content in coated aggregate was about 16-17 %. These differences were attributed to differences in the compaction method, boundary or container-wall effects and the lubricant effect of the bitumen.

- Binder modification by 10 % CRM by weight of bitumen has led to an increase in the optimum binder content from 4.8 % to 5.8 %. Furthermore, at these binder contents the unmodified mixture (Control mix) had 5.5 % voids, whereas the mixtures modified with CRM from truck (CRM mix 1) and from car tyres (CRM mix 2) had 3.5 % voids.

- CRM modification increased the stiffness of the mixtures. ITSM values at the optimum binder contents were 1400 and 1800 for the conventional and the rubber-modified mixtures, respectively. Higher ITSM values were attributed to higher binder stiffness as a result of CRM modification.

- For the materials investigated, CRM does not have an adverse effect on the sensitivity of the mixtures to moisture.

- Based on the RLA test results, permanent deformation for the CRM mixtures was slightly higher than that for the conventional mix, probably due to their higher design binder contents.

Based on the results of four-point bending fatigue testing, several conclusions can be drawn:

- CRM modification improved the fatigue lives of the mixtures. Furthermore, the mixture modified with CRM from truck-tyre rubber showed the longest life. For instance, for controlled strain mode, the strain values at 10^6 cycles (ε_6) were 134, 163 and 149 μm/m for the Control mix, CRM mix 1 and CRM mix 2, respectively.

- A power law relationship was found between the rate of fatigue damage and the initial strain and the applied stress, for strain and stress test modes.

- CRM modification reduced the rate of fatigue damage accumulation. The rates of damage for the CRM modified mixtures were lower than for the conventional one. Also, the mixture modified with CRM from truck-tyre rubber exhibited the lowest damage accumulation rate.

- Differences were found between the rate of damage for controlled strain and stress modes thus, the rate of damage for stress mode was higher than for strain mode. These differences were attributed to dissipated energy effects occurring in

both test modes. Furthermore, these differences were significantly larger for the CRM mixtures.

- Corrections to the damage rate were introduced to counteract the variability due to dissipated energy effects in the two test modes. A unique relationship was found between the corrected damage rate parameter and the initial strain for both, controlled strain and stress modes. Based on this parameter, CRM modification reduced the rate of damage due to fatigue

From the analysis of the fracture test results obtained from three-point bending beam tests on notched asphalt specimens the following conclusions can be drawn:

- CRM modification enhanced the mixtures' resistance to brittle fracture at low temperatures. Fracture toughness, K_{IC}, for the CRM modified mixtures was higher than that for the unmodified one and, the mixture modified with CRM from truck tyres exhibited the highest K_{IC}.

- For all mixtures investigated, K_{IC} decreased with increase in temperature from –5 to 5 ^{0}C. At temperatures above 5 ^{0}C, the K_{IC} criterion was not considered applicable, as the materials did not exhibit linear-elastic behaviour.

- Based on the analysis of load-deflection curves, the critical value of the *J*-integral, J_{IC}, was considered a more appropriate fracture characterization criterion for asphalt mixtures than the K_{IC} criterion.

- Based on the J_{IC} criterion, CRM improved the mixtures' fracture resistance at low temperatures. Also, at temperatures below freezing, the mixture modified with CRM from truck tyre exhibited the highest fracture resistance.

- The change in the mixtures' fracture resistance, J_{IC}, with temperature indicated the higher temperature susceptibility of the conventional mixture.

Furthermore, the mixture containing CRM from truck tyres was the least susceptible of all.

8.2 RECOMMENDATIONS FOR FURTHER WORK

Swelling experiments showed that, after prolonged time in bitumen at high temperatures, the rubber started to degrade. However, the extent and factors affecting rubber degradation could not be determined. Rheological properties were also used to monitor the interactions taking place between rubber and bitumen. The physical and chemical state of the rubber in the bitumen matrix has, however, not been fully characterised. Thus, further work is recommended on the physical and chemical processes that control the interaction between the two materials and on the degradation mechanisms of devulcanization and depolymerization of rubber particles in the bitumen medium.

In this study, it has been established that some CRM particles remained intact, though some degradation occurred, due to blending with bitumen at elevated temperatures. This could lead to separation of the two materials during binder storage, as the rubber tends to settle. It may be possible, however, to chemically degrade the crosslinked networks at the surface of the rubber prior to blending, which could improve the interaction between the rubber and the bitumen and between neighbouring rubber particles. This issue, therefore, should be addressed in any future research programme.

The durability of bituminous mixtures containing CRM is an important aspect that will require considerable attention. For these materials to be used in routine operations they would have to be resistant to changes due to long-term, in-service environmental ageing. Thus, short and long-term ageing simulation tests should be performed in order to assess the ageing susceptibility of the materials. In addition to this, long-term monitoring studies on field trials could provide a reliable basis upon which to assess ageing.

The selection of any pavement material should include an assessment of the possibility of recycling. For bituminous mixtures containing CRM binders to be

fully accepted, they should be capable of being recycled. If not, their benefit will be reduced and a new waste problem will be created. It is, therefore, necessary to investigate this issue through laboratory testing and full-scale road trials.

References

REFERENCES

Abdelrahman, M.A. and Carpenter, S.H., (1999). "Mechanism of interaction of asphalt cement with crumb rubber modifier," Transportation Research Record, TRB, National Research Council, Washington, D.C., pp.106 - 113.

Abdulshafi, A.A. and Majidzadeh, K., (1985). "J-Integral and cyclic plasticity approach to fatigue of asphaltic mixtures," Transportation Research Record 1034, TRB, National Research Council, Washington, D.C., pp.112 - 123.

Aglan, H. and Figueroa. L., (1993). "Damage-evolution approach to fatigue cracking in pavements," Journal of Engineering Mechanics, ASCE, Vol. 119. No. 6, pp. 1243 – 1259.

Anderson, D.A. and Kennedy, T.W., (1993). "Development of SHRP binder specification," Proc., Association of Asphalt Paving Technologists, Vol. 62, pp. 481 – 507.

Anderson, D.A., Christensen, D.W., Bahia, H.U., Dongre, R., Sharma, M.G., Antle, C.E. and Button, J., (1994). " Physical characterization. Binder characterization and evaluation," Strategic Highway Research Program, Report SHRP-A-369, Vol. 3, TRB, National Research Council, Washington, D.C.

Anderson, D.A., Lapalu, L., Maresteanu, M.O., Le Hir, Y.M., Planche, J.P. and Martin, D., (2001). "Low-temperature thermal cracking of asphalt binders as ranked by strength and fracture properties," Transportation Research Record 1766, TRB, National Research Council, Washington, D.C., pp.1 - 6.

Anon, (2000). "Road to the future," Mining, Quarry and Recycling, Vol. 29, No. 5.

Arand, W., (1987). "Influence of bitumen hardness on the fatigue behaviour of asphalt pavements of different thickness due to bearing capacity of subbase, traffic loading, and temperature," Proc., 6th International Conference on Structural Behaviour of Asphalt Pavements, Michigan, pp. 65 – 71.

ASTM, (1993a). "Standard test method for J_{IC}, a measure of fracture toughness," Test designation E813-89, Annual Book of ASTM Standards, Vol. 03.01, American Society of Testing and Materials, Philadelphia.

ASTM, (1993b). "Plane-Strain Fracture Toughness of Metallic Materials," Test designation E399-90, Annual Book of ASTM Standards, Vol. 03.01, American Society of Testing and Materials, Philadelphia.

Bahgat, A.G. and Herrin, M., (1968). "Brittle fracture of asphalt mixtures," Proc., Association of Asphalt Paving Technologists, Vol. 37, pp. 32 – 55.

Bahia, H.U. and Davies, R., (1994). "Effect of crumb rubber modifiers (CRM) on performance-related properties of asphalt binders," Proc., Association of Asphalt Paving Technologists, Vol. 63, pp. 414 - 449.

Bahia, H.U, Perdomo, D. and Turner, P., (1997). "Applicability of superpave binder testing protocols to modified binders," Transportation Research Record 1586, TRB, National Research Council, Washington, D.C., pp. 16 – 23.

Baker, R.F. and Connolly, E., (1995). "Mix designs and air quality emissions tests of crumb rubber modified asphalt concrete," Transportation Research Record 1515, TRB, National Research Council, Washington, D.C., pp. 18 – 27.

Barnes, H.A., Hutton, J.F. and Walters, K., (1989). "An introduction to rheology," Rheology Series 3, Elsevier, Amsterdam.

BBA, (1998). "Guidelines document for the assessment and certification of thin surfacing systems for highway," SG3/98/160, SG3 British Board of Agrèment/Highways Authorities Product Approval Scheme (BBA/HAPAS), Watford.

Begley, J.A. and Landes, J.D., (1972). Special Technical Publication No. 514, American Society of Testing Materials, ASTM, Philadelphia, pp. 1 - 20.

Bell, C.A., Cooper, K.E., Preston, J.N. and Brown, S.F., (1989). "Development of new procedure for bituminous mix design," 4th Eurobitume Symposium, Madrid, pp. 499-504.

Berengier, M., Hamet, J.F. and Bar, P., (1990). "Acoustical Properties of porous asphalts: theoretical and environmental aspects," Transportation Research Record 1265, TRB, National Research Council, Washington, D.C., pp. 9 – 24.

Billiter, T.C., Davison, R.R., Glover, C.J. and Bullin, J.A., (1997**a**). "Physical properties of asphalt-rubber binder," Petroleum Science and Technology, Vol. 15. No. 3&4, pp. 205 – 236.

Billiter, T.C., Chun, J.S., Davison, R.R., Glover, C.J. and Bullin, J.A., (1997**b**). "Investigation of the curing variables of asphalt-rubber binder," Petroleum Science and Technology, Vol. 15, No. 4&5, pp. 445 – 469.

Billiter, T.C., Davison, R.R., Glover, C.J. and Bullin, J.A., (1997**c**). "Production of asphalt-rubber binders by high-cure conditions," Transportation Research Record 1586, TRB, National Research Council, Washington, D.C., pp. 50 – 56.

Björklund, N.A., (1979). "Rubber granulates in wearing courses," Proc., XIV World Road Congress, Vienna, Austria.

Bloomquist, D., Diamond, G., Odin, M., Ruth, B. and Tia, M., (1993). "Engineering and environmental aspects of recycled materials for highway construction," Report FHWA-RD-93-088, Federal Highway Administration, Washington, D.C.

Brown, W.R., Jenkins, R.B. and Park, G.S., (1973). "Sorption and diffusion of small molecules in amorphous and crystalline polybutadienes," Journal of Polymer Science, Part C, Polymer Symposia, No. 41, pp. 45 – 67.

Brown, S.F. and Cooper, K.E., (1994). "Simplified methods for determination of fundamental material properties of asphalt mixes," Proc., Strategic Highway Research Program (SHRP) and traffic safety on two continents, VTI, The Hague, Vol. 1A, Part 3, pp. 124 – 136.

BSI, (1989). "Testing aggregates. Method for determination of the polished-stone value," BS 812: Part 114, British Standard Institution, London.

BSI, (1990a). "Sampling and examination of bituminous mixtures for roads and other paved areas. Method of test for the determination of the composition of design wearing course rolled asphalt," BS 598: Part 107, British Standard Institution, London.

BSI, (1990b). "Testing aggregates. Method for determination of aggregate crushing value (ACV)," BS 812: Part 110, British Standard Institution, London.

BSI, (1990c). "Testing aggregates. Method for determination of aggregate abrasion value (AAV)," BS 812: Part 113, British Standard Institution, London.

BSI, (1990d). "Sampling and examination of bituminous mixtures for roads and other paved areas. Methods of test for the determination of texture depth," BS 598: Part 105, British Standard Institution, London.

BSI, (1991). "Fracture mechanics toughness tests. Method for determination of K_{IC}, critical CTOD and critical J values of metallic materials," BS 7448: Part 1, British Standards Institution, London.

BSI, (1993). "Method for determination of the indirect tensile stiffness modulus of bituminous mixtures," DD 213, British Standards Institution, London.

BSI, (1995). "Testing aggregates. Methods for determination of density," BS 812: Part 2, British Standards Institution, London.

BSI, (1996). "Method for the determining resistance to permanent deformation of bituminous mixtures subject to unconfined dynamic loading," DD 226, British Standards Institution, London.

BSI, (2000a). "Methods of test for petroleum and its products. Bitumen and bituminous binders. Determination of needle penetration," BS 2000: Part 49, British Standard Institution, London.

BSI, (2000b). "Methods of test for petroleum and its products. Bitumen and bituminous binders. Determination of softening point. Ring and ball method," BS 2000: Part 58, British Standard Institution, London.

BSI, (2001). "Coated macadam (asphalt concrete) for roads and other paved areas. Specification for constituent materials and for mixtures," BS 4987: Part 1, British Standard Institution, London.

Buisine, J.M., Joly, G., Eladlani, A., Such, C. Farcas, F., Ramond, G., Claudy, P., Létoffé, J.M., King, G.N., Planche, J.P. and Gemanaud, L., (1993). "Thermodynamica behaviour and physiochemical analysis of eight SHRP bitumens," Transportation Research Record 1386, TRB, National Research Council, Washington, D.C., pp. 1 – 9.

Bukka, K., Miller, J.D. and Oblad, A.G., (1991). "Fractionation and characterization of Utah tar sand bitumens: influence of chemical composition on bitumen viscosity," Energy & Fuels, Vol. 5, pp. 333 – 340.

Bull, A.L. and Vonk, W.C., (1987). "Thermoplastic rubber/bitumen blends for roof and road," Thermoplastic Rubber Technology, Manual TR 8.15, Shell Elastomers, London.

Burgess, R., Kopvillem, O. and Young, F., (1971). "Ste. Anne Test Road: relationship between predicted fracture temperatures and low-temperature field performance," Proc., Association of Asphalt Paving Technologists, Vol. 40, pp. 148 – 193.

Button, J.W., Little, D.A., Kim, Y. and Ahmed, J., (1987). "Mechanistic evaluation of selected asphalt additives," Proc., Association of Asphalt Paving Technologists, Vol. 56, pp. 62 – 90.

Button, J.W., (1992). "Summary of asphalt additive performance at selected sites," Transportation Research Record 1342, TRB, National Research Council, Washington, D.C., pp. 67 – 75.

Cabrera, J.G. and Hamzah, M.O., (1996). Chapter 2 "Aggregate grading design for porous asphalt," Performance and durability of bituminous materials, Edited by J.G. Cabrera and J.R. Dixon. Published by E & FN Spon, London, pp. 10 – 22.

Champagne, P.J., Manolakis, E. and Ternan, M., (1985). "Molecular Weight distributions of athabasca bitumen," Fuel, Vol. 64, No. 3, pp. 423 – 425.

Charantia, E., Cano, J.O. and Schnormeir, R.H., (1991). "Twenty-year study of asphalt rubber pavements in Phoenix, Arizona," Transportation Research Record 1307, TRB, National Research Council, Washington, D.C., pp. 29 – 38.

Child, S. and Hicks, B., (2000). "Colsoft – the quiet road surface coating," Highways and Transportation, Vol. 47, No. 11, p. 16, 18.

Chipps, J.F., Davison, R.R. and Glover, C.J., (2001). "A model for oxidative aging of rubber-modified asphalts and implications to performance analysis," Energy & Fuels, Vol. 15, pp. 637 – 647.

Choi, Y.K., Collop, A.C. and Thom, N.H., (2002). "A simple damage approach to modelling fatigue in bituminous materials," Proc. 6th International Conference on the Bearing Capacity of Roads and Airfields, Lisbon, 2002, Vol. 1, pp. 103 – 111.

Chomton, G. and Valayer, P.J., (1972). "Applied rheology of asphalt mixes – Practical applications," Proc. 3rd International Conference on the Structural Design of Asphalt Pavements, London, pp. 214 – 225.

Christison, J.T., Murray, D.W. and Anderson, K.O., (1972). "Stress prediction and low-temperature fracture susceptibility of asphaltic concrete pavements," Proc., Association of Asphalt Paving Technologists, Vol. 41, pp. 494 – 523.

Chung, K.E., Anderson, L.L. and Wiser, W.H., (1979). "New procedure for molecular-weight determination by vapor-phase osmometry," Fuel, Vol. 58, No. 12, pp. 847 – 852.

Collins, J.H., Boulding, M.G., Gelles, R. and Berker, A., (1991). "Improved performance of paving asphalts by polymer modification," Proc., Association of Asphalt Paving Technologists, Vol. 60, pp. 43 – 79.

Cominsky, R.J., Huber, G.A., Kennedy, T.W. and Anderson, M., (1994). "The Superpave mix design manual for new constructions and overlays," Strategic Highway Research Program, Report SHRP-A-407, National Research Council, Washington, D.C.

Cooper, K.E., Brown, S. F. and Pooley, G. R., (1985). "The design of aggregate gradinds for asphalt basecourses," Proc., Association of Asphalt Paving Technologists, Vol. 54, pp. 324 – 346.

Cooper, K.E. and Brown, S.F., (1989). "Development of a simple apparatus for the measurement of the mechanical properties of asphalt mixes," Proc., 4th Eurobitume symposium, Madrid, pp. 494 – 498.

Corbett, L.W. and Swarbrick, R.E., (1958). "Clues to asphalt composition," Proc. Association of Asphalt Paving Technologists, Vol. 27, p. 107

Cowie, J.M.G., (1991)."Polymers: Chemistry & Physics of Modern Materials," 2nd Ed., Blackie, Glasgow.

Crank, J., (1956). "The mathematics of diffusion," Oxford University Press, London.

Crank, J. and Park, G.S., (1968). "Diffusion in polymers," (Eds: Crank, J. and Park, G.S.), Academic Press, London.

C.R.U.M.B., (2003). Crumb Rubber Universal Marketing Bureau. http://www.recycle.net/price/crumb.htlm

Curtis, C.W., Hanson, D.I., Chen, S.T., Shieh, G-J. and Ling, M., (1995). "Quantitative determination of polymers in asphalt cements and hot-mix asphalt mixes," Transportation Research Record 1488, TRB, National Research Council, Washington, D.C., pp. 52 – 61.

David, T.C. and Petersen, J.C., (1967). "Inverse gas-liquid chromatographic studies of asphalt – comparison with analysis by fractionating," Analytical Chemistry, Vol. 39, pp. 1852 – 1857.

De L. Costello, B.A., (1997). "The use of the method of incomplete creep to asses the resistance to rutting of bituminous materials," Proc., 2nd European symposium, Performance and durability of bituminous materials, Leeds, AEDIFICATIO, pp. 71 – 84.

Del Valle, H., (1985). "Procedure – bulk specific gravity of compacted bituminous materials using Parafilm™ coated specimens," Chevron Research Co., Richmond, California.

Di Benedetto, H., Ashayer Soltani, M.A. and Chaverot, P., (1996). "Fatigue damage for bituminous mixtures: a pertinent approach," Proc., Association of Asphalt Paving Technologists, Vol. 65, pp. 142 – 158.

Di Benedetto, H., Ashayer Soltani, M.A. and Chaverot, P., (1997). "Fatigue damage for bituminous mixtures," Proc., 5th International RILEM Symposium – Mechanical Tests for Bituminous Materials – Lyon, France, pp. 263 – 270.

Dongre, R., Sharma, M.G. and Anderson, D.A., (1989). "Development of fracture criterion for asphalt mixes at low temperatures," Transportation Research Record 1228, TRB, National Research Council, Washington, D.C., pp. 94 - 105.

Dransfield, K.A., Gani, M.J.S., Stachurski, Z.H. and Maccarrone, S., (1995). "The failure resistance of bitumen," Materials Forum, Vol. 1, pp. 241 – 254.

Eckmann, B. and Plaindoux, M., (1983). "Liants bitumen caoutchouc Flexochape – Etude de laboratoire," Revue Générale des Routes et Aérodromes, No. 602.

Emery, J., (1995). "Evaluation of rubber modified asphalt demonstration projects," Transportation Research Record 1515, TRB, National Research Council, Washington, D.C., pp. 37 – 46.

Epps, J.A., (1994). "Uses of recycled rubber tyres in highways," National Cooperative Highway Research Program (NCHRP), Synthesis of Highway Practice 198, Transportation Research Board, National Research Council, Washington, D.C.

Esso Belgium, (1984). "Open-graded and dense-graded mixes with asphalt rubber,".

Faab, T.R.J., (1974). "The influence of mix composition, binder properties and cooling rate on asphalt cracking at low-temperatures," Proc., Association of Asphalt Paving Technologists, Vol. 43, pp. 285 – 331.

Fager, G.A., (1994). "Use of rubber in asphalt pavements: Kansas experience," Transportation Research Record 1436, TRB, National Research Council, Washington, D.C., pp. 88 – 97.

Ferguson, A., Fordyce, D. and Khweir, K., (1999). "Designing stone structure wearing course mixtures," Proc. 3rd European Symposium, Performance and Durability of Bituminous Materials and Hydraulic Stabilised Composites, Leeds, pp. 179 - 194.

Ferry, J.D., (1970). "Viscoelastic properties of polymers," 2nd Edition, John Wiley, New York.

Francken, L., Vanelstraete, A., Léonard, D. and Pilate, O., (2003). "New developments in the PRADO volumetric mix design," Proc. 6th International RILEM Symposium, Performance Testing and Evaluation of Bituminous Materials, Zurich, Switzerland, pp. 292 – 298.

Fuller, W.B. and Thompson, S.E., (1907). "The laws of proportioning concrete," Transactions of the American Society of Civil Engineers, Vol. 59, pp. 67 – 172.

Furnas, C.C., (1931). "Grading aggregates. Mathematical relations for beds of broken solids of maximum density," Industrial and Engineering Chemistry, Vol. 23, pp. 1052 – 1058.

Gowda, G.V., Hall, K.D. and Elliot, R.P., (1996). "Arkansas experience with crumb rubber modified mixes using Marshall and Strategic Highway Research Program Level I Design Methods," Transportation Research Record 1530, TRB, National Research Council, Washington, D.C., pp. 25 – 33.

Griffith, A.A., (1920). "The phenomena of rupture and flow in solids," Philosophical Transactions of the Royal Society, London, Series A, Vol. 221, pp. 163 - 198.

Haas, R. and Phang, W., (1988). "Relationship between mix characteristics and low-temperature pavement cracking," Proc., Association of Asphalt Paving Technologists, Vol. 57, pp. 290 – 319.

Hadipour, K. and Anderson, K.O., (1988). "An evaluation of permanent deformation and low temperature characteristics of some recycled asphalt concrete mixtures," Proc., Association of Asphalt Paving Technologists, Vol. 57, pp. 615 – 645.

Hargrave, S., (1998). "Rubber roads reduce noise," Sunday Times Newspaper, 13 September 1998.

Harogoppad, S.B. and Aminabhavi, T.M., (1991). "Diffusion and sorption of organic molecules through polymer membranes. 5. Neoprene, styrene-butadiene-rubber, ethylene-propylene-diene terpolymer, and natural rubber versus hydrocarbons (C_8-C_{16})," Macromolecules, Vol. 24, No. 9, pp. 2598 – 2605.

Heerkens, J.C.P., (1985). "Open-graded rubberised asphalt for noisy highways," 3rd Eurobitume Symposium, The Hague, pp. 686 – 690.

Heitzman, M., (1992). "Design and construction of asphalt paving materials with crumb rubber modifier," Transportation Research Record 1339, TRB, National Research Council, Washington, D.C., pp. 1 – 8.

Heslop, M.W. and Catt, C.A., (1997). "Specifying durability for bituminous surfacings – the importance of binder rheology," Proc., 2nd European symposium, Performance and durability of bituminous materials, Leeds, AEDIFICATIO, pp. 19 – 38.

Hicks, R.G., Lundy, J.R., Leahy, R.B., Danson, D. and Epps, J., (1995). "Crumb rubber modifiers (CRM) in asphalt pavements: summary of practice in Arizona, California, and Florida," Federal Highway Administration, FHWA-SA-95-056, Washington, D.C.

Hicks, R.G. and Epps, J., (2002). "Life cycle cost analysis of asphalt-rubber pavement materials," Rubber Pavements Association, Tempe, Arizona. http://www.rubberpavements.org/library/index.asp.

Hildebrand, J. H. and Scott, R. L., (1964). "The solubility of non-electrolytes," Dover, New York.

Hills, J.F. and Brien, D., (1966). "The fracture of bitumens and asphalt mixes by temperature induced stresses," Proc., Association of Asphalt Paving Technologists, Vol. 35, pp. 292 – 309.

Hird, A.B., Griffiths, P.J. and Smith, R.A., (2001). "Tyre waste and resource management: a mass balance approach," Viridis Report, Project Report PR/SE/235/01, Biffward Programme on Sustainable Resource Use, TRL.

Hoigber, A.J. and Garris, W.E. Jr, (1949). "Analytical fractionation of asphalts," Analytical Edition, Industrial Engineering Chemistry, Vol. 16, pp. 294 – 302.

Holden, G., Bishop, E.T. and Legge, N.R., (1969). "Thermoplastic elastomers," Journal of Polymer Science, Part C, No. 26, pp. 37 – 57.

Hopman, P.C., Kunst, P.A. and Pronk, A.C., (1989). "A renew interpretation method for fatigue measurements, verification of Miner's Rule," Proc. 4th Eurobitume Symposium, Madrid, pp. 557 – 561.

Hughes, B.P., (1962). "Rational concrete mix design," Proc. Institution of Civil Engineers, Vol. 21, pp. 927 – 952.

Hui, J.C.T., Morrison, G.R. and Hesp, S.A.M., (1994). "Improved low-temperature fracture performance for rubber-modified asphalt binders," Transportation Research Record 1436, TRB, National Research Council, Washington, D. C., pp. 83 - 87.

Irwin, G.R., (1957). "Analysis of stresses and strains near the end of the crack traversing a plate," Journal of Applied Mechanics, Vol. 24, pp. 361 – 364.

Irwin, G.R., (1970). "Fracture strength of relatively brittle structures and materials," Journal of the Franklin Institute, Vol. 290, p. 513.

Janoo, V.C., (1989). "Used of low viscosity asphalts in cold regions," Proc., 5th International Conference on Cold Regions Engineering, ASCE, New York, pp. 70 – 80.

Joseph, P.E., Dickson, J.H. and Kennepohl, G., (1992). "Evaluation of polymer-modified asphalts in Ontario," Proc., Canadian Technical Asphalt Association, Vol. 37, pp. 243 – 264.

Jung, D.H. and Vinson, T.S., (1993). "Thermal stress restrained specimen test to evaluate low-temperature cracking of asphalt-aggregate mixtures," Transportation Research Record 1417, TRB, National Research Council, Washington, D.C., pp. 12 - 20.

Jung, D.H. and Vinson, T.S., (1994). "Low-temperature cracking: test selection," Strategic Highway Research Programme, Report SHRP-A-401, National Research Council, Washington, D.C.

Jung, J.-S., Kaloush, K.E. and Way, G.B., (2002). "Life cycle cost analysis: conventional versus asphalt-rubber pavements," Rubber Pavements Association. http://www.rubberpavements.org/library/index.asp.

Kennedy, T.W., Huber, G.A., Harrigan, E.T., Cominsky, R.J., Hughes, C.S., Von Quintus, H. and Moulthrop, J.S., (1994). "Superior Performing Asphalt Pavements (Superpave): The Product of the SHRP Asphalt Research Program," Strategic Highway Research Program, Report SHRP-A-410 National Research Council, Washington, D.C.

Khalid, H., (2000). Private communication. Department of Civil Engineering, Liverpool University, UK.

Khalid, H., (2000)."A comparison between bending and diametral fatigue tests for bituminous materials," Materials and Structures/Matériaux et Constructions, Vol. 33, pp. 457 – 465.

Khosla, N.P. and Zahran, S.Z., (1989). "A mechanistic evaluation of mixes containing conventional and polymer modified (styrelf) asphalts," Proc., Association of Asphalt Paving Technologists, Vol. 58, pp. 274 - 302.

Kim, K.W. and El Hussein, M., (1997). "Variation of fracture toughness of asphalt concrete under low temperatures," Construction and Buildings Materials, Vol. 11, Nos. 7-8, pp. 403 – 411.

Kim, S., Loh, S., Zhai, H. and Bahia, H.U., (2001). "Advanced characterization of crumb rubber modified asphalts, using protocols developed for complex binders," Transportation Research Record 1767, TRB, National Research Council, Washington, D.C., pp. 15 – 24.

Kliever, J.E., Zeng, H. and Vinson, T.S., (1996). "Aging and low-temperature cracking of asphalt concrete mixture," Journal of Cold Regions Engineering, Vol. 10, No. 3. pp. 134 – 148.

Leech, D. and Nunn, M.E., (1997). "Deterioration mechanisms in flexible roads," Proc., 2nd European Symposium, Performance and durability of bituminous materials, Leeds, AEDIFICATIO, pp. 271 – 292.

Lees, G., (1969). "Influence of boundary effects on the packing and porosity of granular materials," Journal of Engineering Geology, Vol. 2, pp. 129 – 147.

Lees, G., (1970). "The rational design of aggregate grading for dense asphaltic compositions," Proc., Association of Asphalt Paving Technologists, Vol. 39, pp. 60 – 94.

Lefebvre, G., (1993). "Porous asphalt," Permanent International Association of Road Congress, Paris.

Lemaitre, J., (1996). "A course on damage mechanics," Ed. Springer, Berlin.

Liang, R.Y. and Lee, S., (1996). "Short-term and long term aging behaviour of rubber modified asphalt paving mixture," Transportation Research Record 1530, TRB, National Research Council, Washington, D.C., pp. 11 – 17.

Lin, M.S., Chaffin, J.M., Liu, M., Glover, C.J., Davison, R.R. and Bullin, J.A., (1996). "The effect of asphalt composition on the formation of asphaltenes and their contribution to asphalt viscosity," Fuel Science and Technology, Vol. 14, Part 1 – 2, pp. 139 – 162.

Ling, M., Curtis, C.W., Hanson, D.I. and Hool, J.N., (1997). "Quantitative analysis of polymers and crumb rubber in hot-mix asphalts," Transportation Research Record 1586, TRB, National Research Council, Washington, D.C., pp. 57 – 67.

Lu, X. and Isacsson, U., (1997). "Rheological characterization of styrene-butadiene-styrene copolymer modified bitumens," Construction and Building Materials, Vol. 11, No. 1, pp. 23 – 32.

Lu, X. and Isacsson, U., (2001). "Modification of road bitumens with thermoplastic polymers," Polymer Testing, Vol. 20, pp. 77 – 86.

Lu, X., Isacsson, U. and Ekblad, J., (1999). "Phase separation of SBS polymer modified bitumens," Journal of Materials in Civil Engineering, Vol. 11, No. 1, pp. 51 – 57.

Mahboub, K., (1990). "Elasto-plastic fracture characterization of paving materials at low temperatures," Journal of Testing and Evaluation, Vol. 18, No. 3, pp. 210 – 218.

Majidzadeh, K., Ramsamooj, D.V. and Fletcher, T.A., (1969). "Analysis of fatigue of a sand-asphalt mixture," Proc., Association of Asphalt Paving Technologists, Vol. 38, pp. 495 – 518.

Majidzadeh, K., Asp, E.M. and Ramsamooj, D.V., (1971). "Application of fracture mechanics in the analysis of pavement fatigue," Proc., Association of Asphalt Paving Technologists, Vol. 40, pp. 227 – 245.

Marasteanu, M.O. and Anderson, D.A., (2000). "Establishing linear viscoelastic conditions for asphalt binders," Transportation Research Record 1728, TRB, National Research Council, Washington, D.C., pp. 1 – 6.

Marasteanu, M.O. and Anderson, D.A., (2001). "Techniques for determining errors in asphalt binder rheological data," Transportation Research Record 1766, TRB, National Research Council, Washington, D.C., pp. 32 – 39.

Maupin Jr, G.W., (1996). "Hot mix asphalt rubber applications in Virginia," Transportation Research Record 1530, TRB, National Research Council, Washington, D.C., pp. 18 – 24.

McDonald, C.H., (1968). "A new patching material for pavement failures," Highway Research Record 146, Transportation Research Board, Washington, D.C., pp. 1 – 16.

Merkle, J.G., Berggren, R.G. and Stelzman, W.J., (1975). "Compliance and fracture," Heavy-Section Steel Technology Quarterly Progress Report, Oak Ridge National Laboratory, Report TM-4805.

Miner, M.A., (1954). "Cumulative fatigue damage," International Conference on the Fatigue Damage of Metals, London.

Moavenzadeh, F., (1967). "Asphalt fracture," Proc., Association of Asphalt Paving Technologists, Vol. 36, pp. 51 – 79.

Monismith, C.L. and Deacon, J.A., (1969). "Fatigue of asphalt paving mixtures," ASCE Transportation Engineering Journal, Vol. 95:2, pp. 317 – 346.

Monismith, C.L., Secor, G.A. and Secor, K.E., (1965). "Temperature stresses and deformation in AC," Proc., Association of Asphalt Paving Technologists, Vol. 34, pp. 248 – 285.

Monismith, C.L., Epps, J.A. and Finn, F.N., (1985). "Improved asphalt mix design," Proc., Association of Asphalt Paving Technologists, Vol. 54, pp. 347 – 407.

Morris, G.R., (1993). "True cost effectiveness of asphalt-rubber paving systems," Proc., of the Symposium on a Critical Look at the Use of Waste Materials in Hot-Mix Asphalt, ASTM Special Technical Publication, No. 1193, pp. 293 – 302.

Morrison, G.R. and Hesp, S.A.M., (1995). "A new look at rubber-modified asphalt binders," Journal of Materials Science, Vol. 30, No. 10, pp. 2584 – 2590.

Morrison, G.R., van der Stel, R. and Hesp, S.A.M., (1995). "Modification of asphalt binders and asphalt concrete mixes with crumb rubber and chemically devulcanized waste rubber," Transportation Research Record 1515, TRB, National Research Council, Washington, D.C., pp. 56 – 63.

Moschopedis, S., Fryer, J.F. and Speight, J.G., (1976). "Investigation of asphaltene molecular weights," Fuel, Vol. 55, pp. 227 – 232.

Murakami, Y., (1987). "Stress intensity factors handbook," Ed. Pergamon, Oxford.

Nali, M. and Manclossi, A., (1995). "Size exclusion chromatography and vapor pressure osmometry in the determination of asphaltene molecular weight," Fuel Science & Technology International, Vol. 13, No. 10, pp. 1251 – 1264.

Neifar, M. and Di Benedetto, H., (2002). "Complex modulus of bituminous mixes: How to interpret measurements," Proc. 3rd International Conference Bituminous Mixtures and Pavements, Thessaloniki, pp. 409 – 421.

Nijboer, L.W., (1948). "Plasticity as a factor on the design of dense bituminous road carpets," Elsevier Publishing Company, London

Nunn, M.E., (1997). "The indirect tensile stiffness modulus test," Proc., Performance related test procedures for bituminous mixtures, University College Dublin, pp. 125 – 137.

Olabisi, O., Robeson, L.M. and Shaw, M.T., (1979). "Polymer-polymer miscibility," Academic Press, San Diego.

Paris, P.C. and Erdogan, F., (1963). "A critical analysis of crack propagation law," Transactions of the ASME, Journal of Basic Engineering, Series D, 85, No. 3.

Pell, P.S., (1973). "Characterization of fatigue behaviour", in "Structural Design of Asphalt Concrete Pavements to Prevent Fatigue Cracking" Proc. of Symposium, Highway Research Board Special Report 140, Washington, pp. 49 – 64.

Pell, P.S. and Cooper, K.E., (1975). "The effect of testing and mix variables on the fatigue performance of bituminous materials," Proc., Association of Asphalt Paving Technologists, Vol. 44, pp. 1 – 37.

Peramanu, S. and Pruden, B.B., (1999). "Molecular weight and specific gravity distributions for Athabasca and Cold Lake bitumens and their saturate, aromatic, resin, and asphaltene fractions," Industrial and Engineering Chemistry Research, Vol. 38, No. 8, pp. 3121 – 3130.

Peterlin, A., (1975). "Dependence of diffusive transport on morphology of crystalline polymers," Journal of Macromolecular Science – Physics, Vol. B11, No. 1, pp. 57 – 87.

Petersen, J.C., (1984). "Chemical composition of asphalt as related to asphalt durability: state of the art," Transportation Research Record 999, TRB, National Research Council, Washington, D.C., pp. 13 – 30.

Petersen, J. C., Roberson, R. E., Branthaer, J. F., Harnsberger, P. M., Duvall, J. J., Kim, S. S., Anderson, D. A., Christiansen, D. W. and Bahia, H. U., (1994). "Binder characterisation and evaluation," Strategic Highway Research Program, Report SHRP-A-367, Vol. 1, National Research Council, Washington, D.C.

Phillips, M.C. and Robertus, C., (1995). "Rheological characterisation of bituminous binders in connection with permanent deformation in asphaltic pavements; the zero-shear-viscosity concept," Proc., The rheology of bituminous binders workshop, Eurobitume, Brussels, Paper No. 50.

Phillips, M.C. and Robertus, C., (1996). "Binder rheology and asphaltic pavement permanet deformation; the zero-shear viscosity," Proc.,1st Eurasphalt and Eurobitume Congress, Strasbourg. Paper No. 5.134

Philipps, M.C., (1997). "Developments in specifications for bitumens and polymer-modified binders, mainly from a reological point of view," Proc. 2nd European Symposium, Performance and Durability of Bituminous Materials, Leeds, UK, pp. 3 – 18.

Planche, J.P. Lesueur, D., Hines, M.L. and King, G.N., (1996). "Evaluation of elastomer modified bitumens using SHRP binder specifications," Proc. 1st Eurasphalt and Eurobitume congress, Strasbourg, Paper No. 5.121.

Pronk, A.C. and Hopman, P.C., (1990). "Energy dissipation: The leading factor of fatigue". In Highway Research: Sharing the Benefits: Proceedings of a conference of the United States Strategic Highway Research Program, London 1990, pp. 255 – 267.

Pronk, A.C., Krans, R.L. and van Gogh, F., (1996). "Temperature increase in an asphalt beam during fatigue – theory and practice," CROW Wegbouwkundige Werkaden, 1996. Ede: CROW.

Pronk, A.C., (1997). "Comparison of 2 and 4 point fatigue tests and healing in 4 point dynamic bending test based on the dissipated energy concept," Proc. 8th International Conference on Asphalt Pavements, Seattle, pp. 987 – 994.

Raad, L. and Saboundjian, S., (1998). "Fatigue behaviour of rubber-modified pavements," Transportation Research Record 1639, TRB, National Research Council, Washington, D.C., pp. 73 – 82.

Rebala, S.R. and Estakhri, C.K., (1995). "Laboratory evaluation of crumb rubber modified mixtures designed using TxDOT mixture design method," Transportation Research Record 1515, TRB, National Research Council, Washington, D.C., pp. 1 – 10.

Rice, J.R., (1968a). "Treatise on Fracture," Vol. 2, H. Liebowitz, Ed., Academic Press, New York, p. 191.

Rice, J.R., (1968b). "A path independent integral and the approximate analysis of strain concentration by notches and cracks," Journal of Applied Mechanics, Vol. 35, pp. 379 - 386.

RMA, (2002). "U.S. Scrap tyre markets 2001," Rubber Manufactures Association, Washington, D.C.
http://www.rma.org/scraptires

Roff, W.J. and Scott, J.R., (1971). "Fibres, films, plastics and rubbers," Butterworth & Co (Publishers) Ltd, London.

Rostler, F.S. and White, R.M., (1962). "Composition and changes of highway asphalts, 85-100 penetration grade," Proc., Association of Asphalt Paving Technologists, Vol. 31, pp. 35 – 89.

Rowe, G.M., (1993). "Performance of asphalt mixtures in the trapezoidal fatigue test," Proc., Association of Asphalt Paving Technologists, Vol. 62, pp. 344 – 384.

Rowe, G.M. and Bouldin, M.G., (2000). "Improved techniques to evaluate the fatigue resistance of asphaltic mixtures," Proc. 2nd Eurasphalt & Eurobitume Congress, Barcelona, Vol. 1, pp. 754 – 763.

RPA, (2003). "Effectiveness of rubberised asphalt in reducing traffic noise," By the Sacramento County Department of Environmental Review and Assessment and Bollard and Brennan, Inc. Rubber Pavements Association, Tempe, US.
http://www.rubberpavements.org/library

Sainton, A., (1990). "Advantages of asphalt rubber binder for porous asphalt concrete," Transportation Research Record 1265, TRB, National Research Council, Washington, D.C., pp. 69 – 81.

Schmidt, R.J., (1972). "A practical method for measuring the resilient modulus of asphalt-treated mixes," Highway Research Record 404, Highway Research Board, Washington, D.C., pp. 22 – 32.

Schweyer, H.E., Chelton, H. and Brenner, H.H., (1955). "A chromatographic study of asphalt. Proc., Association of Asphalt Paving Technologists, Vol. 24, p. 3.

Shell, (1991). "Preparing blends of CARIFLEX TR and bitumens," Shell Technical Bulletin, TR 6.5.

SHRP-A-404, (1994). "Fatigue response of asphalt-aggregate mixes," Strategic Highway Research Program, Report SHRP-A-404, National Research Council, Washington, D.C.

SIPC, (1989). Shell International Petroleum Company, "Bitumen and asphalt nomographs developed by Shell," BANDS-PC User Manual, London.

SIPC, (1995). Shell International Petroleum Company, "Shell pavement design method – stress and strain calculations in pavement models on a PC", BISAR-PC User Manual, London.

Sisko, A.W. and Brunstrum, L.C., (1969). "Relation of asphalt rheological properties to pavement durability," National Co-operative Highway Research Program Report 67, Highway Research Board, National Research Council, Washington, D.C.

Stern, H.J., (1967). "Rubber: Natural and Synthetic," Maclaren and Sons Ltd, London.

Stroup-Gardiner, M., Newcomb, D.E. and Tanquist, B., (1993). "Asphalt-rubber interactions," Transportation Research Record 1417, TRB, National Research Council, Washington, D.C., pp. 99 – 108.

Stroup-Gardiner, M., Chadbourn, B. and Newcomb, D., (1996). "Babbitt, Minnesota: case study of pretreated crumb rubber modified asphalt concrete," Transportation Research Record 1530, TRB, National Research Council, Washington, D.C., pp. 34 – 42.

Sulaiman, S.J. and Stock, A.F., (1995). "The use of fracture mechanics for the evaluation of asphalt mixes," Proc., Association of Asphalt Paving Technologists, Vol. 64, pp. 500 – 531.

Sumpter, J.D.G. and Turner, C.E., (1976). "Method for laboratory determination of J1c," Cracks and Fracture. ASTM STP 601, American Society for Testing and Materials, pp. 3-18.

TAI, (1988). "Mix design methods for asphalt concrete and other hot-mix types," The Asphalt Institute, Manual series No. 2.

Takallou, H.B. .and Hicks, R.G., (1988). "Development of improved mix and contruction guidelines for rubber-modified asphalt pavements," Transportation Research Record 1171, TRB, National Research Council, Washington, D.C., pp. 113 – 120.

Takallou, H.B. and Sainton, A., (1992). "Advances in technology of asphalt paving materials containing used tire rubber," Transportation Research Record 1339, TRB, National Research Council, Washington, D.C., pp. 23 – 29.

Tayebali, A.A., Rowe, G.M. and Sousa, J.B., (1992a). "Fatigue response of asphalt-aggregate mixtures," Proc., Association of Asphalt Paving Technologists, Vol 61, pp. 333 – 360.

Tayebali, A.A., Deacon, J.A., Coplantz, J.S., Harvey, J.T. and Monismith, C.L., (1992b). "Fatigue response of asphalt aggregate-mixes, Part 1 – Test method selection," Strategic Highway Research Program, SHRP Project A-003A, National Research Council, Washington, D.C.

Tayebali, A.A., Deacon, J.A., Coplantz, J.S and Monismith, C.L., (1993). "Modelling fatigue response of asphalt-aggregate mixtures," Proc., Association of Asphalt Paving Technologists, Vol. 62, pp. 285 – 421.

Thom, N.H., Choi, Y.K. and Harireche, O., (2002). "The influence of aggregate properties on asphalt performance," Proc., 3rd International Conference Bituminous Mixtures and Pavements, Thessaloniki, pp. 593 – 602.

Treloar, L.R.G., (1975). "The physics of rubber elasticity," Oxford University Press, London.

Troy, K., Sebaaly, P.E. and Epps, J.A., (1996). "Evaluation systems for crumb rubber modified binders and mixtures," Transportation Research Record 1530, TRB, National Research Council, Washington, D.C., pp. 3 – 10.

UTGW, (2000). "Fourth Annual Report of the Used Tyre Working Group," http://www.tyredisposal.co.uk/reports.asp

UTGW, (2001). "Fifth Annual Report of the Used Tyre Working Group," http://www.tyredisposal.co.uk/reports.asp

van Dijk, W., Moreaud, H., Quedeville, A. and Uge, P., (1972). "The fatigue of bitumen and bituminous mixes," Proc. 3rd International Conference on the Structural Design of Asphalt Pavements, London, pp. 355 – 366.

van Dijk, W., (1975). "Practical fatigue characterization of bituminous mixtures," Proc., Association of Asphalt Paving Technologists, Vol 44, pp. 38 – 74.

van Dijk, W. and Visser, W., (1977). "The energy approach to fatigue for pavement design," Proc., Association of Asphalt Paving Technologists, Vol 46, pp. 1 – 40.

Vinson, T.S., Janoo, V.C. and Haas, R.C.G., (1989). "Summary report on low temperature and thermal fatigue cracking," Strategic Highway Research Program, Report SHRP-A/IR-90-001, National Research Council, Washington, D.C.

Way, G.B., (1998). "OGFC meets CRM: where the rubber meets the rubber," Rubber Pavement Association. http://www.rubberpavements.org/library/crm.asp

Whiteoak, C.D., (1990). "The Shell Bitumen Handbook," Shell bitumen UK, Chertsey, Surrey.

Woodside, A.R., Woodward, W.D.H., Phillips, P. and Mills, A., (2000). "Sustainable reuse of highway materials in hot and cold bituminous mixtures," Proc. Institution of Civil Engineers, Municipal Engineer, Vol. 139, No. 3, pp. 181 – 186.

Yarranton, H.W. and Masliyah, J.H., (1996). "Molar mass distribution and solubility modelling of asphaltenes," American Institute of Chemical Engineer Journal, Vol. 42, No. 12, pp. 3533 – 3543.

Zanzotto, L. and Kennepohl, G.J., (1996). "Development of rubber and asphalt binders by depolymerization and devulcanization of scrap tires in asphalt," Transportation Research Record 1530, TRB, National Research Council, Washington, D.C., pp. 51 – 58.

Appendices

APPENDIX A. Sample preparation for DSR testing

The method of sample preparation developed here for DSR testing of conventional and crumb-rubber modified binders can be summarised as follows.

Binders modified with CRM were produced in a Silverson mixer under controlled conditions following the procedure explained in Chapter 3, section 3.5.8.1. Immediately after the mixing process finished, around 10 g of binder were poured onto grease-proof paper. The samples were then left to cool to room temperature and then stored in an incubator at 5 ^{0}C. Just before testing, the samples were trimmed by hand, while cold, to the required quantities shown in **Table 4.1**. A digital balance was used to weight the exact masses of binder needed for each test geometry.

The placing of the bitumen samples into the plates also required great care. First the parallel places were cleaned with a suitable solvent to remove any traces of previous samples, and left to dry. In the case of the 1 mm gap settings, the binder sample was place onto the lower plate. Then, both plates were placed in an oven at 150 ^{0}C. Once the binder sample flowed evenly across the entire surface of the plate, the plates were removed from the oven and inserted into the instrument. A period of 5 minutes was allowed before the upper plate was brought into contact with the lower plate. A slight rotation was applied to the upper plate as it was brought into proximity with the lower plate to ensure that the binder correctly filled the gap between the plates. A further 10 minutes was allowed to ensure good adhesion, before the system was flooded with the circulating fluid and test commenced.

In the case of the 2 mm gap setting, the method described above had to be modified to avoid flowing off of the binder from the bottom plate. Instead, the bitumen sample was divided in two parts of equal masses, whose were place onto the bottom plate and onto the face of the inverted upper plate before being place in the oven at 150 ^{0}C. Then both plates were removed from the oven and inserted in the instrument. Hereafter, the same methodology as for the 2 mm gap setting was followed.

.APPENDIX B. Determination of void content in a dry aggregate blend

To determine.the compacted density of the mixed aggregates, cylindrical moulds of 100 mm diameter and a fixed amount of 1250 g of aggregate blends were used. Aggregate blends of different proportions were prepared and placed in the moulds. The specific gravity of the blends (*SGMA*) was calculated from the knowledge of the specific gravities and proportions of the individual aggregate sizes, as follows,

$$SGMA = \frac{100}{\sum_{i=1}^{i=n} \frac{P_i}{SG_i}} \qquad \text{(B.1)}$$

where:

P_i = % by weight of the total blend of aggregate size *i*

SG_i = specific gravity of aggregate size *i*

i = aggregate sizes (14, 10, 6 mm, 3 mm to dust and filler)

The blends were then compacted by a vibrating hammer with a 100 mm foot. After compaction the height of the blend in the mould was measured. Measurements were carried out on triplicate specimens and the average value was taken. The compacted density of the mixed aggregate (*CDMA*) was then obtained knowing the weight of the blend and the volume after compaction, hence,

$$CDMA = \frac{\text{Total weight of aggregate blend}}{\text{Volume after compaction}} \qquad \text{(B.2)}$$

Finally, the voids in mixed aggregate (*VMA*) were calculated as follows,

$$VMA(\%) = \left[\frac{SGMA - CDMA}{SGMA}\right] \times 100 \qquad \text{(B.3)}$$

Figure 5.1 illustrates the procedure for the determination of the void content in an aggregate blend.

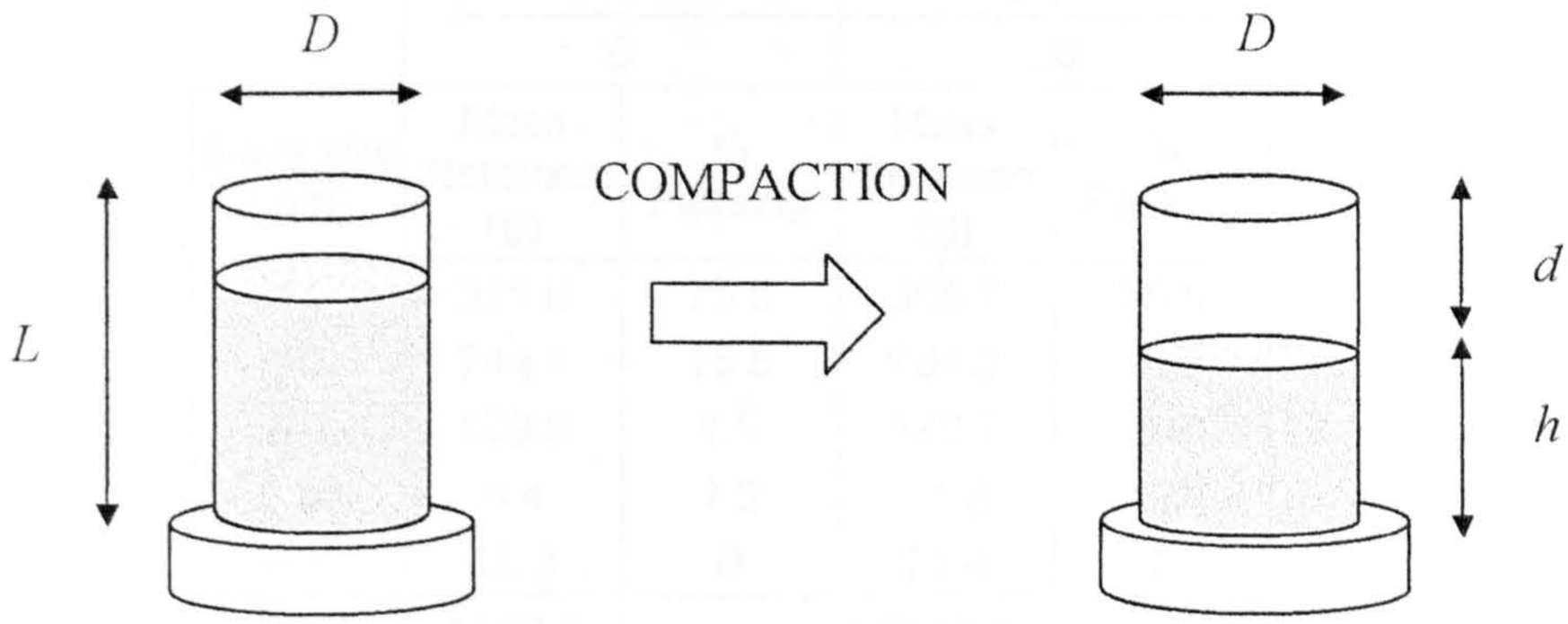

Figure B.1. Determination of dry compacted density of aggregate blends

D = 100 mm

L = 132.5 mm

d = depth after compaction (mm)

h = height after compaction = 132.5 – d (mm)

$$V = \pi\left(\frac{D}{2}\right)^2 \times h = 7.854 \times (132.5 - d) \qquad (\text{cm}^3)$$

APPENDIX C. Sieve analysis results after different compaction times

	Compaction time (sec)			
	0		20	
Sieve size (mm)	Mass Retained (g)	% Passing	Mass Retained (g)	% Passing
14	311.8	75.0	305.7	75.5
10	744.1	15.5	734.2	16.5
6.3	169.8	1.9	172.7	2.6
2.36	8.4	1.2	11.3	1.7
Pan	15.2	0	21.4	0
Total	1249.3		1245.3	

Table C.1. Sample 1 (14/10 mm)

	Compaction time (sec)					
	0		120		300	
Sieve size (mm)	Mass Retained (g)	% Passing	Mass Retained (g)	% Passing	Mass Retained (g)	% Passing
14	311	75.1	266.8	78.6	259.5	79.1
10	750.4	15.0	756.4	17.9	734.3	20.0
6.3	165.5	1.7	176.7	3.7	187.9	4.2
2.36	8.1	1.0	22.4	1.9	30.2	2.4
Pan	13.7	0	23.8	0	30.8	0
Total	1248.7		1246.1		1242.7	

Table C.2. Sample 2 (14/10 mm)

	Compaction time (sec)					
	120		240		420	
Sieve size (mm)	Mass Retained (g)	% Passing	Mass Retained (g)	% Passing	Mass Retained (g)	% Passing
14	390.2	68.7	348.2	72.1	287.8	76.9
10	661.3	15.7	658.5	19.2	693.1	21.2
6.3	150.8	3.6	176.5	5.0	177.8	6.9
2.36	14.8	2.4	23.5	3.1	32.7	4.3
Pan	30.2	0	39.4	0	53.2	0
Total	1247.3		1246.1		1244.6	

Table C.3. Sample 3 (14/10 mm)

APPENDIX D. Void measurements for different aggregate blends

Blend proportions (%)		Depth (mm)	Height (mm)	Volume (cm^3)	Density (g/cm^3)	SGMA	VMA (%)
14 mm	10 mm						
100	0	32.4	100.1	786.2	1.590	2.710	41.3
80	20	36.1	96.4	756.9	1.652	2.710	39.1
60	40	36.6	95.9	753.5	1.659	2.710	38.8
40	60	37.7	94.8	744.8	1.678	2.710	38.1
20	80	36.7	95.8	752.4	1.661	2.710	38.7
0	100	36.1	96.4	757.4	1.650	2.710	39.1

Table D.1. 10 mm added to 14 mm aggregate sizes

Blend proportions (%)		Depth (mm)	Height (mm)	Volume (cm^3)	Density (g/cm^3)	SGMA	VMA (%)
14/10 mm	6 mm						
100	0	37.7	94.8	744.8	1.678	2.710	38.1
80	20	38.3	94.2	740.1	1.689	2.710	37.7
60	40	40.3	92.2	724.4	1.726	2.710	36.3
55	45	39.9	92.6	727.5	1.718	2.710	36.6
40	60	40.3	92.2	723.9	1.727	2.710	36.3
20	80	38.0	94.5	742.2	1.684	2.710	37.9
0	100	36.5	96.0	754.2	1.657	2.710	38.8

Table D.2. 6 mm added to 14/10 mm aggregate sizes

Blend proportions (%)		Depth (mm)	Height (mm)	Volume (cm^3)	Density (g/cm^3)	SGMA	VMA (%)
14/10/6mm	3 mm						
100	0	39.9	92.6	727.5	1.718	2.710	36.6
80	20	53.2	79.3	622.8	2.007	2.706	25.8
70	30	56.2	76.3	599.3	2.086	2.704	22.9
60	40	56.5	76.0	596.9	2.094	2.702	22.5
50	50	59.2	73.3	576.0	2.170	2.700	19.6
40	60	59.5	73.0	573.1	2.181	2.698	19.2
30	70	59.5	73.0	573.1	2.181	2.696	19.1
20	80	57.2	75.3	591.4	2.114	2.694	21.5
0	100	54.4	78.1	613.7	2.037	2.690	24.3

Table D.3. 3 mm added to 14/10/6 mm aggregate sizes

Blend proportions (%)		Depth (mm)	Height (mm)	Volume (cm^3)	Density (g/cm^3)	SGMA	VMA (%)
Blend 1	Filler						
100	0	56.2	76.3	599.3	2.086	2.704	22.9
98	2	58.8	73.7	578.8	2.159	2.704	20.1
96	4	58.5	74.1	581.6	2.149	2.705	20.5
94	6	58.3	74.2	583.0	2.144	2.705	20.7

Table D.4. Blend 1 (70/30)

Blend proportions (%)		Depth (mm)	Height (mm)	Volume (cm^3)	Density (g/cm^3)	SGMA	VMA (%)
Blend 2	Filler						
100	0	56.5	76.0	596.9	2.094	2.702	22.5
98	2	58.9	73.6	578.3	2.161	2.702	20.0
96	4	59.3	73.2	575.2	2.173	2.703	19.6
94	6	59.1	73.4	576.7	2.167	2.703	19.8

Table D.5. Blend 2 (60/40)

Blend proportions (%)		Depth (mm)	Height (mm)	Volume (cm^3)	Density (g/cm^3)	SGMA	VMA (%)
Blend 3	Filler						
100	0	59.2	73.3	576.0	2.170	2.700	19.6
98	2	59.1	73.4	576.7	2.167	2.700	19.2
96	4	61.0	71.5	561.6	2.226	2.701	17.6
94	6	61.3	71.2	558.9	2.236	2.701	17.2

Table D.6. Blend 3 (50/50)

Blend proportions (%)		Depth (mm)	Height (mm)	Volume (cm^3)	Density (g/cm^3)	SGMA	VMA (%)
Blend 4	Filler						
100	0	59.5	73.0	573.1	2.181	2.698	19.2
98	2	61.3	71.2	558.9	2.236	2.698	17.1
96	4	61.7	70.8	555.8	2.249	2.699	16.7
94	6	62.7	69.8	548.5	2.279	2.700	15.6

Table D.7. Blend 4 (40/60)

APPENDIX E. Equations used in the calculation of theoretical void contents

The information provided here is based on a conceptualisation by Khalid (2000) of an aggregate packing model which depends on the dominant aggregate size defining the void structure that is changed by the addition of another aggregate size.

1. Coarse side of voidage profile:

The assumption made here is that the addition of fine aggregates will lead to filling of the voids created by the coarse aggregates. As the fine aggregate content increases, the volume will begin to decrease, as more fine aggregates will replace coarse aggregates. The following equations are used to calculate the theoretical voids at the coarse side end of the pessimum.

The theoretical voids, VMA_{ca}, are obtained as follows,

$$VMA_{ca} = \left[1 - \frac{\text{Total volume excluding voids}}{\text{Bulk volume including voids}}\right] \text{x}100 \qquad \text{(E.1)}$$

The total volume of the aggregate blend excluding voids is given by the volume of solids, thus, the volume of coarse aggregate plus the volume of fine aggregate.

Therefore,

$$\text{Total volume excluding voids} = \frac{\frac{P_{ca}}{SG_{ca}} + \frac{P_{fa}}{SG_{fa}}}{100} \qquad \text{(E.2)}$$

where,

$$\text{Vol.of coarse aggregate} = \frac{\frac{P_{ca}}{SG_{ca}}}{100}$$

$$\text{Vol. of fine aggregate} = \frac{\frac{P_{fa}}{SG_{fa}}}{100}$$

and:

P_{ca} = % by weight of the total blend of coarse aggregate

P_{fa} = % by weight of the total blend of fine aggregate

SG_{ca} = Specific gravity of coarse aggregate

SG_{fa} = Specific gravity of fine aggregate

The bulk volume of the aggregate blend including voids is given by the volume of solids plus the volume of voids. Assuming that fine aggregate fills the voids in the coarse aggregate, thus,

$$\text{Bulk volume of coarse aggregate including voids} = \frac{\frac{P_{ca}}{\rho_{ca}}}{100} \qquad \text{(E.3)}$$

where ρ_{ca} is obtained from coarse aggregate void measurement, as follows,

$$VMA^{*}_{ca}(\%) = \left[1 - \frac{\rho_{ca}}{SG_{ca}}\right] \times 100$$

where:

VMA^{*}_{ca} = measured voids in coarse aggregate (%)

Substituting (E.2) and (E.3) in (E.1),

$$VMA_{ca}(\%) = \left[1 - \frac{\frac{P_{ca}}{SG_{ca}} + \frac{P_{fa}}{SG_{fa}}}{\frac{P_{ca}}{\rho_{ca}}}\right] \times 100 \qquad \text{(E.4)}$$

Finally,

$$VMA_{ca}(\%) = \left[1 - \frac{\frac{100}{P_{ca}/\rho_{ca}}}{SGMA}\right] \times 100 \qquad \text{(E.5)}$$

where,

$$SGMA = \frac{100}{\frac{P_{ca}}{SG_{ca}} + \frac{P_{fa}}{SG_{fa}}}$$

2. Fine side of voidage profile:

The assumption made here is that the addition of coarse aggregate initially leads to discrete particles increasing the bulk volume of the fine aggregates, but as there is no interlock, the packing results in increase in density. This continues to occur until coarse aggregate interlock happens at high stone content, which leads to creation of voidage. However, it is theoretically envisaged that this feature does not happen before the two lines from opposite ends intersect. The following equations are used to calculate the theoretical voids at the fine side end of the pessimum.

The theoretical voids, VMA_{fa}, are obtained as follows,

$$VMA_{fa} = \left[1 - \frac{\text{Total volume of blend excluding voids}}{\text{Bulk volume of blend including voids}}\right] \text{x}100 \qquad \text{(E.6)}$$

$$\text{Bulk volume of blend including voids} = \frac{\frac{P_{ca}}{SG_{ca}} + \frac{P_{fa}}{\rho_{fa}}}{100} \qquad \text{(E.7)}$$

where ρ_{fa} is obtained from fine aggregate void measurement, as follows,

$$VMA^{*}_{fa}(\%) = \left[1 - \frac{\rho_{fa}}{SG_{fa}}\right] \times 100$$

where:

VMA^{*}_{fa} = measured voids in fine aggregate (%)

Substituting (E.2) and (E.7) in (E.6),

$$VMA_{fa}(\%) = \left[1 - \frac{\frac{P_{ca}}{SG_{ca}} + \frac{P_{fa}}{SG_{fa}}}{\frac{P_{ca}}{SG_{ca}} + \frac{P_{fa}}{\rho_{ca}}}\right] \times 100 \qquad \text{(E.8)}$$

Finally,

$$VMA_{fa}(\%) = \left[1 - \frac{\frac{100}{P_{fa}/\rho_{fa} + P_{ca}/SG_{ca}}}{SGMA}\right] \times 100 \qquad \text{(E.9)}$$

The theoretical voidage profile for a blend of fine aggregate, 3 mm to dust, within a blend of coarse aggregate, 14, 10 and 6 mm defined in section 5.2.5, can be calculated from the above equations knowing the voids in the coarse and fine aggregate blends, thus,

$SG_{ca} = 2.710$, $VMA^{*}_{ca} = 36.5$ (measured voids in coarse aggregate), thus,

$\rho_{ca} = 1.721$

$SG_{fa} = 2.696$, $VMA^{*}_{fa} = 24.2$ (measured voids in fine aggregate), thus,

$\rho_{fa} = 2.044$

The theoretical voids are presented in the Table below,

P_{ca}	P_{fa}	$SGMA$	VMA_{ca}	VMA_{fa}
100	0	2.710	36.5	0.0
95	5	2.709	33.1	1.6
90	10	2.709	29.4	3.1
85	15	2.708	25.2	4.6
80	20	2.707	20.5	6.0
75	25	2.707	15.2	7.4
70	30	2.706	9.1	8.8
65	35	2.705	2.1	10.1
60	40	2.704	-6.1	11.4
55	45	2.704	-15.7	12.6
50	50	2.703	-27.3	13.8
45	55	2.702	-41.5	15.0
40	60	2.702	-59.2	16.1
35	65	2.701	-82.0	17.2
30	70	2.700	-112.4	18.3
25	75	2.700	-155.0	19.3
20	80	2.699	-218.8	20.4
15	85	2.698	-325.2	21.4
10	90	2.697	-538.0	22.3
5	95	2.697	-1176.3	23.3
0	100	2.696	-	24.2

Table E.1. Theoretical void contents in dry aggregate blends

APPENDIX F. Sieve analysis results

Sieve size (mm)	Mass Retained (g)	% Retained	Mass Passing (g)	% Passing
14	37	1.2	3026	98.8
10	466	15.2	2560	83.6
6.3	742	24.2	1818	59.4
2.36	968	31.6	850	27.8
1.18	241	7.9	609	19.9
0.3	290	9.5	319	10.4
0.075	168	5.5	151	4.9
Pan	151	4.9	0	0
Total	3063	100		

Table F.1. Blend 1

Sieve size (mm)	Mass Retained (g)	% Retained	Mass Passing (g)	% Passing
14	36	1.2	3024	98.8
10	372	12.2	2652	86.7
6.3	664	21.7	1988	65.0
2.36	913	29.8	1075	35.1
1.18	325	10.6	750	24.5
0.3	384	12.5	366	12.0
0.075	210	6.9	156	5.1
Pan	156	5.1	0	0
Total	3060	100		

Table F.2. Blend 2

Sieve size (mm)	Mass Retained (g)	% Retained	Mass Passing (g)	% Passing
14	28	0.9	3028	99.1
10	320	10.5	2708	88.6
6.3	586	19.2	2122	69.4
2.36	851	27.8	1271	41.6
1.18	400	13.1	871	28.5
0.3	464	15.2	407	13.3
0.075	243	8.0	164	5.4
Pan	164	5.4	0	0
Total	3056	100		

Table F.3. Blend 3

Sieve size (mm)	Mass Retained (g)	% Retained	Mass Passing (g)	% Passing
14	16	0.5	3042	99.5
10	283	9.3	2759	90.2
6.3	421	13.8	2338	76.5
2.36	809	26.5	1529	50.0
1.18	478	15.6	1051	34.4
0.3	573	18.7	478	15.6
0.075	308	10.1	170	5.6
Pan	170	5.6	0	0
Total	3058	100		

Table F.4. Blend 4

APPENDIX G. Preparation of mix specimens

The method for preparing cylindrical specimens from slabs made in the laboratory is presented here.

- For each binder content selected one slab of dimensions 306 x 306 x 64 mm^3 was manufactured.

- The aggregate proportions used are presented in **Table G.1.**

	% Aggregate	
Size (mm)	Blend 1	Blend 2
14	15.1	12.9
10	22.6	19.4
6	30.9	26.5
3	29.4	39.2
Filler	2	2

Table G.1. Aggregate proportions

- The binder quantities presented in **Table G.2** were mixed with 13,284 g of aggregates for blend 1 and with 13,260 g of aggregates for blend 2, proportioned in accordance to **Table G.1**.

Binder content (%)	Binder quantity (g)	
	Blend 1	Blend 2
4.5	/	625
4.8	/	669
5	699	698
5.5	773	772
5.8	/	816
6	848	846

Table G.2. Binder quantities incorporated into mixtures

- Mixing temperatures employed were 155 ^{0}C for the conventional mixes, and 180 ^{0}C for the two crumb-rubber modified mixes, CRM mix 1 and CRM mix 2.

- After mixing, the aggregate-binder mix was poured into heated steel moulds and was compacted under the roller compactor. The compactor applied 20 passes at each four different pressure levels until the mix was compacted to the required thickness.

- The moulds were allowed to cool overnight before the slab was extruded from the mould.

- Finally, five cylindrical specimens were cored from each slab using a diamond tip cored cutter. The finished specimens had a diameter of 99 mm and a height of 64 ± 1 mm.

APPENDIX G

APPENDIX H. Determination of volumetric parameters

The Compacted Density of the Mix (*CDM*) can be calculated as follows,

$$CDM = \frac{Weight_{AIR}}{Weight_{AIR} - Weight_{WATER}} \tag{H.1}$$

and the Compacted Density of Mixed Aggregate (*CDMA*) is given by,

$$CDMA = \frac{CDM(100-b)}{100} \tag{H.2}$$

where b is the % by weight of bitumen of the total mix.

The theoretical Specific Gravity of Mix (*SGM*) is obtained as follows.

$$SGM = \frac{100}{\frac{P_{coarse}}{SG_{coarse}} + \frac{P_{fine}}{SG_{fine}} + \frac{P_{filler}}{SG_{filler}} + \frac{P_{binder}}{SG_{binder}}} \tag{H.3}$$

where:

$P_{coarse}, P_{fine}, P_{filler}, P_{binder}$ = % by weight of the total mix of each constituent

$SG_{coarse}, SG_{fine}, SG_{filler}, SG_{binder}$ = specific gravity of each constituent

Theoretical Voids in Mix (*VIM*),

$$VIM = \frac{SGM - CDM}{SGM} \times 100 \tag{H.4}$$

and, Voids in Mixed Aggregate (*VMA*),

$$VMA = \frac{SGMA - CDMA}{SGMA} \times 100 \tag{H.5}$$

APPENDIX I. Average and standard deviation values for the measured properties in Chapter 5

Binder Content (%)	CDM (g/ml)		VMA (%)		VIM (%)		ITSM (MPa)		Retained ITSM (%)	
	Average	STD	Average	STD	Average	STD	Average	STD	Average	STD
5	2.335	0.006	18.0	0.22	6.6	0.25	1214	92.0	/	/
5.5	2.370	0.010	17.2	0.33	4.5	0.38	960	58.3	/	/
6	2.387	0.008	17.0	0.29	3.1	0.33	688	51.0	/	/

Table I.1. Blend 1

Binder Content (%)	CDM (g/ml)		VMA (%)		VIM (%)		ITSM (MPa)		Retained ITSM (%)	
	Average	STD	Average	STD	Average	STD	Average	STD	Average	STD
4.5	2.352	0.009	16.9	0.33	6.6	0.38	1525	148.5	74	16.7
4.8	2.365	0.006	16.7	0.20	5.7	0.22	1417	229.0	105	20.6
5	2.381	0.010	16.3	0.37	4.7	0.42	1308	147.5	97	19.1
5.5	2.396	0.007	16.2	0.24	3.4	0.28	820	113.2	/	/

Table I.2. Control mix (Blend 2)

Binder Content (%)	CDM (g/ml)		VMA (%)		VIM (%)		ITSM (MPa)		Retained ITSM (%)	
	Average	STD	Average	STD	Average	STD	Average	STD	Average	STD
5	2.341	0.005	17.7	0.17	6.3	0.20	2121	121.4	/	/
5.5	2.375	0.005	16.9	0.17	4.2	0.20	2075	67.8	105	13.8
5.8	2.383	0.002	16.9	0.07	3.5	0.08	1859	147.5	111	6.9
6	2.388	0.005	16.9	0.17	3.0	0.20	1843	124.4	117	14.3

Table I.3. CRM mix 1 (Blend 2)

Binder Content (%)	CDM (g/ml)		VMA (%)		VIM (%)		ITSM (MPa)		Retained ITSM (%)	
	Average	STD	Average	STD	Average	STD	Average	STD	Average	STD
5	2.331	0.009	18.1	0.30	6.7	0.34	1940	103.1	/	/
5.5	2.366	0.004	17.3	0.15	4.6	0.17	1936	96.7	82	23.3
5.8	2.382	0.007	17.0	0.23	3.6	0.27	1808	254.5	115	13.1
6	2.387	0.011	17.0	0.39	3.1	0.46	1783	165.8	105	15.4

Table I.4. CRM mix 2 (Blend 2)

APPENDIX J. The ITSM test

Cooper and Brown (1989) developed the Indirect Tensile Stiffness Modulus (ITSM) test method adopted in the UK, which is carried out in the Nottingham Asphalt Tester (NAT). The test is currently under development to be adopted as a British Standard (BSI, 1993).

In this test the specimens are subjected to a transient load pulse across their vertical diametral axis and the resultant transient deformations along the horizontal diametral axis are measured. The deformation in the horizontal direction is measured by Linear Variable Differential transducers (LVDTs).

The relationship used to calculate the stiffness (Schmidt, 1972) is as follows:

$$E = \frac{P}{\Delta h \cdot t} \times (0.273 + \nu)$$

where:

E	=	Stiffness modulus of the material (N/mm^2)
P	=	Peak vertical load (N)
Δh	=	Peak transient deformation along the horizontal diametral axis
t	=	Specimen thickness (mm)
ν	=	Poisson's ratio (assumed to be 0.35)

The ITSM test is controlled by a computer. Typical requirements and tests conditions include the specimen diameter and thickness along with the "Rise time" and the "Target deformation". The "Rise time" is the time taken for the applied load to reach its maximum value. The "Target deformation" is defined as the horizontal deformation produced by the peak load. Standard values 124 ms and 0.005% of the specimen diameter were used throughout this study.

After the target deformation and the rise-time have been selected, the force applied to the specimen is then automatically calculated by the computer and a

number of conditioning pulses are applied to the specimen. Once the conditioning pulses are complete the system applies five load pulses and the mean stiffness value is recorded as the test result.

The British Standard (BSI, 1993) required the test to be carried out in two orthogonal orientations and allows a repeatability difference of +10 % or –20 % between the mean of the second test and the first. If this condition is met then the mean of the two tests is recorded as the stiffness modulus of the specimen.

Temperature control is essential in the ITSM test. Brown and Cooper (1994) reported a 10 % difference in stiffness modulus resulting from 1 ^{0}C change in temperature. The standard test temperature of 20 ^{0}C was selected for the ITSM test. To ensure that the test specimens were at the right temperature, a period of four hours inside the temperature-controlled cabinet was allowed before testing.

APPENDIX J

APPENDIX K. The sand patch test

In the sand patch test a known volume of sand is spread onto the road surface to form a circular patch so that the depressions are filled to the level of the peaks. The texture depth is determined by dividing the volume of sand by the area of the patch.

Sand patch tests were carried out on slabs made in the laboratory. The volume of sand used was 20 ml, instead of 50 ml as recommended by BS 598: Part 105 (BSI, 1990d). This volume was used to accommodate for the dimensions of the slab.

For this fixed volume of sand, the texture depth of the surface was determined as follows:

$$T_d = \frac{25465}{D^2}$$

where:

T_d = texture depth (mm)

D = diameter of the patch (mm) (average of 4 determinations)

APPENDIX L. Fatigue specimens

Sample	Binder content (%)	SGM	SGMA	CDM (gm/ml)	CDMA (gm/ml)	VMA (%)	VIM (%)
C1	4.8	2.507	2.702	2.357	2.244	16.94	5.96
C2	4.8	2.507	2.702	2.370	2.256	16.51	5.46
C3	4.8	2.507	2.702	2.356	2.243	17.00	6.02
C4	4.8	2.507	2.702	2.357	2.244	16.94	5.96
C5	4.8	2.507	2.702	2.358	2.245	16.91	5.92
C6	4.8	2.507	2.702	2.363	2.249	16.75	5.74
C7	4.8	2.507	2.702	2.368	2.255	16.56	5.52
C8	4.8	2.507	2.702	2.368	2.255	16.56	5.52
C9	4.8	2.507	2.702	2.365	2.252	16.67	5.65
C10	4.8	2.507	2.702	2.381	2.267	16.11	5.01
C11	4.8	2.507	2.702	2.367	2.253	16.61	5.58
C12	4.8	2.507	2.702	2.375	2.261	16.32	5.25
C13	4.8	2.507	2.702	2.383	2.269	16.03	4.92
C14	4.8	2.507	2.702	2.386	2.271	15.95	4.83
C15	4.8	2.507	2.702	2.383	2.269	16.02	4.91
C16	4.8	2.507	2.702	2.394	2.279	15.66	4.50
C17	4.8	2.507	2.702	2.394	2.279	15.65	4.50
C18	4.8	2.507	2.702	2.395	2.280	15.61	4.44
C19	4.8	2.507	2.702	2.395	2.280	15.63	4.47
C20	4.8	2.507	2.702	2.394	2.279	15.66	4.51
Average	**4.8**	**2.507**	**2.702**	**2.375**	**2.261**	**16.30**	**5.23**

Table L.1. Control mix

Sample	Binder content (%)	SGM	SGMA	CDM (gm/ml)	CDMA (gm/ml)	VMA (%)	VIM (%)
RT1	5.8	2.469	2.702	2.393	2.254	16.58	3.10
RT2	5.8	2.469	2.702	2.388	2.249	16.76	3.32
RT3	5.8	2.469	2.702	2.397	2.258	16.43	2.93
RT4	5.8	2.469	2.702	2.398	2.259	16.38	2.88
RT5	5.8	2.469	2.702	2.400	2.261	16.33	2.82
RT6	5.8	2.469	2.702	2.388	2.249	16.76	3.31
RT7	5.8	2.469	2.702	2.388	2.249	16.76	3.31
RT8	5.8	2.469	2.702	2.391	2.253	16.63	3.16
RT9	5.8	2.469	2.702	2.386	2.247	16.83	3.40
RT10	5.8	2.469	2.702	2.391	2.252	16.65	3.19
RT11	5.8	2.469	2.702	2.386	2.247	16.82	3.39
RT12	5.8	2.469	2.702	2.383	2.245	16.90	3.48
RT13	5.8	2.469	2.702	2.385	2.247	16.84	3.41
RT14	5.8	2.469	2.702	2.395	2.256	16.52	3.03
RT15	5.8	2.469	2.702	2.397	2.258	16.43	2.93
RT16	5.8	2.469	2.702	2.369	2.232	17.39	4.05
RT17	5.8	2.469	2.702	2.368	2.231	17.45	4.11
RT18	5.8	2.469	2.702	2.371	2.233	17.35	4.00
RT19	5.8	2.469	2.702	2.365	2.228	17.55	4.23
RT20	5.8	2.469	2.702	2.377	2.239	17.14	3.76
Average	**5.8**	**2.469**	**2.702**	**2.386**	**2.247**	**16.83**	**3.39**

Table L.2. CRM mix 1

Sample	Binder content (%)	SGM	SGMA	CDM (gm/ml)	CDMA (gm/ml)	VMA (%)	VIM (%)
RC1	5.8	2.469	2.702	2.370	2.233	17.36	4.01
RC2	5.8	2.469	2.702	2.367	2.230	17.48	4.15
RC3	5.8	2.469	2.702	2.362	2.225	17.64	4.34
RC4	5.8	2.469	2.702	2.372	2.234	17.32	3.96
RC5	5.8	2.469	2.702	2.375	2.237	17.21	3.84
RC6	5.8	2.469	2.702	2.374	2.237	17.22	3.85
RC7	5.8	2.469	2.702	2.364	2.227	17.57	4.26
RC8	5.8	2.469	2.702	2.363	2.225	17.64	4.33
RC9	5.8	2.469	2.702	2.364	2.227	17.60	4.29
RC10	5.8	2.469	2.702	2.369	2.231	17.42	4.08
RC11	5.8	2.469	2.702	2.381	2.242	17.01	3.60
RC12	5.8	2.469	2.702	2.377	2.239	17.14	3.75
RC13	5.8	2.469	2.702	2.375	2.237	17.21	3.84
RC14	5.8	2.469	2.702	2.381	2.243	16.98	3.57
RC15	5.8	2.469	2.702	2.387	2.249	16.78	3.34
RC16	5.8	2.469	2.702	2.398	2.259	16.39	2.89
RC17	5.8	2.469	2.702	2.396	2.257	16.49	3.00
RC18	5.8	2.469	2.702	2.404	2.264	16.19	2.66
RC19	5.8	2.469	2.702	2.398	2.259	16.38	2.88
RC20	5.8	2.469	2.702	2.400	2.260	16.34	2.83
Average	**5.8**	**2.469**	**2.702**	**2.379**	**2.241**	**17.07**	**3.67**

Table L.3. CRM mix 2

APPENDIX M. PVC fatigue data file

Specimen = PVC

Temperature = 10 ^{0}C

Frequency = 10 Hz

Microstrain = 300

Cycle No.	Stress amp kPa	Stress mean kPa	Strain amp mm/mm	Strain mean mm/mm	Percent Stiffness	Stiffness (kPa)	Phase angle	Hyst Loop Area	Cumulative hyst loop area
50	1090.2	-66.1	0.000297	-0.000047	100			0.022031	0.872055
100	1099.4	-36.1	0.000298	-0.000041	100	3684445	1.65	0.022611	1.770938
150	1100.1	6.9	0.0003	-0.00003	99.6	3671471	1.61	0.022824	3.130094
200	1099.4	26.5	0.0003	-0.000025	99.4	3661626	1.65	0.022814	4.038432
250	1096.3	53.9	0.000299	-0.000018	99.4	3662646	1.67	0.022528	5.39112
300	1097.8	69.8	0.0003	-0.000014	99.2	3656399	1.7	0.022678	6.295945
350	1100.2	65.4	0.000299	-0.000015	99.9	3679519	1.59	0.022559	7.653026
400	1095.3	98.3	0.000299	-0.000006	99.4	3663250	1.77	0.022833	8.566988
450	1100.1	107.5	0.0003	-0.000004	99.6	3667983	1.5	0.022807	9.944701
500	1122.6	89.5	0.000299	-0.000012	101.8	3750463	1.44	0.023027	10.862534
550	1097.2	107.3	0.0003	-0.000004	99.2	3654570	1.6	0.022903	12.241074
600	1100.8	94.1	0.000299	-0.000008	99.8	3677588	1.7	0.022898	13.15291
650	1097.1	116.4	0.000299	-0.000003	99.7	3672786	1.6	0.022755	14.524428
700	1094.3	121.2	0.000298	-0.000001	99.6	3671123	1.81	0.02308	15.445362
750	1101.4	124.7	0.0003	0	99.7	3672167	1.66	0.022982	16.827988
800	1105.5	132.4	0.000301	0.000002	99.6	3670773	1.84	0.023188	17.753785
850	1096.5	126	0.0003	-0.000001	99.1	3652217	1.68	0.022958	19.13719
900	1099.4	128.7	0.0003	0.000001	99.6	3669375	1.73	0.02298	20.059042
950	1094.8	132.6	0.000299	0.000001	99.5	3665168	1.75	0.023066	21.437847
1000	1101.2	130	0.0003	0.000001	99.6	3667898	1.67	0.02288	22.354171
1050	1099.6	126.7	0.0003	-0.000001	99.4	3662410	1.65	0.022821	23.732536
1100	1101.2	123.9	0.000301	-0.000002	99.2	3656704	1.57	0.023122	24.655237
1132	1099.7	120.2	0.0003	-0.000003	99.6	3670161	1.64	0.022986	25.570507

APPENDIX N. File reduction macro

```
Sub Macro1()
'
' Macro1 Macro
' Macro recorded 01/05/2002 by ignacio
'
' Keyboard Shortcut: Ctrl+a
'
    name_initial_sheet = "     "
    number_rows = 10
    first_row = 12

    name_reduced_sheet = name_initial_sheet & "_reduced"


    Sheets("Sheet1").Select
    Sheets("Sheet1").Name = name_reduced_sheet


    Sheets(name_initial_sheet).Select
    Range("B1").Select
    ActiveCell.FormulaR1C1 = "=INT((COUNT(C[-1])-3)/" & number_rows &
")"


    n_iteration = ActiveCell

   For i = 0 To n_iteration
    Sheets(name_initial_sheet).Select
    Rows(first_row + i * number_rows & ":" & first_row + i *
number_rows).Select
    Selection.Copy
    Sheets(name_reduced_sheet).Select
    Range("A" & i + 1).Select
    ActiveSheet.Paste
   Next
'
End Sub
```

APPENDIX O. Reduced fatigue data file

Specimen = C6 (Control mix)

Stress = 3000 kPa (peak-to-peak)

Cycle No.	Stress amp (MPa)	Stress mean (MPa)	Strain amp (με)	Strain mean (με)	Stiff (%)	Stiff (MPa)	Phase angle (^{0})	Hyst Area (J/m^3)	Cumulative area (J/m^3)	Energy Ratio
50	1.58725	0.0083	169.5	-10	100			344.801	16279.086	47.21299
100	1.4949	0.0209	161	-9.5	100	9275.7	21.2	310.675	28787.344	92.66064
150	1.49745	0.032	162	-6.5	99.5	9230.1	21.51	315.371	47618.268	150.9913
200	1.4954	0.03405	163	-6	98.8	9165.4	21.4	319.262	60336.446	188.9872
250	1.4982	0.0374	164.5	-3.5	98.2	9105.5	21.72	323.325	79751.696	246.6611
300	1.4949	0.03815	164.5	-1.5	98	9093.8	21.53	324.203	92703.312	285.9422
350	1.49815	0.03175	165.5	-8	97.7	9062.7	21.83	327.085	112274.1	343.2566
400	1.4973	0.04115	166	-1.5	97.4	9032.3	21.8	327.724	125399.69	382.6381
450	1.49645	0.03935	166.5	1.5	96.9	8985.7	21.88	329.476	145171.82	440.6142
500	1.49955	0.0378	167	3	96.9	8987.6	21.73	332.346	158555.71	477.0802
1000	1.4984	0.0386	172	1	94.1	8724.0	21.91	344.632	327979.73	951.681
1500	1.50335	0.03235	175	-3	92.7	8599.2	22.29	355.11	503742.27	1418.553
2000	1.5022	0.03965	177	0	91.6	8495.7	22.48	362.113	682851.65	1885.742
2500	1.4977	0.0412	178.5	1.5	90.5	8397.4	22.63	366.896	865073.64	2357.817
3000	1.49975	0.0408	180	1.5	89.8	8330.0	22.67	373.626	1050211.4	2810.863
3500	1.49715	0.0391	181.5	-0.5	88.8	8238.3	22.79	378.916	1238142.9	3267.592
4000	1.4947	0.04005	181.5	2.5	88.8	8238.7	22.84	379.673	1427305	3759.301
4500	1.49905	0.0386	182.5	-1.5	88.5	8207.1	22.94	382.193	1618333.7	4234.336
5000	1.50105	0.0403	183.5	0	88.1	8169.9	23.1	389.045	1811266.3	4655.673
5500	1.49945	0.04375	185	2	87.5	8113.8	23.1	390.679	2005805	5134.151
6000	1.4995	0.0425	185	0.5	87.3	8100.6	23.33	393.532	2201772.7	5594.901
6500	1.5016	0.0375	185.5	-3.5	87.3	8098.7	23.35	394.216	2398838.3	6085.086
7000	1.4988	0.04335	186	1.5	86.9	8063.5	23.47	395.372	2596692.7	6567.72
7500	1.4967	0.03465	184.5	-4	87.4	8105.6	23.36	394.155	2795106.2	7091.388
8000	1.49695	0.0425	184	-1	87.6	8127.4	23.45	392.946	2993298.7	7617.583
8500	1.49885	0.04035	185	-4.5	87.4	8103.9	23.44	395.256	3191179.8	8073.704
9000	1.4993	0.042	186	0	86.8	8052.8	23.62	397.887	3390219.2	8520.558
9500	1.4992	0.04475	186.5	1	86.7	8039.1	23.68	400.504	3590171.6	8964.134
10000	1.49825	0.03275	186	-5	86.8	8047.3	23.55	400.267	3790719.6	9470.477
10500	1.4982	0.0414	187.5	-0.5	86.1	7987.8	23.65	402.727	3992674.7	9914.097
11000	1.5002	0.04095	188	0.5	86	7978.7	23.69	406.346	4195147.7	10324.08
11500	1.50045	0.0309	187.5	-5.5	86.4	8012.9	23.58	404.292	4398213	10878.8
12000	1.50105	0.04	188.5	2	85.9	7963.8	23.7	406.202	4601114.7	11327.16
12500	1.4985	0.03325	187.5	-4	86.2	7995.8	23.53	405.065	4804325.9	11860.63
13000	1.50055	0.03825	188.5	0.5	85.9	7967.6	23.62	408.351	5008003.5	12263.97
13500	1.5014	0.04095	189.5	1.5	85.5	7933.2	23.72	409.633	5212241.7	12724.17
14000	1.4768	0.04195	185.5	0	85.9	7964.8	23.61	394.616	5415500.6	13723.47
14500	1.4988	0.0433	189	1.5	85.5	7926.1	23.71	407.73	5619492.4	13782.39
15000	1.49935	0.0411	189	1.5	85.6	7941.7	23.89	408.428	5823651.1	14258.7
15500	1.4996	0.042	189	1	85.6	7936.7	23.8	409.459	6027968.5	14721.79
16000	1.4998	0.0421	189	1.5	85.6	7944.2	23.82	408.588	6232037.9	15252.62
16500	1.5022	0.0341	188	-6	86.2	7996.0	23.7	406.826	6435814.3	15819.57
17000	1.501	0.0436	189.5	2.5	85.3	7911.9	23.85	412.63	6640371.5	16092.8
17500	1.50175	0.0435	190.5	3.5	85.1	7890.3	23.9	414.489	6846581.2	16518.13
18000	1.50135	0.04275	191	1	84.6	7850.2	24.01	415.789	7053670.1	16964.54
18500	1.49995	0.04545	191.5	1	84.5	7836.7	24.16	416.21	7261703	17447.21
19000	1.50045	0.04095	192	1.5	84.2	7814.3	24.02	418.459	7470566.6	17852.57
19500	1.49935	0.0361	192	-3.5	84.1	7802.1	23.85	416.24	7679390.5	18449.43
20000	1.5003	0.045	192	0.5	84.2	7813.3	24.05	418.274	7888693.4	18860.11
20500	1.49995	0.04075	192.5	2	84.1	7799.2	23.98	418.432	8098031.9	19353.28
21000	1.49975	0.043	192.5	2	84.1	7798.2	23.96	419.249	8307545.4	19815.3
21500	1.4985	0.0434	193.5	-1	83.4	7736.0	24.2	421.051	8518004.9	20230.34
22000	1.5033	0.0346	191.5	-5.5	84.5	7841.5	24.05	418.561	8727712.9	20851.71
22500	1.5001	0.03555	192.5	-2.5	84.1	7799.8	24.11	421.072	8937966.9	21226.69
23000	1.49975	0.0416	193	2	83.7	7767.2	24.25	423.717	9149501.8	21593.43
23500	1.50045	0.04045	194.5	0	83.1	7709.4	24.05	424.483	9361461.4	22053.8
24000	1.49765	0.0416	194	0.5	83.2	7719.5	24.19	424.003	9573808.7	22579.58
24500	1.49795	0.04045	194	1.5	83.3	7727.1	24.24	425.709	9786994.3	22989.87
25000	1.5001	0.0416	194.5	0.5	83.2	7719.7	24.36	426.618	10000147	23440.52
25500	1.49875	0.0405	195	-0.5	82.8	7682.5	24.2	428.354	10213849	23844.41
26000	1.50815	0.0313	195.5	-7	83.2	7718.5		395.505	10427649	26365.4

26500	1.4982	0.04405	195.5	2.5	82.7	7667.6	24.41	429.255	10641456	24790.52
27000	1.50025	0.04005	195	1.5	82.8	7684.1	24.21	429.907	10856088	25252.18
27500	1.5008	0.0411	195.5	0.5	82.7	7668.9	24.28	430.411	11071004	25721.93
28000	1.4974	0.0416	195.5	1	82.6	7663.5	24.33	431.108	11286305	26179.76
28500	1.49745	0.0409	196.5	1.5	82.2	7628.0	24.43	434.328	11502855	26484.26
29000	1.50125	0.04095	197.5	-0.5	82	7605.7	24.4	435.743	11720551	26897.85
29500	1.50185	0.0393	198	-0.5	81.8	7585.1	24.44	438.287	11938826	27239.74
30000	1.50015	0.03835	198	1.5	81.7	7576.5	24.46	438.67	12157810	27715.16
30500	1.50105	0.037	198.5	-2	81.6	7569.1	24.38	439.259	12377158	28177.36
31000	1.4997	0.03925	199	-0.5	81.3	7544.9	24.44	440.128	12596841	28620.86
31500	1.4992	0.03895	199	0.5	81.2	7530.8	24.64	442.085	12817550	28993.41
32000	1.5012	0.0339	198.5	-6.5	81.5	7558.2	24.56	440.659	13038663	29589.01
32500	1.5001	0.04	200	3	80.9	7500.7	24.67	445.054	13259879	29793.87
33000	1.5003	0.0401	200	1	80.9	7501.5	24.55	445.51	13481719	30261.32
33500	1.4973	0.0314	199	-6.5	81	7515.3	24.4	443.03	13704321	30933.17
34000	1.50015	0.04255	201	0	80.4	7460.8	24.76	446.337	13925710	31199.99
34500	1.49735	0.04095	200.5	-1.5	80.5	7469.7	24.81	445.805	14149447	31739.09
35000	1.49745	0.0407	201.5	1	80.2	7435.9	24.64	447.458	14374268	32124.28
35500	1.4976	0.03535	201	-7.5	80.2	7442.4	24.64	449.002	14599054	32514.45
36000	1.49965	0.03945	202.5	0.5	79.9	7413.0	24.75	452.813	14825014	32739.82
36500	1.5002	0.04145	202.5	2	79.9	7415.7	24.76	451.967	15050966	33301.03
37000	1.49865	0.0397	203	2	79.7	7391.3	24.75	454.217	15277978	33635.86
37500	1.49915	0.03965	203	1.5	79.5	7377.1	24.71	455.793	15505204	34018.08
38000	1.49895	0.03875	203	1	79.6	7387.3	24.72	453.771	15732368	34670.28
38500	1.5	0.03985	203.5	0.5	79.5	7370.0	24.85	455.226	15959646	35058.73
39000	1.50065	0.0397	204	0.5	79.3	7356.7	24.76	456.996	16187555	35421.66
39500	1.4986	0.03955	204	1.5	79.2	7346.4	24.76	457.279	16416333	35900.04
40000	1.4995	0.0349	201.5	0	80.2	7440.4	24.9	452.892	16644028	36750.54
40500	1.4973	0.0378	202	0.5	79.9	7412.7	24.9	451.679	16870461	37350.55
41000	1.4985	0.03735	203	0.5	79.6	7384.9	24.85	454.637	17097178	37606.22
41500	1.50045	0.03885	203.5	0	79.4	7366.6	24.93	457.584	17325279	37862.51
42000	1.50085	0.0404	204.5	2.5	79.1	7340.9	24.96	460.49	17554478	38121.3
42500	1.49805	0.04505	205	3.5	78.9	7316.2	25.01	461.594	17784958	38529.44
43000	1.49975	0.0406	205.5	1	78.7	7302.8	25.01	462.319	18016426	38969.68
43500	1.4986	0.0422	206	0.5	78.5	7280.7	25.1	463.988	18248363	39329.39
44000	1.49935	0.04115	207	2	78.2	7252.1	25.11	465.929	18481554	39666.03
44500	1.5017	0.0404	207	1.5	78.1	7247.2	25.07	468.737	18715259	39926.99
45000	1.49445	0.03475	206	-7.5	78.3	7260.7	24.91	464.828	18949211	40766.07
45500	1.4979	0.04115	208.5	2	77.5	7186.3	25.24	471.28	19184348	40706.9
46000	1.5012	0.0433	208.5	2	77.5	7191.4	25.29	475.129	19420590	40874.35
46500	1.5003	0.03505	208.5	-5	77.7	7203.2	25.06	471.436	19657518	41697.11
47000	1.49935	0.0418	208.5	0.5	77.5	7187.8	25.26	472.985	19894237	42061.03
47500	1.50015	0.03975	209.5	0	77.2	7165.5	25.21	474.47	20131165	42428.74
48000	1.4986	0.04155	210	0	77	7142.4	25.32	477.278	20369103	42677.65
48500	1.4911	0.04255	209.5	2	76.7	7116.9	25.19	473.188	20608139	43551.69
49000	1.4981	0.0386	211	0.5	76.5	7093.2	25.19	481.944	20847924	43257.98
49500	1.4982	0.04175	211	1.5	76.5	7098.8	25.25	481.748	21088373	43774.7
50000	1.49955	0.0405	212	-3	76.3	7079.6	25.25	483.361	21329989	44128.49
50500	1.49845	0.0408	212.5	1	75.9	7043.7	25.54	486.771	21572651	44317.86
51000	1.49975	0.0401	214	0	75.6	7014.4	25.45	490.743	21817328	44457.75
51500	1.49955	0.04265	215	2.5	75.2	6973.5	25.53	493.693	22063452	44690.63
52000	1.49915	0.0433	215	1	75.2	6971.6	25.6	493.585	22310516	45200.96
52500	1.5002	0.04	215	0.5	75.2	6976.4	25.43	493.329	22555928	45721.88
53000	1.49915	0.0386	215.5	-0.5	75	6956.7	25.36	493.522	22798085	46194.67
53500	1.4995	0.03965	216	-0.5	74.9	6948.3	25.32	496.122	23045297	46450.87
54000	1.49875	0.0413	217	2	74.4	6905.5	25.5	498.708	23294114	46708.92
54500	1.4989	0.03575	217	-9	74.5	6911.1	25.31	497.664	23544537	47310.11
55000	1.49875	0.0436	218.5	-0.5	73.9	6857.0	25.57	501.418	23795463	47456.34
55500	1.50115	0.04075	219	3	73.9	6853.6	25.63	505.938	24046399	47528.35
56000	1.49785	0.0408	219	-1	73.7	6833.9	25.57	505.51	24299319	48068.92
56500	1.49895	0.04125	219.5	1	73.6	6824.6	25.61	507.663	24549768	48358.4
57000	1.4974	0.036	220.5	-4.5	73.2	6788.9	25.44	509.986	24804656	48637.91
57500	1.49895	0.04265	221.5	1.5	73	6767.6	25.65	514.419	25061387	48717.85
58000	1.5013	0.0404	222.5	-0.5	72.7	6741.0	25.7	517.124	25318959	48961.1
58500	1.5016	0.0407	224	1	72.3	6705.4	25.75	521.097	25573319	49075.93
59000	1.50175	0.04065	225	0	72	6678.5	25.89	527.581	25834887	48968.57
59500	1.4998	0.041	226	-1	71.5	6629.1	26.07	529.93	26098611	49249.17
60000	1.50065	0.03915	227.5	-1	71.1	6597.0	25.98	533.902	26364569	49380.91
60500	1.49915	0.04245	228	0.5	70.9	6572.8	26.01	535.322	26631935	49749.37
61000	1.499	0.0416	228.5	1.5	70.8	6563.3	26.11	538.83	26900958	49924.76
61500	1.4997	0.0443	229.5	4	70.5	6535.5	26.21	540.069	27170375	50309.08
62000	1.5015	0.04135	231	0.5	70.1	6504.3	26.08	546.077	27441595	50252.25
62500	1.50105	0.0412	232.5	-0.5	69.6	6459.3	26.19	547.661	27712642	50601.82
63000	1.4992	0.04	233	0	69.4	6438.7	26.22	550.768	27987407	50815.24
63500	1.50145	0.0419	234.5	1	69	6401.9	26.31	554.324	28263190	50986.77

64000	1.5031	0.04055	235.5	-4.5	68.8	6383.8	26.34	556.882	28541256	51251.89
64500	1.4971	0.041	236.5	1.5	68.2	6329.6	26.25	558.742	28820626	51581.28
65000	1.49925	0.04135	238	1	68	6305.9	26.22	564.463	29101149	51555.46
65500	1.49895	0.0416	238	-1	68	6304.7	26.14	562.755	29382709	52212.26
66000	1.4994	0.0423	239.5	1	67.5	6262.0	26.32	567.334	29665733	52289.72
66500	1.5049	0.0418	241.5	-5	67.2	6237.0	26.27	571.661	29950757	52392.51
67000	1.49905	0.04045	239.5	0	67.5	6264.6	26.31	569.121	30236647	53128.68
67500	1.49945	0.0422	241.5	-1	66.9	6206.5	26.39	574.124	30522634	53163.84
68000	1.49955	0.0393	243.5	1	66.4	6160.0	26.38	581.278	30811407	53006.32
68500	1.49795	0.0395	245	-0.5	65.9	6111.0	26.64	585.748	31103792	53100.98
69000	1.49845	0.0382	246.5	2	65.5	6075.1	26.46	590.86	31398216	53139.86
69500	1.50005	0.03885	248	1	65.2	6051.3	26.49	591.065	31693985	53621.83
70000	1.50185	0.0415	250.5	-3	64.7	5999.2	26.62	595.996	31992300	53678.72
70500	1.50045	0.0387	251.5	-0.5	64.3	5960.7	26.58	603.791	32292624	53483.12
71000	1.5001	0.03985	253.5	1	63.7	5912.5	26.66	610.958	32596518	53353.12
71500	1.49895	0.03685	256	-1.5	63.2	5858.4	26.64	616.625	32903508	53360.65
72000	1.5021	0.0406	259	2	62.6	5804.4	26.71	626.402	33214118	53023.65
72500	1.49965	0.03885	261.5	-1	61.8	5730.4	26.91	634.322	33529485	52858.78
73000	1.50075	0.0391	264	0	61.3	5687.9	26.88	642.429	33848711	52688.64
73500	1.5027	0.04155	267.5	0	60.6	5617.0	27.02	653.605	34172011	52282.36
74000	1.50195	0.04005	271	3	59.7	5537.9	27.09	664.888	34500540	51889.25
74500	1.5019	0.0396	274.5	0	59	5475.7	27.2	676.82	34834919	51468.51
75000	1.5003	0.0396	278.5	1.5	58.1	5391.3	27.25	687.574	35175611	51159.02
75500	1.49835	0.03995	282.5	1.5	57.1	5299.6	27.28	702.979	35524311	50533.96
76000	1.4971	0.0406	287.5	0	56.1	5204.7	27.42	717.658	35880297	49996.37
76500	1.4997	0.04065	296	1	54.7	5070.5	27.87	748.085	36247442	48453.64
77000	1.50095	0.0438	303	0.5	53.4	4953.8	27.98	772.686	36628072	47403.57
77500	1.499	0.0421	313	0.5	51.6	4789.7	28.17	804.831	37022531	46000.38
78000	1.4992	0.0421	325	0.5	49.7	4611.7	28.39	844.182	37435634	44345.45

APPENDIX P. Fatigue damage parameters

Sample	Type	ε_0 (με)	E_{00} (MPa)	dE^*/dN	a_T	W_{00} (J/m^3)	dW/dN	a_W	a_F (C=1.95)
C1	Strain	153	8738.4	-0.0102	-1.167E-06	287.47	-0.0002	-6.957E-07	1.380E-06
C2	Strain	151.1	8366.8	-0.0082	-9.801E-07	279.52	-0.0002	-7.155E-07	1.112E-06
C3	Strain	150.7	9113.5	-0.0157	-1.723E-06	287.62	-0.0003	-1.043E-06	1.938E-06
C8	Strain	137.5	8454.9	-0.0039	-4.613E-07	238.59	-0.00008	-3.353E-07	5.189E-07
C7	Strain	135.2	8286.7	-0.0062	-7.482E-07	238.22	-0.0001	-4.198E-07	8.099E-07
C9	Strain	135	8092.3	-0.0049	-6.055E-07	239.27	-0.0001	-4.179E-07	7.359E-07
C10	Strain	125.4	9365.5	-0.0031	-3.310E-07	212.2	-0.00005	-2.356E-07	3.327E-07
C11	Strain	126.8	6934.7	-0.0014	-2.019E-07	193.52	-0.00003	-1.550E-07	2.546E-07
C12	Strain	123 8	8122.1	-0 0016	-1.970E-07	202.29	-0.00003	-1.483E-07	2.558E-07
C13	Strain	176.6	8502.9	-0.0163	-1.917E-06	392.9	-0.0006	-1.527E-06	2.454E-06
C14	Strain	175.5	8197.2	-0.0137	-1.671E-06	373.59	-0.0004	-1.071E-06	1.977E-06
C16	Stress	144.9	9529.8	-0.0143	-1.501E-06	300.32	0.0011	3.663E-06	8.896E-07
C17	Stress	152.2	9388.8	-0.0206	-2.194E-06	312.35	0.0017	5.443E-06	1.655E-06
C6	Stress	161.5	8298.5	-0.0242	-2.916E-06	375.99	0.0021	5.585E-06	1.667E-06
C18	Stress	136.7	8940.9	-0.0077	-8.612E-07	232.22	0.0005	2.153E-06	7.677E-07
C19	Stress	133.7	8879.4	-0.004	-4.505E-07	237.1	0.0002	8.435E-07	3 653E-07
C20	Stress	117.5	8640.1	-0.0039	-4.514E-07	174.35	0.0002	1.147E-06	4.871E-07

Table P.1. Fatigue damage parameters: Control mix

Sample	Type	ε_0 (με)	E_{00} (MPa)	dE^*/dN	a_T	W_{00} (J/m^3)	dW/dN	a_W	a_F (C=2.70)
RT1	Strain	150.2	8331 5	-0 0012	-1.440E-07	261.41	-0.00003	-1.148E-07	2.519E-07
RT2	Strain	150 7	7854 9	-0 0023	-2.928E-07	273.2	-0.00006	-2.196E-07	4.184E-07
RT4	Strain	150 4	8481.1	-0.0014	-1.651E-07	271.66	-0.00003	-1.104E-07	1.886E-07
RT5	Strain	173.7	8622	-0.0046	-5.335E-07	373.98	-0.0001	-2.674E-07	7.219E-07
RT6	Strain	174.8	8871.8	-0.0067	-7.552E-07	367.63	-0.0002	-5.440E-07	1.102E-06
RT3	Strain	175.4	8560.1	-0.003	-3.505E-07	372.48	-0.0001	-2.685E-07	5.070E-07
RT7	Strain	200.3	8760.1	-0.013	-1.484E-06	469.04	-0.0005	-1 066E-06	1.939E-06
RT8	Strain	201.3	7636.2	-0 008	-1.048E-06	454.98	-0.0004	-8.792E-07	1.350E-06
RT9	Strain	200.0	7243	-0.0066	-9.112E-07	440.63	-0.0003	-6.808E-07	1.324E-06
RT10	Stress	143.3	9619.3	-0 0093	-9 668E-07	267.62	0.0008	2 989E-06	2.757E-07
RT11	Stress	130.7	10549	-0.0122	-1.157E-06	235.48	0.0007	2.973E-06	4 687E-07
RT12	Stress	137.2	10121	-0 0086	-8 497E-07	254.82	0.0006	2.355E-06	3.598E-07
RT14	Stress	124	9592 9	-0.004	-4.170E-07	200.1	0.0002	9 995E-07	2.844E-07
RT16	Stress	106.3	10719	-0 0033	-3.079E-07	159 44	0.0001	6.272E-07	1.485E-07
RT15	Stress	116.3	9874.2	-0.0021	-2.127E-07	188.82	0.0001	5.296E-07	8.367E-08
RT17	Stress	174.5	9717.2	-0.0189	-1.945E-06	352.54	0.0019	5.389E-06	1.505E-06
RT18	Stress	159.7	9907.7	-0.0227	-2.291E-06	350.86	0.002	5.700E-06	6.907E-07
RT19	Stress	197.6	7734 8	-0.0409	-5.288E-06	539 55	0.0061	1.131E-05	8.353E-07

Table P.2. Fatigue damage parameters: CRM mix 1

Sample	Type	ε_0 (με)	E_{00} (MPa)	dE^*/dN	a_T	W_{00} (J/m^3)	dW/dN	a_W	a_F (C=3.05)
RC1	Strain	150 5	8261.1	-0 003	-3 631E-07	251.16	-0.00006	-2.389E-07	5.138E-07
RC2	Strain	150 3	8347.8	-0.0018	-2.156E-07	266 62	-0.00004	-1.500E-07	2 743E-07
RC3	Strain	149 6	7546.3	-0.0015	-1.988E-07	243.91	-0.00003	-1.230E-07	2.921E-07
RC4	Strain	175.4	8385.9	-0.0059	-7.036E-07	355.17	-0.0002	-5.631E-07	6.913E-07
RC5	Strain	174.7	7432.1	-0.0026	-3.498E-07	333.19	-0.00009	-2.701E-07	5.927E-07
RC6 I	Strain	175.1	8059	-0.0127	-1.576E-06	339 81	-0.0004	-1.177E-06	2.270E-06
RC20	Strain	199 6	9271.4	-0 0217	-2.341E-06	526 94	-0.001	-1.898E-06	3.287E-06
RC19	Strain	199 4	9089 9	-0.0221	-2.431E-06	524.12	-0 001	-1 908E-06	3.767E-06
RC9 I	Strain	200.9	6402.9	-0.0065	-1.015E-06	407.82	-0.0003	-7.356E-07	1.367E-06
RC10	Stress	147.1	9173.8	-0.0175	-1.908E-06	289.05	0.0014	4.843E-06	2.616E-07
RC11	Stress	139 9	9579.5	-0.0164	-1.712E-06	275.14	0.0011	3.998E-06	2.870E-07
RC12	Stress	137.4	9803.4	-0 0183	-1 867E-06	271.38	0.0011	4.053E-06	5.015E-07
RC13	Stress	130 2	9188.3	-0 0062	-6.748E-07	209 88	0 0003	1.429E-06	4.766E-07
RC14	Stress	125.2	9098 3	-0 0042	-4 616E-07	214.7	0.0002	9.315E-07	1.916E-07
RC15	Stress	122.0	9284.4	-0.0044	-4.739E-07	204.13	0.0002	9.798E-07	1.654E-07
RC16	Stress	86.2	10666	-0.0017	-1.594E-07	116	0.00005	4.310E-07	4.574E-08
RC17	Stress	103 2	9739.9	-0.0037	-3.799E-07	173.3	0.0002	1.154E-06	
RC18	Stress	105 9	9456.7	-0 003	-3.172E-07	195.77	0.00009	4 597E-07	1.172E-07

Table P.3. Fatigue damage parameters: CRM mix 2

APPENDIX Q. Pavement model for the evaluation of the wearing course mixtures

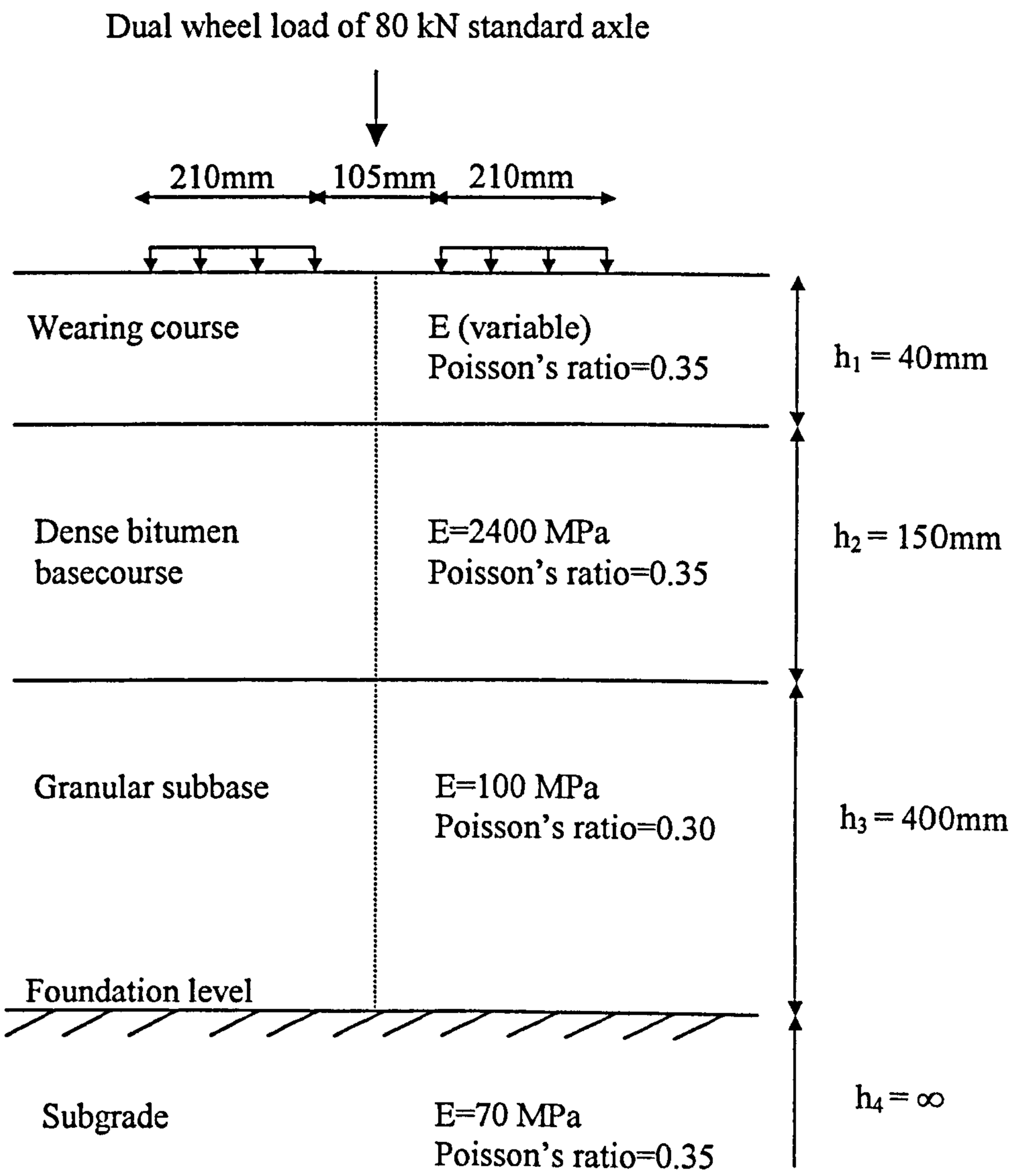

Figure Q.1. Pavement model (after Khalid, 2000)

APPENDIX R. Fracture specimens

Sample	Binder content (%)	SGM	SGMA	CDM (gm/ml)	CDMA (gm/ml)	VMA (%)	VIM (%)
FC1	4.8	2.507	2.702	2.361	2.248	16.81	5.81
FC2	4.8	2.507	2.702	2.384	2.270	16.00	4.89
FC3	4.8	2.507	2.702	2.381	2.267	16.11	5.01
FC6	4.8	2.507	2.702	2.381	2.267	16.11	5.01
FC7	4.8	2.507	2.702	2.387	2.272	15.90	4.77
FC8	4.8	2.507	2.702	2.385	2.271	15.97	4.85
FC9	4.8	2.507	2.702	2.374	2.260	16.36	5.29
FC11	4.8	2.507	2.702	2.364	2.251	16.71	5.69
FC12	4.8	2.507	2.702	2.387	2.272	15.90	4.77
Average	**4.8**	**2.507**	**2.702**	**2.378**	**2.264**	**16.21**	**5.12**
STDEV	**0**	**0**	**0**	**0.010**	**0.009**	**0.34**	**0.39**

Table R.1. Control mix

Sample	Binder content (%)	SGM	SGMA	CDM (gm/ml)	CDMA (gm/ml)	VMA (%)	VIM (%)
FRT1	5.8	2.469	2.702	2.377	2.239	17.13	3.75
FRT2	5.8	2.469	2.702	2.389	2.250	16.71	3.26
FRT3	5.8	2.469	2.702	2.392	2.253	16.61	3.14
FRT5	5.8	2.469	2.702	2.360	2.223	17.72	4.43
FRT6	5.8	2.469	2.702	2.397	2.258	16.43	2.94
FRT7	5.8	2.469	2.702	2.385	2.247	16.85	3.42
FRT10	5.8	2.469	2.702	2.380	2.242	17.03	3.62
FRT11	5.8	2.469	2.702	2.396	2.257	16.47	2.98
FRT12	5.8	2.469	2.702	2.391	2.252	16.64	3.18
Average	**5.8**	**2.469**	**2.702**	**2.385**	**2.247**	**16.84**	**3.41**
STDEV	**0**	**0**	**0**	**0.012**	**0.011**	**0.40**	**0.47**

Table R.2. CRM mix 1

Sample	Binder content (%)	SGM	SGMA	CDM (gm/ml)	CDMA (gm/ml)	VMA (%)	VIM (%)
FRC1	5.8	2.469	2.702	2.368	2.231	17.44	4.11
FRC2	5.8	2.469	2.702	2.378	2.240	17.10	3.70
FRC3	5.8	2.469	2.702	2.380	2.242	17.03	3.62
FRC5	5.8	2.469	2.702	2.391	2.252	16.64	3.18
FRC6	5.8	2.469	2.702	2.396	2.257	16.47	2.98
FRC7	5.8	2.469	2.702	2.395	2.256	16.50	3.02
FRC9	5.8	2.469	2.702	2.382	2.244	16.96	3.54
FRC10	5.8	2.469	2.702	2.395	2.256	16.50	3.02
FRC11	5.8	2.469	2.702	2.393	2.254	16.57	3.10
Average	**5.8**	**2.469**	**2.702**	**2.386**	**2.248**	**16.80**	**3.36**
STDEV	**0**	**0**	**0**	**0.010**	**0.009**	**0.34**	**0.40**

Table R.3. CRM mix 2

Publications

3rd INTERNATIONAL CONFERENCE
BITUMINOUS MIXTURES AND PAVEMENTS
Thessaloniki, Greece, 21-22 November 2002

INFLUENCE OF CRUMB RUBBER MODIFIER (CRM) FROM TYRE WASTE ON THE RHEOLOGICAL PROPERTIES OF BITUMINOUS BINDERS

I. Artamendi
Research Student, Civil Engineering, University of Liverpool
G. C. Eastmond
Honorary Senior Fellow, Chemistry, University of Liverpool
H. Khalid *
Senior Lecturer, Civil Engineering, University of Liverpool
Department of Civil Engineering, University of Liverpool, Liverpool, L69 3GQ, UK
khalid@liv.ac.uk

ABSTRACT
As part of a programme to examine the viability of incorporating crumb tyre rubbers into asphalts, we have investigated interactions between bitumen and both car- and truck-tyre rubbers. Solvent swelling of rubbers was studied to determine their solubility parameters and to predict which components of bitumen will be absorbed. The diffusion of bitumen into tyre rubber monoliths was studied at 180 °C; equilibrium absorptions, achieved after about 1 day, were determined and diffusion coefficients for diffusion of bitumen components into rubbers were estimated. A method was developed to isolate rubber crumb after interaction with bitumen and to isolate the modified bitumen after depletion of the diffusing components. Rheological studies on neat bitumen, crumb rubber – bitumen mixtures and isolated bitumen were determined after various times of heating at 180 °C. Complex moduli were determined at 10 Hz and 45 °C. The normal hardening of bitumen was observed and this was also seen in residual bitumen and mixtures with rubber. Interpretations of the variations in complex moduli for bitmen-rubber mixtures based on modification of the swollen rubber network were developed.

KEYWORDS: rubber, bitumen, diffusion swelling, rheology

1. INTRODUCTION

As land-fill sites become unavailable, the need to dispose of large quantities of waste used car and truck tyres has generated a major environmental problem. A possible method of disposal for a large tonnage of such material is to incorporate it into roads, in either the road bed or surfacing. The rubber, probably in the form of small (crumb) particles, will be in contact with and will modify the bitumen of crumb-rubber-modified (CRM) bitumen binders. While there have been attempts to incorporate rubber into road surfaces, with differing degrees of success, there is limited information on the interaction of rubber with bitumen and its consequences.

There have been several studies relevant to incorporating tyre rubber into bituminous materials, primarily in the USA. Those studies, which involved bitumen-rubber interactions at processing temperatures in excess of 200 °C, identified significant features associated with the bitumen-rubber mixtures.[1-2] However, the temperatures employed exceeded commercial operating temperatures in the UK and degradation of the rubbers was rapid. We have undertaken similar and additional studies at lower temperatures, mainly 180 °C, to study the consequences of interactions closer to normal commercial operating conditions and where rubber degradation is less extensive.

It is common commercial practice to incorporate thermoplastic polymers into polymer-bitumen mixtures. Studies of such mixtures performed over the years have included, for example, styrene-butadiene statistical copolymer, styrene-butadiene-styrene triblock copolymer or ethylene-vinyl acetate copolymer[3] or, more recently, polyethylenes.[4] Such modifiers may or may not be soluble in bitumen and might be dispersed on a molecular scale or as particulates. Although bitumen, or some of its components, might be a solvent for un-crosslinked rubbers, bitumen can only be a swelling agent for vulcanized rubber, as from scrap tyres, prior to rubber degradation.

Bitumen is a mixture of substances and its composition is dependent on its geographical origin, grade and producer. In general terms, bitumen consists of asphaltenes, resins, naphthenics and aromatics and is essentially a mixture of hydrocarbons of different molecular weight and structure;[5] sulfur (up to 8 wt%) is the other main constituent. Rubber waste can consists of natural (truck tyres) and synthetic, (usually styrene-butadiene statistical copolymer in car tyres) rubbers and each will contain additives including carbon black, oils, antioxidants and residues from the crosslinking process; detailed composition of tyre rubber also varies with the manufacturer and grade of tyre. The overall problem of studying complex mixtures can be minimised by materials selection and in this study truck and car-tyre rubbers were used separately.

As part of a programme on Waste Minimization in Industry, sponsored by the Engineering and Physical Sciences Research Council, we investigated interactions between bitumen and tyre rubbers. At ambient temperatures, bitumen is a viscous fluid and crosslinked rubbers are, by definition, above their

glass-transition temperatures. The whole system is, therefore, associated with significant levels of molecular mobility. Diffusion of components between rubber and bitumen phases will only proceed slowly at service temperatures but rapidly when heated for asphalt preparation and road laying. In this communication we report some results of an initial investigation into interactions between bitumens of Kuwaiti origin and car and truck tyre rubbers, separately, at 180 °C; the nature of the diffusive process and the rheological consequences (at lower temperatures) of the interactions are described. These results identify and establish some basic features of the systems and some practical implications. A more detailed investigation of bitumen-rubber interactions is in progress to obtain additional information on the kinetics and long-term consequences of the interactions.

2. EXPERIMENTAL

Samples of bitumen, 50, 100 and 200 pen grades of Kuwaiti origin (KSR), were provided by Shell Bitumen; SARA analysis of 100 pen KSR gave asphaltenes 16.2 wt%, resins 19.1 %, aromatics 57.6 %, saturates 7.1%. Samples of tyre rubbers, as monoliths and as crumb, nominal sizes 300 and 600 microns, produced by buffing scrap tyres, were provided by J. Allcock; car and truck tyres were segregated but grades within those categories were not selected. Solvents were obtained from Aldrich.

Solubility parameters of tyre rubbers were estimated by immersing individual pieces of rubber cut from tyre tread, 0.2 g, approx, in various solvents, 20 ml. Samples were withdrawn after various immersion times, wiped dry with absorbent paper and re-weighed. Diffusion of bitumen into rubbers was also investigated by immersing weighed rubber monoliths, nominal dimensions 15x10x1 mm, in a large excess of bitumen for various times. Samples were removed, cleaned and re-weighed.

Samples of crumb-rubber-bitumen mixtures for rheological studies were prepared by mixing 60 g of crumb rubber (600 microns) in 100 pen bitumen (600 g) in a Silverson mixer at a selected temperature, typically 180 °C. Dynamic mechanical properties of samples were subsequently studied using a Bohlin DSR rheometer; measurements were undertaken at a frequency of 10 Hz and at a temperature of 45 °C with a plate diameter of 25 mm, gap of 1 mm and a controlled strain of 0.001.

3. RESULTS AND DISCUSSION

Consequences of the interactions between bitumen and crosslinked rubber depend on the interaction parameters between rubber and each of the several components in the bitumen. By definition, the rubber, at ambient temperatures, is above its glass-transition temperature and the network chains are inherently mobile. Bitumen is also inherently mobile but highly viscous. Diffusion of

components across the rubber-bitumen interface at processing temperatures might occur rapidly to produce a dispersion of modified rubber in a matrix of modified bitumen. If equilibrium is achieved between bitumen and rubber during asphalt preparation at, say, 180 °C this situation will be effectively frozen in initially but might not represent the equilibrium position at service temperatures. The properties of the rubber-bitumen composite will depend on the consequences of the diffusion processes, which will modify the properties of both the rubber and bitumen phases.

Initially we examined the swelling of samples of rubber in a selection of solvents in order to estimate solubility parameters of the crosslinked rubbers. It has previously been reported that solubility parameters for bitumens are in the range 8.4 to 9.2 and similar to polymers used as modifiers; polymers with solubility parameters outside this range did not give good performances as modifiers.[1] Weighed samples of car and truck tyre rubbers were cut from tyre treads and immersed in solvents for various times. Specific volumes of solvent absorbed per gram of car-tyre rubber were determined as functions of immersion time in the solvents. Swelling by most solvents at room temperature was achieved within two days. The main difference between the two rubbers was the extent of swelling observed in *n*-hexane (δ = 7.3 $cal^{1/2}$ $cm^{-3/2}$) and cyclohexane (δ = 8.2). Solubility parameters of the rubbers were identified as the peaks in the plots of equilibrium specific volumes of solvent absorbed as functions of solubility parameter, Fig 1. Both rubbers showed peaks at a solubility parameter of 9.3, approximately, where samples swell by about 200 vol%. It is clear that the solubility parameters and the cohesive energy densities of the two rubbers are very similar. Greatest swellings were found with chlorinated solvents and tetrahydrofuran, while polar solvents with high solubility parameters($\delta > 9.5$), such as alcohols, acetonitrile and acetone did not swell the rubbers at all. Toluene gave high swellings of both rubbers but aliphatic solvents such as cyclohexane and especially n-hexane swelled truck-tyre rubber far more than they did car-tyre rubber; the low equilibrium swelling of car-tyre rubber by *n*-hexane was achieved rapidly but the greater swelling of truck-tyre rubber was approached more slowly. Although most components of bitumen and rubbers are hydrocarbons, swelling data predict different swelling of the rubbers by bitumen because of the different relative swelling propensities by aliphatic hydrocarbons.

Solvent swelling data suggest that aromatic components of the bitumen will diffuse into the rubbers preferentially and that truck-tyre rubber will also absorb aliphatic components of the bitumen in the early stages. It is established, from concepts of polymer-polymer miscibility that high-molecular-weight components of the bitumen, such as asphaltenes, will not be miscible with the high-molecular-weight rubber.[6] Aromatic components will have a relatively high tendency to diffuse into the rubbers, compared with the aliphatic components but possibly moderated by the molecular weights of the components.

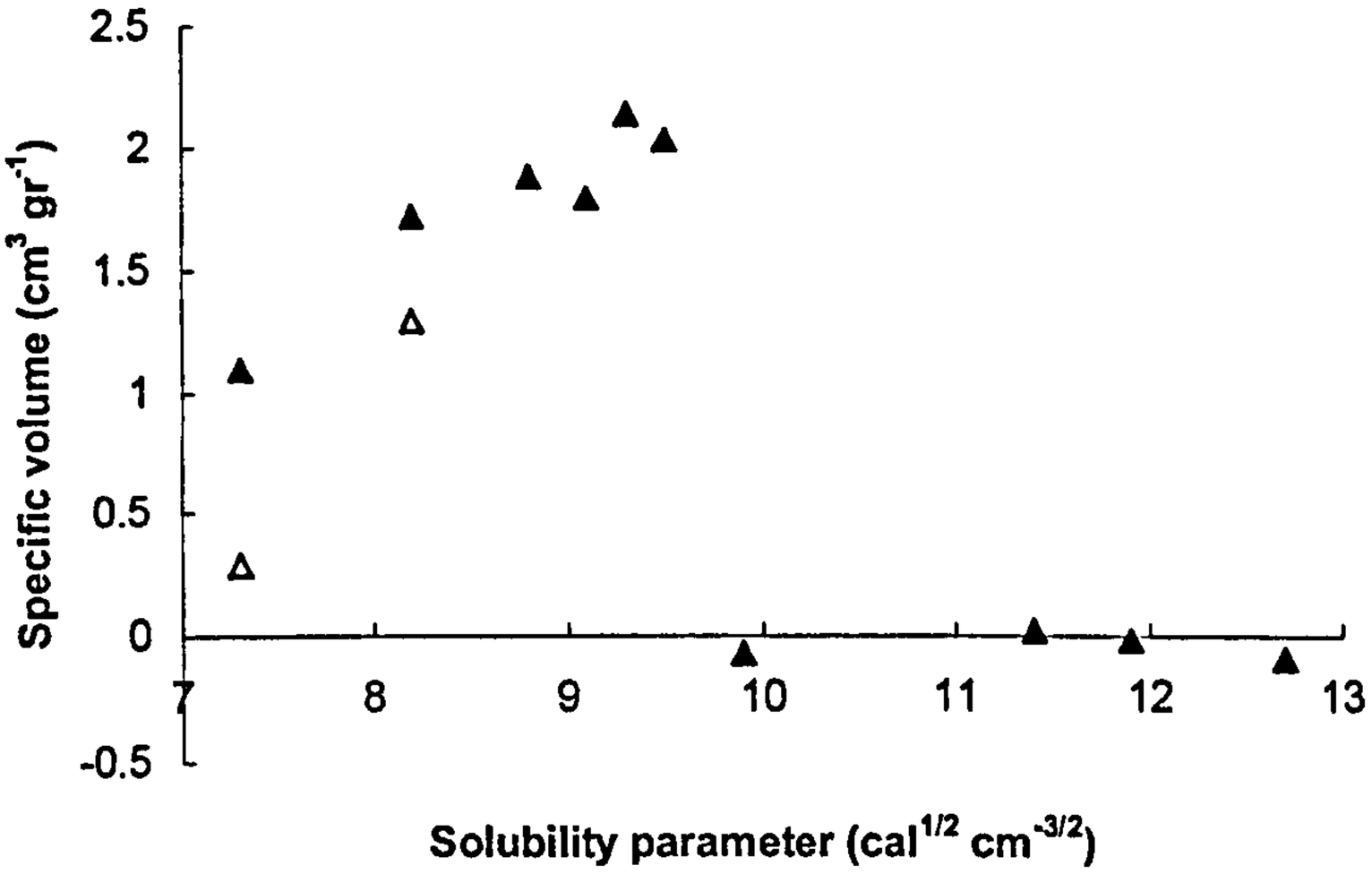

Figure 1. Variation in equilibrium specific volumes of solvent absorbed with solubility parameter for car- and truck-tyre rubbers.

To investigate the absorption of bitumen by rubbers, samples of tyre rubbers were weighed, immersed in bitumen at, say, 180 °C for various times with occasional stirring, removed and cleaned from excess bitumen by wiping with paper while hot and brushing for a few seconds with cold chlorobenzene. Samples were reweighed; separate samples were used for each measurement. Samples were considered as plane sheets with a nominal thickness of 1 mm. Because of difficulty in cutting crosslinked rubber there is some non-uniformity and error in the recorded sample thicknesses but these errors do not affect weight increases or the general conclusions.

Data show that, at elevated temperatures, bitumen is initially absorbed rapidly and then approaches equilibrium. For synthetic car-tyre rubber the equilibrium swelling is well established after about 1 day and is maintained for several (approx. 10) days when the samples were very soft and tacky. After longer periods of immersion samples became mechanically weak and degraded physically on handling; fragments of the rubber could be recovered quantitatively. In the case of truck-tyre (natural) rubber equilibrium was achieved after approximately 1 day but it was more difficult to establish the equilibrium swelling accurately as physical degradation on handling became noticeable within 2 days. The second feature of note was that the equilibrium weight increase for natural rubber (~120 wt%) at 180 °C is greater than that for synthetic rubber (~75 wt%), probably reflecting the greater solubility of bitumens' aliphatic components in the truck tyre rubbers.

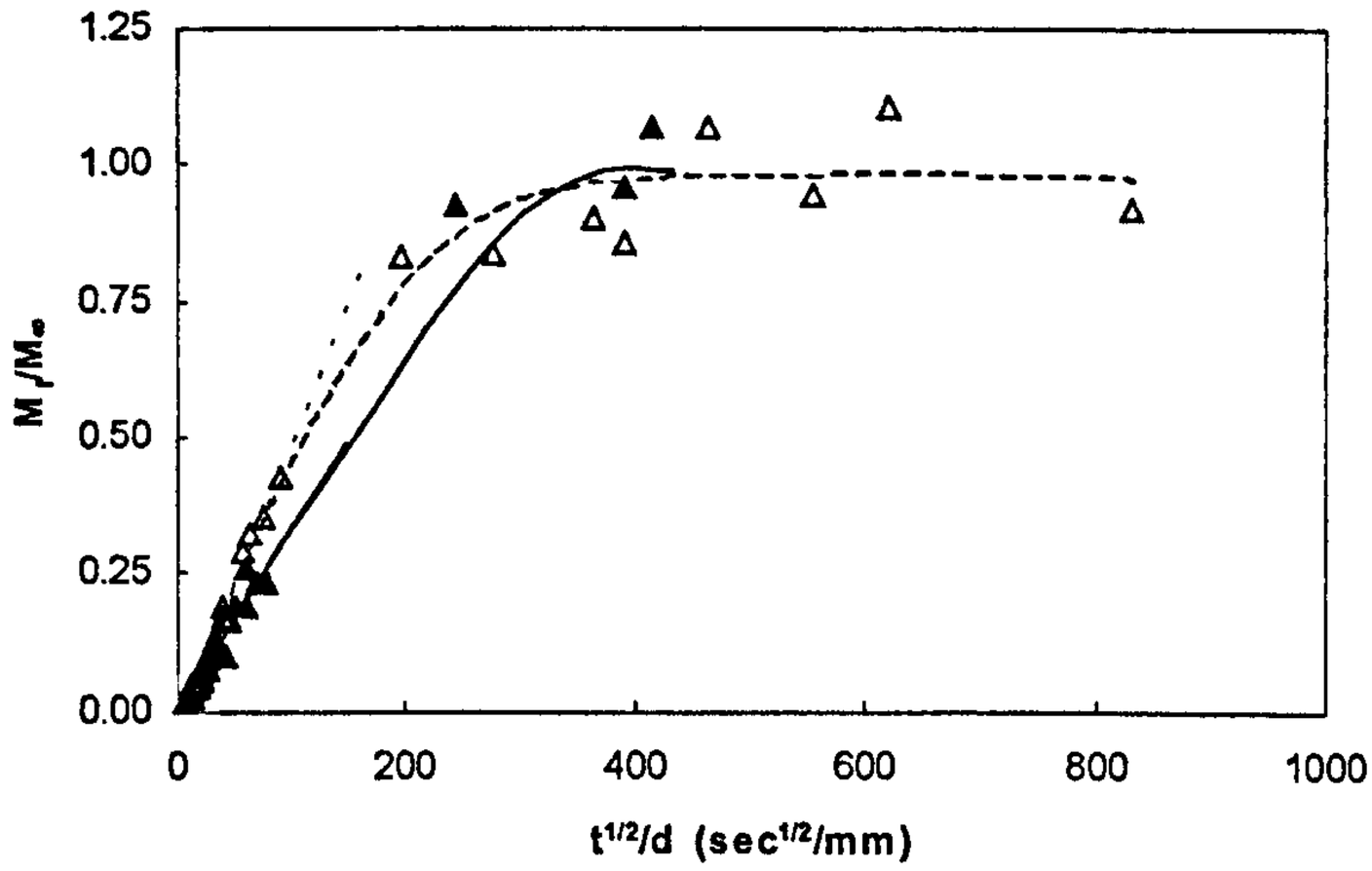

Figure 2. Variations In M_t/M_∞ for absorption of bitumen into car- and truck-tyre rubbers with plane sheet geometry at 180 °C.

In Figure 2 swelling data are normalised and plotted as the variation in M_t/M_∞ with $t^{½}/d$, where t is the immersion time for the rubber in the bitumen and d is the sample thickness of the rubber; M_t, M_∞ are mass increases at time t and at equilibrium. Plots show linear regions in the early stages of swelling and data are consistent with simple Fickian diffusion into the rubbers with plane sheet geometry.[7] Values of apparent diffusion coefficients D for diffusion of bitumen into rubber were determined from the slopes of the linear regions as 5.3×10^{-6} mm^2 s^{-1} (car tyre) and 2.1×10^{-6} mm^2 s^{-1} (truck tyre). Despite the fact that the plots in Fig. 2 are linear for significant times, the estimated diffusion coefficients are considered as apparent for several reasons. First, the equation for Fickian diffusion, used to estimate values of D, assumes: (i) the nature of the matrix does not change, i.e. D does not change, as equilibrium is approached; (ii) systems develop their equilibrium concentrations at samples surfaces virtually instantaneously on immersion into the penetrant. Diffusion of large weight fractions of bitumen into the rubbers markedly change their physical properties as they soften and, inevitably, molecular mobilities within them increase; the theoretical model is more applicable to absorption of small amounts of gases and vapours. The diffusion coefficient cannot be expected to remain constant throughout; the function plotted in Fig. 2 is expected to be linear to about 50% absorption for constant D and to higher extents of absorption if D increases with concentration of penetrant.[8] Where swelling is large corrections for the volume fraction of penetrant absorbed are required to obtain the correct diffusion coefficient.[8] Also, where extensive swelling takes place, it is unreasonable to expect the surface to adopt its equilibrium penetrant

concentration initially when there is little or no swelling of the sample interior.[8] Second, bitumen is a complex material and different components might diffuse into the rubber at different relative rates as the rubber swells. Solvent swelling observations indicate that the lighter aromatic components might diffuse into both rubbers preferentially in the early stages and enhance diffusion of other components in the later stages as the environment within the swollen rubber changes. Aliphatic components might also diffuse into truck rubber in the earlier stages. It has been reported that in cases where the diffusion coefficient is not constant, complexity in the diffusive processes might be manifest as in data for diffusion into synthetic rubber in the initial stages where the data do not extrapolate through the origin.[7] We have noted that the linear data in the earlier stages of diffusion of the bitumen components into truck rubber pass through the origin of Fig. 2. However, data for absorption into car-tyre rubber do not extrapolate through the origin but are associated with a short, reproducible induction period of about 1 minute at 180 °C, possibly associated with initial softening of the rubber surface by aromatic components prior to the absorption of aliphatic components.

Composites produced in consequence of bitumen components diffusing into rubber particles are inevitably heterogeneous (2-phase) systems of rubber particles dispersed within a bitumen matrix. Absorption of bitumen components by the rubber inevitably depletes the bitumen of the absorbed components and modifies the properties of both the rubber and bitumen phases. To assess the consequences we investigated changes in properties of the bitumen phase as well as those of the composite material. Samples of 600 μm car-tyre rubber (10 wt%) and truck-tyre rubber were, separately, mixed with 100 pen bitumen in a Silverson shear mixer at 180 °C. Samples of modified bitumen were isolated by filtering the samples through a polyester cloth filter (50 μm) at 180 °C. It was not possible to isolate samples of modified rubber crumb free of bitumen by simple filtering. While any non-mechanical process might modify the system by diffusion of components, it was necessary to have recourse to the use of solvent to recover modified crumb. Filtered samples were washed free of excess bitumen with chlorobenzene at room temperature. Several short washings were required. The modified crumb rubber particles at this stage were tacky and aggregated on removal of solvent. Addition of methanol in the presence of a little chlorobenzene allowed particles of soft, dry crumb to be isolated. A particle size analysis of the modified crumb rubber has not been undertaken but visual examination of the modified crumb showed a similar distribution of large and small particles as in the initial crumb.

Rheological measurements were undertaken on neat bitumen (i.e. bitumen in the absence of rubber) and on bitumen-rubber mixtures after heating to 180 °C and also on residual bitumens isolated from mixtures with crumb rubber. Values of complex shear modulus G* and phase angle δ were determined at 10 Hz at 45 °C. Fig. 3 compares values of G* for bitumen and bitumen in contact with crumb truck-tyre rubber for various heating times at 180 °C. It is well-known

that bitumen "ages" on heating and this hardening effect is seen in the gradual increase in G* for neat bitumen in Fig. 3. Samples of residual bitumen, depleted of components absorbed into the rubber, have higher values of G* in the bitumen matrix of the composite than neat bitumen. Hardening of this modified bitumen matrix progresses on continued heating with rubber, as with neat bitumen. The overall increase in G* might be seen as premature ageing of bitumen but arises from a different mechanism. Higher values of G* are a result of selective removal of components into the rubber phase and are not true hardening; this general increase in G* could probably be offset in practical situations, if necessary, by using a grade of bitumen containing more of the components which absorb into the rubber.

Dynamic mechanical properties of the total rubber-bitumen mixtures show more complex behaviour. In Fig. 3 it is seen that a high value of G* at 45 °C is achieved within 1 hour of mixing at 180 °C. With longer periods of interaction between the rubber and bitumen G* decreases to about 5 hours mixing time and then increases slowly with further mixing; the latter trend is consistent with normal hardening of the bitumen matrix. Properties of the final composite are intermediate between those of neat bitumen and higher values of G* for the residual bitumen. These results are consistent with incorporating a volume fraction (~20 vol%) softened rubber particles within a hardened bitumen matrix.

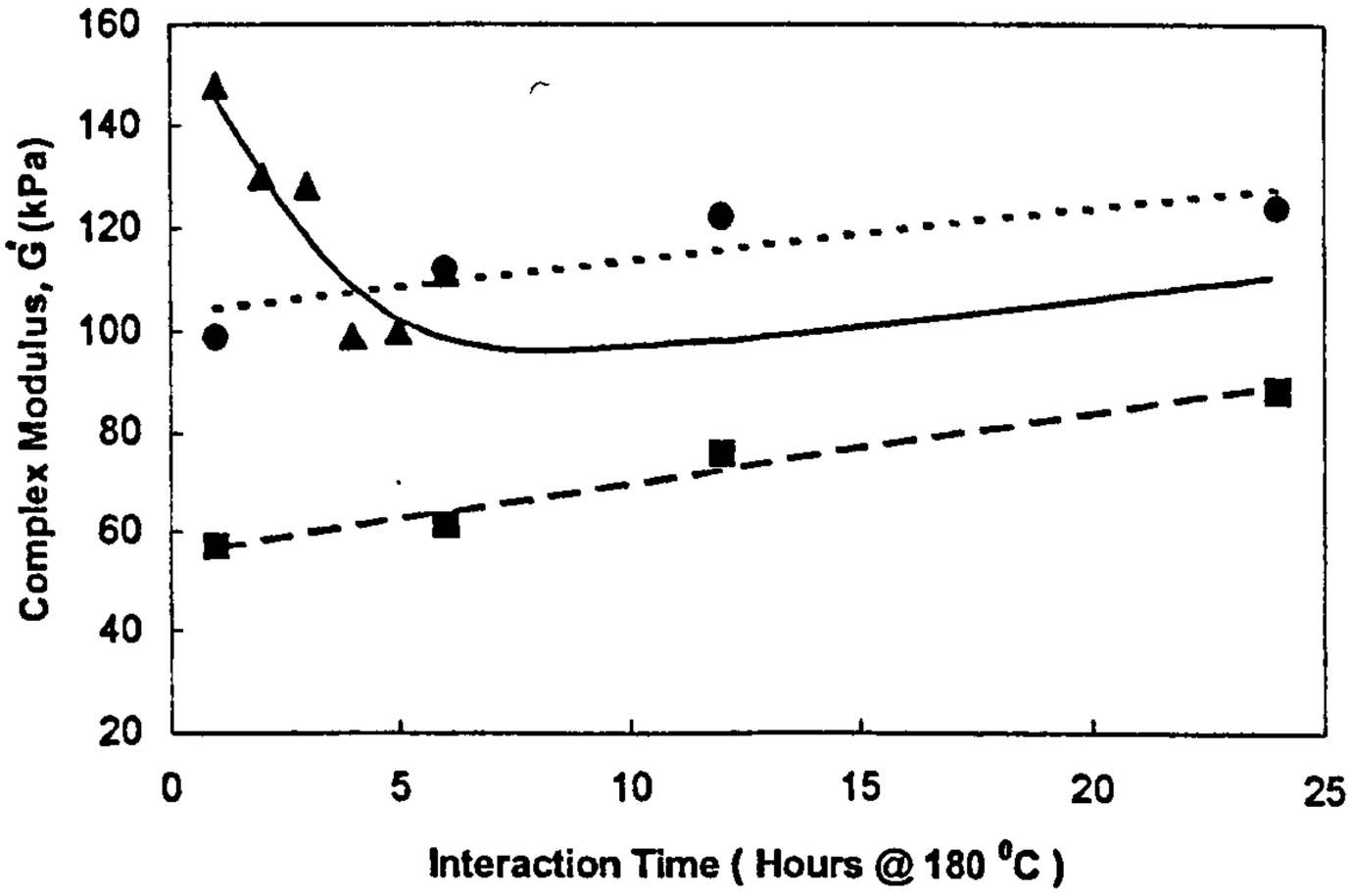

Figure 3. Variations in G* with mixing time at 180 °C for neat bitumen, bitumen-rubber mixtures and residual bitumen at 10 Hz and 45 °C.

Data in Figure 2 were analysed assuming plane sheet geometry. Crumb rubber approximates more closely to spheres of 600 μm diameter. Using the

value of D calculated from Fig. 2 it can be estimated that 90% equilibrium swelling for such spherical particles of truck rubber would be achieved within 2 hours.[9] Crumb rubber particles are not true spheres but have larger surface areas as a result of protrusions on the surfaces of the rough abraded particles and absorption will probably be faster. We therefore estimate that swelling into CRM is complete prior to the first data point in Fig. 3. Consequently, we attribute the reduction in G* for CRM-bitumen mixtures with interaction time at 180 °C to subsequent processes and specifically to some form of polymer degradation.

Two principal modes of degradation could operate: modification of thermally labile -S-S- crosslinks introduced during tyre manufacture or main-chain scission and depolymerization of polymer chains. Bevilaqua reviewed thermal and oxidative degradation processes in different rubbers.[10] Polyisoprene, used in truck tyres, is stable to thermal degradation below 200 °C; SBR rubber, used in car tyres, is more stable. However, in vulcanizates sulfur crosslinks can undergo scission and formation below 200 °C. In effect, crosslinks can reorganize within hot, swollen rubber particles, reducing retractive forces within the swollen polymer networks. Examination of isolated rubber particles showed them to become swollen and soft but not to suffer the degradation which occurred in earlier studies where mixing was performed above 200 °C. We attribute changes in rubber properties between 1 and 5 hours mixing to modification, rather than destruction, of the network structure.

4. CONCLUSIONS

Solvent-swelling studies established that car- and truck-tyre rubbers have solubility parameters of about 9.3 and strongly absorb aromatic solvents. Truck-tyre rubber absorbs aliphatic solvents more strongly that does car-tyre rubber. It is concluded that the same pattern of solubility applies to absorption of bitumen components into rubbers.

At 180 °C truck-tyre rubber absorbs more bitumen (120 wt%) than does car-tyre rubber (75 wt%); equilibrium is achieved in periods of about 1 day. Apparent values of D were determined as 2.13×10^{-6} and 5.30×10^{-6} $mm^2\ s^{-1}$ for car and truck-tyre rubbers, respectively

The rheological properties of crumb-rubber-modified bitumen are determined by the composition of the bitumen matrix and rubber particles modified in consequence of the diffusion processes. These processes result in hardened bitumen matrices modified by softened rubber particles. The composite has a higher modulus than that of neat bitumen.

ACKNOWLEDGEMENTS: The authors wish to acknowledge financial support from EPSRC and support from J. Allcock and Sons, Shell Bitumen UK and Tarmac Ltd.

REFERENCES:

[1] Curtis, C. W., D. I. Hanson, S. T. Chen, G-J. Shieh, and M. Ling, Quantitative determination of polymers in asphalt cements and hot-mix asphalt mixes, *Transportation Record 1488,* 1995, pp 52-61.

[2] See various papers in *Transportation Record*, 1995-1999 and references therein.

[3] Collins J. H., M. G. Bouldin, R. Gelles and A. Berker, Improved performance of paving asphalts by polymer modification, *J. Assoc. Asphalt Paving Technologists*, 1991 **60** 43.

[4] Fawcett A. H., T. McNally, G. M. McNally, F. Andrews and J. Clarke, Blends of bitumen with polyethylenes, *Polymer*, 1999 **40** 6337.

[5] The Shell Bitumen Handbook, Shell Bitumen UK, Chertsey, UK, 1990.

[6] Olabisi,O., L. M. Robeson and M. T. Shaw, "Polymer-Polymer Miscibility", Academic Press, San Diego, 1979.

[7] Crank, J, Mathematics of diffusion, Oxford Univ. Press, London, 1956.

[8] Crank, J. and G. S. Park, Methods of measurement in "Diffusion in polymers" (Eds: Crank, J. and G. S. Park), Academic Press, London 1968, Chapter 1.

[9] Meares, P., "Polymers: Structure and Bulk Properties", Van Nostrand, London, 1965, Chap. 12.

[10] Bevilaqua, E. M., "Thermal and oxidative degradation of natural rubber and allied substances", *Monographs in Macromolecular Chemistry*, (Ed. Conley, R.T.), Marcel Dekker Inc., NY, 1970, Vol. 1.

3rd INTERNATIONAL CONFERENCE
BITUMINOUS MIXTURES AND PAVEMENTS
Thessaloniki, Greece, 21-22 November 2002

EXPLORATORY STUDY TO EVALUATE THE PROPERTIES OF RUBBERISED ASPHALT MODIFIED USING THE WET AND DRY PROCESSES

H.A. Khalid *
Senior Lecturer, Civil Engineering, University of Liverpool, UK
I. Artamendi
Research Student, Civil Engineering, University of Liverpool, UK
* Dept. of Civil Engineering, University of Liverpool, Brownlow St., Liverpool L69 3GQ, U.K., khalid@liv.ac.uk

ABSTRACT

An exploratory laboratory study was undertaken to measure the effect of Crumb Rubber Modifier (CRM) on asphalt properties, modified by the incorporation of CRM using the wet and dry processes. The study commenced with achieving a basic understanding of the net effect of CRM addition on binder properties, in which Brookfield viscosity, penetration and softening point data showed the practicable maximum levels of CRM modification. This was followed by a study of mixture properties with neat and CRM-modified binders, adopting Stone Mastic Asphalt (SMA) and Dense Bitumen Macadam (DBM) wearing course mixtures. The measured properties included volumetric parameters, stiffness modulus, durability and permanent deformation.

For the dry process, roadbase and wearing course DBM and wearing course SMA mixtures were used in the study. CRM was incorporated into the mixture at various levels by replacing equivalent amounts of aggregate particles from the mix, whose particle size distribution resembled that of the added CRM.

Results obtained from this study showed that tyre rubber modification in the dry process had an adverse effect on mixture properties, in contrast to the wet process in which there were no detrimental effects.

KEY WORDS: Rubberised asphalt, wet & dry process, mechanical properties.

1. INTRODUCTION

Major environmental incentives for the use of waste tyre rubber in civil engineering applications continue to evolve, as disposal of shredded tyres in landfill sites will be prohibited by the EU in 2006. This will further encourage the drive to improve the techniques of incorporating tyre rubber in asphalt pavements. The task ahead will thus aim to minimise the risks involved in the use of tyre rubber in asphalt and to maximise the benefit incurred from improved performance.

Crumb Rubber Modifier (CRM) from tyre waste has been used in asphalt mixtures in two approaches, namely the wet process and the dry process. The wet method involves dispersing the CRM particles in the bitumen to produce a rubber-modified binder, which is then mixed with aggregate to form a mixture. In the dry method, on the other hand, the CRM is mixed with the aggregates before introducing the binder to the mixture, i.e. CRM acts as a partial replacement to some of the aggregate sizes. In simple terms, the wet process involves less risk as the interaction between CRM and bitumen can be controlled during the digestion process, whereas in the dry method interaction begins as soon as the bitumen is added to the aggregate blend and is thus more difficult to control. On the other hand, from an application standpoint the wet procedure involves the added step of blending the CRM into the binder prior to adding the binder into the aggregate blend.

The results presented in this paper aim to provide a basic assessment of the effect of CRM addition in the two methods on performance-related properties of typical asphalt pavement materials.

2. ADDITION OF CRM TO BITUMEN

There was a need to establish the net effect of CRM addition on basic bitumen properties, e.g. penetration and softening point, under controlled conditions of mixing duration and temperature. CRM was blended into bitumen at 180°C using a high shear mixer for one hour. CRM of 300μm nominal size from truck tyre origin was blended with two Venezuelan binders of 50 and 100 pen grades. The penetration and softening point of the binders were measured in accordance with BS 2000 [1] and are given in Figure 1, where it can be seen that by adding about 10-15% by weight CRM the binder is lowered by one grade. Figure 2 shows that the Brookfield viscosity, similarly, increases with CRM content. For the range 200 – 500 cP commensurate with mixing conditions, it can be seen that for modified binders with more than 10% CRM these conditions are achievable at temperatures above 180°C. This suggests that at such levels of modification the binders will be too viscous for adequate aggregate coating at practical mixing temperatures.

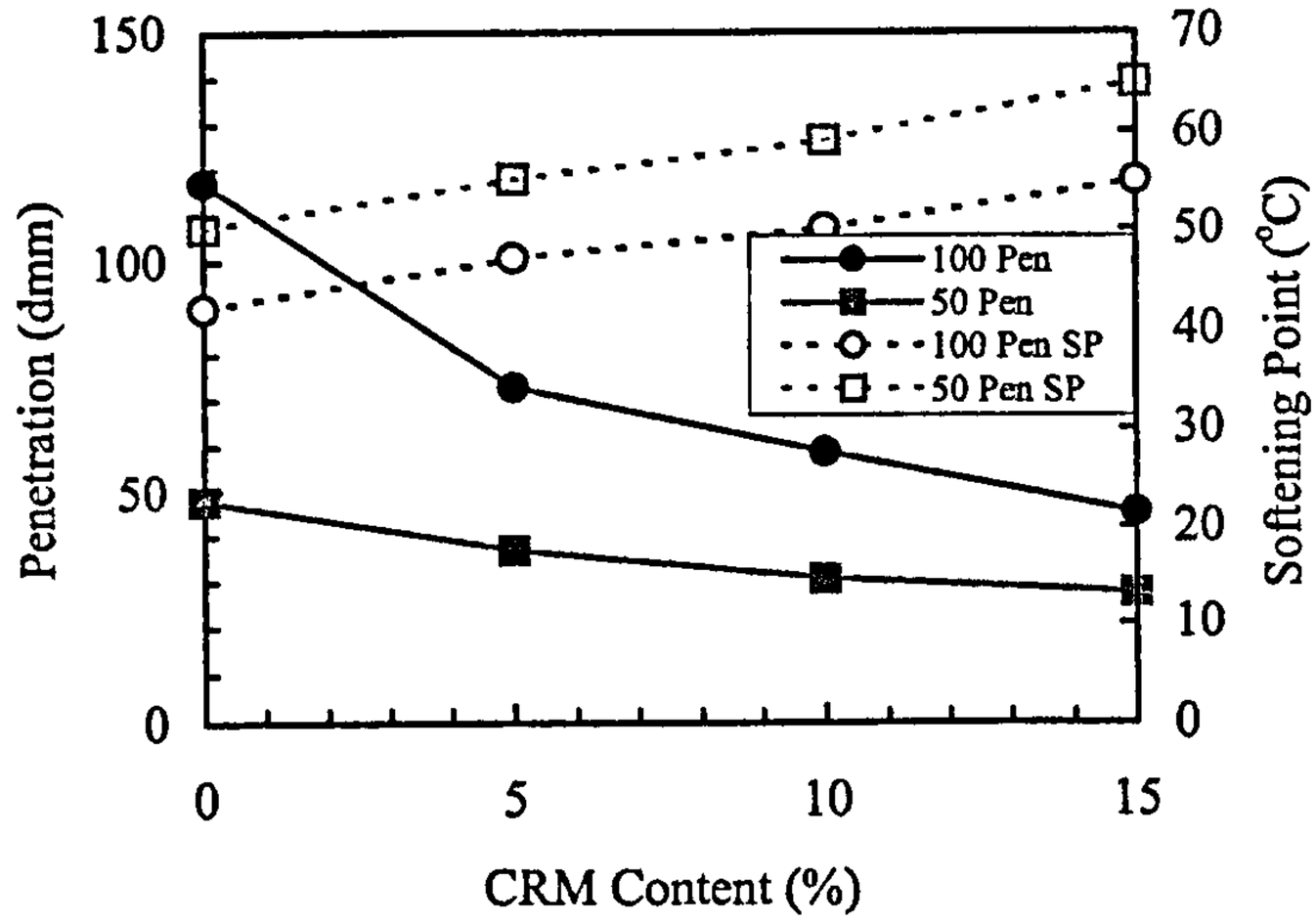

Figure 1. Effect of CRM addition on the penetration and softening point of two binders

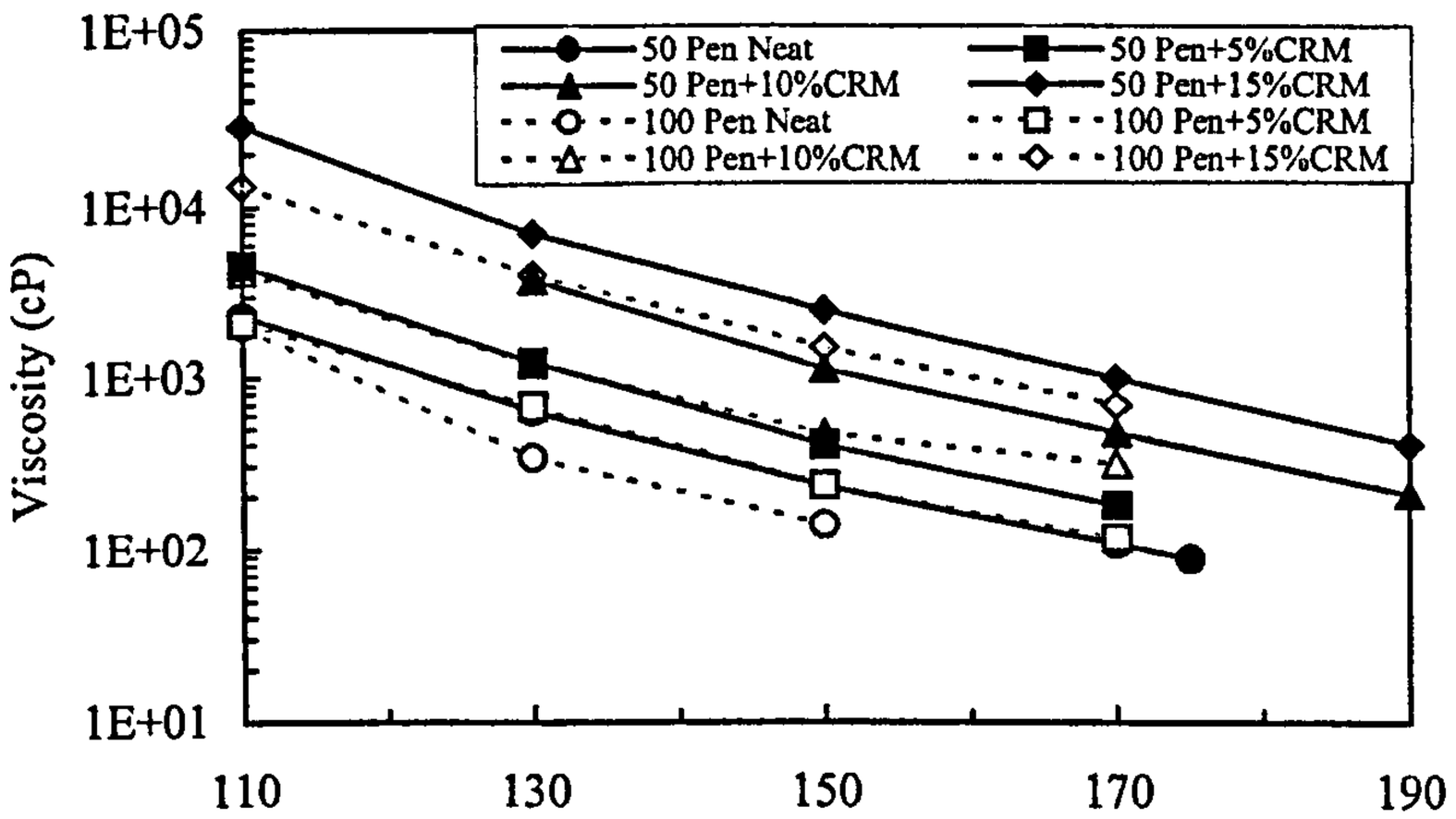

Figure 2. Effect of CRM addition on Brookfield viscosity of two binders

3. ASPHALT MODIFIED BY THE WET PROCESS

The 50 and 100 pen binders were incorporated into 14mm wearing course mixtures in this study, a Stone Mastic Asphalt (SMA) and a Dense Bitumen Macadam (DBM) respectively, whose aggregate gradings are shown in Figure 3. Marshall samples were prepared using 6.8 and 5.1% binder content by weight for the SMA and DBM with the SMA binder containing 0.3% by weight cellulose fibres. Average void contents of 3.4 and 4.3% were obtained for the two mixes (ranges of 2.1-4.7 and 3.5-5.1%). No fibres were included for the modified SMA. The aggregates used were gritstone.

The Indirect Tensile Stiffness Modulus (ITSM) of the prepared samples was measured at 20°C in accordance with BS DD213 [2]. After ITSM measurements some samples were passed through a water immersion regime to evaluate their sensitivity to moisture damage and others were tested for their resistance to deformation in the Repeated Load Axial test (RLA) at 40°C in accordance with BS DD226 [3]. The water immersion regime involved saturating the samples under vacuum pressure, followed by conditioning in a hot water bath at 60°C for 6 hours and then in a cold water bath at 5°C for 16 hours prior to testing for the retained ITSM at 20°C.

Figure 4 shows the initial and conditioned ITSM of the neat and modified SMA and DBM mixes. The histogram shows an increase in the ITSM with CRM content for the two materials. The figure also shows that even though the percentage retained stiffness upon immersion decreases with CRM content (percentage values given on histograms), the retained stiffness values either remain or slightly increase with increase in CRM. Figure 5 indicates that permanent deformation decreases with CRM modification.

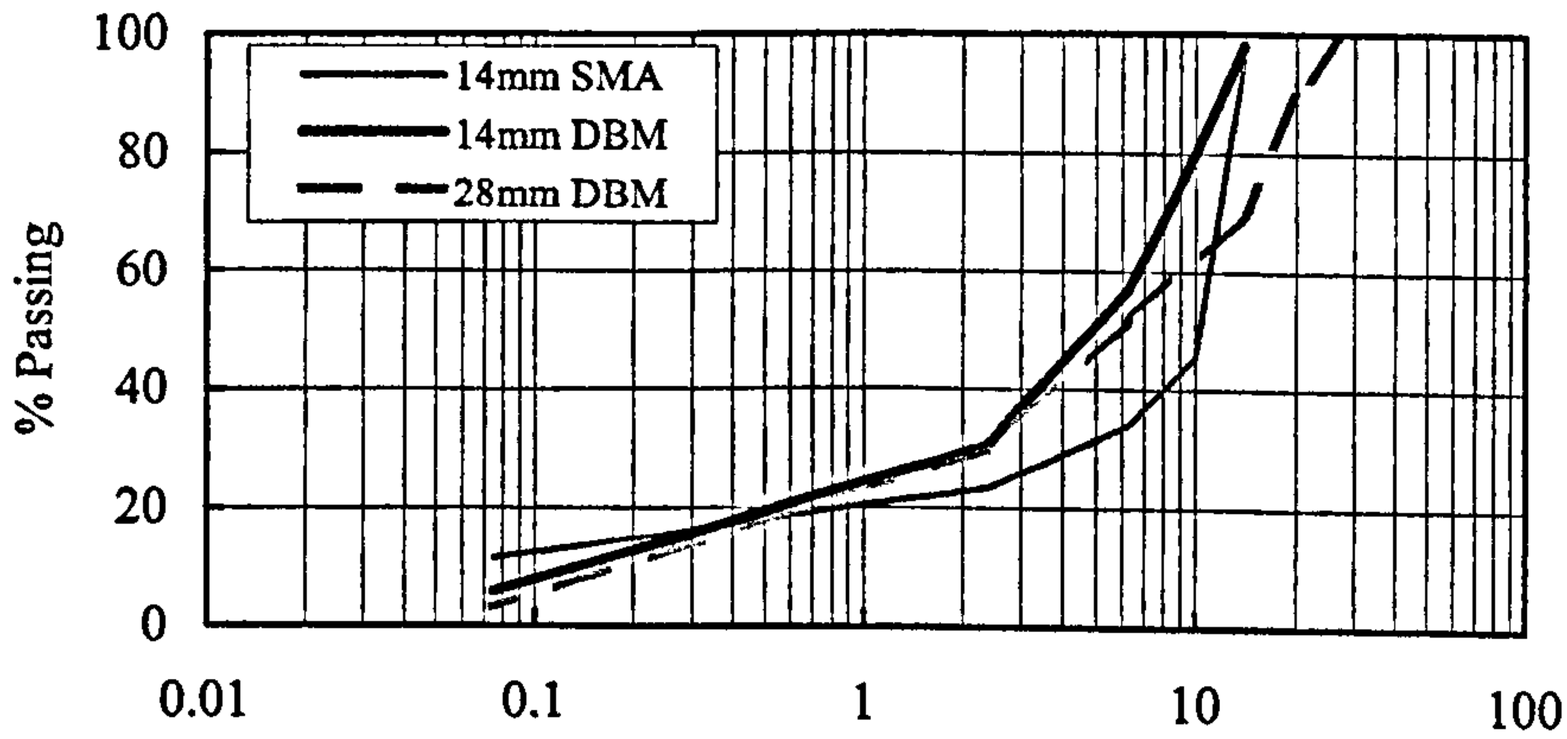

Figure 3. Particle size distribution of the materials used in the study

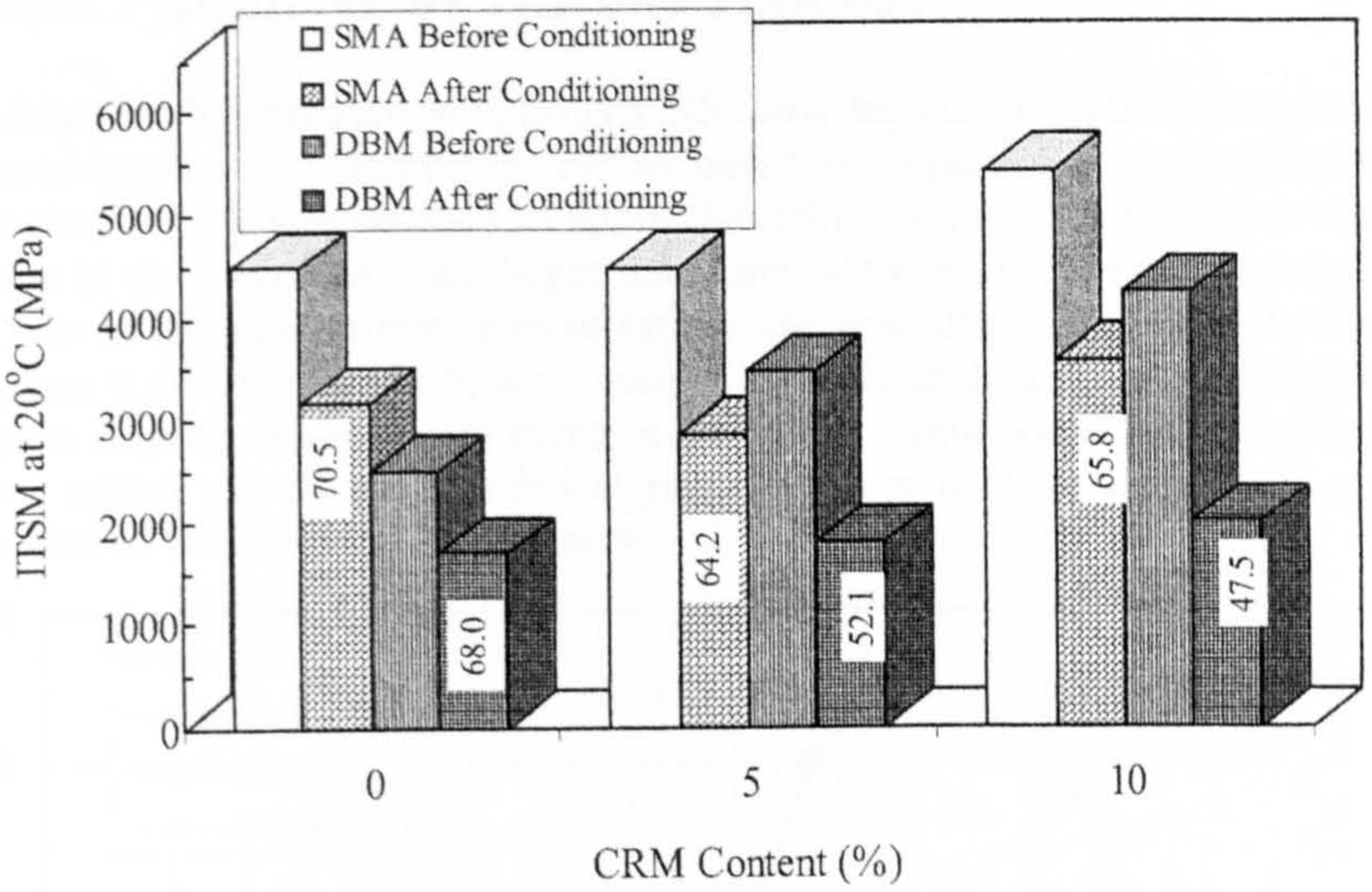

Figure 4. Effect of CRM addition in the wet process on mix stiffness

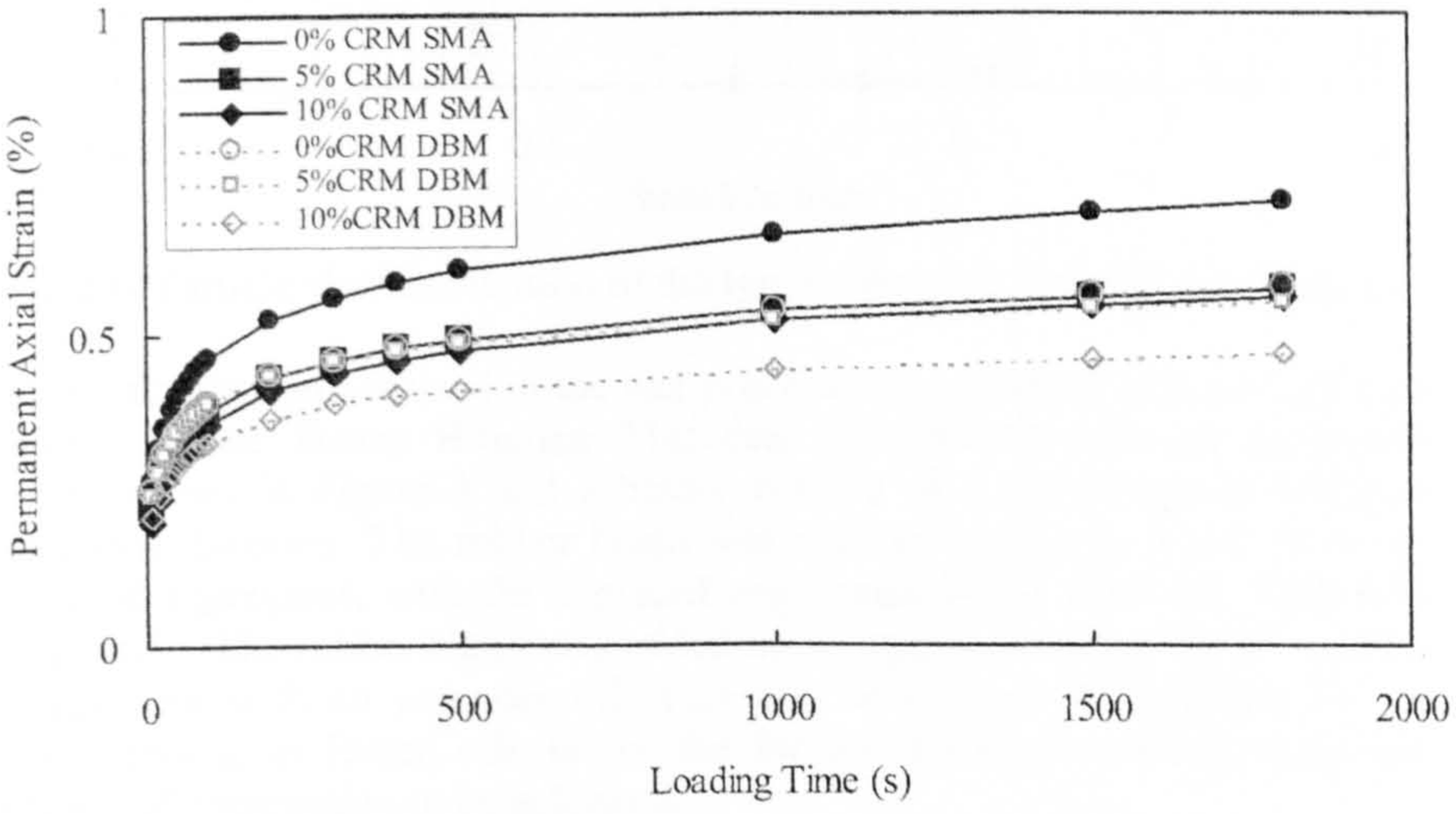

Figure 5. Effect of CRM addition in the wet process on the mix resistance to permanent deformation in the RLA

4. ASPHALT MODIFIED BY THE DRY PROCESS

Tyre rubber can be shredded to various mesh sizes depending on the anticipated use. It was important to identify the rubber based on its particle size distribution and for simplicity it was decided to apply the term 'crumb' to any particle less than 1mm in size, whereas those larger than 1mm were referred to as 'granules'. In this part of the study, three sizes of crumb and granules, whose particle size distribution is given in Figure 6, were used to partially replace the the 3mm-dust aggregates whose grading is also given in the figure. Trials were made in which the three rubber sizes were blended at proportions to achieve a grading very close to that of the 3mm-dust aggregates.

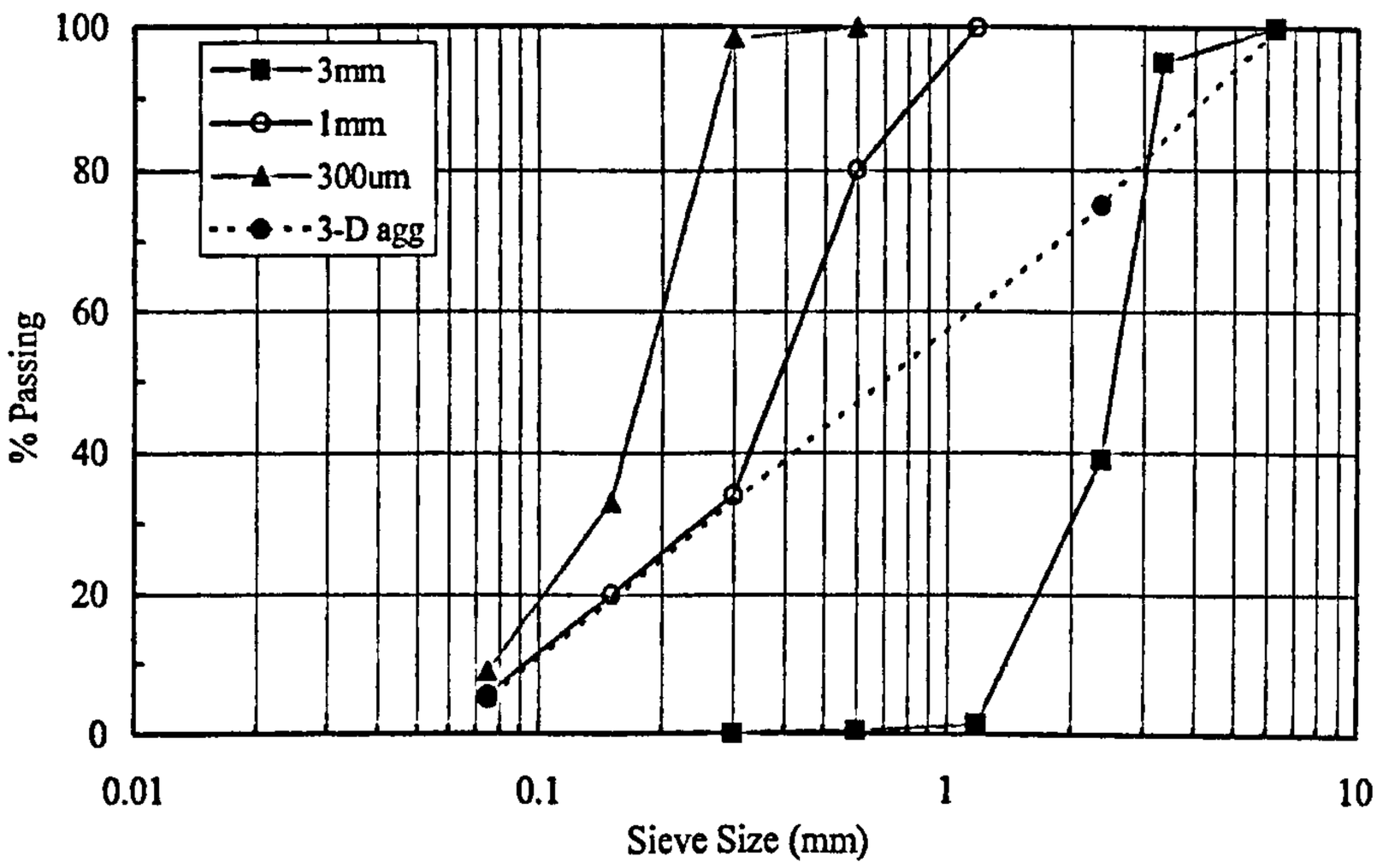

Figure 6. Particle size distribution of the tyre rubber and 3mm-dust aggregates

The same two mixes used in the wet process were adopted here, as well as a 28mm roadbase Dense Bitumen Macadam (DBM-RB) with an aggregate grading shown in Figure 3 and a binder content of 4.5% using the 100 pen Venezuelan bitumen. The rubber blend was used to replace 3, 5 and 10 % by weight of aggregates, with the replaced aggregates being from the 3mm-dust size fraction. The rubber blend was added to the aggregate either 'as is' or after pre-treatment with an extender oil. This was to control the swelling of the rubber leading to lesser effects on the binder, thereby enabling improved coating and compaction to be achieved.

A simple procedure was devised to determine the amount of extender oil required to pre-treat the rubber. It involved a process based on a BS procedure for determinig the specific gravity of fines [4]. Batches of pre-treated rubber were prepared with various percentages of extender oil and the material was

poured into a metal cone and tamped. The optimum extender oil pre-treatment was defined as the percent at which the material just holds its shape. For the truck tyre rubber this was found to be 4%.

For the DBM-RB mix, cylindrical samples of 150mm diameter and approx. 70mm high were prepared using a vibrating hammer compaction method. It was not feasible to compact samples with 10% rubber, as the material crumbled after extraction from the moulds. There were some difficulties in the mixing and compaction of the untreated rubber modified mixtures, which has led to inadequate coating and lower densities compared to the treated rubber modified mixtures which were more convenient to compact. Treated rubber particles were softer and had a less harsh texture than the untreated particles. This has facilitated mixing and compaction and led to better packing. Figures 7 and 8 show the effect of rubber modification on the 3 mixes used, where it can be seen that the stiffness decreases and voids content increases with increase in rubber content. For the treated rubber mixes, however, the reduction in stiffness and increase in voids is seen to be less than that undergone by the untreated rubber mixes.

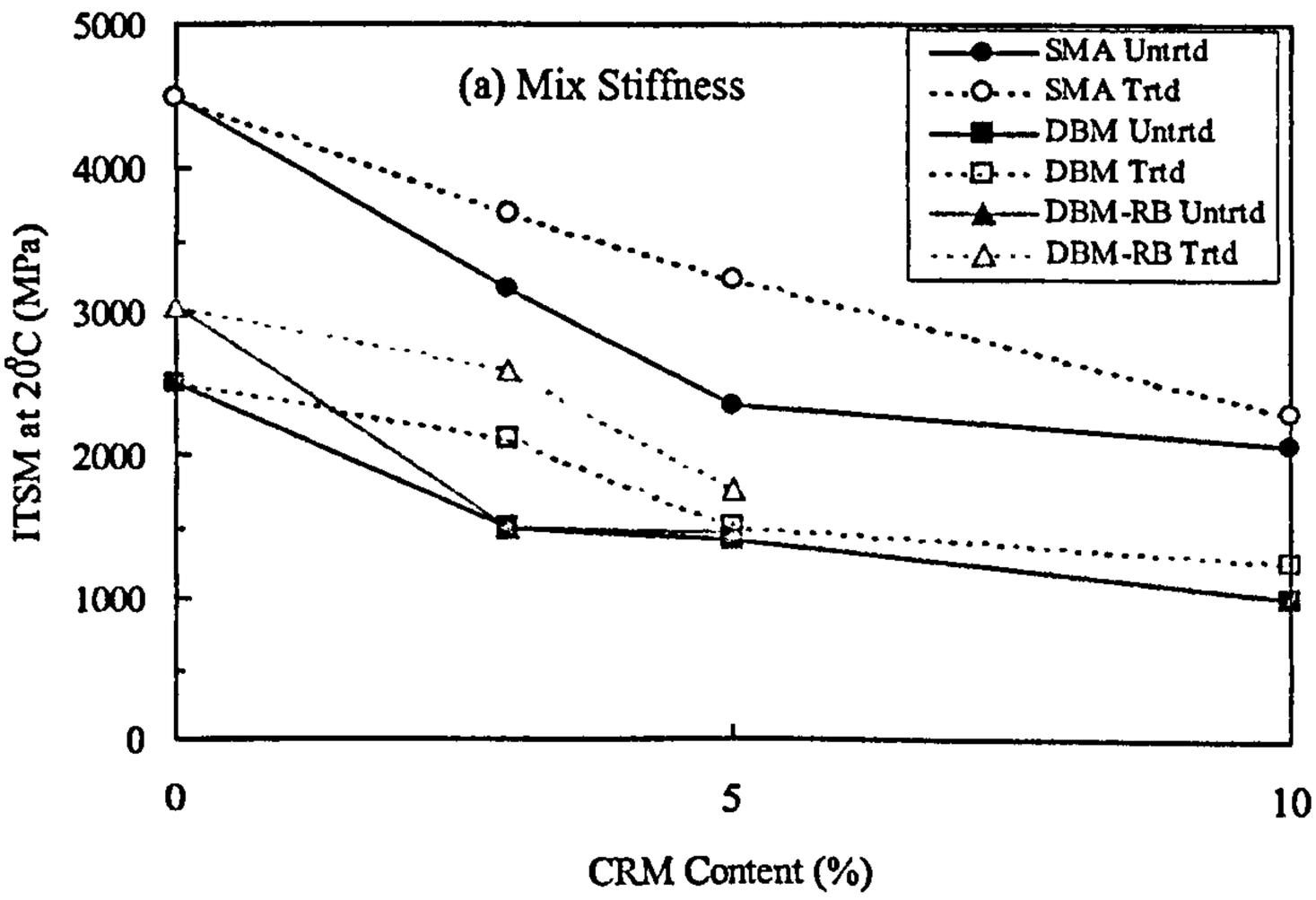

Figure 7. Effect of rubber addition in the dry process on mix stiffness

Half of the samples were then passed through the water immersion regime described in the previous section and the other half were tested in the RLA, with the results presented in Figures 9 and 10. The untreated rubber modified mixes

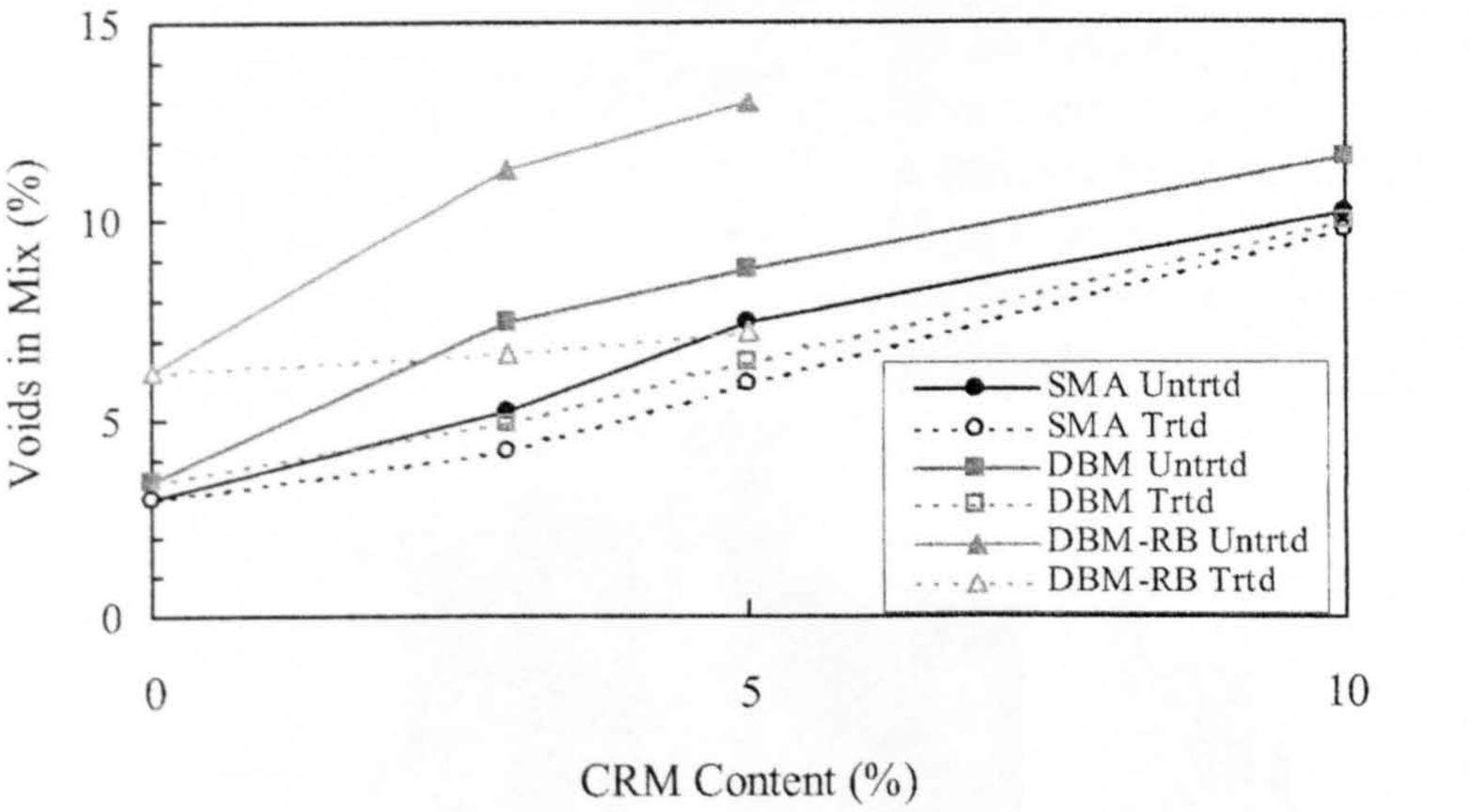

Figure 8. Effect of rubber addition in the dry process on mix voids content

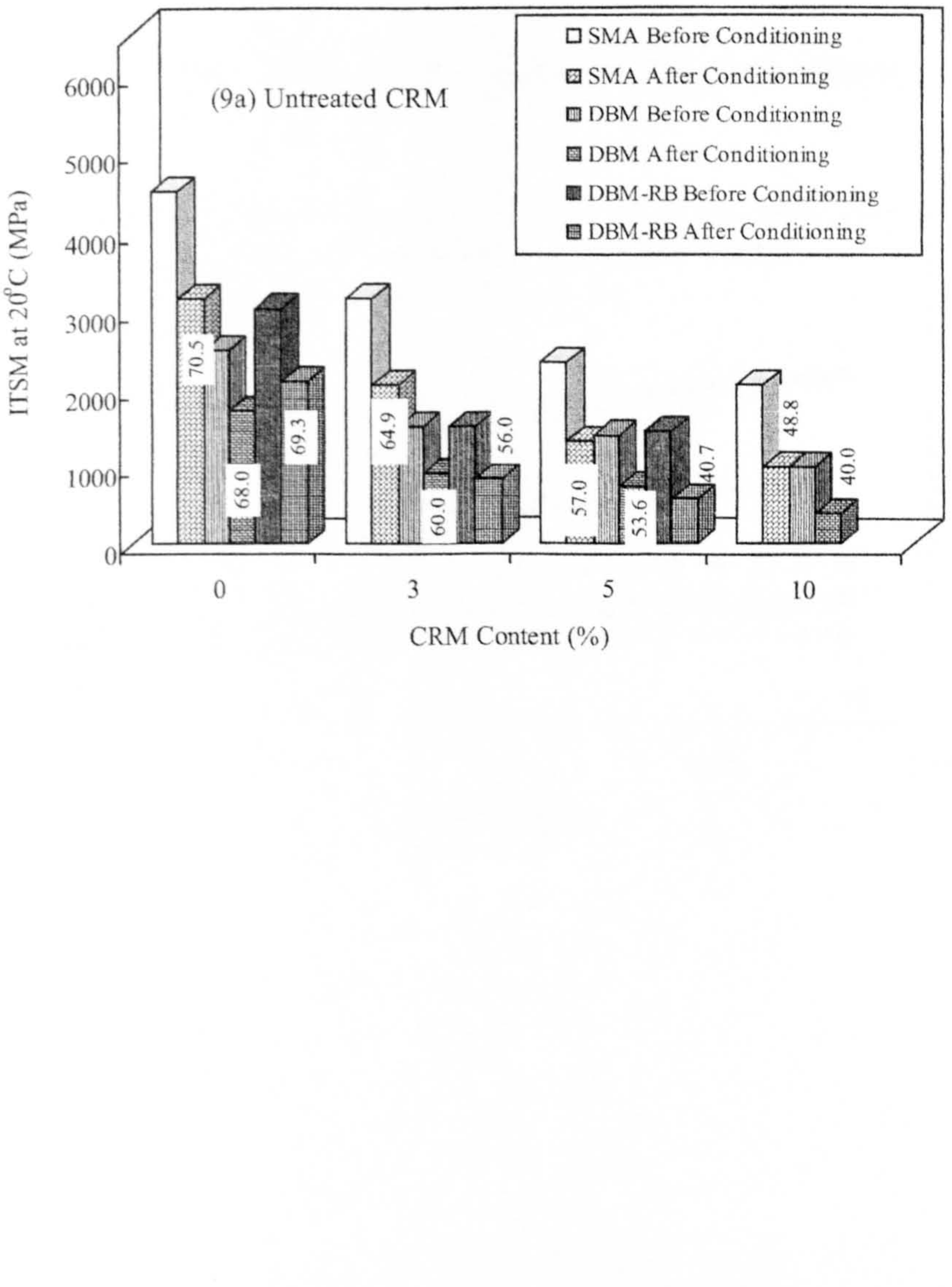

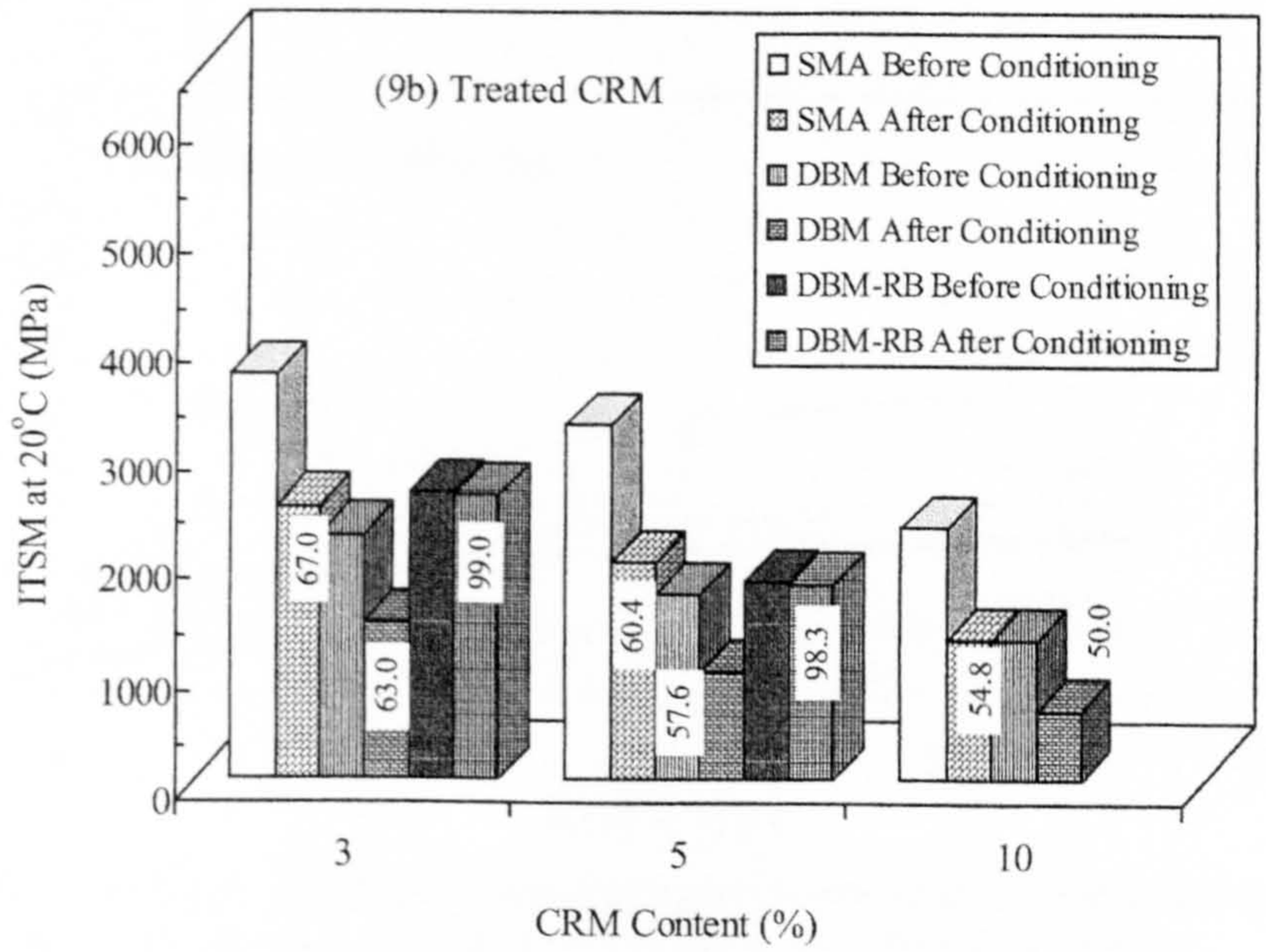

Figure 9. Effect of rubber addition in the dry process on mix stiffness

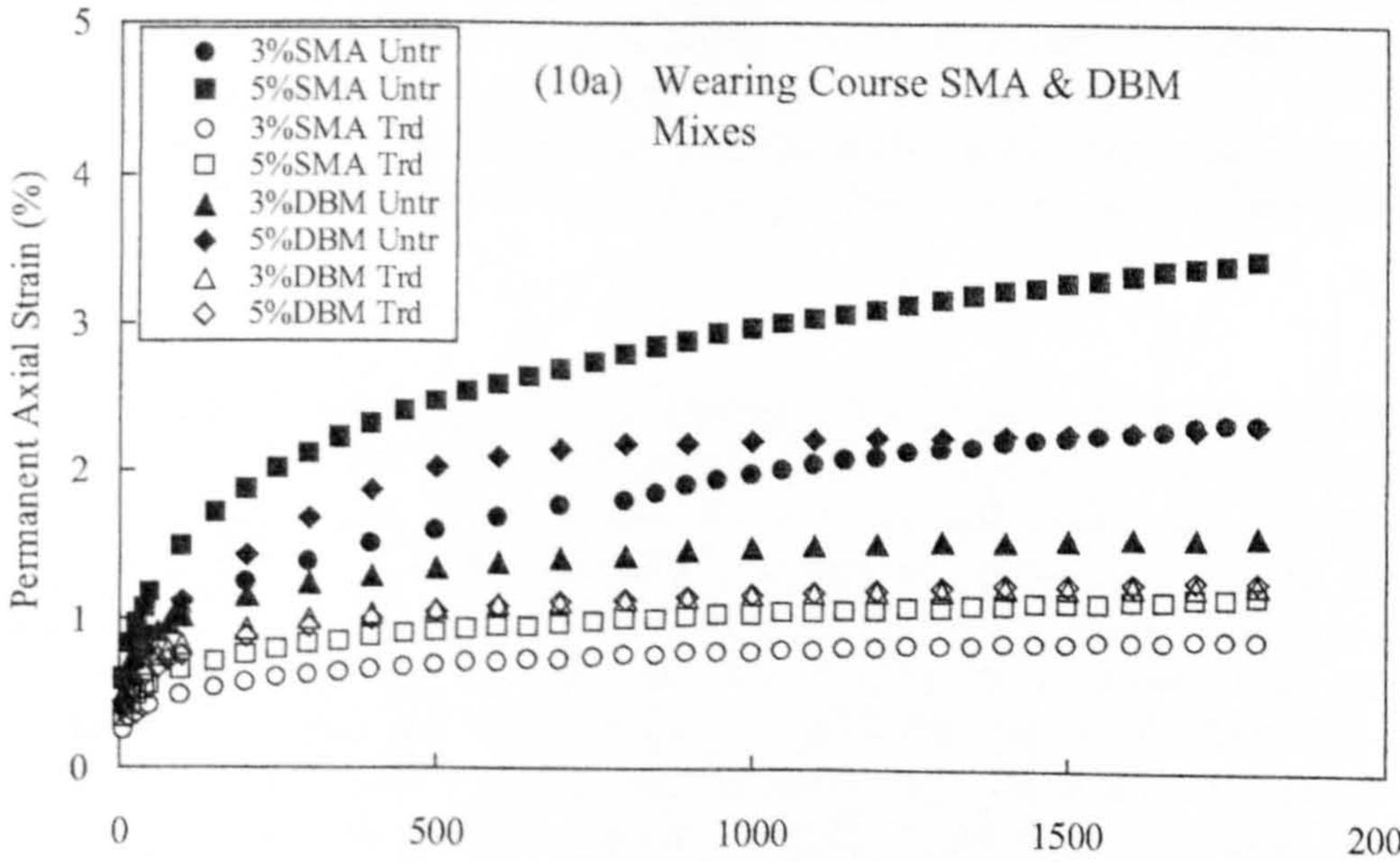

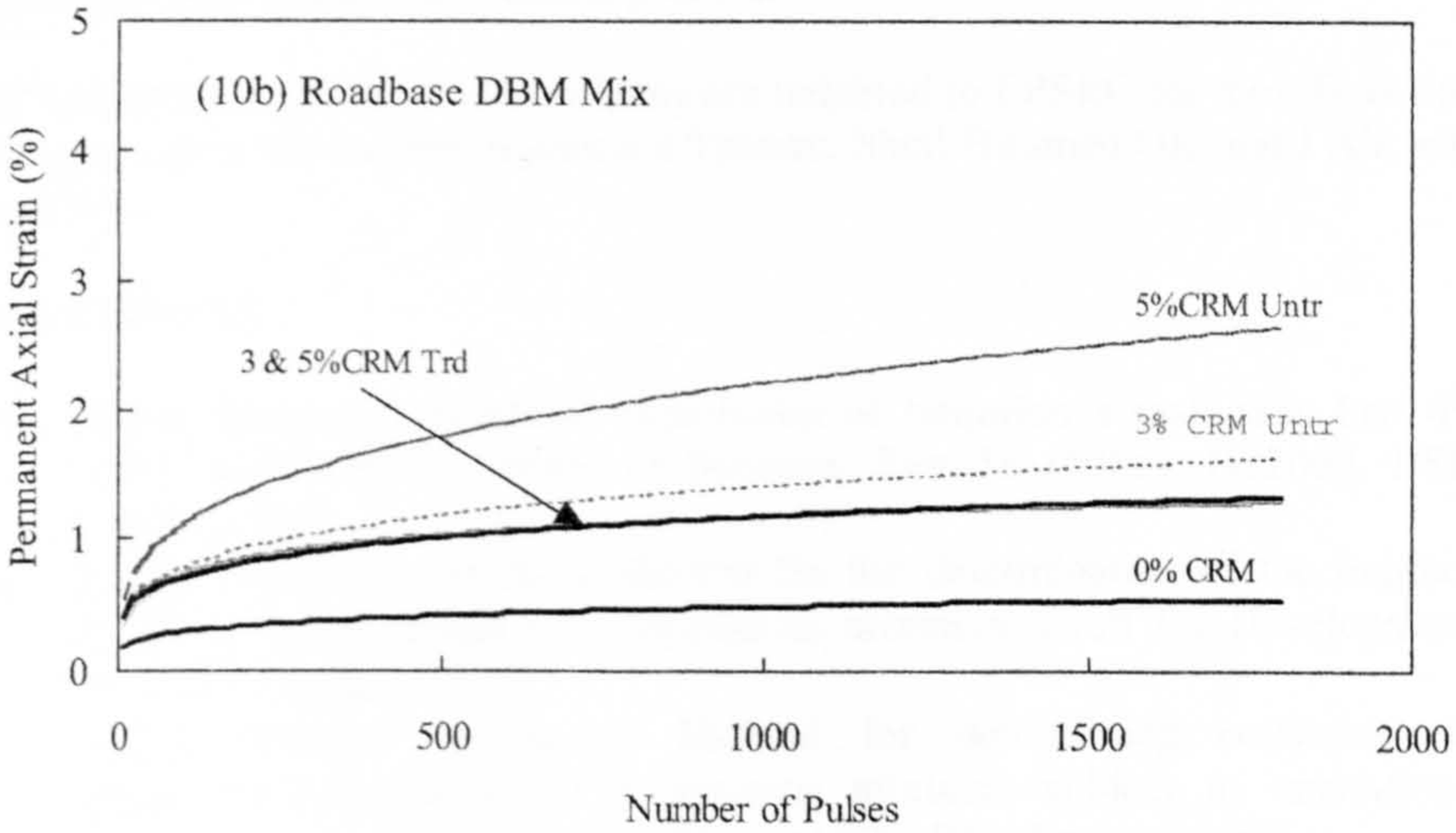

Figure 10. Effect of rubber addition in the dry process on the wearing course and roadbase mixes resistance to permanent deformation in the RLA

undergo larger reduction in stiffness upon immersion than the treated mixes (percentage reduction values given on histograms). The most notable difference between untreated and treated is that of the DBM-RB mix, where the retained stiffness increases from 56 and 40.7% to 99 and 98.3% at 3 and 5% rubber respectively after immersion. The permanent axial strain undergoes a reduction due to treatment for the SMA and DBM mixes, although the strain level is higher than that of the unmodified mixes shown in Figure 5. For the DBM-RB mix, even though treatment is seen to reduce the axial strain, the material's resistance to permanent deformation decreases due to dry process modification.

5. CONCLUSIONS

This study has shown that adding more than 10% CRM to the binder renders it too viscous for practical field applications. In the wet process, the stiffness and resistance to permanent deformation of the SMA and DBM mixes improved with CRM content. Whilst moisture sensitivity increased due to CRM modification, the retained stiffness values either remain or slightly increse with CRM content. In the dry process, the results have shown that rubber modification has an adverse effect on the volumetric, stiffness, durability and permanent deformation properties of the materials used and thus, there is no technical incentive to modify asphalt using this technique. However, it was shown that pre-treatment of the rubber to control its swelling has an improved effect on the untreated rubber, but still gives inferior properties to the neat mix.

Furthermore, pre-treatment with extender oils increases cost and introduces an additional step to the modification process.

ACKNOWLEDGEMENT: The authors are indebted to EPSRC for their financial support and to the Industrial partners Tarmac, Shell Bitumen UK and J Allcock and Sons.

REFERENCES:

[1] British Standars Institution, Penetration of bituminous materials, Part 49 (1983) and softening point of bitumen, Part 58 (1988), BS2000, BSI, London, 1988.
[2] British Standars Institution, Method for the determination of the indirect tensile stiffness modulus of bituminous mixtures, Draft for Development 213, BSI, London, 1993.
[3] British Standars Institution, Method for determining resistance to permanent deformation of bituminous mixtures subject to unconfined dynamic loading, Draft for Development 226, BSI, London, 1996.
[4] British Standars Institution, Method for sampling, BS 812: Part 102, BSI, London 1989.